Diss. ETH No. 6413

Body-Mounted Antennas

The Effect of the Human Body on the RF Transmission of Small Body-Mounted Biotelemetry- and Portable Radio Antennas in the Frequency Range 10-1000 MHz and Safety Considerations

A Dissertation submitted to the

SWISS FEDERAL INSTITUTE OF TECHNOLOGY ZURICH
for the degree of
Doctor of Technical Sciences

presented by

PETER A. NEUKOMM
Dipl. El. Ing. ETH
born July 28, 1943
Citizen of Hallau, Schaffhausen

Accepted on the Recommendation of
Prof. H. Baggenstos, referee
Prof. Dr. E. Baumann, co-referee

Juris Druck + Verlag Zurich
1979

ISBN 3 260 04682 8

PREFACE

This work is an attempt to present a survey on the problems dealing with body-mounted antennas. The effect of the human body on the radiation patterns has been investigated by theoretical models and experiments. A polarization transformation effect has been discovered which leads to a new class of antennas for the resonance frequency range of man. The safety aspects have been investigated by studying the available literature on biological effects of radio- and microwaves.

The author wishes to thank all who have contributed to this work. Valuable scientific support came especially from :

- Prof. H.Baggenstos in electromagnetic theory (ETH, Inst. Electronics)
- Prof. R.F.Harrington in computer programs and theory (Syracuse Univ.)
- Dr. R.M.Bevensee in near-field analysis and computer programs (Lawrence Livermore Laboratory)
- Prof. O.P.Gandhi in resonance absorption (University of Utah)
- Prof. A.W.Guy in phantom techniques (University of Seattle)
- Dr. Z.R.Glaser and Dr. D.L.Conover in safety aspects (NIOSH)

The experiments could be only performed by the technical assistance of:

- R.Graner and M.Knaute in antenna measurements (Division of Military aerodromes)
- W.Kerle in RF-instrumentation (PTT Switzerland)

I extend my thanks to the directors of the Laboratory of Biomechanics, ETH Zürich:

- Dr. B.M.Nigg and the late,much admired, Prof. J.Wartenweiler (ETH) for the general support of this work as a side branch of biomechanics.

Finally I appreciated the valuable comments and suggestions by

- Dr. J.Denoth (ETH, Laboratory of Biomechanics)
- Mrs. P.Fritz (Zürich)
- Prof. E.Baumann (ETH, Institute of Applied Physics)
- Prof. D.Kaufmann (University of Florida, visiting professor ETH)

and the drawing of the figures by Michael Fritz

P.A. Neukomm

to Vreni

CONTENTS

1. INTRODUCTION

Biotelemetry is concerned with the obtaining and transmission of measuring data from a free-moving subject. Among other transmission methods such as infrared and ultrasonic it is utilized for all modulated radiowaves in the frequency range 10 to 1000 MHz.

In radio telemetry one distinguishes between tracking (radio bearing and identification of subjects) and real measuring data transmission. In contrast to voice communication systems a non-interrupted data flow is required from a moving subject, because the redundancy of the signals is small and the test situation happens only once in many cases.

Multichannel telemetry equipment for the continuous recording of physiological, chemical, biomechanical and other data are primarily applied on human subjects in patient monitoring, exercise physiology and sport research. The encumbrance for the subject due to weight and volume of the equipment and the feedback of the apparatus on the measuring data should be as little as possible. With today's technology it is possible to produce miniature transducers and transmitters. Missing are, however, small, body-mounted antennas with good omnidirectional properties.

A small, trunk-mounted, or even a non-visible, efficient antenna on the subject would open new fields of application not only for biotelemetry. Many applications of mobile voice communication for security personnel, police agents, etc.,require a camouflaged antenna (GOUBAU and SCHWERING [32], KING [48]). Experience demonstrates however, that the transmission loss of small, body-mounted antennas amounts up to about 20-30 dB. This means that less than one percent of the RF energy can be utilized for transmission in unfavorable conditions. An enhancement of the power of the transmitter output for the improvement of transmission performance cannot be recommended for two reasons: In modern equipment the battery determines the final weight and volume of the transmitter, and RF-power in excess of 100 mW may exceed the safety limits for uncontrolled RF exposition (DDR-Standard [18], NEUKOMM [64]).

In the last few years various experimentalists attempted to quantify the influence of the human body on the radiation pattern of body-mounted antennas. Azimuthal radiation pattern measurements with horizontal polarized antennas were performed in the frequency range 6 to 280 MHz (BUCHANAN, MOORE and RICHTER [12]). Investigations with vertical polarized $\lambda/2$ dipoles demonstrated a dominant, but not explicable influence of the antenna-body distance at 450 and 900 MHz (KING and WONG [49]). The fitting of relatively large antennas to the body was investigated in the frequency range 33 to 170 MHz by means of the VSWR, and a main resonance of the human body was postulated to occur at 60-80 MHz (KRUPKA [53]). As a result from these works one may conclude, that the human body acts as a director, reflector or absorber at frequencies above 30 MHz. In spite of considerable effort no systematic relationship was found between body geometry, antenna-body-distance, frequency and radiation pattern.

A first attempt to compute the radiation pattern of an antenna-body system came out in 1977 (NYQUIST, CHEN and GURU [66]). The model consisted of a short dipole antenna with assumed sinusoidal current distribution, parallel to a rectangular cylinder subdivided in dielectrical volume elements. By means of tensor Green's functions various results at 50 MHz were computed, such as power depositions in the body, impedance change of the antenna and also the azimuthal radiation pattern for some antenna locations.

Up to now a general theory about the radiation characteristics of an antenna-body system is missing. The reasons for that gap are mainly:

- An antenna is a complicated radiation source. The fields around an antenna can be roughly categorized in near zone ($r<\lambda/2\pi$), far zone ($r>\lambda$) and transition zone. Within the near zone a strong reactive near field exists which is partially converted within the transition zone into an effective, real, radiating field. The final far field in the far zone is clearly described by the antenna parameter, as long as the near zone is not disturbed. But exactly this happens in the practical application of body-mounted antennas. Any antenna, especially an electrically small antenna, will be detuned by the body proximity. In spite of VSWR measurements one knows little about the radiated power and its radiation characteristics. If the antenna is combined with a fix transmitter (e.g., walkie-talkie) it is difficult to define a radiation reference level. If the antenna is remotely fed, surface waves on the feeding coaxial cables may radiate more than the antenna itself. Reflections from the ground effect a further, but estimable influence. In general, it is quite difficult to construct an antenna test set-up for antenna-body distances (d_{at}) below 0.2 m and signal levels below - 15 dB (0 dB = antenna in free space) with a measuring error of less than 3 dB. Therefore, systematic effects could not be detected by experiments in the past.

- Most experiments have been performed at some fixed frequencies and with some fixed antenna-body distances where the future use of the transmitter was planned. A systematic relationship can be recognized only if these parameters are changed in little steps over a large range.
- The human body exhibits a complicated, variable shape. The dielectric inherent properties of the individual body organs vary around 1:10. In addition they are strongly dependent on the frequency, with a distinct change at about 100 MHz (JOHNSON and GUY [45]).
- The frequency range of interest covers the resonance region of the human body. The largest circumference of a body (human body : measured from head to feet) is roughly equal to the wavelength of the first resonant frequency. In fact this is demonstrated by absorption computation and thermographic investigations, where the maximum absorption occurs at about 65 MHz, if a human body model is irradiated by a plane wave (GANDHI, HAGMANN and D'ANDREA [24], CHEN and GURU [14].

From the literature neither analytical resolvable models nor approximative methods are available which explain the radiation characteristics of actual body-mounted antennas in the entire frequency range. The method of NYQUIST, CHEN and GURU [66] could lead to a systematic explanation, if the model could be improved by parameter variation. However, an extension of that method exceeds the limited storage capacity and the computation time limits of our ETH computer. Thus,other models and computation methods have to be found in order to understand the systematic correlations in a antenna-body system and in order to develop new, efficient antenna configurations.

Leer - Vide - Empty

2. PROJECT

The fundamentals have to be prepared for the development of efficient, electrically small, body-mounted antennas with omnidirectional radiation patterns in the horizontal plane.

An antenna-body model has to be created which allows the computation of the systematic relation among frequency, body geometry, relative position of the antenna to the body and transmission loss. The model should be applicable for the entire frequency range from 10 to 1000 MHz.

A measuring method has to be developed which allows radiation pattern recording of body-mounted antennas in the entire frequency range from 10 to 1000 MHz. The measuring error should be less than 3 dB.

An investigation about the possible risks of body-mounted antennas has to be performed. The safety standard of some countries would prohibit the use of transmitters with sufficient power in combination with electrically small antennas. The international findings on biological effects of radio- and microwaves are controversial and the safety standards vary greatly from country to country. Biological effects may have an influence on the accuracy of biotelemetrical data and could lead to health hazards. The investigation should conclude in recommendations for reliable and safe use of transmitting devices with body-mounted antennas.

Leer - Vide - Empty

3. Symbols and Definitions

SYMBOL	NAME AND DEFINITION	UNIT
a	radius	m
a_s	radius of the radiansphere (4.5.) , $\lambda/2\pi$	m
$\vec{a}$	spherical radius vector (5.2.1.)	
ARP	azimuthal radiation pattern (7.2.1.)	
A_1	body-mounted antenna (5.1.2.) , usually electrically small ($h<\lambda/4$)	
A_2	remote antenna (5.1.2., 8.3.3.) , large broadband antenna	
$\vec{A}$	magnetic vector potential (6.3.2.)	Vs/m
$\vec{A}^{scat}$	scattered magnetic vector potential (6.3.2.)	Vs/m
B	bandwidth , $2\Delta f_{450}$ or frequency range between - 3 dB, (4.5.,16.1.)	MHz
BK	wave propagation constant k in computer programs (10.2.2.)	1/m
BMR	basal metabolic rate (4.1.), metabolic power dissipation	W/kg
$\vec{B}$	magnetic induction $\mu_r\mu_0\vec{H}$	Vs/m^2
c	velocity of light in vacuum, $2.9979\cdot10^8$ m/s	m/s
$\overrightarrow{curl}$	curl vector function, $\overrightarrow{curl}\,\vec{E} = \vec{\nabla}\times\vec{E}$	
C	capacitance, 1 Farad = 1 Coulomb/Volt	As/V
C	central nervous system (4.4.)	
CW	continuous wave	
C_{max}	maximum circumference of the body in wavelengths	1
d	transmission distance ($d \gg \lambda$) (5.1.2., 8.2.)	m
div	divergence vector function, div $\vec{E} = \vec{\nabla}\cdot\vec{E}$	
d_{at}	antenna-body distance , distance from A_1 to body surface (5.1.2)	m
d_g	thickness of the reflecting layer (5.3.2.)	m
dB	decibel, relative measure for power or field strength (5.1.2.) power: 10 log (P/P_0), field: 20 log (E/E_0)	1
D	refracted wave (5.3.2.)	
DRP	directive radiation pattern (7.2.1.)	
D_c	diameter of the infinite cylinder IZYL (5.4.1., 6.5.2.)	m
D_h	diameter of the helical antenna (4.5., 16.1.1.)	m
D_B	mean diameter of the trunk of a TS or test body (10.4.9.)	m
DTEST	1/4 of the test segment length in program PANB (6.4.5.1.,10.2.2.)	m

SYMBOL	NAME AND DEFINITION	UNIT
e	constant, e = 2.718	
EEG	electroencephalogram	
EM	electromagnetic (-wave)	
E_o	reference electric field strength for 0 dB, received field strength at optimal antenna polarization in quasi-free-space condition (5.2.1.)	V/m
E_h	horizontal component (ϕ-component) of an E-field near a body (5.2.1.)	V/m
E_n	perpendicular (normal) component of an E-field to a surface (6.3.)	V/m
E_r	radial component of an E-field with respect to body axis (5.2.1.)	V/m
E_t	tangential component of an E-field with respect to a surface (6.3.)	V/m
E_v	vertical component of an E-field near a body (|| body axis) (5.2.1.)	V/m
E_z^{inc}	incident electric field strength in z-direction	V/m
E_z^{ind}	induced electric field strength in z-direction	V/m
E_z^{scat}	scattered electric field strength in z-direction	V/m
E_z^{tot}	total electric field strength in z-direction	V/m
$\underline{\vec{E}}$	electric field intensity, complex vector	V/m
$\underline{\vec{E}}_{inc}$	general incident electric field	V/m
$\underline{\vec{E}}_{ref}$	general reflected electric field	V/m
$\underline{\vec{E}}(\vec{a})$	electric field at the relative position $\vec{a}$ to the body (5.2.1.)	V/m
$\vec{E}_\theta$	θ - ('vertical') polarized incident E-field (6.4.3.)	V/m
$\vec{E}_\phi$	ϕ - ('horizontal') polarized incident E-field (6.4.3.)	V/m
f	frequency in MHz, $f = \omega/2\pi$	1/s
f_{res}	resonant frequency (usually in MHz)	MHz
f_{lim1}	lower frequency limit due to Fresnel condition (5.3.1.)	MHz
f_{lim2}	lower frequency limit due to Rayleigh criterion (5.3.2.)	MHz
f_{lim3}	upper frequency limit due to plane wave condition (5.3.3.)	MHz
f_{lim4}	lower frequency limit due to far-field condition (5.3.3.)	MHz
f_{lim5}	maximum computational frequency in program HARRA (10.3.1.)	MHz
F	frequency in MHz in all computer programs	MHz
FFHD	flat folded helical dipole (16.1.2.)	
FHD	flat helical dipole (16.1.2.)	
FSL	free-space level = E_o = 0 dB (5.1.2.)	dB

SYMBOL	NAME AND DEFINITION	UNIT
FZYL	finite cylinder, computational body model (5.4.1.)	
g_n	Green's function (6.4.2.1.)	
$\overrightarrow{grad}$	gradient vector operator, $\overrightarrow{grad}\ \Phi = \vec{\nabla}\ \Phi$	
G_2	gain of the remote antenna A_2 (5.3.2.)	1
GA	ground plane antenna (16.1.2.)	
G_n	evaluated Green's function (6.4.2.1.)	
$Gain_B$	transmission gain, gain of antenna A_1 when body-mounted with respect to the quasi-free-space performance (5.1.2.)	dB
h	hour	h
h	physical length of an electrically small (monopole) antenna (4.5.)	m
h_1	height of A_1 above ground (5.1.2.)	m
h_2	height of A_2 above ground (5.1.2.)	m
h_{eff}	effective height of an antenna (for U_{ind} computation)	
h_B	relative height of the center of A_1 with respect to the feet of the test body, z-coordinate of A_1 in computation (5.1.2.,10.2.5.)	m
HDR	heat development rate, usually relative value (4.3.)	1
H_n	perpendicular (normal) component of a H-field to a surface (6.3.)	A/m
H_t	tangential component of an H-field with respect to a surface (5.3.)	A/m
H_x^{inc}	incident magnetic field strength in x-direction	A/m
H_x^{scat}	scattered magnetic field strength in x-direction	A/m
H_x^{tot}	total magnetic field strength in x-direction	A/m
$\underline{\vec{H}}$	magnetic field intensity, complex vector	A/m
$\underline{\vec{H}}_{inc}$	general incident magnetic field	A/m
$\underline{\vec{H}}_{ref}$	general reflected magnetic field	A/m
$\underline{H}_n^{(2)}(kr)$	Hankel function, second kind, order n (6.5.2.)	
I	current	A
j	square root of -1, imaginary number	1
$\vec{j}$	electric current density in a volume element (6.3.4.)	A/m^2
J_t	tangential electric current density (6.3.1.)	A/m
$J_n(kr)$	Bessel function, order n (6.5.2.)	
$\vec{J}$	electric current density on a surface (6.3.1.)	A/m
k_m	amount of the wave propagation factor in a medium	1/m

SYMBOL	NAME AND DEFINITION	UNIT
$\vec{k}$	wave propagation factor $2\pi/\lambda$ in free space	1/m
KK	number of regarded modes n in computer program PANB	1
L	inductance, 1 Henry = 1 Vs/A	Vs/A
LPD	logarithmic periodic antenna (remote antenna A_2) (8.3.3.)	
L_B	length of the TS or test body (10.4.9.)	m
$Loss_B$	transmission loss caused by the body, (= - $Gain_B$) (5.1.2.)	dB
L(J)	integro-differential operator (6.4.1.)	
m	refraction index, $m = k_m/k$ (5.3.2.)	1
M	number of division of the interval 0 to π in computer programs	1
MANMOD	conducting human body model, sagittal or lateral view (5.4.1.)	
MET	metallic cylinder (for experiments) (5.4.1.)	
MHz	megahertz, 10^6 Hz	1/s
MW	microwave, frequencies above 300 MHz	
n	mode number (in expansion functions) (6.4., 6.5., 10.3.1.)	1
N	number of tangential units along the contour curve of a body of revolution (6.4.)	1
NN	number of modes to be computed in program HARRA	1
NP	number of body contour points, (NP-1)/2 = N, program HARRA and PANB	1
NPHI	number of division of the interval 0 to π in program HARRA and PANB	1
NNPHI	number of computed azimuthal field points in program PANB and PANC	1
NTEST	number of test segments in program PANB (10.2.4.)	1
N_h	number of turns of a helical monopole antenna (16.1.)	1
P_1	polarization of antenna A_1, orientation of the main polarization axis in the space, vertical, radial or horizontal (5.1.2.,10.2.5.)	
P_2	polarization of antenna A_2, vertical or horizontal (5.1.2.)	
P	real power in watt	VA
PHA	phantom cylinder (for experiments) (5.4.1.)	
P_{abs}	absorbed power in a lossy medium, watt (4.3.)	VA
P_{in}	input power at a transmitting antenna, watt (5.3.2.)	VA
P_{loss}	dissipated power in a transmitting antenna, watt (4.5.)	VA
P_{rad}	radiated power from a transmitting antenna, watt (4.5.)	VA
P_{reac}	reactive power near a transmitting antenna (4.5.)	VA

SYMBOL	NAME AND DEFINITION	UNIT
P_{real}	real power (rad+loss) from and in a transmitting antenna (4.5.)	VA
P_{scat}	total scattered power from an object (5.2.3.)	VA
$\vec{P}$	power density, Poynting vector $\vec{P} = \vec{E} \times \vec{H}$, usually in mW/cm² (4.5.)	VA/m²
$\vec{P}_{real}$	real power density, computed from P_{rad} only, mW/cm² (4.5.)	VA/m²
$\vec{P}_{reac}$	reactive power density, $\lvert\vec{P}_{real}\rvert \cdot Q$, mVA/cm² (4.5.)	VA/m²
Q	Q-factor, ratio f_{res}/B or stored energy/radiated+lossed energy in an RLC network (4.5.)	1
r	radius or distance	m
$\vec{r}$	radius vector from origin of coordinate system (6.3.2.)	m
$\vec{r}'$	radius vector of a source point from origin of coordinate system	m
R	amount of the distance between source and observation point, $\lvert\vec{R}\rvert = \lvert\vec{r} - \vec{r}'\rvert$ (6.3.2., 6.4.)	m
R	resistance, Ohm	V/A
RACS	relative absorption cross section (4.3.)	1
RCS	radar cross section, usually related to shadow area (5.2.3.)	m²
RF	radio frequencies, frequencies below 300 MHz	
RH	radius of a contour point in programs HARRA and PANB (10.2.2.)	m
RHD	round helical dipole (16.1.)	
RTEST	radius of the test segment center point (6.4.5.1., 10.2.2.)	m
R_{loss}	loss resistance of an antenna (4.5., 16.1.1.)	V/A
R_{rad}	radiation resistance of a transmitting antenna (4.5., 16.1.1.)	V/A
$\underline{R}_E$	reflection coefficient of the E-field of a TE-wave (5.2.4.)	1
$\underline{R}_H$	reflection coefficient of the H-field of a TM-wave (5.2.4.)	1
[R]	measurement row matrix (6.4.3.)	
s	distance from ground to feet of TS (5.1.2.)	m
S	surface of a body	m²
SAR	specific absorption rate, in W/m² or W/kg (4.3.)	VA/g
SUB	standard human test subject (5.4.1.)	
t	time	s
t	index, means tangential (to a surface) component (6.3.)	
$\vec{t}_{1,2}$	tangential unit vectors on a surface of a body (6.3.5.)	1
TE	transversal electric mode, horizontal polar. (5.2.4., 5.3.2.)	

SYMBOL	NAME AND DEFINITION	UNIT
TEM	transversal electro-magnetic mode, general case (5.2.4.)	
TM	transversal magnetic mode, vertical polarization (5.2.4., 5.3.2.)	
TS	test subject	
U	voltage	V
U_{ind}	induced voltage at the antenna terminals (5.2.2.)	V
V	volume of a body	m^3
VSWR	voltage standing-wave ratio, ratio of U_{max}/U_{min} (16.1.)	1
V_{eff}	effective volume of an antenna, computational value (4.5.)	m^3
V_s	volume of the radiansphere = $\lambda^3/6\,\pi^2$ (4.5.)	m^3
[V]	excitation matrix (6.4.1.)	
$\vec{W}_i$	testing function (6.4.1.)	
[Y]	admittance matrix (6.4.1., 10.2.2.)	
$Y_n(kr)$	Neumann function (Bessel function of second kind) (6.5.2.)	
Z	Impedance	V/A
ZH	height of a contour point in programs HARRA and PANB (10.2.2.)	m
ZTEST	height of the test segment center point (6.4.5.1., 10.2.2.)	m
Z_0	characteristic impedance of vacuum, Z_0 = 377 Ohm	V/A
Z_m	characteristic impedance of a medium (5.3.2.)	V/A
[Z]	impedance matrix (6.4.1., 10.2.2.)	
α	incident angle with respect to a body surface (5.2.4.)	°
β	phase factor (5.2.2.)	1
$\underline{\alpha}_n$	Fourier coefficient (6.5.2.)	
γ	reflection angle (glancing angle) of a wave to the ground (5.1.2.)	°
γ_B	Brewster angle, total refraction of a TM-wave (5.1.2, 5.3.2.)	°
$\underline{\Gamma}$	refraction coefficient of the air-medium interface at perpendicular (normal) wave incidence (4.2., 5.2.4.)	
δ	penetration depth of a wave into a medium (4.2., 5.2.4., 6.2.)	m
δE	maximum field strength variation along antenna axis (5.2.2.)	dB
$\delta\Phi$	maximum phase variation of the field along antenna axis (5.2.2.) (δE and $\delta\Phi$ are measurements for the field homogeneity, 10.3.5.)	°

SYMBOL	NAME AND DEFINITION	UNIT
ΔU	ratio actual induced voltage U_{ind} to approximated induced voltage $\overline{U}_{ind}$ (from center field) in dB (5.2.2., mean error 10.2.5.)	dB
Δ_{s1}	path difference for the first Fresnel Ellipsoid (5.3.1.)	m
Δ_{s2}	path difference of a rough surface (Rayleigh criterion) (5.3.2.)	m
Δ_{s3}	path difference of a plane wave along the body axis (5.3.3.)	m
$\Delta_{s3'}$	path difference of a spherical wave along body axis (5.3.3.)	m
$\Delta_{\psi 2}$	phase difference due to the reflection of the wave at a rough surface, Rayleigh criterion : $\Delta_{\psi 2} < \pi/2$ (5.3.2.)	°
ε	total permittivity	As/Vm
ε_m	permittivity of a medium (total permittivity)	As/Vm
ε_0	dielectric constant, $\varepsilon_0 = 8.854 \cdot 10^{-12}$ F/m or As/Vm	As/Vm
ε_r	relative dielectric constant of a medium	1
θ_{el}	elevation angle of an incident wave above ground (5.1.2.)	°
θ_d	refraction angle (5.3.2.)	°
θ_i	incident angle of a wave (to the body axis) (5.1.2.)	°
θ_T	angle of the test segment to the body axis (6.4.5.1.)	°
λ	wavelength	m
λ_m	wavelength of a wave in a medium (4.2.)	m
λ_0	wavelength of a wave in vacuum	m
μ	total permeability	Vs/Am
μ_m	permeability of a medium (total)	Vs/Am
μ_0	permeability of vacuum, $\mu_0 = 4\pi \cdot 10^{-7}$ H/m or Vs/Am	Vs/Am
μ_r	relative permeability of a medium	1
ρ	radius of a point on the surface of the body of revolution (6.4.)	m
ρ_m	distributed charges in a medium (charge density) (6.2.)	As/m³
σ, σ_m	conductivity of a medium in S/m or mho/m (4.2.)	A/Vm
σ_{su}	surface charge density on a body (6.3.)	As/m²
ϕ	azimuthal rotation angle (in the horizontal plane) (5.1.2.)	°
Φ	electric potential (6.3.3.)	V
ψ	phase of the reflection coefficient (5.3.2.)	°
$\Psi(z)$	current distribution function along the antenna axis (5.2.2.)	1
ω	angular frequency, $\omega = 2\pi f$ in rad/s	1/s

Leer - Vide - Empty

4. Safety Aspects of Radio- and Microwaves

4.1. INTRODUCTION AND HISTORICAL BACKGROUND

Body-mounted antennas are used in biotelemetry and walkie-talkies. Biotelemetry transmitters are applied on human test subjects and animals in order to record physiological and other data with minimum encumbrance for the test subject. Great efforts are made to reduce the influence of the measuring equipment on the data to be measured. In this chapter we are therefore not only interested in possible health hazards of radio transmitters but also in effects which may falsify the recorded data.

The subject is within the near-zone of a radiating source if body-mounted antennas are used. Due to the smallness of the antenna and due to the small antenna-body distance (d_{at}), the power density ($\vec{P}$) at the subject's surface may exceed the maximum permissible values of some safety standards. As an example the consequent application of the German Democratic Safety Standard [18] prohibit such transmitting devices if the radiated power exceeds a few mW.

The non-ionizing electromagnetic (EM) spectrum encompasses frequencies from 1 Hz to 10^{19} Hz. In general, frequencies from about 0.03 MHz to 300 MHz are called radio frequencies (RF) and frequencies from 300 MHz to 300,000 MHz are designated as microwaves (MW). In analogy to the well established safety standards for ionizing radiation the purpose of the less known safety standards for non-ionizing radiation is to protect a large population from uncontrolled exposure. A safety standard is always a compromise between absolute safety and practical realization. The permissible limits should exclude health hazards based on the present state of science. Under certain, well-described conditions the safety limits may be exceeded willingly if the risks resulting from other factors can be considerably reduced. For example, the application of a powerful ECG telemetry transmitter for the monitoring of heart disease patients is justified if the physician in charge considers a permanent heart monitoring as urgent.

A meaningful application of the safety standard requires the knowledge of the risks and often also the history of the standard's development. Until about 1945 "low-power" non-ionizing EM radiation was generally considered completely harmless. It was known that dielectrical materials can be heated internally with high RF power, an effect which is applied in diathermy for the clinical warming-up of certain body regions (MOOR [60], SCHWAN [73]). During World War II the U.S. Department of Defense medical services became interested and concerned about possible hazards associated with the development, operation and maintenance of the increasing numbers of radar sets and other RF emitting electronic equipment. The main reason for that interest was reports about human microwave cataractogenesis (see MILROY and MICHAELSON [59]), HIRSCH and PARKER [44]) in radar repairmen who have been exposed to power densities in excess of 100 mW/cm^2. After some investigations by the U.S. Navy and the U.S. Air Force, responsibility for research on biomedical aspects was delegated in 1957 to "Tri-Service-Program" directed by the USAF. This program, well described by MICHAELSON [58], included investigations on effects of exposure on whole-body, selective organs and tissues, single cells and enzyme systems, using various power levels, for pulsed and continuous waves in the frequency spectrum from 200 to 24,500 MHz. Basic work for the understanding of thermal effects was performed by SCHWAN and PIERSOL [74] on the field of power matching, absorption, penetration depth, etc.. Non-thermal effects such as field force effects on molecules (pearl chain formation , MUTH [61]), orientation of macromolecules (HELLER [43]), activation of membranes and neurons (e.g., LIVESHITS [55]), macromolecular resonance denaturation (e.g., BACH, LUZZIO and BROWNELL [4]) and many other effects have been investigated in that period. The listed non-thermal effects occurred only at high field intensities, so that the thermal effects were considered as dominant. A safe limit of 10 mW/cm^2 power density was defined which is still valid now (ANSI 1974 [2]) in the USA and in most of the western countries.

The power density number of 10 mW/cm^2 has the following origin: the metabolic processes of the human body amount to about 1 W/kg when averaged over the total body mass for the sleeping state (BELDING and HATCH [8], GUY [35]). This Basal Metabolic Rate (BMR) for the whole body may be exceeded by that of individual organs; for example, the heart muscle has a metabolic rate of 33 W/kg, the brain 11 W/kg, the liver 6.7 W/kg, the skeletal muscle 0.7 W/kg (GUY [35]). As a fundamental, limiting criterion an artifical power deposition of 1 W/kg averaged over the whole body was defined. Such an external heating increases theoretically the head core temperature by about 0.15 ^{o}C and the body muscle temperature by about 1^{o}C (EMERY et al. [22]). This heating is considered harmless since it is comparable with the heat produced by physical exercise. It was argued that since the BMR of the human body is in the order of 75 watts for a 70 kg man with a body surface of about 1.9 m^2, this represents an equivalent areal heat production rate of about 4 mW/cm². Since half of the surface area would be available for single sided exposure to a MW field, by limiting the maximum continuous MW exposure on 10 mW/cm², one would expect no more than a doubling of the BMR in the body. (See limitations of this simplistic model in the next sections and TELL [77].) The philosophy of permissible heat loading concerns mainly the protection against destruction. Furthermore, clearly defined test conditions were choosen, e.g., in animal experiments an isolated test subject was exposed to a plane wave and great effort has been made to keep the field homogeneous. From the power density 10 mW/cm² the equivalent free space field intensities were derived for near-field conditions (E-field 200 V/m, H-field 0.5 A/m).

The Russian and generally the Eastern safety regulations are based on other considerations. The regulations concerning the power density are up to 10,000 times more stringent and the exposure duration is limited. As an example the GDR safety standard [18] demands that the power density in the MW region should not exceed 10 µW/cm² at 8 h/day, and for the same exposure duration the E-field should not exceed 2 V/m in the frequency range 50 to 300 MHz. The H-field is not limited up to now, but since GUY [36] could prove that the H-field induced E-fields inside a human body are larger than the E-field induced E-fields in the frequency range 1 to 20 MHz, an appendix regarding permissible H-fields is to be expected. These very limiting safety standards are based mainly on effects studied in encephalography, biochemistry, cardiovascular pathophysiology etc. and are often connected with investigations in occupational medicine. Soviet investigators have stressed that the central nervous system is highly sensitive to all modes of radiation exposure. Their conceptional approach is based to a large extent on Pavlovian methods as can be seen from the many publications about changes in conditioned reflexes (GORDON, ROSCIN and BYCKOV [30]), see also summary of MICHAELSON [57]). Without discussing the details of the Eastern investigations it is evident that <u>alterations of functions</u> of complicated biological systems occur at much lower field intensities (nonthermal or microthermal effects) than material alterations or destruction. In the late 1960's the Eastern literature was reaching the American microwave community and initiated a broad research on low-level effects. One reason for this new interest was the introduction of microwave ovens in the USA, where the microwave leakage is in the range from 0.7 to 20 mW/cm^2 (CONSUMER REPORTS [17]) in contrast to the reported effects at a power density level of 10 $\mu W/cm^2$ to 5 mW/cm^2 (GORDON [30,31]). In 1971 GLASER [29] from the U.S. Electromagnetic Radiation Project Office began with a bibliography on reported effects and clinical manifestations attributed to MW and RF radiation. During this time the ninth supplement came out so that about 4,600 citations are available.

Some of the Eastern findings could not be reproduced in the West. Criticized were the insufficiently described test methods (see e.g. PROCEEDINGS WARSAW [69]). If more than one animal is kept in a cage for animal experiments, the field homogeneity may be disturbed by a factor of 100. Reflections from the cage walls and ground effects lead to enhanced absorption. If a rat is placed in a reflector corner, an averaged incident power density of 10 mW/cm^2 may lead to an absorption of 200 W/kg (GANDHI [26,27]). On the other hand it must be pointed out, that under working conditions, reflections exist and that no long-term investigations have been performed with controlled conditions. The stringent Eastern safety standards which have been prepared above all for the protection of workers in factories are reasonable from this point of view.

In the following sections the physical background of RF and MW absorption and recent investigations on biological effects will be presented in order to estimate safety recommendations for body-mounted antennas.

4.2. ELECTRIC AND MAGNETIC PROPERTIES OF BIOLOGICAL MATERIALS

The investigations of the electric and magnetic properties were mainly performed during the last 30 years. Only the most important results can be discussed here; additional data and computation formulas can be found e.g., by TOLER and SEALS [79], SCHWAN and LI [75], JOHNSON and GUY [45].

Biological material is non-magnetic and can be characterized by their dielectric properties: conductivity σ and relative dielectric constant ε_r. The dielectric properties depend on the material and the frequency. In TABLE 1 these dielectric properties and the properties of the electromagnetic waves in the media are shown for two typical biological material groups:

PROPERTIES OF ELECTROMAGNETIC WAVES IN TWO GROUPS OF BIOLOGICAL MEDIA								
	GROUP A Muscle,Skin, and Tissue with High Water Content				GROUP B Fat,Bone, and Tissue with Low Water Content			
Frequency f [MHz]	40.7	100	300	915	40.7	100	300	915
Wavelength in Air λ_0 [cm]	738	300	100	32.8	738	300	100	32.8
Wavelength in Media λ_m [cm]	51.3	27.0	11.9	4.5	187	106	41.0	13.7
Relative Diel. Constant ε_r [1]	97.3	71.7	54.0	51.0	14.6	7.5	5.7	5.6
Conductivity σ [mmho/m] or σ [mS/m]	690	890	1370	1600	13-53	19-75	32-107	56-147
Depth of Penetration δ [cm]	11.2	6.66	3.89	3.04	118	60.4	32.1	17.7
Refl.Coeff. $\underline{\Gamma}$ $\lvert\underline{\Gamma}\rvert$ [1] arg($\underline{\Gamma}$) [°]	0.91 +176	0.88 +175	0.83 +175	0.77 +177	0.62 +173	0.51 +168	0.44 +169	0.42 +173

TABLE 1 Properties of electromagnetic waves in two groups of biological media. (Source: JOHNSON and GUY [45]).

The dielectric behavior of the two groups of biological materials listed in TABLE 1 has been evaluated most thoroughly by SCHWAN and his associates [73,74,75]. The biological tissues are composed of cells encapsulated by thin membranes containing an intracellular fluid. The increase of the conductivity σ and the decrease of the relative dielectric constant ε_r with increasing frequency can be explained for group A by the interfacial polarization across the cell membrane. The cell membranes, with a capacity of about 1F/cm^2, act as insulating layers at low frequencies so that currents flow only in the extracellular medium. At higher frequencies the reactance decreases, resulting in increasing currents in the intracellular medium. The most noticeable change can be observed at about 100 MHz. A current density of about 1 mA/cm^2 produces a heat equal to that due to the BMR (SCHWAN [72]).

The depth of penetration δ of RF and MW power into the material is defined as the distance required to reduce the power by e^2. The indicated values are valid only for a plane slab, an extended investigation of KRITIKOS and SCHWAN [52] on the distribution of heating potential inside lossy spheres has revealed hot spots in depths which may be larger than δ. The hot spots appear inside only for spheres with radii from 0.1 to 8 cm and frequencies from 300 to 12,000 MHz and are of importance mainly in animal experiments (see e.g., GUY [35]).

The reflection coefficient $\underline{\Gamma}$ of the air-media interface will be important for the later computation of the scattering properties of a biological body. A $\underline{\Gamma}$ of 0.88/+175° (group A, TABLE 1) means that the reflected wave will be only about 1 dB less than whose reflected from a perfect conductor and will show the same phase (dB: 20 log E/E_0, E_0 reference E-field, E measured E-field, see chapter 5.1.2). For the computation of the absorption of electromagnetic energy in a multi-layer medium, also the reflection coefficients from one layer to the other are of importance as can be seen in the next section.

4.3. ABSORPTION OF ELECTROMAGNETIC ENERGY IN BIOLOGICAL MATERIAL

The determination of the absorbed power in an arbitrarily shaped inhomogeneous biological medium needs a great computational effort. However, the multi-layer plane slab model is well investigated and may serve as a first approach for the absorption phenomena.

A simple plane slab model consists of two infinite layers of a certain thickness which are irradiated perpendicularly by a plane wave. (FIGURE 2: irradiation from the left, first layer = 3 cm fat, second layer = 10 cm muscle)

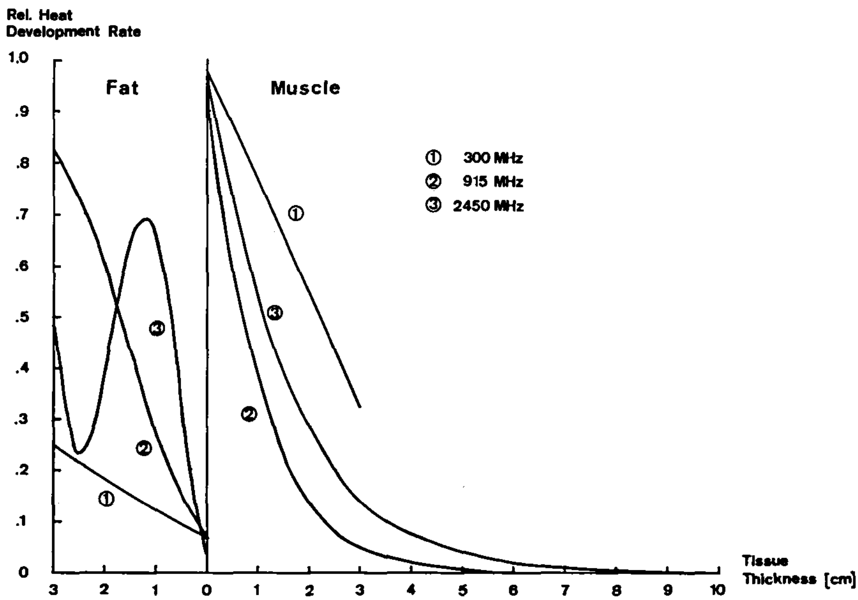

FIGURE 2 Relative Heat Development Rate (HDR) in a two-layer model. (Source: TELL [76], SCHWAN and PIERSOL [74])

The power which is absorbed in a volume element V and which is converted into heat is given by the formula (1):

$$P_{abs} = \frac{1}{2} \int_V \sigma \, |\vec{E}(\vec{r})|^2 \, dV \qquad (1)$$

The specific absorption rate (SAR) can be obtained by relating P_{abs} to the volume (W/cm^3) or to the specific gravity (W/kg). The electric field strength $\vec{E}(\vec{r})$ can be computed by the reflection coefficients and the attenuation factors in the two layers. Since the impedances of the materials are complex, a feasible method of solution is to apply the Smith Chart as demonstrated by TELL [76].

The SAR leads directly to the Relative Heat Development Rate (HDR) by dividing the obtained SAR's by the maximum obtained SAR (FIGURE 2). The heat actually produced could be computed by applying the laws of thermodynamics, but since thermal data (heat conduction, external cooling, etc.) are difficult to obtain with the required accuracy, thermographic methods are better suited (GUY, WEBB and SORENSEN [36]).

In FIGURE 2 it is interesting to see that the HDR in the fat layer depends directly on the intrinsic wavelength λ_m. At 915 MHz the fat layer is about $\lambda_m/4$ (TABLE 1) and acts therefore as a $\lambda/4$ impedance transformer. The result is a high HDR at the irradiated surface and a sharp rise just inside the muscle layer. At 300 MHz the heating in the fat is much less than in the muscle, and at 2,450 MHz the surface heating of the fat layer is about 68 percent of the maximum heating which occurs deeper within the fat.

This simple plane slab model is a good model for local application of a guided plane wave (diathermy applicators etc.), but does not adequately describe RF and MW absorption in complicated biological structures with irregular geometry, especially if the dimension of the body is comparable to the wavelength.

The absorption of EM energy in a three-dimensional body depends greatly on the body geometry and the wavelength. An adequate measure to describe this phenomenon is the Relative Absorption Cross-Section (RACS):

In FIGURE 3 a dielectric sphere with a radius a is shown which is irradiated by a plane wave (SCHWAN [72]). The RACS is defined as the ratio of absorbed power to the incident power. The incident power can be computed from the incident power density (in free space) multiplied by the shadow area πa^2; the absorbed power can be computed by several methods or determined by thermal measurements. An RACS smaller than 1 means that a part of the incident power is reflected or transmitted through the sphere. An RACS greater than 1 means that the effective shadow area is greater than the physical area πa^2 or, in other words, that EM power is extracted also from outer regions around the sphere.

Where are 3 different regions (FIGURE 3) : for small radius a (or for long wavelengths λ) the RACS is small, but increases rapidly with size.

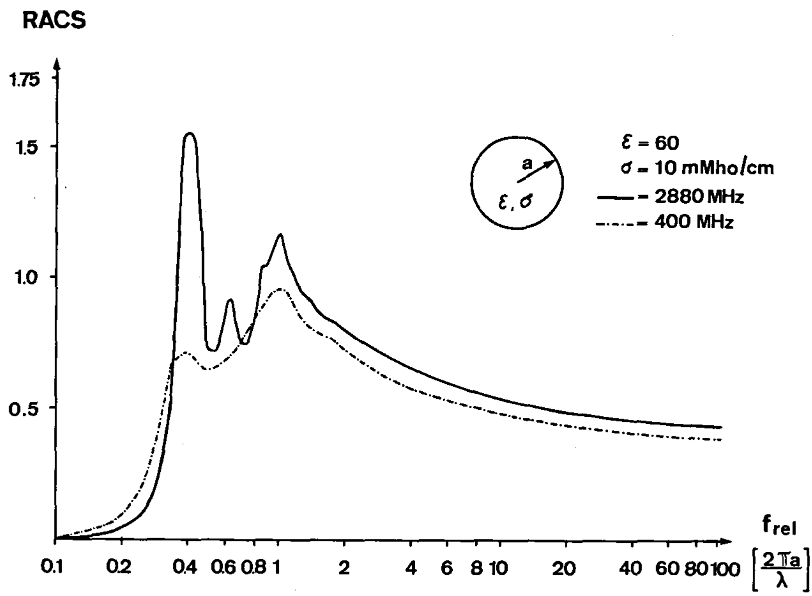

FIGURE 3 Relative Absorption Cross-Section (RACS) of a sphere of tissue-like dielectric properties as a function of the relative frequency f_{rel} (sphere circumference $2\pi a$ /wavelength λ) (Source: SCHWAN [72]).

For large radius a (or short wavelengths λ) the RACS is about 0.5 since the sphere reflects a part of the incident power. High RACS's occur, if the circumference of the sphere is almost equal to the wavelength. For $2\pi a/\lambda$ between 0.4 and 1.5 the RACS may exceed 1. In that resonant case not only is the absorption very high, but also the field homogeneity around the sphere is disturbed; an effect which will be important in the later field computation outside the irradiated body.

GANDHI et al.[25] continued RACS investigations with dielectric ellipsoids and various field polarizations. An ellipsoid with the axis a/b of 6.34 shows an RACS of about 4.2, if the incident E-field is polarized parallel to the main axis a and if the length L (2a) of the ellipsoid is about $\lambda/2$.

Specific Absorption Rates (SAR, see above) of body elements were determined by GANDHI, HAGMANN and D'ANDREA [24] and are shown in FIGURE 4: A saline-filled man model was irradiated in free space with a power density of 1 mW/cm^2. The maximum averaged SAR for the whole body amounts to 0.2 W/kg and occur at 68 MHz for a model length of 1.75 m. The SAR of the leg and of the neck may reach 0.4 W/kg as can be seen from FIGURE 4.

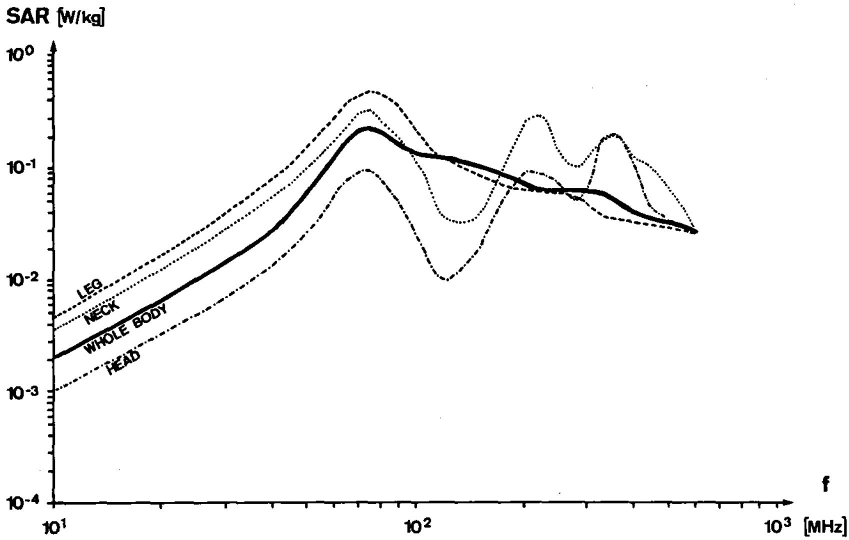

FIGURE 4 Specific Absorption Rate (SAR) for a 1.75 m man model at an incident power density of 1 mW/cm² in free space, vertical polarization. (Source: GANDHI, HAGMANN and D'ANDREA [24])

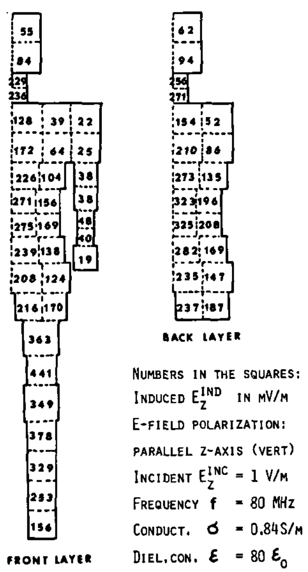

FIGURE 5

The z-component (vertical) of induced electric field. Incident EM-Wave: vertical polarization, incident E_Z^{inc} 1 V/m, 80 MHz.

Compared with FIGURE 4 at an incident power density of 1 mW/cm² and 70 MHz the maximum SAR's occur at the knee (0.4-0.5 W/kg) and in the neck (0.2 W/kg). (Source: CHEN and GURU [15])

In FIGURE 5 the computed induced E-field components in the z-direction are shown in a body model irradiated by a vertical polarized EM-wave (CHEN and GURU [15]. The incident E-field is 1 V/m and the frequency 80 MHz. The highest induced E-field occurs in the knee region and is about 0.44 times the incident field. The computed SAR's agree with the measurement of GANDHI et al. [24,25] . High values are obtained mainly in the leg, the thigh and the neck. At horizontal polarization the largest SAR's occur at about 200 MHz and are located in the chest amounting to 0.4 W/kg at 1 mW^2 incident power density level (CHEN and GURU [15]). The dielectric properties σ and ε in experiment and computation are similar to those of group A in TABLE 1. If the computer capacity is available, they could be varied for each cube for future refinement with more cubes.

Up to here the human body was considered to be in free space. The effects of the presence of reflecting surfaces and ground effects were studied by GANDHI et al. [24,26,27]. The SAR's for the whole body and some intact anatomical parts of a man for an incident power density of 1 mW/cm^2 is shown in FIGUR 6, where man is in good electrical contact with a high conducting ground plane:

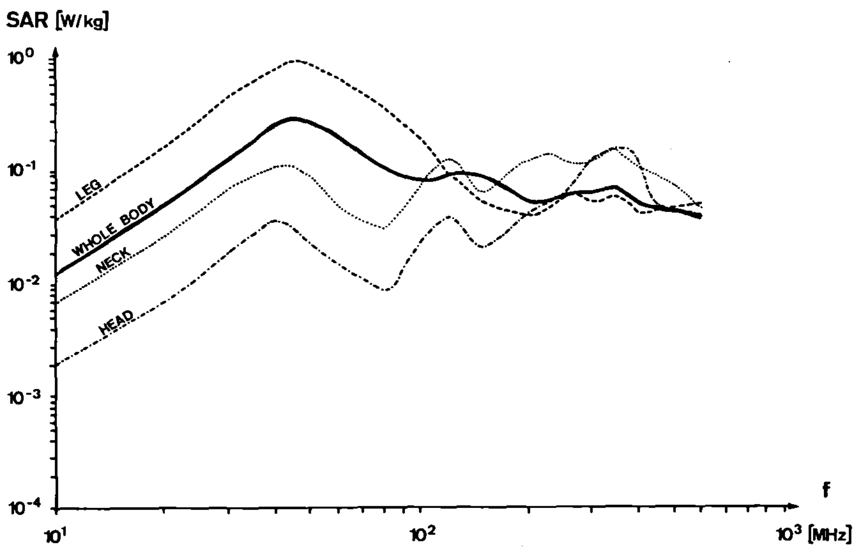

FIGURE 6 Specific Absorption Rate (SAR) for a 1.75 m man model in good electrical contact with a high conducting ground plane. The incident power density is 1 mW/cm^2. (Source: GANDHI, HAGMANN and D'ANDREA [24])

The resonant frequency is now near 35 MHz, and the SAR's are about twice as high than in the ungrounded condition. The SAR of the whole body amounts to about 0.3 W/kg, the SAR of the leg to about 1 W/kg at an incident power density of 1 mW/cm^2. The indicated SAR's are those integrated over basic anatomical structures and do not reveal the worst case.

A further increase of the SAR in the whole body can be observed when the man is placed in front of a flat reflector (1W/kg), in a 90^0 corner reflector (6W/kg) and in a corner reflector with ground contact (12W/kg) (all values related to a power density of 1 mW/cm^2).

In the introduction it has been mentioned that the fundamental, limiting criterion was a power deposition of 1 W/kg which is equal to the BMR. At frequencies below 20 MHz and above 300 MHz the present U.S. safety standard of 10 mW/cm^2 fulfills this criterion. However, a more stringent safety standard seems to be reasonable for the resonance frequency range 20 to 300 MHz.

4.4. OBSERVED BIOLOGICAL EFFECTS OF RF AND MW

Although some thousand recent investigations on biological effects are available (see bibliography of GLASER et al. [29]), the effects at low-power densities are not yet understood in a larger context. Most of the experiments were carried out with small animals at frequencies above 300 MHz, therefore the results of such investigations cannot be transferred directly onto large animals or humans. Some few examples should give an overview on the variety of the documented effects.

The teratogenic effects of MW in insects were studied by LIU, ROSENBAUM and PICKARD [56] by irradiating the pupae of the darkling beetle *Tenebrio Molitor* during its metamorphosis. A statistically significant increase in malformations in the adult insect was observed at power levels as low as 170 $\mu W/cm^2$. The pupation time increased monotonically with the power density at a constant (2 h) irradiation duration. The damages increased linearly with the logarithm of the dosage, and the effects started at approximately 40 $\mu W/cm^2$ power density and 0.1 mWh/cm^2 energy density. Exposure of various durations (max. 16 h) and powers (max. 16 mW/cm^2) strongly suggested that it is the total dosage which determines the level of teratological damage. Since irradiation at 16 mW/cm^2 is known to produce a measured rise in pupal temperature of less than 2^0 C, and since heating by conventional thermal techniques appears not to be teratogenic, the effects seem to be not (macro-) thermal in origin.

A widely observed and accepted biological effect of low-average power EM energy is the auditory sensation evoked in an exposure to MW. Among other researchers GUY et al. [37] describe the effect as an audible clicking or buzzing sensation that originates from within and near the back of the head and that corresponds in frequency to the recurrence rate of the MW pulses. The loudness of the sensation correlates with the average incident power density. The threshold energy density per pulse is about 40 $\mu J/cm^2$ (corresponds to about 0.01 $\mu Wh/cm^2$) and is five order of magnitudes smaller than the permissible U.S. safety standard value of 1 mWh/cm^2 for peak power averaged over any 6-minute period (ANSI [2]). However, it should be mentioned that the average power density for the threshold of 120 $\mu W/cm^2$ (about two order of magnitudes lower than the permissible U.S. safety standard value) requires a pulse width of 1 to 32 μs, with peak power from 1.25 to 40 W/cm^2. The presented data are valid for 2,450 MHz for humans. Experiments at 918 MHz with cats have shown that depending on the pulse width (3 to 32 μs) average energy densities of 17 to 28 $\mu J/cm^2$ per pulse, average densities of 17 to 28 $\mu W/cm^2$ and peak power density of 0.8 to 5.8 W/cm^2 are required to produce the auditory effects. Although an energy density of 40 $\mu J/cm^2$ is capable of increasing the tissue temperature by only $5 \cdot 10^{-6}$ ^0C, the auditory effect could be explained by microthermal expansion of the liquid in the cochlea, producing a pressure wave similar to the normal input of acoustic signals.

Microwave-induced chronotropic effects in the isolated rat heart are described in a recent report by OLSEN, LORDS and DURNEY [68]. Continuous (CW) MW irradiation at 960 MHz causes bradycardia (lowered heart rate) in isolated, perfused rat heart maintained at 20 ^0C. The observed bradycardia occured at a power deposition of 1.3 to 2.2 W/kg that should have caused mild tachycardia (increased heart rate) based on the theromogenic properties of the irradiation. The observed bradycardia, moreover, exhibits neurologic features, because atropinized hearts showed strong tachycardia during irradiation, and hearts treated with propranolol showed significantly stronger bradycardia during irradiation than seen without drugs. It is assumed tha MW interacts with the autonomic nervous system by changing the neurotransmitter release mechanism. Because the temperature rise was limited to 0.1 ^{o}C, macrothermal mechanisms are not possible, but the possibility exists, that microheating, i.e.,strong thermal gradients over small regions could be responsible for this chronotropic effect of MW. Similar effects, but at lower SAR in living rats,are reported by East European researchers [28,29,69].

A considerable body of literature has grown in the East European countries on transient functional changes following low dose RF and MW irradiation. A sample of clinical and experimental data is presented in TABLE 7.

A SAMPLING OF THE GENERAL BIOLOGICAL EFFECTS OF MICROWAVES AT POWER DENSITIES OF 10 mW/cm^2 OR LESS (EAST EUROPEAN SOURCES)	
Clinical Effects	Experimental Effects
I. General subjective complaints (sensations,fatigue,loss of appetite,asthenia, etc.)	I. Decreased physical endurance and retarded weight gain (rats).
II. Functional CNS and perceptual changes.	II. General inactivation of CNS electrical activity; domination of hypothalamic function; altered afferent function (rabbits, cats). Inhibition of conditioned reflexes; increased motor activity; weakening of excitation/inhibition reactions (rats,mice,birds). Morphological changes in nervous systems (rats,guinea pigs,rabbits) Altered reactivity in response to drugs (rats,rabbits).
III. Cardiovascular and associated autonomic changes.	III. Altered blood pressure and heart rate (rats,rabbits).
IV. Altered blood chemistry.	IV. Altered blood neuroendocrine chemistry (rats,rabbits).
V. Altered metabolism.	V. Altered amino acid and ascorbic acid metabolism (rats)
VI. Depressed endocrine function.	VI. Altered reproductive cycle; decreased viability of offspring (rats).
VII. Increased susceptibility to infectious diseases.	VII. Altered immune reactions (rabbits).

TABLE 7 A sampling of the general biological effects of MW power densities of 10 mW/cm^2 or less as reported by Soviet, Czechoslovakian and Polish researchers. (Source: GLASER and DODGE [28,19])

In the Warsaw Proceedings "Biological Effects and Health Hazards of MW Radiation" [69] and in the recent book by BARANSKI and CZERSKI [6] a review of the East European research is presented. GORDON,ROSCIN and BYCKOV [30] describe functional disturbances in the Central Nervous System (CNS), physiological alterations and behavioral changes which occur at power levels down to a few μW/cm². Various low-level effects may be considered as selective absorption of radiation at the interfaces of heterogeneous biological systems, e.g.,hypothalamic-hypophyseal-suprarenal system. Electrophysical investigations of isolated nerves and muscle fibers in frogs at 5 μW/cm² have revealed slowed conduction of impulses, an increased synaptic delay, a lengthening of latent and refractionary periods and changes in action potentials. DUMANSKIJ and SANDALA [20] investigated alterations in the EEG, in conditioned reflex activity (longer latent period, weakend reaction to positive stimuli) and in several metabolic processes in rats and rabbits after irradiation with less than 10 μW/cm² at 50 MHz and 12 h/day exposition. KALADA, FUKOLOVA and GONCAROVA [46] and others [69] demonstrated effects in occupational exposure. The effects are manifested by weakness, fatigue, headache, etc. and dysfunctions in the autonomic nervous system, which are apparently reversible.

As pointed out by many Western researchers some of the Eastern findings could not be reproduced in the West at the same low-power density level (see e.g.,CHOU and GUY [16] and ROMERO-SIERRA, HALTER and TANNER [70]). However, there is an increasing number of investigations in the West which lead now to similar results (EEG-changes, altered conditioned reflexes, behavioral changes, pathological changes in nerve tissue and brain, increased sensitivity to drugs, etc.), and it has been well established that certain birds, fish and invertebrates can exhibit sensitivity at very weak fields of all kinds (see e.g.,discussion by DODGE and GLASER [19]). Very little is known about RF- and MW receptors, the effect of irradiation on children and non-healthy persons, and the significance of long-term irradiation.

4.5. HIGH FREQUENCY FIELDS FROM ELECTRICALLY SMALL ANTENNAS NEAR A BODY

The purpose of this section is to estimate the quantities of the E- and H-fields on the surface of a subject in close contact with a transmitting antenna and to compare these quantities with the safety standards.

Let us consider a small ($2h < \lambda$, see FIGURE 8) dipole antenna A_1 radiating an RF power P_{rad}. In a large distance r ($r \gg \lambda$) from the antenna one may assume that the propagating wave is plane, so that the E- and H-vectors are rectangular to each other and show the same phase. The amount of the vector power density $\vec{P}$ and the amounts of the vectors $\vec{E}$ and $\vec{H}$ can be computed from P_{rad}, r and the characteristic impedance of vacuum Z_0:

$$|\vec{P}| = |P_{rad}| \,/\, 4 \cdot r^2 \cdot \pi \qquad (2)$$

$$\vec{P} = \vec{E} \times \vec{H} \quad \text{(Definition Poynting)} \qquad (3)$$

$$Z_0 = (\mu_0/\varepsilon_0)^{1/2} = |\vec{E}| \,/\, |\vec{H}| \qquad (4)$$

$$|\vec{E}| = (|\vec{P}| \cdot Z_0)^{1/2} \qquad (5)$$

$$|\vec{H}| = (|\vec{P}| / Z_0)^{1/2}$$

In the vicinity of an actual antenna ($r<\lambda$) the $\vec{E}$- and $\vec{H}$-vectors are neither rectangular to each other nor in phase. $\vec{P}$ becomes a rotating vector of variable amount, and the time averaged power density $|\bar{\vec{P}}|$ is

$$|\bar{\vec{P}}| = \tfrac{1}{2}\, |\mathrm{Re}(\vec{E} \times \vec{H}^*)| \qquad (6)$$

The total power density $\vec{P}$ can be considered to be a superposition of a real power density $\vec{P}_{real}$ and a reactive power density $\vec{P}_{reac}$. The energy associated with the reactive power P_{reac} pulses back and forth and represents stored energy (similar to the energy stored in an inductor or capacitor). The energy flow associated with the real power P_{real} is always positive in direction of propagation and represents a real energy flow. For the following estimation we define $\vec{P}_{real}$ as the power density which is produced from a 'hypothetical point source' with the radiating power P_{rad} :

$$|\vec{P}_{real}| = |P_{rad}| \,/\, 4 \cdot r^2 \cdot \pi \qquad (8)$$

An antenna can be considered as a resonator for the nominal frequency f_{res} which loses energy by radiation. In the vicinity of the antenna exists a large reactive power which is converted into radiating (real) power, and at about $r = \lambda/2\pi$ the radiating power dominates over the rapidly decreasing reactive power.

An electrically small antenna is defined as an aerial, one whose size is a small fraction of the wavelength. It is a capacitor or inductor, and is tuned to resonance by a reactor of opposite kind (WHEELER [83]).From this definition it is evident that an electrically small antenna will show a considerable amount of reactive power.

The 'Helical Normal-Mode Antenna' is today one of the most applied type of electrically small antennas for walkie-talkies and biotelemetry transmitters. The dipole version (see FIGURE 8) of the helical antenna consists of a helical conductor in the shape of a long cylinder with the diameter $D_h (D_h \ll \lambda)$ and with the axial length 2h $(2h<\lambda/2)$. The computation of the helical antenna and its features will be discussed in chapter 16.1. At the moment we have to know only, that the main radiation direction is radial to the axis and that the main polarization axis is parallel to the antenna axis (similar to a full-size dipole antenna).

With the theory of WHEELER [83,84,85] the ratio of real to reactive power can be computed in a situation as shown in FIGURE 8.

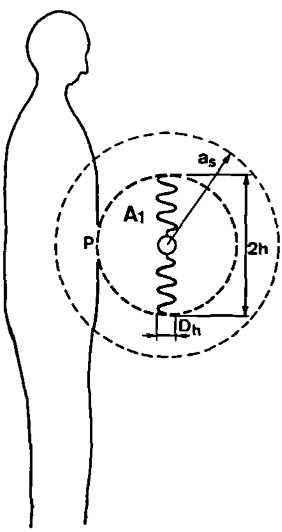

FIGURE 8
Model for the estimation of the near-field reactive power

- A_1 : helical dipole antenna
- 2h : physical antenna length $(<\lambda)$
- D_h : diameter of the helical coil $(<<\lambda)$
- a_s : radius of the radiansphere (see definition in the text, $a_s = \lambda / 2\pi$)
- λ : wavelength
- P : point on the surface of the body, located in a distance h from the antenna

The 'radiansphere' is defined by WHEELER [84] as the boundary between the near field and the far field of a small antenna. Its circumference is λ, and the radius a_s is one radianlength $(\lambda/2\pi)$, at which distance the three terms of the field (from R,L and C of the antenna impedance) are equal in magnitude. The volume V_s of the radiansphere is:

$$V_s = \frac{4\pi}{3}\left(\frac{\lambda}{2\pi}\right)^3 = \frac{\lambda^3}{6\pi^2} \tag{9}$$

An electrically small antenna is somewhat smaller than the radiansphere, but it has a sphere of influence occupying the radiansphere. From the computation of radiation power factor an effective volume V_{eff} has been defined (WHEELER [85]) which is very roughly a value between the physical volume of the antenna and the volume of a sphere containing the antenna:

$$\frac{\pi D h^2}{4} \cdot 2h \ll V_{eff} < \frac{4\pi}{3} \cdot h^3 \tag{10}$$

The effective volume of a slender helical antenna is about $2/3 \cdot h^3 \cdot \pi$.
The ratio between radiating power P_{rad} to reactive power P_{reac} is given by the ratio V_{eff} to V_s as discovered by WHEELER [83,85].

$$\frac{P_{reac}}{P_{rad}} = 4.5\,\frac{V_s}{V_{eff}} \tag{11}$$

An antenna can also be considered as a resonant R-L-C network. The so-called Q-factor of such a network is defined by the ratio of the resonant frequency f_{res} to the bandwidth B and results from the ratio of stored power (in L and C) to real power (in R). The real power is the sum of the radiated power (in the radiation resistance R_{rad}) and the dissipated power P_{loss} (in the loss resistances R_{loss}):

$$Q = \frac{f_{res}}{B} = \frac{\text{stored power}}{\text{real power}} = \frac{P_{reac}}{P_{rad} + P_{loss}} \tag{12}$$

By combining equation (11) and (12) we obtain for the lossless antenna:

$$\frac{f_{res}}{B} = 4.5\,\frac{V_s}{V_{eff}} = \frac{P_{reac}}{P_{rad}} \tag{13}$$

Equation (13) leads to the following interesting conclusions:

1. By decreasing the size of a distinct antenna type the bandwidth decreases considerably, if the resonant frequency is kept constant. This law (WHEELER [83]) is often not noticed in practical antennas, because the radiation resistance decreases and the loss resistance increases.

2. By decreasing the size of a distinct antenna, the reactive power in-

creases considerably, if the radiated power and the resonant frequency are kept constant. The Q of an actual antenna is about 5 to 30, so that the electrically small antenna represents a strong, concentrated reactive power source.

With the assumption that the total real and reactive power is contained in a sphere of radius h (FIGURE 8) and is distributed homogeneously, the averaged quantities of $\vec{P}_{real}$, $\vec{P}_{reac}$, $\vec{H}$ and $\vec{E}$ at the subject's surface point P can be estimated as follows:

a) The radiated power P_{rad} can be computed from the electrical field-strength E_V in the far-field at the distance r: (BECKER [7])

$$P_{rad} \cong \frac{E_V{}^2 \cdot r^2}{45\,\Omega} \quad ; \quad E_V \text{ in mV/m}, \quad r \text{ in m}, \quad P_{rad} \text{ in } \mu\text{W} \tag{14}$$

b) The real power density $\vec{P}_{real}$ originating from an assumed point source with the real radiating power P_{rad} is with equation (8) :

$$|\vec{P}_{real}| = P_{rad} / 4\pi h^2 \tag{15}$$

c) The Q-factor can be obtained by measuring the resonant frequency f_{res} and the - 3 dB bandwidth B. For the lossless antenna we obtain the reactive power density $\vec{P}_{reac}$ with equation (12) :

$$|\vec{P}_{reac}| = |\vec{P}_{real}| \cdot Q \tag{16}$$

For an antenna with high losses it is recommended to determine the losses with the efficiency measuring method or to compute the theoretical Q (see Appendix 16.1.)

d) If we assume that the total reactive power is stored magnetically, the H-field component is about

$$|\vec{H}| \cong Q \cdot (|\vec{P}_{real}|/Z_0)^{1/2} \tag{17}$$

and if we assume that the total reactive power is stored electrically, the E-field component is about

$$|\vec{E}| \cong Q \cdot (|\vec{P}_{real}| \cdot Z_0)^{1/2} \tag{18}$$

The obtained results agree with actual measurements of helical antennas (TELL and O'BRIEN [78]) within a factor of 2. For generally small antennas an error factor of about 5 is to be expected, which is acceptable, because the threshold for biological effects is very variable.

Two typical examples should illustrate the significance of radiation of body-mounted antennas with respect to safety:

Mobile communication systems. Security personnel, police, traffic-control agents, the crew on railroad yards and many other groups are equipped more and more with body-mounted transmitters. The position of the antenna during transmission is close to the hip, chest or head, the standard power is 1 to 5 watts; the standard frequencies are about 170, 450 and recently also 900 MHz. For a 450 MHz walkie-talkie the general specifications are as follows: monopole antenna with a length of h=4 cm, antenna-body distance d_{at}=4 cm (situation as depicted in FIGURE 8), input power 5 W, antenna efficiency 50 percent and bandwidth 10 percent. From these data we compute a radiated power P_{rad} = 2.5 W and a Q-factor of 10. The radiation intensities on the surface of the body computed with equation (15) to (18) are: real power density $\vec{P}_{real}$ = 10 mW/cm², reactive power density $\vec{P}_{reac}$ = 100 mVA /cm² and maximum possible $\vec{E}$ or $\vec{H}$ = 2,000 V/m or 5 A/m.

These intensities are comparable to the measurements of TELL and O'BRIEN [78] at a 3.8 W/450 MHz walkie-talkie equipped with a 15 cm helical antenna. At a distance of 5 cm a maximum power density of 24 mW/cm² was measured with an E-field probe (EDM-3 from NBS, see e.g., [9]).

If we assume a daily transmission duration of 20 minutes, the radiation of standard professional walkie-talkies exeeds the U.S. safety standard by a factor 1 to 10 and the East-European safety standard by a factor of 100 to 1,000. Macro-thermal effects are not to be expected, because the small irradiated area is well-cooled, but micro-thermal or non-thermal effects probably occur. The main risk is not only the high intensities, but the uncontrolled, frequent, world-wide application of walkie-talkies. The actual Polish regulation (see ref. 461 in BARANSKI and CZERSKI [6]) requires that any candidate for work necessitating exposure to MW must undergo a medical examination and obtain a medical certificate for fitness, and periodic examination of MW workers are compulsory. It would be wise to collect medical data on personnel equipped with mobile communication systems in order to decide if similar examinations are necessary for such personnel.

Miniature biotelemetry transmitters. A common antenna for biotelemetry transmitters is a small coil around the housing. We assume the following data: RF-input power 1 mW, antenna diameters $2h = 2$ cm, radiation efficiency 10 percent and a Q-factor of 30. With that data the real power density $\vec{P}_{real}$ is about 0.01 mW/cm^2 and the reactive power density $\vec{P}_{reac}$ is about 0.30 mVA/cm^2.

The radiation intensities of miniature biotelemetry transmitters are between the safety standard limits of the U.S. and East Europe. The radiation duration is generally a few weeks, and often electrodes to sensitive body regions (EEG) are implanted . Often pulse position modulation (sharp peak power) is applied in animal experiments. Health hazards are not likely to occur , but micro-thermal gradients may cause biological effects which may lead to wrong physiological measuring data. Therefore,it would be wise to check the probable influence of the biotelemetry transmitter radiation with respect to artifacts.

The accurate computation of the E- and H-fields near an antenna and near or in the body is complicated and vary from one antenna type to the other. Near-field results of a slender monopole antenna have been presented by CHANG, HALBGEWACHS and HARRISON [13]. NYQUIST, CHEN and GURU [66] investigated the coupling of a 50 MHz $\lambda/4$ dipole antenna with a man-model consisting of dielectrical cubes. At an antenna-body distance of 10 cm they computed a total power deposition of 0.28 W at an input power of 3.14 W. They concluded that an input power of 20 W results in potentially hazardous intensities comparable to a plane-wave irradiation with 10 mW/cm^2. It should be mentioned that a $\lambda/4$ antenna is 1.5 m long so that the critical power level may be expected below 2 W for electrically small antennas.

Accurate near-field measurements in and outside the boby still pose a problem. EGGERT, GOLTZ and KUPFER [21] developed the near-field strength meter NFM-1 which allows E-field measurements 10 cm away from a source with less than 15 percent error in the frequency range 10 to 350 MHz. BELSHER [9] developed the near-field electric energy density meter EDM-2 with a E-probe consisting of three orthogonal miniature dipoles. The probe is imbedded in a 2 cm ø stick and allows E-field measurements with less than 10 percent error in the frequency range 10 to 500 MHz. GREENE [33,34] described an H-field probe and a near-field exposure synthesizer for the frequency range 10 to 40 MHz. The best method to determine the field inside a body is the thermographic recording of the absorption in a model (e.g., GUY, WEBB and SORENSEN [36]).

4.6. CURRENT TRENDS IN INTERNATIONAL SAFETY STANDARD DEVELOPMENT

An overview on the present safety standards and on the actual existing exposures is given in FIGURE 9:

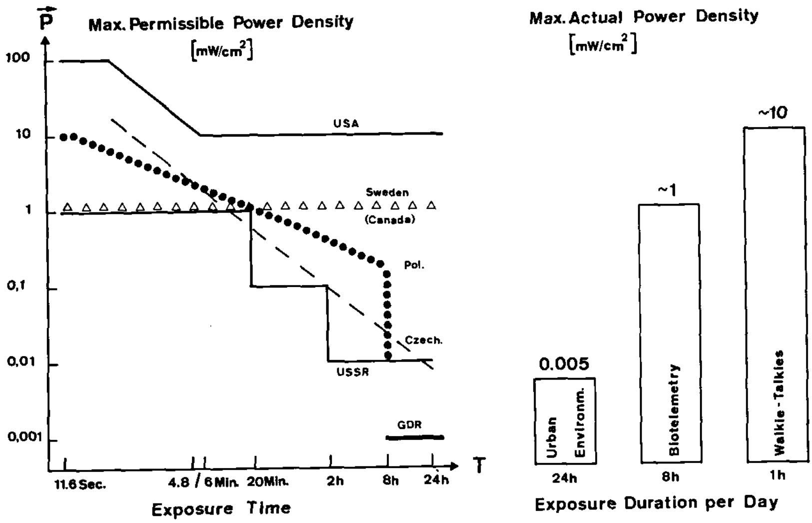

FIGURE 9 International safety standards and actual exposures. Some standards are related gradually to the duration, all are valid for partial and whole body exposure. The GDR limit is valid for pregnant and nursing women. The urban environmental exposure regards approximately 20,000 people in Washington and Chicago. Sources: MICHAELSON [57], DODGE and GLASER [19], ANSI [2], TGL [18], HANKIN et al. [39] and NEUKOMM [64].

The U.S. Safety Standard recommendations (ANSI [2]) apply to all radiation within the frequency range from 10 MHz to 100 GHz except for deliberate exposure of patients by or under the direction of practitioners of the healing arts. The recommendations pertain to both whole body and partial body irradiation. For normal environmental conditions the CW (continuous wave) radiation guide is 10 mW/cm^2, and the equivalent free-space electric and magnetic field strengths are approximately 200 V/m RMS and 0.5 A/m. For modulated fields, the power densities and the field strengths are averaged over any 0.1 hour period, and they should also not exceed an energy density of 1 mWh/cm^2. The US Army (MICHAELSON [57] recommends further, that short exposures should not exceed 100 mW/cm^2, and that the exposure duration (in minutes) is limited by the expression 6000/((x mW/cm^2)^2).

Sweden decreased step by step the maximum permissible power density from 10 mW/cm² (1970) over 5 mW/cm² (1973) to now 1 mW/cm², and Canada intends to follow (DODGE and GLASER [19]).

The East European safety standards in FIGURE 9 apply for all occupational radiation in the frequency range 300 MHz to 300 GHz. Remarkable are the stepped curve (constant dosis) and the low values for permanent exposure. At lower frequencies somewhat higher values are permissible. A typical example for Eastern safety standards is presented in TABLE 10 with the German Democratic Republic's (GDR) safety standard:

FREQUENCY RANGE	MAXIMUM PERMISSIBLE FIELD INTENSITIES IN THE GERMAN DEMOCRATIC REPUBLIC (1978)			
	OCCUPATIONAL EXPOSURE TO IRRADIATION		COMMUNAL HYGIENE (RECOMMENDED)	
	GENERAL	PREGNANT AND NURSING WOMEN	OPEN TERRITORY	DWELLING HOUSES
60 kHz - 3 MHz	50 V/m	10 V/m per 8 h	10 V/m	10 V/m
3 MHz - 30 MHz	20 V/m	4 V/m per 8 h	4 V/m	0.4 V/m
30 MHz - 300 MHz	5 V/m	2 V/m per 8 h	2 V/m	0.2 V/m
300 MHz - 300 GHz	10 µW/cm² per 8 h 100 µW/cm² per 2 h 1 mW/cm² per 0.3 h	1 µW/cm² per 8 h	5 µW/cm² (pulsed, rot. antenna) 1 µW/cm² (CW)	2 µW/cm² (pulsed, rot. antenna) 0.5 µW/cm² (CW)

TABLE 10 Maximum permissible field intensities for RF and MW irradiation in occupational exposure and communal hygiene in the GDR.
(Sources: DDR-Standard and appendix [18])

The actual exposure to RF and MW is shown in FIGURE 8 for three different categories. In urban areas with distributed Radio- and TV stations many thousand people are living day and night in EM fields. HANKIN et al. [39] investigated the power densities of UHF-TV stations and found that about 20,000 people in Washington, 20,000 people in Chicago and 3,000 people in Philadelphia are exposed to more than 4 µW/cm². Up to now little data are available about hazardous effects, from the work of VREELAND, SHEPHERD and HUTCHINSON [82] it is known, however, that TV-stations may affect the correct operation of pacemakers. Mobile communication systems and especially the UHF walkie-talkies are of greater significance as discussed in section 4.5..One may assume, that about 10 million people are exposed to more than 1 mW/cm² by such sources, and it is worth to mention that in the East European countries the power of professional walkie-talkies is legally limited to about 100 mW. Biotelemetry transmitters are relatively safe, but deserve attention to possible artifacts.

4.7. RECOMMENDATIONS FOR SAFETY LIMITS FOR BODY-MOUNTED ANTENNAS

With the present poor knowledge about long-time effects of RF and MW on humans it is very difficult to state generalized recommendations. If very low permissible values are recommended, many sensible applications for biotelemetry and mobile communications have to be excluded. If very high values are recommended, we have to bear the responsibility for health hazards. Summarizing the facts collected in this chapter , we may come to the following conclusions:

Averaged permissible values related to the transmitting frequency: Below 20 MHz the power absorption is about proportional to f^2, is determined mainly by the H-field, and at 10 mW/cm^2 the SAR's are well below 1 W/kg. A maximum power deposition of 10 mW/cm^2 and maximum near-field strengths of 200 V/m and 0.5 A/m are conservative limits.

Above 300 MHz the penetration depth is small, but local hot spots are possible under certain conditions. A maximum power density of 1 mW/cm^2 and maximum near-field strengths of 63 V/m and 0.16 A/m must not be exceeded.

In the resonance region of 20 to 300 MHz excessive local absorption is only possible, if the human body is irradiated by a remote source (whole body exposure), and if the power density is more than 1 mW/cm^2. For partial body exposure, like irradiation from body-mounted antennas, a distribution of the available radiation power may be expected. For low-power transmitters (e.g., < 25 W) the maximum power density should not exceed 1 mW/cm^2 and the near-field strengths should not exceed 63 V/m and 0.16 A/m. For a high-powered transmitter the coupling conditions and the power distribution have to be investigated.

Peak power and dosis: The reported phenomena seem to be effects from the dosis and effects from the peak values. The above indicated maximum ratings are conservative for CW and for maximum 2 hour exposure per day. For shorter durations and pulse modulated sources the above indicated averaged power densities may be multiplied by a factor of 10 and the above indicated averaged field intensities may be multiplied by a factor of 3 in order to obtain the permissible peak values . For long-time exposure, however, the above indicated values should by divided by the factors 10 and 3, respectively.

Risk factors: Some of the risk factors are: conducting objects inside and outside the body (e.g., pace makers, electrodes, microphone cables, headphones, transducers), decreased state of health, extreme environmental conditions (heat), stress, immobility, pregnancy, etc. The present state of bio-research leads to the conclusion that some reversible biological effects may occur, but that real health hazards can be excluded at such low maximum safety limits. With respect to biotelemetry one has to take into account possible artifacts which may lead to wrong results. In animal experiments, especially with small animals, one should consider the wavelength/size ratio, the different biological functions (e.g., thermoregulation, metamorphosis) and the environmental (e.g., cage reflections) conditions.

Leer - Vide - Empty

5. Analysis of the Antenna-Body System

5.1. DESCRIPTION OF THE GENERAL PROBLEM

5.1.1. DEFINITION OF THE BASIC GOALS IN ANTENNA BODY MODELLING

Comparatively speaking, there are two kinds of antenna engineers. First, the experienced practitioner who develops in a short time an exotic, well-operating antenna, but who is not able to deliver computational data, because there are too many variable, undefined parameters. Second, the theoretically-trained engineer, who computes for assumed idealized conditions an excellent theoretical antenna which operates badly under the given difficult environmental conditions.

Similar to above the same dilemma is manifested in our modelling problem:

> The antenna-body model should contain on one hand all significant parameters which describe a realistic situation, on the other hand the selected model should be computable with a reasonable effort.

The basic goals may be defined as follows:

> The computation of the antenna-body model should explain the systematic relation among frequency, body geometry, relative position of the antenna to the body and transmission loss to a remote antenna.
>
> The results of the computation should be verified by a sufficiently accurate measuring method.
>
> The obtained results from both theory and experiment should deliver fundamental data for the development of efficient, electrically small, body-mounted antennas. With the test subject standing on the earth, the antenna-body system should radiate omnidirectionally in the horizontal plane.

5.1.2. PARAMETER DESCRIPTION OF THE GENERAL ANTENNA-BODY SYSTEM

The general test situation is shown in Figure 11. Given is a test subject (TS), a body-mounted antenna (A_1) and a remote antenna (A_2). The TS is electrically isolated from ground by the small space (s) between ground and feet. The relative position of A_1 to the TS is defined by the azimuthal rotation angle (ϕ), the relative antenna height (h_B) and by the antenna-body distance (d_{at}), which is the distance between the center of A_1 and the surface of the TS. The absolute position of the antennas is defined as follows: The transmitting distance (d) is much greater than the wavelength (λ) and d_{at}; therefore we regard d as constant. The antenna height (h_1) is the height of A_1 above ground, the antenna height (h_2) is the height of A_2 above ground. The elevation angle (θ_{el}) is the vertical angle of the beam $\overline{A_1A_2}$ to the horizontal ground; the incident angle (θ_i) is the vertical angle between the beam $\overline{A_1A_2}$ and the vertical body axis. The reflection angle (γ_B) is the Brewster angle (later discussed in 5.3.2.).

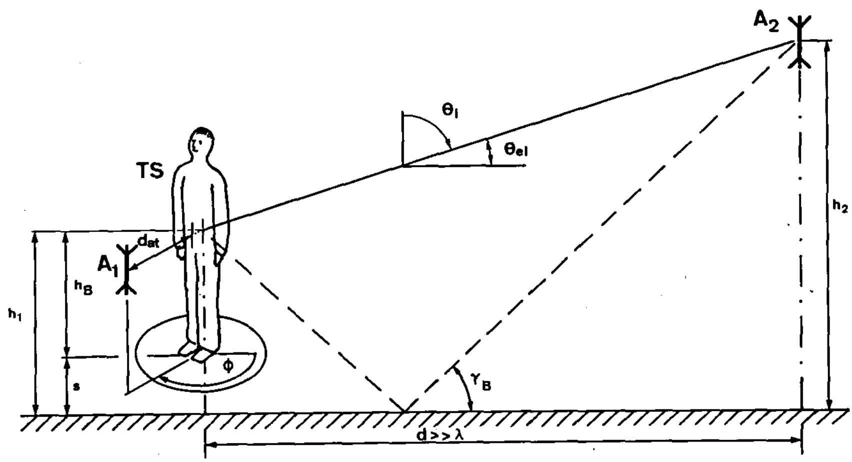

FIGURE 11 General test situation. Parameters described in the text.

The point of interest is the transmission from an EM signal from A_1 to A_2 when a body (TS) is near to the antenna A_1. Because we want to investigate the systematic influence of the TS and not the properties of a specific antenna type, we define the test situation closer :

The two antennas A_1 and A_2 have to fulfill the following requirements:

- The physical size of A_1 should be smaller than any relevant dimension of the test set-up.
- A_1 should have only <u>one</u> dominant E-polarization axis (p_1)
- A_1 should radiate omnidirectionally in free space (e.g., radial radiation independent on the rotation angle of the axis of A_1)
- A_1 should not change its input impedance due to body proximity.
- A_2 should have a strict linear E-polarization (p_2)

As an additional regulation the input power (P_{in}) at A_1, the absolute positions h_1,h_2,d and the polarization p_2 are kept constant for each experiment performed at a given frequency (f).

The reference field strength E_0 is measured at A_2, when no subject is present. A_1 is oriented for maximum radiation in direction of A_2; in the first case (see FIGURE 11) p_1 and p_2 are vertical.

The actual field strength E is measured at A_2 when the TS is positioned, varying d_{at},h_B, ϕ and p_1.

The "transmission loss" ($Loss_B$) and the "transmission gain" ($Gain_B$) is defined as follows:

$$Loss_B = - 20 \log \left(\frac{|E|}{|E_0|}\right) \quad \text{in decibels [dB]} \tag{19}$$

$$Gain_B = 20 \log \left(\frac{|E|}{|E_0|}\right) \quad \text{in decibels [dB]} \tag{20}$$

$Loss_B$ is a measure for the negative (or positive) influence of the TS on the radiation characteristics of the antenna A_1. $Loss_B$ is a function of many parameters which are discussed in TABLE 12. The main radiation pattern of the antenna-body system are described by $Loss_B$ versus ϕ and versus θ_{el}.

Because E_0 represents the maximum possible field strength for a given test antenna in the best practical conditions (near ground, but far away from a body), we call $Loss_B$ of the free antenna (E_0) "free-space level" (FSL):

$$\text{Free-space level (FSL)} = 0 \text{ dB} = \text{reverence level } E_0 \tag{21}$$

The polarization p_2 of A_2 may also be horizontal (parallel to the ground). In that case the FSL (0 dB) is obtained by orienting p_1 of A_1 horizontal, so that p_1 and p_2 are parallel.

In the case of reverse transmission, that is, transmission from A_2 to A_1, the FSL (0 dB) is calibrated to the electrical field strength E_0 of the incident, plane wave in the region, where the TS is intended to be placed.

Finally, it is pointed out once more that E_0 or the FSL is not identical with the field strength produced by an ideal isotropic radiator. At the moment we are not interested in the directional gain and in the efficiency of A_1; such questions will be treated later in Appendix 16.1..

A list of $Loss_B$ determining parameters are presented in TABLE 12:

A SAMPLE OF SIGNIFICANT PARAMETERS DETERMINING GENERALLY THE TRANSMISSION LOSS			
PARAMETER	SYMBOL	RANGE	DESCRIPTION OF THE PARAMETER AND ESTIMATION OF ITS INFLUENCE
Frequency Wavelength	f λ	10-1000 MHz 0.3 - 30 m	At frequencies from 50-300 MHz the dimensions of the human body are in the same order of magnitude as the wavelength. Resonance phenomena of unknown influence are to be expected.
Polarization of A_1 and A_2	p_1 p_2	vert./hor./radial vert./hor.	The main resonance of the human body occurs at vertical polarization, a weaker resonance at horizontal polarization. Field irregularities outside the body may likely occur especially in the case of resonance for p_1 and p_2 vertical.
Body-mounted antenna	A_1	h < 0.15 m	The requirements concerning length, polarization, omnidirectionality and impedance have been defined in 5.1.2. In the experiment A_1 has to be operated off-resonance in order to keep the impedance stable. An antenna for practical use, however, has to be tuned exactly on resonance for the provided mounting. Details are described in section 8. and 16.1.
Remote antenna	A_2	—	A_2 has no influence, if A_2 is a calibrated precision antenna with strict linear polarization p_2.
Height of A_1 above ground	h_1	0.8 - 1.5 m	An h_1 of this range corresponds to 0.03λ up to 5λ. The radiation pattern in the vertical plane will show varying lobes for an elevation angle θ_{el} of 5-20°. The electrical center of the antenna-body system is not known, so that errors of about 4 dB are likely due to ground reflections. See γ_B below.
Height of A_2 above ground	h_2	fix 6.2 m	At frequencies above 20 MHz the h_2 has no influence, as long as h_1, d and thus θ_{el} are kept constant.
Transmission distance	d	fix 31 m	As long as d is greater than λ and if θ_{el} is kept constant, the distance d has no influence. A small variation of the actual A_1-A_2 distance with d_{at} of ± 1 m causes a 0.3 dB change.
Relative A_1 height	h_B	0.6 - 1.3 m	h_B has an influence on h_1 and causes a secondary influence. The primary influence of h_B is a subject of this study.
Azimuthal angle	ϕ	0 - 360°	Experiments showed a large loss in the shadow zone at 180°. The influence of ϕ is a subject of this study.
A_1-body-distance	d_{at}	0.05 - 4 m	Experiments showed a large loss at small d_{at}. A large range variation of d_{at} is a subject of this study.
Space TS to ground	s	0.2 - 1 m	Grounding effects will probably affect $Loss_B$. The TS has to be isolated from the ground to minimize that influence.
Geometry of the TS	L_B D_B	1.5 - 1.5 m 0.2 - 0.5 m	The length L_B and the diameter D_B of the TS might be related to the $\lambda/2$ resonances. A standard TS or phantom is required.
Material of the TS	ε_r σ	6 - 100 0.01-1.6 S/m	See section 4.2. The EM density is so high that the material might be of little significance at large d_{at}.
Elevation angle	θ_{el}	5 - 20°	The elevation angle θ_{el} should be kept constant. See discussion at h_1 above.
Brewster angle	γ_B	12 - 17°	The ground reflected vertically polarized wave is more than 10 dB smaller than the directly transmitted wave, if the Brewster angle γ_B is adjusted properly. For details see section 5.3.2.

TABLE 12 A sample of significant parameters which generally determine the transmission loss ($Loss_B$) in an antenna-body system.

5.2. PARAMETER EVALUATION AND MODELLING OF THE ANTENNA-BODY SYSTEM

5.2.1. TRANSFORMATION OF THE PROBLEM WITH THE RECIPROCITY THEOREM

The EM fields in the vicinity of an electrically small transmitting antenna A_1 are of a complicated nature. If A_1 is in the vicinity of the body, the near-fields are disturbed. The integral effects of the near-fields at the remote antenna A_2 determine the transmission loss $Loss_B$. The computation of this problem is quite difficult and needs much additional input data concerning the specific antenna and the specific body.

Because we are only interested in the transmission loss from a point A_1 to a point A_2, we may ask also for the transmission loss from a point A_2 to a point A_1. If both losses are of the same magnitude, we had only to look at the more simple second case.

The reciprocity theorem (HEILMANN [42]) runs as follows:

> Assumed are two arbitrary antennas A_1 and A_2 at arbitrary relative orientation and distance. If the same voltage is applied either to A_1 or A_2, the same current will flow in the other antenna A_2 or A_1.

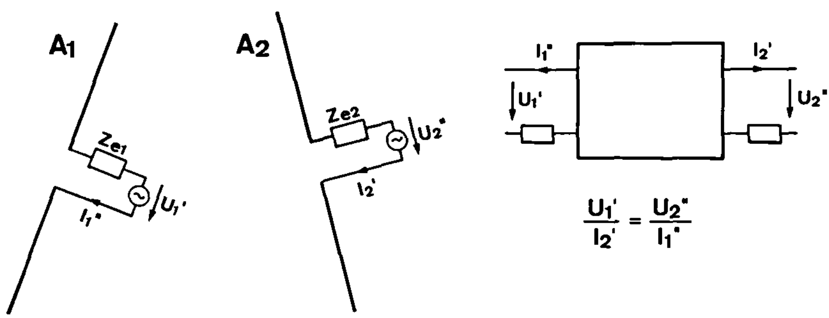

$$\frac{U_1'}{I_2'} = \frac{U_2''}{I_1''}$$

FIGURE 13 Test set-up for the verification of the reciprocity theorem (Source: HEILMANN [42]).

The reciprocity theorem is valid for any linear medium, where μ, ε and k are scalar, but arbitrary quantities. These electromagnetic parameters may depend on their locations, but are not functions of the field vectors.

In our model we can assume that the body material is linear (i.e., not dependent on the magnitude of the EM-field, no thermal alterations of the material) and isotropic (i.e., the properties do not depend on the direction of the EM field vectors). If both antennas are terminated with the same impedance, we may conclude that $Loss_B$ is the same for A_1-A_2 and A_2-A_1 transmission.

As it will be shown in section 9.1.5. the reciprocity theorem is valid for our application. The verification measurements revealed a difference of less than 2 dB when the direction of transmission was reversed (transmitter and receiver changed over, antennas unchanged). This held true for all test bodies (see 5.4.1.), for all measurements at 100 to 1000 MHz, for all d_{at}'s above 0.05 m and for an applied input power P_{in} of 1 mW.

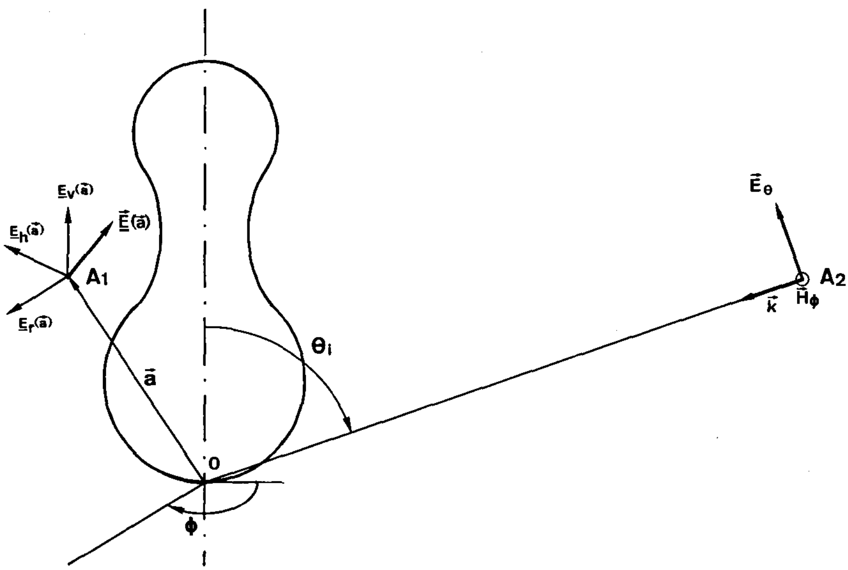

FIGURE 14 Transformed test situation. Antenna A_2 generates a plane wave in the region of the body, the wave is scattered at the body and the disturbed wave is picked-up by antenna A_1.

The transformed problem, which we have to <u>compute</u> in this study is: a body is irradiated by a plane wave with an FSL field strength E_0 at O. We have to quantify the $\vec{\underline{E}}(\vec{a})$ vector components $\underline{E}_v$ (vertical), $\underline{E}_h$ (horizontal) and $\underline{E}_r$ (radial) around the body as a function of $\vec{a}$ (FIGURE 14).

5.2.2. ANTENNA LENGTH AND FIELD HOMOGENEITY

In the test situation FIGURE 14 the monitored E-vector $\underline{\vec{E}}(\vec{a})$ is given by

$$\underline{\vec{E}}(\vec{a}) = \underline{\vec{E}}_{inc}(\vec{a}) + \underline{\vec{E}}_{scat}(\vec{a}) \qquad (23)$$

where $\underline{\vec{E}}_{inc}(\vec{a})$ is the incident E-vector from A_2, and $\underline{\vec{E}}_{scat}(\vec{a})$ is the scattered E-vector from the body. The total E-vector $\underline{\vec{E}}(\vec{a})$ is varying in direction, amount and phase for variable positions $\vec{a}$. Because the antenna A_1 will have a certain length 2h (FIGURE 15), the E-field irradiating A_1 is not constant along the antenna axis.

Because the voltage induced at the terminals of the antenna A_1 will become a measure for the transmission loss, we have to investigate the relation between $\underline{\vec{E}}(\vec{a})$, antenna length 2h and the induced voltage U_{ind}.

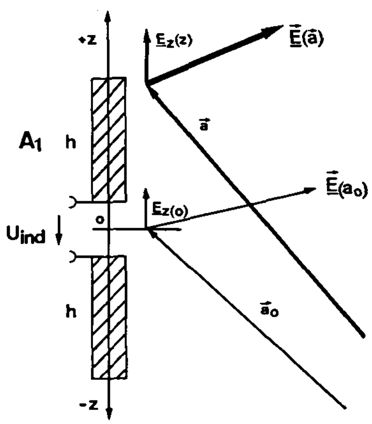

FIGURE 15
Induced voltage in a linear dipole antenna immersed in a inhomogeneous electrical field.

$\underline{\vec{E}}(\vec{a})$	:	variable applied E-field
$\underline{E}_z(z)$	:	z-component of $\underline{\vec{E}}(\vec{a})$ for $\vec{a}$ on the z-axis
z	:	axis of the antenna
2h	:	length of the antenna
U_{ind}	:	induced voltage at the terminal of the antenna
$\vec{a},\vec{a}_0$	:	position vector (see also FIGURE 14)

Let us assume a linear dipole antenna A_1 with the axis z and the length 2h (FIGURE 15). Let us further assume that we know the current distribution function $\Psi(z)$ along the z-axis for an incident plane wave (see e. g., HEILMANN [42]). The induced voltage U_{ind} is then given by:

$$U_{ind} = \int_{-h}^{+h} \underline{E}_z(z)\ \Psi(z)\ dz \qquad (24)$$

If the length 2h of A_1 is adequately small, the variations of $\underline{E}_z(z)$ along the z-axis are so small, that we are allowed to replace $\underline{E}_z(z)$ by the plane wave equivalent field strength $\underline{E}_z(o)$ of $\underline{\vec{E}}(\vec{a}_0)\cdot\vec{e}_z$.

For a given antenna A_1 a certain relation between the axial antenna length 2h and the variability of the axial field $\underline{E}_z(z)$ has to exist, if the above approximation should lead to induced voltages U_{ind} representing the field-strength. We assume the following:

- A_1 should measure the relative field strength $\underline{E}_z(z)$ compared to an FSL reference field E_0 with an accuracy of 2 dB.
- A_1 is small compared with the wavelength ($2h < 0.2\lambda$).
- The total $\vec{\underline{E}}(\vec{a})$-vector is polarized in z-direction, which is the main polarization axis p_1 of A_1.
- We assume for the worst case a constant current distribution function $\Psi(z)$ = constant. An $\underline{E}_z$ at the ends of the antenna has the same weight on U_{ind} as an $\underline{E}_z$ at the antenna center.
- We assume that $\underline{E}_z(+h)=E_0=0$ dB and that $|\underline{E}_z(z)|$ increases monotonously from $-h<z<+h$. $\underline{E}_z(z)$ may be approximated as:

$$|\underline{E}_z(z)| = E(x) = a_0 + a_1 x + a_2 x^2, \quad x = \frac{z+h}{2h}, \quad 0<x<1 \tag{25}$$

- We assume that the phase angle $\arg(\underline{E}_z(z))$ increases monotonously from $-h < z < +h$ and depends linearly on z :

$$\arg(E_z(z)) = \text{const.} + z \cdot \beta \cdot k \quad ; \; 2h \cdot \beta \cdot k < \pi/2 \; , \; \beta = \text{const.} \tag{26}$$

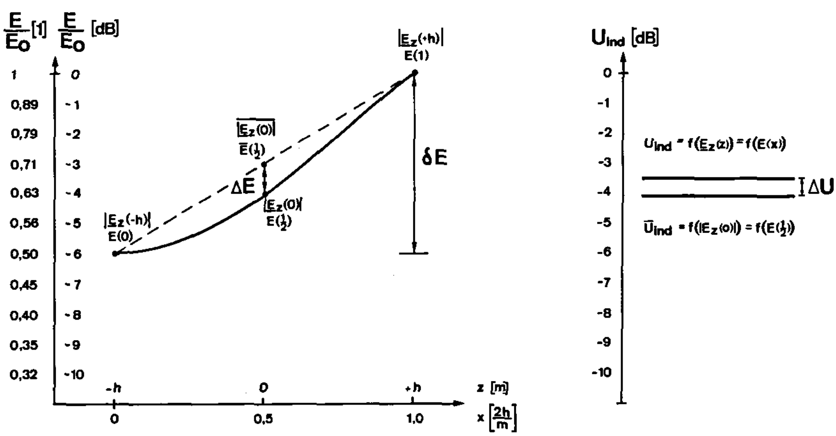

FIGURE 16 Relation among δE, ΔU and ΔE in a worst-case situation as computed later in section 10. The assumed worst case E-field data are:

$$\begin{array}{llll} |\underline{E}_z(-h)| = E(x=0) & = \text{minimum at one antenna end} & = -6.00\text{ dB} & \\ |\underline{E}_z(o)| = E(x=1/2) & = \text{nominal center field} & = -4.08\text{ dB} & \\ |\underline{E}_z(+h)| = E(x=1) & = \text{maximum at other antenna end} & = \;\;0.00\text{ dB} & (27) \\ |\overline{\underline{E}_z(o)}| = \overline{E}(x=1/2) & = \text{logarithmic mean value} & = -3.00\text{ dB} & \end{array}$$

The induced voltage U_{ind} at the antenna terminals is with (25)

$$U_{ind} = \int_{-h}^{+h} \underline{E}_z(z)\, dz = 2h\int_{0}^{+1} E(x)\, dx = 2h\left(a_0 + \frac{a_1}{2} + \frac{a_2}{3}\right) \tag{28}$$

The approximated induced voltage $\overline{U}_{ind}$ with a constant (center) field is

$$\overline{U}_{ind} = \int_{-h}^{+h} \underline{E}_z(o)\, dz = 2h\int_{0}^{+1} E(\tfrac{1}{2})\, dx = 2h\left(a_0 + \frac{a_1}{2} + \frac{a_2}{4}\right) \tag{29}$$

The logarithmic mean value $\overline{|\underline{E}_z(o)|}_{dB} = 20\log\left(\overline{|\underline{E}_z(o)|}/|\underline{E}_z(+h)|\right)$ is

$$\overline{|\underline{E}_z(o)|}_{dB} = \overline{E}(\tfrac{1}{2})_{dB} = \frac{1}{2}\left[20\log 1 + 20\log\left(\frac{a_0}{a_0+a_1+a_2}\right)\right] \tag{30}$$

$$= 20\log\left[\sqrt{1+\frac{a_1}{a_0}+\frac{a_2}{a_0}} \Big/ \left(1+\frac{a_1}{a_0}+\frac{a_2}{a_0}\right)\right]$$

The logarithmic center field strenght $|\underline{E}_z(o)|_{dB}$ is $20\log|\underline{E}_z(o)|/|\underline{E}_z(+h)|$:

$$|\underline{E}_z(o)|_{dB} = E(\tfrac{1}{2})_{dB} = 20\log\left[\left(1+\frac{a_1}{2a_0}+\frac{a_2}{4a_0}\right)\Big/\left(1+\frac{a_1}{a_0}+\frac{a_2}{a_0}\right)\right] \tag{31}$$

From (28) and (29) we obtain the logarithmic difference ΔU :

$$\Delta U = 20\log U_{ind} - 20\log \overline{U}_{ind} = 20\log\left|\frac{1+\frac{a_0}{2a_0}+\frac{a_2}{3a_0}}{1+\frac{a_1}{2a_0}+\frac{a_2}{4a_0}}\right| \tag{32}$$

From (30) and (31) we obtain the logarithmic difference ΔE :

$$\Delta E = 20\log E(\tfrac{1}{2}) - 20\log \overline{E}(\tfrac{1}{2}) = 20\log\left|\frac{1+\frac{a_1}{2a_0}+\frac{a_2}{4a_0}}{\sqrt{1+\frac{a_1}{a_0}+\frac{a_2}{a_0}}}\right| \tag{33}$$

If we replace $\frac{a_1}{a_0}$ by α_1 and $\frac{a_2}{a_0}$ by α_2 , we obtain

$$\Delta U = 20\log\left|\frac{1+\frac{\alpha_1}{2}+\frac{\alpha_2}{3}}{1+\frac{\alpha_1}{2}+\frac{\alpha_2}{4}}\right| \tag{34}$$

$$\Delta E = 20\log\left|\frac{1+\frac{\alpha_1}{2}+\frac{\alpha_2}{4}}{\sqrt{1+\alpha_1+\alpha_2}}\right| \tag{35}$$

As we can see from equation (35), ΔE becomes zero for specific pairs of α_1 and α_2, also when ΔU is not zero. Therefore, the number ΔE cannot be used as an indicator for ΔU.

ΔU, however, varies only little for $0 < \alpha_1, \alpha_2 < 1$. As can be seen from (34), ΔU increases with α_2 and decreases with increasing α_1. A good measure for the maximum $|\Delta U|$ can be obtained with $|\delta E|$, assuming that the E(x) function is of the type $E(x) = a_0 + a_2 x^2$. In FIGURE 16 such a function has been assumed with $a_0 = 0.5$, $a_2 = 0.5$ and thus $\alpha_1 = 0$, $\alpha_2 = 0$. The obtained results δE and ΔU are:

$$|\delta E| = 6 \text{ dB} \quad ; \quad |\Delta U| = 0.56 \text{ dB} \tag{36}$$

If we regard only the $\Delta U/\alpha_2$ ratio of the same quadratic equation $E(x) = a_0 + a_2 x^2$, we obtain for a permissible $|\Delta U|$ of 1 dB an α_2 of 2.3. Thus, the field strength variation δE along the antenna should not exceed :

$$|\delta E| = \left| |\underline{E}_z(-h)|_{dB} - |\underline{E}_z(+h)|_{dB} \right| < 20 \log \left(\frac{1}{1+2.3}\right) = 10 \text{ dB} \tag{37}$$

The permissible phase variation $\delta\Phi$ along the antenna is limited by:

$$|U_{ind}| = \left|\int_{-h}^{+h} \hat{E} \sin(\beta \cdot z \cdot k)\, dz\right| = \left|\frac{\hat{E}}{k} (\cos(2h\beta \cdot k)\right| \tag{38}$$

If we require a resulting real-part variation of less than 10 dB (which causes a $|\Delta U| < 1$ dB, see (37)), we obtain a phase variation limit $\delta\Phi$ of

$$|\delta\Phi| = |\arg(\underline{E}_z(-h)) - \arg(\underline{E}_z(+h))| < \arccos(10^{-\frac{10}{20}}) = 71° \tag{39}$$

For the practical applications the field homogeneity requirements along a dipole test antenna A_1 are completely specified by (38) and (39). Within these limits the field strength $\underline{E}_Z(o)$ at the <u>center</u> of the antenna is <u>representative</u> for the whole field around the antenna, at an accuracy of better than 2 dB. Under these conditions the transmission loss $Loss_B$ for p_1 = z-polarization can be computed as:

$$Loss_B = -20 \log \frac{|\underline{E}_Z(o)|}{|\underline{E}_0|} \qquad \begin{array}{l} E_0 = \text{FSL, } z = \text{polar. axis,} \\ E_Z(o) = \text{center field strength} \end{array} \tag{40}$$

If equations (36) and (38) are not fulfilled, equation (24) has to be evaluated for both theoretical $Loss_B$ and verification experiments.

5.2.3. RELATION OF BODY-DIMENSIONS TO WAVELENGTHS

In section 4.3. and FIGURE 3 it has been shown that the absorption of EM energy inside of a dielectric sphere depends on the ratio of the sphere-circumference $2\pi a$ to the wavelength λ (see RACS).

With the Radar Cross Section (RCS) it should be shown that also the scattered fields outside a body depend on the same ratio. If a body is irradiated by an EM wave, a part of the EM energy will be absorbed as discussed in 4.3. and the remaining EM energy will be scattered in all directions. That part of EM-energy which will be back-scattered toward the EM-source can be quantified by the RCS. The RCS is defined as:

$$RCS = \frac{P_{scat}}{|\vec{P}|} = \lim_{R \to \infty} 4\pi R^2 \frac{|\vec{E}_{scat}|^2}{|\vec{E}_{inc}|^2} \tag{41}$$

P_{scat} is the total scattered power, $\vec{P}$ is the incident power density of the EM wave at the body, R is the distance between the remote source and the body, $\vec{E}_{scat}$ is the back scattered E-field and $\vec{E}_{inc}$ is the incident E-field. The RCS of a sphere is shown in FIGURE 17 versus the ratio $2\pi a/\lambda$.

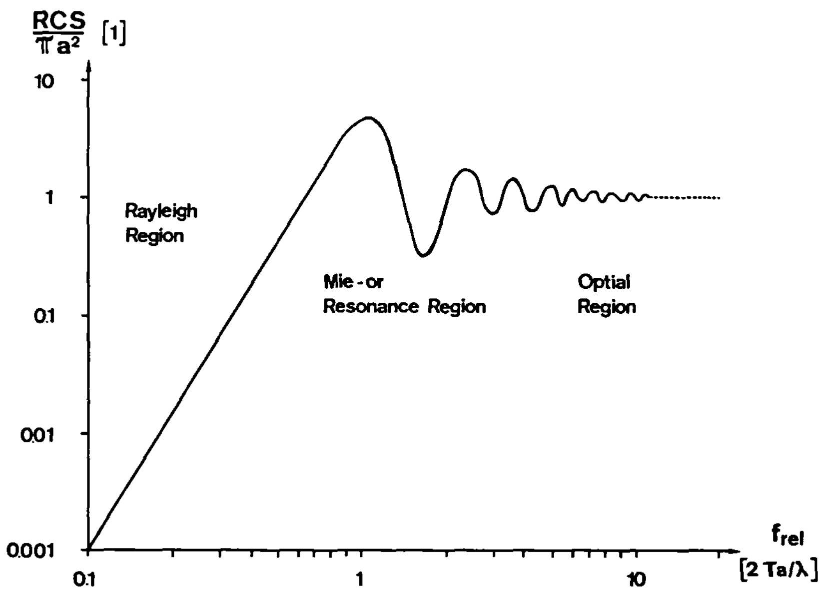

FIGURE 17 Radar Cross Section (RCS) of a sphere with the radius a, related to the shadow area πa^2, versus the relative frequency f_{rel} (sphere circumference $2\pi a$/ wavelength λ). (Source: BECKER [7]).

The shape of the human body can be approximated by an ellipsoid. From the literature it is known that the RCS of an ellipsoid is similar to the RCS of a sphere, if the largest circumference is equal and if the incident wave is polarized parallel to the main axis of the ellipsoid. In FIGURE 18 a simplified man-model is shown and the approximated main resonant frequency for vertical polarization is indicated:

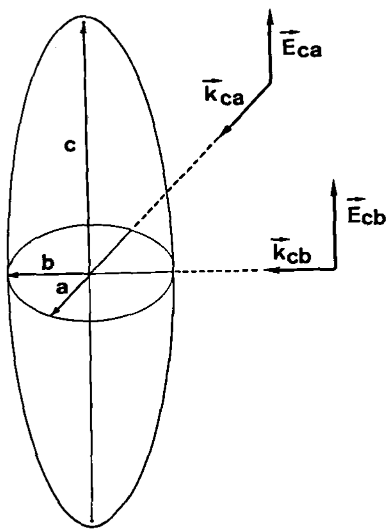

FIGURE 18 Simplified Man-Model

Vertical axis : 2c = 1.8 m
Sagittal axis : 2a = 0.2 m
Lateral axis : 2b = 0.3 m

Incident vertical polarized waves:
Sagittal incidence : $\vec{E}_{ca}, \vec{k}_{ca}$
Lateral incidence : $\vec{E}_{cb}, \vec{k}_{cb}$

Circumferences for vertical polarized incident waves:

$C_{ca} \cong \pi(1.5(c+a)-\sqrt{c \cdot a}) = 3.77$ m
$C_{cb} \cong \pi(1.5(c+b)-\sqrt{c\ b}) = 3.79$ m

Resonant frequency for maximum RCS
$f_{res} \cong 80$ MHz (vertical polar.)

Comparing FIGURE 3 with FIGURE 17 we notice a certain relationship. If the absorption in a body and if the scattered field far away from the body is highly dependent on the circumference/wavelength ratio, we may assume that the scattered fields near the body are also affected by the same ratio:

- At frequencies below 40 MHz the RACS and the RCS are small. That means that the integral effect of the body on the incident EM-wave is small. However, local field disturbances in the vicinity of the body has to be expected, because the body is not transparent to EM-waves.
- At high frequencies above about 200 MHz the RACS and RCS are high but almost constant. The resonance effects may be neglected, and the three dimensional problem may be reduced to a two-dimensional problem, e.g., the scattering from an infinite cylinder.
- In the resonance region, that is about 40 to 200 MHz, both RACS and RCS are high and depend greatly on the frequency. Numerical field computations on a three dimensional model are urgently needed.

5.2.4. INFLUENCE OF THE HUMAN BODY'S MATERIAL ON THE SCATTERED FIELD

The dielectric properties of biological materials have been discussed in section 4.2.. They depend on material and frequency, but, in general, the human body represents a dense, lossy medium. With respect to the field distribution around the irradiated body we have to look closer to the transmission of EM-energy through the body and the reflection of an EM-wave at the body's surface:

The transmission of EM-energy through the body can be estimated as follows: We assume a vertical, circular cylinder, which is irradiated by a plane, vertical polarized wave with the incident E-field $\vec{E}_{inc}$ (FIGURE 19):

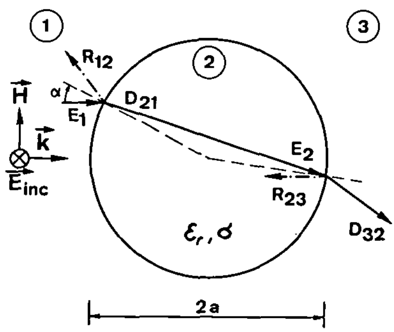

FIGURE 19 Transmission of EM-energy through a circular cylinder.
2a : diameter of the cylinder
1,3: medium air
2 : medium body, lossy material
E_1 : incident wave, $|\vec{E}_{inc}| = 0$ dB
R_{12}: reflected E-field in 1
D_{21}: refracted E-field in 2
E_2 : attenuated E-field in 2
R_{23}: reflected E-field in 2
D_{32}: transmitted E-field in 3

The EM wave enters into medium 2 only for small angles α and is refracted close to the center of the cylinder. The entered wave D_{21} is attenuated during the travelling through the body and amounts finally to E_2. The second refraction produced a small transmitted and scattered wave, D_{32}. Maximum transmission occurs at $\alpha = 0^o$ and at low frequencies. For this case the complex computation of the EM transmission through a plane slab model of 2a thickness was performed by a computer, using the method of TELL [76]:

Input data:		Output data:	
Thickness plane slab	: 2a = 0.25 m	Reflection	R_{12} = -0.8 dB
Frequency	: f = 75 MHz	Attenuated field	E_2 = -38 dB
Material : ε_r = 50 ,	σ = 1.25 S/m	Transmitted field	D_{32} = -52 dB

Without EM-transmission the $Gain_B$(5.1.2.) in the shadow zone amounts up to -30 dB at extremely small d_{at}. Because the transmitted wave amounts to -52 dB, is scattered and is even smaller at higher frequencies, the transmitted wave through the human body has no effect on the transmission $Loss_B$.

The reflection of the incident EM-wave at the surface of the human body determines the scattered field around the body. The EM-wave reflected at the air-body interface is described by the three reflection coefficients $\underline{\Gamma}$ (see TABLE 1) and $\underline{R}_E$,$\underline{R}_H$ (see also section 5.3.2. and FIGURE 24):

- $\underline{\Gamma}$: reflection coefficient for the E-vector of an TEM-wave with rectangular incidence on the surface. The complex number $\underline{\Gamma}$ is derived only from the intrinsic impedances of the interface media (for computation see e.g.,TELL [76]). An average value for our frequency range is about 0.7-0.9 $/\measuredangle 175\text{-}177^0$ (TABLE 1).
- $\underline{R}_E$: reflection coefficient for the E-vector of an TE-wave. Here the E-vector is parallel to the surface. R_E is the ratio of $\underline{E}_{ref}$ to $\underline{E}_{inc}$ and $-\underline{H}_{ref}$ to $\underline{H}_{inc}$. For a vertical body and a vertical polarized incident TE-wave (FIGURE 19) $\underline{R}_E$ is about $1/\measuredangle 180^0$ (larger than $\underline{\Gamma}$) for all angles $\alpha > 10^0$. (For reference see FIGURE 24, horizontal reflection at earth, $\alpha = 90^0 - \gamma$).
- $\underline{R}_H$: reflection coefficient for the H-vector of an TM-wave. Here the H-vector is parallel to the surface. R_H is the ratio of $\underline{H}_{ref}$ to $\underline{H}_{inc}$ and $-\underline{E}_{ref}$ to $\underline{E}_{inc}$. For a vertical body and a horizontal polarized incident TM-wave, $\underline{R}_H$ is near $1 /\measuredangle 0^0$ for all angles α smaller than 70^0. Total refraction and signum change occur only at $\alpha > 80^0$ and are of little significance on the integrally scattered fields. The average reflection coefficient for the E-vector is greater than $\underline{\Gamma}$ and amounts to about $1/\measuredangle 180^0$. (For reference see FIGURE 24, vertical reflection at earth, $\alpha = 90^0 - \gamma$).

The reflection coefficient $\underline{\Gamma}$ represents at least for vertical polarization the smallest occuring reflection coefficient. The reflection coefficient for any incident E-vector at the interface air to a perfect conductor is -1. Compared with $\underline{\Gamma}$ the amplitude of the body-reflected E-vector differs only within - 3 dB. This means that we are allowed to assume the human body as a perfectly conducting body, if we are only interested in the fields outside of the human body.

However, the penetration depth δ of the EM-wave in the human body is not zero as in a perfect conductor. The surface charges and the surface currents (see section 6.) which are responsible for the scattered field are distributed in the outer layers but also with decreasing amplitude in deeper regions (TABLE 1). Therefore, the perfectly conducting man-model is only accurate for $d_{at} > 50$ mm and verification measurements are needed.

5.3. GENERAL CONSIDERATIONS ON ANTENNA MEASUREMENTS

5.3.1. ANTENNA MEASUREMENTS IN PROXIMITY TO THE GROUND

For the field measurements the TS has to be rotated together with the body-mounted antenna A_1, and the antenna-body distance d_{at} must be varied up to 4 m. Theoretically, antenna measurements with quasi-free-space conditions would be possible with anechoic chambers or elevated platforms. However, at measuring frequencies from 10 to 1000 MHz both methods are not suitable. Below 200 MHz an anechoic chamber has to be huge, and the common absorber pyramid plates has to be matched to the frequency (length of an absorber pyramid approximately $\lambda/4$!). An elevated platform is prohibitive due to material and stability problems. Thus, the measurements have to be performed in proximity to the ground, and we have to analyse the influence of the ground on the <u>relative</u> transmitted signal from A_1 to A_2:

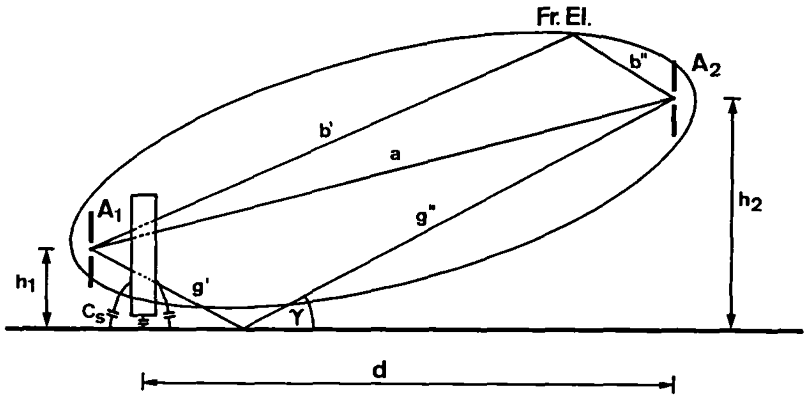

FIGURE 20 Effects in proximity to the ground in antenna measurements.

TS : Test subject   Fr.El.: Fresnel Ellipsoid $(b'+b''-a) = \lambda/2$

A_1 : Body-mounted antenna C_s : stray capacitors from TS to ground

A_2 : Remote antenna γ : reflection angle (glancing angle)

At a small antenna height h_1 (FIGURE 20) disturbing effects occur by:

- Capacitive coupling of the TS to the ground
- Entrance of material into the first Fresnel Ellipsoid

and depending on h_1, h_2 and d :

- Ground reflections with significant interferences if $(g'+g''-a) = n\frac{\lambda}{2}$ and if the reflection coefficient of the ground is high.

The capacitive coupling of the TS to the ground depends on the space s and the material of both the TS and the ground. With great effort the stray capacitors C_s might be computed, but its effect on the scattered field around the TS would require a further study. Because such a study does not help much in the understanding of the antenna-body problem, it is not necessary to further scrutinize an investigation. In order to reduce the capacitive coupling, a constant space s of 0.2 m is now defined for the measurements. Verification measurements with varying s from 0.2 to 1 m will show that the capacitive coupling can be neglected with this restriction.

The first Fresnel Ellipsoid is defined as the geometrical locus for all points which satisfy the condition $(b'+b''-a)=\lambda/2$. (FIGURE 20). If no obstacles interfere with the first Fresnel Ellipsoid, one speaks of optical line-of-sight propagation (BECKER [7]). The lower frequency limit $f_{lim\,1}$ for this free propagation can be approximately determined for the data:

$$\begin{array}{lcll} \text{Antenna height } h_1 & : & 1.16 & \text{m} \\ \text{Antenna height } h_2 & : & 6.2 & \text{m} \\ \text{Distance} \quad d & : & 31 & \text{m} \quad (d_{at} = 0) \end{array} \tag{42}$$

Assuming the ellipsoid touches the ground with the reflected beam $g'+g''$ we obtain the path difference Δs_1 and the frequency limit $f_{lim\,1}$:

$$\Delta_{s1} = g'+g''-a = \sqrt{(h_2+h_1)^2 + d^2} - \sqrt{(h_2-h_1)^2 + d^2} = 0.455 \text{ m} \tag{43}$$

$$f_{lim1} = c/2\Delta_{s1} = 330 \text{ MHz} \tag{44}$$

It has to be clearly stated that accurate absolute antenna measurements are not possible for frequencies below 350 MHz with such a test set-up. However, relative measurements with an accuracy of about 2 dB (experimental experience) are possible, if one looks carefully on the reflection angle γ.

5.3.2. REFLECTIONS FROM THE GROUND AND WAVE POLARIZATION

The following considerations are based on the condition that there is an optical line-of-sight propagation as discussed above.

The antenna measurements are performed on a very large lawn. Because the grass is not an ideal reflector, we have to find out the frequency limit f_{lim2} at which a certain grass thickness d_g changes from an EM smooth to an EM rough surface (Rayleigh criterion, BECKER [7]):

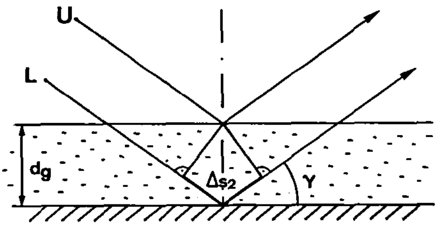

FIGURE 21 Phase difference of two beams, reflected on different heights.
λ : reflection angle
d_g : thickness of the reflecting layer (grass)
U : upper beam
L : lower beam
Δs_2: path difference

In FIGURE 21 an EM-wave is shown which is reflected by the reflection angle γ from a grass surface. The upper beam U is reflected from the top of the grass layer, the lower beam L from the actual earth. We assume a reflection coefficient $\underline{R_E}$ of +1. The path difference Δs_2 depend on γ and d_g:

$$\Delta_{s2} = 2 \cdot d_g \cdot \sin\gamma \tag{45}$$

If the resulting phase difference $\Delta\psi_2$ is near 0, the surface can be regarded as smooth. If $\Delta\psi_2$ is larger than π, the surface is rough and represents a random scatterer. With the Rayleigh criterion $\Delta\psi_2 < \pi/2$ we obtain finally the lower frequency limit $f_{lim\,2}$ for a smooth surface:

$$f_{lim\,2} < \frac{c}{8 \cdot d_g \cdot \sin\gamma} \tag{46}$$

If we assume a thickness $d_g \leqq 0.05$ m and a reflection angle $\gamma \leqq 17^o$ we obtain:

$$f_{lim\,2} < 2500 \text{ MHz} \tag{47}$$

Thus we study the ground reflection at the smooth earth (FIGURE 22):

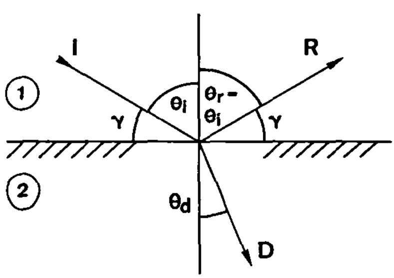

FIGURE 22 Reflection of a wave.
I,θ_i : incident wave and angle
D,θ_d : refracted wave and angle
R,θ_r : reflected wave and angle
1 : medium air $(\varepsilon_1,\mu_1,\sigma_1,m_1)$
2 : medium earth $(\varepsilon_2,\mu_2,\sigma_2,m_2)$
m_1,m_2: refraction indices
γ : reflection angle $90^o-\theta_i$

The computation of reflection and refraction of waves at the interface of two media is completely described by e.g., BAGGENSTOS [5] and BECKER [7]. The derivation of the formulas is quite long, but well known so that only the significant final formulas should be indicated here.

The correlation of the refraction index m, the wave factor k and the characteristic impedance Z_m in a medium is given by BECKER [7] :

$$Z_m = \left(\frac{j\omega \mu_0 \mu_r}{j\omega \varepsilon_0 \varepsilon_r - \sigma} \right)^{1/2} = \frac{\omega \mu_0 \mu_r}{k} = \frac{\mu_r}{m} Z_0 \tag{48}$$

The correlation of the incident angle θ_i with the refraction angle θ_d and with the reflection angle θ_r ($\gamma = 90^0 - \theta_r$) is:

$$\theta_i = \theta_r \ , \quad k_1 \sin\theta_i = k_2 \sin\theta_d \ , \quad m_1 \sin\theta_i = m_2 \sin\theta_d \tag{49}$$

The two different polarizations have to be treated separately (TABLE 23):

THE DIFFERENT REFLECTION OF A VERTICALLY AND A HORIZONTALLY POLARIZED WAVE	
VERTICAL POLARIZATION (TM-WAVE)	HORIZONTAL POLARIZATION (TE-WAVE)
The E-vector is in the plane of incidence. The H-vector is parallel to the interface. Directly computable : reflection coefficient R_H of the H-vector : $R_H = \dfrac{\mu_1 m_2^2 \cos\theta_i - \mu_2 m_1 \left[m_2^2 - m_1^2 \sin^2\theta_i\right]^{1/2}}{\mu_1 m_2^2 \cos\theta_i + \mu_2 m_1 \left[m_2^2 - m_1^2 \sin^2\theta_i\right]^{1/2}}$ For $\mu_1 = \mu_2 = \mu_0$ and $\sigma_1 = \sigma_2 = 0$: $R_H = \dfrac{\tan(\theta_i - \theta_d)}{\tan(\theta_i + \theta_d)}$ If $\theta_i + \theta_d = \pi/2$, the R_H becomes zero and there is no reflected wave. The glancing reflection angle γ ($\gamma = 90^0 - \theta_i$) for which this extinction occurs is here defined as BREWSTER ANGLE γ_B	The H-vector is in the plane of incidence. The E-vector is parallel to the interface. Directly computable : reflection coefficient R_E of the E-vector : $R_E = \dfrac{\mu_2 m_1 \cos\theta_i - \mu_1 m_2 \left\{1 - \left(\frac{m_1}{m_2} \sin\theta_i\right)^2\right\}^{1/2}}{\mu_2 m_1 \cos\theta_i + \mu_1 m_2 \left\{1 - \left(\frac{m_1}{m_2} \sin\theta_i\right)^2\right\}^{1/2}}$ For $\mu_1 = \mu_2 = \mu_0$ and $\sigma_1 = \sigma_2 = 0$: $R_E = -\dfrac{\sin(\theta_i - \theta_d)}{\sin(\theta_i + \theta_d)}$ R_E varies only a little and does not become zero. There is always a ground reflection.

TABLE 23 Computation of the reflected wave for vertically and horizontally polarized incident waves. (Source: BECKER [7]).

The amounts and phases of the reflection coefficients R_H and R_E for a TM- and a TE-wave reflected by a realistic earth surface ($\varepsilon_2 = 10\varepsilon_0$, $\sigma_2 = 1$ mS/m) is shown in FIGURE 24:

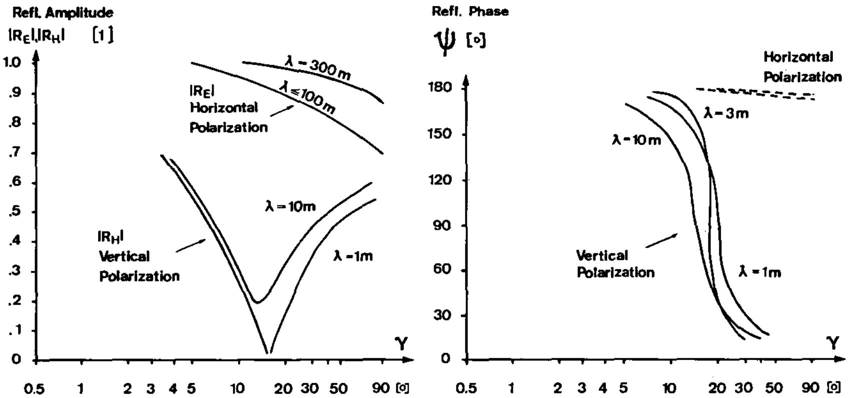

FIGURE 24 Amplitudes R_H and R_E (left) and phases ψ of R_H and R_E (right) versus the glancing reflection angle γ for an average earth surface. (Source: BECKER [7]).

If the conductivity is very low, the refraction index m_2 and the Brewster angle γ_B' become for $\varepsilon_r = 10$, $\mu_r = 0$, $\sigma_2 = 0$: $(\gamma_B' = 90^0 - \gamma_B)$

$$m_2 = \sqrt{\varepsilon_r} \quad ; \quad \gamma_B' = 90^0 - \arctan m_2 \quad = \quad 17^0 \tag{50}$$

which is close to the value depicted in FIGURE 24.

At vertical polarization the influence of the reflected wave is small, if the glancing reflection angle γ is near γ_B'. With the data in FIGURE 24 applied to the antenna configuration in FIGURE 20 we can compute according to BECKER [7] the influence of the reflected wave on the transmission from A_2 to A_1. The field strength E_{oeff}' at A_1 produced by the direct beam (a) from A_2 is (input power P_{in}, antenna gain G_2):

$$|E_{oeff}'| = \frac{(30\ P_{in}\ G_2)^{1/2}}{d} \tag{51}$$

The actual E_{oeff} at A_1 produced by the beams (a) and (g'+g'') is:

$$|E_{oeff}| \approx |E_{oeff}'| \left(1 + 2|R_H| \cos(\psi + \frac{4\pi h_1 h_2}{\lambda d}) + |R_H|^2\right)^{1/2} \tag{52}$$

If we insert the data (42), we obtain a γ of 13.4^0 and thus an $|R_H|$ of less than 0.2 (FIGURE 24). At worst case ψ conditions and for all frequencies between 30 to 1000 MHz the field strength E_{oeff} varies within :

$$0.8\ |E_{oeff}'| < |E_{oeff}| < 1.2\ |E_{oeff}'| \qquad (53)$$

so that $|E_{oeff}|$ differs from -2.0 to +1.6 dB. With respect to the transmission loss determination the effect of the ground reflected wave will be smaller, because the reference E_0 will be determined for each measuring frequency, and because the direct and reflected E-vectors are not parallel.

At horizontal polarization the influence of the reflected wave might be important, if we look on FIGURE 24 and equation (52). With $|R_E| = 1$ we obtain from (52) the interference equation:

$$|E_{oeff}| \approx |E_{oeff}'| \left| 2\sin\left(\frac{2\pi h_1 h_2}{\lambda\ d}\right)\right| \qquad (54)$$

With the data (42) we obtain at 323 MHz a maximum (+6 dB) and at 646 MHz an extinction (< -10 dB). Because h_1 of A_1 is not identical with the height of the antenna-body center, transmission loss measurements are very inaccurate at arbitrary frequencies. Reasonable measurements at horizontal polarizations are only possible at certain selected frequencies and only with large h_1 and h_2. Because the horizontal polarization is of little significance for omnidirectionally radiating antenna-body systems, measurement at horizontal polarization will not be performed.

5.3.3. FIELD HOMOGENEITY ALONG THE BODY AXIS AT VERTICAL POLARIZATION

For the computation a homogeneous, plane wave has been assumed. For the measurements this is not absolutely true as can be seen from FIGURE 25:

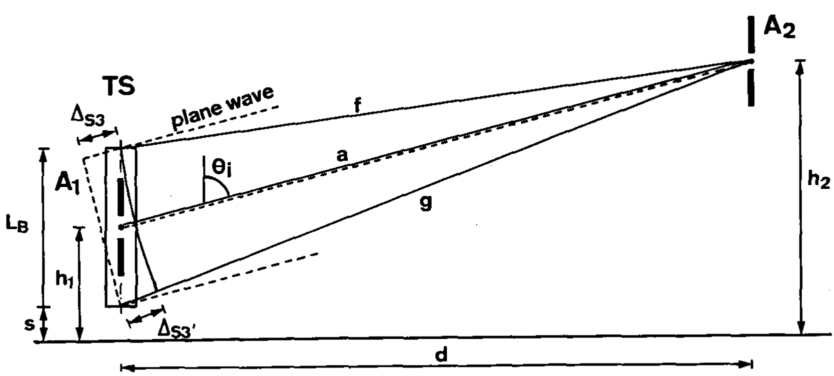

FIGURE 25 Field homogeneity along the body axis of the TS.

For this consideration we assume that A_1 is on the vertical axis of the TS and that the following parameters are given:

$$\begin{array}{lll} p_1, p_2 & : \text{polarization} & = \text{vertical} \\ h_1 & : \text{nominal antenna height} & = 1.16 \text{ m} \\ h_2 & : \text{fixed antenna height} & = 6.2 \text{ m} \\ d & : \text{transmission distance} & = 31 \text{ m} \\ s & : \text{space TS to ground} & = 0.2 \text{ m} \\ L_B & : \text{length of the TS} & = 1.8 \text{ m} \end{array} \tag{55}$$

For the computer computations (section 6.4., FIGURE 33) one assumes a plane wave (dashed lines in FIGURE 25) irradiating the TS with the nominal θ_i:

$$\theta_i = \text{nominal incident irradiation angle} = 80.8^0 \tag{56}$$

The program computes the phase difference among any field point and the origin 0 for the incident plane wave. In this case the path difference Δ_{s3} of the plane wave along the axis of the TS amounts to :

$$\Delta_{s3} = L_B \cos\theta_i = 0.2878 \text{ m} \tag{57}$$

In the actual measurements (solid lines in FIGURE 25) the TS is irradiaated by a spherical wave with an averaged incident angle θ_i. The path difference Δ_{s3}' of the spherical wave along the axis of the TS is:

$$\Delta_{s3'} = g - f = (d^2+(h_2-s)^2)^{1/2} - (d^2+(h_2-L_B-s)^2)^{1/2} = 0.2921 \text{ m} \tag{58}$$

The difference of the plane to the spherical wave is expressed by the difference of the path differences $\Delta_{s3} - \Delta_{s3}'$. If we allow a phase difference of max. $\pi/2$, we obtain a maximum permissible frequency limit $f_{lim\,3}$ for which the spherical wave can be still regarded as a plane wave:

$$f_{lim\,3} \leqq \frac{c}{4|\Delta_{s3} - \Delta_{s3'}|} = 17{,}000 \text{ MHz} \tag{59}$$

In addition we have to fulfill the condition $d > \lambda$, i.e., A_1 has to be outside of the near-field of A_2. For small antennas we obtain the lower limit

$$f_{lim\,4} \geqq \frac{c}{d} = 9.7 \text{ MHz} \tag{60}$$

Neglecting the ground reflections, we may assume a plane wave for both experiment and computation, if the operation frequency f is between:

$$9.7 \text{ MHz} < f < 17{,}000 \text{ MHz} \tag{61}$$

The effect of the ground on the field homogeneity ($E_0(h_1)$) along the vertical axis is described in ARRL [3] for some selected cases. Generally, the field strength $E_0(h_1)$ oscillates around the free space value $E_0(\infty)$, with minima and maxima spaced about $\lambda/2$. Because the field homogeneity is of fundamental interest for the later experiments, the field homogeneity along the vertical axis of the TS (without TS) has been measured by varying h_1 from $\lambda/8$ up to λ with the following method :

Electrically small dipole antennas A_1 ($2h = 0.1$ m) with autonomic RF-oscillators (see section 11.3.) were moved along the vertical axis with a special antenna manipulator (see section 11.2.). The field strength $E_0(h_1)$ was measured with an LPD antenna A_2 (see section 8.3.3.) and was calibrated to the field strength for $h_1 = 1.2$ m . The obtained data are presented in TABLE 26:

VERTICALLY POLARIZED FIELD AMPLITUDE VARIATION AT VARIABLE ANTENNA HEIGHTS H_1						
FREQUENCY [MHz]	RELATIVE FREE-SPACE FIELD STRENGTH $E_0(h_1)$ IN DECIBELS AT HEIGHT					
	$h_1 = 0.8$ m	$h_1 = 1.0$ m	$h_1 = 1.2$ m	$h_1 = 1.4$ m	$h_1 = 1.6$ m	$h_1 = 1.8$ m
65	+ 0.5	+ 0.0	+ 0.0	- 0.0	- 0.5	- 0.5
74	+ 1.0	+ 0.5	+ 0.0	- 0.5	- 1.0	- 1.0
101	+ 1.5	+ 0.5	+ 0.0	+ 0.0	+ 0.0	+ 0.5
164	- 1.5	- 1.0	+ 0.0	+ 0.5	+ 1.5	+ 2.0

TABLE 26 Homogeneity of the field along the vertical axis of the TS at vertical polarization. Values of $E_0(h_1)$ related to E_0 at $h_1 = 1.2$ m. (Measuring data obtained by the standard test set-up, $h_2 = 6.2$ m, $d = 31$ m).

The maximum field strength variation amounts to ± 2 dB in a full $\lambda/2$-h_1 range (TABLE 26: f = 164 MHz). If we apply the equations (52,53),there is a good agreement; the changing factor is R_H, but because $s < h_1 < s+L_B$, the reflection angle is $11.6^0 < \gamma < 14.8^0$ and thus $|R_H| < 0.2$. The variations of $|E_0(h_1)|$ along the vertical axis are the same as given by equation 53 and amount to -2.0 to + 1.6 dB for all frequencies between 30 to 1000 MHz.

As a conclusion from this section 5.3. we may state:

- The test set-up allows antenna measurements with an accuracy of ± 2 dB in the proximity to ground at vertical polarization p_2 of A_2.
- The TS must not be coupled with the ground.

5.4. ANTENNA-BODY MODELS FOR EXPERIMENT AND COMPUTATION

5.4.1. BODY MODELS

An adequate body model should respond to the investigated parameter like the original with a required accuracy but should be so simple that the phenomena can be computed with adequate effort.

The computation of the antenna-body model requires a stepwise increase of the complexity of the body model. In this study we start with a infinite model for two-dimensional computation and we end with a conducting model of human shape for three-dimensional computation.

The experiment with the antenna-body model requires a stepwise decrease of the complexity of the body model. The aim is twofold: at one side the body model should quantify the difference between original and model; on the other hand the model should allow the verification of the computation.

The development of the different body models is depicted in FIGURE 27:

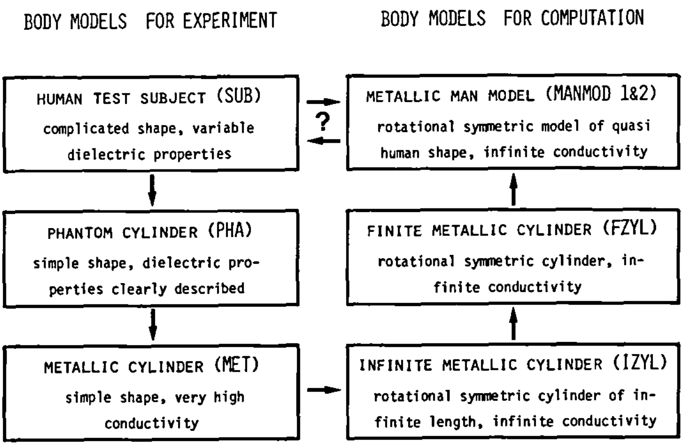

FIGURE 27 Body modelling for experiment and computation.

The different body models are specified as follows:

HUMAN TEST SUBJECT (SUB)

The same TS has been used for all experiments (dress without metallic parts)

Body length	:	1.68 m
Averaged trunk diameter	:	0.25 m
Lateral diameter	:	0.3 m
Sagittal diameter	:	0.2 m

PHANTOM CYLINDER (PHA)

A cylindrical vessel has been constructed using a PVC tube filled with a kind of Ringer solution:

Cylinder length : 1.8 m	Dielectric properties of the Ringer
Cylinder diameter : 0.25 m	solution at 750 MHz:
Wall thickness : 6.0 mm	Relative permittivity ε_r : 50
Relative ε_r of the wall: 2.7	Conductivity σ : 1.25 S/m

The Ringer solution has been composed according to a prescription by GUY [38] and consisted of:

Glycol Ethandiol	$HOCH_2$-CH_2OH	48.2 liters
Destilled water	H_2O	35.4 liters
Natrium Chloride	NaCL	1.86 kg

METALLIC CYLINDER (MET)

A cylindrical vessel without caps has been constructed with copper plates:

Cylinder length : 1.8 m
Cylinder diameter : 0.25 m
Wall thickness : 1.0 mm

INFINITE METALLIC CYLINDER (IZYL)

For the two-dimensional (off-resonance) computation a rotational symmetric cylinder of infinite length and infinite conductivity has been assumed:

Cylinder length : infinite
Cylinder diameter : 0.25 m (nominal value, used as a parameter)

FINITE METALLIC CYLINDER (FZYL)

For the general three-dimensional computations a rotational symmetric cylinder with hemispherical caps and infinite conductivity has been assumed:

Cylinder length : 1.8 m
Cylinder diameter : 0.25 m
Caps diameter : 0.25 m (other caps used as a parameter)

METALLIC MAN MODEL (MANMOD 1 & MANMOD 2)

The sagittal and lateral projection of the human test subject (SUB) was used for modelling rotational symmetric, perfectly conducting body models. The shapes can be seen in FIGURE 28 and are described in section 16.2.4.

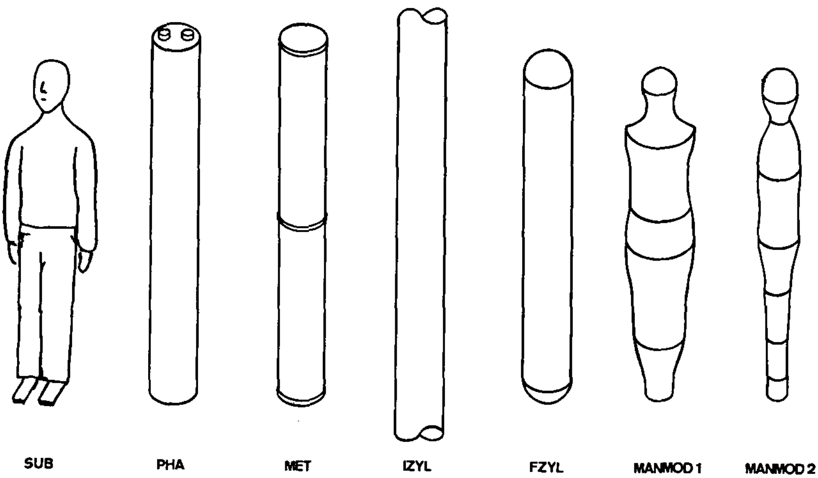

FIGURE 28 Body models used in experiments and computations

5.4.2. ANTENNA-BODY MODELS FOR COMPUTATION

The off-resonance computation for frequencies above 200 MHz can be performed with a two-dimensional antenna-body model, using the body model IZYL. We assume a plane wave with $\theta_i = 90^o$ which is scattered by a vertical cylinder of infinite length. The total field at an arbitrary point outside of the cylinder is the superposition of the incident field and the scattered field. This problem can be analytically solved by Bessel functions.

The general computation has to be performed with a three-dimensional antenna-body model, using the body models FZYL and MANMOD. We assume a plane wave with $\theta_i = 80.8^o$ which is scattered by a rotational symmetric body. The total field at an arbitrary point outside of the cylinder is again the superposition of the incident field and the scattered field. This problem can only be solved by numerical methods, e.g., by the method of moments.

5.4.3. ANTENNA-BODY MODELS FOR EXPERIMENT

The antenna-body model consists of the body models SUB, PHA and MET in a test set-up as shown in FIGURE 11. The parameters d (nominal 31 m), θ_i (nominal 80.8^o) and $\gamma_B'(12\text{-}17^o)$ should be kept as constant as possible during varying d_{at} and ϕ. The antennas have to fulfill the requirements indicated in section 5.1.2..

Leer - Vide - Empty

6. Fundamental Theory for the Computation of Scattering from Conducting Bodies

6.1. PURPOSE OF THE THEORY

The purpose of this theoretical section is to present all needed steps from the Maxwell equations up to the numerical solution concept. The theoretical background is described in BAGGENSTOS [5], VAN BLADEL [81], ANDREASEN [1], KING and WU [50], HARRINGTON and MAUTZ [40] and BEVENSEE [10].

6.2. PENETRATION DEPTH OF THE EM FIELD IN CONDUCTING BODIES

Most of the computations of fields near a conducting body are based on the assumption that the body is a perfect conductor and that there is no field inside the body. This assumption should be proven for our application.

If the conducting body and the observer are not in relative motion to each other and if the conducting body is an isotropic and linear medium, the Maxwell equations within the conducting body can be written as:

$$\overrightarrow{\mathrm{curl}}\ \vec{H} = \sigma_m \vec{E} + \varepsilon_m \frac{\partial \vec{E}}{\partial t} \tag{101}$$

$$\overrightarrow{\mathrm{curl}}\ \vec{E} = - \mu_m \frac{\partial \vec{H}}{\partial t} \tag{102}$$

$$\mathrm{div}\ \vec{H} = 0 \tag{103}$$

$$\mathrm{div}\ \vec{E} = \frac{\rho_m}{\varepsilon_m} \tag{104}$$

In these equations σ_m is the conductivity of the medium, ε_m is the dielectric constant ε_r of the medium multiplied by the permittivity ε_0 of vacuum, μ_m is the relative permeabiltiy μ_r of the medium multiplied by the permeability μ_0 of vacuum and ρ_m is the electric charge density in the medium.

If static fields can be excluded,we obtain with (104) inserted in (101) :

$$\mathrm{div}\ \overrightarrow{\mathrm{curl}}\ \vec{H} = 0 = \frac{\sigma_m}{\varepsilon_m}\rho_m + \frac{\partial \rho_m}{\partial t} \qquad \text{and with}$$

$$\rho_m = \rho_{m_0}\ e^{-t/\tau} \qquad \text{we obtain}$$

$$\tau = \frac{\varepsilon_m}{\sigma_m} \tag{105}$$

Consider now a time interval T in which a charge of the fields E and H should be observed. If this time interval T (usually a fraction of the period time of the applied wave) is large in relation to τ, that is here

$$\frac{T}{\tau} \gg 1 \tag{106}$$

when the electric charge density ρ_m in the medium can be assumed to be zero, since it disappears rapidly.

With the restriction (106) the Maxwell equations inside the medium are:

$$\overrightarrow{\text{curl}}\, \vec{H} = \sigma_m \vec{E} + \varepsilon_m \frac{\partial \vec{E}}{\partial t} \tag{101}$$

$$\overrightarrow{\text{curl}}\, \vec{E} = - \mu_m \frac{\partial \vec{H}}{\partial t} \tag{102}$$

$$\text{div}\, \vec{H} = 0 \tag{103}$$

$$\text{div}\, \vec{E} = 0 \tag{107}$$

Using the curl function on (101) and (102) and the identity

$$- \Delta = \overrightarrow{\text{curl}}\, \overrightarrow{\text{curl}} - \overrightarrow{\text{grad}}\, \text{div}$$

we obtain in a Cartesian coordinate system (x,y,z) the formula

$$\frac{\partial^2 F}{\partial x^2} + \frac{\partial^2 F}{\partial y^2} + \frac{\partial^2 F}{\partial z^2} + \mu_m \sigma_m \frac{\partial F}{\partial t} + \mu_m \varepsilon_m \frac{\partial^2 F}{\partial t^2} = 0 \tag{108}$$

where F stands for $E_x, E_y, E_z, H_x, H_y, H_z$. The solution of this differential equation can be found in the case of a homogeneous body material with

$$F = F_0\, e^{(-\vec{k}_m \cdot \vec{r} + j\omega t)} \qquad \text{where} \tag{109}$$

$$k_m^2 = k_{mx}^2 + k_{my}^2 + k_{mz}^2 = j\omega\mu_m\sigma_m - \varepsilon_m\mu_m\omega^2 \tag{110}$$

$$|\vec{k}_m| = \pm \sqrt{\omega\mu_m\sigma_m} \cdot \sqrt{j - \varepsilon_m\omega/\sigma_m} \tag{111}$$

With the restriction (106) and with the period time T of the applied wave we obtain the maximum frequency f_{max} at which the charge density within a well conducting medium (copper) may be still ignored:

$$T = \frac{2\pi}{\omega} \; ; \; \frac{\omega\varepsilon_m}{2\pi\sigma_m} \ll 1$$

$$\varepsilon_m \sim \varepsilon_0 = 8.86 \cdot 10^{-12} \ \text{A} \cdot \text{s} \cdot \text{V}^{-1} \cdot \text{m}^{-1}$$

$$\sigma_m \sim 10^7 \ \text{A} \cdot \text{V}^{-1} \cdot \text{m}^{-1}$$

$$f_{max} \sim 10^{18} \, \text{Hz} \gg 1000 \ \text{MHz} \tag{112}$$

The wave factor $\vec{k}_m$ from (111) becomes at frequencies well below f_{max}:

$$\vec{k}_m \sim \pm \sqrt{\pi f \mu_m \sigma_m}\ (1+j) \tag{113}$$

Considering a wave travelling in positive direction r within an isotropic medium, we may write:

$$-\vec{k}_m \cdot \vec{r} = -k_m \cdot r$$

The attenuated wave is described by (113) inserted in equation (109):

$$F = F_0\, e^{-\sqrt{\pi f \mu_m \sigma_m} \cdot r} \cdot e^{j(\omega t - \sqrt{\pi f \mu_m \sigma_m} \cdot r)} \tag{114}$$

F_0 may be regarded as a component of $\vec{E}$ or $\vec{H}$ below the surface of the conducting body. The penetration depth δ, defined as the distance which the propagating component will travel before the amplitude is decreased by a factor of e^{-1}, can be quantified as

$$\delta = \frac{1}{\sqrt{\pi f \mu_m \sigma_m}} \tag{115}$$

The lowest frequency in our investigation is 10 MHz. With a permeability $\mu_m = \mu_0$ and with δ we are now able to compute the maximum thickness of the field carrying surface layer of a well conducting medium. In a depth of 5 times δ the fields are almost zero, and this layer thickness 5δ is :

$$5\delta = 5 \cdot \delta_{10\ MHz} \sim 0.2\ mm\ \ (copper) \tag{116}$$

This layer is much smaller than all dimensions of the body (see FIGURE 28) so that the field inside the conducting body models (copper) can be considered to be zero. This means that the computations on a perfectly conducting body will be also representative for an actual metallic body model as used for the experiments.

6.3. CHARGE- AND CURRENT-DENSITIES AT THE SURFACE OF A CONDUCTING BODY

6.3.1. BOUNDARY-VALUE PROBLEM

We apply the Maxwell equations (101) and (102) on the fields near the surface of the medium and assume a thin layer 5δ in which the fields may exist. The deeper regions are field-free as calculated with (114). In the computational model FIGURE 29 we assume that:

a) The E- and H- components within the test area ΔA are finite

b) The E- and H- components within Δl are constant in planes || surface.

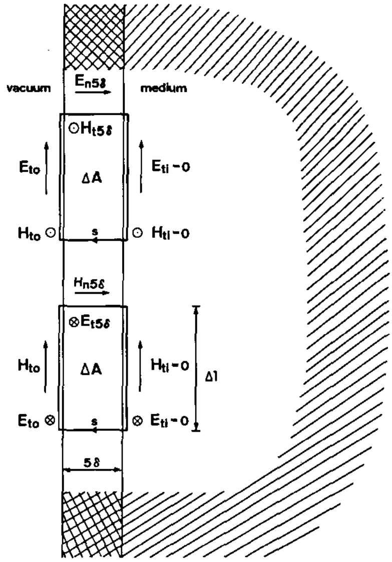

FIGURE 29 Interface between vacuum and a well-conducting medium.

5δ = thickness field-carrying layer
Δl = length of the test area ΔA
ΔA = test area $5\delta \cdot \Delta l$
s = integration path

E_{to} = E-comp. tangential outside
E_{ti} = E-comp. tangential inside
H_{to} = H-comp. tangential outside
H_{ti} = H-comp. tangential inside

$E_{t5\delta}$ = E-comp. tangential in layer
$E_{n5\delta}$ = E-comp. normal in layer
$H_{t5\delta}$ = H-comp. tangential in layer
$H_{n5\delta}$ = H-comp. normal in layer

The integration along s contains the parts :

$$F_{to} \cdot \Delta l - F_{tl} \cdot \Delta l + \int_0^{5\delta} F_{n5\delta}(s)\, ds + \int_{5\delta}^{0} F_{n5\delta}(s)\, ds$$

so that only $F_{to} \cdot \Delta l$ is left. Thus, the integrations of (101) and (102) are:

$$E_{to} = - \frac{\mu_m}{\Delta l} \int_{\Delta A} \frac{\partial \vec{H}}{\partial t} \cdot d\vec{A} \quad ; \quad \vec{H} = H_{t5\delta}(s) \qquad (117)$$

$$H_{to} = \frac{1}{\Delta l} \left(\int_{\Delta A} \sigma_m \vec{E} \cdot d\vec{A} + \varepsilon_m \int_{\Delta A} \frac{\partial \vec{E}}{\partial t} \cdot d\vec{A} \right) \quad ; \quad \vec{E} = E_{t5\delta}(s) \qquad (118)$$

For the integration of the Maxwell equations (103) and (104) we consider a subvolume ΔV containing the field carrying layer (FIGURE 30) :

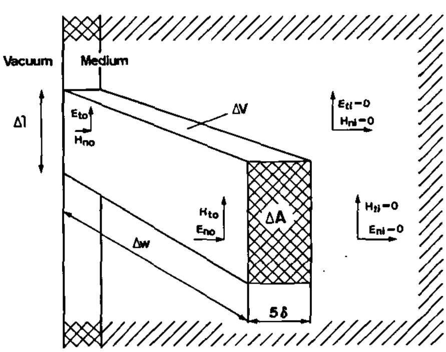

FIGURE 30 Interface between vacuum and medium (see also FIGURE 29 above).

Δw = width of the subvolume ΔV
ΔV = subvolume $\Delta A \cdot \Delta w$

E_{no} = E-comp. normal outside
E_{ni} = E-comp. normal inside
H_{no} = H-comp. normal outside
H_{ni} = H-comp. normal inside

In analogy to the assumptions a) and b) we assume the field conditions:

c) The E- and H-components within the test subvolume ΔV are finite

d) The E- and H-components within $\Delta l \cdot \Delta w$ are constant in planes || surface.

The integrations of (103) and (104) over the layer thickness 5δ lead to :

$$H_{no} = 0 \tag{119}$$

$$E_{no} = \frac{1}{\Delta l \cdot \Delta w} \int_{\Delta V} \frac{\rho_m}{\varepsilon_m} \cdot dV \tag{120}$$

We assume now that there is an outer wave travelling parallel to the surface. The Poynting vector $\vec{P}$ is therefore parallel to the surface, and with FIGURE 30 we obtain the only tangential component P_t :

$$P_t = E_{to} \cdot H_{no} - E_{no} \cdot H_{to} \neq 0$$

Since H_{no} is zero (119) it remains :

$$P_t = - E_{no} \cdot H_{to} \quad \text{and} \quad E_{no} \neq 0 \, , \; H_{to} \neq 0 \tag{121}$$

$E_{no} \neq 0$ means that the right side of (120) is not zero. Since we have proven with (105) that there are no charges ρ_m inside the medium at low frequencies, then charges have to exist on the surface of the medium:

$$E_{no} = \frac{\sigma_{su}}{\varepsilon_m} \quad ; \quad \sigma_{su} = \text{surface charge density } [C \cdot m^{-2}] \tag{122}$$

$H_{to} \neq 0$ means that the right side of (118) is not zero. Thus currents flowing in the outer layer have to exist which can be expressed by:

$$H_{to} = J_t \quad ; \quad \vec{J} = \text{current density vector } [A \cdot m^{-1}] \tag{123}$$

The direction of J_t is tangential to the surface and perpendicular to H_{to}.

Now we consider a wave perpendicular (normal) to the surface. If we neglect the losses in the medium, there is no wave entering the medium and thus the wave will be totally reflected. This means that the Poynting vector has no normal component P_n (see FIGURE 29) :

$$P_n = E_{to} \cdot H_{to} = 0 \quad \text{(upper and lower case)} \tag{124}$$

Either E_{to} or H_{to} could be zero in order to fulfill (124). If H_{to} would be zero, no wave could exist outside the medium since H_{no} is already zero as proven by (119). Because the wave cannot vanish outside the medium, the other field component E_{to} has to be zero, and we obtain:

$$E_{to} = 0 \tag{125}$$

The conclusion of (119,122,123,125) is: at the surface of a good conductor the $\vec{E}$-field has only a component normal to the surface, produced by a surface charge density σ_{su}, and the $\vec{H}$-field has only a component tangential to the surface, produced by the surface current density $\vec{J}$ normal to $\vec{H}$.

This surface charge density σ_{su} and the current density $\vec{J}$ are the origins of the scattered fields from a conducting body which is irradiated by a wave.

6.3.2. THE EFFECT OF THE SURFACE CURRENT DENSITY $\vec{J}$

In FIGURE 31 a conducting body is depicted with the area element dS , containing the surface current density $\vec{J}$ and the surface charge density σ_{su}:

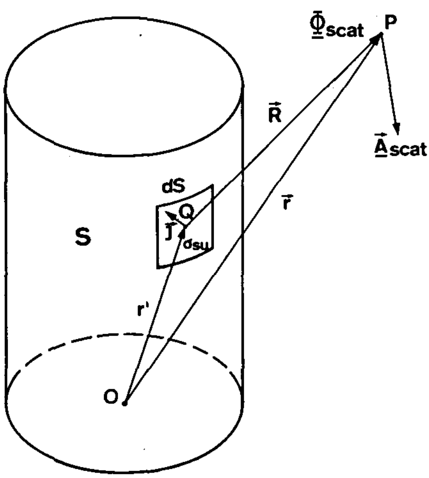

FIGURE 31 Conducting body with $\vec{J}$ and σ_{su} produced by an incident wave, and scattered parameters.

O = Origin of coordinate system
Q = Source point
P = Observation point
r' = Position of the source point
r = Position of the observ.point
$\underline{\Phi}^{scat}$ = Scattered electr. potential
$\underline{\vec{A}}^{scat}$ = Scattered mag.vector pot.
$\vec{J}$ = Surface current density
σ_{su} = Surface charge density
dS = Area element on the body

The source is the current density $\vec{J}$ in the area element dS positioned at $Q(\vec{r}\,')$. The effect is the scattered magnetic vector potential $\underline{\vec{A}}^{scat}$ at the remote observation point $P(\vec{r})$. Because the distance between the source and the observation point is comparable with the wavelength λ, a phase difference occurs which has to be treated by the time retardation t' :

$$t' = t - \frac{R}{c} \quad ; \quad \begin{aligned} R &= |\vec{R}| = |\vec{r} - \vec{r}\,'| \\ t &= \text{actual time} \\ t' &= \text{time retardation} \end{aligned} \qquad (126)$$

The scattered magnetic vector potential $\vec{A}^{scat}$ is defined as

$$\vec{A}^{scat}(\vec{r},t) = \frac{\mu_0}{4\pi} \int_S \vec{J}\,(\vec{r}\,',\vec{t}\,')\,\frac{1}{R}\,dS \qquad (127)$$

From (109) and (123) we obtain the complex surface current density $\underline{\vec{J}}$:

$$\underline{\vec{J}}\,(r',t') = \vec{J}(\vec{r}\,')\,e^{\,j\omega t'} \qquad (128)$$

and using the retardation (126) we insert (128) in (127) :

$$\underline{\vec{A}}^{scat}(\vec{r},t) = \frac{\mu_0}{4\pi}\int_S \vec{J}(\vec{r}\,')\,e^{\,j\omega(t-R/c)}\,\frac{1}{R}\,dS$$

Introducing the wave factor k for free space (111)

$$k = 2\pi/\lambda = \omega/c \qquad (129)$$

the exponential function becomes

$$e^{\,j\omega(t-R/c)} = e^{\,jk(t\cdot c\,-\,R)}$$

and if we delete the time dependency we obtain finally :

$$\underline{\vec{A}}^{scat}(\vec{r}) = \frac{\mu_0}{4\pi}\int_S \vec{J}(\vec{r}\,')\,e^{-jkR}\,\frac{1}{R}\,dS \qquad (130)$$

6.3.3. THE EFFECT OF THE SURFACE CHARGE DENSITY σ_{su}

The treatment of the effect of the charge density σ_{su} is analogous to 6.3.2.. The source is the charge density σ_{su} in the area element dS positioned at $Q(\vec{r})$.The effect is the scattered electric (scalar) potential Φ^{scat} at $P(\vec{r})$.

The scattered electric potential Φ^{scat} is defined as

$$\Phi^{scat}(\vec{r},t) = \frac{1}{4\pi\varepsilon_0}\int_S \sigma_{su}(\vec{r}\,',t')\,\frac{1}{R}\,dS \qquad (131)$$

and analogous to 6.3.2., we obtain with deleted time dependency :

$$\underline{\Phi}^{scat}(\vec{r}) = \frac{1}{4\pi\varepsilon_0}\int_S \sigma_{su}(\vec{r}\,')\,e^{-jkR}\,\frac{1}{R}\,dS \qquad (132)$$

6.3.4. THE FIELD OUTSIDE OF THE CONDUCTING MEDIUM

With the magnetic vector potential $\vec{A}^{scat}$ (130) and the electric potential Φ^{scat} (132) the field strengths of the scattered $\vec{E}^{scat}$ and $\vec{H}^{scat}$ are:

$$\vec{H}^{scat} = \frac{1}{\mu_0}\,\overrightarrow{\mathrm{curl}}\,\vec{A}^{scat} \qquad (133)$$

$$\vec{E}^{scat} = -\frac{\partial\vec{A}^{scat}}{\partial t} - \overrightarrow{\mathrm{grad}}\,\Phi^{scat} \qquad (134)$$

The total fields outside of the conducting medium are the superpositions of the incident and the scattered fields:

$$\vec{E}^{\,tot} = \vec{E}^{\,inc} + \vec{E}^{\,scat} \tag{135}$$

$$\vec{H}^{\,tot} = \vec{H}^{\,inc} + \vec{H}^{\,scat} \tag{136}$$

The index 'tot' means total outer field, 'inc' stands for the incident field and 'scat' stands for the scattered field.

The combinations of (134)(135) and (133)(136) lead to :

$$\vec{E}^{\,tot} = \frac{\partial \vec{A}^{\,scat}}{\partial t} - \overrightarrow{\text{grad}}\,\Phi^{\,scat} + \vec{E}^{\,inc} \tag{137}$$

$$\vec{H}^{\,tot} = \frac{1}{\mu_0}\,\overrightarrow{\text{curl}}\,\vec{A}^{\,scat} + \vec{H}^{\,inc} \tag{138}$$

6.3.5. DETERMINATION OF THE CURRENT DENSITY $\vec{J}$ AND THE CHARGE DENSITY σ_{su}

From equations (119) and (123) we know that at the margin of the conductor only the tangential H-components are existing. Since the coordinate system is not yet choosen, we define $\vec{H}_t$ as a H-vector parallel to the test area dS.

$$\vec{H}_t^{\,tot} = \vec{H}_t^{\,inc} + \vec{H}_t^{\,scat} \tag{139}$$

$$\mu_0\vec{H}_t^{\,tot} = \mu_0\vec{H}_t^{\,inc} + \mu_0\vec{H}_t^{\,scat}$$

With the equation (123) and the relation:

$$\mu_0\vec{H}_t^{\,scat} = \text{Induction } \vec{B}^{\,scat} = \overrightarrow{\text{curl}}_t\,\vec{A}^{\,scat} = \vec{J}_t\,\mu_0$$

$$\overrightarrow{\text{curl}}_t = \text{tangential components of } \overrightarrow{\text{curl}} \tag{140}$$

we obtain finally

$$\vec{J} = \frac{\overrightarrow{\text{curl}}_t\,\vec{A}^{\,scat}}{\mu_0} + \vec{H}_t^{\,inc} \tag{141}$$

Equation (141) is a transcendental differential equation for the two tangential components of $\vec{J}$.

Similar as above we obtain the normal component of $\vec{E}$ at the margin of the conductor with equations (122) and (137) :

$$\overrightarrow{\text{grad}}_n, A_n, E_n = \text{normal component of } \overrightarrow{\text{grad}},\ \vec{A},\ \text{and } \vec{E} \tag{142}$$

$$E_n^{\,tot} = -\frac{\partial \vec{A}_n^{\,scat}}{\partial t} - \overrightarrow{\text{grad}}_n\,\Phi^{\,scat} + E_n^{\,inc} \tag{143}$$

By inserting (122) we obtain a transcendental differential equation :

$$\frac{\sigma_{su}}{\varepsilon_0} = - \frac{\partial \vec{A}_n^{\,scat}}{\partial t} - \overrightarrow{grad}_n \, \Phi^{scat} + \vec{E}_n^{\,scat} \tag{144}$$

Equation (134) can be rearranged considering (109) :

$$\underline{\vec{E}}^{scat}(\vec{r}) = - j\omega \underline{\vec{A}}^{scat}(\vec{r}) - \overrightarrow{grad} \, \underline{\Phi}^{scat}(\vec{r}) \tag{145}$$

and with (135) and (125) are

$$\underline{\vec{E}}^{inc} = \underline{\vec{E}}^{tot} - \underline{\vec{E}}^{scat}$$

$$\underline{\vec{E}}_t^{inc} = \underline{\vec{E}}_t^{tot} - \underline{\vec{E}}_t^{scat} \qquad \text{with } \underline{\vec{E}}_t^{tot} = 0 \tag{146}$$

we obtain with $\underline{\vec{A}}_t$, $\overrightarrow{grad}_t$ = tangential components of $\underline{\vec{A}}$ and $\overrightarrow{grad}$

$$\underline{\vec{E}}_t^{scat}(\vec{r}) = j\omega \underline{\vec{A}}_t^{scat}(\vec{r}) + \overrightarrow{grad}_t \, \underline{\Phi}^{scat}(\vec{r}) \tag{147}$$

We may apply now (147) on a local coordinate system $\vec{t} = \hat{t}_1, \hat{t}_2$ on the surface of the conducting body where the sources are located. Thus, we build the scalar product $\vec{t}$ with $\vec{E}^{inc}$ as follows :

$$\vec{t} \cdot \underline{\vec{E}}^{inc}(\vec{r}) = \vec{t} \cdot \left(j\omega \underline{\vec{A}}^{scat}(\vec{r}) + \overrightarrow{grad}_t \, \underline{\Phi}^{scat}(\vec{r}) \right) \tag{148}$$

By inserting (127) and (132) the equation (148) can be shaped in a form of an integral equation which does no more contain $\underline{\vec{A}}$ and $\underline{\Phi}$:

$$\vec{t} \cdot \underline{\vec{E}}^{inc}(\vec{r}) = \frac{j\omega\mu_0}{4\pi} \vec{t} \cdot \left(\int_S \underline{\vec{J}}(\vec{r}\,') \frac{e^{-jkR}}{R} \, dS + \frac{1}{j\omega\mu_0\varepsilon_0} \overrightarrow{grad}_t \int_S \underline{\sigma}_{su}(r') \frac{e^{-jkR}}{R} \, dS \right) \tag{149}$$

The current density vector $\underline{\vec{J}}$ and the surface charge density $\underline{\sigma}_{su}$ are <u>not</u> independent of each other but are linked by the continuity equation:

$$\frac{\partial}{\partial t} \rho(\vec{r},t) = - \operatorname{div} \vec{j}(\vec{r},t) \tag{150}$$

In our case the continuity equation becomes

$$\frac{\partial}{\partial t} \sigma_{su}(\vec{r},t) = - \operatorname{div}_t \vec{J}(\vec{r},t) \tag{151}$$

By inserting (109) and (122) in equation (151) we obtain

$$\underline{\sigma}_{su}(\vec{r}\,') = - \frac{1}{j\omega} \operatorname{div}_t \underline{\vec{J}}(\vec{r}\,') \tag{152}$$

The surface current density $\underline{\sigma}_{su}$ is now expressed by a function of $\vec{\underline{J}}$ for each position r' of the area element dS. With the free-space wave factor

$$k^2 = \omega^2 \varepsilon_0 \mu_0 \tag{153}$$

we combine (149) with (152). We obtain two equations for the tangential components of the incident E-field as functions of $\vec{\underline{J}}$ only :

$$\vec{t} \cdot \vec{\underline{E}}^{inc}(\vec{r}) =$$

$$\frac{j\omega\mu_0}{4\pi} \vec{t} \cdot \left(\iint_S \vec{\underline{J}}(\vec{r}\,') \frac{e^{-jkR}}{R} \, dS + \frac{1}{k^2} \overrightarrow{\mathrm{grad}}_t \int_S \frac{e^{-jkR}}{R} \, \mathrm{div}_t \vec{\underline{J}}(\vec{r}\,') \, dS \right) \tag{154}$$

The general scattering problem is a very complicated mathematical boundary - value problem which so far has resisted exact analytical treatment except in such special cases as the sphere and the infinite cylinder. For all other cases only numerical methods can be applied.

6.4. SCATTERING FROM BODIES OF REVOLUTION WITH THE METHOD OF MOMENTS

6.4.1. GENERALIZED NETWORK PARAMETERS FOR BODIES OF REVOLUTION

The integral equation (154) can be solved numerically by the method of moments (HARRINGTON [41]). In the years 1968 and 1969 a theory and some computer programs have been developed for the scattering from bodies of revolution by HARRINGTON AND MAUTZ [40]. The following is a summary of this report as it applies to the present problem. The first step is the determination of the generalized network parameters:

The equation (154) can be rewritten in the simpler form:

$$\vec{E}_t^{inc} = L(\vec{J}) \tag{155}$$

where $L(\vec{J})$ is the integro-differential operator and which corresponds to the right side of equation (154). $L(\vec{J})$ is also similar to (148) :

$$L(\vec{J}) = [j\omega \vec{A} + \overrightarrow{\mathrm{grad}}\,\Phi]_t \tag{156}$$

$$\vec{A} = \vec{A}^{scat} \qquad \text{(see (130))}$$

$$\Phi = \Phi^{scat} \qquad \text{(see (132))}$$

A solution of (155) gives the current $\vec{J}$ on the surface S. Usually we are interested in some functional of $\vec{J}$, which can be computed once $\vec{J}$ is known.

In order to effect a solution by the method of moments, let the inner product be defined as : (see definition of <f,g> in HARRINGTON [41])

$$< \vec{W}, \vec{J} > = \int_S \vec{W} \cdot \vec{J} \ dS \qquad (157)$$

Both $\vec{W}$ and $\vec{J}$ are tangential vectors on S. A set of expansion functions $\{\vec{J}_j\}$ is next defined, and the current on S is approximated by

$$\vec{J} = \sum_j I_j \vec{J}_j \qquad (158)$$

I_j are constants to be determined. Equation (158) is substituted into (155) which, because of the linearity of L, reduces to

$$\vec{E}t_{inc} = \sum_j I_j L(\vec{J}_j) \qquad (159)$$

A set of testing functions $\{\vec{W}_i\}$ is defined, and the inner product of (159) with each $\vec{W}_i$ is taken. The result is

$$\sum_j I_j <\vec{W}_i, L\vec{J}_j> = <\vec{W}_i, \vec{E}_{inc}> \qquad i = 1,2,3,\ldots \qquad (160)$$

The index 't' has been dropped from $\vec{E}_{inc}$ because the inner product involves only tangential components. We now define the generalized network matrices

$$[Z] = [<\vec{W}_i, L(\vec{J}_j)>] \qquad (161)$$

$$[V] = [<\vec{W}_i, \vec{E}_{inc}>] \qquad (162)$$

$$[I] = [I_i] \qquad (163)$$

and rewrite the set (160) as

$$[Z] [I] = [V] \qquad (164)$$

[Z] is the generalized impedance matrix , and $[Y] = [Z]^{-1}$ is the generalized admittance matrix. The inverse of (164)

$$[I] = [Y] [V] \qquad (165)$$

gives the coefficients I_j of the current expansion (158) and hence is an approximate solution of the problem.

The impedance elements of (161) are explicitly using (156) and (157) :

$$Z_{ij} = \int_S W_i \cdot (j\omega \vec{A}_j + \overrightarrow{grad} \ \Phi_j) \ dS \qquad (166)$$

The subscript j denotes that $\vec{A}_j$ and Φ_j are potentials due to $\vec{J}$ and σ_{su}. In order to match the equations in 6.3. to those used in [40] we replace

$$\begin{aligned} \overrightarrow{\text{grad}}\ \Phi &= \vec{\nabla}\Phi \\ \text{div}\ \vec{J} &= \vec{\nabla}\cdot\vec{J} \end{aligned} \qquad (167)$$

Regarding $\vec{W}_i$ as a current density from σ_{su}, we rewrite (152) with (167)

$$\sigma_{su_i} = \frac{-1}{j\omega}\vec{\nabla}\cdot\vec{W}_i \qquad (169)$$

Now (166) can be written as

$$Z_{ij} = j\omega\int_S (\vec{W}_i\cdot\vec{A}_j + \sigma_{su_i}\Phi_j) \qquad (170)$$

Equation (170) is more convenient for computation than (166) or (154).

So far the discussion has been for an arbitrary conducting body. Now we restrict considerations to the surface S generated by revolving a plane curve about the z-axis. The surface and the coordinate systems are shown in FIGURE 32:

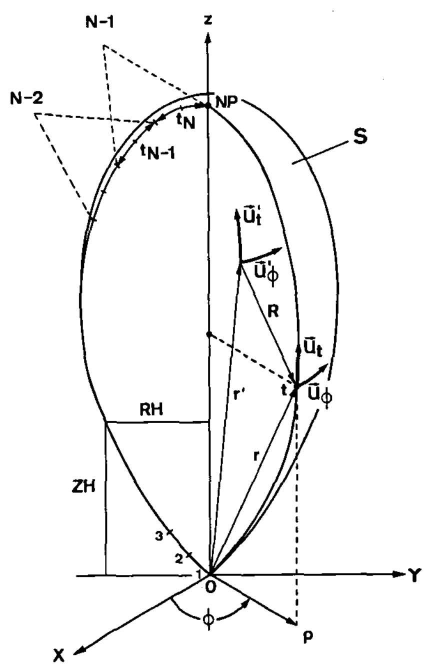

FIGURE 32 Body of revolution and coordinate systems.

S = surface of the body

NP = number of points describing the generating curve

RH = radius parameter of gen.curve

ZH = height parameter of gen.curve

t_N = tangent unit elements, $N = (\frac{NP-1}{2})$

t = length variable along the curve generating S

ρ = radius of a point on S

ϕ = angle of a point on S

z = height of a point on S

$\vec{u}_t$ = local tangential coord. syst.

$\vec{u}_\phi$ = local tangential coord. syst. (suffix ' = source point)

$\overset{N-1}{\wedge}$ = triangle function (182), N-1 peaks at 1,2,...N-1.

The body of revolution is described by the generating curve given by the curve parameters RH and ZH. The variable 't' is now a tangential length variable along the curve generating the surface S. We desire the expansion (158) to be general enough to approximate an arbitrary $\vec{J}$ on S. Hence, independent sets of functions are defined as

$$\vec{J}^{t}_{mj} = \vec{u}_t \, f_j(t) \, e^{jm\phi} \tag{171}$$

$$\vec{J}^{\phi}_{mj} = \vec{u}_\phi \, f_j(t) \, e^{jm\phi} \tag{172}$$

where u_t and u_ϕ are unit vectors t-directed and ϕ-directed, respectively. The $f_j(t)$ has been chosen in both sets to be the same, but it is not necessary to do so [40]. The current expansion (158) now becomes

$$\vec{J} = \sum_{m,j} (I^{t}_{mj} \vec{J}^{t}_{mj} + I^{\phi}_{mj} \vec{J}^{\phi}_{mj}) \tag{173}$$

For testing functions, choose

$$\vec{W}^{t}_{ni} = \vec{u}_t \, f_i(t) \, e^{-jn\phi} \tag{174}$$

$$\vec{W}^{\phi}_{ni} = \vec{u}_\phi \, f_i(t) \, e^{-jn\phi} \tag{175}$$

which differ from (171,172) only in the sign of the exponent. The $\vec{W}_n$ are orthogonal to $\vec{J}_m$, $m \neq n$, over 0 to 2π on ϕ, and also to $L(\vec{J}_m)$ (the field from $\vec{J}_m$). Hence,all impedance elements are zero except those for which m = n, and each mode n can be treated separately. This is the major simplification introduced by the rotational symmetry of the body. For the computation of non-rotational symmetric bodies, such as shown in FIGURE 18, the further procedure had to be already changed here.

The use of (171)(172)(174) and (175) to evaluate the elements of (170) results in the partitioned matrix equation

$$\begin{bmatrix} [Z_n{}^{tt}] & [Z_n{}^{t\phi}] \\ [Z_n{}^{\phi t}] & [Z_n{}^{\phi\phi}] \end{bmatrix} \begin{bmatrix} [I^{t}_{n}] \\ [I^{\phi}_{n}] \end{bmatrix} = \begin{bmatrix} [V^{t}_{n}] \\ [V^{\phi}_{n}] \end{bmatrix} \tag{176}$$

Here the elements of the Z submatrices are

$$(Z^{tt}_{n})_{ij} = \langle \vec{W}^{t}_{ni}, L(\vec{J}^{t}_{nj}) \rangle \text{, etc. for } t\phi, \phi t \text{ and } \phi\phi \tag{178}$$

The elements of the I submatrices are the coefficients in (173), and the elements of the V submatrices are

$$
\begin{aligned}
(V_n^t)_i &= \langle \vec{W}_{ni}^t , \vec{E}_{inc} \rangle \\
(V_n^\phi)_i &= \langle \vec{W}_{ni}^\phi , \vec{E}_{inc} \rangle
\end{aligned}
\tag{179}
$$

Note that, for N terms in the Fourier series of ϕ, there are N sets of matrix equations (176).

The solution to (176) can be also written in partitioned form as

$$
\begin{bmatrix} [I_n^t] \\ [I_n^\phi] \end{bmatrix} = \begin{bmatrix} [Y_n^{tt}] & [Y_n^{t\phi}] \\ [Y_n^{\phi t}] & [Y_n^{\phi\phi}] \end{bmatrix} \begin{bmatrix} [V_n^t] \\ [V_n^\phi] \end{bmatrix}
\tag{180}
$$

The Y submatrices must in general be obtained after inversion of the entire Z matrix and are not the inverse of the corresponding Z submatrices. However, as shown in [40], the -n mode matrices are related to the +n mode matrices, so that only the $n \geq 0$ mode matrices need to be inverted.

Finally, for an explicit solution one has to choose the t expansion functions $f_i(t)$. A triangle expansion function gives a piecewise-linear approximation which converges rapidly:

$$
f_i(t) = \frac{1}{\rho}\, T(t - t_i) \tag{181}
$$

$$
T(t) = 1 - |t| \quad \text{for } |t| < 1 \quad \text{and} \quad 0 \text{ for } |t| > 1 \tag{182}
$$

When using these functions, distance and frequency are scaled so that the t_i's are one unit apart. The generating curve is determined by NP body points (FIGURE 32). There are $(NP-1)/2 = N$ tangential units, and if one triangle function covers 2 units, there are N-1 peaks at 1,2,3...N-1.

6.4.2. IMPEDANCE MATRICES

6.4.2.1. EVALUATION OF THE IMPEDANCES

The generalized impedances for a body of arbitrary shape is the integral over all source points (dS') and the integral over all field points (dS) :

$$
Z_{ij} = \int_S dS' \int_S dS \left[j\omega\mu_0\, \vec{W}_i \cdot \vec{J}_j + \frac{1}{j\omega\varepsilon_0} (\vec{\nabla}' \cdot \vec{W}_i)(\vec{\nabla} \cdot \vec{J}_j) \right] \frac{e^{-jkR}}{4\pi R} \tag{183}
$$

For bodies of revolution the integrals have the t-elements 0 to N and the ϕ-

elements 0 to 2π. The radius R (see FIGURE 32) can be expressed by $\vec{r} - \vec{r}'$:

$$R = \left[\rho^2 + \rho'^2 - 2\rho\rho' \cos(\phi - \phi') + (z - z')^2\right]^{1/2} \tag{184}$$

The inner products in (183) are of the type

$$\vec{\nabla} \cdot \vec{J} = \frac{1}{\rho}\frac{\partial}{\partial t}(\rho J_t) + \frac{1}{\rho}\frac{\partial}{\partial \phi}(J_\phi) \tag{185}$$

Four types of impedances are defined by (178). To evaluate them, we use (171)(172) and (174)(175) to obtain the $\vec{W} \cdot \vec{J}$ terms in (183) as

$$\vec{W}^p_{ni} \cdot \vec{J}^q_{nj} = e^{jn(\phi-\phi')} f_i(t') f_j(t) \vec{u}'_p \cdot \vec{u}_q \tag{186}$$

where p and q represent permutations of t and ϕ. The unit vector inner products in terms of the body coordinates defined by FIGURE 32 are

$$\begin{aligned} \vec{u}'_t \cdot \vec{u}_t &= \sin v \sin v' \cos(\phi-\phi') + \cos v \cos v' \\ \vec{u}'_t \cdot \vec{u}_\phi &= - \sin v' \sin(\phi-\phi') \\ \vec{u}'_\phi \cdot \vec{u}_t &= \sin v \sin(\phi-\phi') \\ \vec{u}'_\phi \cdot \vec{u}_\phi &= \cos(\phi-\phi') \end{aligned} \tag{187}$$

Here v is the angle between the t direction and the z axis, being positive if $\vec{u}_t$ points away from the z-axis. Changing $(\phi-\phi')$ to a new variable, and expressing the sine and cosine terms of (187) as exponentials, one ϕ integration of (183) can be performed. The remaining ϕ integration defines the Green's function :

$$g_n = \int_0^{\pi} d\phi \, \frac{e^{-jkR_o}}{R_o} \cos n\phi \tag{188}$$

where R_o is given by (184) with $\phi'=0$. With f_i given by (181), the resultant expression for the impedance elements (178) are (only $(Z^{tt}_n)_{ij}$ shown):

$$(Z^{tt}_n)_{ij} = \int_0^N dt' \int_0^N dt \left[j\omega\mu_0 T(t'-i)\, T(t-j) (\sin v \sin v' \, \frac{g_{n+1} + g_{n-1}}{2} + \cos v \cos v' \, g_n) + \frac{1}{j\omega\varepsilon_0} T'(t'-i)\, T'(t-j)\, g_n \right] \tag{189}$$

Here T' is the derivative of the triangle function

$$T'(t) = \begin{cases} 1, & -1 < t < 0 \\ -1, & 0 < t < 1 \\ 0, & |t| > 1 \end{cases} \tag{190}$$

The integrations of (189) involve many different integrands, and to reduce the number of integrations the following approximations are made. For the t-integration, the T function is approximated by four pulses of amplitude 1/4, 3/4, 3/4, 1/4, and the derivative of T (denoted here as T') is represented exactly by four pulses of amplitude 1, 1, - 1, - 1. The functions ρ, $\sin v$, and $\cos v$ are assumed constant over each pulse, equal to their values at the midpoints of the pulses. For the t' integration, the T - function is approximated by four impulse functions of strengths 1/8, 3/8, 3/8, 1/8, and the derivative of T is approximated by four impulse functions of strengths 1/2, 1/2, -1/2, -1/2 (T_1, T_2, T_3, T_4 and T_1', T_2', T_3', T_4').

The midpoints of the pulses and the pulse Green's functions are defined :

$$t_p = i + \frac{p-2.5}{2} \quad ; \quad t_q = j + \frac{q-2.5}{2} \tag{191}$$

$$G_n = 2\int_{j+\frac{q-3}{2}}^{j+\frac{q-2}{2}} dt \int_0^{\pi} d\phi \, \frac{e^{-jkR_p}}{R_p} \cos n\phi \tag{192}$$

$$R_p = \left[\rho^2 + \rho_p^2 - 2\rho\rho_p \cos\phi + (z-z_p)^2\right]^{1/2} \tag{193}$$

In terms of these definitions and approximations, the matrix elements of (189) reduce to:

$$(Z_n^{tt})_{ij} = \sum_{p=1}^{4}\sum_{q=1}^{4}\Big[j\omega\mu_0 \, T_pT_q \left(\sin v_p \sin v_q \frac{G_{n+1}+G_{n-1}}{2} + \cos v_p \cos v_q \, G_n\right) + \frac{1}{j\omega\varepsilon_0} T_p' \, T_q' \, G_n\Big] \tag{194}$$

$$(Z_n^{t\phi})_{ij} = \sum_{p=1}^{4}\sum_{q=1}^{4}\Big[-\omega\mu_0 \, T_pT_q \sin v_p \frac{G_{n+1}-G_{n-1}}{2} + \frac{n}{\omega\varepsilon_0} T_p' \frac{T_q}{\rho_q} G_n\Big]$$

$$(Z_n^{\phi t})_{ij} = \sum_{p=1}^{4}\sum_{q=1}^{4}\Big[+\omega\mu_0 \, T_pT_q \sin v_q \frac{G_{n+1}-G_{n-1}}{2} - \frac{n}{\omega\varepsilon_0} \frac{T_p}{\rho_p} T_q' G_n\Big]$$

$$(Z_n^{\phi\phi})_{ij} = \sum_{p=1}^{4}\sum_{q=1}^{4}\Big[j\omega\mu_0 \, T_pT_q \frac{G_{n+1}-G_{n-1}}{2} + \frac{n^2}{j\omega\varepsilon_0} \frac{T_p}{\rho} \frac{T_q}{\rho} \, G_n\Big]$$

Here ρ_p, v_p, ρ_q, v_q are the ρ and v evaluated at t_p and t_q respectively.

Finally, the G_n (192) was prepared for the numerical computation by dividing the integration interval 0 to π into M equal intervals. In the actual computer program the G_n's were further divided by k in order to make them insensitive to the absolute size of the body. In addition , the T_p and the T'_p were modified, as can be seen in the description of the computer program A by HARRINGTON and MAUTZ [40].

6.4.2.2. LIMITATIONS OF THE NUMERICAL COMPUTATIONS OF THE IMPEDANCES

The computer program HARRA is based on the above theory. It will be discussed later in section 10.2.. The purpose of the program HARRA is to compute the four Z-matrices (194) and its inverse four Y-admittance matrices (164). The Y-matrices for each mode n from 0 to n_{nn}(192) are stored in a file for the later use by following programs computing the scattering.

Because the solution for the Y-matrices are obtained by matrix inversions, the matrix size has to be limited to a reasonable value in order to save computation time and storage capacity. The body shape will be approximated by 20 tangents (N=20), thus one obtaines 4 matrices of the size 19 x 19 for each mode. The integral intervals of the G_n's of 0 to π will be divided into 20 subintervals (M=20).

With these specifications acurate Y-matrices up to the mode n=6 can be obtained for a conducting model of man up to frequencies of 400 MHz. The proof for these statments will be presented in the program description in section 10.3.1.

6.4.3. MEASUREMENT MATRICES

Any linear measurement of the field from the current $\vec{J}$ on the body S can be expressed as a linear functional of $\vec{J}$, that is

$$\text{measurement} = \int_S \vec{E}^r \cdot \vec{J} \;\; dS \qquad (195)$$

where $\vec{E}^r$ is a known function. For a moment solution, the current is given by a superposition $J = \Sigma_j \, I_j \vec{J}_j$, and (195) reduces to

$$\text{measurement} = [R] \;\; [I] \qquad (196)$$

where [I] is the matrix (163) and [R] is a measurement row matrix:

$$[R] \;\; = \;\; [< \vec{J}_j, \vec{E}^r >] \qquad (197)$$

[R] is similar to the excitation matrix [V] (162), and with the matrix solution (165) substituted in (196), one has

$$\text{measurement} = \;\; [R] \; [Y] \; [V] \qquad (198)$$

For bodies of revolution, the expansion for $\vec{J}$ can be separated into t and ϕ directed components, according to (173). It is then convenient to partition [R] into t and ϕ component terms as

$$(R_n^t)_i = \langle \vec{J}_{ni}^t , \vec{E}^r \rangle \qquad (R_n^\phi)_i = \langle \vec{J}_{ni}^\phi , \vec{E}^r \rangle \tag{199}$$

The analogous partition for excitation [V] is given by (179). Now one can rewrite (198) in the partitioned form as

$$\text{measurement} = \begin{bmatrix} [R_n^t] & [R_n^\phi] \end{bmatrix} \begin{bmatrix} [Y_n^{tt}] & [Y_n^{t\phi}] \\ [Y_n^{\phi t}] & [Y_n^{\phi\phi}] \end{bmatrix} \begin{bmatrix} [V_n^t] \\ [V_n^\phi] \end{bmatrix} \tag{200}$$

where the Y submatrices are obtained after the Z matrix is inverted and are not the inverses of the corresponding Z submatrices.

An important special case is that of radiation field measurements. HARRINGTON [41] has shown that the radiation field from currents $\vec{J}$ on S is given by (201) :

$$\vec{E} \cdot \vec{u} = \frac{-j\omega\mu_0}{4\pi r} e^{-jkr} [R] [I] \tag{201}$$

where the elements of [R] are given by (197) with

$$\vec{E}^r = \vec{u}\, e^{-j\vec{k}\cdot\vec{r}} \tag{202}$$

This is a unit plane wave with polarization vector $\vec{u}$ and propagation vector $\vec{k}$. An arbitrary plane wave is a superposition of two orthogonal components :

$$\vec{E}_\theta = \text{'vertical' polarization (see 5.3.2.)} \tag{203}$$

$$\vec{E}_\phi = \text{'horizontal' polarization (see 5.3.2.)} \tag{204}$$

Hence, one can treat the general case as two applications of (202), one for $\vec{u} = \vec{u}_\theta$ and the other for $\vec{u} = \vec{u}_\phi$. To distinguish between the two cases let us denote the measurement matrices as follows: (205),(206)

θ-polarized case	φ-polarized case	
$(R_n^{t\theta})_i = \langle \vec{J}_{ni}^t , \vec{E}_\theta^r \rangle$	$(R_n^{t\phi})_i = \langle \vec{J}_{ni}^t , \vec{E}_\phi^r \rangle$	θ: (205)
$(R_n^{\phi\theta})_i = \langle \vec{J}_{ni}^\phi \; \vec{E}_\theta^r \rangle$	$(R_n^{\phi\phi})_i = \langle \vec{J}_{ni}^\phi \; \vec{E}_\phi^r \rangle$	φ: (206)

The excitation matrices can now be evaluated as follows. Let

$$\vec{E}_\theta^r = \vec{u}_\theta^r \, e^{jk(\rho \sin\theta_r \cos\phi + z\cos\theta_r)} \tag{207}$$

where θ_r and $\phi_r = 0$ are the angles to the field point of measurement. The inner products required in (205) are given by

$$\begin{aligned} \vec{u}_t \cdot \vec{u}_\theta^r &= \cos\theta_r \sin v \cos\phi - \sin\theta_r \cos v \\ \vec{u}_\phi \cdot \vec{u}_\theta^r &= -\cos\theta_r \sin\phi \end{aligned} \tag{208}$$

Using the integral formula for Bessel functions

$$J_n(\rho) = \frac{j^n}{2\pi} \int_0^{2\pi} e^{-j\rho\cos\phi} e^{-jn\phi} \, d\phi \tag{209}$$

one can evaluate the ϕ integrations in (205), obtaining

$$\begin{aligned} (R_n^{t\theta})_i &= 2\pi j^{n+1} \int_0^N dt\, \rho f_i(t) e^{jkz\cos\theta_r} \left[\cos\theta_r \sin v \, \frac{J_{n+1} - J_{n-1}}{2} \right. \\ &\qquad\qquad \left. + j \sin\theta_r \cos v \; J_n \right] \\ (R_n^{\phi\theta})_i &= -2\pi j^{n+1} \int_0^N dt\, \rho f_i(t) e^{jkz\cos\theta_r} \cos\theta_r \, \frac{J_{n+1} + J_{n-1}}{2j} \end{aligned} \tag{210}$$

and one can similarly evaluate the ϕ integration for the ϕ case :

$$\begin{aligned} (R_n^{t\phi})_i &= 2\pi j^{n+1} \int_0^N dt\, \rho f_i(t) \, e^{jkz\cos\theta_r} \sin v \, \frac{J_{n+1} + J_{n-1}}{2j} \\ (R_n^{\phi\phi})_i &= 2\pi j^{n+1} \int_0^N dt\, \rho f_i(t) \, e^{jkz\cos\theta_r} \, \frac{J_{n+1} - J_{n-1}}{2} \end{aligned} \tag{211}$$

where J_n is

$$J_n = J_n(k\rho \sin\theta_r) \tag{212}$$

For computations, the $\rho f_i(t)$ in (210) and (212) were the triangle functions (182). For plane-wave excitation of the body the excitation matrix [V] is

$$(V_n^{pq})_i = (R_{-n}^{pq})_i \tag{213}$$

where pq represents $t\theta$, $\phi\theta$, $t\phi$, or $\phi\phi$. Equation (213) means that the V_i are given by (210) and (211) with n replaced by -n and θ_r by θ_t .

6.4.4. GENERAL PLANE-WAVE SCATTERING

The radar scattering problem consists of a plane wave incident on a scattering body, plus measurement of the far-zone scattering. Because we are interested in the measurement of the near-zone scattering, only a few details should be discussed here. The solution of this radar scattering problem requires the determination of the t-directed and ϕ-directed surface currents. In program B the currents are computed and printed for the axial incidence of a plane wave, and in program D the currents are partly computed for an oblique incidence (HARRINGTON and MAUTZ [40])

Using the formulas (127),(132) and the continuity equation (152), the scattered field in a point near the body (see FIGURE 31) could be computed if J^t and J^ϕ are known at the peaks of each triangle function. A special program E (not enclosed in this book) has been prepared to compute these currents for arbitrary wave incidence. In principle, the current densities for each mode are obtained by program D, have to be summed over all needed modes and transferred in program B for linearization and printing.

6.4.5. NEAR-FIELD COMPUTATION

6.4.5.1. METHOD OF SOLUTION

The solution of our actual problem, that is the computation of the scattered field and the incident field near the conducting body became possible with the extension of the theory by BEVENSEE [10] (see FIGURE 33) :

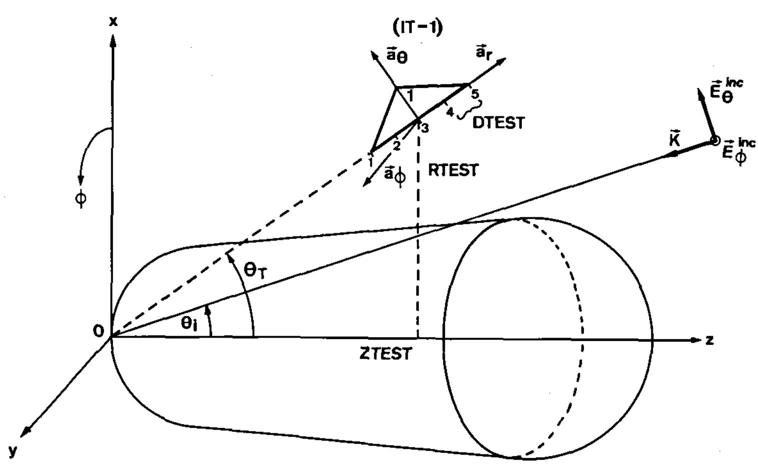

FIGURE 33 Coordinates and nomenclature for near-field computations at oblique incidence of a plane wave. (Source: BEVENSEE [10])

The method of solution (BEVENSEE [10] is an extension of the method by HARRINGTON and MAUTZ [40] discussed above in sections 6.4.1. to 6.4.3.. The formulas (155) up to (163) can be summarized as follows:

The operation equation

$$\vec{E}_t^{inc} = L(\vec{J}) , \quad L(\vec{J}) = (j\omega\vec{A} + \vec{\nabla}\Phi)_t \tag{214}$$

is solved by expanding

$$\vec{J} = \sum_j I_j \vec{J}_j \tag{215}$$

for the n^{th} azimuthally varying mode by a set of functions : $\vec{J}_j = \vec{u}\, f_j\, e^{jn\phi}$ ($\vec{u}$ = unit vector in the t- or ϕ-direction on the surface of the body) and by a set of functionals $\vec{W}_j = \vec{u}\, f_j\, e^{-jn\phi}$ in succession :

$$< \vec{W}_i , \vec{E}_t^{inc} > = \sum_j < \vec{W}_i , L(\vec{J}_j) > I_j , \; i = 1,2,.. N \tag{216}$$

The < > denotes a spatial integral over the localized range of the W_i-function. Defining Z_{ij} as $< \vec{W}_i , L(\vec{J}_j) >$ one obtains the network representation of (214) as :

$$V_i = \sum_j Z_{ij}\, I_j , \quad V_i = < \vec{W}_i , \vec{E}_t^{inc} > \tag{217}$$

Analogously, <u>a test segment, subscript T</u> , is inserted to measure the scattered field $\vec{E}^{scat} = L(\vec{J})$ as (BEVENSEE [10])

$$< \vec{W}_T , \vec{E}^{scat} > = < \vec{W}_T , -L(\vec{J}) > = -\sum_j < \vec{W}_T , L(\vec{J}_j) > I_j \tag{218}$$

Defining the measurement matrix [ZM] as $(ZM)_{1j} = -< \vec{W}_T , L(\vec{J}_j) >$, where the index '1' means test segment 1 and 'j' the source element (166), one has

$$< \vec{W}_T , \vec{E}^{scat} > = \sum_j (ZM)_{1j}\, I_j \tag{219}$$

and the electric field in the T-direction along the test segment is approximately

$$\vec{E}_T^{scat} = \frac{1}{< \vec{W}_T >} \sum (ZM)_{1j}\, I_j \tag{220}$$

As the area $< \vec{W}_T >$ of the test segment approaches zero, $\vec{E}_T^{scat}$ approaches the correct scattered field value.

The computation of the fields at a point near the conducting body (see FIGURE 33) involves the following steps:

First, the [Z] matrices (194) and its inverse [Y] matrices have to be computed for all needed modes. This computation is only dependent on the dimensions of the body and the applied frequency but not on the irradiation angle θ_i or the polarization.

Second, the [R] matrices (210) and (211) have to be computed for a specific incident wave in order to obtain the exitation matrices [V] and the coefficient [I] of the current expansion (164).

Third, at a given test point a test segment is defined by five points and four sections of equal length DTEST (FIGURE 33). This test segment is first positioned along the spherical radius vector $\vec{a}_r$ (for IT = 1, as shown in FIGURE 33) to measure the $\vec{a}_r$- and $\vec{a}_\phi$-components of the $\vec{E}$ field. It is then positioned along the spherical $\vec{a}_\theta$-vector (for IT = 2) to measure the $\vec{a}_\theta$- and $\vec{a}_\phi$-components of the $\vec{E}$ field. The two measured E_ϕ fields approach each other as the test segment length 4DTEST approaches zero; their discrepancy gives an estimate of the accuracy obtained with this segment.

The total E-field $\vec{E}^{tot}$ along an $\vec{a}$-vector is the superposition of $\vec{E}^{inc}$ and $\vec{E}^{scat}$ (see (135)). The $\vec{E}^{inc}$- components are obtained by using the subroutine PLANE (which computes the [R] and [V] matrices, see (213)) applied a second time on the test segment. The $\vec{E}^{scat}$-components are computed with a new subroutine NEARZ which is well described by BEVENSEE [10]

The matrix elements of [ZM] (220) are determined similar to the elements of [Z] (194) but with an altered Green's function G_{nT}. If we denote a surface element on the body as $2\, y_o \cdot x_o$ ($2\, y_o$ = 2 tangent units as in FIGURE 32, x_o = circumference unit $\rho_q \pi/M$, M = number of π intervals), the G_{nT} for the test segment may be written in the form

$$G_{nT}^{(1)} = \frac{1}{2\rho_q y_o} \int_{-yo}^{+y_o} dy \int_0^{xo} dx \; \frac{1 + jk\left[x^2 + (y-ya)^2 + \Delta_a^2\right]^{1/2}}{\left[x^2 + (y-y_a)^2 + \Delta_a^2\right]^{1/2}} \qquad (221)$$

where $dx = \rho_q d\phi$, x,y = center of a local coordinate system at the center of the J^{th} source element, y_a = tangential distance from the test section and Δ_a = projection distance from the test section (see FIGURE 34). Equation (221) can be evaluated as follows:

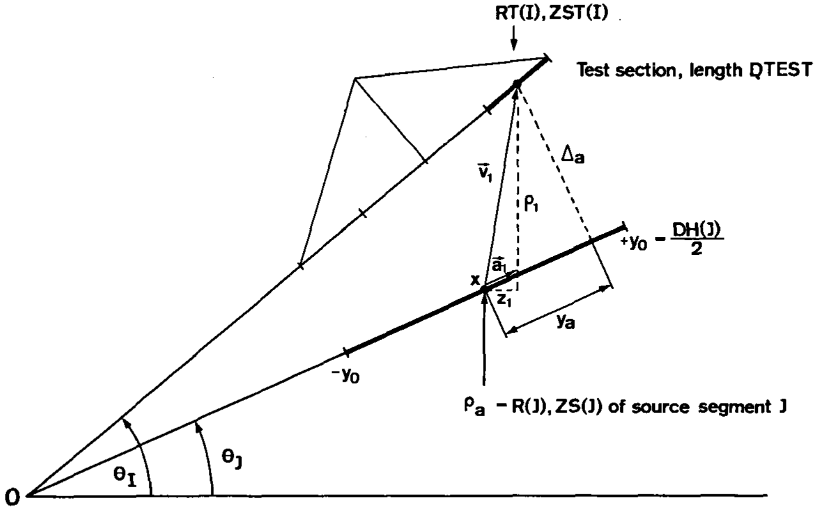

FIGURE 34 Coordinates and nomenclature for a test segment section very near to a triangle segment on the body. The x and y of the local coordinate system are measured from the center of the source segment J.
$y_a = \vec{v}_1 \cdot \vec{a}_1$, $|\vec{a}_1| = 1$, $\Delta_a^2 = v_1^2 - y_a^2$ (Source : BEVENSEE [10])

With $y_A = y_o + y_a \geq 0$ and $y_B = y_o - y_a \geq 0$ one obtains:

$$G_{nT}^{(1)} = \frac{1}{2\,\rho_q\, y_o} \int_{-y_A}^{y_B} dy \int_0^{x_o} dx \;\frac{1 - jk\left[x^2 + y^2 + \Delta_a^2\right]^{1/2}}{\left[x^2 + y^2 + \Delta_a^2\right]^{1/2}} \tag{222}$$

In NEARZ the near-charge contribution (222) of source segment J to the potenial at test section I is computed only if all three of these conditions are true : K = 1 ($0 \leq \phi \leq \pi/M$ in the azimuthal integration over the source), Δ_a < DTEST (the center of the test section is closer to the source segment than the test section length), and $|y_A| \leq$ DH(J)/2 (i.e., a perpendicular dropped from the test section falls somewhere on the source segment). If one or more of these conditions is not valid the standard G_n (192) will be computed by the distant-source formulas . The evaluation of G_n for the numerical computation is described in HARRINGTON and MAUTZ [40] and that of $G_{nT}^{(1)}$ in BEVENSEE [10].

Because of the approximations in separating the charge contributions to the potential on the test segment into a smoothed near-charge and discrete far-charge components, the test fields should be regarded as suspect unless $\Delta_a/\lambda > 1$ and also 4 DTEST/λ < 1/4, where 4 DTEST is the full length of the test segment in FIGURE 33.

The remainder of NEARZ is essentially the same as in program A and HARRA (6.4.2.2.) except that the measurement matrix [ZM] is computed for the test segment instead of the impedance matrix [Z] of the body.

The output of the source program HARRDF (BEVENSEE [10]) consists of the field components $E^{inc}, E^{scat}, E^{tot}$ in the directions of $\vec{a}_\theta, \vec{a}_r$ and (2x) $\vec{a}_\phi$ for $\phi = 0^o$, a selected incident angle θ_i and the selected mode n.

The extended program PANB computes these quantities for all needed modes n and for ϕ = 0, 5, 10,..180^o. The contribution of each mode is summed separately, and one obtains the complete E^{tot} in $\vec{a}_\theta, \vec{a}_r$ and $\vec{a}_\phi$ (mean value) directions. After coordination transformation the $E^{tot}(\phi)$ are available in vertical, horizontal and radial directions. The amounts of $E^{tot}(\phi)$ related to $|E|$ of the incident plane wave deliver the chosen transmission $Loss_B$ for the three polarization axes p_1 of the antenna A_1 in FIGURE 11.

6.4.5.2. LIMITATIONS OF THE NEAR-FIELD COMPUTATIONS

The basic limitations are already given by the computation of the [Z] matrices with program HARRA (see discussion in section 6.4.2.2.)

A further problem is to select the "best" segment length. If the segment is short, one would measure fluctuating components of the tangential fields, since the boundary condition of $E_t = 0$ (125) is only satisfied in an integral sense with respect to the triangle functions. If the segment is long, one obtains an averaged value of the surrounding fields of the test point. Near field computations of a point field with a test segment tend to be inaccurate unless both these conditions are fulfilled:

a.) Minimum distance of the test segment center to the body surface > λ.
b.) Test segment length < $\lambda/4$.

The accuracy of the obtained results will be discussed in section 10.3.. In general, the field components can be computed with less than 2 dB error for a human-sized conducting model, if the frequency is below 500 MHz and if the distance of the test segment (antenna-body distance d_{at}) from the surface is larger than 0.1 m. It is required to investigate the influence of each additional mode n and to perform two computations with different test segment lengths, in our case 0.08 and 0.2 m, to check fluctuations.

6.5. SCATTERING FROM LONG CIRCULAR CYLINDERS: AN ANALYTICAL APPROACH

6.5.1. PURPOSE OF THE ANALYTICAL APPROACH

The numerical computation of a finite body of revolution according to section 6.4. is primarily limited by computation time and storage capacity of the computer. Tremendous efforts are needed if the frequency is above 400 MHz and if the antenna-body distance is smaller than 0.1 m.

On the other hand, as shown in section 5.2.3., the human body is large compared with the wavelength at frequencies above 200 MHz if we consider the radar cross section as a measure for quasi-off-resonance behavior.

If we neglect the resonance phenomena and are looking only on the total field at vertical polarization at frequencies above 200 MHz, the three-dimensional problem can be converted in a more simple two-dimensional problem. Thus, the adequate model is an infinite, circular cylinder, which is irradiated by a plane wave at an angle $\theta_i = 90^0$. The theory to solve this problem originates from KING and WU [50] and VAN BLADEL [81].

6.5.2. METHOD OF SOLUTION

The scattered fields associated with a circular cylindrical scattered can be determined by separation of variables. The configuration of interest is shown in FIGURE 35 , the body model is the IZYL defined in 5.4.1.:

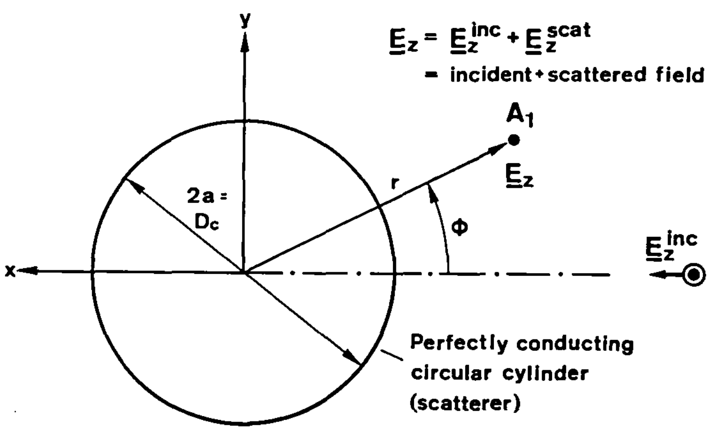

FIGURE 35 Two-dimensional model of man for analytical computation (IZYL). Vertical infinite cylinder in a vertical polarized incident plane wave: D_c = cylinder diameter, A_1 = antenna positioned at r,ϕ, $\underline{E}_z^{inc}$ = incident $\vec{E}$

For the following computation it is convenient to operate with the angle ϕ' and the cylinder radius a :

$$\phi' = \phi + \pi \quad ; \quad a = D_c/2 \tag{223}$$

The incident $\vec{E}$-wave has only a z-component and is of the type :

$$\underline{E}_z^{inc} = e^{-jkx} = e^{-jkr\cos\phi'} \tag{224}$$

The incident field is expanded in a Fourier series in ϕ' whose r-dependent coefficients are found by insertion in the wave equation to satisfy Bessel's equation. Thus, with $\underline{E}_z^{inc}$ finite at r = 0

$$\underline{E}_z^{inc} = \sum_{n=-\infty}^{\infty} j^{-n} J_n(kr)\, e^{jn\phi'} \tag{225}$$

where $\underline{J}_n(kr)$ is a Bessel function of order n. The scattered field must have a Fourier series of the form

$$\underline{E}_z^{scat} = \sum_{n=-\infty}^{\infty} \underline{\alpha}_n\, j^{-n}\, \underline{H}_n^{(2)}(kr)\, e^{jn\phi'} \tag{226}$$

where $\underline{H}_n^{(2)}(kr)$ is a Hankel function of the second kind and order n. The value of $\underline{\alpha}_n$ follows directly from the boundary condition (125) :

$$\underline{E}_z = \underline{E}_z^{inc} + \underline{E}_z^{scat} = 0 \quad \text{at} \quad r = a \tag{227}$$

according to which the $\underline{\alpha}_n$ are

$$\underline{\alpha}_n = - \frac{J_n(ka)}{\underline{H}_n^{(2)}(ka)} \tag{228}$$

The above formulas by KING and WU [50] and VAN BLADEL [81] are now evaluated for near-field conditions with respect to the computer program PANA (see also program description in section 7.3. and listings in 16.2.1.)

A series of complex parameters can be expressed as

$$\sum_{-\infty}^{+\infty} \underline{c}_n = \underline{c}_n + \sum_{n=1}^{+\infty} (\underline{c}_n + \underline{c}_{-n}) \tag{229}$$

In equation (225) the $\underline{c}_n$ and $\underline{c}_{-n}$ are

$$\begin{aligned} \underline{c}_n &= j^{-n} J_n(kr)\, e^{jn\phi'} \\ \underline{c}_{-n} &= j^{-n} J_{-n}(kr)\, e^{-jn\phi'} = j^n (-1)^n J_n(kr)\, e^{-jn\phi'} \end{aligned} \tag{230}$$

With the relations $(-j)^n = (j)^{-n}$ and $e^{jn\phi'} = \cos\phi' = e^{-jn\phi'}$, $\underline{E}_z^{inc}$ becomes

$$\underline{E}_z^{inc} = J_o(kr) + 2\sum_{n=1}^{+\infty} j^{-n} J_n(kr) \cos n\phi' \qquad (231)$$

The series for $\underline{E}_z^{scat}$ is evaluated as follows:

$$\underline{c}_n = \underline{\alpha}_n \; j^{-n} \; \underline{H}_n^{(2)}(kr) \; e^{jn\phi'}$$

$$\underline{c}_{-n} = \underline{\alpha}_{-n} \; j^{n} \; \underline{H}_{-n}^{(2)}(kr) \; e^{-jn\phi'}$$

$$\underline{H}_{-n}^{2}(kr) = e^{-jn\pi} \; \underline{H}_n^{(2)}(kr) \qquad (232)$$

Because $(-1)^n = (e^{j\pi})^n$, $(-1)^n e^{jn\pi} = (e^{j2\pi})^n = +1$, the $\underline{\alpha}_{-n}$ becomes

$$\underline{\alpha}_{-n} = -\frac{(-1)^n J_n(ka)}{e^{-jn\pi} \underline{H}_n^{(2)}(ka)} = (-1)^n e^{jn\pi} \underline{\alpha}_n = \underline{\alpha}_n \qquad (233)$$

and the $\underline{c}_{-n}$ becomes

$$\underline{c}_{-n} = \underline{\alpha}_n \, j^n \, e^{-jn\pi} \; \underline{H}_n^{(2)}(kr) \; e^{-jn\phi'} \qquad (234)$$

With the relations $e^{-jn\pi} = (-1)^n$, $j^n e^{-jn\pi} = j^{-n}$ one obtains for $\underline{E}_z^{scat}$

$$\underline{E}_z^{scat} = \underline{\alpha}_o \underline{H}_o^{2}(kr) + 2\sum_{n=1}^{+\infty} \underline{\alpha}_n \; \underline{H}_n^{(2)}(kr) \; j^{-n} \cos n\phi' \qquad (235)$$

The combined fields from (231) and (235) represent the solution $\underline{E}_z(r,\phi')$ at the location of the antenna A_1.

For the computer program the Hankel function may be replaced by the expression:

$$\underline{H}_n^{(2)}(kr) = J_n(kr) - j\, Y_n(kr) \qquad (236)$$

where J_n is a Bessel function of the first kind and order n, and Y_n is a Bessel function of the second kind and order n or a Neumann function.

6.5.3. LIMITATIONS OF THE ANALYTICAL NEAR-FIELD COMPUTATION

The convergence of the series (231) and (235) is quite slow ($r \gg a$) for big values of ka. Whereas six terms (modes n) give satisfactory results for ka = 3, over 1000 terms are needed for ka = 100 (KING and WU [50]). Our ka is about 3 at 1000 MHz, and accurate near-field data are possible with $n \leq 25$.

Leer - Vide - Empty

7. Two-Dimensional Computation of Scattering from an Infinite Circular Cylinder

7.1. COMPUTATIONAL MODEL AND GOALS

The antenna-body model consists of a perfectly conducting, circular cylinder of infinite length (FIGURE 28: Model IZYL), a small antenna A_1 polarized parallel to the cylinder axis with the coordinates r (radius) and ϕ (azimuthal angle), and an incident plane wave with the E-field polarized parallel to the cylinder axis. The computational situation is shown in FIGURE 35, and the method of solution is described in section 6.5..

The selection of this model follows from the analysis in section 5.2.3. and 5.2.4. The vertical IZYL represents a standing human TS at frequencies above 200 MHz, irradiated by a plane wave with the incident angle $\theta_i = 90°$.

The model allows the computation of all vertical polarized E-field components and should give a preliminary answer about the correlation among antenna-body distance d_{at}, azimuthal angle ϕ, frequency f, cylinder diameter D_c and transmission Gain_B .

7.2. COMPUTER PROGRAM PANA: NEAR-FIELD PATTERN COMPUTATION OF THE INFINITE CYLINDER IZYL

7.2.1. COMPUTATIONAL FORMULAS AND PARAMETERS

The total field (vertical component always) $\underline{E}(r,\phi')$ at the antenna A_1 is determined by the formulas (223) to (236) in section 6.5.. With $\phi' = \phi + \pi$:

$$\underline{E}(r,\phi') = \underline{E}^{inc}(r,\phi') + \underline{E}^{scat}(r,\phi') \qquad (= 0 \text{ at } r = a) \tag{227}$$

$$\underline{E}^{inc}(r,\phi') = J_0(kr) + 2\sum_{n=1}^{+\infty} j^{-n}\, J_n(kr)\cos n\phi' \tag{231}$$

$$\underline{E}^{scat}(r,\phi') = \underline{\alpha}_0\, \underline{H}_0^{(2)}(kr) + 2\sum_{n=1}^{+\infty} \underline{\alpha}_n\, \underline{H}_n^{(2)}(kr)\, j^{-n} \cos n\phi' \tag{235}$$

$$\underline{\alpha}_n = -\frac{J_n(ka)}{\underline{H}_n^{(2)}(ka)} \qquad ; \quad a = D_c/2 \tag{228}$$

$$\underline{H}_n^{(2)}(kr) = J_n(kr) - j\, Y_n(kr) \tag{236}$$

The transmission $Gain_B$ (see definition (20) in section 5.1.2.) is then:

$$Gain_B = 20 \log \left| 1 + \frac{\underline{E}^{scat}(r,\phi')}{\underline{E}^{inc}(r,\phi')} \right| \tag{237}$$

In the program the variables and parameters are denoted as follows:

INPUT	PARAMETER NAME	MEANING	UNITS
*	A (REAL)	a, radius of the cylinder	[m]
	AK (REAL)	ka	
	DAT (REAL)	d_{at}, antenna-body distance	[m]
*	DMAX1 (REAL)	maximum d_{at} for ARP	[m]
*	DMAX2 (REAL)	maximum d_{at} for DRP	[m]
*	DMIN1 (REAL)	minimum d_{at} for ARP	[m]
*	DMIN2 (REAL)	minimum d_{at} for DRP	[m]
	EZI (COMPL)	E^{inc}	
	EZSC (COMPL)	E^{scat}	
*	F (INTEG)	f, integer number for the frequency	[MHz]
	G (REAL)	$Gain_B$	[dB]
	HNKR (COMPL)	H_n, Hankel function, second kind	
	JN (REAL)	J_n, Bessel function, first kind	
	K (REAL)	k, wave propagation factor	
	LAM (REAL)	λ, wavelength	[m]
*	M1 (INTEG)	maximum mode n for ARP	
*	M2 (INTEG)	maximum mode n for DRP	
*	MR1 (INTEG)	number of d_{at} for ARP	
*	MR2 (INTEG)	number of d_{at} for DRP	
	PHI (INTEG)	ϕ, integer azimuthal angle, 0,5,10,.. 180	[°]
	PHH (REAL)	ϕ', $\phi+\pi$	[°]
	RK (REAL)	kr	
	YN (REAL)	Y_n, Bessel function, second kind	

TABLE 36 Variables and parameters used in program PANA
(ARP: Azimuthal radiation pattern, DRP: Directive radiation pattern)

7.2.2. PROGRAM DESCRIPTION PANA

The listing of the program PANA is enclosed in Appendix 16.2.1. It consists of one main program and one subroutine BESS. The main program consists of two parts preceded by an input section.

PANA 44 to 60 : Input and preliminary computations
PANA 61 to 98 : Computation of the azimuthal radiation pattern
PANA 100 to 143 : Computation of the directive radiation pattern

The input data set consists of the following punched cards (PANA 174-179):

NAMES INPUT PARAMETER				FORMATS INPUT PARAMETER				SAMPLE INPUT PARAMETER			
DMIN1	DMAX1	MR1	M1	F6.2	F6.2	I4	I4	0.05	0.25	05	12
DMIN2	DMAX2	MR2	M2	F6.2	F6.2	I4	I4	0.05	1.00	20	25
A				F7.3				0.125			
F				I3				150			
:				:				:			
F				I3				250			

TABLE 37 Input parameter set (punched cards PANA 174-179)

Card No. 1 : data for the azimuthal radiation pattern

Card No. 2 : data for the directive radiation pattern

Card No. 3 : data for the cylinder radius

Card No. 4+i : data for the frequencies to be computed (i = 0,1,2,..)

In the present program the azimuthal radiation pattern computation (part 1) consists of the computation of the ϕ-dependence of $Gain_B$ for five (MR1) fixed d_{at}'s of 0.05 to 0.25 m in the ϕ-range 0 to 180°. The spacing of the ϕ-steps is determined to 5° due to the statement

```
      DO 2 I=1,37                                                    PANA 81
```

The maximum number of d_{at}'s (MR1) is limited by the output procedure PANA 69-71; the values of the d_{at}'s may vary from 0.01 to 9.99 m (PANA 70).

In the present program the directive radiation pattern computation (part 2) consists of the computation of the d_{at}-dependence of $Gain_B$ at the irradiated side (ϕ = 0°) and in the shadow zone (ϕ = 180°) of the cylinder. The d_{at}'s vary from 0.05 to 1.00 m in 0.05 m steps, determined by the input cards. The maximum number of d_{at}'s (MR2) is limited only by the computational time; the values of the d_{at}'s may vary from 0.01 to 9.99 m (PANA 109).

The program computes the two radiation patterns for as many frequencies as frequency input cards are added in the data set. If the last frequency is executed, the program stops due to the statements:

```
      IF(EOF (1)) 52,53                                              PANA 55
   52 STOP                                                           PANA 145
```

The radius a (A) is limited by PANA 64 and 104 and may vary from 0.005 to 4.999 m . The frequency f (F) may vary from 1 to 999 MHz (PANA 62 and 101).

The computation of the first $Gain_B$ for the azimuthal radiation pattern starts with the defining of AK (PANA 60), selecting the first d_{at} (PANA 78 and 79) and selecting the first $\phi = 0°$ (PANA 81 and 82). The corresponding RK is given by PANA 88 and the PHH by PANA 83. The maximum mode number M1 is transferred to M, and the computation parameters M,AK,RK,PHH are transferred to the subroutine BESS for the computation of $Gain_B$ (G) :

```
     CALL BESS(M,AK,RK,PHH,EZI,EZSC,V,G)                     PANA 89
```

The subroutine BESS will be discussed below. The result G ($Gain_B$) is returned from the subroutine and is checked for correct size in printing (PANA 90) and plotting (PANA 92). With the statements

```
      DO 3 L=1.31                                           PANA 85
    3 D1(L)=1H                                              PANA 86
      KK=IFIX(G+30.5)                                       PANA 93
      D1(KK)=1RO+J)                                         PANA 94
```

the number J (first J = 1) of the J-th d_{at} is plotted as an amplitude marker in the $Gain_B$ versus ϕ diagram in FIGURE 38.

The computation of the first $Gain_B$ for the directive radiation pattern uses the same AK and starts with the defining of the first d_{at} (PANA 124) and the first PHH (PANA 118) . The corresponding RK is computed in PANA 131 and 132. The following computation of $Gain_B$ in the subroutine BESS and the plotting of $Gain_B$ as an amplitude marker in the $Gain_B$ versus d_{at} diagram is similar to above with the exception that a (*) is printed. The complete diagram is shown in FIGURE 39.

The subroutine BESS uses the routine BESYN of the library BRUSLIB VIMCODE C306. Because other Bessel routines might be used in other computer centers, a few comments are helpful. In FORTRAN IV the transfer of the parameter 0 causes difficulties. Thus, the mode numbers n = 0,1,2,...M are changed into MP1 = 1,2,3,...M+1 (PANA 153). The statement

```
     CALL BESYN(-AK,MP1,JN,YN)                               PANA 154
```

executes the computation of $J_n(ka)$ and $Y_n(ka)$ for the modes 0,1,2,..MP1-1. With PANA 156 one obtains the $\underline{\alpha}_n$ of (228) in array AN(I). Similarly

```
     CALL BESYN(-RK,MP1,JN,YN)                               PANA 157
```

executes the computation of $J_n(kr)$ and $Y_n(kr)$. Finally, the $\underline{E}^{inc}$ and $\underline{E}^{scat}$ are computed in PANA 158-167. The returned G in PANA 169 represents $Gain_B$ of equation (237) for the selected r and ϕ'.

7.2.3. PROGRAM LIMITATIONS AND ACCURACY

The convergence of the series in equation 231 and 235 is quite slow for large values of kr and similar in equation 228 for large values of ka. The mimimum required modes n_{min} to solve equation 237 accurately depends therefore primarily on the maximum frequency f and the maximum d_{at}. The subroutine BESS allows the computation of maximum 99 modes, and since the computational time increases with n, n_{min} should be evaluated as follows:

For large values of d_{at}'s (or distance r) $Gain_B$ should approach 0 dB for $\phi = 180^0$ (shadow zone). If the chosen n_{min} is too small, $Gain_B$ increases first monotonously with increasing d_{at} as expected; it begins to oscillate for larger d_{at}'s, and finally the program stops with an error message. Introducing the additional statements:

```
  GOTO 5                    before  PANA  61
5 CONTINUE                  before  PANA 100
  IJ=IJ+2                   before  PANA 118
```

the program executes only the directive radiation pattern computation for $\phi = 180^0$. At a given frequency f, a given radius a and a chosen minimum mode number n_{min} (M2) the largest correctly computed d_{at} can be seen in the $Gain_B$ versus d_{at} diagram (e.g., FIGURE 39,bottom, if M2 would be <12).

In our application it was found that even for the maximum frequency 999 MHz a mode number of 25 (M2 = 25) is sufficient for d_{at} below 2 m, with a = 0.125 m and an accuracy of better than 0.1 dB.

The dimensions of the input parameters depend mainly on the selected output formats and have been discussed in 7.2.2.. The units are [m] and [MHz]:

DMIN1	: 0.01	DMIN2	: 0.01	A	: 0.005-4999	
DMAX1	: 9.99	DMAX2	: 9.99	F	: 1 - 999	(238)
MR1	: 1 - 5	MR2	: 1 - ∞	No. of F	: 1 - ∞	
M1	: 1-99	M2	: 1-99	$\Delta\phi$ steps	: 1 - ∞ (PANA 81)	

Scaled model computations are possible with a factor c_{scale}:

$$
\begin{aligned}
F_{model} &= F_{actual} \cdot c_{scale} \\
A_{model} &= A_{actual} \div c_{scale} \\
R_{model} &= R_{actual} \div c_{scale} \quad (R = d_{at} + a)
\end{aligned}
\tag{239}
$$

The execution of the program PANA on a CDC 6500 computer requires a storage of 20,000 to 60,000 octal, depending on the compiler. The standard program (with 3 frequencies) requires 30 s excecution time.

7.3. COMPUTED RESULTS OF THE TWO-DIMENSIONAL MODEL IZYL

7.3.1. AZIMUTHAL AND DIRECTIVE RADIATION PATTERNS OF ANTENNA-IZYL MODEL

Samples for the frequency 567 MHz (FIGURES 38 and 39) and 150 MHz (FIGURES 40 and 41) are presented here; additional samples are in Appendix 16.2.1..

A Z I M U T H A L   R A D I A T I O N   P A T T E R N   F R E Q U E N C Y 567 M H Z

TWO-DIMENSIONAL ANTENNA-BODY SYSTEM

TESTBODY: INFINITE ROT.SYM.CYLINDER — DIAMETER: .25 M

NUMBER OF MODI: 12

POLARIZATION: VERTICAL/VERTICAL

DAT(I) : ANTENNA-BODY DISTANCE IN METERS

GAI(I) : GAIN, FIELD STRENGTH AT THE ANTENNA A1 IN DB, 0 DB = FREE SPACE

PHI : HORIZONTAL ROTATION ANGLE IN DEGREES

	DAT(1) .050	DAT(2) .100	DAT(3) .150	DAT(4) .200	DAT(5) .250
PHI	GAI(1)	GAI(2)	GAI(3)	GAI(4)	GAI(5)
0	.5	3.9	3.7	.5	-5.3
5	.5	3.9	3.7	.5	-5.3
10	.4	3.9	3.7	.6	-5.1
15	.3	3.8	3.8	.8	-4.9
20	.2	3.8	3.8	1.1	-4.4
25	.0	3.7	3.8	1.4	-3.9
30	-.2	3.5	3.9	1.8	-3.1
35	-.5	3.4	3.9	2.1	-2.3
40	-.8	3.2	3.9	2.5	-1.3
45	-1.1	3.0	3.9	2.8	-.4
50	-1.5	2.7	3.8	3.1	.4
55	-1.9	2.4	3.7	3.3	1.2
60	-2.4	2.0	3.6	3.5	1.9
65	-2.9	1.6	3.4	3.5	2.4
70	-3.5	1.2	3.1	3.5	2.9
75	-4.1	.6	2.7	3.4	3.1
80	-4.8	.1	2.3	3.3	3.3
85	-5.5	-.6	1.8	3.0	3.3
90	-6.3	-1.3	1.2	2.6	3.1
95	-7.1	-2.0	.6	2.1	2.9
100	-7.9	-2.8	-.1	1.5	2.5
105	-8.8	-3.6	-.8	.9	2.0
110	-9.7	-4.5	-1.7	.2	1.4
115	-10.7	-5.5	-2.6	-.7	.7
120	-11.8	-6.5	-3.5	-1.6	-.2
125	-12.9	-7.6	-4.7	-2.6	-1.2
130	-14.2	-8.9	-5.9	-3.8	-2.3
135	-15.6	-10.3	-7.3	-5.2	-3.7
140	-17.1	-11.8	-8.8	-6.8	-5.2
145	-18.7	-13.4	-10.5	-8.4	-6.9
150	-20.2	-15.0	-12.1	-10.1	-8.6
155	-21.4	-16.2	-13.4	-11.5	-10.1
160	-21.9	-16.8	-14.1	-12.3	-11.0
165	-21.8	-16.8	-14.1	-12.4	-11.2
170	-21.5	-16.5	-13.9	-12.2	-10.9
175	-21.2	-16.2	-13.6	-11.9	-10.6
180	-21.0	-16.1	-13.4	-11.7	-10.5

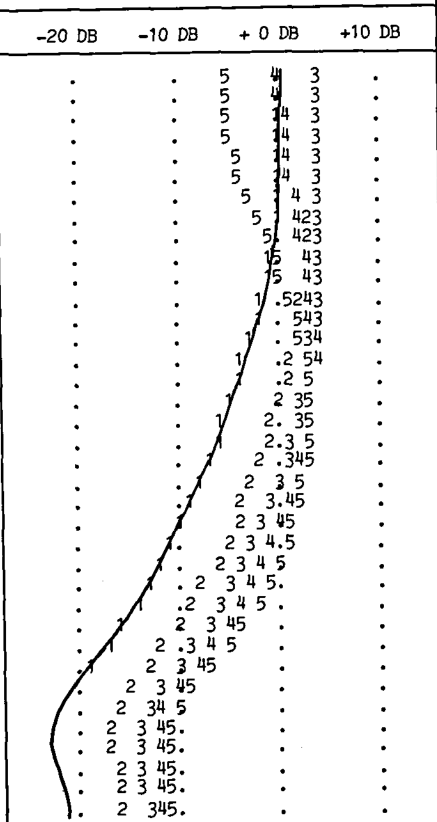

FIGURE 38 Azimuthal radiation pattern at 567 MHz (result of program PANA)
Left: $Gain_B$ for 5 d_{at}'s and $\phi = 0 - 180°$, right: $Gain_B$ versus ϕ for 5 d_{at}'s.

In FIGURE 38 and 39 the diameter of the IZYL is 0.25 m and the frequency is 567 MHz. The azimuthal radiation pattern (FIGURE 38) shows a clear minimum of the gain (GAI(I)) at ϕ = 160-165°, decreasing with decreasing d_{at} (DAT(I)). The directive radiation pattern (FIGURE 39) at ϕ = 0° reveals a gain oscillation, with maxima at d_{at} of about $\lambda/4 + n\cdot\lambda/2$.

D I R E C T I V E R A D I A T I O N P A T T E R N F R E Q U E N C Y 567 M H Z

TWO-DIMENSIONAL ANTENNA-BODY SYSTEM

ROT.ANGLE PHI : 0 ABOVE,180 BELOW

TESTBODY: INFINITE ROT.SYM.CYLINDER
DIAMETER: .25 M

NUMBER OF MODI: 25
POLARIZATION: VERTICAL/VERTICAL

DAT(I) M	GAI(I) DB	PHI DEG
1.00	-.48	0
.95	1.67	0
.90	1.93	0
.85	.14	0
.80	-2.73	0
.75	-1.46	0
.70	1.43	0
.65	2.38	0
.60	1.06	0
.55	-2.45	0
.50	-2.85	0
.45	1.02	0
.40	2.84	0
.35	2.15	0
.30	-1.57	0
.25	-5.30	0
.20	.45	0
.15	3.68	0
.10	3.92	0
.05	.48	0
0.00		
.05	-21.04	180
.10	-16.06	180
.15	-13.44	180
.20	-11.74	180
.25	-10.52	180
.30	-9.60	180
.35	-8.87	180
.40	-8.27	180
.45	-7.78	180
.50	-7.35	180
.55	-6.99	180
.60	-6.67	180
.65	-6.39	180
.70	-6.14	180
.75	-5.91	180
.80	-5.71	180
.85	-5.52	180
.90	-5.35	180
.95	-5.20	180
1.00	-5.06	180

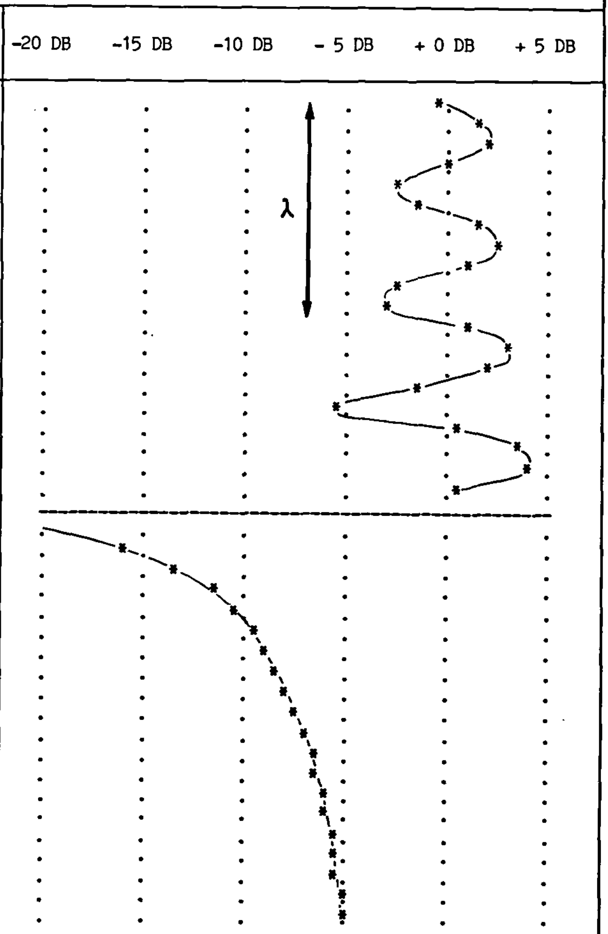

FIGURE 39 Directive radiation pattern at 567 MHz (result of program PANA).
Above: $Gain_B$ versus d_{at} at $\phi = 0°$, below: $Gain_B$ versus d_{at} at $\phi = 180°$.

In FIGURE 40 and 41 the same IZYL is shown at a frequency of 150 MHz. This frequency is just below the application range of this two-dimensional computational model. The data obtained with this model should be compared with the data from the three-dimensional model in section 10.4..FIGURE 40 shows the azimuthal- and FIGURE 41 the directive radiation pattern:

A Z I M U T H A L R A D I A T I O N P A T T E R N F R E Q U E N C Y 150 M H Z

TWO-DIMENSIONAL ANTENNA-BODY SYSTEM

TESTBODY: INFINITE ROT.SYM.CYLINDER — NUMBER OF MODI: 12
DIAMETER: .25 M — POLARIZATION: VERTICAL/VERTICAL
DAT(I) : ANTENNA-BODY DISTANCE IN METERS
GAI(I) : GAIN, FIELD STRENGTH AT THE ANTENNA A1 IN DB, 0 DB = FREE SPACE
PHI : HORIZONTAL ROTATION ANGLE IN DEGREES

	DAT(1) .050	DAT(2) .100	DAT(3) .150	DAT(4) .200	DAT(5) .250	
PHI	GAI(1)	GAI(2)	GAI(3)	GAI(4)	GAI(5)	-20 DB -10 DB + 0 DB +10 DB
0	-8.2	-3.3	-.8	.8	1.9	. . 1 2 3.45 .
5	-8.2	-3.3	-.8	.8	1.9	. . 1 2 3.45 .
10	-8.3	-3.4	-.8	.8	1.8	. . 1 2 3.45 .
15	-8.3	-3.4	-.9	.7	1.8	. . 1 2 3.45 .
20	-8.4	-3.5	-1.0	.6	1.7	. . 1 2 3.45 .
25	-8.6	-3.7	-1.1	.5	1.6	. .1 2 3.45 .
30	-8.7	-3.8	-1.2	.4	1.5	. .1 2 34 5 .
35	-8.9	-4.0	-1.4	.2	1.4	. .1 2 345 .
40	-9.1	-4.2	-1.6	.0	1.2	. .1 2 3 45 .
45	-9.4	-4.5	-1.9	-.2	1.0	. .1 2 3 45 .
50	-9.7	-4.7	-2.1	-.4	.8	. 1 2 3 45 .
55	-10.0	-5.0	-2.4	-.7	.5	. 1 2 34.5 .
60	-10.3	-5.4	-2.7	-1.0	.2	. 1 2 3 45 .
65	-10.7	-5.8	-3.1	-1.4	-.1	. 1. 2 3 45 .
70	-11.1	-6.2	-3.5	-1.7	-.5	. 1. 2 3 4 5 .
75	-11.6	-6.6	-3.9	-2.2	-.9	. 1 . 2 3 45. .
80	-12.1	-7.1	-4.4	-2.6	-1.3	. 1 . 2 34 5. .
85	-12.6	-7.6	-4.9	-3.1	-1.8	. 1 . 2 3 45 . .
90	-13.1	-8.2	-5.5	-3.7	-2.3	. 1 . 2 34 5 . .
95	-13.7	-8.7	-6.0	-4.2	-2.9	. 1 .2 3 45 . .
100	-14.3	-9.3	-6.6	-4.8	-3.5	. 1 .2 3 45 . .
105	-14.9	-10.0	-7.3	-5.5	-4.1	. 1 2 3 45 . .
110	-15.6	-10.6	-7.9	-6.2	-4.8	. 1 2. 3 45 . .
115	-16.2	-11.3	-8.6	-6.8	-5.5	. 1 2.3 45 . .
120	-16.8	-11.9	-9.3	-7.5	-6.2	. 1 2 .34 5 . .
125	-17.4	-12.5	-9.9	-8.2	-6.9	. 1 2 3 45 . .
130	-18.0	-13.1	-10.5	-8.8	-7.5	. 1 2 3.45 . .
135	-18.5	-13.6	-11.0	-9.4	-8.1	. 1 2 3.45 . .
140	-18.9	-14.0	-11.5	-9.8	-8.6	.1 2 345 . .
145	-19.1	-14.3	-11.8	-10.2	-9.0	.1 2 3 45 . .
150	-19.4	-14.6	-12.1	-10.4	-9.3	.1 2 3 45 . .
155	-19.5	-14.7	-12.2	-10.6	-9.5	.1 2 34.5 . .
160	-19.6	-14.8	-12.3	-10.7	-9.6	1 2 345 . .
165	-19.6	-14.8	-12.3	-10.7	-9.6	1 2 345 . .
170	-19.6	-14.8	-12.3	-10.7	-9.6	1 2 345 . .
175	-19.6	-14.8	-12.3	-10.7	-9.6	1 2 345 . .
180	-19.6	-14.8	-12.3	-10.7	-9.6	1 2 345 . .

FIGURE 40 Azimuthal radiation pattern at 150 MHz (result of program PANA). Left: Gain_B for 5 d_{at}'s and $\phi = 0 - 180°$, right: Gain_B versus ϕ for 5 d_{at}'s.

The azimuthal radiation pattern (FIGURE 40) shows a clear minimum of the gain (GAI(I)) at $\phi = 180^0$, decreasing with decreasing d_{at} (DAT(I)). The minimum gain amounts to -19.6 dB, compared with -21.9 dB at 567 MHz. FIGURE 41 shows at $\phi = 0^0$ a maximum gain at $d_{at} = \lambda/4$ (0.375 m). The shadow zone $\phi = 180^0$ is within 1.5 dB identical with those at 567 MHz.

D I R E C T I V E R A D I A T I O N P A T T E R N F R E Q U E N C Y 150 M H Z

TWO-DIMENSIONAL ANTENNA-BODY SYSTEM — ROT.ANGLE PHI : 0 ABOVE, 180 BELOW

TESTBODY: INFINITE ROT.SYM.CYLINDER — NUMBER OF MODI: 25
DIAMETER: .25 M — POLARIZATION: VERTICAL/VERTICAL

DAT(I) M	GAI(I) DB	PHI DEG
1.00	-3.07	0
.95	-3.42	0
.90	-3.17	0
.85	-2.41	0
.80	-1.38	0
.75	-.31	0
.70	.67	0
.65	1.52	0
.60	2.20	0
.55	2.71	0
.50	3.06	0
.45	3.23	0
.40	3.22	0
.35	3.02	0
.30	2.59	0
.25	1.89	0
.20	.83	0
.15	-.77	0
.10	-3.31	0
.05	-8.20	0
0.00		
.05	-19.59	180
.10	-14.80	180
.15	-12.32	180
.20	-10.74	180
.25	-9.61	180
.30	-8.75	180
.35	-8.08	180
.40	-7.53	180
.45	-7.07	180
.50	-6.68	180
.55	-6.34	180
.60	-6.05	180
.65	-5.79	180
.70	-5.56	180
.75	-5.36	180
.80	-5.17	180
.85	-5.00	180
.90	-4.84	180
.95	-4.70	180
1.00	-4.57	180

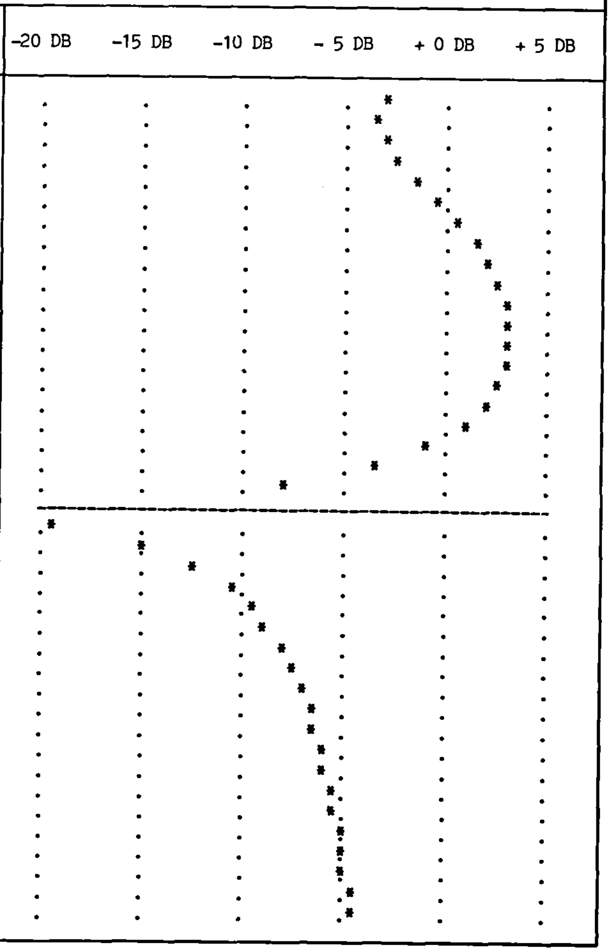

FIGURE 41 Directive radiation pattern at 150 MHz (result of program PANA).
Above: $Gain_B$ versus d_{at} at $\phi = 0^0$, below: $Gain_B$ versus d_{at} at $\phi = 180^0$.

7.3.2. MINIMUM GAIN DEPENDING ON FREQUENCY AND CYLINDER RADIUS

The minimum $Gain_B$ occurs at frequencies above 300 MHz not at $\phi = 180°$ but at about 165° as shown in FIGURE 42 (dashed lines: model not accurate). Small diameter changes are of little significance at all d_{at}'s (FIGURE 43).

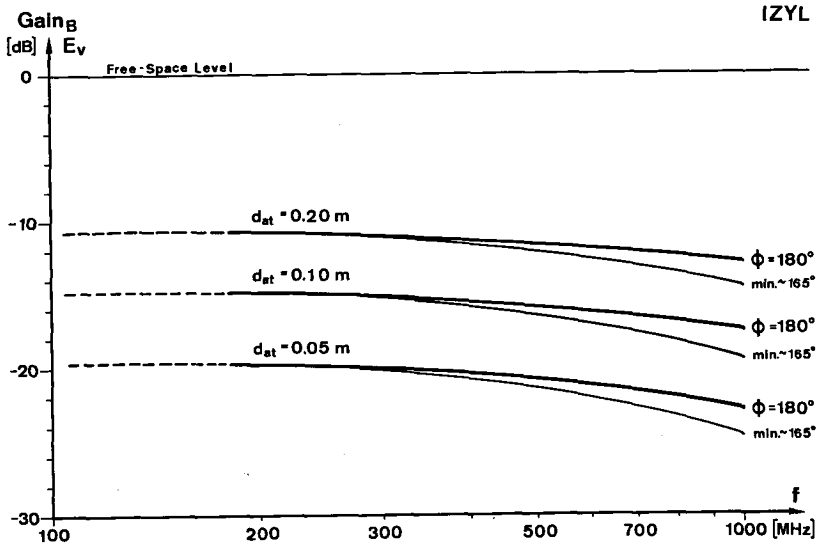

FIGURE 42 $Gain_B$ versus f in the shadow zone of the IZYL.

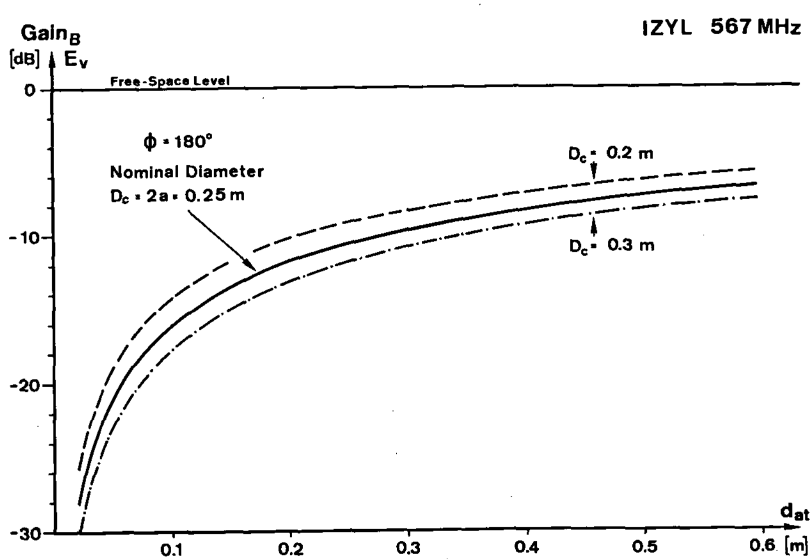

FIGURE 43 $Gain_B$ versus d_{at} for different cylinder diameters D_c ($\phi = 180°$).

8. MEASURING METHOD

8.1. PURPOSE OF THE EXPERIMENT

The experiments should answer the following questions:

Assumption verification : The computational models are based on assumptions which need to be verified. The main assumptions, as discussed in section 5.2., are reciprocity, quasi-perfect conductivity, and simplified body shape.

Off-resonance model verification : The two-dimensional computation of the radiation characteristics of the IZYL-antenna model (section 7.) delivers data for frequencies above 200 MHz. The experiment at frequencies above 200 MHz should deliver near-field data for large scale d_{at} and ϕ variation. If an acceptable correlation between experiment and computation exists, an extension of the theory on three dimensional computation of conducting bodies is reasonable.

Resonance phenomena : The analysis of the antenna-body system (section 5.2.3.) predicts resonance effects at about 40 to 200 MHz. The experiment should verify this prediction.

Practical body-mounted antennas : A practical body-mounted antenna is usually a monopole antenna mounted on a transmitting device. If the housing of the transmitter is small (e.g., maximum dimension about 0.25 m), the counterpoise for the monopole antenna is not ideal (too small) for frequencies below 300 MHz. Thus, the experiment should also deliver data for standardized transmitting devices operating in proximity to the body in the entire regarded frequency range.

8.2. DESCRIPTION OF THE ANTENNA-BODY TEST SET-UP

Real-size antenna-body experiments have to be performed outdoors and in proximity to the ground. The reasons for this decision and the problems dealing with ground reflections have been discussed in section 5.3..
The outdoor FR experiments are performed on a military airport (AMF Dübendorf). With respect to RF-emissions one has to act very cautiously. Not only the RF-power emitted at the measuring frequency has to be kept within permissible limits but also unwanted harmonic distortions have to be controlled. On the other hand there are at any frequency distortions from the outside. Our experiment requires a signal/noise (S/N) ratio of > 30 dB

since the effect to be studied are up to 25 dB below the maximum field strength level. Further, one is obliged to apply small radiation sources (electrically small antennas, limited counterpoise) with a generally limited efficiency. Thus, the accurate measuring frequency and the necessary RF-power cannot be determined in advance.

Quartz-stabilized RF-generators for all measuring frequencies are out of question. The manufacturing of miniaturized transmitters is too expensive (especially for frequencies above 200 MHz), the frequency is fixed and the power can only be controlled within small margins (see section 11.3.).

Free-oscillating RF-generators tend to be unstable with respect to power and frequency, need a careful tuning in order to avoid harmonic distortions and get detuned if the antenna environment is disturbed. Thus, such transmitting devices are not suited for our experiments.

In order to choose arbitrary antennas, frequencies and power levels, a dummy system (FIGURE 44) is used instead of an autonomic RF-generator. The monopole antenna A_1 and its counterpoise represent an idealized field point source (transmitting case) or a small field probe (receiving case). A_1 is connected by a long coaxial cable to a precision RF-generator or in the receiving case to a field strength meter.

Let us first consider A_1 as a transmitting antenna. Remote feeding causes severe problems concerning radiation from the feeding coaxial cable, if A_1 is a monopole with an electrically small ($< \lambda/2$ diameter) counterpoise. For the experiments A_1 has to be approached up to 0.05 m to the test body. As a consequence, the counterpoise in FIGURE 44, No. 2, represents the maximum acceptable size with a diameter of 70 mm and a length of 100 mm. If no precautions would be taken, the outer sleeve of the cable would become a part of the counterpoise at frequencies below 500 MHz. Radiating currents on the outer sleeve of the cable would make accurate field measurements impossible. Methods for attenuating such sleeve currents are described in ARRL [3], KRUPKA [53] and ROTHAMMEL [71]. Usually a $\lambda/4$ hollow cylinder is mounted around the coax, opened towards the antenna and contacted with the coax on the opposite cylinder side. Such a $\lambda/4$ RF choke is efficient if the diameter is about 3-times the coax diameter. A smaller RF-choke can be obtained if the feeding coax cable is shaped in a coil (FIGURE 44, No. 4) of an electrical length of $\lambda/4$. The design of such a helical RF-choke is similar to that of a helical antenna and will be discussed in 8.3.2.. Because the helical RF-choke radiates itself a certain amount of RF power, it is covered by an absorbing tube (FIGURE 44, No.5.). The remaining surface waves on the feeding coax are attenuated by covering the whole coax with absorber material in the proximity of the antenna A_1. Finally load variations for the coax and the generator are prevented by inserting a 20 dB attenuator (FIGURE 44, No.3) below the antenna's foot point.

The complete antenna test set-up is shown in FIGURE 44. It follows the specifications evaluated in section 5.3. and allows measurements of vertical polarized E-fields in the frequency range 10-1000 MHz. The dummy system discussed above has a shape of a circular cylinder of 70 mm diameter and is supported by an antenna holder (No.6.). Depending on the frequency the test antenna A_1 (No.1.) is a helical monopole as shown or a whip (see 8.3.1.). The revolving stage (No.7.) rotates the test-body together with the antenna A_1. A directive, broadband antenna (8.3.3.) A_2 (No.8.) completes the antenna test set-up.

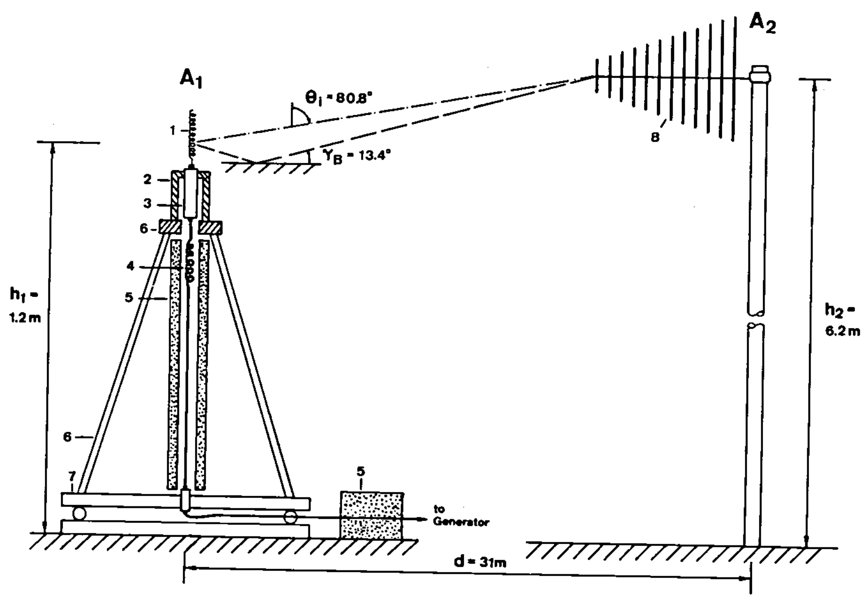

FIGURE 44 Measuring antenna test set-up

1: test (body-mounted) antenna A_1
2: electrical counterpoise for A_1
3: 20 dB attenuator in series
4: matched RF-choke
5: EM absorber material
6: wooden antenna holder
7: wooden revolving stage
8: remote antenna A_2

For the computational models the transmission distance d has been defined in section 5.1.2. as follows:

$$\left.\begin{array}{l}\text{Transmission distance d}\\ \text{for computational models}\end{array}\right\} : \begin{array}{l}\text{Horizontal distance between}\\ \text{the center of the body and } A_2\end{array} \qquad (240)$$

For the experiment it is better to keep the distance between A_1 and A_2 constant, thus we define the experimental transmission distance d:

$$\left.\begin{array}{l}\text{Transmission distance d}\\ \text{for experiments}\end{array}\right\} : \begin{array}{l}\text{Horizontal distance between}\\ \text{the centers of } A_1 \text{ and } A_2\end{array} \qquad (241)$$

Essentially there is no difference between (240) and (241), because d_{at} is small compared with d and because we are not interested in the absolute phase of the fields. However, the reference field strength E_0 is more constant when the antennas and the cables are not moved.

The experiments require rotation of the antenna-body system (ϕ = variable, d_{at} = parameter) and translation of the body in respect to the antenna A_1 (d_{at} = variable, ϕ = parameter). These two experiments are shown schematically in FIGURE 45:

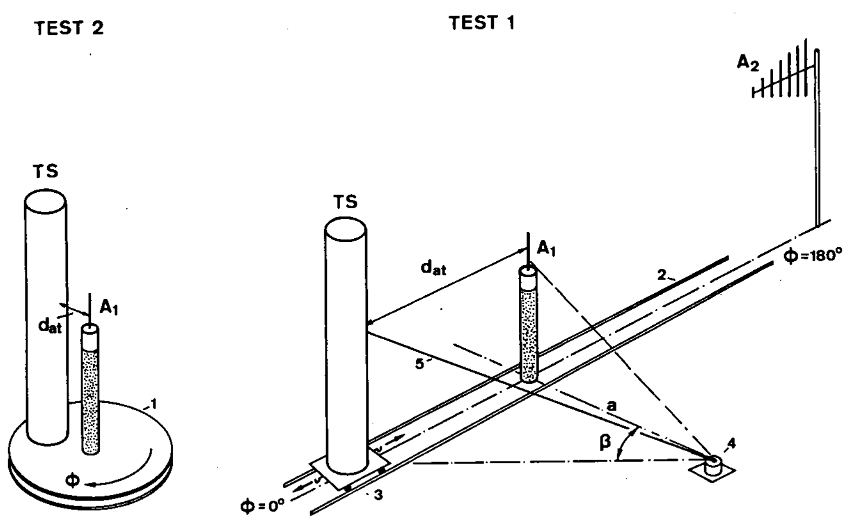

FIGURE 45 Rotation and translation of test bodies

1: wooden revolving stage
2: plastic trackway section
3: wagon
4: displacement transducer (rubber band goniometer)
5: rubber thread

8.3. ANTENNAS AND FEEDING

8.3.1. BODY-MOUNTED ANTENNA A_1

Theoretically the body-mounted antenna A_1 should fulfill the following requirements as defined in section 5.1.2. :

- The radiation intensity should be constant, but the efficiency is not of interest.
- The physical size of A_1 should be smaller than any relevant dimension of the test set-up.
- Only one dominant E-polarization axis p_1 should exist.
- The antenna should radiate omnidirectionally.
- The impedance and thus the radiation should not change due to body proximity.

In practice there are physical and technical limitations:

- The efficiency should be so high, that the radiation of A_1 is much higher (30 dB) than the leakage radiation of all involved equipment. Such an efficiency can only be obtained if A_1 is operated near resonance.
- An antenna length h of 0.15 m is acceptable for the purpose of the experiment. This antenna length corresponds to $\lambda/4$ at 500 MHz. Thus, efficient, resonant (no external tuning), electrically small antennas have to be used for all frequencies below 500 MHz.
- A strict linear polarization is difficult to obtain with resonant electrically small antennas. Any internal frequency tuning element leads to certain field irregularities.
- Omnidirectional radiation in a horizontal plane depends not only on the antenna but also on the feeding cable. A dipole antenna is not suited because the cable had to be mounted rectangular to the antenna axis. Thus, monopole antennas have to be used with a limited counterpoise.
- If an antenna has to be operated near resonance, the impedance depends on body proximity, because the bandwidth of any electrically small antenna is narrow (see section 4.5.).

The normal mode helical monopole (16.1.) offers a good compromise for antenna lengths $h > \lambda/20$. The polarization is elliptical, with a dominant vertical E-component which is larger than that of an equal-sized whip.

Ant. Type No.	Resonant Frequency f_{res}[MHz]	Approx.-3 dB Bandwidth min/max[MHz]	Antenna length h [mm]	Antenna diameter D_h [mm]	Number of turns N_h	Wire diam. d_w[mm]
AT1 hel.	120 ± 3	110 - 125	185	11.5	42	1.5
AT2 hel.	180 ± 3	170 - 185	155	12.0	26	2.0
AT3 hel.	210 ± 2	190 - 215	145	12.0	24	2.0
AT4 hel.	298 ± 2	260 - 310	145	12.0	13	2.0
AT5 hel.	363 ± 4	335 - 403	130	12.0	8	2.0
AT6 whip	490 ± 5	450 - 560	150	-	-	1.5
AT7 whip	630 ± 5	605 - 700	110	-	-	2.0
AT8 whip	1060 ± 8	960 -1150	75	-	-	1.0

TABLE 46 Monopole antennas A_1 for field experiments. The resonant frequency f_{res} and the bandwidth have been measured with a network analyser, when A_1 was mounted on the counterpoise, with RF-choke, but without attenuator, and in an anechotic chamber.

The specifications of the experimental antennas A_1 are shown in TABLE 46. It should be mentioned that these data may vary from the theoretical data in section 16.1., because the antennas A_1 are operated on the later used limited counterpoise.

8.3.2. RF-CHOKES

The purpose of the RF-chokes is to attenuate surface currents on the feeding coaxial cable. They are constructed from an RG-58 coaxial cable, wrapped in a helical shape. The specifications are shown in TABLE 47:

RF Choke No	Operating Range f_c [MHz]	Choke length l_c[mm]	Choke diameter d_c [mm]	Cable length l_f[mm]	Number of turns n_c	Cable diam. d_f [mm]
CH1	50 - 150	100	20	1000	14	6
CH2	100 - 200	70	16	700	12	6
CH3	150 - 200	50	16	500	8.5	6
CH4	200 - 250	37	16	330	6	6
CH5	250 - 350	22	16	220	4	6
CH6	350 - 500	13	16	130	3	6

TABLE 47 RF-chokes for field experiments. f_c theoretical values.

The effectiveness of the coax-line RF-chokes in TABLE 47 decreases at higher frequencies because of the distributed capacitance among the turns. Since they have to be mounted in absorbing tubes (attenuation of the choke radiation), the Q-factor is not very high, resulting in a favourable broad band range, but with further decreases effectiveness. There is a simple method to test RF-chokes: when the complete antenna test set-up according to FIGURE 44 is assembled for the selected test frequency, the received field strength should not change more than 2 dB if the coaxial feeding cable is touched by hand at any location along the cable.

8.3.3. REMOTE ANTENNA A_2

Because the helical antennas A_1 are elliptically polarized and we have to measure only the vertical polarized E-field component, the remote antenna A_2 has to be strictly linear polarized. In addition A_2 should be a directive antenna with broadband characteristics. It was found that a logarithmic periodic antenna (LPD) fulfills these requirements best. The chosen Cross LPD (R. GRANER, AMF) operates from 100 to 1000 MHz with a directive gain of about 6 dB (aperture angle $\pm 60^o$). By simple line-switching the vertical polarization and the horizontal polarization can be measured independently, which is needed to check the radiation properties of A_1 before the actual experiment can be started.

8.4. MEASURING EQUIPMENT

8.4.1. REVOLVING STAGE FOR ANTENNA-BODY ROTATION

In cooperation with R. GRANER from the AMF a revolving stage and an electronic plotter control unit has been developed. It consists of

- revolving stage with basement, stage, engine and angle sensors (see FIGURE 48, shown with inverted separate stage).
- angle data transmitter, combined with remote control of the stage rotator and with an intercom system
- plotter control unit with angle display, synchronizer and x-y driver (see FIGURE 49).

This equipment allows the automatic plotting of azimuthal gain charts when combined with the RF-equipment and the power supply for the stage engine. The control unit synchronizes on the zero marker (FIGURE 48) and plots one full 0-360^o E/ϕ sequence with 1^o resolution on an ordinary x-y recorder in a rectangular diagram as recommended by CEI Publication 138.

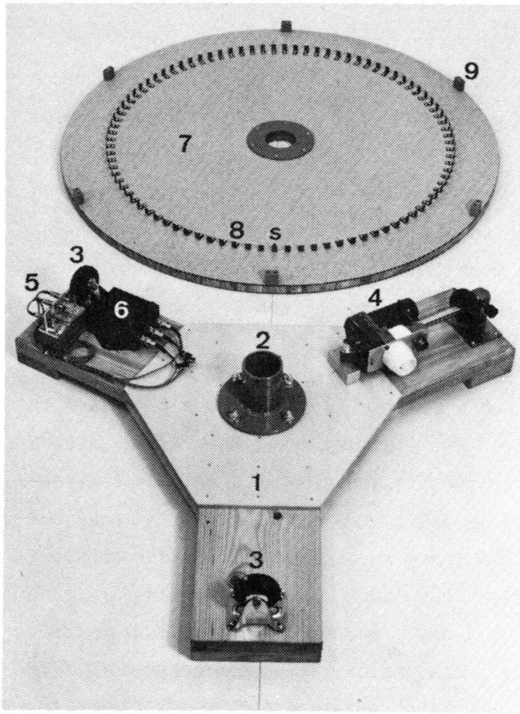

FIGURE 48 Revolving stage

1 : basement

2 : hollow axle (for antenna coaxial cable with rotational N-connector)

3 : supporting wheels

4 : engine with driving wheel (24 V DC)

5 : angle sensors with sensor protection bolts

6 : line driver and intercom station

7 : stage platform (upside down)

8 : angle markers (s: synchronization marker)

9 : angle marker protection

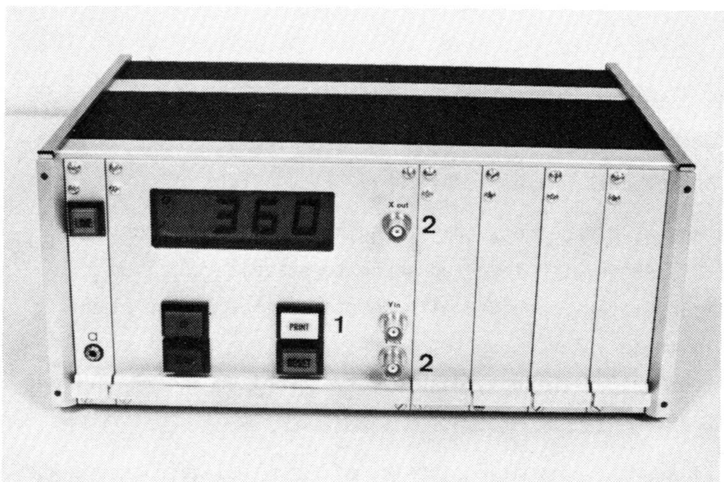

FIGURE 49 Plotter control unit

1 : command switch : next revolution = plot diagram

2 : x-y driver output

8.4.2. TRACKWAY FOR ANTENNA-BODY TRANSLATION

According to FIGURE 45 a trackway was constructed in order to move the heavy test subject (phantom weight 90 kg !) continuously toward the stationary antenna A_1. A wooden basement of 5 meter length equipped with plastic rails was mounted on the ϕ-coordinates 0-180° and later 90-270°. A small, ball-bearing equipped wagon carried the test subjects, with the footpoint spaced $s = 0.2$ m appart from the ground. By help of deflection pullies, mounted each 10 meters away from A_1 on the trackway axis, and long plastic strings the wagon could be precisely moved manually.

The monitoring of d_{at}, which is the distance from the center of A_1 and the nearest surface of the test body, is not easy. First,this distance has to be actually measured and not e.g., the position of the wagon, because of practical accuracy considerations. Second, the space between A_1 and TS should not be disturbed by measuring devices, because any metallic or dielectric material causes field disturbances. Third, an accuracy of ± 10 mm is required at least in the low d_{at} regions.

The rubber band goniometry, developed by NEUKOMM [65] for the biomechanical research, solves this difficult problem with little effort. A low torque conductive plastic potentiometer is mounted rectangularly to the trackway axis in the distance $a = 2$ m from the vertical A_1 axis. (FIGURE 45, No. 4.). At the vertical axis of the potentiometer a beryllium bronze arm of 0.1 mm thickness and 100 mm length is attached. The arm can be bent up and down without angular changes or significant forces on the axle. From this arm a thin rubber thread ($\varnothing < 0.3$ mm) is stretched (about 1 N tensil force) to the test point on the TS and fixed with self-adhesive tape (see FIGURE 45, No. 5.). The linear motion d_{at} is thus transformed into an angular motion β according to

$$\beta = \mathrm{arctg}(d_{at}/a) \qquad (242)$$

There is a non-linear, but one-to-one correspondence between β and d_{at}. In a linear β presentation the interesting range $0 < d_{at} < 0.35$ m corresponds to $0 < \beta < 10°$ but contains also the large range $0.35 < d_{at} < 2.38$ m corresponding to $10 < \beta < 50°$. The accuracy in the low d_{at} range is better than 10 mm, because the hysteresis of the rubber band goniometer is less than 0.3°, the resolution is quasi-infinite (better than 0.01°). The non-linearity of the potentiometer of 0.5 % F.S. would cause moderate errors in (242), thus the β-scale is calibrated directly in the actual d_{at}-scale.

The mechanical β signal is converted by the potentiometer into a proportional electrical tension, and with the built-in impedance converter the signal is transmitted over a long shielded cable to the x-imput of the plotter. If the field strength signal is on the y-imput of the plotter, one obtains a calibrated E/d_{at} plot with $0 < d_{at} < 2.3$ m for $\phi = 0^{o}$ and $\phi = 180^{o}$. Of course, the switching from $\phi = 0^{o}$ to $\phi = 180^{o}$ requires a tip down of the A_1 antenna tower and to connect the rubber thread on the reverse side of the test body when it has been rolled over with the wagon. The d_{at}-scale has to be calibrated once by means of markers on the middle line of the trackway.

8.4.3. FIELD MEASURING EQUIPMENT

Besides the mentioned antennas and ϕ/d_{at} recording devices the following materials have been applied in the experiments:

- Field-strength measuring unit: main unit RHODE + SCHWARZ VHF-UHF ESUM BN 15076/5/P with the plug-in units 25-230 MHz, 160-470 MHz, and 850-1300 MHz. The effective accuracy (as tested) is $\pm$ 0.5 dB in the +5 to -20 dB range and $\pm$ 2 dB in the -20 to -35 dB range. (0 dB = 80 % full scale of the recorder output, operating on the self calibrated "linear" range of the ESUM)
- RF-Generator : HEWLETT PACKARD 8640B, 25-1000 MHz. The stability of the amplitude is specified to $\pm$0.1 dB and could be checked by a free space recording before and after an experiment at a specific frequency (over-all test revealed a stability of $\pm$ 0.5 dB at frequencies above 200 MHz, depending mostly on the antenna A_1)
- X-Y-Recorder: BRYANS 26000 A3. The accuracy is specified to $\pm$ 1mm which could be affirmed by a test,
- Absorber material: blocks of 0.3 x 0.3 x 1 m. Standard absorbers of the PTT antennna development division, efficient above about 100 MHz. Has been used to attenuate sleeve currents on the feeding coaxial cable (see FIGURES 44 and 53).
- Coaxial cables: double shielded coax of 9 mm diameter with N-connectors. Standard materials of the AMF antenna development division. At frequencies below 30 MHz the RF-radiation leakage cannot be neglected if inefficient antennas and cable lengths in excess of 40 m are used.

8.5. ANTENNA SET-UP TESTING AND EXPERIMENTAL PROCEDURE

Field measurements with non-resonant antennas in proximity to the ground require careful preliminary tests in order to exclude artifacts. With a human test subject TEST 1 (FIGURE 45, ϕ= 0.90,180,270°, d_{at} = 0 to 4 m) and TEST 2 (FIGURE 45, d_{at} = 0.035,0.077,0.135 m) have been performed at the frequencies 25,50,75,100,150,200,300,400,600,700,800 and 900 MHz. In October 1976 a further experiment with the three test bodies SUB, PHA and MET (see specifications in section 5.4.1) was performed according TEST 1 (FIGURE 45, ϕ = 0 and 180°, d_{at} = 0.035 to 2 m) at 11 frequencies from 74 to 897 MHz. TABLE 50 shows the preliminary test preparations, TABLE 51 the antenna parameter and TABLE 52 the experiment check list.

1. LABORATORY PREPARATIONS
1.1. Computation and construction of antennas A_1 1.2. Network analysis in anechoic chamber (TABLE 46) 1.3. Construction and testing of RF-chokes (TABLE 47) 1.4. Construction of rubber band goniometer with lawn anchor 1.5. Goniometer test with 100 m cable and strong RF disturbances
2. MEASURING SET-UP PREPARATIONS
2.1. Warming-up of RF equipment and recorder, initial calibration 2.2. Trackway mounting with levelling rod under 100 kg load 2.3. Goniometer mounting with levelling rod. (In this test series is a=1m, corresponding to d_{at} : 2 m $\hat{=}$ β : 63.43°) 2.4. Calibration of the d_{at} scale with reference markers on trackway 2.5. Verification of the d_{at} accuracy when rubber thread is attached on phantom at h_1 = 1.2 m.
3. TRANSMISSION TEST (for each measuring frequency)
3.1. Search for a free RF-channel 3.2. Evaluation of antenna A_1 and RF choke, sleeve current tests. 3.3. Checking if no obstacles are around within a radius of 50 m. 3.4. Polarization and reciprocity test: Transmitter out on A_1, polarization A_2 = vertical , reading: Receiver input on A_1, polarization A_2 = vertical , reading: Receiver input on A_1, polarization A_2 = horizontal , reading: Transmitter out on A_1, polarization A_2 = horizontal , reading: 3.5. RF-leakage test: A_1 replaced by a 50 Ω terminator Transm. out on A_1 cable, polar. A_2 = vertical , reading: Receiv. in on " " " " = vertical , reading: Receiv. in on " " " " = horizontal , reading: Transm. out on A_1 cable, polar. A_2 = horizontal , reading:

TABLE 50 Preliminary test preparations and checks

The accuracy of the data obtained in the following antenna-body experiments depends directly on the results of the transmission test 3.4. and 3.5. in TABLE 50. The field strength at vertical polarization should be at least 15 dB higher than the field strength at horizontal polarization, and should be at least 20 dB higher than the noise or the residual signal picked-up when A_1 (transmitting and receiving case) is replaced by a 50 Ω terminator. The reciprocity test reveals RF-leakage in the control center, theoretically the transmission in both directions should give the same reading. These important antenna parameters are listed in TABLE 51 :

Freq [MHz]	A_1 No.	RF choke No.	A_1 = transmitting antenna				A_1 = receiving antenna			
			A_2 : verti.		A_2 : horiz.		A_2 : verti.		A_2 : horiz.	
			ANT [dB]	TERM [dB]	ANT [dB]	TERM [dB]	ANT [dB]	TERM [dB]	ANT [dB]	TERM [dB]
74	AT1	2x CH1	25	3	13	0	17	25	18	20
101	AT1	3x CH1	25	10	0	0	26	15	0	0
125	AT1	2x CH1	25	0	6	0	25	0	6	0
158	AT2	CH1	25	0	4	0	26	0	3	2
205	AT3	CH2	25	2	9	0	25	7	9	0
250	AT4	CH3	25	0	2	0	25	0	3	0
300	AT4	CH3	25	3	5	0	24	7	5	0
400	AT5	CH4	25	0	0	0	25	0	0	0
562	AT6	CH5	25	3	11	0	24	0	7	0
700	AT7	CH6	25	0	0	0	25	0	5	0
897	AT8	CH6	25	0	2	0	25	0	0	0

TABLE 51 Antenna parameter of the test set-up used in the later antenna-body experiments. ANT: specified antenna A_1 connected to generator or receiver, TERM: A_1 replaced by a 50 Ω terminator. Frequency 74 allows no accurate measurements (but qualitative measurements for A_1 = transmitting antenna), 101 MHz is at the border line of the applicability.

If we compare TABLE 51 with TABLE 46, one can predict that the frequency

300 MHz may cause difficulties, because AT4 resonates at 298 MHz. A change in the proximity of the antenna (body) will effect an important change of the antenna impedance. The specifications at 74 MHz are not satisfactory not only due to AT1, but also due to the lower frequency limit of 100 MHz of the remote antenna A_2.

The check list for the actual antenna-body experiment (TEST 1 in FIGURE 45) is shown in the next TABLE 52 :

4. ANTENNA-BODY EXPERIMENT CHECK LIST (for each measuring frequency)
4.1. Final calibration of RF-equipment and recorder 4.2. Repetition of points 3.4. and 3.5. according TABLE 50 4.3. Zero calibration of the goniometer 4.4. Calibration of the FSL (free-space level) on + 15 dB for A_1 = transmitting antenna and A_2 = vertical polarization 4.5. Experiments with the test bodies MET, PHA and SUB in the d_{at}-interval 0.035 up to 2 m: (A_2 = always vertical polarization) 4.5.1.1. MET, $\phi = 0^\circ$, A_1 = transmitting antenna 2. A_1 = receiving antenna 4.5.2.1. PHA, $\phi = 0^\circ$, A_1 = transmitting antenna 2. A_1 = receiving antenna 4.5.3.1. PHA, $\phi=180^\circ$, A_1 = receiving antenna 2. A_1 = transmitting antenna 4.5.4.1. MET, $\phi=180^\circ$, A_1 = transmitting antenna 2. A_1 = receiving antenna 4.5.5.1. SUB, $\phi=180^\circ$, A_1 = receiving antenna 2. A_1 = transmitting antenna 4.5.6.1. SUB, $\phi= 0^\circ$, A_1 = transmitting antenna 2. A_1 = receiving antenna 4.6. When all test bodies are dislocated, reading of the FSL for A_1 = transmitting antenna. 4.7. Reading of the goniometer at $d_{at} = 0$.

TABLE 52 Antenna-body experiment check list (shortened)

The procedure for TEST 2 (FIGURE 45) is similar to TABLE 50, 51, and 52. In FIGURE 53 a picture is shown of such a TEST 2. The measured results are discussed in the next section together with the theoretical predictions. The sketch in FIGURE 54 is not only a joke : the directive gain from the bodies of three men amounts to about 4 to 6 dB as measured with a MOTOROLA HT 220 walkie-talkie with a 4 inch helix at 174 MHz.

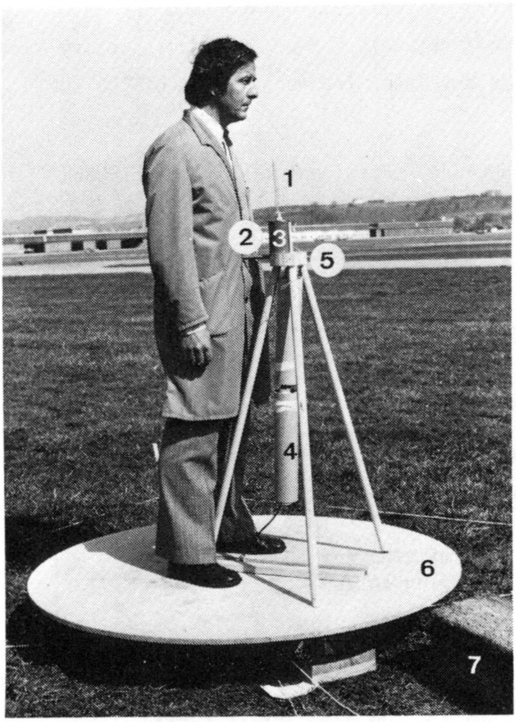

FIGURE 53
Test set-up for azimuthal radiation experiments

1: test antenna A_1
2: spacer (d_{at} = parameter)
3: electrical counterpoise with attenuator
4: absorber tubes (RF-choke within the tubes)
5: wooden antenna holder
6: wooden revolving stage
7: absorber blocks on feeding coaxial cable

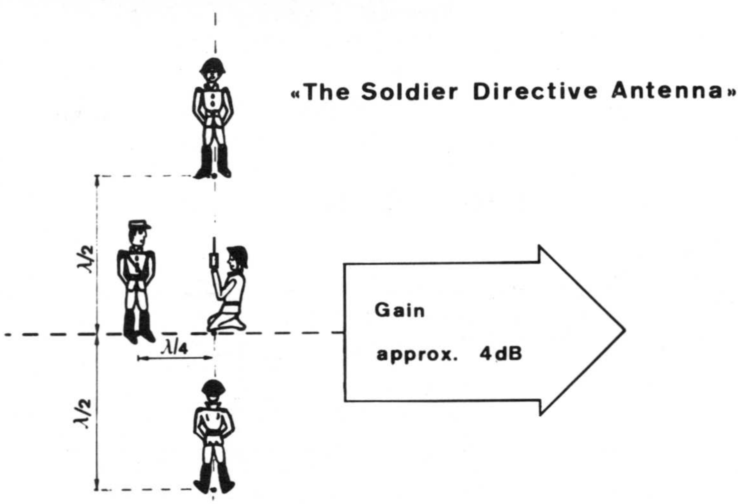

FIGURE 54 "The soldier directive antenna". An application of the $Gain_B$ obtained at $d_{at} = \lambda/4$ at $\phi = 0^o$ and $d_{at} = \lambda/2$ at $\phi = 90$ and 270^o.

9. Comparison of Experimental Data with Theoretical Data

9.1. Investigated Parameters

9.1.1. Effect of Frequency and Body Material

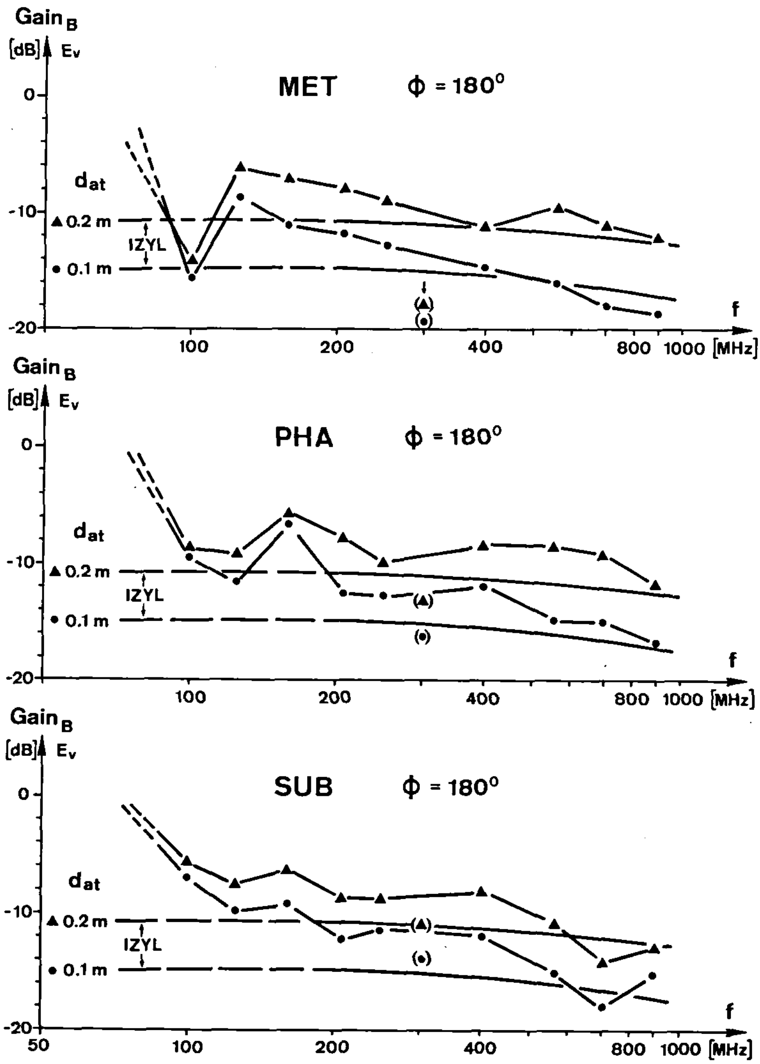

FIGURE 55 $Gain_B$ versus f in the shadow zone from the three test bodies MET, PHA, SUB (measured data) compared with the computed data from IZYL. Parameter: $d_{at} = 0.1$ and $0.2\,m$. E_V: E-field strength, vertical polarization.

FIGURE 55 is a comparison between the experimental data for the three test bodies MET, PHA, SUB and the computational data for the IZYL (see definition of the bodies in 5.4.1.). Shown are the data for the constant parameter d_{at} = 0.1 m and 0.2 m in the shadow zone $\phi = 180^{0}$, obtained from the $Gain_B/d_{at}$ experiment in FIGURES 56,57 and 58.

The experiment, performed according to the check lists in 8.5., includes the experimental frequencies (74), 101, 125, 158, 205, 250, (300), 400, 562, 700 and 897 MHz. The results at (74) and (300) MHz are not accurate enough for a quantitative consideration, the reasons are mentioned below TABLE 51 and in section 9.2..

The computational data for the infinite cylinder (IZYL) are valid only for frequencies above 200 MHz for finite bodies of more than 1.8 m length, as explained in section 7.1.. The most interesting result is the parallelism of the $Gain_B$ curves for d_{at} = 0.1 m and 0.2 m. The difference is almost constant versus the frequency and amounts to 4 ± 0.5 dB.

The experimental data reveal a similar tendency. For all test bodies the gain difference between d_{at} = 0.1m and d_{at} = 0.2m amounts to 4 ± 3 dB and often to 4 ± 1 dB. Thus, one may assume for a first approach that the measuring accuracy is better than ± 3 dB.

The experimental data oscillate around the computed data, at frequencies below 200 MHz with a considerable amplitude and above 200 MHz with a much smaller amplitude. The experimental data reveal clearly four regions:

- $\lambda/2$ resonance at 74 to 101 MHz (exp. data of insufficient accuracy)
- $3\,\lambda/4$ anti-resonance at about 101 to 125 MHz
- λ second resonance at about 125 to 158 MHz
- $> \lambda$ off-resonance at frequencies above 200 MHz.

The MET and PHA have the same length of 1.8 m, the SUB is only 1.68 m long. It seems that the body material does not influence the resonant frequencies much, and that the anti-resonance is especially weaker in lossy materials.

Above 200 MHz the difference between experiment and theory is less than ± 3 dB for all three test bodies. Taking into account that field measurements in the shadow zone are very difficult due to the large field gradients, the correlation is encouraging.

9.1.2. EFFECT OF ANTENNA-BODY DISTANCE AND BODY MATERIAL

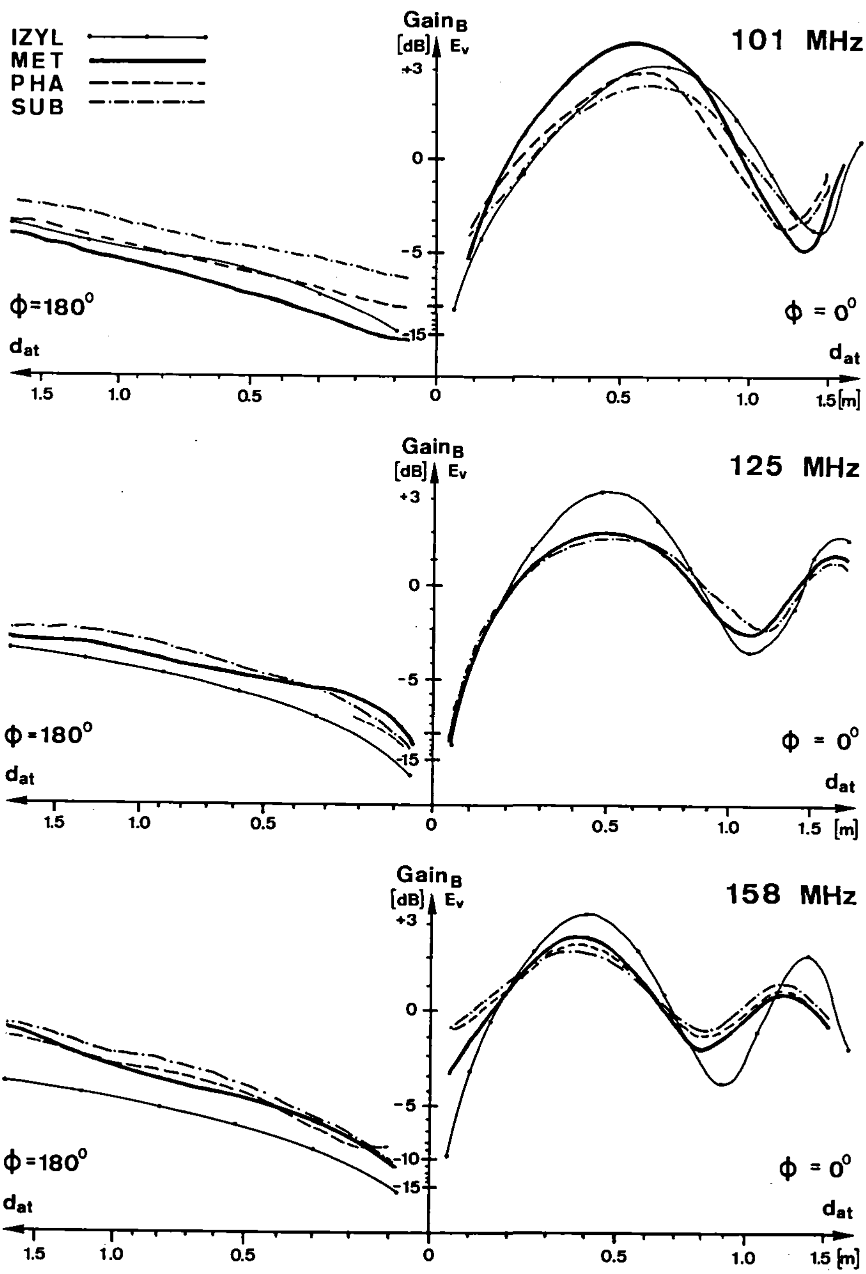

FIGURE 56 Gain$_B$ versus d_{at} at ϕ = 0 and 180° from the three test bodies MET, PHA. SUB (measured data) compared with the computed data from IZYL.

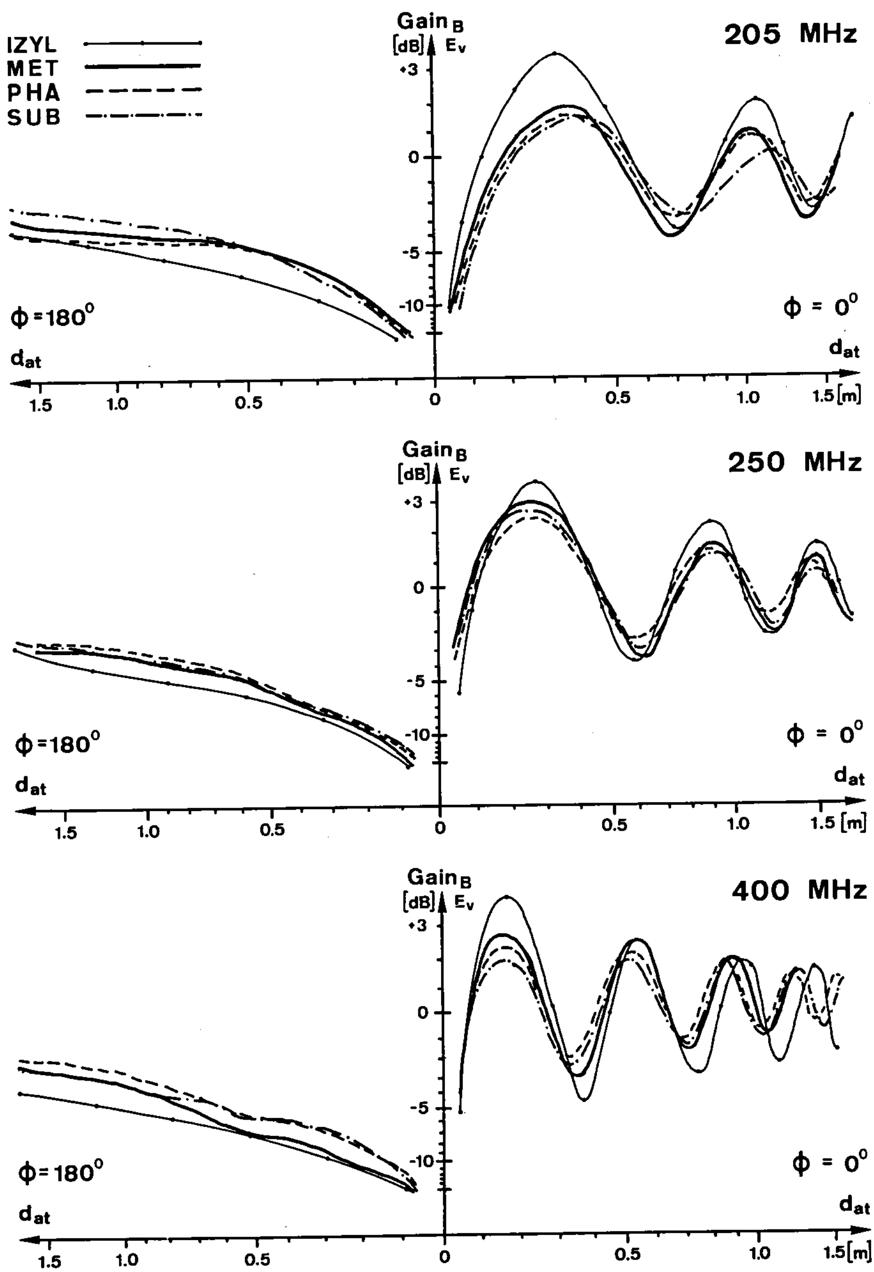

FIGURE 57 Gain$_B$ versus d_{at} at ϕ = 0 and 180° from the three test bodies MET, PHA, SUB (measured data) compared with the computational data from IZYL (continuation of FIGURE 56).

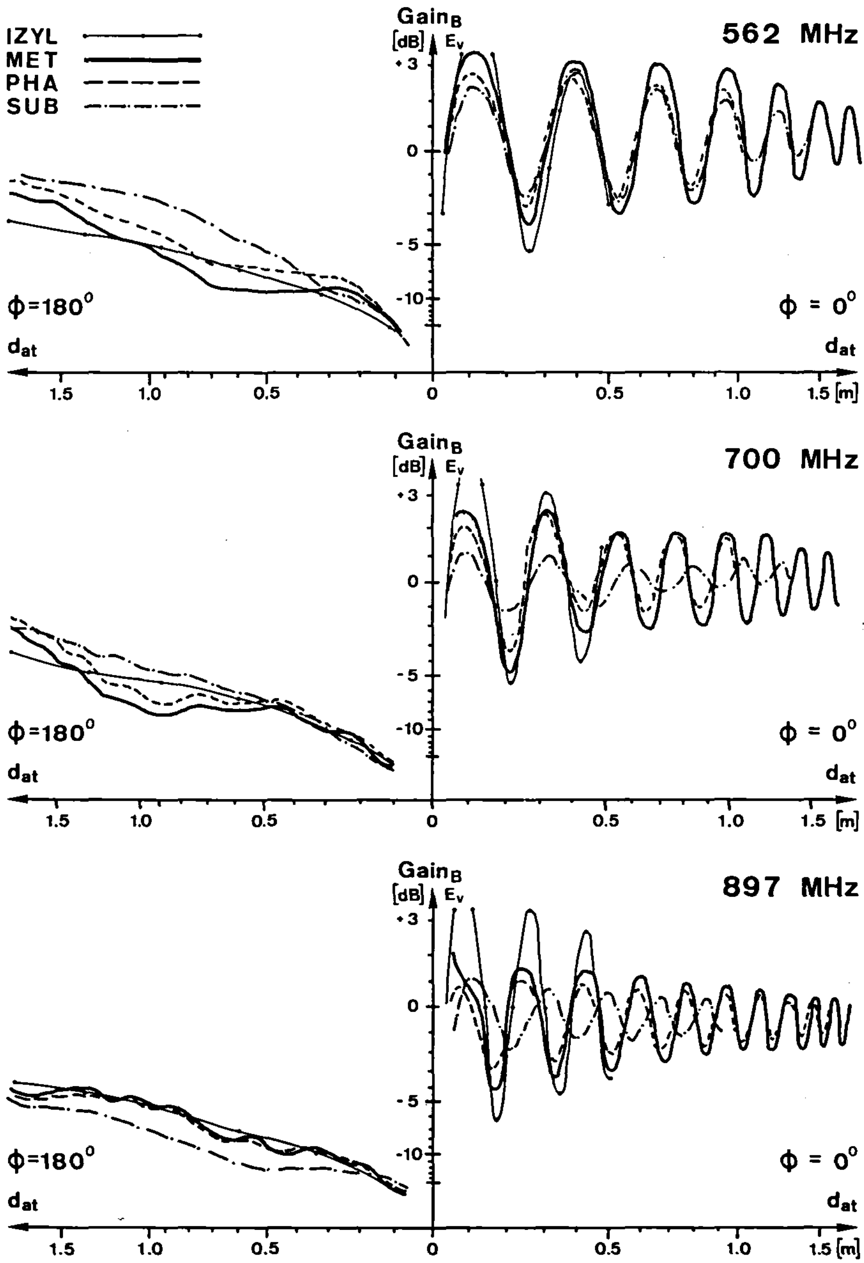

FIGURE 58 $Gain_B$ versus d_{at} at ϕ = 0 and 180° from the three test bodies MET, PHA, SUB (measured data) compared with the computational data from IZYL (continuation of FIGURES 56 and 57).

FIGURES 56,57 and 58 are comparisons between the experimental data for the three test bodies MET,PHA,SUB and the computational data for the IZYL.

The experiments include the experimental frequencies 101, 125, 158, 205, 250, 400, 562, 700 and 897 MHz and were performed according to the check lists in section 8.5..

The computational data for the infinite cylinder (IZYL) are valid only for frequencies above 200 MHz, as explained in section 7.1.. The $Gain_B$ decreases with decreasing d_{at} in the shadow zone $\phi = 180^o$ and oscillates around the FSL in the irradiated zone $\phi = 0^o$, with maxima at $d_{at} \sim n\lambda/4$, $n = 1,3,5,....$ and minima at $d_{at} \sim n\lambda/2$, $n = 0,1,2,....$

The experimental data agree qualitatively with the theoretical data for all frequencies and antenna-body distances. The quantitative agreement depends on the frequency range:

- Resonance region below 200 MHz. At $\phi = 0^o$ the differences are smaller than 2 dB, except for 158 MHz at d_{at} below 0.1 m. At $\phi = 180^o$ the differences amount up to about 5 dB at d_{at} above 0.2 m. Generally, $Gain_B$ decreases from SUB to PHA to MET. The somewhat larger differences at very small d_{at}'s seem to be caused by near-field effects.
- Off-resonance region between 200 and 400 MHz. There is an excellent agreement between experiment and theory. Generally, the accuracy is better than 3 dB for all d_{at}'s and ϕ's. There are no significant differences between the three test bodies.
- High frequencies above 400 MHz. It should be mentioned that the test antenna A_1 has a length of $\sim \lambda/4$ in this frequency region, so that A_1 cannot be regarded as an actual point source. However, the difference amounts to less than 4 dB. The data for MET and PHA are very similar but differ from SUB, leading to the hypothesis that the shape of the body becomes more important than the body material.

The $Gain_B$ versus d_{at} diagrams demonstrate clearly a formerly unknown, systematical relation between these two quantities.

Analogous experiments at $\phi = 90^o$ and 270^o revealed similar results as shown at $\phi = 0^o$, with maxima at $d_{at} \cong n\lambda/2$, $n = 1,3,..$as predicted. An application of these maxima at 0, 90 and 270^o is shown in FIGURE 54. Similar effects occur also, if a person approaches a mobile receiver (FM, 80 - 120 MHz) when tuned to a weak radio station (Try it with your radio !).

9.1.3. EFFECT OF THE AZIMUTHAL ANGLE

If one speaks of the influence of the human body on the radiation pattern of body-mounted antennas, one means generally the azimuthal radiation pattern. Such experiments were performed by many authors, e.g., BUCHANAN, MOORE and RICHTER [12], KING and WU [50], etc.. Generally, the published results differed greatly, offering hypotheses about directive properties of the human body and impedance changes.

After the discovery of the dominant d_{at} effect, the azimuthal radiation pattern is well explainable in the off-resonance region. FIGURE 59 shows a typical azimuthal radiation pattern recording for d_{at}=0.035, 0.077 and 0.135 m compared with the computed results at d_{at}=0.050 and 0.150 m :

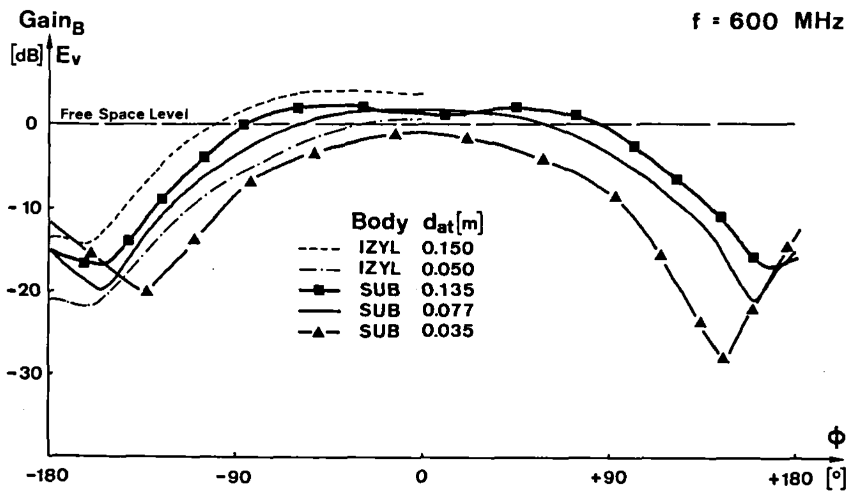

FIGURE 59 Azimuthal radiation pattern at 600 MHz. Gain$_B$ versus ϕ for the human test subject SUB compared with the computational data from IZYL.

The experimental data SUB, d_{at} = 0.077 and 0.135 m are in between the computational data from IZYL, d_{at} = 0.05 and 0.15 m. Thus, the agreement between experiment and computation is better than 3 dB for d_{at} above 0.05 m. The antenna-body system is an efficient directive antenna with a front-to-back ratio of up to 20 dB and a gain up to 2-3 dB. The main- and side-lobes are completely controlled by d_{at} for a given ϕ (FIGURES 59, 38 and the other computer results in Appendix 16.2.1.). The experimental difference in gain and ϕ, and the asymmetric shape of the curve at d_{at} = 0.035 m may be caused by the asymmetry of the SUB and by an inclination of A_1.

A summary of the results obtained by TEST 2 (see FIGURE 45) is shown in TABLE 60. Listed are the minimum $Gain_B$ measured with the human test subject SUB at d_{at} = 0.035, 0.077 and 0.135 m and the minimum $Gain_B$ computed from IZYL :

MINIMUM GAIN AT VERTICAL POLARIZATION IN SHADOW ZONE FOR SUB AND IZYL														
Frequency	[MHz]	25	50	75	100	150	200	300	400	500	600	700	800	900
SUB, $Gain_B$ d_{at} = 0.035 m	[dB]	0	-8	+2	-4	-18	-20	-23	-20	-22	-28	-23	-21	-26
SUB, $Gain_B$ d_{at} = 0.077 m	[dB]	0	-3	+4	-7	-13	-17	-21	-19	-18	-21	-21	-18	-24
SUB, $Gain_B$ d_{at} = 0.135 m	[dB]	0	-4	--	-5	-12	-11	-15	-18	-17	-17	-21	-16	-20
IZYL, $Gain_B$ d_{at} = 0.100 m	[dB]	-	-	-	-	-	-15	-15	-16	-17	-17	-18	-18	-19

TABLE 60 Minimum $Gain_B$ at vertical polarization in the shadow zone $135^o < \phi < 225^o$. Comparison between measured data (SUB) and computational data (IZYL) at different antenna-body distances d_{at}.

The experimental minima occur somethere between $135 < \phi < 225^o$. They are symmetrical for $d_{at} > 0.05$ m (see also FIGURE 59, the most asymmetrical recording of the whole test series). In contrast, the computed minima are always near $\pm 165^o$ (see also section 10.4.) in the IZYL-model. Nevertheless, the IZYL data agree within 3 dB with the averaged experimental data at d_{at} 0.077 and 0.135 m. Taking into account the small signals (up to -26 dB below FSL), and the large field gradients, the agreement is satisfactory for frequencies above 200 MHz (IZYL-model limit).

9.1.4. EFFECT OF THE BODY MATERIAL

In the analysis 5.2.4. it was shown that the reflection coefficient for TEM, TE and TM waves is close to -1 for the E-vector and that probably differences occur only due to larger penetration depth δ. In fact, the experimental results prove these hypotheses. The differences among MET, PHA and SUB are generally below $\pm$ 3 dB (FIGURES 56,57,58 and also 55) at d_{at} above 0.1 m. Below 200 MHz and at extreme small d_{at}'s there are somewhat larger differences caused perhaps by δ, but also by the different shapes of the bodies. From the practical point of view, these differences are of little interest, as long as the antenna-body distance is above approximately 0.050 m. Smaller d_{at} are only sensible with much smaller antennas, but one should take into account that $Gain_B$ becomes very small and that the antenna gets detuned due to the extreme body proximity.

9.1.5. VERIFICATION OF THE RECIPROCITY THEOREM

The complete test series TEST 1 in section 9.1.2. was performed for both transmission directions (A_1 = transmitting antenna / A_2 = receiving antenna and A_1 = receiving antenna / A_2 = transmitting antenna). The transmission loss (or $Gain_B$) differed only within ± 2 dB (usually ± 0.5 dB). This holds true for all three test bodies, for all frequencies above 100 MHz and for all antenna-body distances above 0.05 m. The RF-power was always below 1 mW; it might be that at higher power levels with considerable heating effects significant differences could occur, but such power levels are beyond our application.

9.2. DISCUSSION OF THE LIMITATIONS OF EXPERIMENT AND COMPUTATION

The agreement between experiment and theory is ± 3 dB at frequencies above 200 MHz and antenna-body distances above 0.1 m. Taking into account the large signal range from -26 dB up to + 4 dB, the agreement is more than satisfactory. A difference of ± 3 dB around the - 20 dB level corresponds to a power variation of only ± 1%, related to 0 dB = FSL = 100 %.

The relative simple IZYL model explains the off-resonance effects at frequencies above 200 MHz, at d_{at} above 0.1 m and for all test bodies.

The assumptions in section 5.2. could be verified. The reciprocity theorem is valid for our application as shown in 9.1.5.. The human body can be regarded as a perfectly conducting body with respect to scattering, at least for d_{at} above 0.05 m as shown in 9.1.1. and 9.1.2..

Experimental data at frequencies between 100 and 900 MHz (except 300 MHz) could be measured accurately at distances from 4 m up to 0.1 m. The lower frequency limit is mainly determined by the performance of the test antenna A_1 and also by the remote antenna A_2. The main problem is the bad efficiency of electrically small antennas when operated off - resonance. Measurements with antennas tuned on resonance tend to be inaccurate as can be seen in FIGURE 55 at 300 MHz: the extreme loss with MET is caused by detuning effects due to body proximity, less accentuated with PHA and

SUB. The experimental lower limit for d_{at} is determined by the antenna dimensions and by the extremely low signal level in the shadow zone.

A problem related to all frequencies below 300 MHz is the insufficient counterpoise of the monopole antennas A_1. With the precautions in FIGURE 44 the resulting radiation from the feeding coaxial cable could be attenuated. A better solution with dipole antennas and built-in RF-generators will be shown in section 11.3..

The IZYL-antenna model has proven its usability for two-dimensional off-resonance computations at vertical E-field polarization at $\theta_i = 90^o$. An extension of the computations for frequencies at or below resonance, for arbitrary polarizations and arbitrary wave incidence is only possible with a finite body-antenna model. Such three-dimensional computations and experiments of verifications will be performed in the next sections.

10. Three-Dimensional Computation of Scattering From Finite Bodies of Revolution

10.1. COMPUTATIONAL MODELS AND GOALS

The antenna-body models consist of perfectly conducting, finite bodies of revolution (FIGURE 28: Body models FZYL, MANMOD 1 and MANMOD 2), a small antenna A_1 positioned at h_B,d_{at} and ϕ, and an incident plane wave with an irradiation angle θ_i to the vertical axis of the body. The computational situation is shown in the FIGURES 14 and 33 : the E-field vector of the incident wave may be θ-polarized ('vertical', def. 203) or ϕ-polarized ('horizontal', def. 204); the E-field components at A_1 are computed in $\vec{a}_\theta$, $\vec{a}_r$ and $\vec{a}_\phi$ directions by help of test segments located at RTEST and ZTEST, rotated with the angle ϕ around the z-axis. With these data one obtains the vertical, radial and horizontal field components E_v,E_r and E_h at A_1.

The method of solution is described in section 6.4. and is based on the extended works of HARRINGTON and MAUTZ [40] and BEVENSEE [10]. The purpose of the following (very expensive) computation is to collect numerical data in the important frequency range 10 to 500 MHz (extended resonance region of man) with regard to near-field components which influence $Gain_B$. The parameters of interest are the body geometry (actual shape of the body), frequency f, antenna-body distance d_{at}, azimuthal angle ϕ,antenna polarization p_1 and p_2, incident irradiation angle θ_i and the relative antenna height h_B.

10.2. COMPUTER PROGRAMS FOR NEAR-FIELD COMPUTATIONS

10.2.1. GENERAL OVERVIEW

Due to storage capacity- and computational time limits the computation is split-up into three independent programs connected by one file:

- Program HARRA : computation of the Y-matrices
- Program PANB : computation of near-field data for some A_1-positions
- Program PANC : computation of the field homogeneity along A_1.

These programs are written in Fortran IV for a CDC 7600 computer and require a minimum storage capacity of 160,000 octal in the core memory. The data are stored in a COLLECT FILE, catalogued in HARRA, read and extended in PANB and read in PANC. There is only an auxiliary print output in HARRA and PANB, because the final data are plotted by a special routine.

The following subroutines are used several times in program HARRA,PANB:

- Subroutine LINEQ : replaces a 19 by 19 matrix Z by its inverse
- Subroutine PLANE : provides the measurement matrices for the body of revolution and for the test segments
- Subroutine PROGA : prepares the matrix variables in order to accommodate the Y-matrices read from the file
- Subroutine REORD : arranges a number of values in descending order (needed if no plotter is available)
- Subroutine NEARZ : computes the coordinates for the test segments, similar to the body coordinates in HARRA.

The complete programs and output samples are enclosed in Appendix 16.2.. Not enclosed is the plot routine, because its application is limited to the ETH computer center. The procedure to compute the near-field data can be summarized as follows:

- definition of the body geometry and frequency in HARRA
- computation of the Y-matrices for some modes and storage in a collect file in HARRA
- definition of the test segments (location and length) in PANB
- computation of the near-fields for each mode, manual test of the convergence of the results in PANB
- summation of contribution of each mode and for each azimuthal angle, manual checking of the minimum number of needed modes in PANB
- coordinate transformation of the results in order to obtain the E-field components in vertical, radial and horizontal direction, separate storage of the data in the collect file in PANB
- auxiliary output of $Gain_B$ for some significant cases in PANB
- reading of the file data, final processing and plotting or
- reading of the file data, final processing of the field homogeneity and printing in PANC.

10.2.2. PARAMETER DESCRIPTION

The input parameters are described in TABLE 61; the body parameters for FZYL, MANMOD 1 and MANMOD 2 are enclosed in the listings of PANC in Appendix 16.2.4.. CAUTION: For convenience the computational frequency is ten times smaller than the actual frequency, and all computational dimensions are ten times larger than actual. This means that the input data have to be scaled to the computational data. The output tables describing the body parameters, the tables with the complex field data for each test segment for the convergence test and the tables showing the contribution of each mode are presented in the computational scale. However, the final graphical outputs and the final result tables about the field homogeneity are presented in the actual scale.

INPUT PARAMETER	MEANING	UNITS
BK (REAL)	Computational wave factor = $2\pi/\lambda_{actual}$ * 0.1.	[1/m]
DTEST (REAL)	Test segment length, see FIGURE 33, computational DTEST = actual size * 10 .	[m]
F (REAL)	Computational frequency = f_{actual} *0.1 in HARRA. Only used for data card identification.	[MHz]
F (REAL)	Actual frequency used in PANC.	[MHz]
KK (INTEGER)	Number of computed modes. KK = 8 means that the modes 0,1,2,...7 are executed, if the correspon-ding Y-matrices are available.	
NN (INTEGER)	Mode number. NN is the same as n appearing in (194).	
NNPHI (INTEGER)	Number of azimuthal angle ϕ steps in the range from 0^o to 180^o. The standard NNPHI is 37.	
NP (INTEGER)	Number of points describing the generating curve, see FIGURE 32. The arc length t_{tot} along this curve is divided in (NP-1)/2 = N tangential unit elements t from one peak of a triangle function to the next peak. It is <u>not</u> necessary that the body points are equally spaced. Standard NP is 41.	
NPHI (INTEGER)	Number of equal subdivisions of the body ϕ axis from 0 to π. The standard NPHI is 20.	
NT (INTEGER)	Number of irradiation angles. The standard NT is 1, but the program is prepared for larger NT's.	
NTEST (INTEGER)	Number of test points (A_1 positions d_{at}'s and h_B's). The standard NTEST is 9 for PANB and 5 for PANC.	
RH (REAL)	Radius of the points describing the generation curve, see FIGURE 32. The computational RH is the actual body radius * 10.	[m]
RTEST (REAL)	Radius from the body axis to the test point, see FIGURE 33. The computational RTEST is the actual radius * 10.	[m]
RUN (INTEGER)	Control variable. If RUN = 1, program PANB com-putes the scattering from the direct incident wave , if RUN = 2, of the ground reflected wave.	
ZH (REAL)	Height of the points describing the generation curve, see FIGURE 32. The computational ZH is the actual height * 10.	[m]
ZTEST (REAL)	Height h_B of the test point, see FIGURE 33. The computational ZTEST is $h_{Bactual}$ * 10.	[m]

TABLE 61 Input parameter names used in programs HARRA, PANB and PANC

OUTPUT AND FILE PARAMETER NAMES	MEANING	UNITS
DA (REAL)	length of the body in z-axis, actual scale	[m]
DAV (REAL)	logarithmic difference $\delta E, p_1$ vertical or hor.	[dB]
DAR (REAL)	logarithmic difference $\delta E, p_1$ radial	[dB]
DI (REAL)	antenna-body distance d_{at}, from body point No. 22, def. at PANB 336, actual scale	[m]
DU (REAL)	diameter of the body, at body point No. 20, def. at PANB 332, actual scale	[m]
DPV (REAL)	phase variation $\delta\Phi$ along the antenna axis, p_1 vertical or horizontal	[°]
DPR (REAL)	phase variation $\delta\Phi$ along antenna axis, p_1 rad.	[°]
EAV (REAL)	logarithmic difference ΔU, p_1 vertical or hor.	[dB]
EAR (REAL)	actual to averaged U_{ind} p_1 radial	[dB]
EPH (COMPLEX)	E-field $\vec{a}_\phi$-direction amplitude of one mode, of	[V/m]
ERAD "	" $\vec{a}_r$ " one test point, for ϕ =	
ETH "	" $\vec{a}_\theta$ " $0°$, θ_i, E_θ^{inc} and E_ϕ^{inc}	
EPTOT (COMPLEX)	E-field $\vec{a}_\phi$-direction added amplitudes up to	[V/m]
ERTOT "	" $\vec{a}_r$ " the last computed mode,	
ETTOT "	" $\vec{a}_\theta$ " else identical to above	
EHTOT (COMPLEX)	E-field horizontal field strength components	[V/m]
ESTOT "	" radial including all modes for	
EVTOT "	" vertical all ϕ's, one test point	
GHTOT (REAL)	E-field horizontal amounts of the components	[V/m]
GSTOT "	" radial in dB, including all modes	
GVTOT "	" vertical for all ϕ's, one test p.	
PHTOT (REAL)	Phase horizontal phases of the field com-	[°]
PSTOT	of radial ponents GHTOT, GSTOT and	
PVTOT	E-field vertical GVTOT	
HO (REAL)	relative antenna height h_B, actual size	[m]
IT (INTEGER)	control variable for test segment orientation	
ITE (INTEGER)	index test point	
L (INTEGER)	index irradiation angle	
M (INTEGER)	index mode	
NST (INTEGER)	number of stored final data: NTEST*NNPHI(H,S,V)	
NZ (INTEGER)	number of stored Y-elements: $(NP-3)^2$(Y1,Y2,Y3,Y4)	
POL (INTEGER)	control variable: 1=E_θ^{inc}, 2=E_ϕ^{inc} (p_2)	
SYH (COMPLEX)	stored final data, horizontal components	[V/m]
SYS (COMPLEX)	stored final data, radial components	[V/m]
SYV (COMPLEX)	stored final data, vertical components	[V/m]
TJ (REAL)	arc length along generating curve to the j^{th} triangle function (HARRA), computational scale	[m]
X1 (REAL)	irradiation angle θ_i or $180°-\theta_i$, (RUN 1,2)	[°]
Y1-4 (COMPLEX)	Y-matrices elements $(Y_n^{tt})_{ij}$, $(Y_n^{\phi t})_{ij}$, $(Y_n^{t\phi})_{ij}$,	
Z (COMPLEX)	$(Y_n^{\phi\phi})_{ij}$, first run n = 0, next run n = 1,2,..NN	
S164M07 (FILE)	S = code MANMOD 2, 164 = 164 MHz, M07 = max.mode 7	
S164D9 (FILE)	S = code MANMOD 2, 164 = 164 MHz, D9 = 9 d_{at}'s	
F100D5 (FILE)	F = code FZYL, 100 = 100 MHz, D5 = 5 d_{at}'s	

TABLE 62 Output and file parameter names in programs HARRA,PANB,PANC

10.2.3. PROGRAM DESCRIPTION HARRA

The computer program HARRA is based on the theory in section 6.4.1. and 6.4.2.. In the presented form (Appendix 16.2.2.) it computes the Z-matrices for the body MAMMOD 2 for the actual frequency 164 MHz, performs the matrix inversion and stores the Y-matrices Y1 to Y4 for the modes 0 to 7 in the collect file AMAT2 with the code name S164M07.

The source program is the program A developed and well described by HARRINGTON and MAUTZ [40]. It runs on an IBM computer. Because our computer center is equipped with a CDC-computer, the source program has been altered to the present program HARRA. The modifications regard mainly the structure of the program parts, the conversion of some characters and the file generation. Only the input and file procedure are discussed here; details can be studied in the above mentioned source program description.

Punched card data about mode number, number of body points, ϕ-subdivisions, k-factor and frequency (computational scale) is read early in the main program:

```
   50 READ (1,51) NN, NP, NPHI, BK, F                      HARRA 47
   51 FORMAT (3I3, E14.7, F8.2)                            HARRA 48
```

The number F is only used for punched card data identifications and is not used for computations. Because we need all modes from 0,1,2,...7 in our example, there are 8 data cards, only differing in the first number for NN. If the last mode is executed, the program stops due to the statement:

```
      IF (EOF (1)) 52,49                                   HARRA 49
   49 CONTINUE                                             HARRA 50
   52 STOP                                                 HARRA259
```

Punched card data about the body contour (MANMOD 2) is read later:

```
      READ (1,53) (RH(I),I=1,NP)                           HARRA 51
      READ (1,53) (ZH(I),I=1,NP)                           HARRA 52
   53 FORMAT (10F8.4)                                      HARRA 53
```

For each mode a complete set of data is required. With an earlier reading of the number NP only one reading of the body data would be required, but for a better overview on the program the presented procedure is more convenient.

For each mode the Y-matrices are computed and printed separately. The output (see example in Appendix 16.2.2.) consists of the listing of the input data, the 19 arc lengths along the generation curve and 4 Y-matrices of 19 x 19 complex elements (see theory in section 6.4.2.2.). The Y-matrices are stored on the collect file according to:

```
PERMF,AMAT2.          (first run)                  HARRA   4
PUBLIC,COLLECT.       (first run)                  HARRA   7
COLLECT,N=AMAT2.      (first run)                  HARRA   8
CATALOG,AMAT2.        (first run)                  HARRA   9
                           or
ATTACH,AMAT2,PW..     (following runs)             HARRA  13
PUBLIC,COLLECT.       (following runs)             HARRA  16
COLLECT,M=AMAT2.      (following runs)             HARRA  17

PROGRAM HARRA (....TAPE 6 = DISK)                  HARRA  21

   WRITE (6) (Z(I),I=1,NZ)                         HARRA242

ADD, S164M07, DISK, RO.                            HARRA334
LIST                                               HARRA335
END                                                HARRA336
```

Due to the LIST statement all existing names of the files in AMAT2 are listed.

10.2.4. PROGRAM DESCRIPTION PANB

The computer program PANB is based on the theory in section 6.4.5.. In the presented form (Appendix 16.2.3.) it reads the Y-matrices from the collect file, computes the current densities on the body of revolution MANMOD 2 for the specified incident wave, computes the incident, the scattered and the total E-field at a specified test segment near the body, determines the field components in vertical, radial and horizontal directions, delivers some tables for accuracy considerations, prints an auxiliary output and stores the final data in the same collect file AMAT2 with the code name S164D9 (or in a new collect field HOMOG with the code name F100D5, see description program PANC).

The source program is the program HARRDF, developed and well described by BEVENSEE [10]. HARRDF is an extension of the program D by HARRINGTON and MAUTZ [40], so that both reports have to be consulted for a detailed understanding. HARRDF runs on an IBM computer and delivers the field components in $\vec{a}_\theta$, $\vec{a}_r$ and $\vec{a}_\phi$ directions at one test point, for $\phi = 0^o$ and for each single mode. The source program has been altered to the present program PANB. The modifications regard mainly the structure of the program parts, the preceding computation of the Y-matrices (now in HARRA), the conversion of some characters (CDC-notations), the θ_i-handling, the extension on the computation of the ϕ-dependence, the summation of the contributions of each mode, the coordinate transformation of the results, the output procedure and the file generation. A major problem was the reduction of the storage requirement from the original 662,513 octal to 160, 000 octal. Only the input and some important procedures are discussed here; the principle of the method is described in section 6.4.5. and the computational details in the above mentioned reports.

Punched card data about the number of modes, number of body points, ϕ-subdivisions, number of incident angles, number of test points, number of azimuthal steps, k-factor and wave origin is read early in the main program in computational scale:

```
50 READ (1,51) KK, NP, NPHI, NT, NTEST, BK, RUN                PANB  62
51 FORMAT (6I3, E14.7, 2X, I2)                                 PANB  63
```

Usually only one corresponding data card is necessary, but more than one is possible simliar to the input section in program HARRA. Next the card data about the body contour (MANMOD 2) are read:

```
   READ (1,53) (RH(I),I=1,NP)                                  PANB  67
   READ (1,53) (ZH(I),I=1,NP)                                  PANB  68
53 FORMAT (10F8.4)                                             PANB  69
```

Next an integer array TEXT(9) is filled with the letters for the words "VERTIKAL","HORIZONTAL","RADIAL","DIREKTE EINSTRAHLUNG" (means direct irradiation) and "REFLEKTIERTE EINSTRAHLUNG" (means irradiation by a wave reflected from the ground) to be used in the output tables. The input data appear first in the output listing due to the statements

```
   JA=RUN*3+1                                                  PANB  79
   :                                                             :
   WRITE (3,46) (ZH(I),I=1,NP)                                 PANB  91
```

The irradiation angle θ_i is set to 80.78^o (direct wave, RUN = 1) and 103.36^o (reflected wave, RUN = 2) due to the statements

```
   DT = 0.394                     [DT = PI/(NT-1)    ]         PANB 111
   DO 1 J=1,NT                    [DO 1 J=1,NT       ]         PANB 112
   THR(J) = DT*(J-1) + 1.410      [THR(J) = DT*(J-1)]          PANB 113
   IF(RUN.EQ.2) THR(J) = DT*J+1.410                            PANB 114
```

For equally spaced θ_i-steps the [statements] must be used and all arrays concerning the θ_i-variable (L=1,NT) have to be changed (PANB 39 to 50).

After some initial computations the punched card data about the 9 test points are read :

```
      READ (1,49) (RTEST(J), ZTEST(J), DTEST(J), J=1,NTEST        PANB 173
   49 FORMAT (3F8.4)                                              PANB 174
```

For a given mode subroutine PLANE is called with its 5th argument IT=1 to compute the incident plane wave components VVR(1,J) on the J^{th} field triangle on the body:

```
      CALL PLANE (VVR,THR,NP,NT,1,R,ZS,SV,CV,T,TR)                PANB 199
```

In contrast to the source program the Y-matrices are read from the collect file, called by PROGA which prepares only the matrices accommodations.

```
      CALL PROGA                                                  PANB 200
  127 READ (6) (Y(I),I=1,NZ)                                      PANB 202
```

In the DO 41 loop E3(L,J) and E3(L,J+NM) measure the current densities for the L^{th} incident angle of the E_θ^{inc} (p_2 = vertical, see FIGURE 33) while E4(L,J) and E4(L,J+NM) measure corresponding current densities of the E_ϕ^{inc} (p_2 = horizontal, see FIGURE 33) in $\vec{t}$ and $\vec{\phi}$ directions (FIGURE 32):

```
      E3(L,J) = E3(L,J) + Y(J1)*VVR(1,I1)-Y(J2)*VVR(1,I2)         PANB 221
      E4(L,J) = E4(L,J) - Y(J1)*VVR(1,I3)+Y(J2)*VVR(1,I4)         PANB 222
```

With J_t and J_ϕ the current densities per unit length in azimuth and along t, respectively, at the peak of the J^{th} triangle, for a certain θ^{inc},

E_θ^{inc} polarization

$$J_{Jt}(\phi) \begin{cases} \dfrac{E3(L,J)}{RH(J2)} & NN = n = 0 \\ \dfrac{E3(L,J)}{RH(J2)}\, 2\cos n\phi & n \geq 1 \end{cases} \tag{240}$$

$$J_{J\phi}(\phi) \begin{cases} 0 & n = 0 \\ \dfrac{E3(L,J+NM)}{RH(J2)}\, j\, 2\sin n\phi & n \geq 1 \end{cases} \tag{241}$$

These formulas are similar for E_ϕ^{inc} polarization (see BEVENSEE [10]) and can be used to compute the current density $\vec{\underline{J}}$ in equation 128 at any point on the body surface, if one sums the contributions of all modes for each azimuthal angle separately.

In the following discussions only the E_θ^{inc} polarization will be considered, but all the data from E_ϕ^{inc} are computed, printed and stored. With E3(L,J) stored for a given mode, for each incident angle 1, and for each triangle function J, the scattered field for that mode can be determined from them for all test segments in succession. Thus, the DO loop 7100 over the test segments, NEARZ determines the near-field matrix ZM for a given test segment, and PLANE yields its sampled incident field for all angle of incidence. Both test segment orientations for IT = 1 and IT = 2 are treated:

```
      DO 706 IT=1,2                                               PANB 251
```

The test segment fields are approximated according to equation 220. The ESC(IT,1) and ESC(IT,2) at PANB 257 are proportional to the scattered field mode amplitudes in the $\vec{a}_r$ and $\vec{a}_\phi$-directions for IT = 1, and in the $\vec{a}_\theta$ and $\vec{a}_\phi$-directions for IT = 2, respectively. From statement 702 to 711 the incident, the scattered and the total E-fields in $\vec{a}_r$ (ERAD), $\vec{a}_\theta$ (ETH) and twice in $\vec{a}_\phi$ (EPH) - directions are computed and printed for the regarded mode M, irradiation angle L, test segment ITE and both wave polarizations. The use of the two EPH's will be discussed in section 10.3.4.2..

With the advice of BEVENSEE [10] the program has been extended to compute the total field components for different azimuthal angles. The key formulas are: (ERAD:ETR, ETH:ETH, EPH: ETP1 and ETP2 inside the program)

$$E_r^{tot}(r_T,z_T,\phi) = \sum_{M=0}^{KK-1} ETR(M,ITE,L) \begin{matrix} \cos M\phi, E_\theta^{inc} \\ j \sin M\phi,\ E_\phi^{inc} \end{matrix} \tag{242}$$

$$E_\theta^{tot}(r_T,z_T,\phi) = \sum_{M=0}^{KK-1} ETH(M,ITE,L) \begin{matrix} \cos M\phi, E_\theta^{inc} \\ j \sin M\phi,\ E_\phi^{inc} \end{matrix} \tag{243}$$

$$E_\phi^{tot}(r_T,z_T,\phi) = \sum_{M=0}^{KK-1} ETP_2^1(M,ITE,L) \begin{matrix} j \sin M\phi,\ E_\theta^{inc} \\ \cos M\phi, E_\phi^{inc} \end{matrix} \tag{244}$$

These computations are performed by the statements

```
  909 DO 506 M=1,KK                                               PANB 361
      NN = M-1                                                    PANB 362
      ERTOT = ERTOT + ETR(M,ITE,L)*COPHI(M,J)                     PANB 363
      ETTOT = ETTOT + ETT(M,ITE,L)*COPHI(M,J)                     PANB 364
      EPTOT = EPTOT + ETP(M,ITE,L)*SIPHI(M,J)                     PANB 365
```

where ETP is the averaged value of the two EPH's and the trigonometric functions COPHI and SIPHI are the previously computed numbers:

```
      EPR = (ETP1R+ETP2R)/2 $ EPI = (ETP1I+ETP2I)/2               PANB 295
      ETP(M,ITE,L) = COMPLX(EPR,EPI)                              PANB 296
      COPHI(M,J) =   COS(NN*PHI(J))                               PANB 189
      SIPHI(M,J) = U*SIN(NN*PHI(J))                               PANB 190
```

In order to monitor the contribution of each mode (see later in section 10.3.4.1.) the continuously summed up field components are listed in the output for $\phi = 0$, 90 and 180°. The sample output shows the results for one θ_i, the 9 test points (h_B = constant = 1 m, d_{at} = DIST = parameter), for E_θ^{inc} and for the actual frequency 164 MHz, according to:

```
  40 CONTINUE                                               PANB 330
     F=3000.*BK/(2*PI)                                      PANB 331
     :                                                         :
     IF(J.EQ.19) WRITE (3,545) NN,ERTOT,EPTOT,ETTOT         PANB 376
 913 CONTINUE                                               PANB 378
```

From the last ERTOT, EPTOT, ETTOT the corresponding field components are computed in vertical, horizontal and radial directions : EVTOT, EHTOT and ESTOT. They are also stored as SYV(JDI), SYH(JDI) and SYS(JDI) :

```
     JDI=0                                                  PANB 350
     JDI=JDI+1                                              PANB 379
     EVTOT = ERTOT * COTN(ITE) - ETTOT * SITN(ITE)          PANB 380
     SYV(JDI) = EVTOT                                       PANB 381
     EHTOT = EPTOT                                          PANB 382
     SYH(JDI) = EPTOT                                       PANB 383
     ESTOT = ERTOT * SITN(ITE) + ETTOT * COTN(ITE)          PANB 384
     SYS(JDI) = ESTOT                                       PANB 385
```

The numbers COTN(ITE) and SITN(ITE) are the sin and cos of the a-vector already computed in PANB 177 for the different test points. Next the field components are scaled in dB and the phase angles are computed:

```
     PP = CMPLX(1.0E-32, 1.0E-32)                           PANB 333
     QQ = 1.0E-32                                           PANB 334
     IF(CABS(EVTOT).LT.QQ) EVTOT = PP                       PANB 386
     :                                                         :
     GVTOT(ITE,L,J) = 20.*ALOG10(CABS(EVTOT))               PANB 389
     :                                                         :
     PVTOT(ITE,L,J) = ATAN2(REAL(EVTOT),AIMAG(EVTOT))*PR    PANB 392
     :                                                         :
 504 CONTINUE                                               PANB 396
```

For the later use of the results in the plot programs or in PANC,the complex original data are stored in the collect file:

```
  ATTACH,AMAT2,PW..                                         PANB   4
  CALL,S164M07,P=AMAT2,B=DISK.  (for Y-matrices)            PANB   5
  PROGRAM PANB (..TAPE 6 = DISK, TAPE 7 = RESULT)           PANB  13
     WRITE (7) (SYV(I),I=1,NST)                             PANB 397
     WRITE (7) (SYH(I),I=1,NST)                             PANB 398
     WRITE (7) (SYS(I),I=1,NST)                             PANB 399
  ADD, S164D9, RESULT,RO.       (or S100D5 for later PANC)  PANB 768
```

The remaining of the program PANB is concerned with the graphical output of the amplitude and the phase of $Gain_B$. Due to the statements

```
DO 918 I=1,3                                                  PANB 400
J = (I*18)-17                                                 PANB 401
```

only the results for $\phi = 0, 90$ and 180^o are printed. By changing these cards into DO 918 I=1,37 and J = I all azimuthal results would be printed. Only the p_1 = vertical polarization is executed by the output procedure. By changing PANB 402, 403 and 431 and duplicating the program from PANB 404 to 463 (change labels) one also obtains the other p_1-data. The E_ϕ^{inc} output (p_2 = horizontal) is already incorporated in the program due to the DO loop 912 in PANB 239,but not shown in the sample output.

Similarly, the results for the next program PANC are computed for all p_1 and p_2. The only difference is, that the results are stored in the collect file HOMOG, and that only 5 test points are needed.

10.2.5. PROGRAM DESCRIPTION PANC

The computer program PANC is an extension to program PANB and is based on the investigation in section 5.2.2.. It reads the vertical polarized E-data of P1, P4 , P5, the radial polarized E-data of P1, P2, P3 and the horizontal polarized E-data of P1 (see FIGURE 63) for all azimuthal angles $0 \leq \phi \leq 180^o$ (J = 1, NNPHI) from the collect file HOMOG. It computes the horizontal E-data of P6 and P7, so that the fields at the center and at the ends of a dipole antenna of $2h = 0.1$ m are available for p_1 = vertical/radial at p_2 = vertical and p_1 = horizontal/radial at p_2 = horizontal. Then it computes the amplitude variation δE and the phase variation $\delta\Phi$ along the antenna polarization axes, the logarithmic difference ΔU between the induced voltage computed by $E_{center} \cdot 2h$ and the numeric integral $\int_{-h}^{+h} E(\xi) \cdot d\xi$ where $\vec{\xi} = p_1$, and prints all data versus ϕ in tables which can be directly applied for field homogeneity considerations and antenna design. The sample program is specified for the body model FZYL at 100 MHz and $d_{at} = 0.1$ m. The listing of the program and results for the frequencies 65,75,100,125,300 and 425 MHz are enclosed in Appendix 16.2.4..

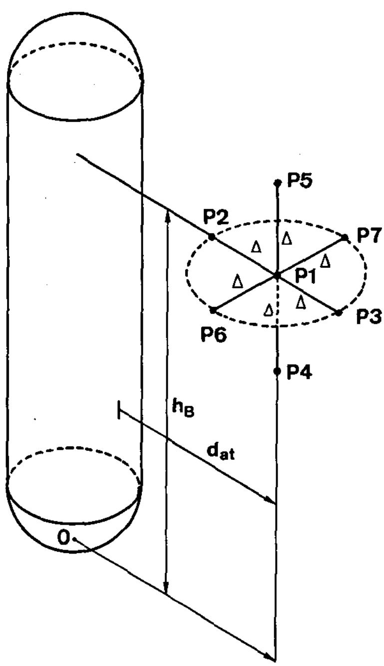

FIGURE 63

Body model FZYL and antenna A_1 with its center at P1.

Antenna polarization p_1:

p_1 = vertical : P4, P1, P5

p_1 = radial : P2, P1, P3

p_1 = horizontal: P6, P1, P7

Antenna length $2h = 2\Delta = 0.1$ m

Antenna height $h_B = 1$ m

Ant.body dist. $d_{at} = 0.1$ m

Body diameter $D_B = 0.25$ m

Body length $L_B = 1.8$ m

There is only one punched card data read concerning the actual frequency:

```
    READ (1,10) F                                          PANC 45
 10 FORMAT (2X, F5.1)                                      PANC 46
```

The other parameters as used in PANB for the field computations are defined by statements:

```
    DA = 1.8 $  DI(1) = 0.1 $ DU = 0.25 $ HO = 1.0 $ X1 = 80.8      PANC 47
    NNPHI = 37 $ NST = 185
```

DA is the body length, DI(1) the d_{at} of the center of the antenna, DU the body diameter, HO the relative antenna height h_B, X1 the irradiation angle θ_i, NNPHI the number of azimuthal ϕ-steps and NST the number NTEST x NNPHI of stored data for each p_1 at p_2 = vertical (POL = 1) and horizontal (POL = 2). In order to compute the missing field data at P6 and P7 the arc length CS between P1(J) and P1(J+1) is determined by

```
    CS = (DU/2.+DI(1))*PI/(NNPHI-1)                        PANC 50
```

In FIGURE 61 the approximation method is shown for the computation of the field data at P6 and P7:

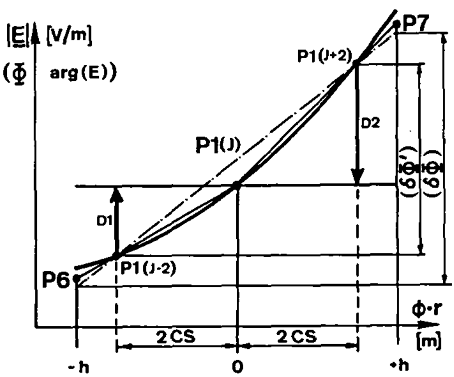

FIGURE 64 Approximation method for the E-field data at P6 and P7 (p_1 = horizontal, amplitude |E| and phase Φ) from the data at P1(J-2), P1(J) and P1(J+2).
Correction factor FAC : 2h/4CS where CS is the arc length between P1(J) and P1(J+1)
|E| at P6 : |E| at P1(J) - FAC*D1
|E| at P7 : |E| at P1(J) - FAC*D2
δΦ : FAC*δΦ'

The correction factor is computed by (here 2h = d_{at} = 0.1 m)

```
    FAC = DI(1)/(4.*CS)                                    PANC 51
```

In the first run POL =1 (PANC 58) the p_2 = vertical- data are read from the collect file by:

```
    READ (6) (SYV(I), I=1,NST)                             PANC 59
    READ (6) (SYH(I), I=1,NST)                             PANC 60
    READ (6) (SYS(I), I=1,NST)                             PANC 61
```

After the statements describing the output the field data are rearranged.

In the DO loop 700 the J-dependent variables ITE1 for P1, ITE2 for P2,.. ITE5 for P5 are computed by the statements PANC 97 to 101. For each azimuthal angle $0 \leq \phi \leq 180^{o}$ (J = 1,NNPHI) the amounts of the fields at P1,P5,P4 (vertical components) and at P1,P3,P2 (radial components) are computed according to

```
AMV1 = CABS(SYV(ITE1))  $  AMR1 = CABS(SYS(ITE1))          PANC 114
AMV5       "    ITE5    $  AMR3       "    ITE3            PANC 115
AMV4       "    ITE4    $  AMR2       "    ITE2            PANC 116
```

The phases of the fields at these points are computed due to

```
PV1  = ATAN2(REAL(SYV(ITE1)),AIMAG(SYV(ITE1))) * PR        PANC 117
 :                                                             :
```

The phase differences $\delta\Phi$ along the p_1-vertical/radial axes is computed by:

```
DPV1 = ABS(PV5-PV4)  $ DPV2 = 360.-DPV1                    PANC 123
 .                                                            .
IF(ABS(DPV2).LT.ABS(DPV1)) DPV1 = DPV2  $ DPV = ABS(DPV1)  PANC 125
 .                                                            .
```

Then the dB-values of the fields are computed according to

```
AV1 = 20.*ALOG10(AMV1)  $ AR1 = 20.*ALOG10(AMR1)           PANC 133
 .                                                            .
```

The numerical integration of the E-field along the antenna axis is simply the sum of (AMV5+AMV1)·h/2 + (AMV4+AMV1)·h/2 and corresponds to the actual induced voltaged U_{ind} (see section 5.2.2.). The mean induced voltage $\overline{U}_{ind}$ is AMV1·2h. The logarithmic difference ΔU in dB is 20 log $(\overline{U}_{ind}/U_{ind})$:

```
EAV = 20.*ALOG10((4.*AMV1)/(AMV5+AMV4+2.*AMV1))            PANC 136
EAR       "         "    R1      R3   R2      R1           PANC 137
```

The amplitude variation δE is computed according to

```
DAV = ABS(AV5-AV4)  $ DAR = ABS(AR3-AR2)                   PANC 138
```

After the checking of the size of AV1 and AR1 (PANC 139 and 142) the results ϕ, E(dB) center, Φ center, ΔU, δE and $\delta\Phi$ are printed for p_1 = vertical and radial at p_2 = horizontal due to the statement PANC 145.

In the second run POL = 2 (PANC 58) the p_2 = horizontal data are read from the collect file by the same statements PANC 59,60 and 61. After the output statements the field data are rearranged as follows in DO loop 700:

```
IH1 = J-2 $ IH2 = J+2 $ NC = NNPHI-1                       PANC 94
IF(J.EQ.1)  IH1 = J+2 $ IF(J.EQ.2)    IH1 = J              PANC 95
IF(J.EQ.NC) IH2 = J   $ IF(J.EQ.NNPHI) IH2 = J-2           PANC 96
```

At POL = 2 the vertical components SYV(J) are not used. In order to apply the same procedure as for POL = 1 the horizontal components around the center point P1 ($\phi = \pm 10^{o}$, see FIGURE 64) P1(J-2), P1(J) and P1(J+2) are transferred into the vertical component arrays of P1, P5 and P4:

```
      IF(POL.EQ.1) GOTO 4                                    PANC 103
      SYV(ITE1) = SYH(ITE1)                                  PANC 104
      SYV(ITE5) = SYH(IH1)                                   PANC 105
      SYV(ITE4) = SYH(IH2)                                   PANC 106
    4 CONTINUE                                               PANC 107
```

Now the amplitude difference D1 and D2 (FIGURE 64) is computed and the approximated amounts at P6 (now called P5) and P7 (now called P4) are determined, and the phase difference $\delta\Phi$ is obtained by $\delta\Phi' \cdot FAC$:

```
      IF(POL.EQ.1) GOTO 5                                    PANC 127
      D1 = AMV1-AMV5  $ D2 = AMV1-AMV4                       PANC 128
      AMV5 = AMV1-D1*FAC $ AMV4 = AMV1-D2*FAC                PANC 129
      IF(AMV5.LT.QQ) AMV5 = QQ  $ IF(AMV4.LT.QQ) AMV4 = QQ   PANC 130
      DPV = DPV*FAC                                          PANC 131
    5 CONTINUE                                               PANC 132
```

The rest of the procedure is analogous to the computation of the field parameters at p_2 = vertical.

The output consists of two tables. The first table contains the field data p_1 = vertical/radial at p_2 = vertical , and the second table contains the field data p_1 = horizontal/radial at p_2 = horizontal. The model body and the antenna positions are explained in the table head. The data are ranging from $0 \leq \phi \leq 180^{o}$. The output parameters are:

GAIN CENTER DB	= amount of the field at P1 in [dB]
PHASE CENTER DEG	= phase of the field at P1 in [^{o}]
MEAN ERROR DB	= logarithmic difference ΔU in [dB]
MAXIMUM GAINVAR DB	= logarithmic difference δE in [dB]
MAXIMUM PHASEVAR DEG	= phase variation $\delta\Phi$ in [^{o}]

The results of PANC are discussed in section 10.3.5.1.

10.3. INVESTIGATION OF PROGRAM LIMITATIONS AND COMPUTATIONAL ACCURACY

10.3.1. PROGRAM LIMITATIONS

The limitations of the program HARRA and PANB are defined by BEVENSEE [10] and HARRINGTON and MAUTZ [40] and are interpreted as follows:

- The programs are written for perfectly conducting bodies of revolution in free space.
- The wave-number $k = 2\pi/\lambda$ should be such that the peaks of the triangle functions are not more than $\lambda/2\pi$ apart. For a given λ this condition determines the number NP (number of points describing the generation curve). The arc length along the generation curve t_{tot} (see FIGURE 32) is divided in HARRA by $(NP-1)/2 = N$ tangential unit elements t of equal lengths. This length should not be larger than $\lambda/2\pi$ in order to prevent field oscillation between two peaks of the triangle functions. If we assume the standard NP of 41 and an arc length of the human body of $t_{tot} = 2\,m$, we obtain the maximum permissible frequency f_{lim5}:

$$f_{lim5} = \frac{(NP-1)/2 \cdot c}{t_{tot} \cdot 2\pi} = 500 \text{ MHz} \tag{243}$$

- The number of subdivisions of the ϕ-axis, NPHI, should be large enough so that $\pi(n_{max})/NPHI < 1$ rad, n_{max} being the number of the last azimuthal mode employed. In addition, $(2\pi/\lambda)\ (\pi/NPHI) \cdot \rho_{max} < 1$ rad, ρ_{max} being the maximum radial cylindrical coordinate of the body contour. These conditions are interpreted as follows:
- We assume a plane wave at $\theta_i = 90^o$, $\vec{k} \| x$-axis. The ϕ-axis is subdivided in $\pi \cdot n_{max}/NPHI$ sectors with the arc length w and the angle ϕ_W. The phase along w should not vary more than $\lambda/2\pi$ in order to prevent field oscillations within a sector. For small ϕ_w the projection of w to the $\vec{k}$-axis amounts to $w \cdot \sin\phi$. The maximum permissible n_{max} for a given $f = 300$ MHz, $\rho_{max} = 0.125\,m$ and $NPHI = 20$ for all sectors amounts to:

$$n_{max} = \frac{\lambda \cdot NPHI}{2\pi \cdot \pi \cdot \rho_{max}} \cdot \frac{1}{\sin\phi} = 8 \tag{244}$$

Equation (244) is valid for all ϕ. If we consider the interesting special case $\phi = 0^o$ (or 180^o) and $d_{at} < 0.2$ m, the sectors with ϕ near 0^o (or 180^o) are of greater influence than those with ϕ near $\pi/2$. Thus, n_{max} may be as large as 10 for 500 MHz without large accuracy loss.

- The convergence of the computed current densities to their correct values along the surface increases with NP and NPHI and should be rapid if both circumferences ($2 \cdot t_{tot}$ and $\rho_{max} \cdot 2\pi$) remain < λ. In our case with $\theta_i \sim 90^0$ the body radius sets the limit. With a $\rho_{max} = 0.125$ m the convergence may worsen at frequencies above 380 MHz.
- Near-field computations of a point field with a test segment tend to be inaccurate unless both these conditions are fulfilled:

  a.) minimum distance of the test segment center to the body surface > λ

  b.) test segment length < $\lambda/4$.

  When the test segment is very near to the body surface it usually does not measure the point field accurately. But if it has a length equal to one of the triangle functions it measures, at the position of that triangle function, the integral of electric field according to the network equation obtained with that function. The length of a triangle element is about 0.09 m (actual) and the length of a test segment is 4•DTEST = 0.08 and 0.20 m (actual) which is smaller than $\lambda/4$ at frequencies below 375 MHz. The distance of the test segment to the body surface, however, is generally much smaller than λ (d_{at} from 0.05 m to about 1 m). Thus, computations have to be performed with different test segment lengths, at test frequencies around the wanted frequency and the influence of each mode has to be monitored.

The program PANC is limited on d_{at} = 0.1 m but is valid for all frequencies. For other d_{at}'s see the program description in 10.2.5..

10.3.2. COMPUTATIONAL TIME LIMITATIONS

With the standard NP of 41 and the standard NPHI of 20 one obtains for each mode 4 matrices of the size 19 x 19 (complex elements). The computational time depends on the matrix inversion time and thus on the matrix size and on the number of modes. As an example program HARRA requires for the computation of 9 modes at the computational frequency 16.4 MHz 325 sec on a CDC 6500. The execution of program PANB at the same frequency for 7 test points with the modes 0 to 7 requires 320 sec. The execution of program PANC needs only about 5 sec. Thus, one should limit n_{max} on the absolutely needed number (increases with d_{at} and frequency, see 10.3.4.1.), and one should limit the number of test segments, especially those with large d_{at}.

10.3.3. STORAGE CAPACITY LIMITATIONS

The original program by BEVENSEE [10] requires a total storage of 662,513 octal which exceeds the permissible limit of 160,000 octal of the ETH computer by a factor of 4. With the assistance of BEVENSEE and the specialists at the computer center the storage requirement could be reduced. The main steps of reduction were:

- Separate computation of the Y-matrices in HARRA
- Reduction of the ZM-matrix from (2 x 10,000) to (2 x 76)
- Reduction of NT to 2, KK to 13 and NTEST to 9
- Reduction of the VVR from (2 x 14,400) to (2 x 760), Y from (10,000) to (1,444), and G from (30,603) to (4764)
- Extensive use of the COMMON BLANK and COMMON/A

The reduction of the array sizes and the COMMON operations is critical with respect to writing over the reserved array lengths. Several debugging procedures are needed which cannot be discussed here.

The final storage requirements of the programs in Appendix 16.2. are:

- Program HARRA: 61,200 octal (specified 70,000)
- Program PANB : 121,600 octal (specified 130,000)
- Program PANC : < 10,000 octal (specified 70,000)

10.3.4. INVESTIGATION OF THE COMPUTATIONAL ACCURACY

10.3.4.1. MINIMUM MODE NUMBER KK

The preliminary study in section 7.2.3. has shown that up to 25 modes contribute to the total field at $f \leq 1000$ MHz and $d_{at} \leq 2$ m. It is not possible to compute so many modes due to the limitations mentioned above. With the following method the absolutely needed minimum KK is evaluated:

Program PANB offers for p_1 = vertical and horizontal a table denoted as "Einfluss der Anzahl der berücksichtigten Modi auf E^{tot}" (see Appendix 16.2.3.) For each test segment the values for ERTOT,EPTOT and ETTOT are listed for the azimuthal angles ϕ = 0, 90 and 180^0 as the summation from the modes 0 to M, where $0 \leq M \leq$ (KK-1). In each column one checks first if the (KK-1) result is $>10^{-3}$ and if the (KK-2) result differs not more than ±1%. Then one chooses that result in the column which is not more than ±5 % different from the (KK-1) result and notes the corresponding minimum M.

TABLE 65 shows the evaluation of the minimum mode number from the data in Appendix 16.2.3. for the actual frequency 164 MHz and for 5 % relative accuracy.

TEST SEGMENT No.	d_{at} [m]	ERTOT-comp.at 0° M	90° M	180° M	EPTOT-comp.at 0° M	90° M	180° M	ETTOT-comp.at 0° M	90° M	180° M	Recommended KK (M+1)
1	0.08	3	1	3	0	3	(3)	1	2	3	$\geq$ 4
2	0.13	2	2	3	0	3	(3)	2	2	2	$\geq$ 4
3	0.18	3	4	3	0	3	(4)	2	2	3	$\geq$ 4
4	0.28	3	4	4	0	3	(4)	3	3	3	$\geq$ 5
5	0.38	3	2	4	0	3	(4)	4	3	4	$\geq$ 5
6	0.53	4	4	4	0	3	(4)	4	4	4	$\geq$ 5
7	0.68	4	4	5	0	5	(5)	4	4	6	$\geq$ 7
8	0.83	6	5	6	0	5	(6)	5	4	6	$\geq$ 7
9	1.03	7	6	6	0	7	(7)	6	6	7	$\geq$ 8

TABLE 65 Determination of the minimum mode number KK for 5 % relative accuracy at 9 d_{at}'s at the actual frequency 164 MHz and model MANMOD 2.

In general it is sufficient to monitor the results at $\phi = 180°$. In the example in TABLE 65 (164 MHz, p_1 = vertical, $\theta_i = 80.8°$) the horizontal component EPTOT is very small (10^{-7}) so that those differences are of little meaning. Very roughly the minimum KK increases linarly with d_{at} and frequency. The computational data in section 10.4. at d_{at} from 0.1 to 0.4 m were computed with the NN and KK listed in TABLE 66, checked according to TABLE 65 at a 2% level below 300 MHz and 5% level above 300 MHz.

FREQUENCY RANGE	MAXIMUM NN in HARRA		SELECTED KK in PANB	
1 to 30 MHz	4	ok	5	ok
50 to 100 MHz	5	ok	6	ok
101 to 200 MHz	7	ok	8	ok
250 to 300 MHz	9	ok	10	ok
350 to 500 MHz	10	∿ok	11	∿ok
600 to 800 MHz	12	(?)	13	(?)

TABLE 66 Mode number NN and KK versus frequency at d_{at} from 0.1 to 0.4 m. At frequencies below 500 MHz the relative accuracy is better than 5 % , the absolute accuracy (FSL = 100 %) is better than 0.2 % .

10.3.4.2. DIFFERENCE BETWEEN THE TWO AZIMUTHAL FIELD COMPONENTS

Program PANB computed the azimuthal field components EPH twice (for E^{inc}, E^{scat} and E^{tot}, for $\phi = 0^o$), first for IT = 1 (test segment oriented along the $\vec{a}_r$-vector) and then for IT = 2 (test segment oriented along the $\vec{a}_\phi$-vector) for both incident polarizations ETHETA INC (p_2 = vertical) and EPHI INC (p_2 = horizontal). The results are listed after the output of the body contour (see Appendix 16.2.3.) as follows:

θ SIG θθ MAG Sθθ SIG ϕϕ MAG Sϕϕ MODE NN = 0

RTEST = 1.7500 ZTEST = 10.0000 DTEST = 0.2000

EINC ETHETA INC
ERAD(x,x), EPH (x,x), ETH(x,x), EPH (x,x)
ESCAT ETHETA INC
ERAD(x,x), EPH (x,x), ETH(x,x), EPH (x,x)
ETOT ETHETA INC
ERAD(x,x), EPH (x,x), ETH(x,x), EPH (x,x)

etc. for EPHI INC

RTEST = 2.2500 ZTEST = 10.0000 DTEST = 0.2000

etc. for all RTEST up to

RTEST = 11.2500 ZTEST = 10.0000 DTEST = 0.2000

and the same output is now repeated for all modes up to MODE NN = 7

The data in Appendix 16.2.3. were used as an indicator for the computational accuracy. The results, obtained with the following method, are listed in TABLE 67 :

EPH1 = first EPH (IT = 1), EPH2 = second EPH (IT = 2),
Data from ETOT and ETHETA INC (E^{tot} and p_1 = vertical) (245)

$$\text{Error in } {}^o/oo = \left| |EPH1| - |EPH2| \right| \cdot 1000\, E_0 \qquad (246)$$

The results in TABLE 67 are therefore related to the free-space level = 1000 ^{o}/oo = 0 dB. Generally, the error increases with decreasing dat, and the first modes determine the final accuracy. Below 500 MHz an increase of the error could not be noticed depending on the frequency . In normal conditions (see next section) the total error is well below 1 %.

TEST SEGMENT No.	d_{at} [m]	Difference between the two EPH in $^{0}/oo$ at 164 MHz. Mode: NN = 0	NN = 1	NN = 2	NN = 3	NN = 4	NN = 5	NN = 6	NN = 7
1	0.08	0	1.926	0.257	0.029	0.016	<0.03	~ 0	~ 0
2	0.13	0	0.273	0.103	0.045	0.021	~ 0	~ 0	~ 0
3	0.18	0	0.011	0.065	0.041	0.024	~ 0	~ 0	~ 0
4	0.28	0	0.061	0.060	0.024	<0.03	~ 0	~ 0	~ 0
5	0.38	0	0.053	0.047	0.012	~ 0	~ 0	~ 0	~ 0
6	0.53	0	0.034	0.036	<0.03	~ 0	~ 0	~ 0	~ 0
7	0.68	0	0.029	0.017	~ 0	~ 0	~ 0	~ 0	~ 0
8	0.83	0	0.026	<0.03	~ 0	~ 0	~ 0	~ 0	~ 0
9	1.03	0	<0.03	~ 0	~ 0	~ 0	~ 0	~ 0	~ 0

TABLE 67 Computational error in $^{0}/oo$ versus mode number NN and versus d_{at} at the actual frequency 164 MHz and model MANMOD 2 .

Considering the results in TABLE 67 one could conclude that the computational accuracy is satisfactory for all applications, but this is not absolutely true. The exceptions are mentioned in 10.3.4.3..

10.3.4.3. DIFFERENCE BETWEEN RESULTS AT DIFFERENT TEST SEGMENT LENGTHS

Due to the approximation method by BEVENSEE [10] (see description in 6.4. 5.1. and program limitations in 10.3.1.) problems may occur at some few frequencies at small d_{at}. Without checking carefully the result according to the method in 10.3.4.2. the computational error had to be specified to about 10 %. With the following method inaccurate results can be detected easily:

All computations are performed twice, first with a test segment length of 0.08 m (DTEST = 0.2) and second with 0.2 m (DTEST = 0.5). The results of the test points are plotted versus the frequency (all results in section 10.4. contain the computational data from both test segments). At some arbitrary frequencies discrepancies occur between the two results (see FIGURE 80,82). If the difference exceeds 1 dB, the results are checked according to 10.3.4.2.. Up to now the inaccuracy was always manifested by a large EPH difference, in all of the 11 problematic cases of about 100 complete near-field computations. The computations are repeated at a new frequency, differing from the "disturbed" frequency by about 2 %. There is no strict rule to prevent "disturbed" frequencies, but d_{at}'s below 0.2 m , frequencies above 300 MHz and complicated body shapes are risk factors.

10.3.5. FIELD HOMOGENEITY AROUND A NEAR FIELD POINT

10.3.5.1. SIGNIFICANCE OF THE FIELD HOMOGENEITY AND COMPUTATIONAL DATA

The body-mounted antenna A_1 is not infinitesimally small. Thus, the induced voltage at the anntenna terminals (receiving case) depends generally not only on the field at the (computed) antenna center, but also on the field along the antenna axis. The study in section 5.2.2. concluded in the statements:

If the amount of the E-field can be described by a polynome of second degree and if the phase of the E-field changes monotonously along the antenna axis, the logarithmic difference ΔU (i.e., the ratio induced voltage from center field / induced voltage from actual field , see 5.2.2.) is less than 1 dB, if the following conditions are fulfilled:

δE =	variation of the amount of the E-field along the antenna axis in direction of the regarded p_1	< 10 dB	(37)
$\delta\Phi$ =	phase variation of the E-field along the antenna axis in direction of the regarded p1	< 71 °	(38)

In section 10.2.5. the near-field data along the p_1-axis vertical, radial and horizontal were computed at the center and at the ends of a dipole antenna of the length 2h = 0.1 m, with test segment lengths of 0.08 m. The test segments at +h and -h are separated by a gap of 0.02 m, so that oscillations (if existing) can be detected without computational artifacts which may occur at smaller test segments (10.3.1.). The quantities ΔU,δE and δΦ were computed for d_{at} = 0.1 m, h_B = 1.0 m, θ_i = 80.8° and for the body model FZYL at several frequencies (see TABLE 68, 69 and the results in Appendix 16.2.4.).

The computational results confirm the validity of equation (37) and (38). At p_1 = vertical and radial the δE and δΦ are below the critical level and thus ΔU remains smaller than 1 dB. With p_1, p_2 = horizontal the antenna A_1 is oriented perpendicular to the E^{tot} wavefront at about ϕ = 80 to 100°, resulting in large phase changes and thus large ΔU. The significant data of the homogeneity investigation are summarized in TABLE 70 for the frequencies 65, 75, 100, 125, 150, 300 and 425 MHz.

A Z I M U T H A L R A D I A T I O N P A T T E R N F R E Q U E N C Y 150 M H Z

HOMOGENEITY CHECK OF THE FIELD ALONG A 0.1 METER DIPOLE ANTENNA

TESTBODY: ROT.SYM.CYLINDER
AXIAL LENGTH = 1.80 M
DIAMETER = .25 M

FIELD POINT
DAT = .10 M
HB =1.00 M

INCIDENT WAVE
POLAR. = VERTICAL
THETA = 80.8 DEG

PHI	VERTICAL POLARIZED ANTENNA					RADIAL POLARIZED ANTENNA				
	GAIN CENTER	PHASE CENTER	MEAN ERROR	MAXIMUM GAINVAR	MAXIMUM PHASEVAR	GAIN CENTER	PHASE CENTER	MEAN ERROR	MAXIMUM GAINVAR	MAXIMUM PHASEVAR
DEG	DB	DEG	DB	DB	DEG	DB	DEG	DB	DB	DEG
0	-3.6	151.9	.00	.4	2.8	1.4	40.8	-.26	4.1	.2
5	-3.6	152.0	.00	.4	2.8	1.4	40.8	-.25	4.1	.2
10	-3.7	152.4	.00	.4	2.7	1.4	40.9	-.25	4.1	.1
15	-3.7	153.2	.00	.4	2.7	1.4	41.1	-.25	4.1	.0
20	-3.9	154.2	.00	.4	2.6	1.3	41.3	-.25	4.1	.2
25	-4.0	155.4	.00	.4	2.5	1.3	41.6	-.25	4.1	.4
30	-4.1	157.0	.00	.4	2.3	1.2	41.9	-.25	4.1	.7
35	-4.3	158.8	.00	.4	2.1	1.2	42.3	-.24	4.0	.9
40	-4.6	160.8	.00	.4	1.9	1.1	42.7	-.24	4.0	1.2
45	-4.8	163.1	.00	.4	1.7	1.1	43.0	-.23	4.0	1.5
50	-5.1	165.7	.00	.4	1.5	1.0	43.4	-.23	4.0	1.8
55	-5.4	168.5	.00	.3	1.2	.9	43.8	-.23	4.0	2.1
60	-5.8	171.5	.00	.3	.9	.8	44.1	-.22	3.9	2.4
65	-6.2	174.8	.00	.3	.7	.7	44.4	-.22	3.9	2.6
70	-6.6	178.3	.00	.3	.4	.6	44.7	-.22	4.0	2.8
75	-7.1	-178.0	.00	.3	.0	.5	44.8	-.21	4.0	3.0
80	-7.6	-174.0	.00	.2	.3	.4	44.9	-.21	4.0	3.0
85	-8.2	-169.8	.00	.2	.6	.3	44.8	-.21	4.0	3.0
90	-8.8	-165.3	.00	.1	.9	.1	44.7	-.21	4.0	2.9
95	-9.5	-160.5	.00	.1	1.2	.0	44.5	-.21	4.0	2.8
100	-10.2	-155.3	.00	.0	1.4	-.1	44.2	-.21	4.1	2.5
105	-10.9	-149.8	-.00	.1	1.7	-.2	43.7	-.21	4.1	2.2
110	-11.6	-143.9	-.00	.2	1.8	-.3	43.2	-.21	4.1	1.7
115	-12.4	-137.4	-.00	.3	1.9	-.3	42.6	-.21	4.1	1.3
120	-13.2	-130.4	-.00	.4	1.9	-.4	42.0	-.21	4.1	.8
125	-13.9	-122.9	-.00	.5	1.7	-.4	41.4	-.21	4.1	.3
130	-14.6	-114.9	-.01	.6	1.3	-.5	40.7	-.21	4.1	.2
135	-15.2	-106.6	-.01	.7	.8	-.5	40.0	-.22	4.1	.7
140	-15.6	-98.1	-.01	.8	.1	-.5	39.4	-.22	4.0	1.2
145	-15.9	-89.9	-.01	.8	.6	-.5	38.8	-.22	4.0	1.6
150	-16.1	-82.3	-.01	.9	1.3	-.5	38.3	-.22	4.0	1.9
155	-16.2	-75.5	-.01	.9	2.0	-.5	37.8	-.23	3.9	2.2
160	-16.2	-69.8	-.01	.8	2.5	-.5	37.4	-.23	3.9	2.4
165	-16.2	-65.4	-.01	.8	2.8	-.5	37.1	-.23	3.9	2.6
170	-16.1	-62.2	-.01	.8	3.1	-.5	36.9	-.23	3.9	2.7
175	-16.1	-60.3	-.01	.8	3.2	-.5	36.8	-.23	3.9	2.8
180	-16.1	-59.7	-.01	.8	3.3	-.5	36.7	-.23	3.9	2.8

TABLE 68 Field homogeneity at 150 MHz at $d_{at} = 0.1$ m and p_2 = vertical. Left: p_1 = vertical, right: p_1 = radial; dB-values related to 0 dB = FSL. Gain center: $Gain_B$ [dB], Phase center: phase Φ [^{o}], Mean error: ΔU [dB], Maximum gainvar: δE [dB], Maximum phasevar: $\delta\Phi$ [^{o}].

A Z I M U T H A L R A D I A T I O N P A T T E R N F R E Q U E N C Y 150 M H Z

HOMOGENEITY CHECK OF THE FIELD ALONG A 0.1 METER DIPOLE ANTENNA

TESTBODY: ROT.SYM.CYLINDER
AXIAL LENGTH = 1.80 M
DIAMETER = .25 M

FIELD POINT
DAT = .10 M
HB =1.00 M

INCIDENT WAVE
POLAR. = HORIZONTAL
THETA = 80.8 DEG

PHI DEG	HORIZONTAL POLARIZED ANTENNA GAIN CENTER DB	PHASE CENTER DEG	MEAN ERROR DB	MAXIMUM GAINVAR DB	MAXIMUM PHASEVAR DEG	RADIAL POLARIZED ANTENNA GAIN CENTER DB	PHASE CENTER DEG	MEAN ERROR DB	MAXIMUM GAINVAR DB	MAXIMUM PHASEVAR DEG
0	-4.7	16.8	.10	0.0	0.0	*****	******	*****	*****	******
5	-4.7	17.1	.10	.4	2.6	-19.4	36.2	-.18	2.7	17.1
10	-4.8	17.9	.10	.8	5.2	-13.4	36.6	-.18	2.7	16.8
15	-5.0	19.1	.09	1.2	7.9	-9.9	37.2	-.18	2.6	16.5
20	-5.3	20.9	.09	1.6	10.5	-7.4	38.1	-.18	2.6	16.0
25	-5.7	23.3	.08	2.0	13.2	-5.5	39.3	-.18	2.6	15.4
30	-6.1	26.1	.08	2.5	15.9	-4.0	40.7	-.18	2.6	14.6
35	-6.6	29.5	.07	3.0	18.8	-2.8	42.3	-.18	2.5	13.8
40	-7.2	33.5	.07	3.5	21.7	-1.8	44.1	-.17	2.5	12.8
45	-8.0	38.0	.06	4.1	24.8	-.9	46.1	-.17	2.5	11.8
50	-8.8	43.2	.05	4.8	28.4	-.1	48.3	-.17	2.4	10.7
55	-9.8	49.0	.04	5.6	32.6	.6	50.6	-.17	2.4	9.5
60	-11.0	55.8	.03	6.6	38.1	1.1	53.0	-.17	2.3	8.2
65	-12.3	63.6	.00	7.9	46.2	1.6	55.6	-.17	2.3	6.9
70	-13.9	73.1	-.07	9.4	59.5	2.0	58.2	-.17	2.3	5.5
75	-15.9	85.3	-.28	10.5	82.8	2.3	60.9	-.17	2.2	4.2
80	-18.1	102.5	-.89	8.9	116.6	2.5	63.7	-.17	2.2	2.8
85	-20.3	128.7	-1.96	4.1	142.9	2.7	66.5	-.17	2.2	1.4
90	-21.0	164.7	-2.44	1.6	149.0	2.8	69.3	-.17	2.1	.0
95	-19.3	-162.4	-1.61	7.2	134.2	2.8	72.1	-.17	2.1	1.4
100	-16.8	-140.5	-.69	11.1	101.8	2.7	74.8	-.17	2.1	2.7
105	-14.4	-125.9	-.26	11.3	70.4	2.6	77.5	-.17	2.1	4.0
110	-12.4	-115.4	-.10	9.8	51.2	2.4	80.1	-.17	2.1	5.3
115	-10.8	-107.1	-.03	8.2	40.1	2.2	82.6	-.17	2.1	6.6
120	-9.3	-100.3	.01	7.0	33.0	1.8	85.0	-.17	2.1	7.7
125	-8.1	-94.5	.03	5.9	28.1	1.3	87.3	-.17	2.1	8.8
130	-7.1	-89.4	.05	5.1	24.2	.8	89.5	-.17	2.1	9.9
135	-6.2	-85.1	.06	4.4	21.0	.1	91.4	-.17	2.1	10.9
140	-5.4	-81.2	.07	3.7	18.2	-.7	93.3	-.17	2.1	11.8
145	-4.7	-77.9	.08	3.1	15.6	-1.7	94.9	-.17	2.1	12.5
150	-4.2	-75.1	.08	2.6	13.2	-2.9	96.3	-.17	2.1	13.3
155	-3.7	-72.8	.09	2.1	10.9	-4.3	97.5	-.17	2.1	13.9
160	-3.4	-70.9	.09	1.7	8.7	-6.1	98.6	-.17	2.1	14.4
165	-3.1	-69.4	.10	1.2	6.5	-8.6	99.4	-.17	2.1	14.8
170	-2.9	-68.3	.10	.8	4.3	-12.0	99.9	-.17	2.1	15.0
175	-2.8	-67.7	.10	.4	2.1	-18.0	100.3	-.18	2.1	15.2
180	-2.7	-67.5	.10	0.0	0.0	*****	******	*****	*****	******

TABLE 69 Field homogeneity at 150 MHz at $d_{at} = 0.1$ m and p_2 = horizontal. Left: p_1 = horizontal, right: p_1 = radial; dB-values related to 0 dB = FSL. Gain center : $Gain_B$ [dB]. Phase center: phase Φ [°], Mean error: ΔU [dB], Maximum gainvar: δE [dB], Maximum phasevar: $\delta\Phi$ [°].

The maximum ratings of the computed field homogeneity parameters are listed in TABLE 70 :

FRE-QUEN-CY [MHz]	Maximum ratings p_2 = VERTICAL						Maximum ratings p_2 = HORIZONTAL					
	p_1 = VERTICAL			p_1 = RADIAL			p_1 = HORIZONTAL			p_1 = RADIAL		
	ΔU [dB]	δE [dB]	δΦ [°]	ΔU [dB]	δE [dB]	δΦ [°]	ΔU [dB]	δE [dB]	δΦ [°]	ΔU [dB]	δE [dB]	δΦ [°]
65	0.1	1.0	10	0.3	4.5	4	8.7	29.9	200	0.2	2.1	7
75	0.2	3.8	18	0.3	4.3	2	7.6	25.0	194	0.2	2.1	8
100	0.0	1.3	3	0.3	4.5	2	5.4	18.1	180	0.2	2.3	11
125	0.0	1.9	5	0.4	4.5	3	3.7	13.5	165	0.2	2.5	14
150	0.0	0.8	3	0.3	4.1	3	2.4	11.3	149	0.2	2.7	17
300	0.0	1.2	8	0.5	5.1	31	>10	>20	222	0.3	2.2	45
425	0.1	1.7	19	1.0	5.9	65	3.1	13.3	100	0.3	2.3	50

TABLE 70 Maximum ratings from the field homogeneity computations. The data concern the model FZYL with the antenna position d_{at} = 0.1 m and h_B = 1.0 m, related to a 2h = 0.1 m dipole antenna A_1.

The field homogeneity is satisfactory except for p_1 = p_2 = horizontal which is not suited for omnidirectional transmission. From the data in TABLE 70 one can conclude that all further computations have only to be performed for the center test point which is representative for the field around the test point, if d_{at} is larger than 0.1 m and if the frequency is below 500 MHz.

10.3.5.2. COMPUTATIONAL DATA FOR ANTENNA DESIGN

With the knowledge of the amplitude- and especially the phase conditions along a certain antenna axis the design of radiation systems become possible which perform better than an usual antenna in the proximity to a body. If we look at TABLE 68 at p_1 = radial we notice a field amplification effect produced by the body. There is strong radial field around the body, differing only from +1.4 to -0.5 dB at $0 < \phi < 180^o$. The δE and the δΦ are within reasonable limits (4 dB and 3^o), so that an excellent antenna with omnidirectional radiation characteristics could be designed. In the following study the near-field data are discussed and compared with experimental data; a special radial antenna will be shown in 13.3.3..

Leer - Vide - Empty

10.4. RESULTS FROM THREE-DIMENSIONAL COMPUTATIONS ON ANTENNA-BODY MODELS

10.4.1. OVERVIEW OF INVESTIGATED PARAMETERS AND EXPLANATIONS

In the following sections the influence of certain parameters on the near-field will be demonstrated by computer plots. Unless otherwise specified, the regarded body model is the finite conducting cylinder (FZYL), the irradiation angle ϕ amounts to 80.8^o, p_2 is vertical (E_θ^{inc}) and the relative antenna height h_B is 1.0 m. The field data are related to the free-space level FSL = 0 dB and specify the E-field in dB in direction of the investigated polarization axis p_1 = vertical, radial or horizontal.

The computations were performed according to section 10.2. and 10.3., and the results were checked according to 10.3.4.. The accuracy of the following data is better than ±1 %, corresponding to ±1 dB at signal levels above - 21 dB, at frequencies from 10 to 500 MHz. All data have been computed with two different test segment lengths (0.08 m and 0.2 m, actual scale) and generally both results are plotted, as can be noticed by the thicker or double lines in the plots. The accuracy of the frequencies above 500 MHz is in the region of 5 % F.S. and was not further investigated, because the previous computational model presented in section 7. covers the frequency range from 200 to 1000 MHz, and because the interesting effects occur below 500 MHz. In addition, more accurate computations above 500 MHz are prohibitive due to storage and computational time limitations (see limitations in section 10.3.2. and 10.3.3.).

The following sections treat the specific effects:

- 10.4.2. Effect of the frequency on vertical and radial field
- 10.4.3. Effect of the antenna-body distance
- 10.4.4. Effect of the azimuthal angle
- 10.4.5. Effect of the irradiation angle
- 10.4.6. Effect of the relative antenna height
- 10.4.7. Effect of the frequency on the azimuthal radiation patterns
- 10.4.8. Effect of the frequency on the directive radiation patterns
- 10.4.9. Effect of different body shapes on the fields in the shadow zone
- 10.4.10. Effect of different body shapes on azimuthal radiation patterns

10.4.2. EFFECT OF THE FREQUENCY ON VERTICAL AND RADIAL FIELD

FIGURE 71 provides a first impression. The $Gain_B$ data are shown for 4 d_{at}'s of 0.1, 0.2, 0.3 and 0.4 m in the shadow zone ϕ = 180^o at p_1,p_2 = vertical.

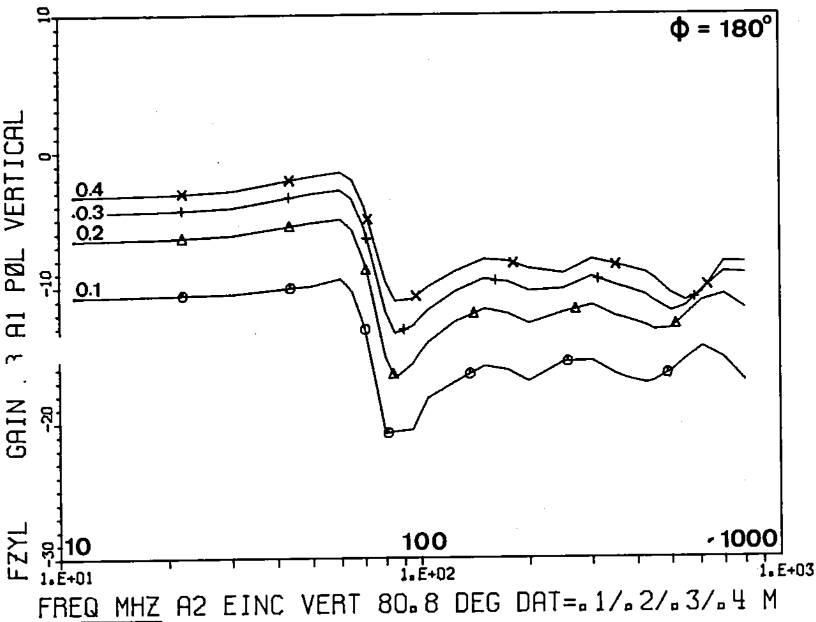

FIGURE 71 Vertical field component E_V versus frequency, parameter d_{at}.

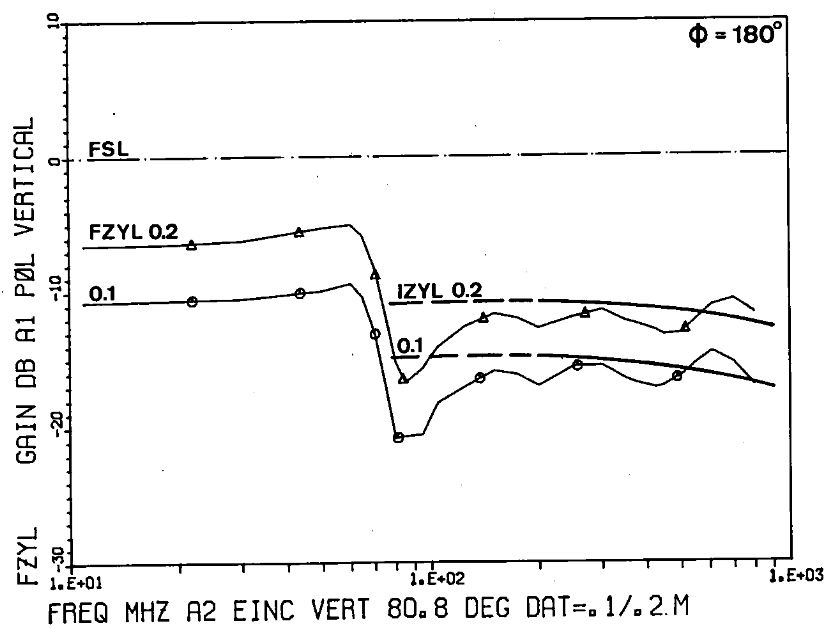

FIGURE 72 Comparison between IZYL and FZYL computation (same parameters).

Unless otherwise specified one always considers the E-field components E_v, E_r and E_h in the shadow region $\phi = 180^o$. In FIGURE 71 one distinguishes 5 frequency regions similar to those noticed in the experiments in section 9.

- < $\lambda/2$ below resonance at frequencies below 50 MHz
- $\lambda/2$ first resonance at about 65 MHz
- 3 $\lambda/4$ anti-resonance at about 80 to 110 MHz
- λ second resonance at about 140 MHz
- > λ off-resonance at frequencies above 200 MHz

If we compare the FZYL results with the previous IZYL results in FIGURE 72 one observes an oscillation of the FZYL data around the IZYL data with an amplitude of maximum 2.5 dB at frequencies above 200 MHz. This means that both computational methods agree at higher frequencies. From the practical point of view this agreement is disappointing for two reasons: first, there is no theoretical chance to operate with vertical polarized antennas above 75 MHz due to the high transmission losses, second, the experimental data do not agree with the computational data below 150 MHz.

Fortunately, an astonishing radial field effect occurs in the resonance region which provides new hope for both application and experiment :

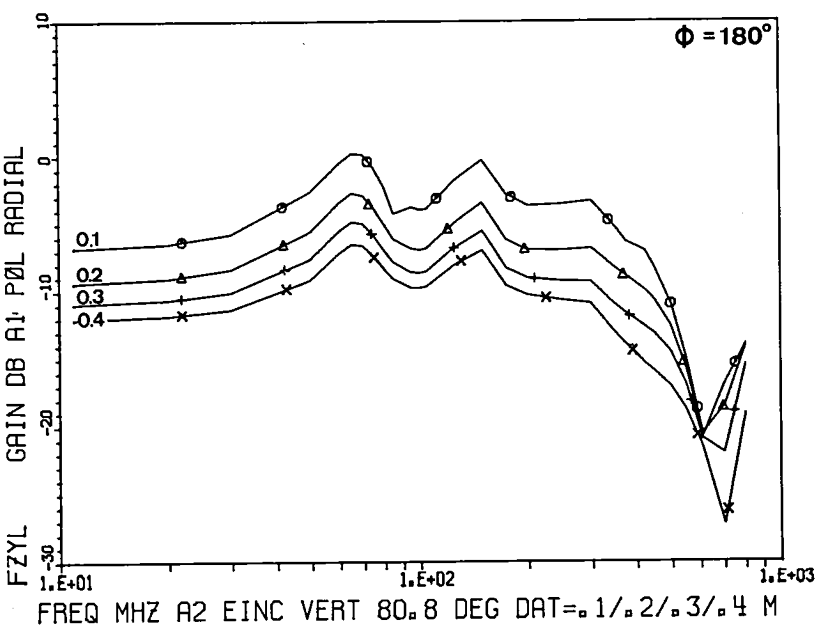

FIGURE 73 Radial field component E_r versus frequency f, parameter d_{at}.

As can be seen in FIGURE 73 a radial field component E_r is developed at frequencies from about 40 to 300 MHz, caused by a vertical polarized incident wave and the body. In the proximity to the body this E_r is very strong (-4 to 0 dB at $d_{at} = 0.1$ m) and decreases with increasing d_{at}. Below 30 MHz the E_r is small (< -12 dB at $d_{at} > 0.3$ m) and above 500 MHz the E_r is extremely small (< - 16 dB at d_{at} > 0.3 m). The significance of the strong E_r is demonstrated in the next section.

10.4.3. EFFECT OF THE ANTENNA-BODY DISTANCE

Let us consider first the vertical (E_v) and radial (E_r) field component within the resonance region at 150 MHz and at $\phi = 0^o$ (irradiated zone) and at $\phi = 180^o$ (shadow zone). FIGURE 74 shows the dependence of the field components from the antenna-body distance d_{at} :

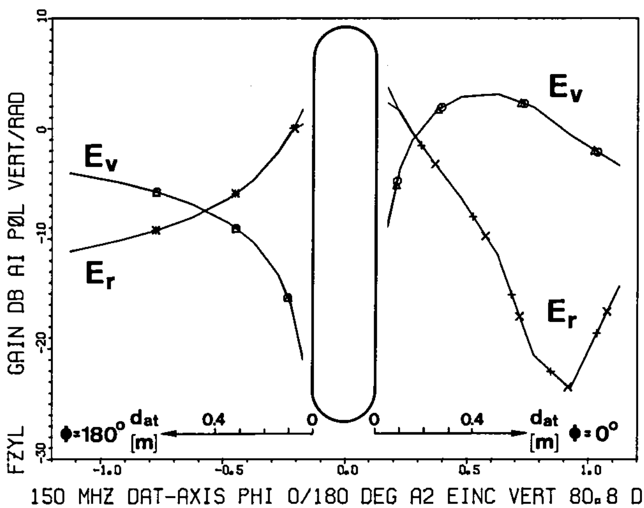

FIGURE 74 Vertical (E_v) and radial (E_r) field component versus d_{at}.
Parameter: E_v and E_r at A_1 at $\phi = 180^o$ (left) and 0^o (right)
Constant : frequency = 150 MHz, p_2 = vertical, θ_i = 80.8^o, h_B = 1.0 m

At $\phi = 0^o$ the E_r becomes larger than E_v at $d_{at} < 0.15$ m and at $d_{at} = 0.05$ m E_r is about 12 dB larger than E_v. The situation is even more extreme at $\phi = 180^o$; the E_r becomes larger than E_v at $d_{at} < 0.42$ m and at $d_{at} = 0.05$ m E_r is about 22 dB larger than E_v! This effect explains the discrepancy of the experimental results at small d_{at}, because the transverse sensitivity of a probe antenna A_1 is rarely below -15 dB. It is not possible to measure an E_v of only -20 dB, if there is also an E_r of about 0 dB.

10.4.4. EFFECT OF THE AZIMUTHAL ANGLE

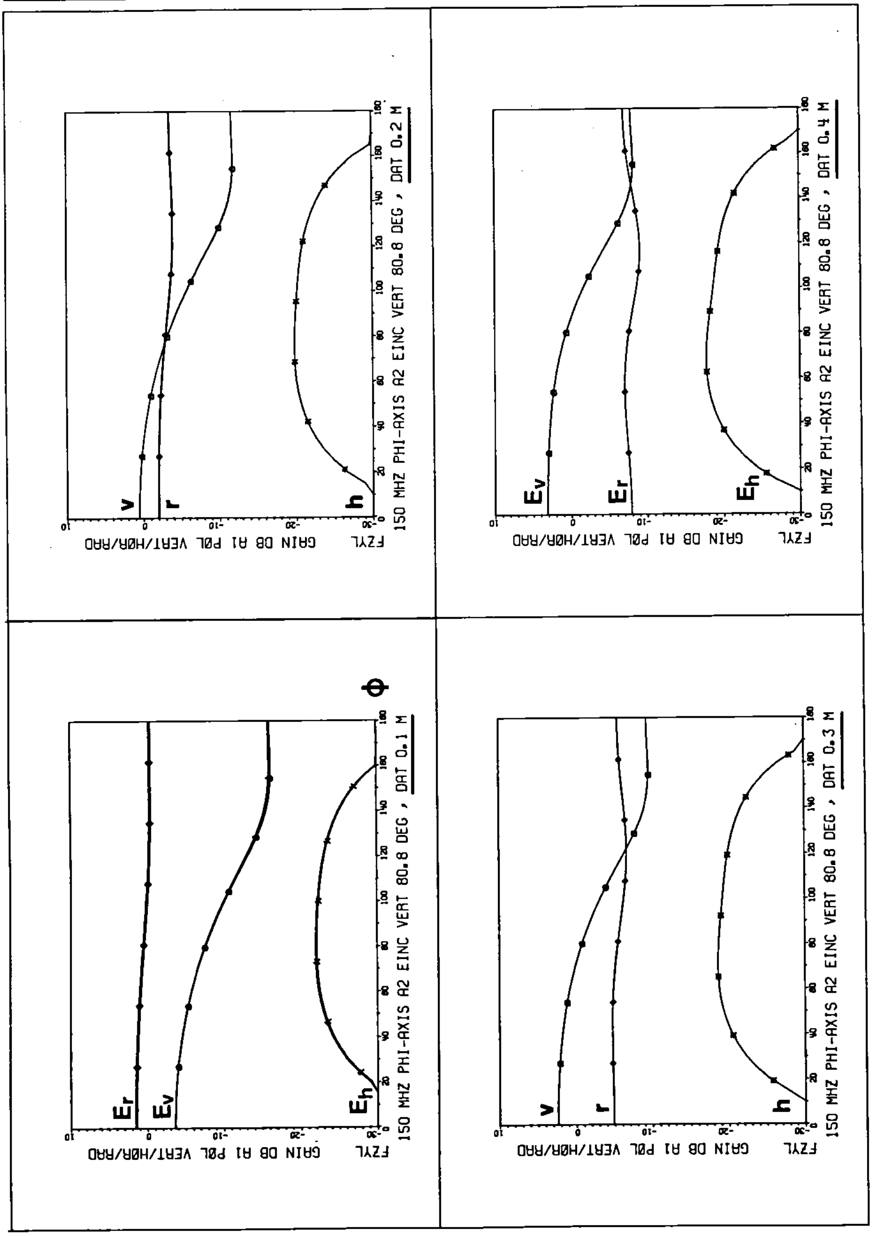

FIGURE 75 Vertical (E_v),radial (E_r) and horizontal (E_h) field components versus azimuthal angle ϕ. Parameter: E_v,E_r,E_h and d_{at} = 0.1,0.2,0.3,0.4 m. Constant: frequency = 150 MHz, p_2 = vertical, θ_i = 80.8°, h_B = 1.0 m. The E_r component is almost constant throughout the full ϕ = 0-180° range.

10.4.5. EFFECT OF THE IRRADIATION ANGLE

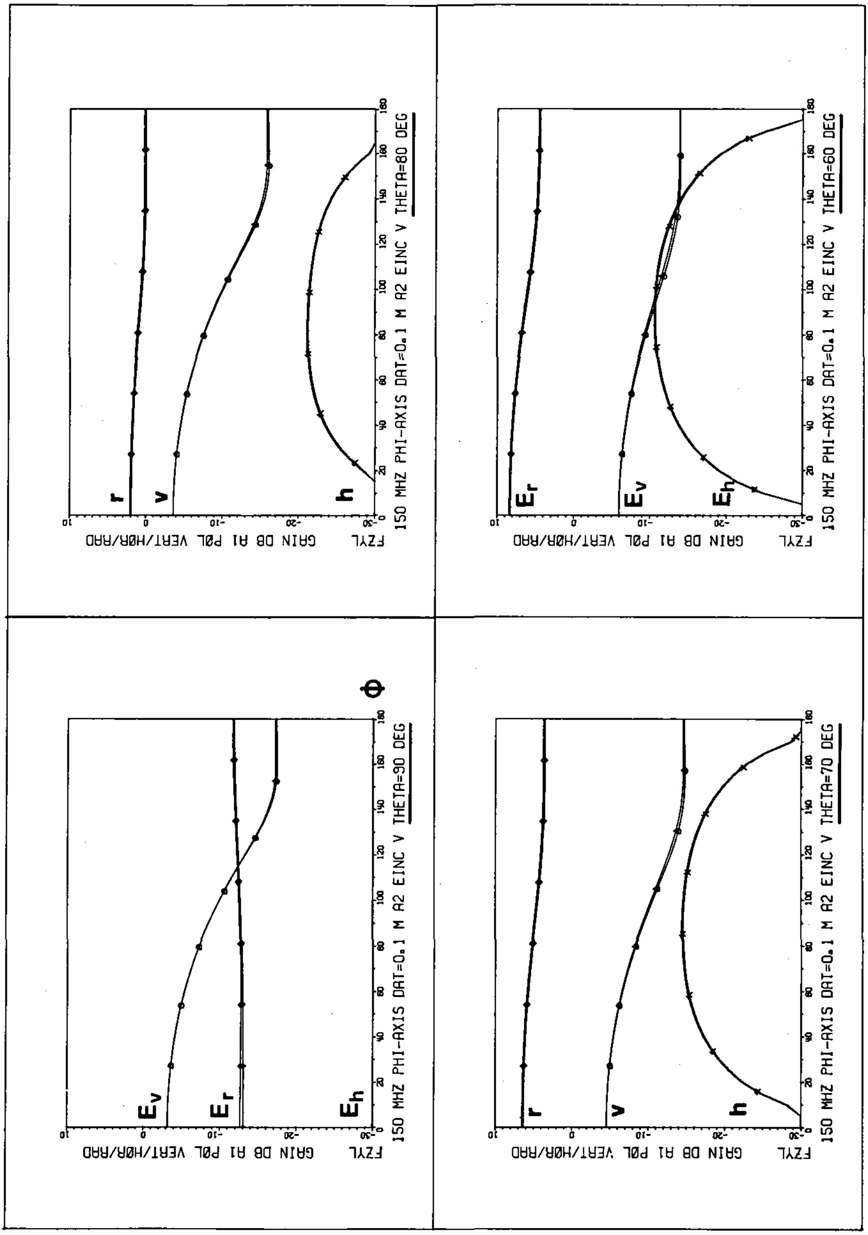

FIGURE 76 Vertical (E_v), radial (E_r) and horizontal (E_h) field components at constant $d_{at} = 0.1$ m versus ϕ for different irradiation angles $\theta_i = 90, 80, 70$ and 60^o. Constant: f = 150 MHz, p_2 = vertical, $h_B = 1.0$ m. E_r increases with decreasing θ_i, E_v remains about constant, E_h disappears at $\theta_i = 90^o$.

10.4.6. EFFECT OF THE RELATIVE ANTENNA HEIGHT

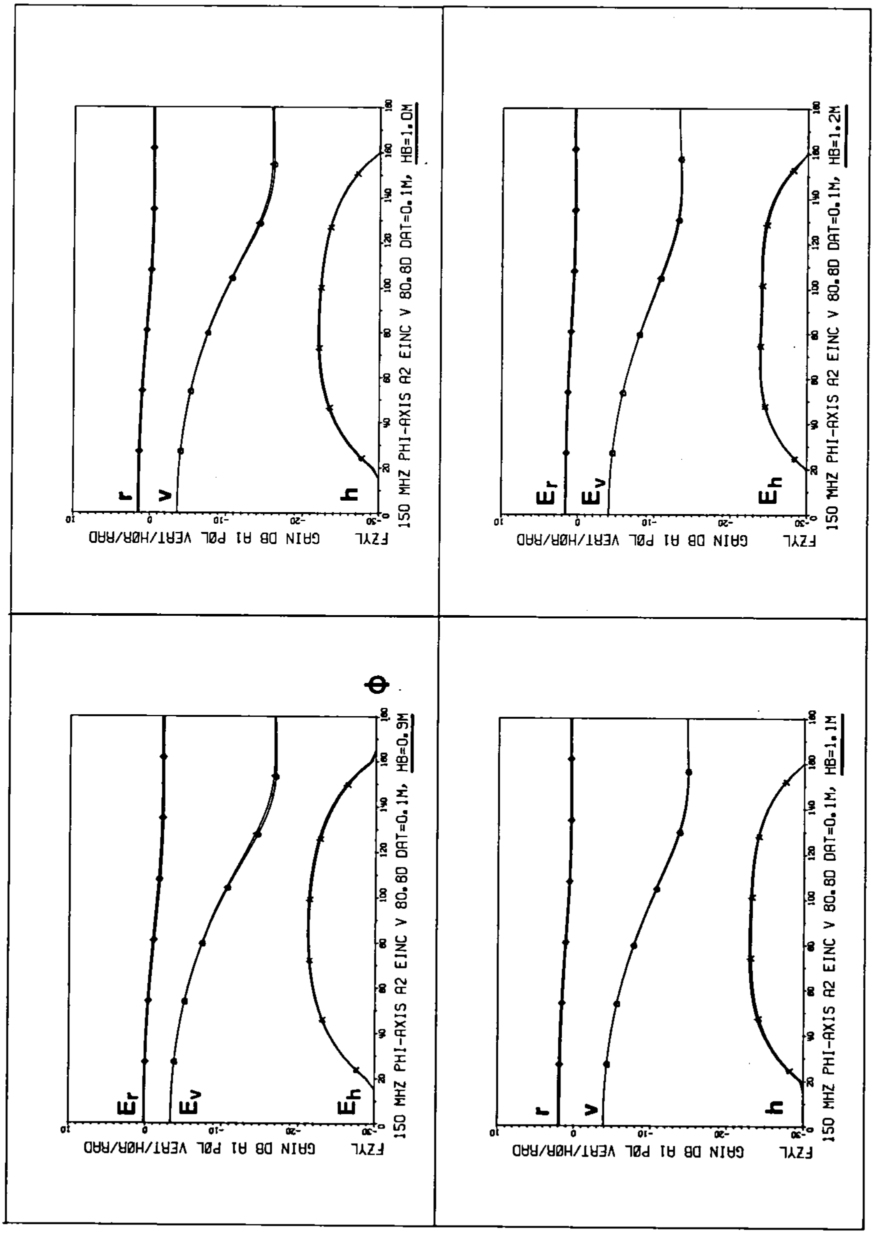

FIGURE 77 Vertical (E_v), radial (E_r) and horizontal (E_h) field components at constant d_{at} = 0.1 m versus ϕ for different relative antenna heights h_B=0.9, 1.0, 1.1 and 1.2 m. Constant: f = 150 MHz, p_2 = vertical, θ_i = 80.8°. Even at h_B = 0.9 (body center) all field components are only little influenced by h_B.

10.4.7. EFFECT OF THE FREQUENCY ON THE AZIMUTHAL RADIATION PATTERN

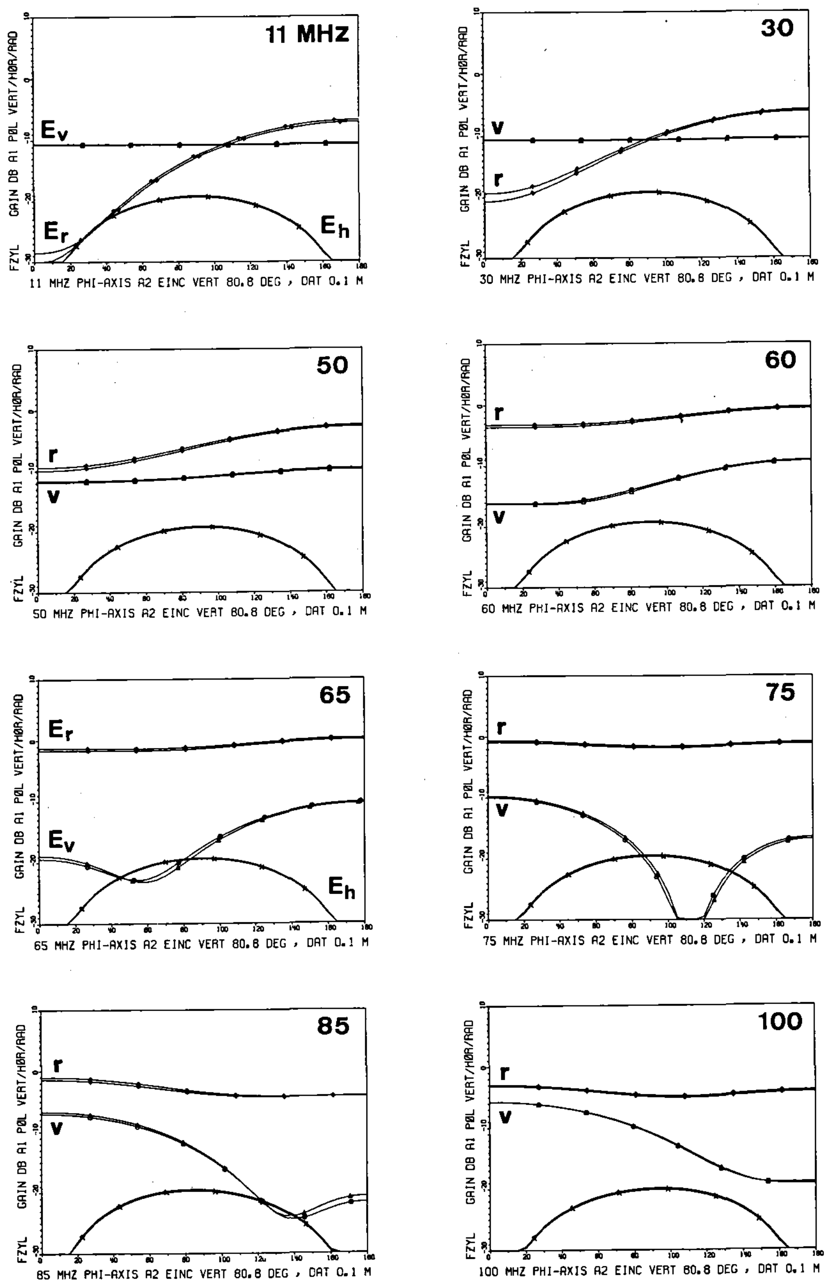

FIGURE 77a Field components E_v, E_r and E_h versus ϕ with the parameter f 11 to 100 MHz. Constant: d_{at} = 0.1 m, p2 = vertical, θ_i = 80.8°, h_B = 1.0 m .

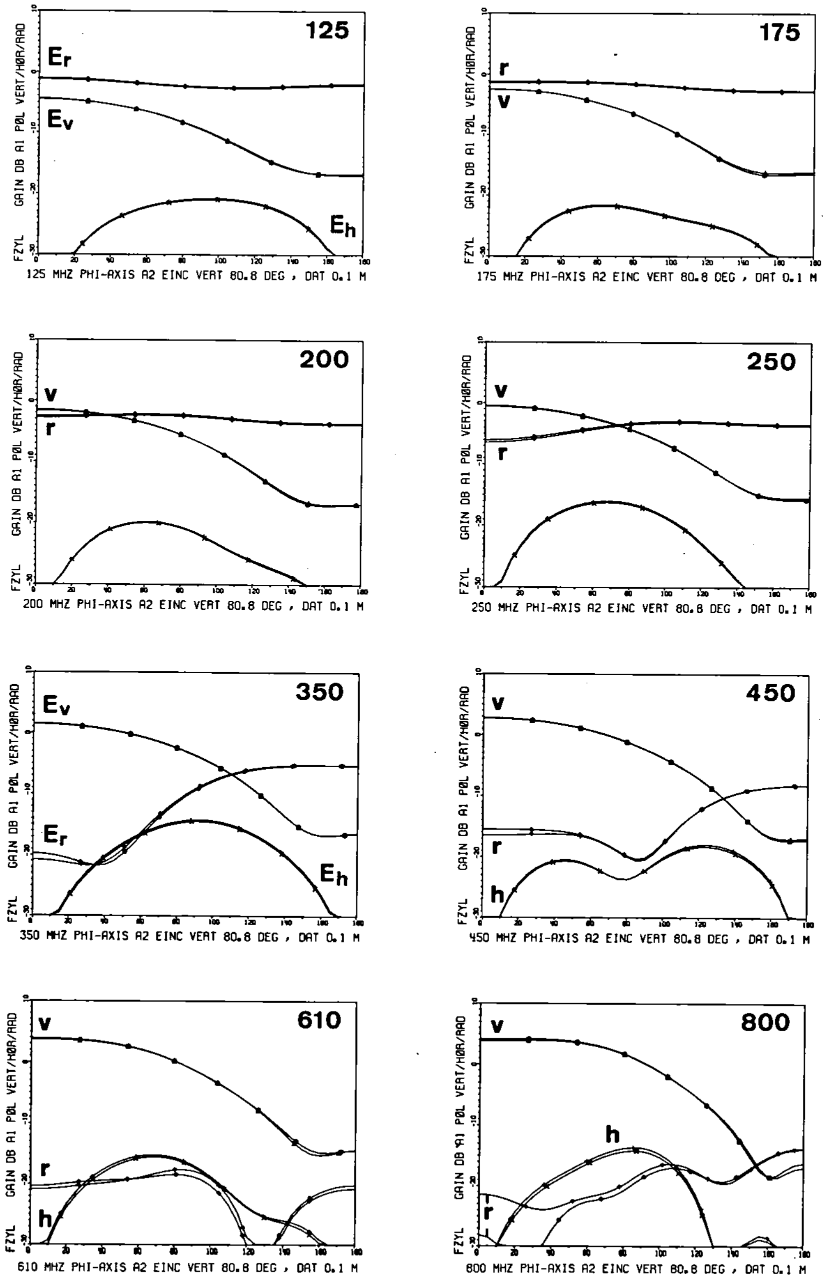

FIGURE 77b Field components E_v, E_r and E_h versus ϕ with the parameter f 125 to 800 MHz. Constant: $d_{at} = 0.1$ m, p_2 = vertical, $\theta_i = 80.8^o$, $h_B = 1.0$ m.

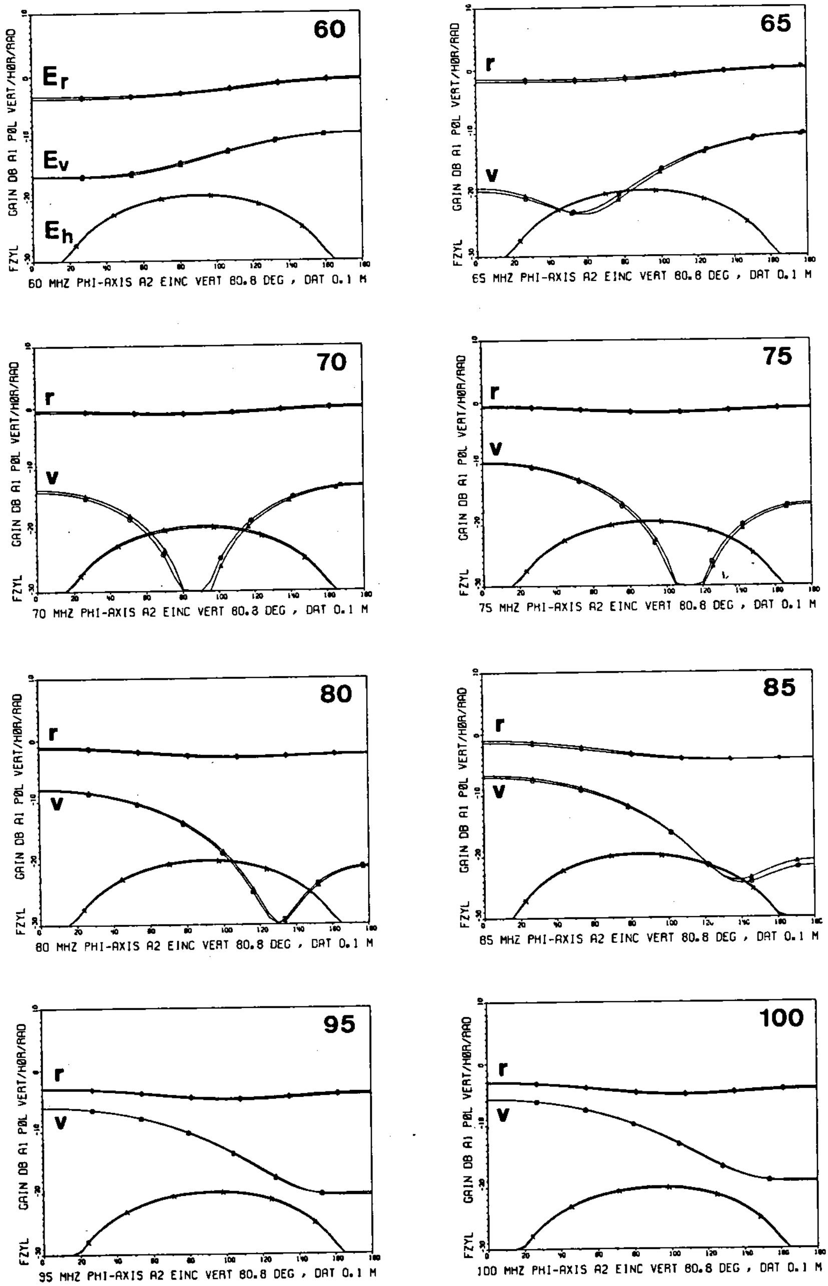

FIGURE 77c Field components E_v, E_r and E_h versus ϕ with the parameter f 60 to 100 MHz. Constant: $d_{at} = 0.1$ m, p_2 = vertical, $\theta_i = 80.8^o$, $h_B = 1.0$ m .

FIGURES 77a and 77b show the azimuthal radiation pattern with constant d_{at} of 0.1 m in the full frequency range 11 to 800 MHz, FIGURE 77c in the resonance frequency range 60 to 100 MHz.

Vertical E-field component E_v

- Below resonance: at frequencies below 50 MHz E_v depends not on ϕ. Although the far-field scattering (RCS, see section 5.3.2.) is small, the attenuation of the near-field is considerable (-11 dB). However, omnidirectional transmission is possible with a reasonable transmission loss.
- Above first resonance: at frequencies above 60 MHz E_v depends much on ϕ. Generally E_v decreases with increasing ϕ and the maximum difference amounts to 12 dB at 125 MHz up to 23 dB at 800 MHz from $0 < \phi < 180^o$. Thus, omnidirectional transmission is difficult due to the large E_v variation and due to the small E_v (minimum: - 19 dB/800 MHz). Compared with the IZYL data the FZYL data vary not more than 2.5 dB above 125 MHz.

Radial E-field component E_r

- Below resonance: at frequencies below 50 MHz E_r depends much on ϕ. Generally E_r is very small at $\phi = 0^o$ (-30 dB at 11 MHz, but increases with f up to -10 dB at 50 MHz) and is relatively high at $\phi = 180^o$ (-7 dB at 11 MHz and -3 dB at 50 MHz). E_r increases with ϕ, and the maximum difference within $0^o < \phi < 180^o$ amounts to 23 dB at 11 MHz and 7 dB at 50 MHz. E_r becomes permanently larger than E_v above 50 MHz and is therefore suited for omnidirectional transmission above 50 MHz.
- Above first resonance: at frequencies from (60)-200 MHz E_r depends not much on ϕ and is always larger than -4 dB. These properties of E_r are ideal for omnidirectional transmission. Above 250 MHz E_r depends on ϕ, first decreases E_r at $\phi = 0^o$, becomes small at $0 < \phi < 180^o$ and above 500 MHz (Appendix 16.2.5.) the minimum E_r becomes very small (-30 dB).

Horizontal E-field component E_h

- At all frequencies the E_h depends much on ϕ and is smaller then -14 dB.

Resonance region 60 to 100 MHz

- Vertical E_v component: with increasing frequency the minimum shifts from $\phi=0^o$ to $\phi=180^o$. The minimum occurs at about 73 MHz (at about $\phi = 90^o$) and is smaller than -30 dB. The maximum E_v amounts to -7 dB at 100 MHz, $\phi = 0^o$.
- Radial E_r component: E_r depends little on ϕ and is always >4.5 dB.

10.4.8. EFFECT OF THE FREQUENCY ON THE DIRECTIVE RADIATION PATTERN

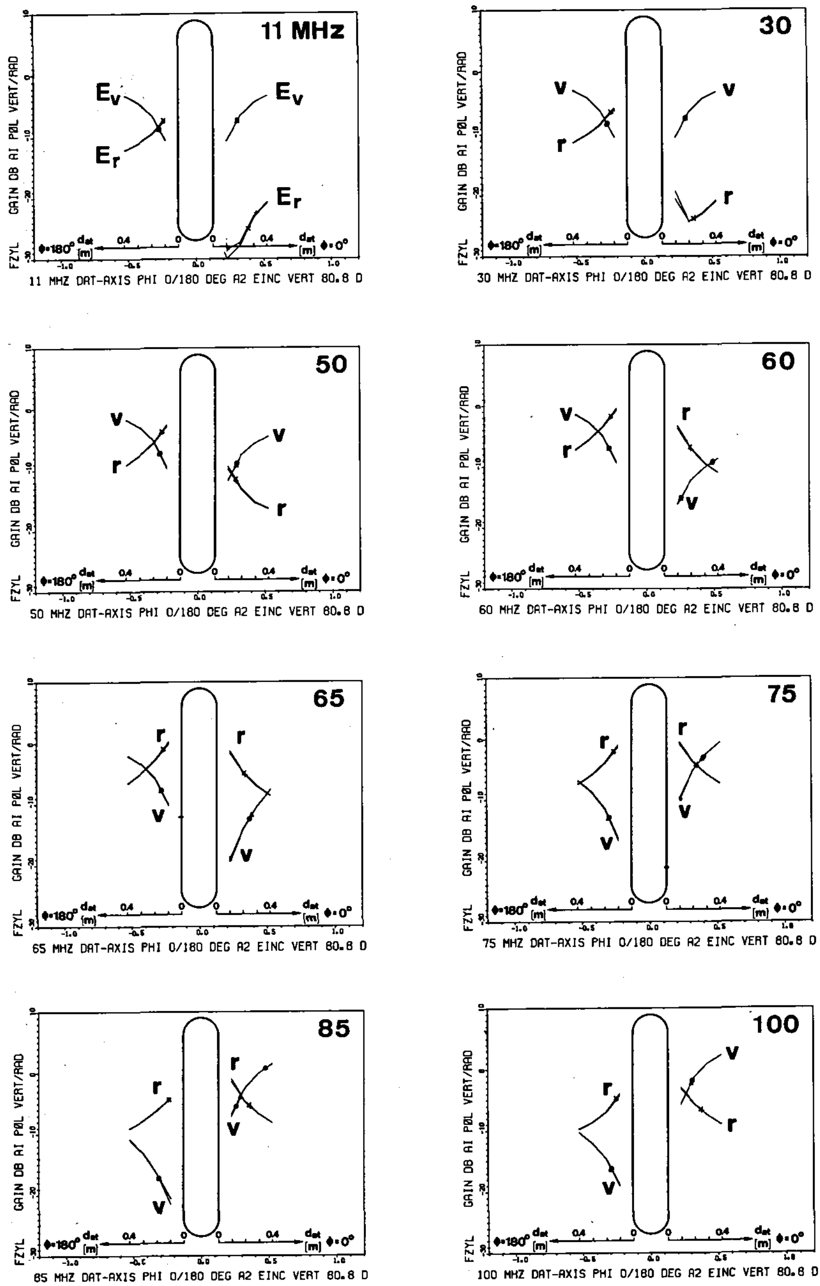

FIGURE 78a Field components E_v and E_r versus d_{at} at $\phi = 0$ and 180^0, with the parameter f 11 to 100 MHz. Constant: p_2 = vertical, $\theta_i = 80.8^0$, $h_B = 1.0$ m .

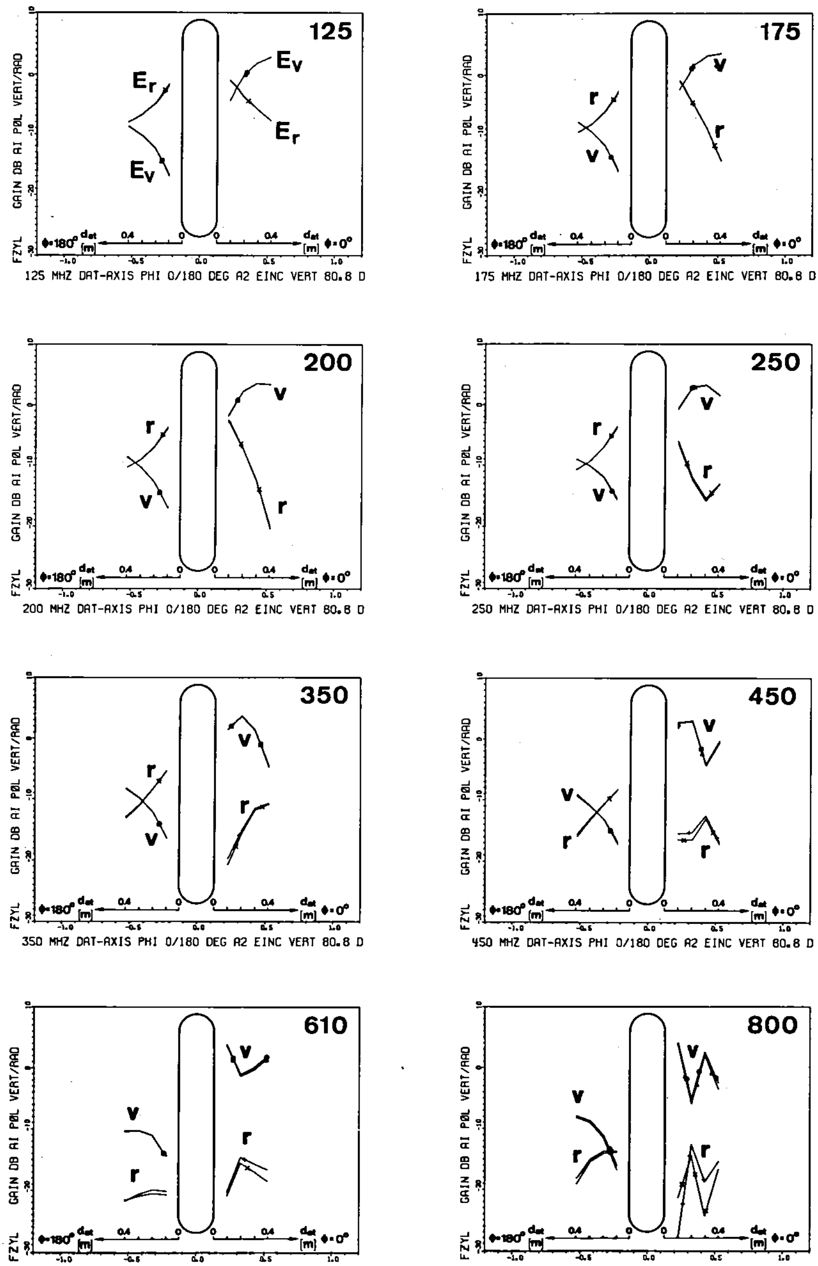

FIGURE 78b Field components E_v and E_r versus d_{at} at $\phi = 0$ and 180^0, with the parameter f 125 to 800 MHz. Constant: p_2 = vertical, $\theta_i = 80.8^0$, $h_B = 1.0$ m.

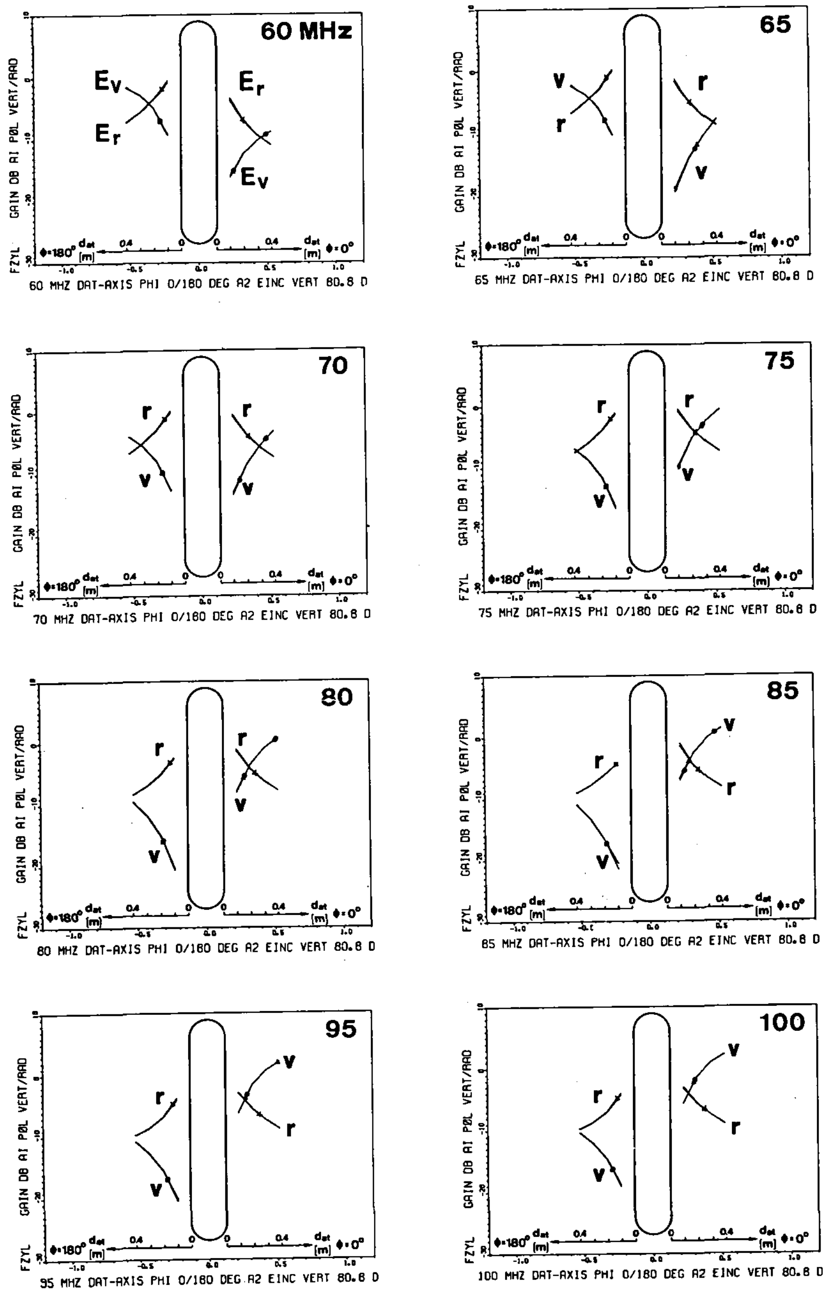

FIGURE 78c Field components E_V and E_r versus d_{at} at $\phi = 0$ and 180^0, with the parameter f 60 to 100 MHz. Constant: p_2 = vertical, $\theta_i = 80.8^0$, $h_B = 1.0$ m .

FIGURES 78a and 78b show the directive radiation pattern at $\phi = 0^{o}$ and 180^{o} at variable d_{at} in the full frequency range from 11 to 800 MHz, FIGURE 78c in the resonance frequency range 60 to 100 MHz.

Vertical E-field component E_V

- Below resonance : Below 30 MHz the E_V's at $\phi = 0$ and 180^{o} are symmetrical, are largest with large d_{at} (- 3 dB at $d_{at} = 0.4$ m) and decrease with decreasing d_{at} (- 11 dB at $d_{at} = 0.1$ m). Above 50 MHz the two E_V's become asymmetric but still decrease with decreasing d_{at}. Thus, the body shows no directive characteristics, and the body has little influence on E_V as long as d_{at} is larger than 0.4 m.
- Above first resonance: At frequencies above 125 MHz E_V is always smaller at $\phi = 180^{o}$ than at $\phi = 0^{o}$. At $\phi = 180^{o}$ E_V decreases constantly with decreasing d_{at}, with an amplitude of about -11 dB at $d_{at} = 0.4$ m and of about -18 dB at $d_{at} = 0.1$ m. At $\phi = 0^{o}$ E_V oscillates around 0 dB according to the results in section 7.3.1.: maxima occur at $d_{at} \sim n \cdot \lambda/4$, $n = 1,3,5,..$ and minima at $d_{at} \sim n \cdot \lambda/2$, $n = 0,1,2,...$ The body acts like an efficient reflector if d_{at} amounts to $n \cdot \lambda/4$ and is a good absorber if $d_{at} < 0.2$ m. As an example the forward/backward ratio is 17 dB at $d_{at} = 0.2$ m /350MHz.

Radial E-field component E_r

- Below resonance: at 11 MHz E_r is very small at $\phi = 0^{o}$ but increases with increasing frequency. Above 50 MHz both E_r's increase with decreasing d_{at} and become larger than E_V at about $d_{at} < 0.15$ m. Above 60 MHz both E_r's are about symmetrical with about -2 dB at $d_{at} = 0.1$ and -9 dB at $d_{at} = 0.4$ m. At very small d_{at} the body acts like a director (11 MHz) and as a director/reflector (> 60 MHz).
- Above first resonance: from (60) to 200 MHz both E_r's at $\phi = 0$ and 180^{o} are about symmetrical with high values at small d_{at}. Generally the E_r's are larger than the E_V's at $d_{at} < 0.1$ m (< 0.3 at $\phi = 180^{o}$), and the body acts like a director/reflector for small d_{at}'s. Above 250 MHz E_r decreases first at $\phi = 0^{o}$ and above 350 MHz also at $\phi = 180^{o}$. Above 450 MHz and $d_{at} > 0.3$ m the E_r's become very small, smaller than the E_V's.

Resonance region 60 to 200 MHz

- Vertical E_V components: if $d_{at} < \lambda/4$, the E_V's decrease with decreasing d_{at} and are smallest at about 85 MHz at $\phi = 180^{o}$ (-22 dB at $d_{at} = 0.1$ m).
- Radial E_r components: Both E_r's are larger (> - 5 dB) at $d_{at} < 0.15$ m .

10.4.9. EFFECT OF DIFFERENT BODY SHAPES ON THE FIELDS IN THE SHADOW ZONE

The former computations with the simple body model FZYL revealed the systematic relations between antenna location and field quantities. The most important results are summarized in FIGURE 80 for $\phi = 180^o$:

- E_v/f diagram: sharp anti-resonance at about 75-105 MHz, recovery of E_v at frequencies above 125 MHz and oscillation around - 16 dB ($d_{at} = 0.1$ m)
- E_r/f diagram: two peaks, one around 70 MHz (+0.5 dB) and a second of similar amplitude around 150 MHz (+0 dB) at $d_{at} = 0.1$ m.
- E_v-E_r/f diagram at $d_{at} = 0.1$ m : E_r is up to 16 dB larger than E_v at frequencies below 550 MHz
- E_v-E_r/f diagram at $d_{at} = 0.4$ m : E_r is usually smaller than E_v

The corresponding data has been computed for the man-models in FIGURE 79:

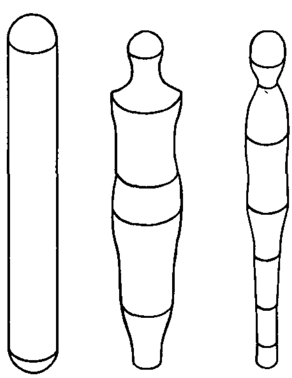

FZYL MANMOD 1 MANMOD 2

FIGURE 79 Computational body models

- FZYL : finite rotational symmetric cylinder with round end caps $L_B = 1.8$ m , $D_B = 0.25$ m .
- MANMOD 1 :rotational symmetric human body, front view = contour curve $L_B = 1.68$ m , $D_B = 0.296$ m at $d_{at} = 1.0$ m.
- MANMOD 2 :rotational symmetric human body, side view = contour curve $L_B = 1.68$ m , $D_B = 0.196$ m at $d_{at} = 1.0$ m.

(dimensions listed in Appendix 16.2.4.)

Comparing FIGURE 81 (MANMOD 1) with FIGURE 80 (FZYL) we find:

- E_v/f diagram: there is still an anti-resonance at about 80-125 MHz but less sharp and without recovery. E_v drops with increasing frequency.
- E_r/f diagram: only the first peak is well developed, amounts to +3 dB at $d_{at} = 0.1$ m and occurs at 75 MHz.
- E_r-E_v diagram at $d_{at} = 0.1$ m : $E_r > E_v$ (max.16 dB) above 600 MHz

Comparing FIGURE 82 (MANMOD 2) with FIGURE 80 (FZYL) we find:

- E_v/f diagram: very similar to FZYL (but shifted in frequency)
- E_r/f diagram: very similar to FZYL but larger amplitude variations. First peak around 80 MHz(+ 4 dB) and second peak around 160 MHz(+2.5 dB).

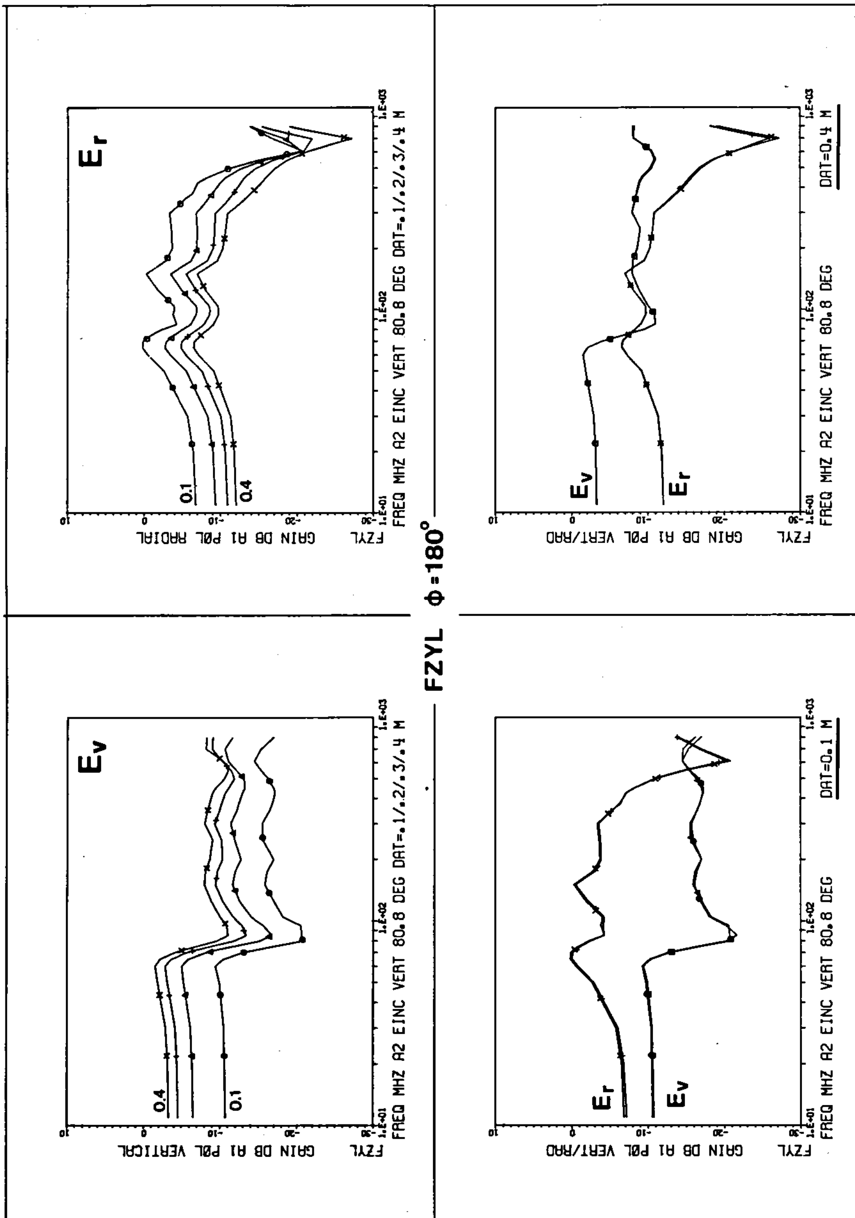

FIGURE 80 Summarized computational results from body model FZYL

E_v versus f, parameter d_{at} — E_r versus f, parameter d_{at}

E_v and E_r at d_{at} = 0.1 m — E_v and E_r at d_{at} = 0.4 m

Constant: $\phi = 180^o$, p_2 = vertical, $\theta_i = 80.8^o$, h_B = 1.0 m.

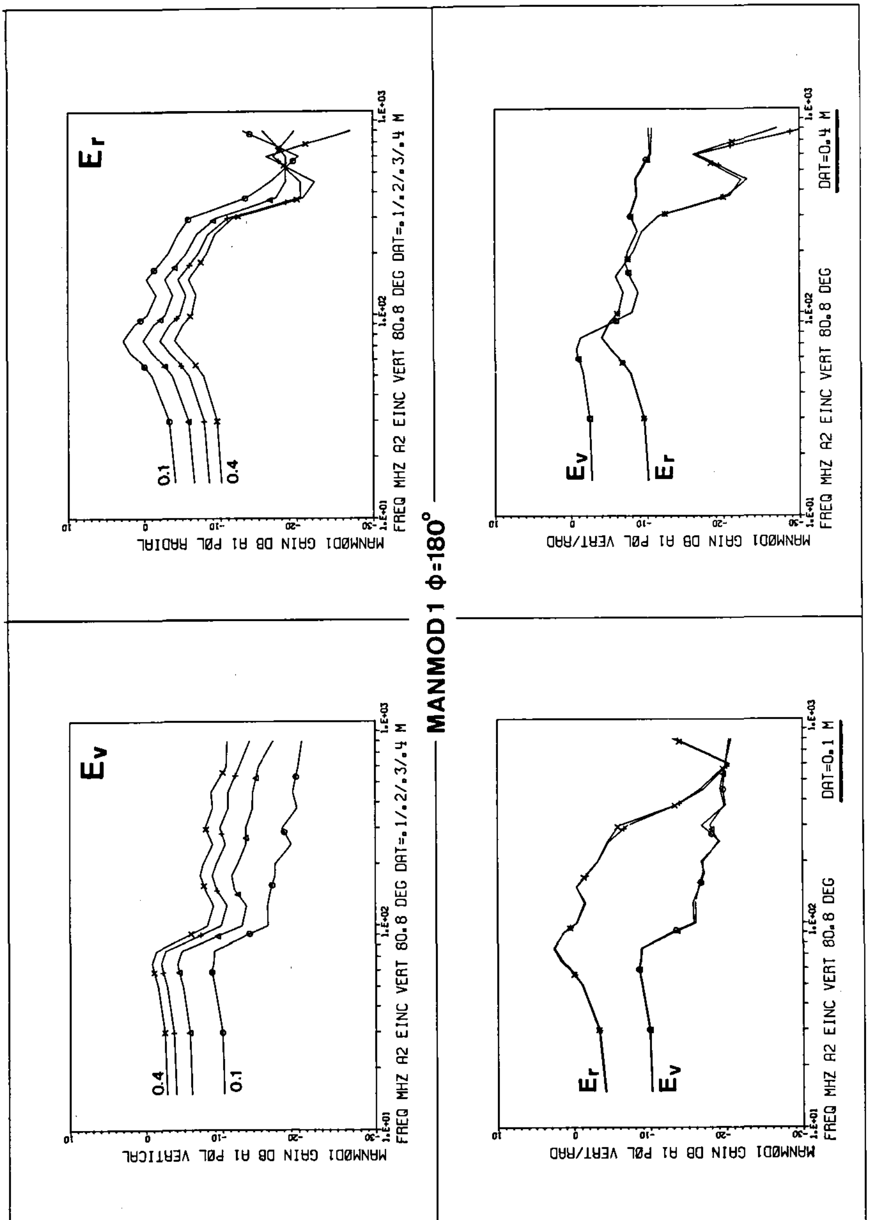

FIGURE 81 Summarized computational results from body model MANMOD1

E_v versus f, parameter d_{at} | E_r versus f, parameter d_{at}

E_v and E_r at d_{at} = 0.1 m | E_v and E_r at d_{at} = 0.4 m

Constant: $\phi = 180^o$, p_2 = vertical, $\theta_i = 80.8^o$, h_B = 1.0 m.

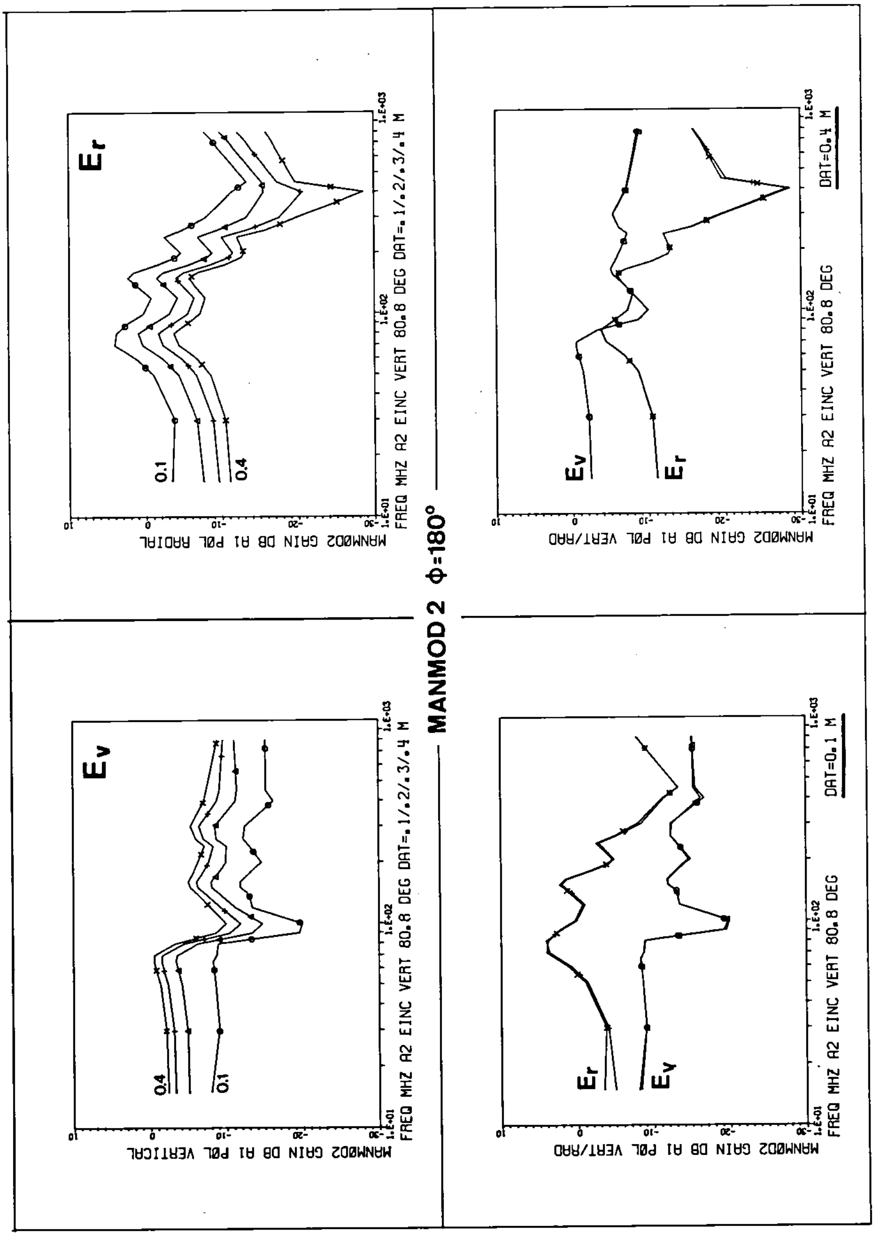

FIGURE 82 Summarized computational results from body model MANMOD 2

E_v versus f, parameter d_{at} — E_r versus f, parameter d_{at}

E_v and E_r at d_{at} = 0.1 m — E_v and E_r at d_{at} = 0.4 m

Constant: $\phi = 180^o$, p_2 = vertical, θ_i = 80.8^o, h_B = 1.0 m.

10.4.10. EFFECT OF DIFFERENT BODY SHAPES ON AZIMUTHAL RADIATION PATTERNS

If we look at the azimuthal radiation patterns in 10.4.7.,we notice the following frequency dependent changes of the field components:

- E_v changes drastically between 60 and 100 MHz
- E_r changes rapidly at about 50 MHz and above 250 MHz
- E_h shows the same pattern up to 350 MHz

Changes of the field components occur only if the body dimensions are in a special relation to the wavelength. If the vertical circumference ($\sim 2\,L_B$, see also FIGURE 18) is about λ, the E_v and E_r are affected. If the horizontal circumference $D_B \cdot \pi$ is about λ, E_h and E_r are affected.

Considering these facts it is easy to understand the changes in the azimuthal radiation patterns due to body shape alterations. Small changes of L_B and D_B provokes similar effects like small changes of the frequency.

Significant azimuthal radiation patterns are shown for the three bodies FZYL, MANMOD 1 and MANMOD 2 in FIGURES 83 a,b,c at 65 MHz and in FIGURES 84 a,b,c at 150 MHz. Additional samples for 11, 50, 75, 85, 200 and 800 MHz are presented in FIGURES 100 to 105 in Appendix 16.2.5..

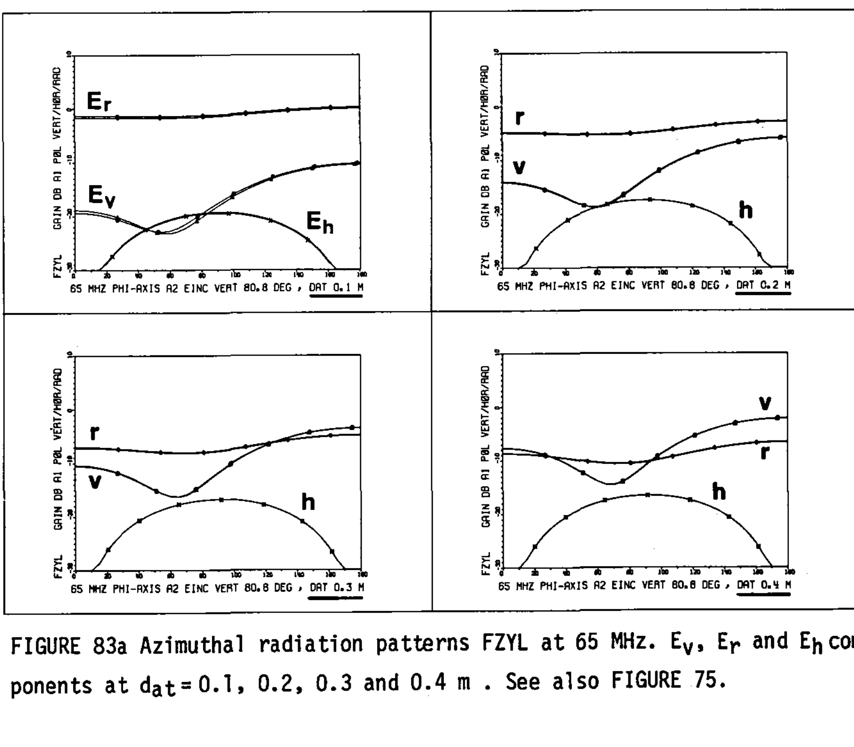

FIGURE 83a Azimuthal radiation patterns FZYL at 65 MHz. E_v, E_r and E_h components at d_{at} = 0.1, 0.2, 0.3 and 0.4 m . See also FIGURE 75.

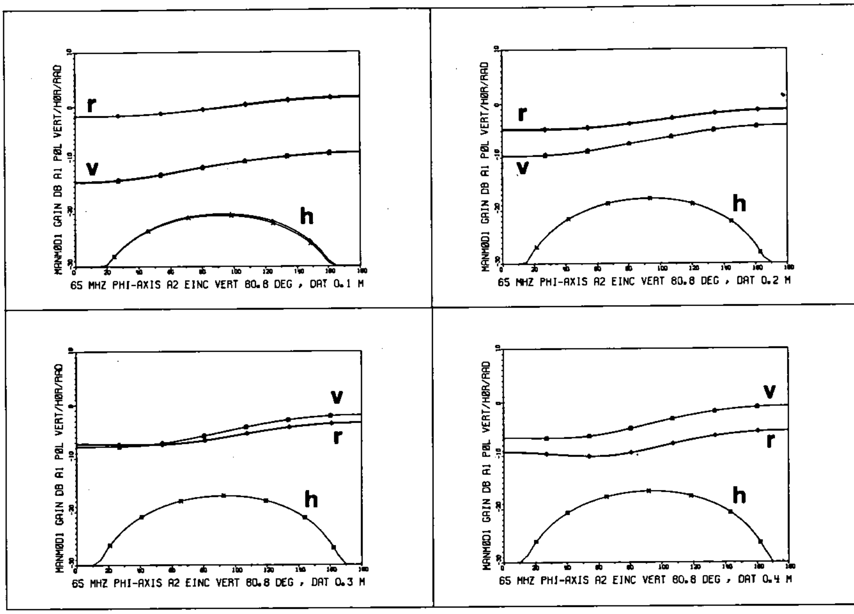

FIGURE 83b Azimuthal radiation patterns MANMOD1 at 65 MHz.

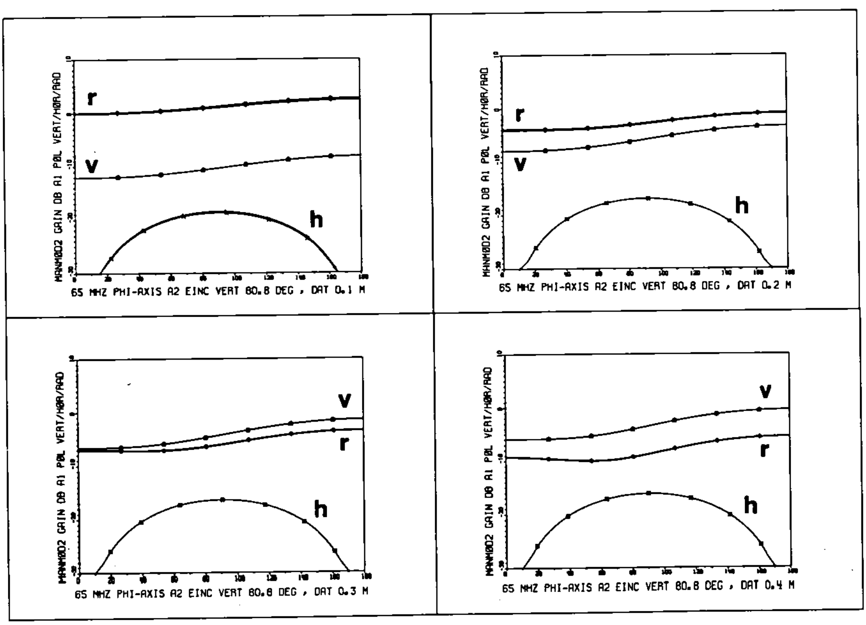

FIGURE 83c Azimuthal radiation patterns MANMOD2 at 65 MHz.

Comparing FIGURES 83a,b,c at 65 MHz we observe an L_B-effect:

- E_v changes drastically from FZYL to MANMOD 1 (L_B = 1.8 and 1.68 m), but there are only small differences between MANMOD 1 and 2 (L_B = 1.68 m). As can be seen in Appendix 16.2.5., FIGURE 102, the MANMOD's resonate at about 75 MHz in contrast to FZYL at 65 MHz due to the 6.7% shorter L_B.
- E_r varies only within 2 dB.
- E_h varies only within 2 dB.

Comparing FIGURES 84a,b,c at 150 MHz we observe an L_B and D_B-effect:

- E_v varies within 5 dB at $\phi = 180°$. The second (λ) resonance is best developed at MANMOD 2 which has the largest L_B/D_B-ratio. The weakest λ resonance occurs at MANMOD 1 with the smallest L_B/D_B-ratio.
- E_r varies within 3 dB, and the values of FZYL are between those of MANMOD 1 and 2, corresponding to the D_B ratio of the three bodies.
- E_h varies within 3 dB. The theoretical horizontal resonant frequencies are 301 MHz (MANMOD 1), 380 MHz (FZYL) and 487 MHz (MANMOD 2). The asymmetry of E_h of MANMOD 1 is caused by a subresonance, because 150 MHz is close to 301 MHz, the E_h of FZYL is already better and the E_h of MANMOD 2 is very symmetrical because 150 MHz is well below 487 MHz.

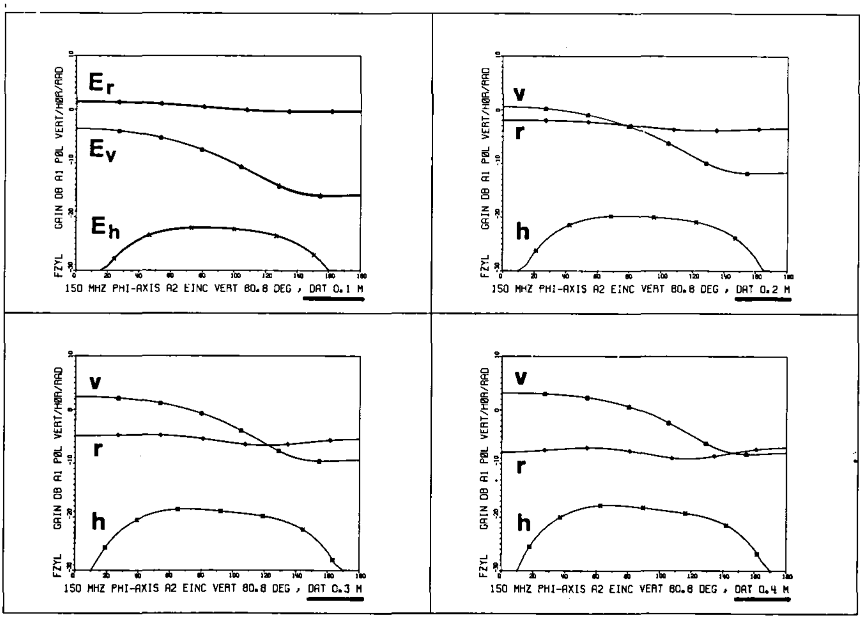

FIGURE 84a Azimuthal radiation patterns FZYL at 150 MHz. E_v, E_r and E_h components at d_{at} = 0.1, 0.2, 0.3 and 0.4 m. See also FIGURE 75.

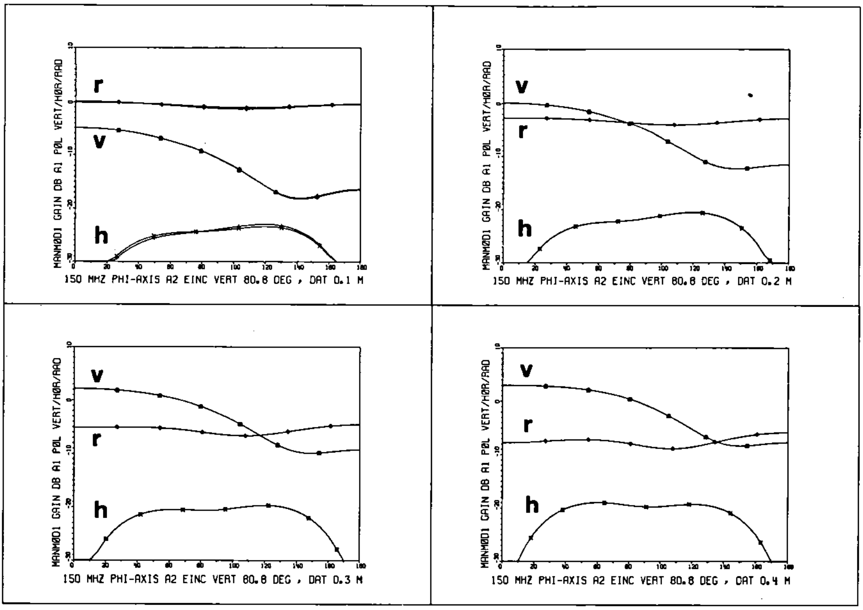

FIGURE 84b Azimuthal radiation patterns MANMOD1 at 150 MHz.

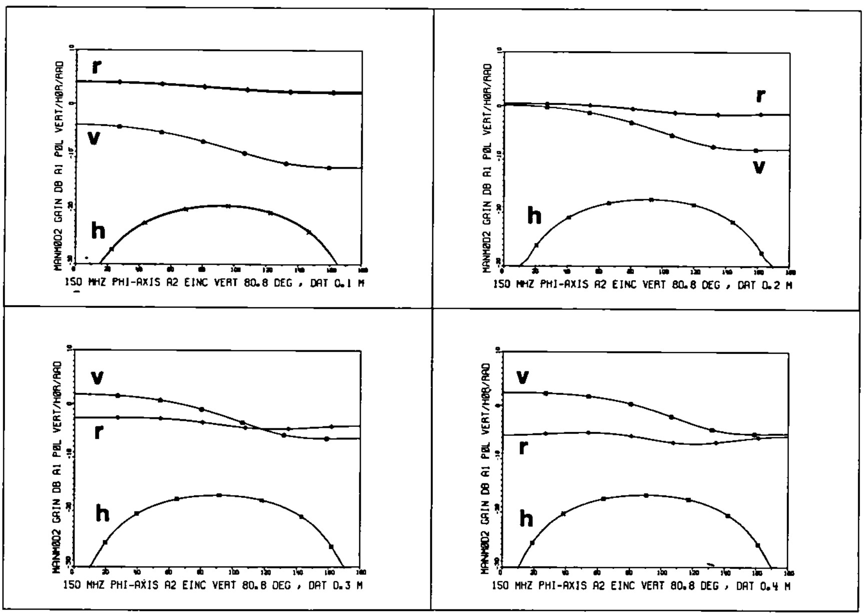

FIGURE 84c Azimuthal radiation patterns MANMOD2 at 150 MHz.

Leer - Vide - Empty

11. Extended Measuring Method for Field Components Separation

11.1. PURPOSE OF THE EXTENDED EXPERIMENTS

The experimental data in section 9. were obtained with the measuring method described in section 8. The computational data agreed with the experimental data within ± 3 dB for all three test bodies, but only at frequencies above 200 MHz and antenna-body distances above 0.1 m.

A poor agreement between experimental data and computation was noticed at frequencies below 200 MHz if d_{at} was smaller than 0.2 m. The reasons for this discrepancy can now be explained by the computational data found in section 10.:

- In the extreme proximity of the body the radial field exceeds the vertical polarized field, especially at $\lambda/2$ resonance ($\sim$ 65 MHz) and at λ resonance ($\sim$ 150 MHz)
- Electrically small monopole antennas with insufficient counterpoise exhibit a considerable transverse sensitivity (receiving case) or radiate a not wholly pure vertical polarized field (transmitting case). The antenna tests in TABLE 51 tell us that the horizontal (or radial) sensitivity is only about 0-12 dB below the vertical sensitivity at 75 MHz, 19 dB at 125 MHz and 16-18 dB at 205 MHz. The antenna data at 101 MHz (25 dB) and 158 MHz (21 dB) are satisfactory, resulting in a better agreement as can be seen in FIGURES 56 and 57.
- Remotely fed test antennas disturb the fields in the proximity of the body, and especially at low signal levels a part of the signal is picked up by the feeding cable, even when surface waves are attenuated according to FIGURE 44.

Another problem was the fixed relative (h_B) and absolute (h_1) antenna height and the missing data concerning the field homogeneity.

The purpose of the extended experiments are therefore defined as:

- Separate measurement or generation of radial and vertical field components in the frequency region 50 to 200 MHz without disturbing the fields around the test body.
- Measurement of the h_1 and h_B-dependence of the field components with and without test bodies for field homogeneity studies.

In section 9.1.5. the reciprocity theorem has been verified, so that the test antenna could be a receiving or a transmitting antenna for our extended experiments. Both methods have their advantages for special applications:

Probe receiving antenna A_1 . A common probe antenna consists of a small dipole (whip, helical or conical for broadband) equipped with a rectifier attached to highly resistive, twisted cables. A remote precision DC amplifier measures the signal without range switching from about 1 mV to 1 V (see e.g. BELSHER [9]) almost linearly. The problem is the very low signal at A_1 (e.g. E_v at 100 MHz and $d_{at} < 0.1$ m) and the relative high field around the connecting cables. A better method would be to build the DC-amplifier and a fiber-optic transmitter close to A_1, but then problems have to be solved concerning power consumption (LED's!) and amplifier stability. This method would be best if broadband characteristic is urgently required and if the signal to be measured is much larger than the other RF-signals in the air. Selective built-in receivers cannot be recommended due to limited amplitude range, tuning problems and stability.

Probe transmitting antenna A_1 . Free-oscillating miniature transmitters cannot be recommended due to amplitude and especially frequency stability problems, because the antenna load is not stable. Quartz-stabilized frequency synthesizers are not suited due to power consumption and space requirements. Thus separate, quartz-stabilized fixed-frequency transmitters offer the best solution concerning volume, power consumption, stability and costs. The main problem is the preset frequency, but on the other hand each probe transmitter can be matched properly to the suited antenna with best long-time stability. Such probe transmitters will be shown in section 11.3. and were used in the following experiments.

11.2. ANTENNA MANIPULATOR

A special antenna manipulator (FIGURE 85 and 86) has been developed with the following features:

- Translation of a complete transmitter along the vertical axis from $0.1 < h_B < 1.7$ m. Continuous remote translation with permanent h_B recording (rubber band goniometry, accuracy better than 5 cm)
- Rotation of A_1 around the antenna center for p_1 vertical to radial
- Accurate and stable positioning of d_{at} at 0.1, 0.2, 0.3 and 0.4 m .

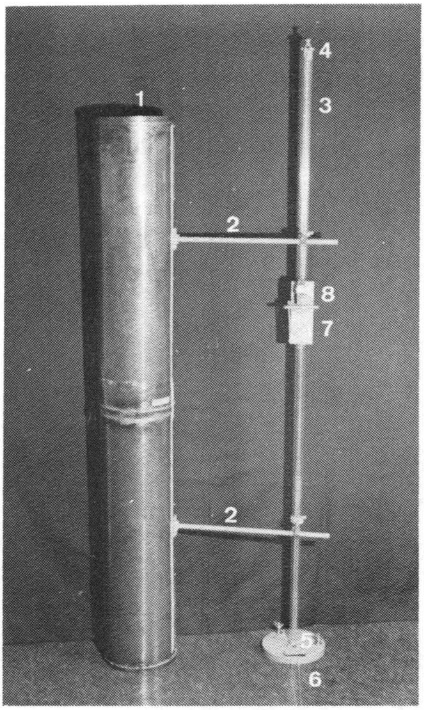

FIGURE 85 Antenna manipulator

1 : test body MET
2 : d_{at}-spacers, 15 mm ∅ PVC tubes screwed perpendicular to the surface of the test body
3 : vertical trackway, three 15 mm ∅ plexiglass tubes
4 : anchoring strings and deflection pully for strings (6)
5 : basement with deflection pully (screwed on revolving stage)
6 : thin plastic strings for remote manual up/down pulling of the wagon carrying the antenna
7 : wagon, PVC plate with four PVC wheels shaped like cotton reels
8 : small revolving disk with lock for antenna rotation around the antenna center (details:FIG.86)

The main parts of the antenna manipulator are shown in FIGURE 85. In addition a rubber band goniometer (similar to FIGURE 45) in the horizontal plane on the basement (5) measures the antenna height. For outdoor experiments the top (4) of the trackway is fixed to the revolving stage by stretched strings to prevent mechanical oscillations.

For the experiments with standard body-earth spacing s ($s = 0.2$ m) the test body is standing directly on the supporting revolving stage (FIGURE 45) for experiments with $s = 0.7$ m on wooden precision spacers.

11.3. ELECTRICALLY SMALL DIPOLE ANTENNAS WITH BUILT-IN OSCILLATORS

A test transmitter consists of an electrically small dipole antenna and of an autonomous RF-generator (FIGURE 86). The test transmitters have been developed in order to obtain very stable, independent and miniature field sources and are denoted as AO 1 (65 MHz), AO 2 (74 MHz), AO 3 (101 MHz) and AO 4 (164 MHz). The helical dipole antenna of $2h < 0.1$ m and $D_h = 11$ mm have been tuned to resonance (TABLE 88) and the RF-generators are mounted perpendicular to the center of the antennas in the neutral antenna plane.

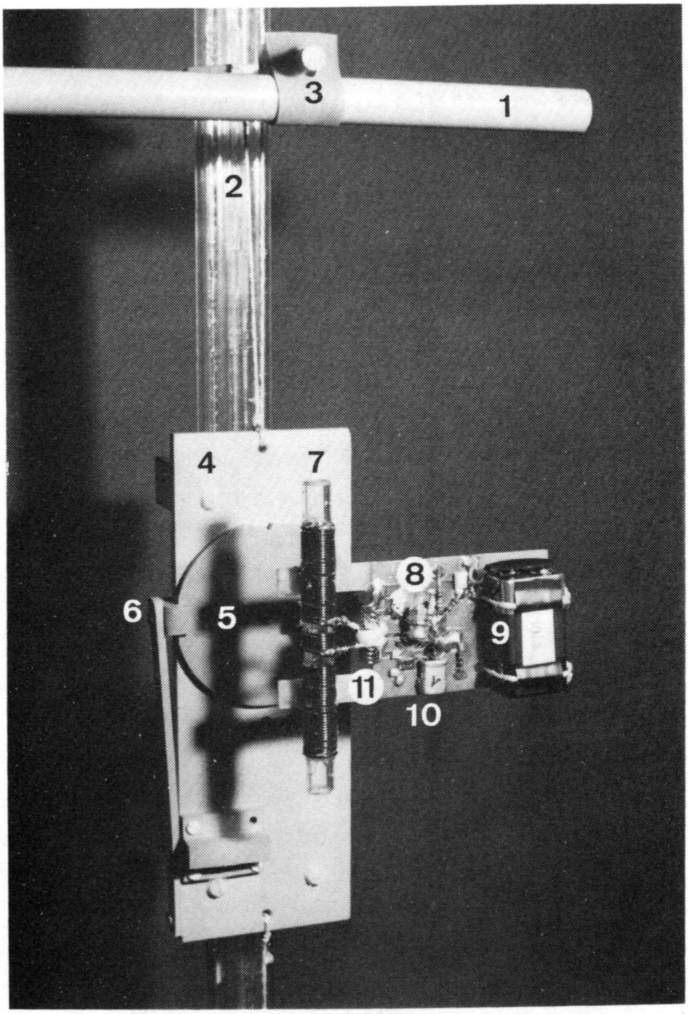

FIGURE 86 Test antenna A_1 with built-in oscillator on antenna manipulator

1 : d_{at}-spacer (see also FIGURE 85)

2 : plexiglass vertical trackway

3 : quick-fixing device for d_{at}

4 : antenna wagon with pulling strings

5 : small revolving disk carrying A_1 for p_1 = vertical to radial

6 : lock of the revolving disk

7 : helical dipole antenna A_1

8 : RF-generator with:

9 : 9V alkaline battery 540 mAh

10 : quartz (3^{th} harmonic mode)

11 : RF-antenna coupler

The construction of miniature, unshielded RF-generators of high amplitude stability is quite difficult at frequencies above 50 MHz. A solution was found in the modification of available high-standard RF-suboscillators of professional walkie-talkies (65,74 and 164 MHz) and in a special construction for 101 MHz. The main specifications of the final RF-oscillators are listed in TABLE 87, the output power amounts to 1 - 10 mW.

FREQ [MHz]	SUBOSCILLATOR manufacturer type	ADDITIONAL ELEMENTS (RF-coupling etc.)	INPUT CURR. [mA]	AMPLITUDE STABILITY (*) [dB]	DIMENSIONS without bat. [mm]
65	AUTOPHON (special)	ferrit 50 to 50 Ω balun,mod.TV balun	7	0.5	27 x 27 x 30
74	MOTOROLA KXN1067A	external 5 V reg., antenna center coil used as oscil. coil	8	0.1	19 x 9 x 28
101	WAFFEN FABRIK THUN (spec.)	inductive coupling 3 turns around osc.	6	1.0	50 x 40 x 10 (few elem.)
164	MOTOROLA KXN1041A 54.667 MHz	5 V reg.,RF-amplif. freq. multiplier antenna center coil used as 164 MHz coil	40	0.5 (*): during 2 hours	19 x 9 x 28 + 25 x 17 x 15

TABLE 87 Specifications of the built-in quartz RF oscillators

The helical dipole antennas were computed according to Appendix 16.1. and tuned with the help of a network analyser. The application of lossy conductors (PVC insulation) increases the bandwidth (damping effect in a resonante RLC network) but decreases the (non important) efficiency.The data of the antennas are listed in TABLE 88.

FREQ [MHz]	TOTAL TURNS No.	CENTER TURNS No.	TOTAL LENGTH [mm]	CENTER LENGTH [mm]	CONDUCTOR MATERIAL DIAMETER,INSULAT. [mm]	-3 dB BANDWIDTH (analyser data) [MHz]
65	121	7	90	8	0.4 PVC center sec. 0.2 enamelled wire for 2x22 end turns	64 to 66
74	97	7	94	9	0.5 enamelled wire	72 to 75
101	72	6	82	9	0.8 enamelled wire	99 to 102
164	45	5	95	9	0.8 PVC	159 to 167

TABLE 88 Specifications of the helical dipole antennas A_1

During the network analyser measurements the center turns of the dipole antenna were coupled to the 50 Ω coaxial measuring cable with a miniature 50 to 50 Ω ferrit balun (Appendix 16.1.1.). The obtained - 3 dB bandwidth may be different when coupled to the actual RF-oscillator and is generally larger at imperfect matching (reduced efficiency).

From the test transmitters AO 1 to AO 4 one cannot expect a totally omnidirectional radiation pattern with strict linear polarization. The transmitter's tests, however, revealed a very stable (0.5 dB) azimuthal radiation pattern at p_1 = vertical (see TABLE 90), and the actual experiments revealed that the transverse polarization (polarization perpendicular to the antenna axis) is about 10 to 15 dB smaller than the main polarization.

11.4. TEST PROGRAM AND SOME EXPERIMENTAL RESULTS OBTAINED WITH AO 1 TO AO 4

1. PREPARATIONS
1.1. Mounting of the h_1-goniometer and calibrations
1.2. Warming-up of the RF-equipment and recorder, initial calibrations
1.3. Measuring of the FSL at p_1 = vertical and radial versus ϕ at h_1 = 1.2 m and p_2 = vertical. (see results in TABLE 90)
1.4. Field homogeneity measurements at $0.7 < h_1 < 2.0$ m at $\phi = 0^0$
1.5. Calibration of FSL to 0 dB at p_1 = vertical, h_1 = 1.2 m, $\phi = 0^0$
2. TRANSMISSION EXPERIMENTS WITH VARIABLE ANTENNA HEIGHTS h_1
2.1. MET at $\phi = 0^0$, d_{at} = 0.1 m, s = 0.2 m, p_1 = vertical/radial, $0.7<h_1<1.5$
2.2. " " d_{at} = 0.2 m, " " " "
2.3. " $\phi=180^0$, d_{at} = 0.1 m, " " " "
2.4. " " , d_{at} = 0.2 m, " " " "
2.5. " $\phi = 0^0$, d_{at} = 0.1 m, s = 0.7 m, p_1 = vertical/radial, $1.2<h_1<2.0$
2.6. " " , d_{at} = 0.2 m, " " " "
2.7. " $\phi=180^0$, d_{at} = 0.1 m, " " " "
2.8. " " , d_{at} = 0.2 m, " " " "
3. TRANSMISSION EXPERIMENTS WITH VARIABLE AZIMUTHAL ANGLE ϕ
3.1. MET at d_{at} = 0.1 m, s = 0.2 m, h_1 = 1.2 m, p_1 = vertical/radial, $0<\phi<360^0$
3.2. " d_{at} = 0.2 m, " " " " "
3.3. " d_{at} = 0.3 m, " " " " "
3.4. " d_{at} = 0.4 m, " " " " "
3.5. " d_{at} = 0.1 m, s = 0.7 m, h_1 = 1.7 m, p_1 = vertical/radial, $0<\phi<360^0$
3.6. " d_{at} = 0.2 m, " " " " "
3.7. SUB at d_{at} = 0.1 m, s = 0.2 m, h_1 = 1.2 m, p_1 = vertical/radial, $0<\phi<360^0$
3.8. " d_{at} = 0.2 m, " " " " "
3.9. " d_{at} = 0.1 m, s = 0.7 m, h_1 = 1.7 m, p_1 = vertical/radial, $0<\phi<360^0$
3.10. " d_{at} = 0.2 m, " " " " "

TABLE 89 Summarized experiments with test transmitters AO 1, AO 2, AO 3, AO 4

The test set-up consists of a revolving stage, carrying the test body and the antenna manipulator, and the remote receiving antenna A_2 at d = 31 m and $h_2 = 6.2$ m as shown in the similar test set-up in FIGURE 44. The performance of the LPD-antenna A_2 is only specified for 100 - 1000 MHz . Below 100 MHz A_2 is suited for relative field measurements of vertical polarized field components (p_2 = vertical) but will also pick-up field components of other polarizations. The performance of the test transmitters AO 1 to AO 4 was measured by recording the azimuthal radiation pattern at p_1 = vertical/radial without TS. If both A_1 and A_2 would be strictly linear polarized, and if there would be no ground reflections, the following data had to be obtained: 1.) p_1 = vertical : E_0 stable at 0 dB from 0 $< \phi < 360^o$. 2.) p_1 = radial : A maximum of - 16 dB ($E_0 \cos\theta_i$) should occur at $\phi = 0$, 180 and 360^o, and the signal should drop to $-\infty$ dB at $\phi = 90$ and 270^o. The actual experimental data are listed in TABLE 90 :

FREQ. [MHz]	VERTICAL POL. Amplitude [dB]	RADIAL POLARIZATION Maximum Signal Amplitude [dB]	Maximum Signal Angle ϕ [^{o}]	Minimum Signal Amplitude [dB]	Minimum Signal Angle ϕ [^{o}]
65	± 0.5	-1, -3	80, 260	-9, -10	165, 350
74	± 0.25	-10, -7	45, 220	-15, -32	115, 320
101	± 0.5	-6,-9,-6	0,185,360	-16, -13	105, 260
164	± 0.25	-6,-8,-6	0,190,360	-14, -12	110, 270

TABLE 90 Experimental data of the performance of the test transmitters AO 1 to AO 4 at $h_1 = 1.2$ m, p_2 = vertical, $\theta_i = 80.8^o$ in proximity to ground.

The test transmitters AO 3 and AO 4 perform best because the azimuthal radiation patterns are symmetrical and follow the predicted pattern. The test transmitters AO 1 (65 MHz) and AO 2 (74 MHz) have a disturbed azimuthal radiation pattern at p_1 = radial, caused primarily by ground reflections and by the elliptical polarization of the helical A_1 antennas. However, measurements of the dominant field components in the proximity of the TS should be possible with a reduced accuracy.

The next test is concerned with the field homogeneity at p_1 = vertical and radial at variable antenna heights without TS. The results are shown in TABLE 91 for both polarizations at $0.8 < h_1 < 1.8$ m.

VERTICALLY POLARIZED FIELD AMPLITUDE VARIATION AT VARIABLE ANTENNA HEIGHTS H_1						
FREQUENCY [MHz]	RELATIVE FREE-SPACE FIELD STRENGTH $E_0(h_1)$ IN DECIBELS AT HEIGHT h_1 = 0.8 m	h_1 = 1.0 m	h_1 = 1.2 m	h_1 = 1.4 m	h_1 = 1.6 m	h_1 = 1.8 m
65	+ 0.5	+ 0.0	+ 0.0	- 0.0	- 0.5	- 0.5
74	+ 1.0	+ 0.5	+ 0.0	- 0.5	- 1.0	- 1.0
101	+ 1.5	+ 0.5	+ 0.0	+ 0.0	+ 0.0	+ 0.5
164	- 1.5	- 1.0	+ 0.0	+ 0.5	+ 1.5	+ 2.0

TOTAL FIELD AMPLITUDE AT P1 = RADIAL / P2 = VERTICAL AT VARIABLE ANTENNA HEIGHTS						
FREQUENCY [MHz]	RELATIVE FREE-SPACE FIELD STRENGTH RELATED TO Ev AT H_1 = 1.2m, $\phi = 0^o$ h_1 = 0.8 m	h_1 = 1.0 m	h_1 = 1.2 m	h_1 = 1.4 m	h_1 = 1.6 m	h_1 = 1.8 m
65	-10.5	-10.2	-10.0	- 9.5	- 9.0	- 8.2
74	-14.5	-13.5	-13.0	-12.5	-12.0	-11.0
101	- 7.0	- 6.6	- 6.0	- 5.0	- 4.5	- 4.5
164	- 6.0	- 5.5	- 6.0	- 7.0	- 8.0	- 9.0

TABLE 91 Field homogeneities of the field components at p_1 = vertical (above) and p_1 = radial (below), measured along the theoretical vertical axis of the TS (without TS) at $\phi = 0^o$ and p_2 = vertical. The reference field strength is the FSL (0 dB), measured with p_1 = vertical at h_1 = 1.2 m.

The upper data in TABLE 91 show that the field homogeneity at $p_1 = p_2$ = vertical is within 1.5 dB at antenna heights h_1 from 0.8 to 1.6 m.

The data below in TABLE 91 are a measure for the transversal $Gain_T$ of the antenna A_1, if A_2 is assumed to be strictly linear polarized. The measured E_{tot} is the superposition of:

$$E_{tot} = E_o \cos\theta_i \;+\; E_o \sin\theta_i \;\cdot \cos\Delta\psi \cdot Gain_T \qquad (245)$$

$\Delta\psi$ is the unknown argument of the transversal $Gain_T$. With (245), E_{tot} and $\Delta\psi = 0^o$ one obtains a $Gain_T$*, which is the minimum of the actual $Gain_T(\Delta\psi)$:

Measured E_{tot} at p_1 = radial, p_2 = vert.	Minimum transversal $Gain_T$
< - 6.8 dB	> - 10.5 dB
< - 9.9 dB	> - 14.0 dB
< -11.8 dB	> - 20.0 dB

Thus, one may assume that the transverse polarization is about - 9 to -20 dB (mean values of TABLE 91, which are depending on the ground reflection)

12. Comparison of Improved Experimental Data with Three-Dimensional Computational Data

12.1. INVESTIGATED PARAMETERS

12.1.1. EFFECT OF THE FREQUENCY ON THE FIELD COMPONENTS AT FZYL AND MET

Let us first compare the previous experimental data of section 9. with the new FZYL computational data of section 10.4.:

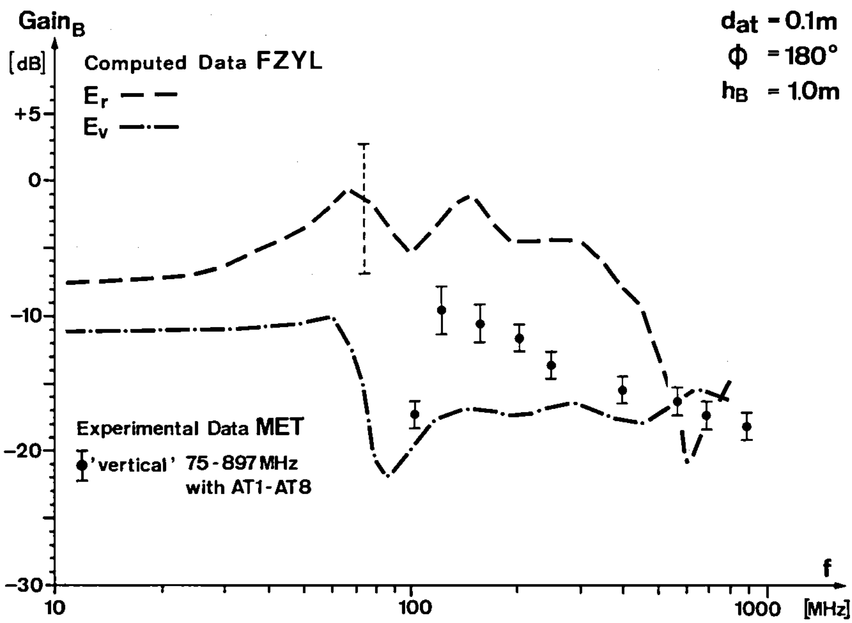

FIGURE 92 Gain$_B$ versus f at $d_{at} = 0.1$ m and $\phi = 180^o$. Comparison between experimental MET data (9.1.1.) and computational FZYL data E_v and E_r.

FIGURE 92 shows the experimental MET data measured with the previous monopole antennas AT1 to AT8 (8.3.1.) at 74, 101, 125, 158, 205, 250, 400, 562, 700 and 897 MHz. Theoretically these measuring data should be close to the computes E_v curve. In fact, a good agreement is achieved at higher frequencies 250, 400, 562, 700 and 897 MHz. At lower frequencies, however, the agreement is poor; the experimental data are generally much higher than the computed E_v's. It seems to be evident that the monopole antennas with their insufficient counterpoise do not only respond to the weak vertical field component but also to the very strong radial field component.

The experiments with the new test transmitters AO1 to AO4 prove the existence of the strong radial field components. The experiments are based on the verified reciprocity theorem (9.1.5.) and in order to quantify the effect of the proximity to the ground the experiments have been performed twice: first experiment with $s = 0.2\,m$, $h_l = 1.2\,m$ ($h_B = 1.0\,m$) and second experiment with $s = 0.7\,m$, $h_l = 1.7\,m$ ($h_B = 1.0\,m$). The results of the experiments are shown in FIGURE 93 :

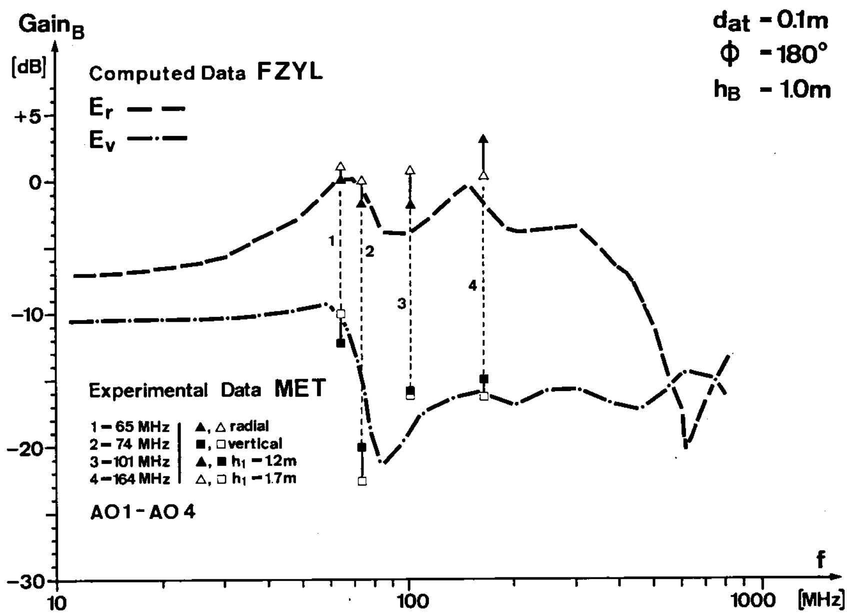

FIGURE 93 Gain$_B$ versus f at $d_{at} = 0.1\,m$ and $\phi = 180^o$. Comparison between experimental MET data (obtained with the test transmitters AO1 to AO4) and computational FZYL data at vertical and radial polarizations. Standard experiments : full symbols, $h_l = 1.2\,m$, $h_B = 1.0\,m$, $s = 0.2\,m$. Experiments with reduced ground effects: empty symbols, $h_l = 1.7\,m$, $h_B = 1.0\,m$, $s = 0.7\,m$. (Test body separated by wooden spacers from the stage)

<u>Vertical field components E_V</u> : The experimental data agree within 3 dB with the computational data, except at 75 MHz where the difference amounts to 5 dB. If one would shift the computed FZYL-data by 5 % to the left the agreement would be 2 dB. Thus, it could be that the actual resonant frequency is about 5 % lower than computed. The effect of the proximity to the ground is not very important, the differences are smaller than 3 dB.

Radial field components E_r : FIGURE 93 proves the existence of the theoretical predicted radial field components. The E_r are more than 10 dB larger than E_v at $d_{at} = 0.1$. The experimental data agree within 2.5 dB with the computational data, except at 164 MHz where the difference amounts to 4 dB. Similar to the E_v-components, a better agreement could be achieved (but only for 65, 74 and 101 MHz) by shifting the FZYL-data by about 5 % to the left. The proximity to the ground results in a 2 dB difference at 65 and 74 MHz and a 4 dB difference at 101 and 164 MHz (s : 0.7/0.2 m).

12.1.2. EFFECT OF ANTENNA HEIGHT AND PROXIMITY TO THE GROUND

The computational data are valid for a body in free space, for a standard relative antenna height $h_B = 0.1$ m and for a standard irradiation angle θ_i of 80.8^0. The experimental data are obtained from a test body in proximity to the ground due to the reasons explained in section 5.3.1.. The antenna-body system is a resonant circuit as we can see from FIGURE 93. Any resonant system is very sensitive to external influences so that in our case the antenna-body system may change its function (e.g., resonant frequency) in proximity to the ground. In order to check if h_B is an exceptional relative antenna height (i.e., not a representantive height) and in order to quantify the effect of the proximity to the ground both h_B (relative antenna height) and h_1 (absolute antenna height) were varied and compared with the computational data in FIGURES 94 a,b,c,d.

Effect of the proximity to the ground : The FSL vary only by $\Delta < 2$ dB from $1.2 < h_1 < 1.7$ m . The computed data are calibrated to FSL (s = 0.2 m) and to 'FSL' (s = 0.7 m). A strong influence of the proximity of the ground is only noticed at E_v (65 MHz) and E_v (74 MHz) due to the different $E_v(h_B)$ pattern. At a fixed h_B of 1.0 m the differences due to ground proximity are well below 3 dB for all E_v and E_r.

Effect of the relative antenna height : Generally, the E_r components increase with increasing h_B (except at 164 MHz, where E_r is almost constant) and vary up to ± 5 dB in the range $0.8 < h_B < 1.2$ m. The E_v components are much lower than E_r and vary up to ± 5 dB in the same range. An h_B of 1.0 m is not an extraordinary antenna height: only at 74 MHz the E_v of the isolated body (s = 0.7 m) is close to a point of inflexion.

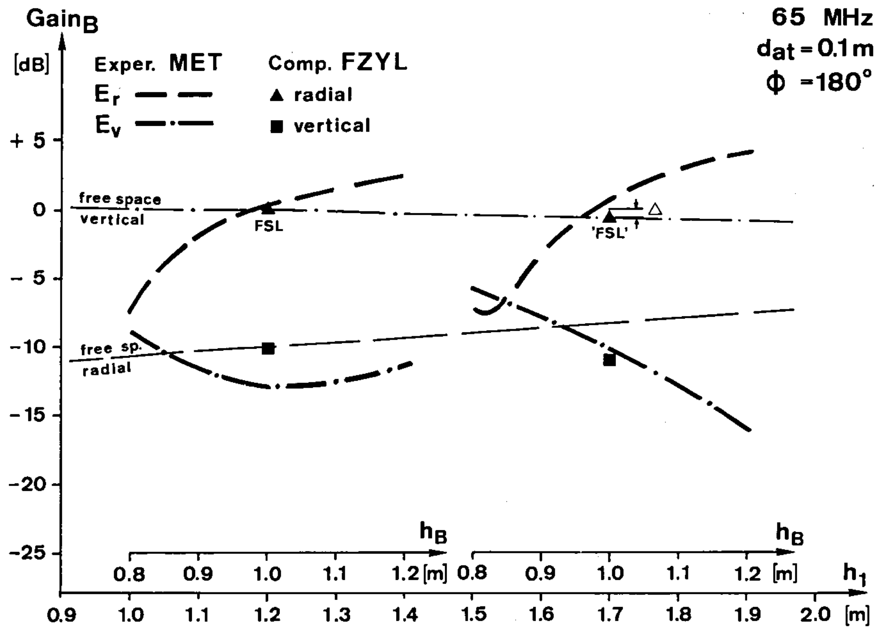

FIGURE 94 a Effect of ground proximity and relative antenna height, 65 MHz

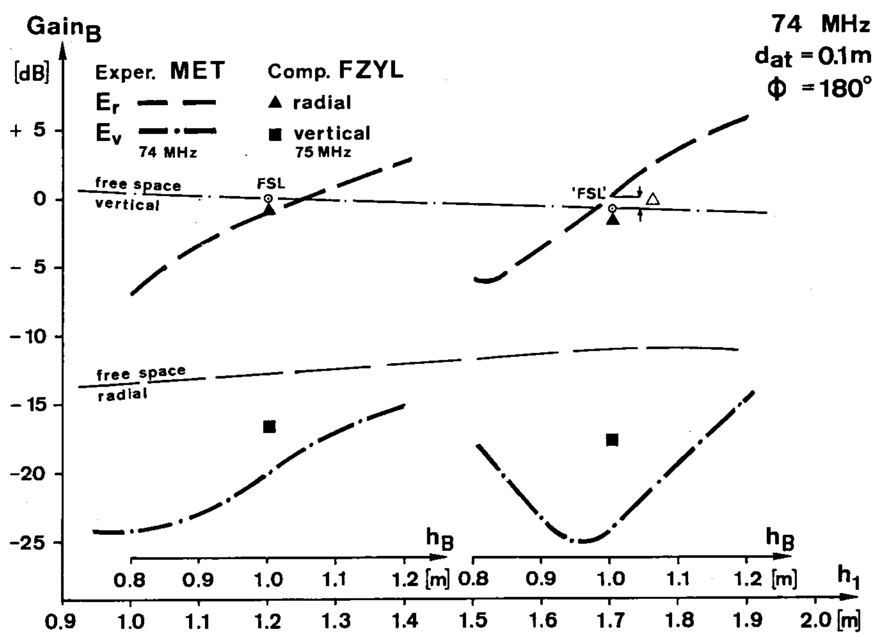

FIGURE 94 b Effect of ground proximity and relative antenna height, 74 MHz

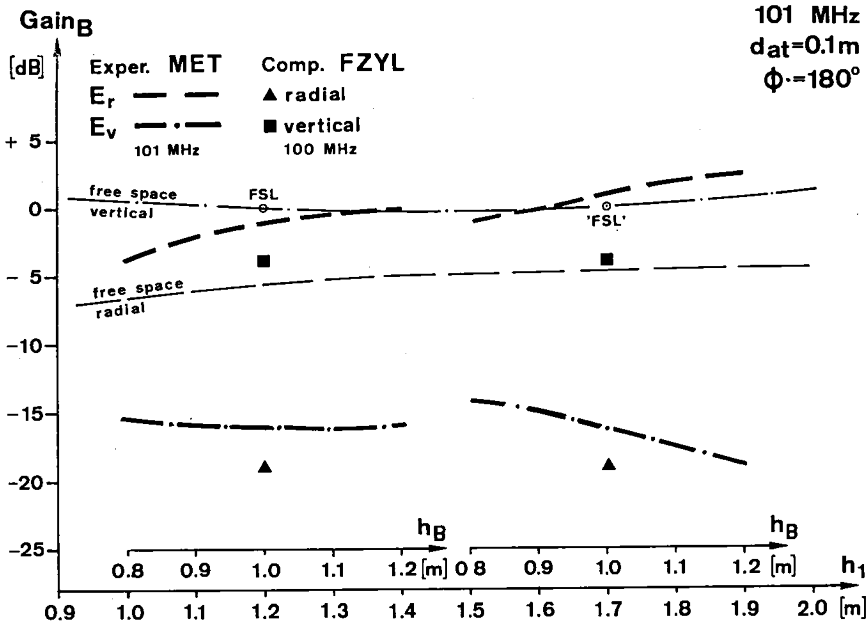

FIGURE 94 c Effect of ground proximity and relative antenna height, 101 MHz

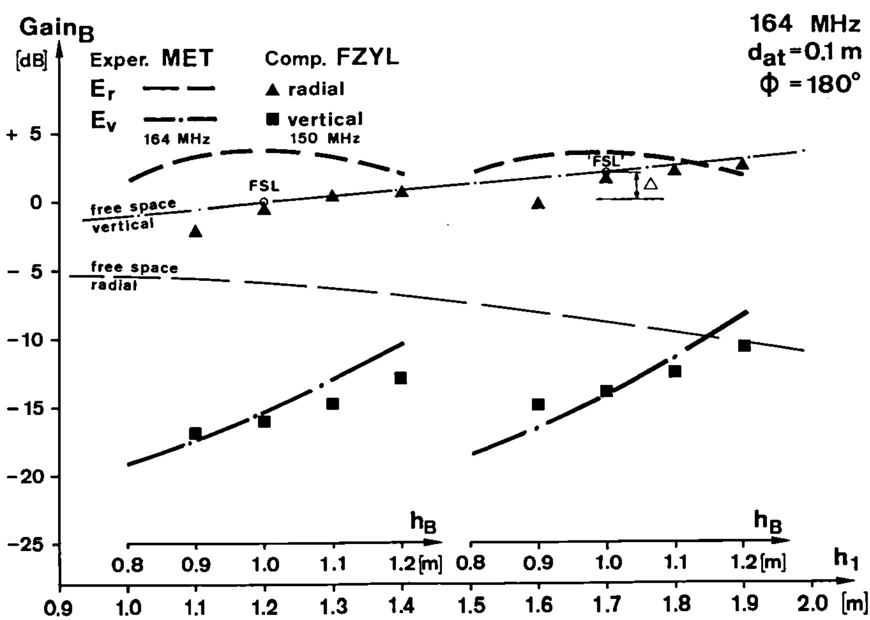

FIGURE 94 d Effect of ground proximity and relative antenna height, 164 MHz

12.1.3. EFFECT OF THE ANTENNA-BODY DISTANCE

FIGURE 92 and 93 revealed very low E_v's above 100 MHz and large E_r's at frequencies between 50 to 300 MHz at d_{at} = 0.1 m and $\phi = 180^0$. FIGURES 95 a, b and c show the corresponding data for d_{at} = 0.2, 0.3, and 0.4 m. Similar to FIGURE 92 the experimental E_v data above 250 MHz agree best with the computational data, the typical error is less than 2 dB. At lower frequencies the experimental E_r and E_v follow the computed patterns and the agreement between experiment and computations is generally better than 4 dB. The comparison of the experimental and computational pattern leads to the assumption that the MET body resonates about 5 % lower than the FZYL. This effect could be explained by the larger circumference of MET (sharp cylinder ends) compared with FZYL (round end caps). FIGURES 95 a,b,c show clearly the increase of E_v with increasing d_{at} and the decrease of E_r with increasing d_{at}. FIGURE 95 c demonstrates the equilibrium of E_v and E_r at d_{at} = 0.4 m in the frequency region 75 to 170 MHz experimentally and theoretically. At smaller d_{at} the radial component E_r is dominant and can be observed from minimum 40 MHz to maximum 500 MHz.

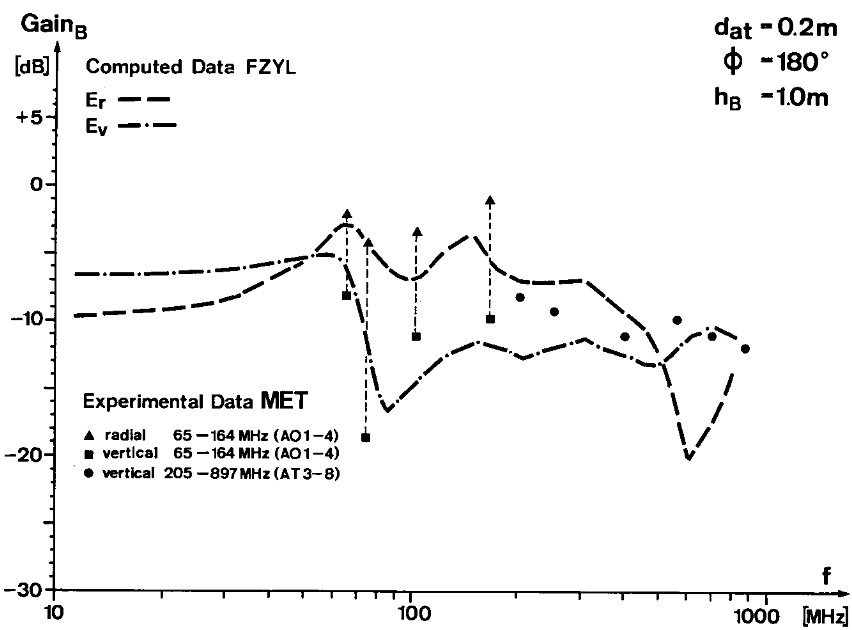

FIGURE 95 a Gain_B versus f at $\phi = 180^0$ and d_{at} = 0.2 m. Comparison between experimental MET data and computational FZYL data. Standard experiments with $\theta_i = 80.8^0$, h_1 = 1.2 m, s = 0.2 m, h_B = 1.0 m with AO 1-4 and AT 3-8.

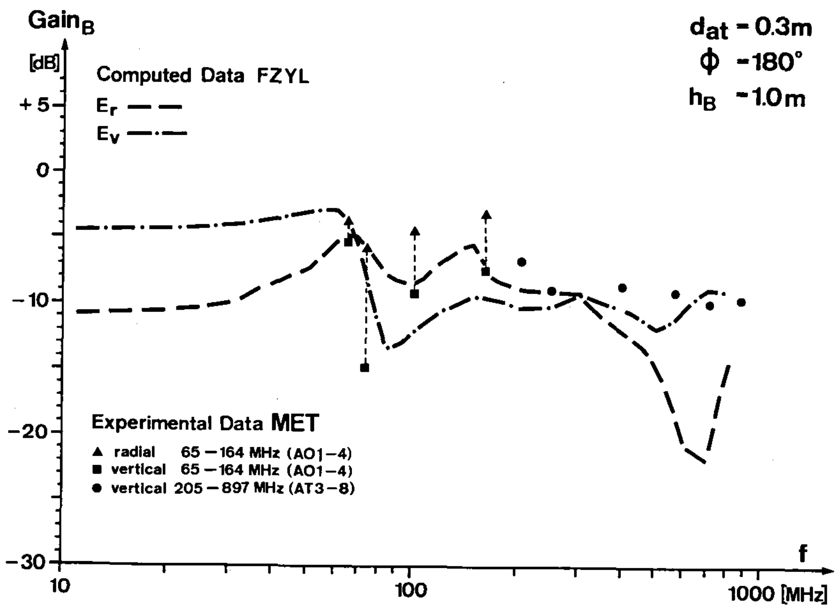

FIGURE 95 b Gain$_B$ versus f at $\phi = 180^0$ and $d_{at} = 0.3$ m. Comparison like 95 a.

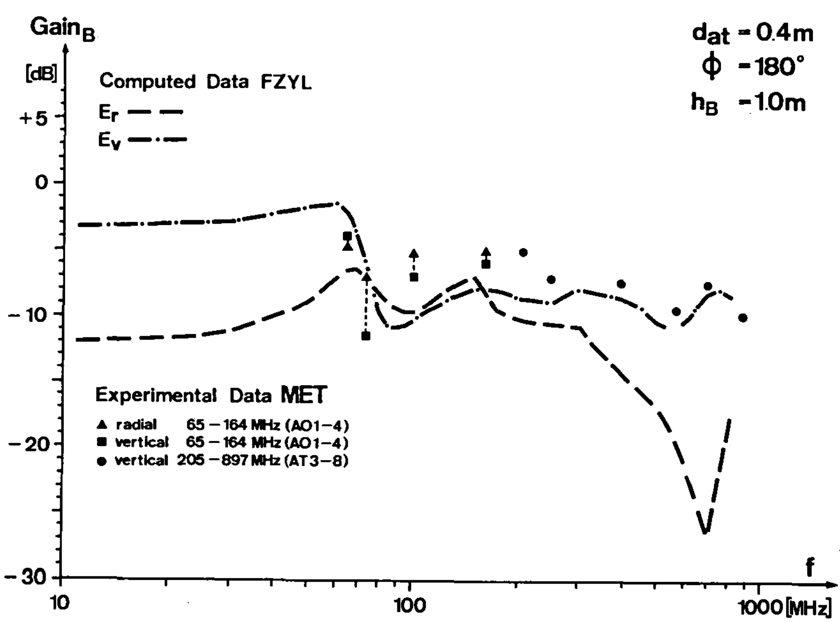

FIGURE 95 c Gain$_B$ versus f at $\phi = 180^0$ and $d_{at} = 0.4$ m. Comparison like 95 a.

12.1.4. EFFECT OF THE FREQUENCY ON THE FIELD COMPONENTS AT A HUMAN BODY

The experimental data in section 9.1.2. revealed only small differences between the test bodies MET, PHA and SUB at larger d_{at}'s. Thus, the experimental SUB data and the two computational data MANMOD 1 and 2 are presented in FIGURE 96 for the most critical antenna-body distance $d_{at} = 0.1$ in the shadow zone $\phi = 180^{\circ}$:

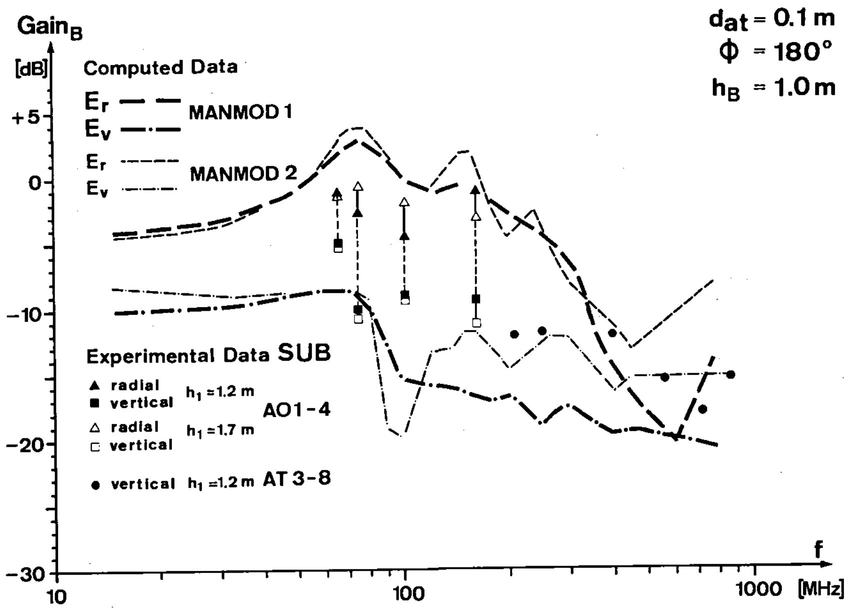

FIGURE 96 $Gain_B$ versus f at $d_{at} = 0.1$ and $\phi = 180^{\circ}$. Comparison between experimental SUB data and computational MANMOD 1 & 2 data for E_r and E_v at two different absolute antenna heights. Full symbols : $h_1 = 1.2$ m, $h_B = 1.0$ m, s = 0.2 m ; empty symbols : $h_1 = 1.7$ m, $h_B = 1.0$ m, s = 0.7 m.

Vertical field components E_v: 9 of the 11 experimental data agree with the the MANMOD 1 or 2 - data within 3 dB. The experimental 400 MHz E_v is 4.5 dB higher than computed and the experimental 101 MHz E_v is 6.5 dB larger.

Radial field components E_r : All investigated frequencies prove the existence of the very large radial field components. The maximum difference between experiment and theory amounts to 3 dB (s = 0.7) and 5 dB (s = 0.2 m). The radial field component at a human body is up to 10 dB larger than the vertical component. Much higher radial fields were recorded with decreased d_{at} , but are not presented here due to insufficient accuracy.

12.1.5. AZIMUTHAL RADIATION PATTERNS OF MET, SUB, FZYL AND MANMOD 1 & 2

The azimuthal radiation patterns at frequencies above 200 MHZ (above resonance) have been treated in section 9.1.2. (TABLE 60) and 9.1.3. (FIGURE 59) since they could be explained with the simple two-dimensional computations on the IZYL model.

The following FIGURES 97 a,b,c,d show the experimental and the computational azimuthal radiation patterns at 65, 74, 101 and 164 MHz at d_{at} = 0.1 m of MET and FZYL, and FIGURES 98 a,b,c,d that of SUB and MANMOD 1 & 2. The experimental data have been recorded with the test transmitters A0 1 to A0 4 (11.3.) in proximity to the ground ($s = 0.2$ m, $h_1 = 1.2$ m) and represent realistic azimuthal radiation patterns for practical applications. Because complete 0-180-360^0 revolutions have always been recorded, two 0-180^0 recordings may appear for the vertical component E_v and the radial component E_r due to the asymmetry of the test set-up (antenna manipulator, radial antenna not perfectly adjusted in the horizontal plane). For the following discussion of the comparison between experimental data (MET and SUB) and computational data (FZYL and MANMOD 1 & 2) the mean value of the experimental data at the distinct angle ϕ will be regarded.

65 MHz : The MET E_v agree with FZYL E_v at $\phi > 100^0$ within 3 dB, but at 0^0 the MET E_v are up to 14.5 dB higher than computed. Comparing MET with the FZYL data at 50 and 60 MHz one may assume that the discrepancy is caused by a lower resonant frequency of MET. The MET E_r agree, however, with FZYL E_r for all ϕ's within 3 dB.

The SUB E_v agree with MANMOD 1 & 2 at $\phi > 90^0$ within 4 dB, but at 0^0 the SUB E_v are up to 10 dB higher than computed. The SUB E_r agree, however, with MANMOD 1 E_r for all ϕ's within 3 dB.

The minimum radial component is always stronger than the maximum vertical component. Using the radial component for omnidirectional transmission an improvement of 7 to 13 dB (MET) and of 0 to 4 dB (SUB) can be achieved in realistic conditions.

74 MHz : The MET E_v agree with FZYL E_v at $\phi > 140^0$ within 3 dB, but do not show the extreme loss at 110^0, caused perhaps by a cross talk of the horizontal component of the elliptical polarized A_1 antenna. The SUB E_r agree with the FZYL E_r for all ϕ's within 4.5 dB.

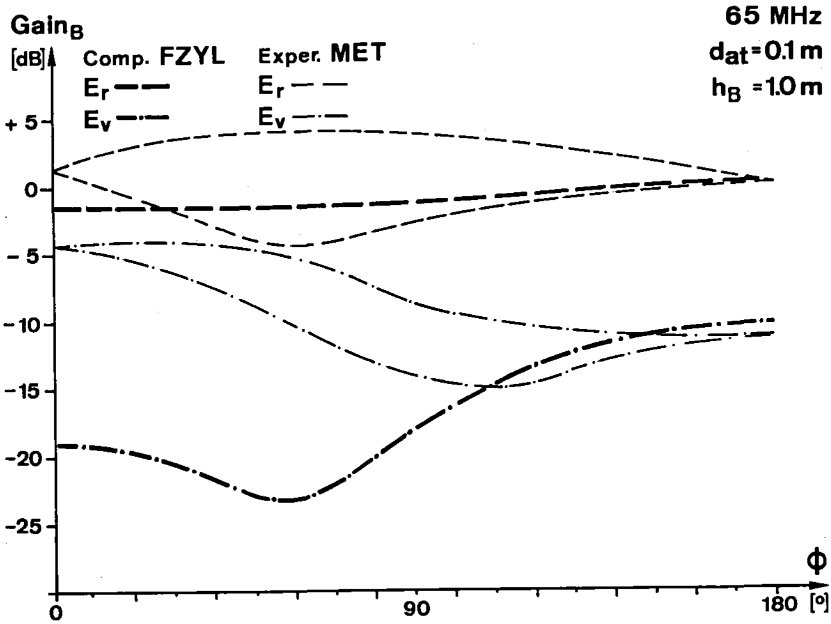

FIGURE 97 a Azimuthal radiation pattern MET and FZYL at $d_{at} = 0.1$ m, 65 MHz.

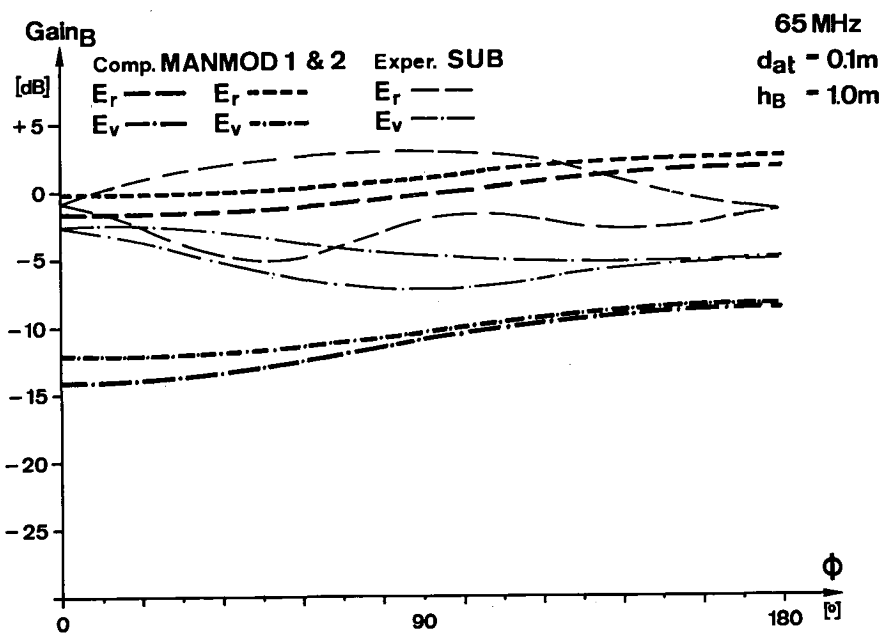

FIGURE 98 a Azimuthal radiation pattern SUB and MANMOD 1 & 2, same d_{at} and f.

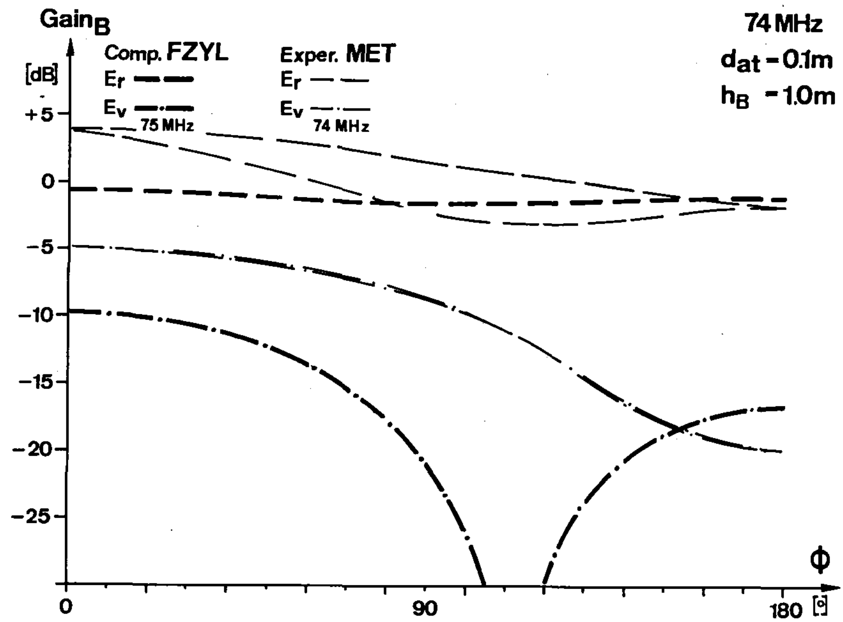

FIGURE 97 b Azimuthal radiation pattern MET and FZYL at d_{at} = 0.1 m, 74 MHz.

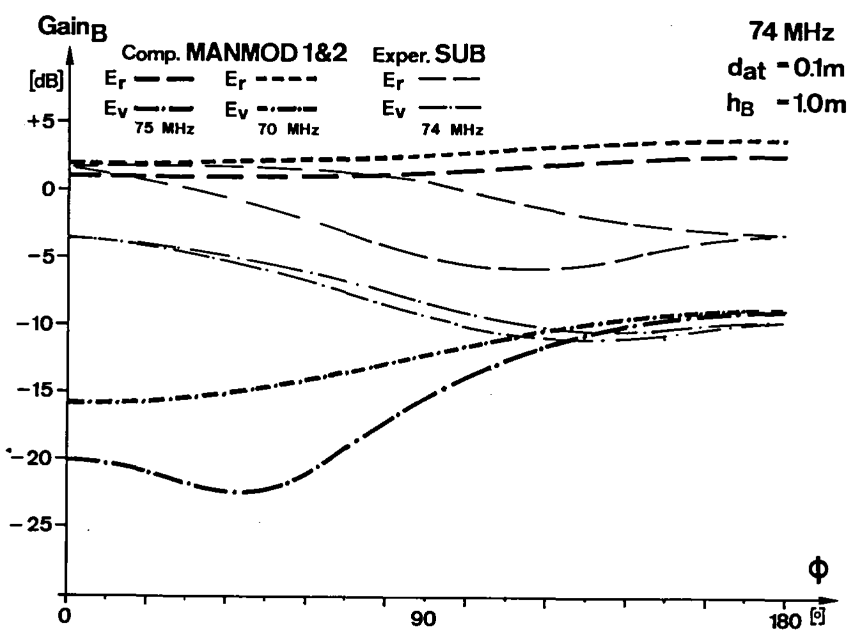

FIGURE 98 b Azimuthal radiation pattern SUB and MANMOD 1 & 2, same d_{at} and f.

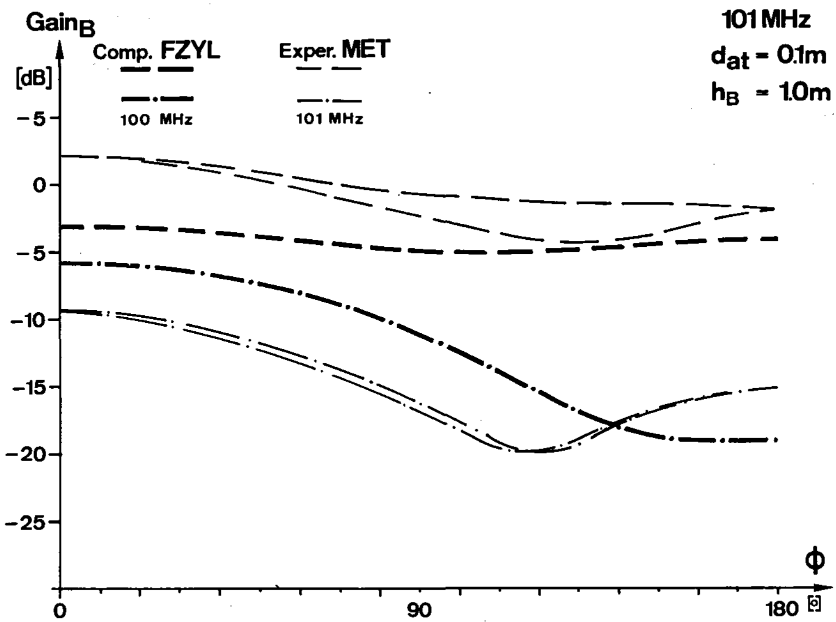

FIGURE 97c Azimuthal radiation pattern MET and FZYL at d_{at} = 1.0m, 101 MHz.

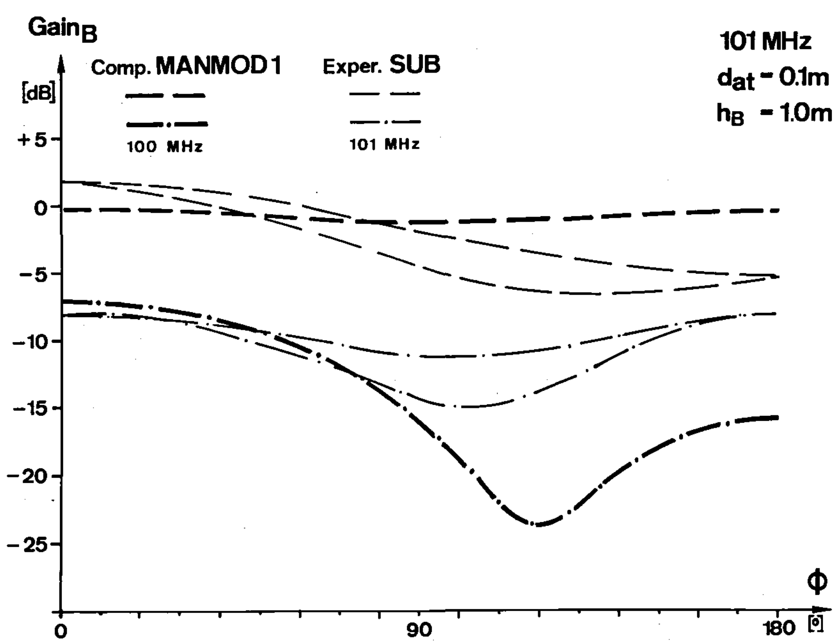

FIGURE 98c Azimuthal radiation pattern SUB and MANMOD1 , same d_{at} and f.

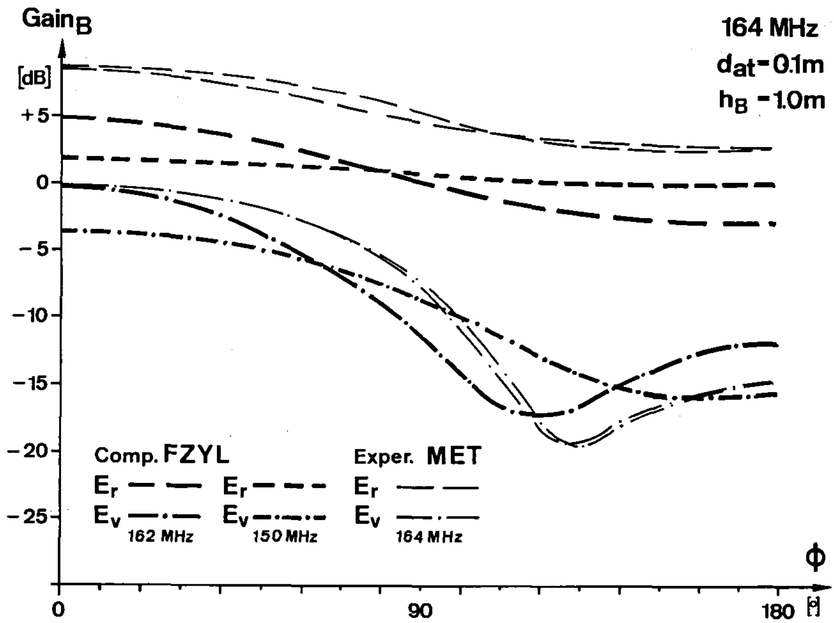

FIGURE 97 d Azimuthal radiation pattern MET and FZYL at d_{at} = 0.1 m, 164 MHz.

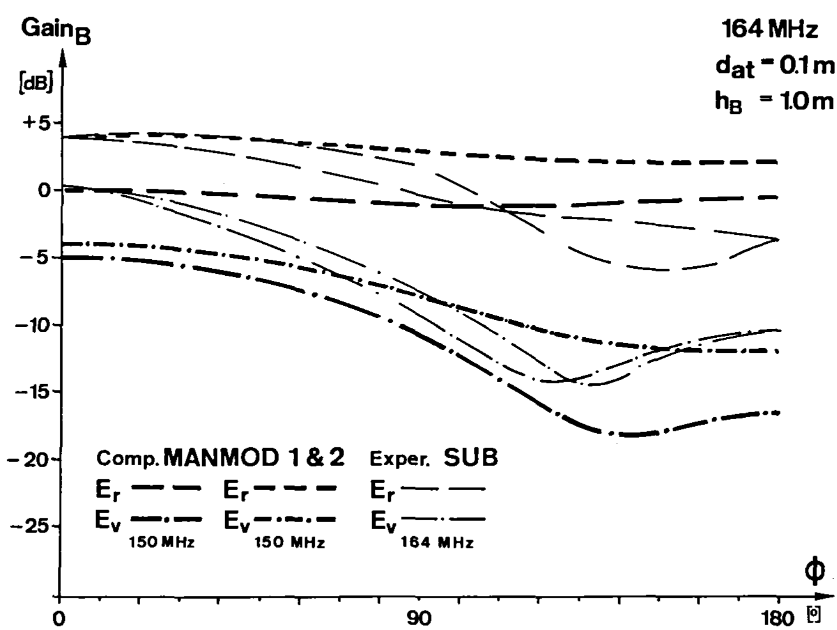

FIGURE 98 d Azimuthal radiation pattern SUB and MANMOD 1 & 2, same d_{at} and f.

74 MHz : (continued) The SUB E_v agree with MANMOD 2 E_v at $\phi > 90^0$ within 3 dB, but at 0-90° the SUB E_v are up to 13 dB higher than computed. The SUB E_r agree with MANMOD 1 E_r for all ϕ's within 6 dB.

Generally the minimum radial component is always stronger than the maximum vertical component (except SUB: $\phi = 0^0$). Using the radial component, the omnidirectional transmission can be improved by 12 to 14 dB (MET) and 5.5 to 8 dB (SUB) in realistic conditions.

101 MHz : The MET E_v agree with FZYL E_v at all ϕ's within 5 dB. A much better agreement could be achieved by comparing MET E_v with FZYL E_v at 85 to 95 MHz (see FIGURE 77 c). One may assume that MET resonates 10 % lower than computed (MET: sharp cylinder ends, FZYL: round end caps). The MET E_v agree with FZYL E_r at all ϕ's within 5 dB, compared with FZYL E_r at 95 MHz within 3 dB.

The SUB E_v agree with MANMOD 1 E_v at $\phi < 90^0$ within 3 dB, but at 90 to 180° the SUB E_v are up to 8 dB higher than computed. The SUB E_r agree with MANMOD 1 E_r at all ϕ's within 5 dB.

The minimum radial component is always stronger than the maximum vertical component. Using the radial component, the omnidirectional transmission can be improved by 15 to 17 dB (MET) and 5 to 8 dB (SUB) in realistic conditions.

164 MHz : The MET E_v agree with FZYL E_v(150 MHz) at all ϕ's within 5 dB, and with FZYL E_v (162 MHz) within 3 dB. The MET E_r agree with FZYL E_r (162 MHz) at all ϕ's within 5 dB.

The SUB E_v agree with MANMOD 2 E_v at all ϕ's within 4 dB. The SUB E_r agree with MANMOD 1 E_r at all ϕ's within 3.5 dB. (Only MANMOD 1 & 2 data at 150 MHz are available)

Generally the minimum radial component is always stronger than the maximum vertical component (except SUB: $\phi = 0^0$). Using the radial component, the omnidirectional transmission can be improved by 14 to 21 dB (MET) and 9 to 11 dB (SUB) in realistic conditions.

12.2. DISCUSSION OF THE LIMITATIONS OF EXPERIMENT AND COMPUTATION

Generally, the experimental data agree with the computational data within ± 3 dB at all frequencies and antenna-body-distances as small as 0.1 m.

Some experimental data in the resonance region differ more than 3 dB from the computational data, especially E_V at $\phi = 0^o$ in proximity to the ground is larger than computed. However, the important data from the shadow zone and the big difference between E_V and E_r are of satisfactory agreement. Taking into account the large signal range from -24 to + 6 dB the agreement between experiment and theory is satisfactory. A difference of ± 3 dB corresponds to a power variation of only 1% F.S., related to 0 dB = FSL = 100 %.

The experimental errors are caused mainly by five reasons:

- Capacitive coupling of the body with the ground. The resonant frequency depends on the proximity to the ground, as demonstrated by GANDHI et al. [24] in FIGURES 4 and 6. In our experiments with s = 0.2 and 0.7 m the difference amounts to maximum 3 dB at $\phi = 180^o$.
- Transverse polarization of the test antenna A_1. The applied helical monopole and dipole antennas are elliptically polarized, so that theoretical signals below -10 dB can be superimposed by stronger transversally polarized field components which determine the recorded data.
- Transverse polarization of the remote antenna A_2. The LPD antenna is only specified for the 100-1000 MHz range. A cross-talk of transversally polarized field components (see TABLE 91) is very probable.
- Symmetry of fields in the proximity of the test body. The antenna-manipulator contains no metallic parts, but the dielectric material may cause field disturbances. The test transmitters are not infinitesimally small and the orientation of the antenna A_1 may vary from the ideal value by about 5^o, causing phase errors and thus amplitude errors.
- Position and shape of the test bodies. The metallic cylinder with its sharp ends (vessel without top and bottom plates) does not correspond completely to the computational cylinder FZYL with its round end caps. The human test subject is not rotationally symmetric and during the measurements a change of the position (vertical axis inclined by a few degrees) and a change of the shape (breathing, etc.) cannot be excluded. The shape of the human body is a very important factor in the resonance region, and the computational differences between MANMOD 1 and MANMOD 2 are in the same order of magnitude as the difference between the experimental SUB and computational MANMOD data.

The limitations and the accuracy of the computational model have been discussed in section 10.3.4.. Principally, the accurate computation is limited to frequencies below 500 MHz with the standard parameter set and each computational result needs to be carefully checked. The computation of a test point is not accurate a priori: only if the frequency, the position of the test point and the test segment length have been varied, without large changes of the result, are the computational data reliable.

The computational errors are caused mainly by three reasons:

- At small d_{at} one can only compute the averaged field components in the environment of the selected test point.
- The computational field data depend very much on the shape of the body. If the body model is of complicated shape (MANMOD 1 & 2) the standard number of contour points is at the lower limit and the field data vary greatly at small variations of d_{at}, h_B and f. The experiments in 9.1.1. have lead to the conclusion that the body material is of little significance at d_{at} above 0.05 m and f above 200 MHz. Thus, the computational model for a human body should be first adapted to the asymmetric body shape and for frequencies below 200 MHz later on to the body material. However, an improvement of the body model is of secondary significance with respect to the practical applications of the obtained data, because the agreement between experimental and computational data is already satisfactory for the fields <u>outside</u> the human body.
- Computational effort. The present state of art allows the computation of 4 test points with a computational time of about 700 seconds on a CDC 6500 computer. More accurate computations are only possible with considerably improved computers with higher speed and more storage capacity.

13. Conclusions and Perspectives

13.1. IMPORTANT INVESTIGATED PARAMETERS OF THE ANTENNA-BODY SYSTEM

13.1.1. OVERVIEW OF THE INVESTIGATED ANTENNA-BODY SYSTEM

The purpose of the antenna-body study has been defined in section 2.. A standard test situation according to FIGURE 11 has been selected which represents the actual operational conditions on one hand and which could be computed on the other hand. Different antenna-body models have been computed and the results have been compared with corresponding experimental data obtained with representative body models. A relatively simple, analytically treatable, computational model was found which explains the effects of the human body on the EM field at frequencies above 200 MHz. A more complicated, numerically treatable, computational model was found which explains the effects in the entire investigated frequency range from 10 to 1000 MHz. Reliable experiments could be performed in the frequency range from 65 to 900 MHz. The agreement between theory and experiment was generally better than 3 dB (corresponding to a 1 % F.S. accuracy at power levels ranging from -25 to + 6 dB) with some few exceptions at extremely small antenna-body distances (see section 9. and 12.).

Interesting systematic computable correlations were found among frequency, body geometry, relative position of the antenna and transmission loss. The main question concerned the worst-case transmission loss in the azimuthal radiation pattern $0 < \phi < 180^{\circ}$. The parameters determining the performance may be listed in the order of their importance as follows:

- frequency (f) and size (length) of the test subject (L_B)
- antenna-body distance (d_{at})
- polarization of the body-mounted antenna (p_1)
- relative antenna height of the body-mounted antenna (h_B)
- lateral and sagittal diameter of the test subject (D_B)
- body material

The most interesting feature of the human body is the field polarization transformation effect which will lead to a new class of electrically small antennas for extremely close mounting on the human body. As found by computations and experiments, omnidirectional transmissions with less than 6 dB transmission loss are practically possible with antennas of less

6 x 6 x 6 cm dimensions mounted directly on the surface of the body. These antennas can be used for transmitters and receivers in the frequency range from about 60 to 160 MHz if the remote antenna A_2 is vertical polarized, without biological problems at power levels up to about 2 W.

13.1.2. THE EFFECT OF THE FREQUENCY ON THE FIELD DISTRIBUTION

In the following discussions we regard only the p_2 = vertical polarization at p_1 = vertical, radial and horizontal. The p_2 = horizontal polarization is of little practical interest with respect on omnidirectional transmission, as can be seen from the data in section 10.3.5..

At p_2 = vertical the wavelength of frequencies between 10 and 1000 MHz are of comparable magnitude like the circumference (from head to feet) of the human body. Thus one distinguishes three principal frequency regions:

- below 50 MHz : Rayleigh region (below first resonance)
- 50 to 200 MHz : Mie- or resonance region (including first resonance at about 65 MHz, second resonance at about 140 MHz, and first anti-resonance at about 100 MHz)
- above 200 MHz : Optical region (above second resonance)

Vertical polarized E-field components (p_1 = vertical) : Considering FIGURE 77 one notices the largest transmission $Loss_B$ above 85 MHz at $\phi \sim 180^0$. Comparing the d_{at} dependences in FIGURE 78 one notices the largest $Loss_B$ at minimum d_{at}. Thus, we have to look at only the $Gain_B$ versus f diagrams at $\phi = 180^0$ at d_{at} = 0.1 m for maximum $Loss_B$ considerations, e.g., FIGURES 92, 93 and 96. At a given (small) d_{at} the $Loss_B$ is relatively small (10 dB) and almost constant from 10 to 50 MHz. Below the first resonance a body is not transparent for EM-waves as could be assumed from the well-known radar cross section (RCS) pattern in FIGURE 17, if we regard small d_{at}'s. From 50 to 65 MHz $Loss_B$ decreases a few, but less than could be assumed by the RCS pattern. At 65 to 120 MHz $Loss_B$ increases drastically (especially at $\phi \sim 90^0$, see FIGURE 77c), amounting to 15-20 dB at d_{at} = 0.1 m. From about 150 to 1000 MHz $Loss_B$ remains large as demonstrated best by FIGURE 72. The best agreement between theory and experiment is obtained at frequencies above 200 MHz, due to the small radial E_r's above 200 MHz.

Radial polarized E-field components (p_1 = radial) : The radial $Loss_B$ versus f pattern is completely different from the vertical $Loss_B$ pattern.

The radial field is maximum at minimum d_{at} and is almost independent f ϕ in the frequency range from 60 to 250 MHz. At frequencies below 30 Ml the radial component is small and the minimum is located at $\phi = 0^{o}$ (FIGl 77) The radial component becomes interesting above 50 MHz, and its pr perties are best demonstrated in the $Gain_B$ versus f diagrams at $\phi = 18($ (FIGURES 92, 93 and 96). $Loss_B$ decreases considerably from 50 to 65 MHz and at d_{at}=0.1m an actual gain of some dB can be observed. A first Los maximum of about 5 dB occurs at about 100 MHz, but not so accentuated a in the vertical polarization. A second $Loss_B$ minimum is at about 150 Mh with about 1 to 3 dB. With increasing frequency $Loss_B$ increases, too. A frequencies above 250 MHz $Loss_B$ is higher than 6 dB ($\phi = 0^{o}$, FIGURE 77 b and above 350 MHz the maximum radial $Loss_B$ is larger than the maximum vertical $Loss_B$. However, at $\phi = 180^{o}$ the radial $Loss_B$ remains small up t about 400 MHz (FIGURES 93 and 96).

The experimental and computational azimuthal radiation patterns in FIGURES 97 and 98 reveal excellent omnidirectional characteristics with up to 11 dB (human test subject) and 21 dB (metallic cylinder) better performance than compared with the vertical component. For practical appli cations the radial component is limited to frequencies between first and second resonance, that is about 50 to 200 MHz.

Horizontal polarized E-field components (p_1 = horizontal): The transmission $Loss_B$ at horizontal polarization is of little practical significanc as demonstrated with FIGURE 77. At $\phi = 0$ and 180^{o} $Loss_B$ is very high, onl at $\phi = 90^{o}$ a $Loss_B$ of less than 20 dB is noticed. Small losses, but only for ϕ around 0 and 180^{o}, are only obtained at p_2 = horizontal which we do not discuss here. Some data for that case are to be found in TABLES 69 and 70 and in the Appendix 16.2.4. for the frequencies 65 to 425 MHz.

13.1.3. THE EFFECT OF THE ANTENNA-BODY DISTANCE

In the following discussion we regard again only the p_2 = vertical polarization. From the practical point of view the small d_{at}'s are of main interest, but only the knowledge of the $Gain_B$-d_{at} dependence lead to an understanding of the shape of the azimuthal radiation patters.

Vertical polarized E-field components (p_1 = vertical): As long as d_{at} is smaller than $\lambda/4$ the transmission $Loss_B$ increases with decreasing d_{at}. At larger d_{at}'s standing waves with highly varying $Loss_B$ are observed.

The human body consists of a material which reflects an EM wave similar to a perfect conductor (see details in section 5.2.4.). The reflection factor for the E-component is thus -1, so that the superimposed signal from scattered and incident field is maximum at $d_{at} \sim \lambda/4$ at $\phi = 0$ (see FIGURES 56,57 and 68). A similar situation occurs at $\phi = 90^o$, where the maximum is at $d_{at} \sim \lambda/2$. At such extraordinary d_{at}/ϕ conditions the transmission $Loss_B$ is very low or even a gain of some dB can be measured, so that the human body can be regarded as a reflector similar to the reflector of a Yagi antenna. A quasi-parabolic antenna can be arranged with 3 persons (FIGURE 54), effecting a directive gain of more than 4 dB. Considering the fact that + 3 dB is the double power, this result is quite interesting. This $\lambda/4$ to $\lambda/2$-effect (depending on ϕ) is also observed in daily life, if one approaches a mobile receiver (e.g. FM, 80 to 120 MHz) which is tuned to a weak radio station : at some distances the signal is very clear and varying some centimeters distortions can be heard. Thus, for frequencies above 300 MHz practical antenna-body distances may be larger than $\lambda/4$, effecting large $Loss_B$ variations in the azimuthal radiation patterns (see e.g. FIGURE 59), which can now be understood and well predicted.

Radial polarized E-field components (p_1 = radial): The radial field effect occurs only in the proximity to the body, as can be seen in FIGURE 78. At very small d_{at} and frequencies between 50 to 250 MHz the $Loss_B$ is very low or even a gain can be observed, independent on ϕ. In this frequency range $Loss_B$ decreases considerably with decreasing d_{at}, e.g. from 11 dB/d_{at} = 1.0 m to -2 dB/d_{at} = 0.05 m at f = 150 MHz and $\phi = 180^o$. At about d_{at} = 0.3 m the amplitude of the radial components are as large as the amplitude of the vertical components, and above 250 MHz a similar, but inverted pattern like the $d_{at}/Gain_B$ versus λ in the vertical component can be noticed.

Horizontal polarized E-field components (p_1 = horizontal): The horizontal components depend little on d_{at}, because they are essentially only the residual, little disturbed horizontal components of the incident field (see effect of the irradiation angle in FIGURE 76).

13.1.4. THE DOMINANT RULE OF THE RADIAL E-FIELD COMPONENT

At frequencies from about 50 to 200 MHz (first to second resonance of the human body) the human body acts like a very efficient polarization converter. The only conditions are : d_{at} below 0.3 m and p_2 = vertical. At d_{at} = 0.1 m the transmission loss amounts to ± 5 dB which is much better than the widely varying transmission $Loss_B$ of - 4 dB to - 20 dB obtained with a vertical polarized antenna. The mechanism of the polarization transformation effect can be briefly summarized as follows:

- Receiving case: We assume a standing human test subject, irradiated by a plane, mostly vertical polarized wave by a remote antenna with an incident angle of 70 to 90°. At frequencies from about 50 to 200 MHz the relative and the specific absorption cross section (FIGURES 3 and 4) is high. Thus, the body collects not only RF-energy corresponding to its shadow area, but also from outer regions similar to a good receiving antenna with a large effective area. The RF- currents are flowing mainly in the outer layers of the body and surface charges are generated. Both currents and charges produce a scattered field around the body. Because the human body is now the new RF-source, it is not astonishing that a certain field component is largest very close to the surface, and because the vertical and the horizontal components are weak, the radial component must be large due to the total collected RF-energy (this explanation is logical for a metallic body, but only partially acceptable for biological bodies). The source of the tremendous radial field component must be the surface charges. The integral effect is completely described by the Maxwell equations and is proven by experiments. It explains the practically important transmission loss or gain, but a further study on the detailed mechanism may be interesting from the scientific point of view.

- Transmitting case: The reciprocity theorem (section 5.2.1.) says that the transmission loss from A_2 to A_1 is the same as from A_1 to A_2. With this answer the explanation is given why a radial transmitting antenna performs best, because the receiving case is mathematically clear. However, the detailed mechanism is not clear at all, only in the integral sense is this explanation satisfactory if we speak only of the transmission loss, which was the purpose of this study. It might be that a radial antenna produces above all large surface charges which evoke axial currents. These currents are comparable to those in a thick mono- or dipole, producing a vertical polarized far field. As we shall see in section 13.3.2., an applicable radial antenna will be equipped with a metallic plate on the surface of subject, so that biological problems can be excluded at reasonable RF-power (body shielded from the large reactive near-field of the antenna). However, a future study on the detailed coupling mechanism might be of scientific interest. In this context it should be mentioned that some unexplainable (parapsychological ?) effects occured with the test transmitters described in section 11. 3. : Some test subjects complained to feel an irritating sensation when the antenna was held radial to the head. Further, an irregular signal could be heard on the monitor receiver if the transmitter was positioned at two distinct points of the upper forehead and to the wrist of the hands. It should be mentioned that the transmitters were quartz stabilized (modulation only possible by selective RF-absorption) and that the CW power was much less than 10 mW.

- Practical significance : The polarization transformation effect is not only very important for specially designed radial antennas, but also for most of the generally applied electrically small antennas, such as the helical monopole antennas of walkie talkies : If self-resonant, electrically small antennas are developed, it is very difficult to obtain a strictly linear polarization. There is always a transverse polarization, e.g., in the case of helical antennas with its elliptical polarization (see Appendix 16.1.) the secondary polarization axis increases with $\pi^2 D_h{}^2/p\lambda$, where p is the pitch and D_h is the helical diameter. Greatly simplified, the transverse polarization is relatively large compared with the desired axial polarization, if the helical antenna length h is small compared with $\lambda/4$. In addition, a helical monopole antenna would require a counterpoise of about $\lambda/2$ diameter in order to operated properly. Transmitting devices are, however, generally much smaller than $\lambda/4$ (maximum housing dimension), so that the electromagnetic counterpoise is not sufficient. As a consequence, the antenna does not radiate the computed elliptical polarized field, but also additional field components of arbitrary polarizations. For constant antenna and transmitter length the ratio of radial to vertical polarization increases with decreasing frequency. At frequencies of 100 MHz this ratio may amount to about -5 dB, at 200 MHz to about -10 dB and at 400 MHz to about -20 dB. Due to this inevitable transverse sensitivity (receiving case) and transverse radiation (transmitting case) the transmission loss does not sharply increase above 75 MHz (FIGURE 96) but increases slowly up to about 300 MHz (FIGURE 92). Above 250 MHz not only the investigated radial effect is of smaller influence, but also the antenna and its counterpoise approaches an ideal, strictly linear polarized radiation system. In this case, the computed $Gain_B/f$ dependence for vertical polarization becomes accurate also for practically realizable mobile radio sets. Thus, the unexpected good performance of practical body-mounted antennas in the proximity of a human test subject at frequencies between 50 and 200 MHz can be now explained by the polarization transformation effect and the technically inevitable transverse polarization of electrically small antennas.

- Perspectives : The polarization transformation effect is of great practical significance and could be proven theoretically and experimentally. Only roughly has the dependence of the relative antenna height been studied (FIGURES 94 a,b,c,d) and little is known about this effect in extreme proximity to the human body. A future study of the parameters d_{at} (0 to 0.1 m), h_B (0.8 to 1.8 m), θ_i (70 to 90°), body-geometry and body material would be of great interest. Because the computational cost would be very high (improved model of man with more than 200 contour points required, investigation of the significance of the body material, many d_{at} and h_B steps necessary), such a future study should start with experiments. Test transmitters similar to those described in section 11., but of reduced size, and an improved antenna manipulator would be required.

13.2. INTERESTING ADDITIONAL FEATURES OF THE ANTENNA-BODY SYSTEM

13.2.1. THE BROAD-BAND CHARACTERISTICS OF THE HUMAN BODY

The presented study dealt with an antenna-body system where the antenna A_1 was separated from the body. In an other study the active radiation of the human body was investigated (NEUKOMMM [63]). Briefly summarized, the main results of that study are:

- A thick monopole antenna was mounted on a large counterpoise and fed properly by a continuously enlarge coaxial line according to HEILMANN

[42], page 110. The radiation pattern of metallic rotational cylinder of a diameter $D_B = 0.25\,m$ (diameter of a human body) and a monopole length 1/2 $L_B = 0.9\,m$ (1/2 human size) was an omnidirectional pattern in the azimuthal plane, with a gain of more than -3 dB at frequencies between 60 to 200 MHz at an elevation angle of about 0 to 10^0. At frequencies above 200 MHz a side lobe at an elevation angle of about 45^0 is developed, causing high losses at 0 to 10^0. The results agreed partially with whose of KRAUS [51].

- The same experiment was repeated with a phantom (comparable with PHA in section 5.4.1., but equipped with a similar feeding as mentioned above). The astonishing result was, that the phantom showed almost the same broad-band characteristics, with only little additional losses: from 60 to 180 MHz an omdirectional radiation pattern was obtained with a gain of more than -5 dB (reference: isotropic antenna).
- Actual experiments with human test subject could not be performed, but there is no doubt that the human body would show a similar performance. If an RF-current is flowing along the vertical axis of the human body, it flows not only in the outer layers, but also in depths of some centimeters (TABLE 1). Thus, the current carrying area is relatively large, resulting in a small resistance R_{loss}. Due to the shape of the human body ('thick cylinder') the radiation resistance is relatively large compared.with the reactive impedance (general theory of thick monopoles and dipoles). This means that the human body is an efficient broad-band antenna for the frequency range 60 to 180 MHz, as proven with the phantom experiments.

Unfortunately, the practical feeding of the human body causes severe problems. Theoretical and experimental investigations by FISCHER and CASTELLI [23] revealed the impossibility of the RF-coupling by means of a toroid. This idea looks very promising at first sight: A toroid coil generates a circular H-field in the horizontal plane and is theoretically appropriated to induce an axial current in a body situated in the center of the toroid. However, in the regarded frequency range 60 to 200 MHz the circumference around the hip is larger than 0.12 λ. Because of the helical construction of the toroid a phase difference of mimimum 90^0 occur because the signal velocity along the toroid is reduced by a factor of 2 to 5 (see Appendix 16.1.), so that the induced axial currents are not in phase. Several improved feeding methods were suggested , including segmental toroids and capacitive coupling, but up to now a practically applicable solution is missing (FISCHER and CASTELLI [23]).

The broad-band characteristics of the human body has its main significance for personal radio sets with inefficient, poorly matched antennas, as for instance wireless microphones in the frequency range 30 to 150 MHz. Below 100 MHz the design of tuned, efficient and body-mounted antennas for vertical polarization is very difficult. The main problems are the detuning effect of the body proximity and the efficiency at small h/λ ratio. If a short monopole or dipole cable antenna is in the proximity of the human body, the body acts like a lengthening of the antenna, as can be noticed with any short-wave or ultra-short-wave receiver. If the original antenna is relatively bad (general situation), the human body is a considerable improvement. Since many transmitters operated with such cable antennas (e.g. biotelemetry in the 37 MHz band), an investigation of the active radiation pattern of the human body and a detailed study on the coupling mechanism would be sensible. Principally, there are two ways for a theoretical analysis:

- Integration of the near-field data of section 10.4. along a multidimensional antenna. By designing a special antenna with matched amplitude- and phase- correlations along the selected polarization axes the desired coupling might be obtained.
- Computing of aperture radiation according to HARRINGTON and MAUTZ [40]. In this case the RF-energy has to be coupled into the body by means of surface electrodes or capacitive plates. This method seems to be risky with respect to biological effects and encumbrance, but perhaps an acceptable solution is possible.

13.2.2. BODY-MOUNTED ANTENNA ARRAYS

The presented study dealt essentially with body-mounted antennas of very small dimensions, after having proved the field homogeneity around the test points. The data computed in section 10.3.5. may be also used for larger antennas, antenna arrays and antennas with more than one polarization axes. Such antennas would be of interest, if quasi-isotropic transmission is required. For such applications the computer programs are already prepared to compute similar data for changing incident angles θ_i.

13.3. PROPOSALS FOR EFFICIENT, BODY-MOUNTED ANTENNAS

13.3.1. VERTICAL POLARIZED ANTENNAS

Most of the currently used antennas are vertical polarized. Constructional details can be found by GOUBAU and SCHWERING [32], KANDOIAN and SICHAK [47], LI and BEAM [54], NEUKOMM [62,63], OEHEN and BALZARINI [67], TONG [80] and WHEELER [85]. It is not possible to discuss these antennas here, but the main limitations should be mentioned:

- Transmission loss of the vertical polarized E-field component. As studied in this report, the transmission loss increases with increasing frequency and with decreasing antenna-body distance. Above 100 MHz and d_{at} below 0.1 m it is not possible to obtain a worst-case transmission loss of less than 10 dB. Usually the transmission loss is physically limited on 10 to 30 dB at higher frequencies and smaller d_{at}'s, and the largest loss occurs usually in the shadow zone.
- Bandwidth. If an electrically small antenna occupies only a small fraction of the radiansphere (WHEELER [85]), the bandwidth decreases with decreasing volume (at constant frequency), if no additional resistive elements are involved. If a body is near to the near-field zone of the antenna, severe detuning effects are most probable.
- Efficiency. Usually, the radiation resistance is small, decreasing with decreasing volume of the antenna (at constant frequency).Each additional loss (ohmic losses in the conductor, earth losses,matching losses, etc.) decreases the efficiency. At frequencies below 200 MHz an important loss is caused by the insufficient counterpoise of monopole antennas.

A comparison of some helical antennas is given in Appendix 16.1.2. A special group of non-resonant antennas are the cable antennas for frequencies below 100 MHz: in contrast to the resonant antenna they may perform better in proximity to the body as in free-space, but also here the overall loss, compared with an ideal dipole in free-space,is in the region of 5 to 20 dB.

13.3.2. RADIAL POLARIZED ANTENNAS

These antennas are up to now little explored. The test transmitters of section 11.3. are not developed for optimal efficiency and are not intended for practical applications. FISCHER and CASTELLI [23] tried to design some radial polarized antennas for practical applications and performed some experiments with metallic and lossy body models (1/3 scale of MET and PHA, see also section 5.4.1.). In principle, these antennas are short helical monopoles with a top capacitor, mounted on a limited counterpoise and feed from a 50 Ω coaxial cable (FIGURE 99).

Top C-Helix mounted on Phantom

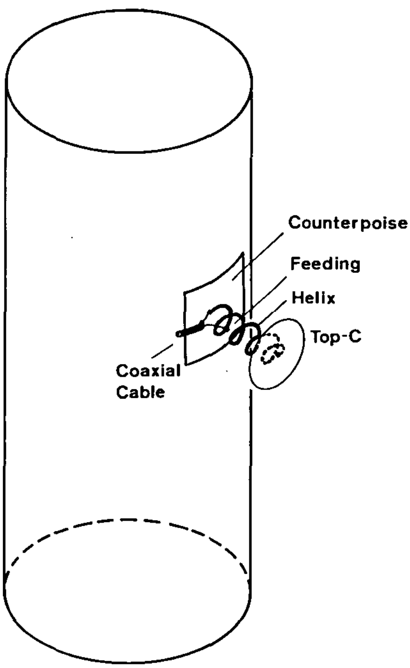

FIGURE 99

Radial polarized antenna (Top C-Helix) mounted on a Phantom.

Antenna dimensions:

h : 34 mm (monopole length)

D_h : 12 mm (helical diameter)

n : 1/2 to feeding point
5 1/2 to top C
(number of turns)

D_C : 47 mm (top C diameter)

L_C : 100 x 100 mm (dimensions of the counterpoise)

Body dimensions: (1/3 scale PHA)

L_B : 0.6 m (length)

D_B : 0.084 m (diameter)

(Source: FISCHER and CASTELLI [23])

The experimental data are of limited accuracy, because the measurements have been performed in a very small anechoic chamber:

Bandwidth on metallic cylinder (1/3 MET)	: 311 to 319 MHz
Bandwidth on model phantom (1/3) PHA)	: 313 to 321 MHz
Minimum/maximum azimuthal gain on 1/3 MET	: -12 dB / -5 dB
Minimum/maximum azimuthal gain on 1/3 PHA	: -16 dB / -9 dB
Bandwidth when mounted on a large c-poise	: 309 to 317 MHz
Gain at vertical polarization " "	: - 0.5 dB

All gain data are related to the ideal, isotropic radiator (0 dB), and not to the FSL as usually used in this study. The comparison of the data with those studied in section 12. lead to the following conclusions:

- The experiments of FISCHER and CASTELLI [23] are comparable to the experiments in section 12. performed at 101 MHz (1/3 of the model size = 1/3 of the nominal frequency). At this frequency the radial $Gain_B$ is minimum and amounts to -5 dB. The new measured data are about 7 to 11 dB lower in the worst case.
- The efficiency of the presented radial antenna could be improved by a larger counterpoise. The increase of the center frequency from 313 to 315 to 317 MHz from mounting on a large counterpoise to 1/3 MET to 1/3 PHA points to a too small counterpoise and efficiency loss.

The presented radial antenna is a promising solution, albeit the predicted high gain could not be achieved completely. However, comparing the radial antenna with a standard vertical polarized antenna of similar volume and mounting, the radial antenna prototype is already better in many respects:

- High absolute gain when mounted very close to the body, little variation of the field amplitude from $0 < \phi < 360^0$
- Human body well shielded from the near-fields of the antenna (Safety)
- Simple mounting, small volume and little encumbrance
- little or no detuning of the resonant frequency when counterpoise is sufficiently large
- Constant VSWR, direct matching to a 50 Ω coaxial line
- Little difference in gain when separated from the body (however, axis of the antenna must be vertical when separated from the body).

The physically given disadvantage of all electrically small antennas, the limited bandwidth, is of minor importance , because there are only very small detuning effects from the body. The reduced efficieny (in context with the extremely small length/λ ratio) is balanced by a better matching but is still a subject for improvement.

The improvement of the radial antenna and the optimization of h_B and d_{at} for frequencies between 50 and 200 MHz would be an interesting field of research. The literature on electrically small antennas and the experimental and theoretical data in this study may lead to practical body-mounted antenna with better performance and less biological risks.

13.4. THE OPTIMAL FREQUENCY RANGE FOR BODY-MOUNTED ANTENNAS

13.4.1. CONCLUSIONS FROM THE OBTAINED DATA

As a result of this study the optimal frequency range for omni-directional transmission with body-mounted antennas can be defined as follows:

OPTIMAL FREQUENCY RANGE : 35 TO 180 MHz

Some remarks are needed with respect to the practical use of personal radio sets. The antenna type, the antenna efficiency, the dimension of the radio set, the matching of the antenna to the RF-terminal and some other factors may lead to a slightly different choice. Thus, we may define four categories of optimal frequencies:

- 35 to 65 MHz : Strictly vertical polarized, well-matched, efficient, electrically small antennas (very theoretical, exist very seldom in practice).The transmission loss is minimum at 65 MHz and increases slightly with decreasing frequency. The lower the frequency, the more difficulties occur with bandwidth, detuning and efficiency.
- 50 to 200 MHz : Strictly radial polarized antennas. Good (experimentally proved) and excellent (predicted theoretically) performance can be obtained at small antenna-body distances in this range.
- 60 to 150 MHz : Technically realizable antennas with dominant vertical polarization but additional transverse (radial) polarization,such as helical monopoles on small transmitting and receiving devices, especially small walkie-talkies. The unexpectedly good performance in moderate proximity to the human body is mainly caused by a cross-talk of the radial component. Usually the transverse polarization was considered as an unavoidable lack of electrically small antennas. Above 150 MHz the design of more vertically polarized antennas becomes possible. As a consequence, the performance becomes better in free space, but worse in the proximity to the body, because both transverse polarization and radial component decreases with increasing frequency.
- 20 to 100 MHz : Cable antennas, inefficient, usually not matched antennas of less than $\lambda/4$ length (wireless microphones, biotelemetry transmitters in the 37 MHz band). The human becomes a part of the antenna due to different effects with resulting better performance.

13.4.2. FUTURE FREQUENCIES FOR BIOTELEMETRY

As a member of the working group TC 62 of the IEC the author took part in the preparation of the IEC document 62(Secretariat) 38 . This document recommends new biotelemetry frequencies to be proposed at the ITU world conference of frequency allocation. The official proposal concludes with:

8.1. A frequency band, ranging from 36.7 to 37.9 MHz, power 50 mW ERP, should be reserved and allocated for biotelemetry.

8.2. Two frequency bands between 70 to 200 MHz, each of 1 MHz width and with a power of 50 mW ERP, should be reserved and allocated for biotelemetry.

The IEC document explains the special needs of biotelemetry, especially the urgently requested international standardization of frequencies which allow omnidirectional transmission with body-mounted antennas. It points to the potential risks of frequencies above 300 MHz at power densities above 10 $\mu W/cm^2$ and recommends therefore lower frequencies with only 50 mW effective radiated power (ERP). If the IEC recommendations became accepted at the ITU conference, at least 110 small band channels (37 MHz) 40 medium band channels (70 - 200 MHz) and 9 broad band channels (37, 70-200 MHz) would be internationally usable during the next 20 years.

14. SUMMARIES

14. SUMMARY

The influence of the human body on the radiation pattern of body-mounted antennas has been investigated in the frequency range 10 to 1000 MHz (below, up to above main resonances of the human body). An analytically formulated, computable antenna-body-model has been developed which explains the correlations between the electrical field (amplitude and phase) and antenna location (antenna-body distance d_{at} and azimuthal rotation angle ϕ) at frequencies above 200 MHz (above resonance region) at vertical polarization (E-field parallel to the largest axis of the body). With the method of moments a computational antenna-body model has been investigated which explains the correlations among electrical field, antenna location (d_{at}, ϕ, and relative antenna height h_B) and irradiation angle θ_i, at all polarization axes and frequencies, especially within the resonance region. Experimental data with human test subjects and body models have been collected with special measuring antennas and field generators at frequencies between 25 to 900 MHz, whereby d_{at}, ϕ and h_B have been varied continuously (or in small steps) within large limits. The agreement between theoretical and experimental data amounted to 3 dB, except at extreme conditions (measuring range: -20 to +5 dB). The main conclusions from the complete study are: 1. There is a mathematical correlation between transmission loss (from a body-mounted to a remote antenna) and frequency, antenna location, body geometry, and polarization. 2. Within 50 to 200 MHz (just below first, up to just above second resonance) the human body (and other, in material and geoemetry comparable bodies) acts like an efficient polarization transformer. At d_{at} below 0.3 m a radial polarized, small antenna allows omnidirectional (i.e. little depending on ϕ) transmission, where the transmission loss decreases with decreasing d_{at}. Even a gain compared with an ideal isotropic radiator in free space can be achieved. 3. The antenna-body distance d_{at} is the parameter of greatest influence in antennas close to a body. Especially at frequencies above 200 MHz and vertical polarization the d_{at} determines the different reflections of the E-field at the body and determines the azimuthal radiation pattern of the antenna-body system. 4. The shape of a (lossy) body is much more important than the (biological) material. 5. The reciprocity theorem is applicable on body-mounted antennas, as experimentally proven at low power,

at frequencies between 65 and 900 MHz, and at d_{at} ranging from 0.05 - 4 m.
6. The optimal frequency range for omnidirectional transmission with body-mounted, electrically small antennas is between 35 to 180 MHz, as resulting from both theoretical and experimental data.

The order of magnitude of electric and magnetic field strengths of the near-fields of electrically small antennas have been approximatively determined and compared with the maximum permissible limits of international safety standards. At higher transmitter power (above approximately 100 mW, very much depending on antenna type and location) these limits may be exceeded, especially by walkie-talkies with vertical polarized helical antennas. Based on the recent results on the biological significance of non-ionizing radiation, RF-induced biological effects are possible, above all at frequencies above the first resonance. These effects may lead to artifacts (Biotelemetry transmitter) and perhaps to health hazards (transmitters of walkie-talkies). Comparing a standard antenna (e.g. vertical polarized helical antenna) with a radial antenna at the same extreme antenna-body distance (below 0.1 m) and at the same input power, the radial antenna does not only decrease the risk, but also offers a smaller transmission loss.

14.2. ZUSAMMENFASSUNG

Der Einfluss des menschlichen Körpers auf das Strahlungsmuster von körpernahen Antennen wurde im Frequenzbereich 10 bis 1000 MHz (unterhalb bis oberhalb der Hauptresonanzen des menschlichen Körpers) untersucht. Es wurde ein analytisch beschreibbares, berechenbares Antennen-Körper-Modell entwickelt, das die Zusammenhänge zwischen elektrischem Feld (Amplitude und Phase) und Antennenposition (Antennen-Körperabstand d_{at} und azimutalem Drehwinkel ϕ) bei Frequenzen oberhalb der Hauptresonanz ab 200 MHz bei vertikaler Polarisation (E-Feld parallel zu Körperlängsachse) erklärt. Mit der 'Method of Moments' wurde ein numerisch berechenbares Antennen-Körper-Modell untersucht, das die wichtigen Zusammenhänge zwischen elektrischem Feld, Antennenposition (d_{at}, ϕ und relativer Antennenhöhe h_B) und Einstrahlungswinkel θ_i bei allen Polarisationsrichtungen und Frequenzen, insbesondere im Resonanzbereich, erklärt. Experimentelle Daten mit Versuchspersonen und Körpermodellen wurden im Frequenzbereich 25 bis 900 MHz mit Hilfe von speziell entwickelten Messantennen und Feldgeneratoren gesammelt, wobei d_{at}, ϕ und h_B kontinuierlich (oder in feinen Abstufungen) in weiten Grenzen variiert wurden. Mit Ausnahme bei extremen Bedingungen wurde eine Uebereinstimmung von 3 dB (Messbereich -20 bis +5 dB) zwischen den experimentellen und berechneten Daten erzielt. Die wichtigsten Folgerungen aus der gesamten Untersuchung lauten: 1. Es besteht ein mathematischer Zusammenhang zwischen Uebertragungsverlust (von körpernaher Antenne zu entfernter Antenne), der Frequenz, der Antennenposition, der Körpergeometrie und den Polarisationsrichtungen. 2. Innerhalb 50 bis 200 MHz (knapp unterhalb erster bis knapp oberhalb zweiter Resonanz) wirkt der menschliche Körper (und andere, geometrisch und materiell vergleichbare Körper) als effizienter Polarisations-Transformator: Bei d_{at} unterhalb 0.3 m erlaubt eine radial polarisierte (d.h. E-Feld radial zur Körper-Längsachse) kleine Antenne eine omnidirektionale (d.h. wenig von ϕ abhängige) Uebertragung, wobei der Uebertragungsverlust mit abnehmendem d_{at} abnimmt und sogar ein Gewinn gegenüber einer idealen, isotropen Antenne im freien Raum möglich ist. 3. Der Antennen-Körperabstand d_{at} ist der wichtigste Parameter bei körpernahen Antennen. Speziell bei Frequenzen oberhalb 200 MHz und vertikaler Polarisation bestimmt d_{at} die unterschiedlichen Reflexionen des E-Feldes am Körper und damit die Azimutal-Strahlungsdiagramme des Antennen-Körper-Systems. 4. Die Form des (verlustbehafteten) Körpers ist von weitaus grösserer Bedeutung als das (biologische) Körpermaterial.

5. Experimente im Frequenzbereich 65 bis 900 MHz bei kleinen Leistungen (1 - 10 mW) und d_{at} von 0.05 bis 4 m haben gezeigt, dass das Reziprozitätsgesetz auch für elektrisch kleine, körpernahe Antennen gilt. 6. Aus Theorie und Experiment geht hervor, dass der optimale Frequenzbereich für omnidirektionale Uebertragung mit kleinen, körpernahen Antennen zwischen 35 und 180 MHz liegt.

Die Grössenordnung der elektrischen und magnetischen Feldstärken im Nahfeld elektrisch kleiner Antennen wurde abgeschätzt und mit den entsprechenden zulässigen Grenzwerten internationaler Sicherheitsvorschriften verglichen. Bei höherer Sendeleistung (ab ca. 100 mW, Grenze sehr stark von Antennentyp und Position zu Körper abhängig) werden diese Grenzwerte überschritten, besonders von Funksprechgeräten mit vertikal polarisierten Helix-Antennen. Auf Grund der neuesten Erkenntnisse sind, vor allem bei Frequenzen oberhalb der ersten Resonanz, HF-induzierte biologische Effekte möglich, die zu Artefakten (Biotelemetrie-Sender) und Gesundheitsschäden (Funksprech-Sender) führen können. Vergleicht man eine Standardantenne (z.B. vertikal polarisierte Helix-Antenne) mit einer Radial-Antenne bei extrem kleinen Antennen-Körperabständen (d_{at} kleiner als 0.1 m) so kann mit der Radial-Antenne bei gleicher Eingangsleistung nicht nur das Sicherheitsrisiko, sondern auch der Uebertragungsverlust verringert werden.

15. References

[1] ANDREASEN M.G. Scattering from Bodies of Revolution. IEEE Trans., Vol. AP-15, No.2, March 1965, pp. 303-310.

[2] ANSI American National Standards Institute: Safety Level of Electromagnetic Radiation with Respect to Personnel. ANSI C95.1-1974, IEEE, New York, 1974.

[3] ARRL The ARRL Antenna Book. American Radio Relay League, Newington, Conn., 1974.

[4] BACH S.A., LUZZIO A.J., BROWNELL A.S. Effects of Radiofrequency Energy on Human Gamma Globulin. In: Biological Effects of Microwave Radiation, (Ed. M.F. Peyton), Plenum, New York, 1961.

[5] BAGGENSTOS H. Vorlesung Elektromagnetische Felder, ETH 1977, Kapitel 4: Rasch veränderliche Felder. Electr. Dept., Swiss Federal Institute of Technology, Zurich, 1977.

[6] BARANSKI S., CZERSKI P. Biological Effects of Microwaves. Dowden,Hutchinson & Ross, Inc., Stroudsburg, Pa., 1976.

[7] BECKER K.D. Ausbreitung Elektromagnetischer Wellen. Springer Verlag, Berlin, 1974.

[8] BELDING H.A., HATCH T.R. Index for Evaluating Heat Stress in Terms of Resulting Physiological Strains. Heating,Piping,Air Conditioning, Aug. 1955, pp.129-136.

[9] BELSHER D.R. Development of Near-Field Electric Energy Density Meter Model EDM-2. HEW Publ. No.(NIOSH) 75-140, 1975.

[10] BEVENSEE R.M. The Syracuse Computer Code for Radiation and Scattering from Bodies of Revolution, Extended for Near-Field Computations. Report UCRL-51622, TID-4500, UC-32, Lawrence Livermore Laboratory, 1974.

[11] BRONSTEIN I., SEMENDJAJEW K. Taschenbuch der Mathematik, Verlag Harri Deutsch, Zürich, 1975.

[12] BUCHANAN H., MOORE W.F., RICHTER C.R. Human Body Effect on Signal Patterns of Personal Telemetry Transmitters. Report SAM-TR-70-4, USAF School of Aerospace Medicine, Aerospace Medical Division (AFSC), Brooks Air Force Base, Texas, Jan. 1970.

[13] CHANG D.C., HALBGEWACHS R.D., HARRISON C.W. The Electromagnetic Field Very Near to a Monopole. IEEE Trans., Vol. EMC-17, No.2, May 1975, pp. 97-105.

[14] CHEN K.M., GURU B.S. Internal EM Field and Absorbed Power Density in Human Torsos Induced by 1-500-MHz EM Waves. IEEE Trans., Vol. MTT-25, No. 9, Sept. 1977, pp. 746-756.

[15] CHEN K.M., GURU B.S. Induced EM Fields Inside Human Bodies Irradiated by EM waves of up to 500 MHz. Internal Report by the Department of El.Eng. and Syst. Sci., Michigan State Univ., 1977.

[16] CHOU C.K.
GUY A.W.
The Effect of the Electromagnetic Fields on the Nervous System. Scientific Report No.6, Aug. 1975, Bioelectromagnetic Res. Lab., Univ. of Washington School of Medicine, Seattle, Wash.98195.

[17] CONSUMER REPORTS
Microwave Ovens: We can tell you how well they performed - but no one really knows how safe they are. Consumer Reports, (USA), June 1976, pp. 314-321.

[18] DDR-STANDARD
Arbeitshygiene: Elektrische, Magnetische und Elektromagnetische Felder und Wellen. TGL 32602/01. Staatsverlag DDR,Berlin,1975. Zusätze: ASAO 5: MfGe Nr.1/1977, Gesetzesblatt 109, 17. März 1978, Teil 1, Nr.8.

[19] DODGE C.H.
GLASER Z.R.
Trends in Nonionizing Electromagnetic Radiation Bioeffects. Research and Related Occupational Health Aspects. J. of Microwave Power, Vol. 12(4), Dec. 1977, pp. 319-334.

[20] DUMANSKIJ J.D.
SANDALA M.G.
The Biologic Action and Hygienic Significance of Electromagnetic Fields of Superhigh and Ultrahigh Frequencies in Densely Populated Areas. In: ref. [69], pp. 289-293.

[21] EGGERT S.
GOLTZ S.
KUPFER J.
Results at the Development of One Near-Field Strength Meter at the Measurement of the Electrical Component of the Electromagnetic RF Field in the GDR. Proc. of the 1977 USNC/URSI Meeting, Arlie, Va. (in press). See also: Nahfeldstärke-Messgerät NFM-1, Zentralinst.f.Arbeitsmed.der DDR,Berlin,1976.

[22] EMERY A.F.
SHORT R.E.
GUY A.W.
KRANING K.K.
LIN J.C.
The Numerical Thermal Simulation of the Human Body When Absorbing Non-ionizing Microwave Irradiation - With Emphasis on the Effect of Different Sweat Models. In: Biological Effects of Electromagnetic Waves, Vol.II, Selected Papers of the 1975-USNC/URSI Annual Meeting, Boulder, Colo.1976,pp. 96-118.

[23] FISCHER T.
CASTELLI J.
Aktivierung des menschlichen Körpers als Sendeantenne. Study work at the Electronics Inst. and Biomechanics Lab., ETH Zurich, 1979.

[24] GANDHI O.P.
HAGMANN M.J.
D'ANDREA J.A.
Some Recent Results on Deposition of Electromagnetic Energy in Animals and in Models of Man. In: Abstracts of Scientific Papers, International USNC/URSI Symposium on the Biological Effects of Electromagnetic Waves, Arlie, Va., 1977.

[25] GANDHI O.P.
SEDIGH K.
BECK G.S.
HUNT E.L.
Distribution of Electromagnetic Energy Deposition in Models of Man with Frequencies Near Resonance. In: Biological Effects of Electromagnetic Waves, selected papers of the 1975-USNC/URSI Annual Meeting, Boulder, Colo.,(HEW publ. (FDA) 77-8011), pp.44-67.

[26] GANDHI O.P.
HUNT E.L.
D'ANDREA J.A.
Deposition of Electromagnetic Energy in Animals and in Models of Man With and Without Grounding and Reflector Effects. Radio Science Vol. 12, No. 6 (S), 1977, pp. 39-47.

[27] GANDHI O.P. — Recent Results on Deposition of Electromagnetic Energy in Animals and in Models of Man. Lecture presented at the ETH, Aug.17, 1978.

[28] GLASER Z.R., DODGE C.H. — Biomedical Aspects of Radio Frequency and Microwave Radiation: A Review of Selected Soviet, East European, and Western References. In: Biological Effects of Electromagnetic Waves. Selected papers of the 1975-USNC/URSI meeting, Boulder,Colo.Vol.1,Dec.1976 (HEW publ. (FDA) 77-8011), pp. 2-34.

[29] GLASER Z.R., BROWN P.F., ALLAMONG J.M., NEWTON R.C. — Bibliography of Reported Biological Phenomena ('Effects') and Clinical Manifestations Attributed to Microwave and Radio-Frequency Radiation. Ninth Supplement, Nov.1977. DHEW (NIOSH) Publ. No. 78-126. First bibliog.: Res.Rep.No.2, NMRI,Bethesda,Md.1971. Available from NTIS,Springfield,Va. 22151.

[30] GORDON Z.V., ROSCIN A.V., BYCKOV M.S. — Main Directions and Results of Research Conducted in tne USSR on the Biologic Effects of Microwaves. In: ref. [69], pp. 22-35.

[31] GORDON Z.V. — Biological Effect of Microwaves in Occupational Hygiene. Izdatel'stvo Meditsina, Leningrad, 1966. US-Translation TT 70-50087,NASA TT F-633, 1970.

[32] GOUBAU G., SCHWERING F. — Proceedings of the ECOM-ARO Workshop on Electrically Small Antennas. U.S. Army Electronics Command, Fort Monmouth, May 1976.

[33] GREEN F.M. — Development of Magnetic Near-Field Probes. HEW Publ. No. (NIOSH) 75-127, 1975.

[34] GREEN F.M. — Development of an RF Near-Field Exposure Synthesizer (10 to 40 MHz). Interagency Agreement NIOSH-IA-75-16. Available from NIOSH, Cincinnati,Ohio 45226.

[35] GUY A.W. — Quantitation of Induced Electromagnetic Field Patterns in Tissue and Associated Biological Effects. In: ref.[69], pp. 203-217.

[36] GUY A.W., WEBB M.D., SORENSEN C.C. — Determination of Power Absorption in Man Exposed to High Frequency Electromagnetic Fields by Thermographic Measurements on Scale Models. IEEE Trans., Vol. BME-23, No.5, Sept. 1976, pp.361-371.

[37] GUY A.W., CHOU C.K., LIN J.C., CHRISTENSEN D. — Microwave-Induced Acoustic Effects in Mammalian Auditory Systems and Physical Materials. Ann. of the N.Y. Acad. of Sciences, Vol. 242, Febr. 1975, pp. 194-218.

[38] GUY A.W. — Phantom Models for Muscle, Brain, Fat, and Bone at MW Frequencies, Private communication, 1976.

[39] HANKIN N.N., TELL R.A., ATHEY T.W., JANES D.E. — High Power Radiofrequency and Microwave Radiation Sources: A Study of Relative Environmental Significance. Operational Health Physics, Proc. Ninth Midyear Topical Symp. of the Health Physics Society. (Compilated by P.L. Carson et al.), Febr. 1976.

[40] HARRINGTON R.F. MAUTZ J.R. — Radiation and Scattering from Bodies of Revolution. Rep. AFCRL-69-0305, 1969, and : Generalized Network Parameters for Bodies of Revolution. Rep. TR-68-7, 1968, Syracuse Univ., El. Eng.Dept. Syracuse, N.Y.

[41] HARRINGTON R.F. — Field Computation by Moment Methods, Macmillian Co., N.Y., 1968 (Second printing: write to the author).

[42] HEILMANN A. — Antennen I. BI Hochschultaschenbücher 140/140a, Mannheim, 1970.

[43] HELLER J.H. — The Effect of Electromagnetic Fields on Unicellar Organisms. In: IRE,AIEE,ISA Conf.Electrical Technology in Medicine and Biology, Vol.7, 1959.

[44] HIRSCH F.G. PARKER J.T. — Bilateral Lenticular Opacities Occurring in a Technician Operating a Microwave Generator. AMA Arch. Ind.Hyg.Occup. Med.6:1952, pp. 512-517.

[45] JOHNSON C.C. GUY A.W. — Nonionizing Electromagnetic Wave Effects in Biological Materials and Systems. Proc. IEEE, Vol.60, No.6, 1972, pp. 692-718.

[46] KALADA T.V. FUKOLOVA P.P. GONCAROVA N.N. — Biologic Effects of Radiation in the 30-300 MHz Range. In: ref.[69], pp. 52-57.

[47] KANDOIAN A.G. SICHAK W. — Wide-Frequency-Range Tuned Helical Antennas and Circuits. IRE Nat. Conv. Rec. Part 2, Antennas and Components, 1953, pp. 42-47.

[48] KING H.E. — Characteristics of Body-Mounted Antennas for Personal Radio Sets. IEEE Trans.,Vol.AP-23, 1975, pp. 242-244.

[49] KING H.E. WONG J.L. — Effects of a Human Body on a Dipole Antenna at 450 and 900 MHz. IEEE Trans.,Vol.AP-25,1977,pp.376-379.

[50] KING R.W.P. WU T.T. — The Scattering and Diffraction of Waves. Harvard Univ. Press, Cambridge, Mass., 1959, Chapter 2.

[51] KRAUS J.D. — Antennas. McGraw Hill, 1950, Chapter 9.

[52] KRITIKOS H.N. SCHWAN H.P. — The Distribution of Heating Potential Inside Lossy Spheres., IEEE Trans., Vol.BME-22, No.6, Nov. 1975, pp. 457-463.

[53] KRUPKA Z. — The Effect of the Human Body on the Radiation Properties of Small-Sized Communication Systems. IEEE Trans., Vol. AP-16, 1968, pp. 154-163.

[54] LI T. BEAM R.E. — Helical Folded Dipoles and Unipoles. Proc. Nat. Electr. 13: 1957, pp. 89-105.

[55] LIVESHITS N.N. — Conditioned Reflex Activity in Dogs under Local Influence of a VHF Field upon Certain Zones of the Cerebral Cortex. Biophys. J., Vol.2,1957, p. 198.

[56] LIU L.M. ROSENBAUM H.J. PICKARD W.F. — The Relation of Teratogenesis in Tenebrio Molitor to the Incidence of Low-Level Microwaves. IEEE Trans., Vol. MTT-23, Nov. 1975, pp. 929-931.

[57] MICHAELSON S.M. Effect of Exposure to Microwaves: Problems and Perspectives. Environmental Health Persp. Vol.8, 1974, pp. 133-156.

[58] MICHAELSON S.M. The Tri-Service Program - A Tribute to George M. Knauf, USAF (MC). IEEE Trans., Vol. MTT-19, No. 2, Febr. 1971, pp. 131-146.

[59] MILROY W.C., MICHAELSON S.M. Microwave Cataractogenesis: A Critical Review of the Literature. Aerospace Medicine, Vol. 43, No.1, 1972, pp. 67-75.

[60] MOOR F.B. Microwave Diathermy. In: Therapeutic Heat and Cold, (Ed.:Licht S.), New Haven, Conn, 1965, Sec. 12, pp. 310-320.

[61] MUTH E. Appearance of Pearl-Chain Formation of Particles in Emulsions Caused by Alternating Fields. Kolloid-Z., Vol. 41, 1927, p. 97.

[62] NEUKOMM P.A. Body-Mounted Transmitting Antennas: Radiation Patterns and Design of Helical Dipole Antennas. In : Biotelemetry III (Eds.:Fryer T.B. , H.A. Miller and H.Sandler), Acad, Press, Inc,N.Y.,1976,pp. 345-348.

[63] NEUKOMM P.A. Biotelemetry Antennas: The Problem of Small Body-Mounted Antennas. Proc.int.conf. BIOSIGMA 78, Vol. 2, Paris 1978, pp. 99-106.

[64] NEUKOMM P.A. Artifacts from RF and MW Telemetry: Estimation of Safety Aspects and Review on Biological Effects.In: Biotelemetry IV (Eds.: Klewe H.J. and H.P.Kimmich), Döring-Druck,Druckerei und Verlag,Braunschweig,1979.

[65] NEUKOMM P.A. The Rubber Band Goniometry. J.Biotelemetry 1, 1974, pp. 12-20.

[66] NYQUIST D.P., CHEN K.M., GURU B.S. Coupling Between Small Thin-Wire Antennas and a Biological Body. IEEE Trans., Vol.AP-25, No.6, Nov. 1977, pp. 863-866.

[67] OEHEN W., BALZARINI N. Helix Biotelemetrie Antennen. Study work at the Lab. Microwave Tech. and Biomechanics Lab., ETH Zurich, 1975.

[68] OLSEN R.G., LORDS J.L., DURNEY C.H. Microwave-Induced Chronotropic Effects in the Isolated Rat Heart. Ann. of Biomed. Engineering 5, 1977, pp. 396-409.

[69] PROCEEDINGS WARSAW Biologic Effects and Health Hazards of Microwave Radiation. Proc. Int.Symposium Warsaw, 15-18 Oct., 1973, Polish Medical Publishers, Warsaw, 1974.

[70] ROMERO-SIERRA C., HALTER S., TANNER J.A. Effect of an Electromagnetic Field on the Sciatic Nerve of the Rat. In: The Nervous System and Electric Currents,(Ed.:Wulfsohn N.L.),Vol.2, Plenum, N.Y., 1971, pp. 81-85.

[71] ROTHAMMEL K. Antennenbuch. Telekosmos-Verlag, Franckh'sche Verlagshandlung, Stuttgart, 1976.

[72] SCHWAN H.P. — Microwave Radiation: Biophysical Considerations and Standards Criteria. IEEE Trans.,Vol.BME-19, No.4, July 1972, pp. 304-312.

[73] SCHWAN H.P. — Biophysics of Diathermy. In: Therapeutic Heat and Cold, (Ed.: Licht S.),New Haven, Conn.,1965, Sec.3, pp. 63-125.

[74] SCHWAN H.P., PIERSOL G.M. — The Absorption of Electromagnetic Energy in Body Tissues. Int. Review of Physical Medicine and Rehabilitation, Vol. 33, 1954, pp. 371-404.

[75] SCHWAN H.P., LI.K. — Capacity and Conductivity of Body Tissues at Ultrahigh Frequencies. Proc. IRE, Vol. 41, Dec. 1953, pp. 1735-1740.

[76] TELL R.A. — Microwave Energy Absorption in Tissue. Report by the Environ. Protection Agency, Twinbrook Res. Lab., 12709 Twinbrook Parkway,Rockville,Md.20852.Feb.1972.

[77] TELL R.A. — An Analysis of Radiofrequency and Microwave Absorption Data with Consideration of Thermal Safety Standards. (Draft). U.S. Environ. Protection Agency,Las Vegas, Nev. 89114, P.O. Box 15027, Dec. 1977.

[78] TELL R.A., O'BRIEN P.J. — Radiation Intensities Due to Mobile Communication Systems. U.S. Environ. Protection Agency, Office of Radiation Program, Silver Spring,Md 20910, 1976.

[79] TOLER J., SEALS J. — RF Dielectric Properties Measurement System: Human and Animal Data. DHEW (NIOSH) Publ. No. 77-176,1977.

[80] TONG D.A. — The Normal Mode Helical Aerial. Radio Communication, July 1974, pp. 432-437.

[81] VAN BLADEL J. — Electromagnetic Fields. McGraw-Hill, 1964, Chapt.12.

[82] VREELAND R.W., SHEPHERD M.D., HUTCHINSON J.C. — The Effects of FM and TV Broadcast Stations upon Cardiac Pacemakers. IEEE Symp. Record (Publ. No. IEEE 74CH0803-7 EMC), 1974.

[83] WHEELER H.A. — Fundamental Limitations of Small Antennas. Proc. IRE, Dec. 1947, pp. 1479-1484.

[84] WHEELER H.A. — The Radiansphere Around a Small Antenna. Proc. IRE, Aug. 1959, pp. 1325-1331.

[85] WHEELER H.A. — Small Antennas. IEEE Trans., Vol.AP-23, No.4, July 1975, pp. 462-469.

16. APPENDIX

CONTENTS page

Leer - Vide - Empty

16.1. HELICAL ANTENNAS

16.1.1. PROPERTIES, DESIGN, EFFICIENCY MEASUREMENT AND MATCHING

A helical antenna is a typical electrically small antenna. Its maximum dimension is a small fraction of the wavelength. The "normal mode" helical antenna (FIGURE 106) consists of a helical conductor in the shape of a long cylinder with the diameter D_h ($D_h << \lambda$) and with the axial (monopole) length h ($h < \lambda/4$). The polarization of the radiated E-field is elliptical, with a dominant axis parallel to the helical cylinder axis (see FIGURE 106, bottom). The radiation pattern is very similar to that of an ordinary whip antenna. i.e. maximum radiation radial to the helical axis.

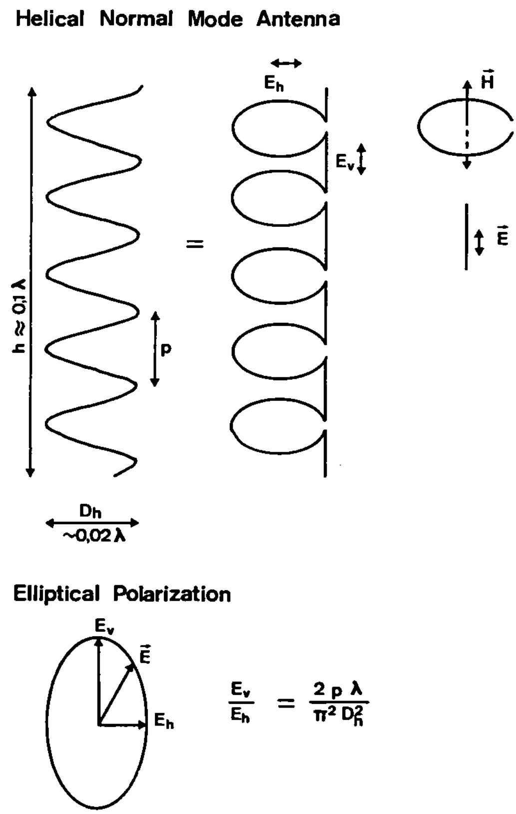

FIGURE 106

Helical Normal Mode Antenna

Vertical E_v far-field generated from the vertical flowing antenna currents,
Horizontal E_h far-field generated from the horizontal flowing antenna currents.

p = pitch

The helix is a slow-wave structure. When used as a waveguide, the axial phase velocity of the wave guided by the helix is less than the velocity of light in free space. Accordingly, the resonant length of a helix is shorter than the corresponding resonant length of a linear wire antenna. Thus, one may reduce the axial length h by a factor of 3 to 8 without adding external tuning elements. Compared with the short (non-resonant) whip antenna one obtains a better current distribution (see FIGURE 107), resulting in a higher radiation resistance:

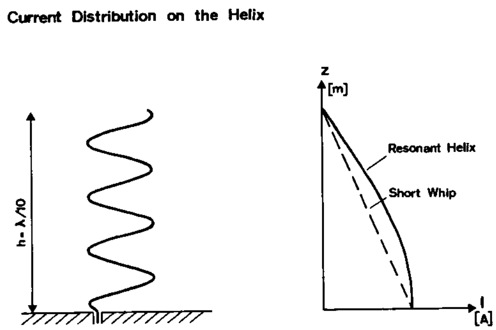

FIGURE 106
Current distribution on the helical antenna
z: vertical antenna axis
I: current in the conductor

The radiation resistance of a half-wave helical dipole can be evaluated by integrating the far-field Poynting vector over a large spherical surface. For a thin half-wave helical dipole of length 2h, an approximate expression for the radiation resistance is : (LI and BEAM [54])

$$R_{rad}\ \text{Helix} = 1280\ (h/\lambda)^2\ \ [\text{Ohm}] \tag{246}$$

As a comparison, the radiation resistance of a small linear dipole of the length 2h and with linear (triangular) current distribution is

$$R_{rad}\ \text{Whip} = 790\ (h/\lambda)^2\ \ [\text{Ohm}] \tag{247}$$

Hence the radiation resistance of a small-diameter half-wave helical dipole is approximately 62 percent greater than that of a small linear dipole of the same length. If the antennas are operated above a perfect ground, the radiation resistances are reduced by a factor of 2 and one obtains the values of KANDOIAN and SICHAK [47]

$$R_{rad}\ \text{Helix above ground} = (25.3\ h/\lambda)^2\ \ [\text{Ohm}] \tag{248}$$

$$R_{rad}\ \text{Whip above ground} = (20\ h/\lambda)^2\ \ [\text{Ohm}] \tag{249}$$

Principally, there are four methods to design a helical antenna:

1. Computation with the method of moments: OEHEN and BALZARINI [67] adapted an existing antenna modelling program (BURKE and SELDEN, Microfiches AD - 767 420, 1973) to the helical dipole problem. This method is very

accurate, if the number of subsegments is large enough ($\sim$ 200) and offers many results : impedance, gain, bandwidth, effect of near-by conducting surfaces, etc. The ROUND HELICAL DIPOLE (RHD) in FIGURE 107 has been computed with this method, and the experimental data (16.1.2.) agree quite well with the computed data. However, this method is very expensive and should only be applied for antenna optimization.

2. Analytical approach. LI and BEAM [54] investigated the characteristic equation for helical waveguide and presented the results in nomograms. This method offers an insight in the complicated correlations between antenna geometry, bandwidth and general performance.

3. Approximative computation. KANDOIAN and SICHAK [47] evaluated approximative computational methods, which were adapted by TONG [80] for computation on pocket calculators. For a given antenna length (h), diameter (D_h) and wavelength (λ) the number of turns (N_h) respectively the number $n_h = N_h/h$ can be approximatively computed for long helices:

$$\log n_h = 0.4 \left(\log\left(\frac{\lambda}{h} - 4\right) + \log\left(\frac{\lambda}{h} + 4\right) + 0.5 \log \lambda - 3 \log D_h\right) - 1 \quad (250)$$

This method offers data for design with an accuracy of about 20 %, if h/λ is not smaller than 1/10 and if D_h is smaller than 0.3 h.

4. Experimental approach. If a network analyser and a small anechoic chamber is available, a well performing helical antenna can be designed as follows: For a monopole helical antenna a wire of a length of $\lambda/2$ is wrapped in a shape of a helix with the desired D_h and h. The 'hot end' is contacted on a large counterpoise, and the feeding coaxial cable (inner conductor) is contacted at the m^{th} turn ($m \cong N/10$) from the now grounded 'hot end'. The Smith Chart (see FIGURE 109) shows the resonance frequency, the bandwidth and the input impedance (transformed $R_{rad} + R_{loss}$ at f_{res}). Varying the feeding point (changing m) one obtains a match to 50 Ohm (with a resulting relative bandwidth) and by cutting the upper antenna ends one obtains the wanted resonance frequency, because the initial f_{res} is usually $\sim$ 30% too small.

The problems of all helical antennas are : 1.) small bandwidth , 2.) reduced efficiency, 3.) low radiation resistance, 4.) sensitivity to detuning effects from proximity to obstacles, 5.) transverse polarization. Because the helical is an electrically small antenna the fundamental laws

HELICAL DIPOLE ANTENNA RHD

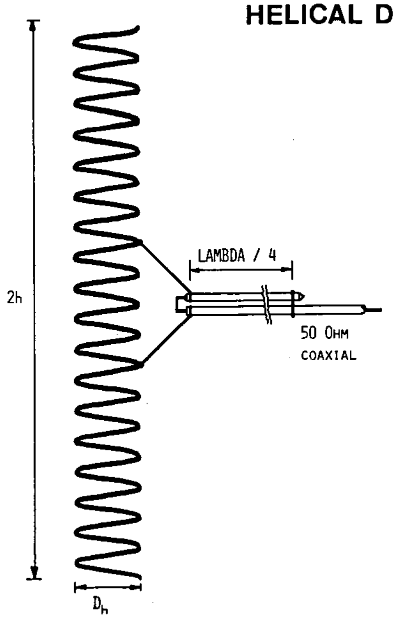

Specifications:

GEOMETRY :

LENGTH	$2h$	:	22 CM
DIAMETER	D_h	:	2 CM
WIRE DIAMETER	D_w	:	2 MM
NUMBER OF TURNS	$2N_h$	:	18

COMPUTER DATA :

EFFICIENCY	EFF	:	94 %
GAIN VERT. POLARIZATION	G_{VERT}	:	+1.4 DB
GAIN HOR. POLARIZATION	G_{HOR}	:	- 17 DB
RADIATION RESISTANCE	R_R	:	9.2 OHM

NETWORK ANALYSER DATA :

RESONANT FREQUENCY	F_{RES}	:	236 MHz
BANDWIDTH (-3 DB)	Bw	:	17 MHz
INPUT RESISTANCE	R_I	:	24 OHM

Azimuthal Radiation Pattern of the Helical RHD Dipole Antenna

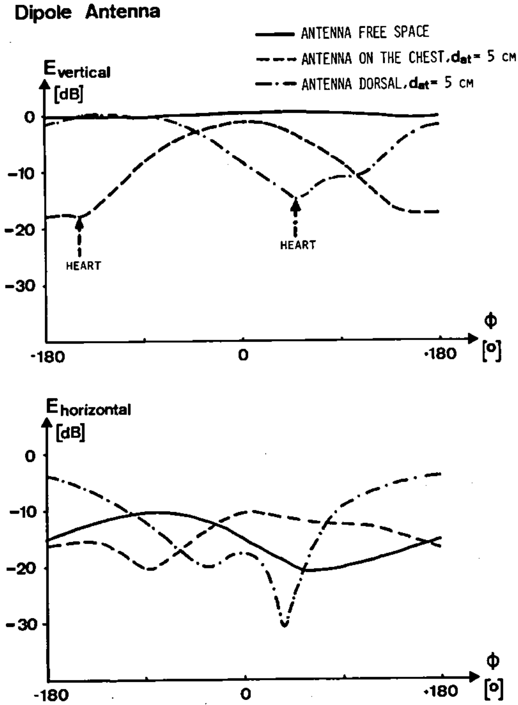

FIGURE 107 (above)

FIGURE 108 (left)

Round helical dipole (RHD)

mechanical details, computer predictions (antenna modelling program, see [67]) network analyser data and (left) performance of the antenna mounted on the human test subject (0 dB : isotropic radiator)

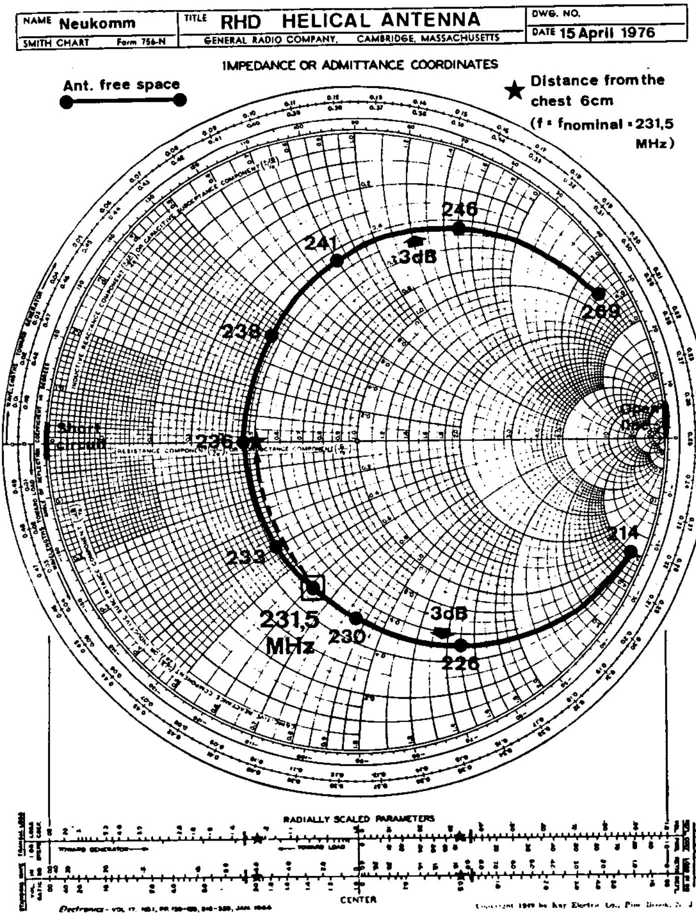

FIGURE 109 Smith Chart of the round helical dipole antenna RHD. Solid line : antenna in free space (anechoic chamber), dashed line : antenna mounted on human test subject at d_{at} = 6 cm . Due to the losses effected by the body the resistance increases with decreasing d_{at} and the resonant frequency lowers with decreasing d_{at}.

found by WHEELER [83,85] must be considered. The bandwidth is determined by the h/λ ratio (see equations 9 to 13 in section 4.5) but can be controlled within small limits with matching (good match = smaller bandwidth and perhaps a better efficiency) and increasing the radiation resistance (higher radiation resistance = smaller bandwidth). The efficiency is mainly determined by ground losses, by losses in the matching network and, in complicated helical structures (double helix, etc.), by resistive losses in the antenna conductor. An example may illustrate the importance of the ground losses:

The standard helical monopole antenna of 173 MHz walkie-talkie (MOTOROLA HT 220) is specified as:

h_t = 114 mm (total length)
h = 106 mm (length of the helix)
N_h = 42 (total number of turns)
D_w = 1.2 mm (wire diameter)
D_h = 9.6-6.7 mm (tapered helical diameter)

The computation according to equation 250 and 246 result in an N_h of $\sim$40 and a radiation resistance of 5.5 Ohm. The housing of the walkie talkie is maximum 180 mm $\hat{=}$ $\lambda/10$. The VSWR of the complete antenna-transmitter system is close to 1:1, so that the ground losses amount to about 44.5Ω. The efficiency in radiation is thus 5.5 / 44.5 + 5.5 = 11 % , so that the complete system radiates about -9.5 dB less than an ideal dipole. A helical dipole according to FIGURE 107 has an efficiency of about 94 (theoretical) and 89 % (measured) and a gain of - 0.75 dB (theoretical) and - 2 dB (measured) compared with an ideal full-length dipole.

The low radiation resistance is a potential source of bad efficiency, if the match to the feeding line is poor , if there are losses in the antenna conductor or in the matching network and if (in the case of monopole antennas) the counterpoise is not large enough. According to LI and BEAM [54] special helical antennas with multi-conductors were designed. As can be seen in the comparison FIGURE 110, 16.1.2., a higher gain can be obtained, but paying the price of a very small bandwidth.Thus, a maximum radiation resistance or a perfect matching is not very sensible with respect to detuning sensitivity: the more the antenna is "improved" for free-space operation, the more delicate it responds to external influencies. One further problem could be the transverse polarization. If the height is about 0.9 times the diameter, the antenna becomes circular polarized. However, as discussed in section 13.1.4., a transverse polarization at frequencies between 50 to 200 MHz may be even an advantage at small antenna-body distances, also when the radiation is reduced at axial polarization. The transverse polarization could be computed by the formulas indicated in FIGURE 106,[54] and [74], but the agreement with the experimental data is so poor, that one should trust only the actually measured data. The same situation happens with the actual bandwidth: it is better not to cite the formulas here. If the bandwidth becomes really very important, one should use the accurate method of moments or one should perform representative experiments.

An important point is the matching of a dipole antenna on a 50 Ω coaxial cable and the determination of the efficiency. Below 1 Watt power and below 300 MHz a ferrit 1 : 1 balun (manufactured from a 0.5 cm^3 standard 1:4 balun for TV-application) leads to very good results. The additional loss is below 10 % , the volume of the network is very small and is not critical with respect to bandwidth. The parallel λ/4 bazooka in FIGURE 106 is only a few percent better, but cumbersome and of limited bandwidth. However, an investigation by the author has shown, that the total bandwidth of dipole antenna plus bazooka is slightly larger than that of the antenna alone, because the reactance of the antenna is partially compensated by the reactance of the bazooka at changing input frequencies. The best method to determine the efficiency follows from the application of the equations by WHEELER [85]: The Smith Chart of the antenna in free-space is recorded, and one reads the real part of the impedance R at resonant frequency f_{res}. The antenna is then located in a conducting vessel with the dimension of the radiansphere (see section 4.5.). The Smith Chart is again recorded, and the highest ohmic resistance near f_{res} represents the total loss resistance R_{loss}. The efficiency Eff can be calculated with

$$\text{Efficiency} = \frac{R - R_{loss}}{R} \tag{251}$$

The absolute accuracy is in the region of 25 %, but the relative accuracy is much better than 5 %, e.g.,if only the feeding point of an antenna is varied . If one combines the efficiency measurement with transmission tests (network analyser, second input channel), the actual performance of a helical antenna can be reliably quantified.

16.1.2. COMPARISON OF SOME ANTENNA TYPES

Five antennas have been selected for a discussion of the performance: The GROUNDPLANE ANTENNA GA is a vertical λ/4 whip on 4 ground rods, each λ/4 of length and at an angle of 135° to the radiating whip. The HELMET ANTENNA HGA is a vertical $\lambda/4$ whip (32.6 cm) on a plastic helmet, coated with a copper mesh. The ROUND HELICAL DIPOLE RHD is the antenna shown in FIGURE 107. The FLAT HELICAL DIPOLE FHD is a flat helix with $2N_h = 10.5$ turns, $2h = 20$ cm, $D_{h1} = 0.5$ cm, $D_{h2} = 5.3$ cm. In the center section the antenna conductor is parallel to the antenna axis at a total length of 6 cm, representing the feeded antenna segment (Δ-match with bazooka, similar to the feeding in FIGURE 107). The FLAT FOLDED HELICAL DIPOLE FFHD consists of a 240 Ω parallel line with the shape of a helix, with single conductors at the antenna ends (see LI and BEAM [54]).The size of the FFHD is the same as that of the FHD, but $2N_h$ is 13.5.

COMPARISON OF SOME BODY-MOUNTED ANTENNNAS USED IN BIOTELEMETRY										
ANT. TYPE	ANTENNA DATA IN FREE SPACE WITHOUT TEST SUBJECT					VERTICAL ANTENNA MOUNTED DORSALLY ON THE TEST SUBJECT WITH $d_{at} = 57$ mm, $h_B = 1.4$ m, $\phi = 180°/0°$				
	RES. FREQ. [MHz]	BAND-WIDTH [MHz]	GAIN [dB]	EFFI-CIEN-CY [%]	VSWR [1]	RES. FREQ. [MHz]	BAND-WIDTH [MHz]	GAIN at ϕ 180° [dB]	GAIN at ϕ 0° [dB]	FREQ. SHIFT [MHz]
GA	220	65	2.15	-	1:1.4	-	-	-	-	-
HGA	237	47	+0.5	-	1:1.3	-	-	-	-	-
RHD	236.3	18	+0.2	89	1:2.5	229.2	23	-20	-7.7	7.1
FHD	237.5	25	+0.8	79	1:4.0	231.8	24	-21	-6.1	5.7
FFHD	242.1	8.8	+1.0	78	1:1.3	236.8	9.6	-20	-4.0	5.3

TABLE 110 Comparison of some body-mounted antennas.

TABLE 110 shows the performance of these antennas. The helical antennas were mounted on the phantom PHA, the antenna center was spaced 57 mm from the surface of the phantom. These results hold true within 2 dB when mounted dorsally on a human test subject SUB. The performance of the GA was measured at an absolute antenna height of 1.4 m, and the helmet antenna HGA was mounted at the head of the SUB, with the head at the same absolute antenna height. This comparison shows clearly that a good antenna in free space may perform poorly in extreme proximity to a body. The interesting FFHD with its high gain and its excellent VSWR cannot be applied in practice, because varying antenna-body distances may detune the antenna in excess of its bandwidth. A good compromise seems to be the flat helical dipole FHD.

16.2. COMPUTER PROGRAMS AND ADDITIONAL RESULTS

General remarks

In the following sections the listings of the used computer programs are presented with all necessary comments. The source programs are those of HARRINGTON and MAUTZ [40] (program A is essentially the here presented program HARRA) and of BEVENSEE [10] (program HARRDF is a part of the here presented program PANB). Program PANA and PANC are new programs.

The programs are written in FORTRAN IV for a CDC computer. Card decks are available from HARRINGTON, BEVENSEE or from the author. Depending on your computer system, some of the characters need to be changed or the punched characters do not agree with the listing obtained from the punched cards. Please check above all the following characters:

C : for comment
= : might be printed (and read) as a >
* : might be printed (and raad) as a ↑
+ : might be printed (and read) as a {

If you notice some differences between your listing (from the card deck) and the presented listing, use a subroutine DECODE for character replacement. Such subroutines should be available at your computer center.

Depending on your computer system, the organisation of the main programs and the subroutines may be different. Problems may occur with the COMMON statements. Check the listings and ask the specialists of the computer center. Before actual computing the punched cards beginning with a C,R or E must be replaced by the corresponding control cards :

C : This card is only a comment card and has no influence on the computation
R : Replace that card by an appropriate control card
E : Take this punched card out of the program

Except program PANA, the execution of the programs is quite expensive. The minimum computational time on a CDC 6500 for a series of 4 test points at one single frequency is in the order of 1000 seconds.

16.2.1. PROGRAM PANA AND IZYL RESULTS

```
E PROGRAM *PANA*, COMPUTATION OF THE TWO-DIMENSIONAL MODEL
E ************************************************************          PANA
E CONTROL CARDS                                                          PANA
PAN,3571,CM60000,CT15.                                                   PANA
FTN.                                                                     PANA
PUBLIC,BRUSLIB.                                                          PANA
PUBLIC,FTNLIB.                                                           PANA
LDSET,LIB=BRUSLIB/FTNLIB.                                                PANA
LGO.                                                                     PANA
R HERE END OF RECORD CARD                                                PANA
C ***************                                                        PANA
      PROGRAM PANA (INPUT,OUTPUT,TAPE1=INPUT,TAPE3=OUTPUT)               PANA
C ***************                                                        PANA
C THIS PROGRAM COMPUTES THE SCATTERING OF A PLANE WAVE FROM A PERFECTLY PANA
C CONDUCTING,CIRCULAR CYLINDER OF INFINITE LENGTH. COMPUTED ARE THE     PANA
C E-FIELD COMPONENTS PARALLEL TO THE CYLINDER AXIS (VERT.POLARISATION)  PANA
C THE INPUT DATA SET CONSISTS OF THE FOLLOWING PARAMETERS:              PANA
C F     = FREQUENCY IM MHZ                                               PANA
C A     = RADIUS OF THE CYLINDER IN METERS                               PANA
C DMIN1 = MINIMUM ANTENNA-BODY SURFACE DISTANCE FOR PART 1               PANA
C DMAX1 = MAXIMUM ANTENNA-BODY SURFACE DISTANCE FOR PART 1               PANA
C MR1   = NUMBER OF COMPUTED ANTENNA-BODY DISTANCES FOR PART 1           PANA
C M1    = NUMBER OF REGARDED MODI FOR PART 1                             PANA
C DMIN2 = MINIMUM ANTENNA-BODY SURFACE DISTANCE FOR PART 2               PANA
C DMAX2 = MAXIMUM ANTENNA-BODY SURFACE DISTANCE FOR PART 2               PANA
C MR2   = NUMBER OF COMPUTED ANTENNA-BODY DISTANCES FOR PART 2           PANA
C M2    = NUMBER OF REGARDED MODI FOR PART 2                             PANA
C THE OUTPUT OF THIS PROGRAM PANA IS THE FIELD STRENGTH AT THE BODY-    PANA
C MOUNTED RECEIVING ANTENNA WITH THE FOLLOWING PARAMETERS:              PANA
C PHI   = HORIZONTAL ROTATION ANGLE IN DEGREES                           PANA
C DAT   = DISTANCE OF THE ANTENNA FROM THE CYLINDER SURFACE             PANA
C GAI   = FIELD STRENGTH IN DB AT THE ANTENNA, (O DB = FREE SPACE VALUE)PANA
                                                                         PANA
C THE FIRST PART CONSISTS OF THE COMPUTATION OF THE AZIMUTHAL RADIATION PANA
C PATTERN FOR FIVE (MR1) ANTENNA-BODY DISTANCES PRESENTED IN A TABLE    PANA
C AND IN A GRAPH.                                                        PANA
C THE SECOND PART CONSISTS OF THE COMPUTATION OF REFLECTING PROPERTIES  PANA
C (PHI = 0 DEG) AND DIRECTING PROPERTIES (PHI = 180 DEG) OF THE ANTENNA-PANA
C CYLINDER SYSTEM AT TWENTY (MR2) ANTENNA-BODY DISTANCES.               PANA
                                                                         PANA
C THIS PROGRAM TAKES USE OF THE LIBRARY BRUSLIB VIMCODE C306 FOR THE    PANA
C COMPUTATION OF THE BESSEL AND HANKEL FUNCTIONS.                       PANA
C ****************                                                       PANA
                                                                         PANA
      COMPLEX EZI,EZSC                                                   PANA
      REAL DAT1(5),DAT2(20),GAI1(5)                                      PANA
      REAL RK,LAM,AK,A,K,G                                               PANA
      INTEGER F,D1(41),D2(51),D3(51),PHI                                 PANA
      READ(1,48) DMIN1,DMAX1,MR1,M1                                      PANA
      READ(1,48) DMIN2,DMAX2,MR2,M2                                      PANA
   48 FORMAT(2F6.2,2I4)                                                  PANA
      READ(1,49) A                                                       PANA
   49 FORMAT(F7.3)                                                       PANA
   50 READ(1,51) F                                                       PANA
   51 FORMAT(2X,I3)                                                      PANA
      IF(EOF (1)) 52,53                                                  PANA
   53 CONTINUE                                                           PANA
      DU=2.*A                                                            PANA
      LAM=300./F                                                         PANA
      K=6.28318/LAM                                                      PANA
      AK=K*A                                                             PANA
  520 FORMAT(1H1,1X,*A Z I M U T H A L  R A D I A T I O N  P A T T E R NPANA
     1  F R E Q U E N C Y*,I4,* M H Z*,/1H0,1X,*TWO-DIMENSIONAL ANTENNA-PANA
     2BODY SYSTEM*,/1H0,1X,*TESTBODY: INFINITE ROT.SYM.CYLINDER*,7X,    PANA
     3*NUMBER OF MODI:*,I3,/1H ,11X,*DIAMETER:*,F4.2,* M*,17X,          PANA
     4*POLARISATION: VERTICAL/VERTICAL*)                                 PANA
  521 FORMAT(1H0,1X,*DAT(I)  : ANTENNA-BODY DISTANCE IN METERS*,/1H ,1X,PANA
     1*GAI(I)  : GAIN, FIELD STRENGTH AT THE ANTENNA A1 IN DB, 0 DB = FRPANA
     2EE SPACE*/1H ,1X,*PHI     : HORIZONTAL ROTATION ANGLE IN DEGREES*)PANA
  522 FORMAT(1H0,1X,*    DAT(1) DAT(2) DAT(3) DAT(4) DAT(5)*,/,1H ,4X,  PANA
     15F7.3,/,1H0,1X,*PHI GAI(1) GAI(2) GAI(3) GAI(4) GAI(5)*,5X,*-20 DBPANA
     2*,4X,*-10 DB*,4X,*+ 0 DB*,4X,*+10 DB*,/,)                          PANA
  523 FORMAT(1H ,1X,I3,5F7.1,08X,*.*,9X,*.*,9X,*.*,9X,*.*)              PANA
  524 FORMAT(1H+,38X,41(R1))                                             PANA
      WRITE(3,520) F,M1,DU                                               PANA
      WRITE(3,521)                                                       PANA
      M=M1                                                               PANA
      DM=(DMAX1-DMIN1)/(MR1-1)                                           PANA
      DO 7 JJ=1,MR1                                                      PANA
    7 DAT1(JJ)= DMIN1+(DM*(JJ-1))                                        PANA
      WRITE(3,522) (DAT1(I),I=1,MR1)                                     PANA
      DO 2 I=1,37                                                        PANA
      PHI=(I-1)*5                                                        PANA
      PHH=180.-((I-1)*5.)                                                PANA
C DURING THE COMPUTATION THE ARGUMENT (PHI+PI) IS REPLACED BY PHH       PANA
      DO 3 L=1,41                                                        PANA
    3 D1(L)=1H                                                           PANA
      DO 4 J=1,MR1                                                       PANA
      RK=(DAT1(J)+A)*K                                                   PANA
      CALL BESS(M,AK,RK,PHH,EZI,EZSC,V,G)                                PANA
      IF(G.GT.10..OR.G.LT.-99.) GOTO 2                                   PANA
      GAI1(J)=G                                                          PANA
      IF(G.GT.10..OR.G.LT.-20.) GOTO 4                                   PANA
      KK=IFIX(G+30.5)                                                    PANA
      D1(KK)=1R0+J                                                       PANA
    4 CONTINUE                                                           PANA
      WRITE(3,523) PHI,(GAI1(II),II=1,MR1)                               PANA
      WRITE(3,524) (D1(L),L=1,41)                                        PANA
    2 CONTINUE                                                           PANA
                                                                         PANA
  620 FORMAT(1H1,1X,*D I R E C T I V E  R A D I A T I O N  P A T T E R NPANA
     1  F R E Q U E N C Y*,I4,* M H Z*,/1H0,1X,*TWO-DIMENSIONAL ANTENNA-PANA
     2BODY SYSTEM*,10X,*ROT.ANGLE PHI : 0 ABOVE,180 BELOW*,/1H0,1X,     PANA
     3*TESTBODY: INFINITE ROT.SYM.CYLINDER*,10X,*NUMBER OF MODI:*,I3,/, PANA
```

```
     41H ,11X,*DIAMETER:*,F4.2,* M*,20X,*POLARISATION: VERTICAL/VERTICAL
     5*,/)
  621 FORMAT(1H0,1X,*DAT(I)  GAI(I)  PHI*,5X,*-20 DB*,4X,*-15 DB*,4X,*-1
     10 DB*,4X,*- 5 DB*,4X,*+ 0 DB*,4X,*+ 5 DB*,/1H ,3X,*M*,6X,*DB*,
     25X,*DEG*,/,)
  623 FORMAT(1H ,1X,F4.2,F9.2,3X,I3,08X,*.*,9X,*.*,9X,*.*,9X,*.*,9X,*.*,
     19X,*.*)
  624 FORMAT(1H+,29X,51(A1))
  625 FORMAT(1H ,1X,*0.00*,23X,51(A1))
      WRITE(3,620) F,M2,DU
      WRITE(3,621)
      M=M2
      DM=(DMAX2-DMIN2)/(MR2-1)
      DO 100 IJ=1,3
      PHH=IJ*90.+90.
      PHI=IJ*90-90
      IF(IJ.EQ.1) GOTO 60
      IF(IJ.EQ.2) GOTO 70
      IF(IJ.EQ.3) GOTO 80
   60 DO 61 J=1,MR2
   61 DAT2(J)= DMAX2-(DM*(J-1)) $ GOTO 90
   70 DO 71 L=1,51
   71 D3(L)=1H-
      WRITE(3,625) (D3(L),L=1,51) $ GOTO 100
   80 DO 81 J=1,MR2
   81 DAT2(J)= DMIN2+(DM*(J-1)) $ GOTO 90
   90 DO 91 J=1,MR2
      DAT=DAT2(J)
      RK=(DAT+A)*K
      CALL BESS(M,AK,RK,PHH,EZI,EZSC,V,G)
      DO 93 L=1,51
   93 D2(L)=1H
      IF(G.GT.5..OR.G.LT.-20.) GOTO 92
      KK=IFIX(G*2.+40.5)
      D2(KK)=1H*
   92 CONTINUE
      WRITE(3,623) DAT,G,PHI
      WRITE(3,624) (D2(L),L=1,51)
   91 CONTINUE
  100 CONTINUE
      GOTO 50
   52 STOP
      END
C ****************
E SUBROUTINE
      SUBROUTINE BESS(M,AK,RK,PHH,EZI,EZSC,V,G)
      REAL JN(100),YN(100)
      COMPLEX  EZI,EZSC,BN,AN(100),HNKR(100)
      P=3.1415926*PHH/180.
      MP1=M+1
      CALL BESYN(-AK,MP1,JN,YN)
      DO 1 I=1,MP1
1     AN(I)=-JN(I)/CMPLX(JN(I),-YN(I))
      CALL BESYN(-RK,MP1,JN,YN)
      DO 2 I=1,MP1
2     HNKR(I)=CMPLX(JN(I),-YN(I))
      EZSC=AN(1)*HNKR(1)
      EZI=JN(1)
      DO 3 N=1,M
      NU=N+1
      BN=-CMPLX(0.,N*3.1415926/2.)
      BN=2.*COS(N*P)*CEXP(BN)
      EZI=EZI+BN*JN(NU)
3     EZSC=EZSC+BN*HNKR(NU)*AN(NU)
      V=CABS(1.+EZSC/EZI)
      G=(ALOG10(V)*20.)
      RETURN  $  END
C ***************
R HERE END OF RECORD CARD
E DATA CARDS
  0.05  0.25  05  12
  0.05  1.00  20  25
  0.125
  150 MHZ
  205 MHZ
  250 MHZ
R HERE END OF INFORMATION CARD
```

A Z I M U T H A L   R A D I A T I O N   P A T T E R N   F R E Q U E N C Y 125 M H Z

TWO-DIMENSIONAL ANTENNA-BODY SYSTEM

TESTBODY: INFINITE ROT.SYM.CYLINDER — DIAMETER: .25 M
NUMBER OF MODI: 12
POLARISATION: VERTICAL/VERTICAL

DAT(I) : ANTENNA-BODY DISTANCE IN METERS
GAI(I) : GAIN, FIELD STRENGTH AT THE ANTENNA A1 IN DB, 0 DB = FREE SPACE
PHI : HORIZONTAL ROTATION ANGLE IN DEGREES

	DAT(1) .050	DAT(2) .100	DAT(3) .150	DAT(4) .200	DAT(5) .250
PHI	GAI(1)	GAI(2)	GAI(3)	GAI(4)	GAI(5)
0	-9.3	-4.4	-1.8	-.1	1.0
5	-9.3	-4.4	-1.8	-.1	1.0
10	-9.4	-4.4	-1.8	-.2	1.0
15	-9.4	-4.5	-1.9	-.2	.9
20	-9.5	-4.6	-2.0	-.3	.9
25	-9.7	-4.7	-2.1	-.4	.8
30	-9.8	-4.9	-2.3	-.6	.6
35	-10.0	-5.1	-2.4	-.7	.5
40	-10.2	-5.3	-2.6	-.9	.3
45	-10.5	-5.5	-2.9	-1.1	.1
50	-10.7	-5.8	-3.1	-1.4	-.2
55	-11.0	-6.1	-3.4	-1.7	-.4
60	-11.4	-6.4	-3.8	-2.0	-.7
65	-11.7	-6.8	-4.1	-2.3	-1.1
70	-12.1	-7.2	-4.5	-2.7	-1.4
75	-12.6	-7.6	-4.9	-3.1	-1.8
80	-13.0	-8.0	-5.4	-3.6	-2.3
85	-13.5	-8.5	-5.8	-4.1	-2.7
90	-14.0	-9.0	-6.4	-4.6	-3.2
95	-14.5	-9.6	-6.9	-5.1	-3.8
100	-15.1	-10.1	-7.5	-5.7	-4.4
105	-15.6	-10.7	-8.0	-6.3	-5.0
110	-16.2	-11.3	-8.6	-6.9	-5.6
115	-16.8	-11.9	-9.2	-7.5	-6.2
120	-17.3	-12.4	-9.8	-8.1	-6.8
125	-17.8	-12.9	-10.3	-8.6	-7.4
130	-18.2	-13.4	-10.8	-9.1	-7.9
135	-18.6	-13.8	-11.3	-9.6	-8.4
140	-18.9	-14.1	-11.6	-10.0	-8.8
145	-19.2	-14.4	-11.9	-10.3	-9.1
150	-19.4	-14.6	-12.1	-10.5	-9.3
155	-19.5	-14.7	-12.2	-10.6	-9.5
160	-19.5	-14.8	-12.3	-10.7	-9.5
165	-19.6	-14.8	-12.3	-10.7	-9.6
170	-19.6	-14.8	-12.3	-10.7	-9.6
175	-19.6	-14.8	-12.3	-10.7	-9.6
180	-19.6	-14.8	-12.3	-10.7	-9.6

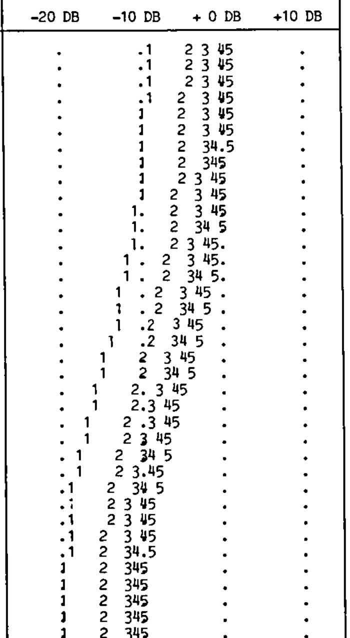

D I R E C T I V E   R A D I A T I O N   P A T T E R N   F R E Q U E N C Y 125 M H Z

TWO-DIMENSIONAL ANTENNA-BODY SYSTEM
ROT.ANGLE PHI : 0 ABOVE, 180 BELOW

TESTBODY: INFINITE ROT.SYM.CYLINDER — DIAMETER: .25 M
NUMBER OF MODI: 25
POLARISATION: VERTICAL/VERTICAL

DAT(I) M	GAI(I) DB	PHI DEG
1.00	-2.07	0
.95	-1.24	0
.90	-.38	0
.85	.43	0
.80	1.16	0
.75	1.78	0
.70	2.29	0
.65	2.68	0
.60	2.96	0
.55	3.12	0
.50	3.16	0
.45	3.07	0
.40	2.84	0
.35	2.45	0
.30	1.86	0
.25	1.04	0
.20	-.12	0
.15	-1.79	0
.10	-4.39	0
.05	-9.30	0
0.00		
.05	-19.60	180
.10	-14.81	180
.15	-12.34	180
.20	-10.75	180
.25	-9.62	180
.30	-8.77	180
.35	-8.09	180
.40	-7.54	180
.45	-7.08	180
.50	-6.69	180
.55	-6.36	180
.60	-6.06	180
.65	-5.80	180
.70	-5.57	180
.75	-5.37	180
.80	-5.18	180
.85	-5.01	180
.90	-4.85	180
.95	-4.71	180
1.00	-4.58	180

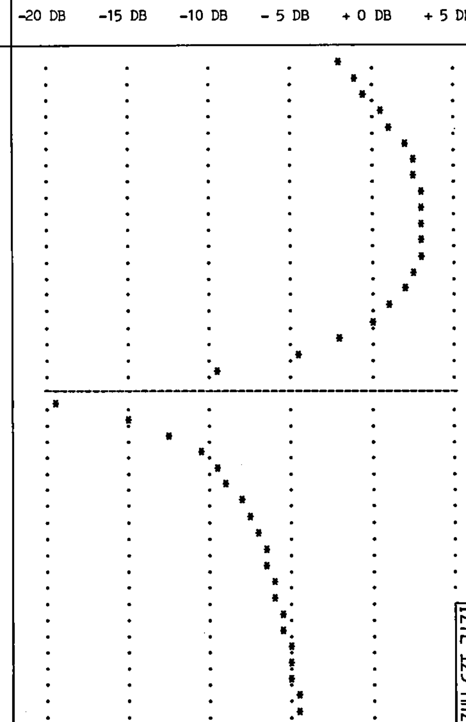

IZYL 125 MHz

A Z I M U T H A L   R A D I A T I O N   P A T T E R N   F R E Q U E N C Y 300 M H Z

TWO-DIMENSIONAL ANTENNA-BODY SYSTEM

TESTBODY: INFINITE ROT.SYM.CYLINDER   NUMBER OF MODI: 12
DIAMETER: .25 M   POLARISATION: VERTICAL/VERTICAL

DAT(I) : ANTENNA-BODY DISTANCE IN METERS
GAI(I) : GAIN, FIELD STRENGTH AT THE ANTENNA A1 IN DB, 0 DB = FREE SPACE
PHI : HORIZONTAL ROTATION ANGLE IN DEGREES

	DAT(1) .050	DAT(2) .100	DAT(3) .150	DAT(4) .200	DAT(5) .250
PHI	GAI(1)	GAI(2)	GAI(3)	GAI(4)	GAI(5)
0	-3.8	.8	2.8	3.6	3.5
5	-3.8	.8	2.8	3.6	3.6
10	-3.9	.7	2.8	3.6	3.6
15	-4.0	.7	2.7	3.5	3.6
20	-4.1	.5	2.6	3.5	3.6
25	-4.2	.4	2.5	3.4	3.6
30	-4.4	.2	2.4	3.4	3.6
35	-4.7	.0	2.2	3.3	3.5
40	-4.9	-.2	2.0	3.1	3.5
45	-5.2	-.5	1.8	3.0	3.4
50	-5.5	-.7	1.6	2.8	3.4
55	-5.9	-1.1	1.3	2.6	3.2
60	-6.3	-1.4	1.0	2.4	3.1
65	-6.7	-1.9	.6	2.1	2.9
70	-7.2	-2.3	.2	1.7	2.6
75	-7.7	-2.8	-.2	1.4	2.4
80	-8.3	-3.3	-.7	.9	2.0
85	-8.9	-3.9	-1.2	.5	1.6
90	-9.5	-4.5	-1.8	-.1	1.1
95	-10.2	-5.2	-2.4	-.6	.6
100	-10.9	-5.9	-3.1	-1.3	.0
105	-11.7	-6.7	-3.9	-2.0	-.7
110	-12.6	-7.5	-4.7	-2.8	-1.5
115	-13.5	-8.4	-5.6	-3.7	-2.3
120	-14.5	-9.4	-6.6	-4.7	-3.2
125	-15.5	-10.4	-7.6	-5.7	-4.3
130	-16.5	-11.5	-8.7	-6.8	-5.4
135	-17.5	-12.5	-9.7	-7.9	-6.5
140	-18.5	-13.5	-10.7	-8.9	-7.6
145	-19.2	-14.3	-11.6	-9.8	-8.5
150	-19.8	-14.9	-12.3	-10.5	-9.3
155	-20.1	-15.2	-12.6	-11.0	-9.8
160	-20.2	-15.3	-12.8	-11.2	-10.0
165	-20.2	-15.3	-12.8	-11.2	-10.0
170	-20.1	-15.2	-12.7	-11.1	-9.9
175	-20.0	-15.2	-12.6	-11.0	-9.9
180	-20.0	-15.1	-12.6	-11.0	-9.8

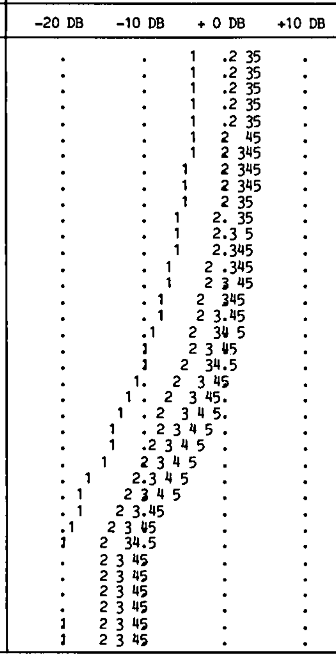

D I R E C T I V E   R A D I A T I O N   P A T T E R N   F R E Q U E N C Y 300 M H Z

TWO-DIMENSIONAL ANTENNA-BODY SYSTEM   ROT.ANGLE PHI : 0 ABOVE, 180 BELOW

TESTBODY: INFINITE ROT.SYM.CYLINDER   NUMBER OF MODI: 25
DIAMETER: .25 M   POLARISATION: VERTICAL/VERTICAL

DAT(I) M	GAI(I) DB	PHI DEG
1.00	-2.71	0
.95	-2.49	0
.90	-1.00	0
.85	.62	0
.80	1.78	0
.75	2.35	0
.70	2.31	0
.65	1.60	0
.60	.18	0
.55	-1.95	0
.50	-4.00	0
.45	-3.59	0
.40	-1.11	0
.35	1.19	0
.30	2.75	0
.25	3.55	0
.20	3.60	0
.15	2.80	0
.10	.78	0
.05	-3.81	0
0.00		
.05	-19.97	180
.10	-15.13	180
.15	-12.61	180
.20	-10.99	180
.25	-9.84	180
.30	-8.97	180
.35	-8.28	180
.40	-7.72	180
.45	-7.25	180
.50	-6.85	180
.55	-6.51	180
.60	-6.21	180
.65	-5.95	180
.70	-5.71	180
.75	-5.50	180
.80	-5.31	180
.85	-5.14	180
.90	-4.98	180
.95	-4.83	180
1.00	-4.70	180

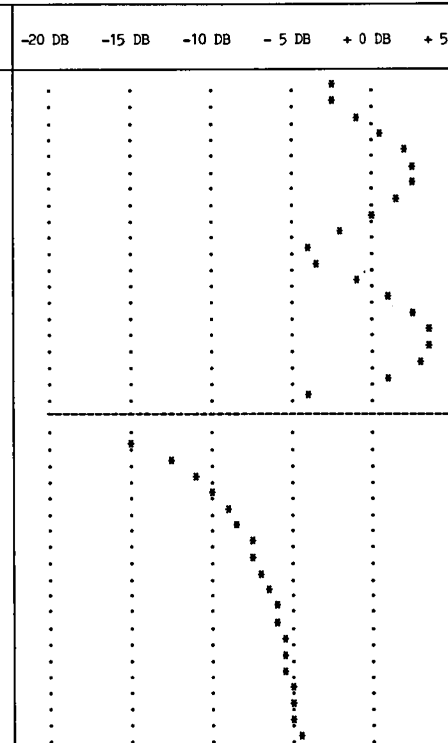

IZYL 300 MHz

A Z I M U T H A L   R A D I A T I O N   P A T T E R N   F R E Q U E N C Y 400 M H Z

TWO-DIMENSIONAL ANTENNA-BODY SYSTEM

TESTBODY: INFINITE ROT.SYM.CYLINDER
DIAMETER: .25 M

NUMBER OF MODI: 12
POLARISATION: VERTICAL/VERTICAL

DAT(I) : ANTENNA-BODY DISTANCE IN METERS
GAI(I) : GAIN, FIELD STRENGTH AT THE ANTENNA A1 IN DB, 0 DB = FREE SPACE
PHI : HORIZONTAL ROTATION ANGLE IN DEGREES

	DAT(1) .050	DAT(2) .100	DAT(3) .150	DAT(4) .200	DAT(5) .250
PHI	GAI(1)	GAI(2)	GAI(3)	GAI(4)	GAI(5)
0	-1.9	2.4	3.8	3.6	2.1
5	-1.9	2.4	3.8	3.6	2.1
10	-1.9	2.3	3.8	3.6	2.2
15	-2.0	2.3	3.7	3.7	2.3
20	-2.2	2.2	3.7	3.7	2.4
25	-2.3	2.0	3.6	3.7	2.6
30	-2.5	1.9	3.5	3.7	2.7
35	-2.8	1.7	3.4	3.7	2.9
40	-3.1	1.4	3.3	3.7	3.1
45	-3.4	1.2	3.1	3.7	3.2
50	-3.7	.9	2.9	3.6	3.3
55	-4.1	.5	2.6	3.5	3.4
60	-4.6	.2	2.3	3.3	3.4
65	-5.1	-.3	2.0	3.1	3.4
70	-5.6	-.7	1.6	2.8	3.3
75	-6.1	-1.2	1.2	2.5	3.2
80	-6.7	-1.8	.7	2.2	2.9
85	-7.4	-2.4	.2	1.7	2.6
90	-8.0	-3.0	-.4	1.3	2.3
95	-8.8	-3.7	-1.0	.7	1.8
100	-9.5	-4.4	-1.7	.1	1.3
105	-10.3	-5.2	-2.4	-.6	.7
110	-11.2	-6.1	-3.3	-1.4	-.0
115	-12.2	-7.0	-4.2	-2.3	-.9
120	-13.2	-8.1	-5.2	-3.2	-1.8
125	-14.4	-9.2	-6.3	-4.3	-2.9
130	-15.5	-10.4	-7.5	-5.5	-4.0
135	-16.8	-11.6	-8.8	-6.8	-5.3
140	-18.0	-12.9	-10.1	-8.1	-6.7
145	-19.2	-14.1	-11.3	-9.4	-8.0
150	-20.1	-15.1	-12.3	-10.5	-9.2
155	-20.6	-15.6	-13.0	-11.3	-10.0
160	-20.8	-15.9	-13.3	-11.6	-10.4
165	-20.7	-15.8	-13.3	-11.6	-10.4
170	-20.6	-15.7	-13.1	-11.5	-10.3
175	-20.4	-15.5	-13.0	-11.3	-10.1
180	-20.4	-15.5	-12.9	-11.3	-10.1

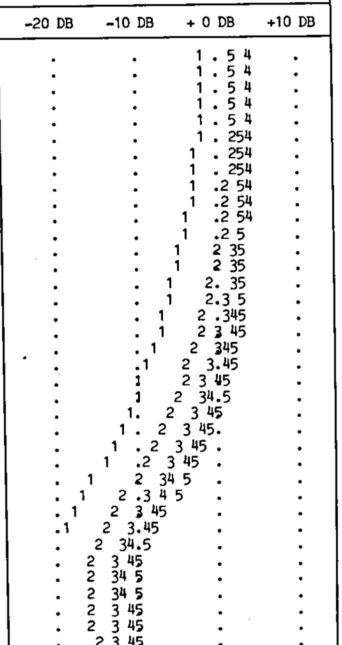

D I R E C T I V E   R A D I A T I O N   P A T T E R N   F R E Q U E N C Y 400 M H Z

TWO-DIMENSIONAL ANTENNA-BODY SYSTEM

ROT.ANGLE PHI : 0 ABOVE, 180 BELOW

TESTBODY: INFINITE ROT.SYM.CYLINDER
DIAMETER: .25 M

NUMBER OF MODI: 25
POLARISATION: VERTICAL/VERTICAL

DAT(I) M	GAI(I) DB	PHI DEG
1.00	.98	0
.95	2.00	0
.90	2.01	0
.85	.95	0
.80	-1.11	0
.75	-3.11	0
.70	-2.22	0
.65	.27	0
.60	2.02	0
.55	2.63	0
.50	2.06	0
.45	.15	0
.40	-3.15	0
.35	-4.53	0
.30	-.98	0
.25	2.07	0
.20	3.63	0
.15	3.80	0
.10	2.40	0
.05	-1.86	0
0.00		
.05	-20.35	180
.10	-15.47	180
.15	-12.91	180
.20	-11.26	180
.25	-10.09	180
.30	-9.20	180
.35	-8.50	180
.40	-7.92	180
.45	-7.44	180
.50	-7.04	180
.55	-6.69	180
.60	-6.38	180
.65	-6.11	180
.70	-5.87	180
.75	-5.65	180
.80	-5.46	180
.85	-5.28	180
.90	-5.12	180
.95	-4.97	180
1.00	-4.83	180

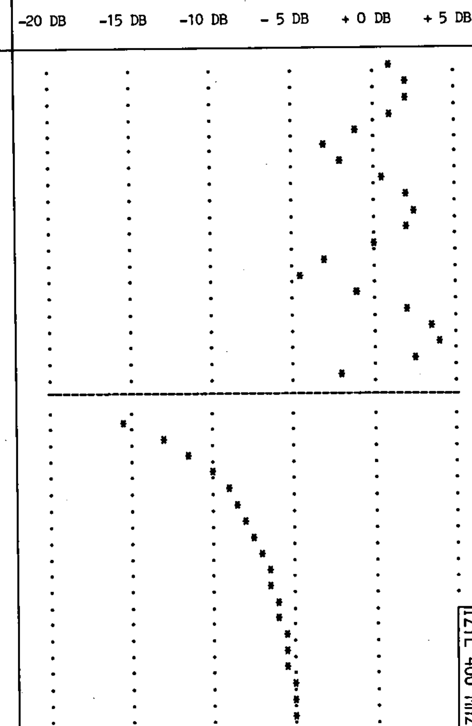

A Z I M U T H A L   R A D I A T I O N   P A T T E R N   F R E Q U E N C Y 700 M H Z

TWO-DIMENSIONAL ANTENNA-BODY SYSTEM

TESTBODY: INFINITE ROT.SYM.CYLINDER
DIAMETER: .25 M

NUMBER OF MODI: 12
POLARISATION: VERTICAL/VERTICAL

DAT(I) : ANTENNA-BODY DISTANCE IN METERS
GAI(I) : GAIN, FIELD STRENGTH AT THE ANTENNA A1 IN DB, 0 DB = FREE SPACE
PHI : HORIZONTAL ROTATION ANGLE IN DEGREES

	DAT(1) .050	DAT(2) .100	DAT(3) .150	DAT(4) .200	DAT(5) .250
PHI	GAI(1)	GAI(2)	GAI(3)	GAI(4)	GAI(5)
0	1.8	4.3	2.0	-5.4	-.7
5	1.8	4.3	2.0	-5.4	-.8
10	1.8	4.3	2.1	-5.1	-1.0
15	1.7	4.3	2.2	-4.8	-1.4
20	1.5	4.3	2.4	-4.2	-2.0
25	1.4	4.2	2.6	-3.5	-2.7
30	1.2	4.2	2.9	-2.7	-3.6
35	.9	4.1	3.1	-1.8	-4.5
40	.6	3.9	3.3	-.8	-5.2
45	.3	3.8	3.5	.1	-5.3
50	-.1	3.6	3.7	.9	-4.5
55	-.6	3.3	3.8	1.7	-3.2
60	-1.1	3.0	3.8	2.3	-1.7
65	-1.6	2.7	3.8	2.8	-.3
70	-2.2	2.2	3.6	3.2	.9
75	-2.9	1.8	3.4	3.4	1.9
80	-3.6	1.2	3.1	3.5	2.5
85	-4.3	.6	2.7	3.4	3.0
90	-5.2	-.2	2.2	3.2	3.2
95	-6.0	-.9	1.6	2.8	3.2
100	-7.0	-1.8	.9	2.3	3.0
105	-7.9	-2.7	.1	1.7	2.6
110	-8.9	-3.6	-.8	1.0	2.1
115	-10.0	-4.6	-1.7	.2	1.4
120	-11.0	-5.7	-2.7	-.7	.6
125	-12.2	-6.8	-3.8	-1.8	-.3
130	-13.4	-8.0	-5.0	-2.9	-1.4
135	-14.8	-9.4	-6.3	-4.2	-2.7
140	-16.4	-11.0	-7.9	-5.8	-4.2
145	-18.2	-12.8	-9.7	-7.6	-5.9
150	-20.1	-14.7	-11.6	-9.5	-7.9
155	-21.7	-16.4	-13.5	-11.4	-9.9
160	-22.7	-17.5	-14.7	-12.8	-11.4
165	-22.7	-17.6	-14.9	-13.1	-11.8
170	-22.2	-17.2	-14.5	-12.7	-11.5
175	-21.8	-16.7	-14.0	-12.3	-11.0
180	-21.6	-16.5	-13.9	-12.1	-10.9

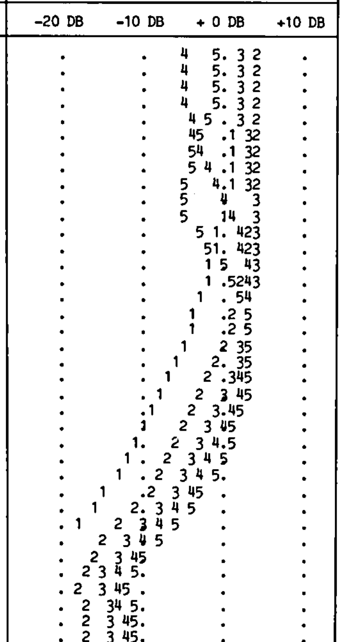

D I R E C T I V E   R A D I A T I O N   P A T T E R N   F R E Q U E N C Y 700 M H Z

TWO-DIMENSIONAL ANTENNA-BODY SYSTEM

ROT.ANGLE PHI : 0 ABOVE, 180 BELOW

TESTBODY: INFINITE ROT.SYM.CYLINDER
DIAMETER: .25 M

NUMBER OF MODI: 25
POLARISATION: VERTICAL/VERTICAL

DAT(I) M	GAI(I) DB	PHI DEG
1.00	1.01	0
.95	1.95	0
.90	-.12	0
.85	-2.77	0
.80	.28	0
.75	2.21	0
.70	.89	0
.65	-2.93	0
.60	-.81	0
.55	2.27	0
.50	1.89	0
.45	-2.24	0
.40	-2.46	0
.35	2.15	0
.30	2.90	0
.25	-.74	0
.20	-5.42	0
.15	1.97	0
.10	4.34	0
.05	1.84	0
0.00		
.05	-21.58	180
.10	-16.53	180
.15	-13.85	180
.20	-12.11	180
.25	-10.86	180
.30	-9.91	180
.35	-9.16	180
.40	-8.55	180
.45	-8.04	180
.50	-7.60	180
.55	-7.22	180
.60	-6.90	180
.65	-6.61	180
.70	-6.35	180
.75	-6.11	180
.80	-5.90	180
.85	-5.71	180
.90	-5.54	180
.95	-5.38	180
1.00	-5.23	180

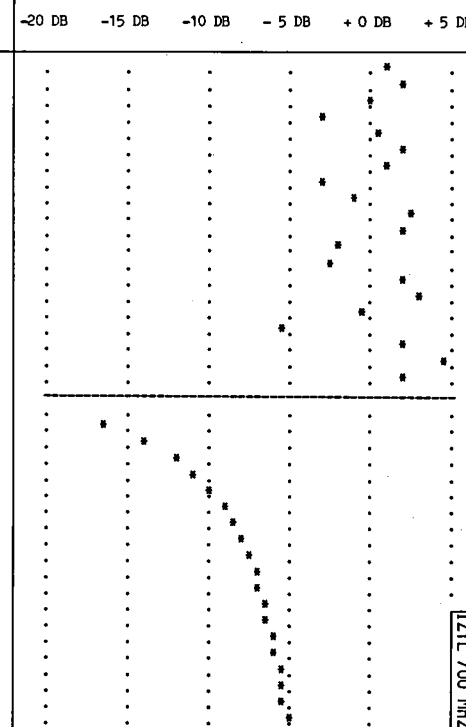

AZIMUTHAL RADIATION PATTERN FREQUENCY 897 MHZ

TWO-DIMENSIONAL ANTENNA-BODY SYSTEM

TESTBODY: INFINITE ROT.SYM.CYLINDER DIAMETER: .25 M
NUMBER OF MODI: 12
POLARISATION: VERTICAL/VERTICAL

DAT(I) : ANTENNA-BODY DISTANCE IN METERS
GAI(I) : GAIN, FIELD STRENGTH AT THE ANTENNA A1 IN DB, 0 DB = FREE SPACE
PHI : HORIZONTAL ROTATION ANGLE IN DEGREES

	DAT(1) .050	DAT(2) .100	DAT(3) .150	DAT(4) .200	DAT(5) .250
PHI	GAI(1)	GAI(2)	GAI(3)	GAI(4)	GAI(5)
0	3.3	3.8	-4.4	.0	3.3
5	3.3	3.8	-4.3	-.0	3.3
10	3.2	3.9	-4.0	-.3	3.3
15	3.1	3.9	-3.5	-.7	3.3
20	3.0	4.0	-2.9	-1.3	3.2
25	2.9	4.1	-2.1	-2.0	3.1
30	2.7	4.1	-1.3	-3.1	2.8
35	2.4	4.2	-.4	-4.3	2.4
40	2.1	4.2	.4	-5.4	1.8
45	1.8	4.2	1.2	-5.9	.9
50	1.4	4.1	1.9	-5.2	-.4
55	1.0	4.0	2.5	-3.7	-2.0
60	.5	3.9	3.0	-1.9	-3.8
65	-.1	3.6	3.4	-.4	-5.0
70	-.7	3.3	3.6	.9	-4.3
75	-1.3	2.9	3.7	2.0	-2.4
80	-2.1	2.4	3.6	2.7	-.5
85	-2.9	1.8	3.4	3.1	1.1
90	-3.8	1.1	3.1	3.4	2.1
95	-4.7	.4	2.6	3.3	2.8
100	-5.7	-.5	2.0	3.1	3.1
105	-6.8	-1.5	1.2	2.6	3.1
110	-8.0	-2.5	.3	1.9	2.8
115	-9.1	-3.7	-.7	1.1	2.2
120	-10.3	-4.8	-1.8	.2	1.5
125	-11.5	-6.0	-2.9	-.9	.6
130	-12.8	-7.2	-4.1	-2.0	-.5
135	-14.1	-8.6	-5.4	-3.2	-1.7
140	-15.7	-10.1	-6.9	-4.7	-3.1
145	-17.4	-11.9	-8.7	-6.5	-4.8
150	-19.5	-14.0	-10.8	-8.6	-6.8
155	-21.8	-16.3	-13.1	-10.9	-9.3
160	-23.6	-18.2	-15.2	-13.1	-11.5
165	-24.0	-18.8	-15.9	-14.0	-12.6
170	-23.4	-18.2	-15.4	-13.6	-12.3
175	-22.6	-17.5	-14.7	-12.9	-11.6
180	-22.4	-17.2	-14.4	-12.6	-11.4

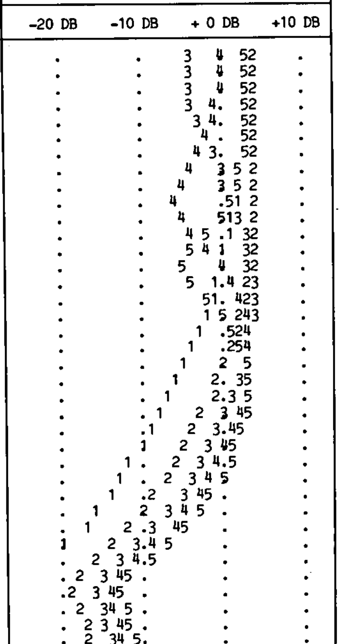

DIRECTIVE RADIATION PATTERN FREQUENCY 897 MHZ

TWO-DIMENSIONAL ANTENNA-BODY SYSTEM
ROT.ANGLE PHI : 0 ABOVE, 180 BELOW

TESTBODY: INFINITE ROT.SYM.CYLINDER DIAMETER: .25 M
NUMBER OF MODI: 25
POLARISATION: VERTICAL/VERTICAL

DAT(I) M	GAI(I) DB	PHI DEG
1.00	-2.53	0
.95	.91	0
.90	1.74	0
.85	-1.97	0
.80	-.45	0
.75	2.20	0
.70	-.39	0
.65	-2.30	0
.60	2.06	0
.55	1.26	0
.50	-3.68	0
.45	1.22	0
.40	2.52	0
.35	-2.70	0
.30	-.60	0
.25	3.31	0
.20	.03	0
.15	-4.37	0
.10	3.81	0
.05	3.28	0
0.00		
.05	-22.36	180
.10	-17.19	180
.15	-14.43	180
.20	-12.63	180
.25	-11.34	180
.30	-10.35	180
.35	-9.57	180
.40	-8.93	180
.45	-8.40	180
.50	-7.95	180
.55	-7.56	180
.60	-7.21	180
.65	-6.91	180
.70	-6.64	180
.75	-6.40	180
.80	-6.18	180
.85	-5.96	180
.90	-5.77	180
.95	-5.63	180
1.00	-5.62	180

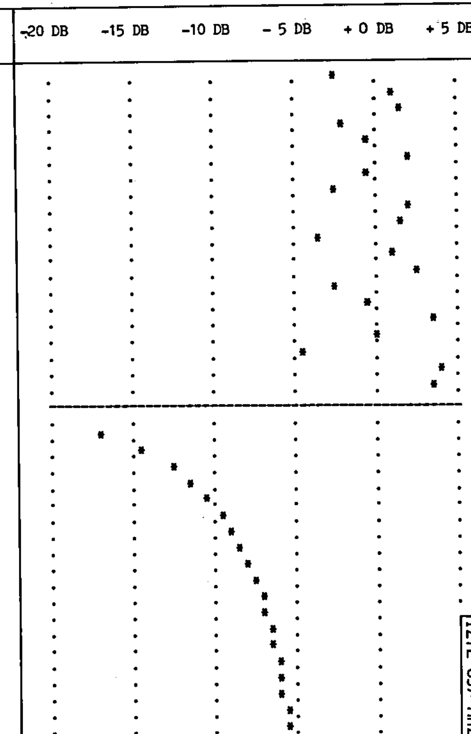

IZYL 897 MHz

16.2.2. PROGRAM HARRA AND OUTPUT SAMPLE

```
E PROGRAM *HARRA*, COMPUTATION OF THE Y-MATRIX
E ********************************************             HARRA   1
E CONTROL CARDS (START RUN)                                  HARRA   2
PAN,3571,CM70000,CT240.                                     HARRA   3
PERMF,AMAT2.                                                HARRA   4
FTN.                                                        HARRA   5
LGO.                                                        HARRA   6
PUBLIC,COLLECT.                                             HARRA   7
COLLECT,N=AMAT2.                                            HARRA   8
CATALOG,AMAT2.                                              HARRA   9
R HERE END OF RECORD CARD                                   HARRA  10
E CONTROL CARDS (FOLLOWING RUNS)                            HARRA  11
PAN,3571,CM70000,CT240.                                     HARRA  12
ATTACH,AMAT2,PW=3571                                        HARRA  13
FTN.                                                        HARRA  14
LGO.                                                        HARRA  15
PUBLIC,COLLECT.                                             HARRA  16
COLLECT,M=AMAT2                                             HARRA  17
R HERE END OF RECORD CARD                                   HARRA  18
C ****************                                          HARRA  19
      PROGRAM HARRA (INPUT,OUTPUT,DISK,TAPE1=INPUT,TAPE3=OUTPUT,HARRA  20
     1TAPE6=DISK)                                           HARRA  21
C ****************                                          HARRA  22
C SOURCE PROGRAM IS DESCRIBED IN REPORT *RADIATION AND SCATTERING HARRA 23
C FROM BODIES OF REVOLUTION* BY R.F. HARRINGTON AND J.R. MAUTZ, JULY HARRA 24
C 1969, ELECTRICAL ENG. DEPT., SYRACUSE UNIV.,SYRACUSE, N.Y. HARRA  25
C MODIFICATIONS BY P.A. NEUKOMM AT BIOMECHANICS LABORATORY,SWISS FEDE- HARRA 26
C RAL INSTITUTE OF TECHNOLOGY PROVIDE THE SAME RESULTS ON THE CDC COM- HARRA 27
C PUTER OF THE ETH-Z. THE MODIFICATIONS IN THIS PROGRAM *HARRA* REGARD HARRA 28
C MAINLY THE CONVERSION FROM IBM TO CDC STANDARD AND FILE GENERATION. HARRA 29
C THE RESULTS OF THIS PROGRAM ARE THE Y-ADMITTANCE-MATRICES FOR THE HARRA 30
C MODI O UP TO KK FOR A GIVEN BODY AND A GIVEN FREQUENCY. IN THIS CASE HARRA 31
C THE BODY IS MANMOD2, THE FREQUENCY 164  MHZ, THE MAXIMUM MODE KK IS 7 HARRA 32
C AND THE RESULTS ARE STORED IN THE FILE S164M07 IN THE COLLECT FILE HARRA 33
C AMAT2.                                                    HARRA  34
C ATTENTION: SCALING IN THE PROGRAM: PHYSICAL DIMENSIONS 10 TIMES HARRA 35
C ACTUAL SIZE, FREQUENCY 10 TIMES LOWER THAN ACTUAL.         HARRA  36
C ****************                                          HARRA  37
                                                            HARRA  38
      COMPLEX A3,A4,Z,GS(40),G,U                            HARRA  39
      COMPLEX G1,G2,G3,TV(50)                               HARRA  40
      COMMON//G(5292),Z(1600)                               HARRA  41
      DIMENSION RH(43),ZH(43),DH(43),TJ(20)                 HARRA  42
      DIMENSION SV(42),CV(42),ZS(42),R(42),ANG(40),AC(40),CSM(120) HARRA 43
      DIMENSION TP(80),T(80),TR(80),JK(4)                   HARRA  44
      REWIND 6                                              HARRA  45
      U=(0.,1.)                                             HARRA  46
   50 READ (1,51) NN,NP,NPHI,BK,F                           HARRA  47
   51 FORMAT(3I3,E14.7,F8.2)                                HARRA  48
      IF(EOF(1)) 52,49                                      HARRA  49
   49 CONTINUE                                              HARRA  50
      READ(1,53)(RH(I),I=1,NP)                              HARRA  51
      READ(1,53)(ZH(I),I=1,NP)                              HARRA  52
   53 FORMAT(10F8.4)                                        HARRA  53
   76 WRITE(3,54) NN,NP,NPHI,BK,F                           HARRA  54
   54 FORMAT(1X//* NN=*,I3,* NP=*,I3,* NPHI=*,I3,* BK=*,E14.7, HARRA 55
     1 * FREQENCY = *,F6.2,* MHZ*)                          HARRA  56
   55 FORMAT(1X/* RH*)                                      HARRA  57
      WRITE(3,55)                                           HARRA  58
      WRITE(3,46)(RH(I),I=1,NP)                             HARRA  59
   46 FORMAT(1X,10F8.4)                                     HARRA  60
      WRITE(3,56)                                           HARRA  61
   56 FORMAT(1X/* ZH*)                                      HARRA  62
      WRITE(3,46)(ZH(I),I=1,NP)                             HARRA  63
      IF((RH(1)-RH(NP)).NE.0..OR.(ZH(1)-ZH(NP)).NE.0.) GO TO 58 HARRA 64
      RH(NP+1)=RH(2)                                        HARRA  65
      ZH(NP+1)=ZH(2)                                        HARRA  66
      RH(NP+2)=RH(3)                                        HARRA  67
      ZH(NP+2)=ZH(3)                                        HARRA  68
      NP=NP+2                                               HARRA  69
   58 DO 57 I=2,NP                                          HARRA  70
      I2=I-1                                                HARRA  71
      RR1=RH(I)-RH(I2)                                      HARRA  72
      RR2=ZH(I)-ZH(I2)                                      HARRA  73
      DH(I2)=SQRT(RR1*RR1+RR2*RR2)                          HARRA  74
      ZS(I2)=.5*(ZH(I)+ZH(I2))                              HARRA  75
      R(I2)=.5*(RH(I)+RH(I2))                               HARRA  76
      SV(I2)=RR1/DH(I2)                                     HARRA  77
      CV(I2)=RR2/DH(I2)                                     HARRA  78
   57 CONTINUE                                              HARRA  79
      KG=NP-1                                               HARRA  80
      N=KG/2                                                HARRA  81
      NM=N-1                                                HARRA  82
      NM2=NM*2                                              HARRA  83
      NM4=NM*4                                              HARRA  84
      NZ=NM2*NM2                                            HARRA  85
      NG=KG*KG                                              HARRA  86
      M5=NN+2                                               HARRA  87
      M6=NN+4                                               HARRA  88
      FM=NN                                                 HARRA  89
      FM2=NN*NN                                             HARRA  90
      PI=3.141593                                           HARRA  91
      ETA=376.707                                           HARRA  92
      DP=PI/NPHI                                            HARRA  93
      CA=BK*BK*ETA                                          HARRA  94
      CQ=ETA                                                HARRA  95
      SS=0.                                                 HARRA  96
      DO 117 I=1,NM                                         HARRA  97
      I1=2*(I-1)+1                                          HARRA  98
      I2=I1+1                                               HARRA  99
      SS=SS+DH(I1)+DH(I2)                                   HARRA100
      TJ(I)=SS                                              HARRA101
  117 CONTINUE                                              HARRA102
      WRITE(3,118)                                          HARRA103
```

```
118 FORMAT(1X/* TJ*)                                                 HARRA104
    WRITE(3,46) (TJ(I),I=1,NM)                                       HARRA105
    DO 2 J=1,NPHI                                                    HARRA106
    ANG(J)=(J-.5)*DP                                                 HARRA107
    AC(J)=COS(ANG(J))                                                HARRA108
  2 CONTINUE                                                         HARRA109
    M3=0                                                             HARRA110
    DO 10 MM=M5,M6                                                   HARRA111
    M1=MM-3                                                          HARRA112
    M2=M3*NPHI                                                       HARRA113
    DO 11 K=1,NPHI                                                   HARRA114
    K1=M2+K                                                          HARRA115
    CSM(K1)=DP*COS(M1*ANG(K))                                        HARRA116
 11 CONTINUE                                                         HARRA117
    M3=M3+1                                                          HARRA118
 10 CONTINUE                                                         HARRA119
    DO 16 J=1,KG                                                     HARRA120
    DEL=.5*DH(J)                                                     HARRA121
    DEL1=DH(J)*BK                                                    HARRA122
    AA=DP*R(J)*DEL*BK                                                HARRA123
    DO 17 I=1,KG                                                     HARRA124
    Z3=ZS(J)-ZS(I)                                                   HARRA125
    RR1=SV(J)*R(J)+CV(J)*Z3                                          HARRA126
    RR2=-SV(J)*R(I)                                                  HARRA127
    RR3=R(J)*R(J)+R(I)*R(I)+Z3*Z3                                    HARRA128
    RR4=-2.*R(J)*R(I)                                                HARRA129
    X1=ABS(R(J)-R(I))+ABS(Z3)                                        HARRA130
    DO 5 K=1,NPHI                                                    HARRA131
    IF(K.NE.1.OR.X1.NE.0.) GO TO 7                                   HARRA132
    X=R(J)*DP                                                        HARRA133
    XX=SQRT(DEL*DEL+X*X)                                             HARRA134
    W1=(X*ALOG((DEL+XX)/X)+DEL*ALOG((X+XX)/DEL))/AA                  HARRA135
    W2=-1.                                                           HARRA136
    GS(1)=W1+U*W2                                                    HARRA137
    GO TO 5                                                          HARRA138
  7 Y=ABS(RR1+AC(K)*RR2)                                             HARRA139
    RD=RR3+RR4*AC(K)                                                 HARRA140
    RK=BK*SQRT(RD)                                                   HARRA141
    D2=RD-Y*Y                                                        HARRA142
    Y1=Y-DEL                                                         HARRA143
    Y2=Y+DEL                                                         HARRA144
    R1=SQRT(Y1*Y1+D2)                                                HARRA145
    R2=SQRT(Y2*Y2+D2)                                                HARRA146
    IF(Y1) 72,73,73                                                  HARRA147
 72 TIN=ALOG((-Y1+R1)*(Y2+R2)/D2)                                    HARRA148
    GO TO 25                                                         HARRA149
 73 TIN=ALOG((Y2+R2)/(Y1+R1))                                        HARRA150
 25 SN=SIN(RK)                                                       HARRA151
    CS=COS(RK)                                                       HARRA152
    GS(K)=(CS-U*SN)*(TIN-U*(BK*DH(J)-RK*TIN))/DEL1                   HARRA153
  5 CONTINUE                                                         HARRA154
    M3=(J-1)*KG+I                                                    HARRA155
    DO 68 MM=1,3                                                     HARRA156
    M1=MM-1                                                          HARRA157
    M4=M1*NPHI                                                       HARRA158
    M2=M1*NG+M3                                                      HARRA159
    G(M2)=0.                                                         HARRA160
    DO 13 K=1,NPHI                                                   HARRA161
    K2=K+M4                                                          HARRA162
    G(M2)=G(M2)+GS(K)*CSM(K2)                                        HARRA163
 13 CONTINUE                                                         HARRA164
 68 CONTINUE                                                         HARRA165
 17 CONTINUE                                                         HARRA166
 16 CONTINUE                                                         HARRA167
    DO 74 J=1,NM                                                     HARRA168
    J2=2*(J-1)+1                                                     HARRA169
    J3=J2+1                                                          HARRA170
    J4=J3+1                                                          HARRA171
    J5=J4+1                                                          HARRA172
    J6=4*(J-1)+1                                                     HARRA173
    J7=J6+1                                                          HARRA174
    J8=J7+1                                                          HARRA175
    J9=J8+1                                                          HARRA176
    DEL1=DH(J2)+DH(J3)                                               HARRA177
    DEL2=DH(J4)+DH(J5)                                               HARRA178
    TP(J6)=DH(J2)/DEL1                                               HARRA179
    TP(J7)=DH(J3)/DEL1                                               HARRA180
    TP(J8)=-DH(J4)/DEL2                                              HARRA181
    TP(J9)=-DH(J5)/DEL2                                              HARRA182
    T(J6)=DH(J2)*DH(J2)/2./DEL1                                      HARRA183
    T(J7)=DH(J3)*(DH(J2)+DH(J3)/2.)/DEL1                             HARRA184
    T(J8)=DH(J4)*(DH(J5)+DH(J4)/2.)/DEL2                             HARRA185
    T(J9)=DH(J5)*DH(J5)/2./DEL2                                      HARRA186
 74 CONTINUE                                                         HARRA187
    DO 75 J=1,NM4                                                    HARRA188
    TR(J)=T(J)                                                       HARRA189
 75 CONTINUE                                                         HARRA190
115 IF((ZH(1)-ZH(NP-2)).EQ.0..AND.(RH(1)-RH(NP-2)).EQ.0.) GO TO 78   HARRA191
    IF(RH(1)) 77,23,77                                               HARRA192
 77 DEL1=DH(1)+DH(2)                                                 HARRA193
    TR(1)=DH(1)*(1.+(DH(2)+DH(1)/2.)/DEL1)                           HARRA194
    TR(2)=DH(2)*(1.+DH(2)/2./DEL1)                                   HARRA195
 23 IF(RH(NP)) 79,78,79                                              HARRA196
 79 J1=(N-2)*4+3                                                     HARRA197
    J2=J1+1                                                          HARRA198
    DEL2=DH(NP-2)+DH(KG)                                             HARRA199
    TR(J1)=DH(NP-2)*(1.+DH(NP-2)/2./DEL2)                            HARRA200
116 TR(J2)=DH(KG)*(1.+(DH(NP-2)+DH(KG)/2.)/DEL2)                     HARRA201
 78 DO 30 J=1,NM                                                     HARRA202
    JL=(J-1)*NM2                                                     HARRA203
    J3=(J-1)*4                                                       HARRA204
    J1=2*(J-1)                                                       HARRA205
    DO 31 I=1,NM                                                     HARRA206
    L1=JL+I                                                          HARRA207
```

```
      L2=L1+NM                                                          HARRA208
      L3=NM*NM2+L1                                                      HARRA209
      L4=L3+NM                                                          HARRA210
      Z(L1)=0.                                                          HARRA211
      Z(L2)=0.                                                          HARRA212
      Z(L3)=0.                                                          HARRA213
      Z(L4)=0.                                                          HARRA214
      I1=2*(I-1)                                                        HARRA215
      I3=(I-1)*4                                                        HARRA216
      DO 70 JJ=1,4                                                      HARRA217
      J2=J1+JJ                                                          HARRA218
      J7=J3+JJ                                                          HARRA219
      DO 71 II=1,4                                                      HARRA220
      I2=I1+II                                                          HARRA221
      I7=I3+II                                                          HARRA222
      J4=(J2-1)*KG+I2                                                   HARRA223
      J5=J4+NG                                                          HARRA224
      J6=J5+NG                                                          HARRA225
      SS=SV(I2)*SV(J2)                                                  HARRA226
      CC=CV(I2)*CV(J2)                                                  HARRA227
      A3=.5*(G(J6)+G(J4))                                               HARRA228
      A4=.5*(G(J6)-G(J4))                                               HARRA229
      Z(L1)=Z(L1)+(CA*T(I7)*T(J7)*(SS*A3+CC*G(J5))-CQ*TP(I7)*TP(J7)*G(J5HARRA230
     1))*U                                                              HARRA231
      Z(L2)=Z(L2)+CA*SV(J2)*TR(I7)*T(J7)*A4-FM*CQ*G(J5)*TR(I7)*TP(J7)/R(HARRA232
     1I2)                                                               HARRA233
      Z(L3)=Z(L3)-CA*SV(I2)*T(I7)*TR(J7)*A4+FM*CQ*G(J5)*TP(I7)*TR(J7)/R(HARRA234
     1J2)                                                               HARRA235
      Z(L4)=Z(L4)+(CA*A3-FM2*CQ/R(I2)/R(J2)*G(J5))*TR(I7)*TR(J7)*U      HARRA236
   71 CONTINUE                                                          HARRA237
   70 CONTINUE                                                          HARRA238
   31 CONTINUE                                                          HARRA239
   30 CONTINUE                                                          HARRA240
   81 CALL LINEQ(NM2,Z)                                                 HARRA241
      WRITE(6)(Z(I),I=1,NZ)                                             HARRA242
      JK(1)=1                                                           HARRA243
      JK(2)=N                                                           HARRA244
      JK(3)=NM2*NM+1                                                    HARRA245
      JK(4)=JK(3)+NM                                                    HARRA246
      DO 93 J=1,4                                                       HARRA247
      K1=JK(J)                                                          HARRA248
      WRITE(3,24) J                                                     HARRA249
   24 FORMAT(1X/* Y*,I1)                                                HARRA250
      DO 92 I=1,NM                                                      HARRA251
      K2=K1+NM-1                                                        HARRA252
   96 WRITE(3,88)(Z(K),K=K1,K2)                                         HARRA253
   88 FORMAT(1X,10G11.4)                                                HARRA254
      K1=K1+NM2                                                         HARRA255
   92 CONTINUE                                                          HARRA256
   93 CONTINUE                                                          HARRA257
      GO TO 50                                                          HARRA258
   52 STOP                                                              HARRA259
      END                                                               HARRA260
C ****************                                                      HARRA261
E SUBROUTINE                                                            HARRA262
      SUBROUTINE LINEQ(LL,C)                                            HARRA263
      COMPLEX C(1),STOR,STO,ST,S                                        HARRA264
      DIMENSION LR(58)                                                  HARRA265
      DO 20 I=1,LL                                                      HARRA266
      LR(I)=I                                                           HARRA267
   20 CONTINUE                                                          HARRA268
      M1=0                                                              HARRA269
      DO 18 M=1,LL                                                      HARRA270
      K=M                                                               HARRA271
      DO 2 I=M,LL                                                       HARRA272
      K1=M1+I                                                           HARRA273
      K2=M1+K                                                           HARRA274
      IF(CABS(C(K1))-CABS(C(K2))) 2,2,6                                 HARRA275
    6 K=I                                                               HARRA276
    2 CONTINUE                                                          HARRA277
      LS=LR(M)                                                          HARRA278
      LR(M)=LR(K)                                                       HARRA279
      LR(K)=LS                                                          HARRA280
      K2=M1+K                                                           HARRA281
      STOR=C(K2)                                                        HARRA282
      J1=0                                                              HARRA283
      DO 7 J=1,LL                                                       HARRA284
      K1=J1+K                                                           HARRA285
      K2=J1+M                                                           HARRA286
      STO=C(K1)                                                         HARRA287
      C(K1)=C(K2)                                                       HARRA288
      C(K2)=STO/STOR                                                    HARRA289
      J1=J1+LL                                                          HARRA290
    7 CONTINUE                                                          HARRA291
      K1=M1+M                                                           HARRA292
      C(K1)=1./STOR                                                     HARRA293
      DO 11 I=1,LL                                                      HARRA294
      IF(I-M) 12,11,12                                                  HARRA295
   12 K1=M1+I                                                           HARRA296
      ST=C(K1)                                                          HARRA297
      C(K1)=0.                                                          HARRA298
      J1=0                                                              HARRA299
      DO 10 J=1,LL                                                      HARRA300
      K1=J1+I                                                           HARRA301
      K2=J1+M                                                           HARRA302
      C(K1)=C(K1)-C(K2)*ST                                              HARRA303
      J1=J1+LL                                                          HARRA304
   10 CONTINUE                                                          HARRA305
   11 CONTINUE                                                          HARRA306
      M1=M1+LL                                                          HARRA307
   18 CONTINUE                                                          HARRA308
      J1=0                                                              HARRA309
      DO 9 J=1,LL                                                       HARRA310
      IF(J-LR(J)) 14,8,14                                               HARRA311
```

```
  14 LRJ=LR(J)                                                      HARRA312
     J2=(LRJ-1)*LL                                                  HARRA313
  21 DO 13 I=1,LL                                                   HARRA314
     K2=J2+I                                                        HARRA315
     K1=J1+I                                                        HARRA316
     S=C(K2)                                                        HARRA317
     C(K2)=C(K1)                                                    HARRA318
     C(K1)=S                                                        HARRA319
  13 CONTINUE                                                       HARRA320
     LR(J)=LR(LRJ)                                                  HARRA321
     LR(LRJ)=LRJ                                                    HARRA322
     LR(J)=LR(LRJ)                                                  HARRA323
     LR(LRJ)=LRJ                                                    HARRA324
     IF(J-LR(J)) 14,8,14                                            HARRA325
   8 J1=J1+LL                                                       HARRA326
   9 CONTINUE                                                       HARRA327
     RETURN                                                         HARRA328
     END                                                            HARRA329
C ****************                                                  HARRA330
R HERE END OF RECORD CARD                                           HARRA331
E DATA CARDS                                                        HARRA332
000041 20 0.3434808E+00    16.4 MHZ
  0.000   0.500   0.515   0.515   0.500   0.500   0.515   0.515   0.525   0.525
  0.575   0.600   0.625   0.660   0.710   0.780   0.925   1.050   1.050   1.000
  0.980   0.980   1.020   1.085   1.100   1.070   1.040   1.000   0.930   0.850
  0.630   0.480   0.490   0.620   0.760   0.850   0.870   0.820   0.700   0.500
  0.000
  0.000   0.000   0.350   0.760   1.270   1.740   2.180   2.580   3.120   3.680
  4.260   4.840   5.500   5.960   6.510   7.060   7.630   8.240   8.700   9.200
  9.740  10.270  10.770  11.340  11.820  12.270  12.550  12.820  13.190  13.510
 13.920  14.310  14.550  14.700  15.000  15.400  15.700  16.050  16.420  16.680
 16.800
001041 20 0.3434808E+00    16.4 MHZ
  0.000   0.500   0.515   0.515   0.500   0.500   0.515   0.515   0.525   0.525
  0.575   0.600   0.625   0.660   0.710   0.780   0.925   1.050   1.050   1.000
  0.980   0.980   1.020   1.085   1.100   1.070   1.040   1.000   0.930   0.850
  0.630   0.480   0.490   0.620   0.760   0.850   0.870   0.820   0.700   0.500
  0.000
  0.000   0.000   0.350   0.760   1.270   1.740   2.180   2.580   3.120   3.680
  4.260   4.840   5.500   5.960   6.510   7.060   7.630   8.240   8.700   9.200
  9.740  10.270  10.770  11.340  11.820  12.270  12.550  12.820  13.190  13.510
 13.920  14.310  14.550  14.700  15.000  15.400  15.700  16.050  16.420  16.680
 16.800
002041 20 0.3434808E+00    16.4 MHZ
  0.000   0.500   0.515   0.515   0.500   0.500   0.515   0.515   0.525   0.525
  0.575   0.600   0.625   0.660   0.710   0.780   0.925   1.050   1.050   1.000
  0.980   0.980   1.020   1.085   1.100   1.070   1.040   1.000   0.930   0.850
  0.630   0.480   0.490   0.620   0.760   0.850   0.870   0.820   0.700   0.500
  0.000
  0.000   0.000   0.350   0.760   1.270   1.740   2.180   2.580   3.120   3.680
  4.260   4.840   5.500   5.960   6.510   7.060   7.630   8.240   8.700   9.200
  9.740  10.270  10.770  11.340  11.820  12.270  12.550  12.820  13.190  13.510
 13.920  14.310  14.550  14.700  15.000  15.400  15.700  16.050  16.420  16.680
 16.800
003041 20 0.3434808E+00    16.4 MHZ
  0.000   0.500   0.515   0.515   0.500   0.500   0.515   0.515   0.525   0.525
  0.575   0.600   0.625   0.660   0.710   0.780   0.925   1.050   1.050   1.000
  0.980   0.980   1.020   1.085   1.100   1.070   1.040   1.000   0.930   0.850
  0.630   0.480   0.490   0.620   0.760   0.850   0.870   0.820   0.700   0.500
  0.000
  0.000   0.000   0.350   0.760   1.270   1.740   2.180   2.580   3.120   3.680
  4.260   4.840   5.500   5.960   6.510   7.060   7.630   8.240   8.700   9.200
  9.740  10.270  10.770  11.340  11.820  12.270  12.550  12.820  13.190  13.510
 13.920  14.310  14.550  14.700  15.000  15.400  15.700  16.050  16.420  16.680
 16.800
004041 20 0.3434808E+00    16.4 MHZ
  0.000   0.500   0.515   0.515   0.500   0.500   0.515   0.515   0.525   0.525
  0.575   0.600   0.625   0.660   0.710   0.780   0.925   1.050   1.050   1.000
  0.980   0.980   1.020   1.085   1.100   1.070   1.040   1.000   0.930   0.850
  0.630   0.480   0.490   0.620   0.760   0.850   0.870   0.820   0.700   0.500
  0.000
  0.000   0.000   0.350   0.760   1.270   1.740   2.180   2.580   3.120   3.680
  4.260   4.840   5.500   5.960   6.510   7.060   7.630   8.240   8.700   9.200
  9.740  10.270  10.770  11.340  11.820  12.270  12.550  12.820  13.190  13.510
 13.920  14.310  14.550  14.700  15.000  15.400  15.700  16.050  16.420  16.680
 16.800
```

EACH MODE COMPLETE DATA SET UP TO LAST MODE NN= 7

```
007041 20 0.3434808E+00    16.4 MHZ
  0.000   0.500   0.515   0.515   0.500   0.500   0.515   0.515   0.525   0.525
  0.575   0.600   0.625   0.660   0.710   0.780   0.925   1.050   1.050   1.000
  0.980   0.980   1.020   1.085   1.100   1.070   1.040   1.000   0.930   0.850
  0.630   0.480   0.490   0.620   0.760   0.850   0.870   0.820   0.700   0.500
  0.000
  0.000   0.000   0.350   0.760   1.270   1.740   2.180   2.580   3.120   3.680
  4.260   4.840   5.500   5.960   6.510   7.060   7.630   8.240   8.700   9.200
  9.740  10.270  10.770  11.340  11.820  12.270  12.550  12.820  13.190  13.510
 13.920  14.310  14.550  14.700  15.000  15.400  15.700  16.050  16.420  16.680
 16.800
R HERE END OF RECORD CARD                                           HARRA333
ADD,S164M07,DISK,RO.                                                HARRA334
LIST                                                                HARRA335
END                                                                 HARRA336
R HERE END OF INFORMATION CARD                                      HARRA337
```

```
NN=  0 NP= 41 NPHI= 20 UK=  .3434808E+00 FREQENCY =  16.40 MHZ

RH
   0.0000    .5000    .5150    .5150    .5000    .5000    .5150    .5150    .5250    .5250
    .5750    .6000    .6250    .6600    .7100    .7800    .9250   1.0500   1.0500   1.0000
    .9800    .9800   1.0200   1.0350   1.1000   1.0700   1.0400   1.0000    .9300    .8500
    .6300    .4800    .4900    .6200    .7600    .8500    .8700    .8200    .7000    .5000
   0.0000

ZH
   0.0000   0.0000    .3500    .7600   1.2700   1.7400   2.1800   2.5800   3.1200   3.6800
   4.2600   4.8400   5.5000   5.9600   6.5100   7.0600   7.6300   8.2400   8.7000   9.2000
   9.7400  10.2700  10.7700  11.3400  11.8200  12.2700  12.5500  12.8200  13.1900  13.5100
  13.9200  14.3100  14.5500  14.7000  15.0000  15.4000  15.7000  16.0500  16.4200  16.6800
  16.8000

TJ
    .8503   1.7705   2.6808   3.6209   4.7630   6.0041   7.0177   8.1602   9.2429  10.2858
  11.3174  12.3713  13.1039  13.7534  14.5486  15.2066  15.7362  16.4463  17.1894

Y1
   .2244E-04  .1244E-03  .4878E-04  .2618E-04  .6413E-04  .1155E-04  .7421E-04 -.9309E-05  .7697E-04 -.2810E-04
   .6853E-04 -.4244E-04  .5337E-04 -.4761E-04  .3018E-04 -.4682E-04 -.5359E-05 -.3697E-04 -.3335E-04 -.2418E-04
  -.5427E-04 -.1061E-04 -.7186E-04  .5896E-05 -.7854E-04  .1634E-04 -.7967E-04  .2295E-04 -.7610E-04  .2660E-04
  -.7341E-04  .2686E-04 -.6710E-04  .2621E-04 -.4755E-04  .2154E-04 -.1628E-04  .8630E-05
   .4800E-04  .2554E-04  .1048E-03  .1614E-03  .1382E-03  .3021E-04  .1605E-03 -.7142E-05  .1673E-03 -.5013E-04
   .1501E-03 -.8221E-04  .1195E-03 -.9502E-04  .6887E-04 -.9597E-04 -.7186E-05 -.7882E-04 -.6739E-04 -.5463E-04
  -.1127E-03 -.2809E-04 -.1512E-03  .4984E-05 -.1662E-03  .2632E-04 -.1692E-03  .4015E-04 -.1620E-03  .4818E-04
  -.1564E-03  .4900E-04 -.1431E-03  .4828E-04 -.1017E-03  .4045E-04 -.3493E-04  .1647E-04
   .6322E-04  .1124E-04  .1335E-03  .3032E-04  .1832E-03  .1445E-03  .2134E-03  .3560E-06  .2233E-03 -.5105E-04
   .2018E-03 -.9729E-04  .1621E-03 -.1163E-03  .9590E-04 -.1209E-03 -.4160E-05 -.1031E-03 -.8369E-04 -.7508E-04
  -.1439E-03 -.4311E-04 -.1956E-03 -.2263E-05 -.2162E-03  .2462E-04 -.2207E-03  .4241E-04 -.2119E-03  .5325E-04
  -.2647E-03  .5464E-04 -.1875E-03  .5446E-04 -.1335E-03  .4665E-04 -.4598E-04  .1936E-04
   .7320E-04 -.9384E-05  .1609E-03 -.7333E-05  .2135E-03  .1438E-06  .2496E-03  .1096E-03  .2625E-03 -.4571E-04
   .2399E-03 -.9465E-04  .1940E-03 -.1219E-03  .1181E-03 -.1319E-03  .2557E-05 -.1180E-03 -.8968E-04 -.9065E-04
  -.1600E-03 -.5764E-04 -.2210E-03 -.1399E-04 -.2458E-03  .1551E-04 -.2520E-03  .3552E-04 -.2426E-03  .4838E-04
  -.2345E-03  .5038E-04 -.2150E-03  .5116E-04 -.1535E-03  .4537E-04 -.5303E-04  .1936E-04
   .7583E-04 -.2786E-04  .1676E-03 -.5031E-04  .2233E-03 -.5114E-04  .2623E-03 -.4609E-04  .2778E-03  .7752E-04
   .2557E-03 -.7838E-04  .2106E-03 -.1025E-03  .1331E-03 -.1229E-03  .1433E-04 -.1189E-03 -.8114E-04 -.9853E-04
  -.1546E-03 -.7045E-04 -.2193E-03 -.3079E-04 -.2465E-03 -.2747E-05 -.2542E-03  .1706E-04 -.2457E-03  .3077E-04
  -.2378E-03  .3740E-04 -.2133E-03  .3564E-04 -.1565E-03  .3436E-04 -.5431E-04  .1558E-04
   .6764E-04 -.4188E-04  .1507E-03 -.8221E-04  .2021E-03 -.9706E-04  .2392E-03 -.9433E-04  .2561E-03 -.7809E-04
   .2490E-03  .8612E-04  .2021E-03 -.5870E-04  .1351E-03 -.8296E-04  .3089E-04 -.9858E-04 -.5371E-04 -.9244E-04
  -.1198E-03 -.7660E-04 -.1795E-03 -.4951E-04 -.2056E-03 -.2828E-04 -.2143E-03 -.1207E-04 -.2088E-03  .5896E-06
  -.2024E-03  .3678E-05 -.1854E-03  .7637E-05 -.1345E-03  .1302E-04 -.4701E-04  .7634E-05
   .5311E-04 -.4709E-04  .1196E-03 -.9535E-04  .1620E-03 -.1165E-03  .1937E-03 -.1221E-03  .2105E-03 -.1031E-03
   .2018E-03 -.5835E-04  .1749E-03  .1281E-03  .1250E-03 -.4212E-04  .4551E-04 -.6394E-04 -.1989E-04 -.7528E-04
  -.7214E-04 -.7240E-04 -.1209E-03 -.6174E-04 -.1435E-03 -.4946E-04 -.1524E-03 -.3850E-04 -.1504E-03 -.2823E-04
  -.1463E-03 -.2504E-04 -.1353E-03 -.1988E-04 -.9862E-04 -.8723E-05 -.3487E-04 -.7550E-06
   .2964E-04 -.4622E-04  .6888E-04 -.9617E-04  .9573E-04 -.1210E-03  .1178E-03 -.1319E-03  .1329E-03 -.1232E-03
   .1349E-03 -.8256E-04  .1248E-03 -.4303E-04  .1010E-03  .1961E-03  .6191E-04 -.1790E-04  .2758E-04 -.3938E-04
  -.1764E-05 -.5886E-04 -.3179E-04 -.6850E-04 -.4773E-04 -.6327E-04 -.5614E-04 -.6629E-04 -.5893E-04 -.6030E-04
```

RESULTS FROM HARRA

ONLY MODE NN = 0 SHOWN HERE

-.5814E-04	-.5739E-04	-.5439E-04	-.5137E-04	-.4186E-04	-.3446E-04	-.1550E-04	-.1099E-04		
-.5304E-05	-.3644E-04	-.7133E-05	-.7894E-04	-.4074E-05	-.1031E-03	.2628E-05	-.1178E-03	.1437E-04	-.1189E-03
.3110E-04	-.9822E-04	.4548E-04	-.6394E-04	.6183E-04	-.1867E-04	.8120E-04	.2613E-03	.9355E-04	.1534E-04
.9900E-04	-.1916E-04	.9803E-04	-.6252E-04	.9295E-04	-.8156E-04	.8602E-04	-.9052E-04	.7663E-04	-.9171E-04
.7260E-04	-.8975E-04	.6451E-04	-.8390E-04	.4295E-04	-.6242E-04	.1358E-04	-.2261E-04		
-.3290E-04	-.2384E-04	-.6745E-04	-.5491E-04	-.8361E-04	-.7519E-04	-.8953E-04	-.9068E-04	-.8112E-04	-.9865E-04
-.5330E-04	-.9238E-04	-.1934E-04	-.7537E-04	.2748E-04	-.3945E-04	.9363E-04	.1552E-04	.1434E-03	.2707E-03
.1769E-03	.1762E-04	.1996E-03	-.3856E-04	.2037E-03	-.7549E-04	.1984E-03	-.9438E-04	.1842E-03	-.1023E-03
.1764E-03	-.1017E-03	.1596E-03	-.9702E-04	.1104E-03	-.7574E-04	.3687E-04	-.2876E-04		
-.5363E-04	-.1034E-04	-.1131E-03	-.2803E-04	-.1442E-03	-.4299E-04	-.1602E-03	-.5745E-04	-.1550E-03	-.7032E-04
-.1197E-03	-.7653E-04	-.7254E-04	-.7337E-04	-.2119E-05	-.5900E-04	.9912E-04	-.1942E-04	.1771E-03	.1719E-04
.2322E-03	.2637E-03	.2735E-03	-.1522E-04	.2851E-03	-.4963E-04	.2815E-03	-.7989E-04	.2641E-03	-.9428E-04
.2536E-03	-.9532E-04	.2304E-03	-.9301E-04	.1611E-03	-.7595E-04	.5445E-04	-.3000E-04		
-.7078E-04	.5810E-05	-.1513E-03	.4730E-05	-.1953E-03	-.2519E-05	-.2205E-03	-.1421E-04	-.2191E-03	-.3098E-04
-.1786E-03	-.4980E-04	-.1208E-03	-.6174E-04	-.3190E-04	-.6852E-04	.9813E-04	-.6236E-04	.1996E-03	-.3793E-04
.2729E-03	-.1527E-04	.3318E-03	.2658E-03	.3495E-03	.5030E-05	.3480E-03	-.3107E-04	.3286E-03	-.5870E-04
.3161E-03	-.6252E-04	.2879E-03	-.6597E-04	.2026E-03	-.5920E-04	.6899E-04	-.2528E-04		
-.7742E-04	.1618E-04	-.1655E-03	.2631E-04	-.2161E-03	.2454E-04	-.2455E-03	.1545E-04	-.2465E-03	-.2750E-05
-.2050E-03	-.2854E-04	-.1436E-03	-.4937E-04	-.4797E-04	-.6919E-04	.9304E-04	-.8159E-04	.2037E-03	-.7530E-04
.2846E-03	-.4982E-04	.3436E-03	.5785E-05	.3718E-03	.2791E-03	.3719E-03	.2279E-04	.3522E-03	-.1069E-04
.3391E-03	-.1973E-04	.3093E-03	-.2768E-04	.2183E-03	-.3505E-04	.7462E-04	-.1758E-04		
-.7853E-04	.2273E-04	-.1635E-03	.4020E-04	-.2207E-03	.4239E-04	-.2518E-03	.3551E-04	-.2542E-03	.1713E-04
-.2137E-03	-.1233E-04	-.1525E-03	-.3837E-04	-.5642E-04	-.6618E-04	.8610E-04	-.9058E-04	.1985E-03	-.9427E-04
.2811E-03	-.8001E-04	.3483E-03	-.3083E-04	.3719E-03	.2349E-04	.3729E-03	.2542E-03	.3539E-03	.3377E-04
.3410E-03	.3217E-04	.3113E-03	.1544E-04	.2201E-03	-.7189E-05	.7546E-04	-.8503E-05		
-.7512E-04	.2634E-04	-.1625E-03	.4828E-04	-.2122E-03	.5325E-04	-.2427E-03	.4837E-04	-.2461E-03	.3083E-04
-.2085E-03	.2640E-06	-.1507E-03	-.2817E-04	-.5926E-04	-.6028E-04	.7683E-04	-.9189E-04	.1845E-03	-.1024E-03
.2640E-03	-.9443E-04	.3293E-03	-.5847E-04	.3527E-03	-.1051E-04	.3545E-03	.3520E-04	.3370E-03	.2291E-03
.3248E-03	.9558E-04	.2956E-03	.7434E-04	.2102E-03	.2611E-04	.7219E-04	.2336E-05		
-.7243E-04	.2662E-04	-.1568E-03	.4916E-04	-.2049E-03	.5472E-04	-.2345E-03	.5047E-04	-.2381E-03	.3356E-04
-.2021E-03	.3455E-05	-.1456E-03	-.2499E-04	-.5847E-04	-.5730E-04	.7271E-04	-.8992E-04	.1766E-03	-.1018E-03
.2534E-03	-.9555E-04	.3156E-03	-.6252E-04	.3395E-03	-.1976E-04	.3413E-03	.3160E-04	.3246E-03	.9673E-04
.3129E-03	.2434E-03	.2859E-03	.9344E-04	.2026E-03	.4003E-04	.6965E-04	.6265E-05		
-.6604E-04	.2594E-04	-.1432E-03	.4839E-04	-.1872E-03	.5450E-04	-.2145E-03	.5122E-04	-.2181E-03	.3581E-04
-.1857E-03	.7486E-05	-.1353E-03	-.1963E-04	-.5509E-04	-.5115E-04	.6453E-04	-.8379E-04	.1594E-03	-.9693E-04
.2297E-03	-.9310E-04	.2877E-03	-.6505E-04	.3089E-03	-.2780E-04	.3108E-03	.1501E-04	.2958E-03	.7446E-04
.2852E-03	.9264E-04	.2636E-03	.2582E-03	.1849E-03	.5277E-04	.6360E-04	.1362E-04		
-.4683E-04	.2125E-04	-.1018E-03	.4046E-04	-.1334E-03	.4657E-04	-.1533E-03	.4529E-04	-.1564E-03	.3436E-04
-.1340E-03	.1277E-04	-.9855E-04	-.8643E-05	-.4199E-04	-.3435E-04	.4289E-04	-.6241E-04	.1104E-03	-.7561E-04
.1607E-03	-.7587E-04	.2026E-03	-.5901E-04	.2182E-03	-.3489E-04	.2200E-03	-.7122E-05	.2097E-03	.2658E-04
.2023E-03	.4048E-04	.1850E-03	.5157E-04	.1315E-03	.2600E-03	.4535E-04	.2641E-04		
-.1626E-04	.8615E-05	-.3546E-04	.1666E-04	-.4659E-04	.1953E-04	-.5370E-04	.1952E-04	-.5504E-04	.1572E-04
-.4750E-04	.7577E-05	-.3535E-04	-.7839E-06	-.1573E-04	-.1113E-04	.1380E-04	-.2291E-04	.3741E-04	-.2907E-04
.5510E-04	-.3031E-04	.6938E-04	-.2547E-04	.7565E-04	-.1766E-04	.7648E-04	-.8485E-05	.7306E-04	.2628E-05
.7051E-04	.6544E-05	.6454E-04	.1383E-04	.4598E-04	.2716E-04	.1591E-04	.1438E-03		

Y2

0.	0.	0.	0.	0.	0.	0.	0.	0.	0.
0.	0.	0.	0.	0.	0.	0.	0.	0.	0.
0.	0.	0.	0.	0.	0.	0.	0.	0.	0.
0.	0.	0.	0.	0.	0.	0.	0.		
0.	0.	0.	0.	0.	0.	0.	0.	0.	0.

```
 *           *           *           *           *           *           *           *           *           *
 0.          0.          0.          0.          0.          0.          0.          0.          0.          0.
 0.          0.          0.          0.          0.          0.          0.          0.

Y3
 0.          0.          0.          0.          0.          0.          0.          0.          0.          0.
 0.          0.          0.          0.          0.          0.          0.          0.          0.          0.
 0.          0.          0.          0.          0.          0.          0.          0.          0.          0.
 0.          0.          0.          0.          0.          0.          0.          0.
 0.          0.          0.          0.          0.          0.          0.          0.          0.          0.
 *           *           *           *           *           *           *           *           *           *
 0.          0.          0.          0.          0.          0.          0.          0.          0.          0.
 0.          0.          0.          0.          0.          0.          0.          0.

Y4
 .7626E-05 -.6989E-02  .5123E-05  .3512E-02  .5558E-05 -.1293E-02  .4970E-05  .4850E-03  .5030E-05 -.1680E-03
 .4773E-05  .8202E-04  .4037E-05 -.2933E-04  .5103E-05  .1461E-04  .4589E-05 -.7221E-05  .2053E-05  .1093E-05
 .1712E-05 -.2978E-05  .7497E-05 -.1866E-05  .7681E-07 -.2151E-05 -.3567E-06 -.1508E-05 -.3191E-05 -.5899E-06
-.1039E-06 -.1679E-06 -.6358E-06 -.8655E-06 -.1108E-05 -.7057E-06 -.7133E-06 -.1406E-06
 .5186E-05  .3563E-02  .3162E-05 -.8527E-02  .4095E-05  .4048E-02  .3284E-05 -.1379E-02  .3638E-05  .5401E-03
 .3495E-05 -.2277E-03  .3155E-05  .9787E-04  .4131E-05 -.3695E-04  .4067E-05  .1897E-04  .2050E-05 -.8153E-05
 .1904E-05  .2336E-05  .1309E-05 -.3232E-05  .6462E-06 -.5229E-06  .2470E-06 -.1577E-05 -.5470E-07 -.3685E-06
-.1510E-07 -.2228E-06 -.1819E-06 -.7835E-06 -.5520E-06 -.8499E-06 -.4486E-06 -.3178E-06
 .5581E-05 -.1309E-02  .4172E-05  .4026E-02  .4445E-05 -.8587E-02  .4491E-05  .3684E-02  .4420E-05 -.1337E-02
 .4719E-05  .6131E-03  .4149E-05 -.2373E-03  .5667E-05  .1112E-03  .5727E-05 -.4542E-04  .3030E-05  .1967E-04
 .2910E-05 -.9037E-05  .2241E-05  .2598E-05  .1275E-05 -.3715E-05  .7133E-06 -.8193E-06  .7692E-07 -.9708E-06
 .3094E-07 -.7514E-07  .6684E-08 -.1165E-05 -.4597E-06 -.1232E-05 -.4786E-06 -.5502E-06
 .4901E-05  .4973E-03  .3343E-05 -.1393E-02  .4526E-05  .3739E-02  .3788E-05 -.7425E-02  .4642E-05  .3365E-02
 .4248E-05 -.1445E-02  .4218E-05  .6053E-03  .5689E-05 -.2512E-03  .6144E-05  .1201E-03  .3412E-05 -.4719E-04
 .3429E-05  .2067E-04  .2939E-05 -.1156E-04  .1869E-05  .3942E-05  .1272E-05 -.3327E-05  .2990E-06  .1253E-06
 .1065E-06 -.5729E-06  .3793E-06 -.9639E-06 -.3727E-07 -.1453E-05 -.2886E-06 -.6823E-06
 .4972E-05 -.1737E-03  .3745E-05  .5481E-03  .4300E-05 -.1364E-02  .4708E-05  .3377E-02  .4846E-05 -.6642E-02
 .5842E-05  .3451E-02  .4858E-05 -.1360E-02  .7357E-05  .6214E-03  .7953E-05 -.2607E-03  .4672E-05  .1149E-03
 .4803E-05 -.4584E-04  .4453E-05  .2419E-04  .3019E-05 -.1294E-04  .2259E-05  .3114E-05  .6508E-06 -.2493E-05
 .2277E-06  .5967E-06  .9436E-06 -.1624E-05  .5276E-06 -.1686E-05 -.7641E-07 -.1031E-05
 .4695E-05  .8444E-04  .3536E-05 -.2311E-03  .4598E-05  .6250E-03  .4316E-05 -.1453E-02  .5714E-05  .3457E-02
 .5707E-05 -.7229E-02  .6407E-05  .3629E-02  .8331E-05 -.1505E-02  .1012E-04  .7151E-03  .6107E-05 -.2809E-03
 .6580E-05  .1277E-03  .6541E-05 -.6074E-04  .4721E-05  .3147E-04  .3810E-05 -.1201E-04  .1254E-05  .4023E-05
 .4347E-06 -.2324E-05  .1952E-05 -.2669E-06  .1676E-05 -.2281E-05  .4616E-06 -.1182E-05
 .4100E-05 -.3073E-04  .3317E-05  .1005E-03  .4094E-05 -.2450E-03  .4351E-05  .6147E-03  .4829E-05 -.1376E-02
 .6428E-05  .3637E-02  .5276E-05 -.8257E-02  .9703E-05  .4584E-02  .1029E-04 -.1971E-02  .6720E-05  .8499E-03
 .7187E-05 -.3453E-03  .7539E-05  .1872E-03  .5587E-05 -.8779E-04  .4672E-05  .3384E-04  .1619E-05 -.1356E-04
 .5602E-06  .6143E-05  .2532E-05 -.3219E-05  .2480E-05 -.8398E-06  .8920E-06 -.1526E-05
 .4925E-05  .1527E-04  .4169E-05 -.4031E-04  .5404E-05  .1151E-03  .5625E-05 -.2574E-03  .7121E-05  .6325E-03
 .8131E-05 -.1520E-02  .9265E-05  .4608E-02  .1257E-04 -.9265E-02  .1786E-04  .5423E-02  .1090E-04 -.2183E-02
 .1246E-04  .9671E-03  .1329E-04 -.4708E-03  .1021E-04  .2458E-03  .8817E-05 -.8481E-04  .3211E-05  .3571E-04
 .1109E-05 -.1634E-04  .5233E-05  .6809E-05  .5505E-05 -.4036E-05  .2332E-05 -.1049E-05
 .4605E-05 -.7493E-05  .4276E-05  .1952E-04  .5687E-05 -.4688E-04  .6340E-05  .1221E-03  .8043E-05 -.2636E-03
 .1036E-04  .7174E-03  .1024E-04 -.1969E-02  .1798E-04  .5388E-02  .2115E-04 -.1079E-01  .1600E-04  .6027E-02
 .1695E-04 -.2419E-02  .1936E-04  .1331E-02  .1573E-04 -.6116E-03  .1417E-04  .2490E-03  .5425E-05 -.9076E-04
 .1876E-05  .4511E-04  .9043E-05 -.1357E-04  .1033E-04  .7469E-05  .4932E-05 -.2855E-05
```

.1978E-05	.1213E-05	.2030E-05	-.8335E-05	.2915E-05	.2028E-04	.3402E-05	-.4807E-04	.4604E-05	.1162E-03
.6056E-05	-.2819E-03	.6610E-05	.8432E-03	.1079E-04	-.2173E-02	.1600E-04	.6041E-02	.9559E-05	-.1118E-01
.1348E-04	.6380E-02	.1443E-04	-.3144E-02	.1212E-04	.1617E-02	.1113E-04	-.5671E-03	.4452E-05	.2391E-03
.1527E-05	-.1077E-03	.7516E-05	.5119E-04	.9062E-05	-.1113E-04	.4652E-05	.5176E-05		
.1693E-05	-.3009E-05	.1976E-05	.2430E-05	.2855E-05	-.9286E-05	.3482E-05	.2104E-04	.4803E-05	-.4646E-04
.6630E-05	.1284E-03	.7091E-05	-.3457E-03	.1246E-04	.9640E-03	.1681E-04	-.2427E-02	.1357E-04	.6380E-02
.1370E-04	-.1202E-01	.1940E-04	.8195E-02	.1514E-04	-.3916E-02	.1442E-04	.1522E-02	.5788E-05	-.5816E-03
.2021E-05	.2804E-03	.9900E-05	-.9754E-04	.1227E-04	.4931E-04	.6506E-05	-.8695E-05		
.7181E-06	-.1784E-05	.1331E-05	-.3233E-05	.2157E-05	.2771E-05	.2922E-05	-.1168E-04	.4376E-05	.2433E-04
.6483E-05	-.6054E-04	.7310E-05	.1858E-03	.1319E-04	-.4655E-03	.1956E-04	.1325E-02	.1433E-04	-.3121E-02
.1896E-04	.8152E-02	.2162E-04	-.1608E-01	.2045E-04	.1102E-01	.1894E-04	-.3826E-02	.8051E-05	.1607E-02
.2721E-05	-.7291E-03	.1376E-04	.3347E-03	.1774E-04	-.7940E-04	.9915E-05	.3867E-04		
.8733E-07	-.2195E-05	.7034E-06	-.6003E-06	.1304E-05	-.3736E-05	.1963E-05	.3868E-05	.3127E-05	-.1282E-04
.4926E-05	.3099E-04	.5653E-05	-.8572E-04	.1064E-04	.2400E-03	.1600E-04	-.5981E-03	.1264E-04	.1583E-02
.1507E-04	-.3835E-02	.2115E-04	.1037E-01	.1673E-04	-.2289E-01	.1798E-04	.1228E-01	.7257E-05	-.4659E-02
.2664E-05	.2237E-02	.1292E-04	-.8147E-03	.1726E-04	.3609E-03	.9924E-05	-.7506E-04		
-.3769E-06	-.1470E-05	.2373E-06	-.1612E-05	.6735E-06	-.7701E-06	.1252E-05	-.3345E-05	.2219E-05	.3061E-05
.3794E-05	-.1184E-04	.4534E-05	.3333E-04	.8842E-05	-.8265E-04	.1396E-04	.2441E-03	.1119E-04	-.5550E-03
.1423E-04	.1493E-02	.1933E-04	-.3779E-02	.1747E-04	.1232E-01	.1611E-04	-.2037E-01	.7954E-05	.1098E-01
.2302E-05	-.5075E-02	.1323E-04	.2211E-02	.1769E-04	-.6703E-03	.1047E-04	.2305E-03		
-.2993E-06	-.5613E-06	-.4966E-07	-.3607E-06	.7805E-07	-.9323E-06	.2928E-06	.1476E-06	.6307E-06	-.2451E-05
.1224E-05	.4004E-05	.1531E-05	-.1333E-04	.3147E-05	.3506E-04	.5203E-05	-.8956E-04	.4377E-05	.2354E-03
.5579E-05	-.5737E-03	.8013E-05	.1596E-02	.7215E-05	-.4691E-02	.7898E-05	.1100E-01	.2584E-05	-.1727E-01
.1656E-05	.1054E-01	.5059E-05	-.3764E-02	.7504E-05	.1538E-02	.4518E-05	-.3885E-03		
-.1360E-06	-.2102E-06	-.2455E-07	-.2708E-06	.3163E-07	-.1283E-06	.1270E-06	-.6249E-06	.2772E-06	.5047E-06
.5399E-06	-.2296E-05	.6773E-06	.5834E-05	.1390E-05	-.1554E-04	.2298E-05	.4350E-04	.1905E-05	-.1027E-03
.2450E-05	.2696E-03	.3356E-05	-.7016E-03	.3020E-05	.2194E-02	.2949E-05	-.4925E-02	.1755E-05	.1025E-01
.1651E-07	-.1972E-01	.3051E-05	.1044E-01	.3505E-05	-.3693E-02	.2219E-05	.1044E-02		
-.6116E-06	-.8233E-06	-.1811E-06	-.7798E-06	.7266E-08	-.1102E-05	.3641E-06	-.9457E-06	.9120E-05	-.1572E-05
.1991E-05	-.2447E-06	.2436E-05	-.3133E-05	.5117E-05	.6629E-05	.8628E-05	-.1332E-04	.7307E-05	.4979E-04
.9425E-05	-.9547E-04	.1339E-04	.3282E-03	.1217E-04	-.8136E-03	.1256E-04	.2174E-02	.5490E-05	-.3718E-02
.2507E-05	.1065E-01	.9275E-05	-.2104E-01	.1483E-04	.1093E-01	.8697E-05	-.2915E-02		
-.1104E-05	-.7011E-06	-.5708E-06	-.8846E-06	-.4471E-06	-.1214E-05	-.4064E-07	-.1480E-05	.5386E-06	-.1698E-05
.1717E-05	-.2291E-05	.2446E-05	-.8563E-06	.5651E-05	-.3960E-05	.1032E-04	.7368E-05	.9226E-05	-.1064E-04
.1226E-04	.4846E-04	.1818E-04	-.7680E-04	.1699E-04	.3614E-03	.1783E-04	-.6628E-03	.8303E-05	.1538E-02
.2682E-05	-.3778E-02	.1520E-04	.1092E-01	.2062E-04	-.1725E-01	.1379E-04	.6656E-02		
-.7057E-06	-.1329E-06	-.4635E-06	-.3257E-06	-.4686E-06	-.5361E-06	-.2983E-06	-.6876E-06	-.7924E-07	-.1029E-05
.4649E-06	-.1192E-05	.3601E-06	-.1594E-05	.2368E-05	-.1095E-05	.4878E-05	-.2808E-05	.4694E-05	.5011E-05
.6456E-05	-.8423E-05	.1011E-04	.3806E-04	.9733E-05	-.7440E-04	.1050E-04	.2258E-03	.4961E-05	-.3813E-03
.1770E-05	.1055E-02	.8941E-05	-.2894E-02	.1374E-04	.6639E-02	.8414E-05	-.9653E-02		

NN= 1 NP= 41 NPHI= 20 D<= .3434808E+00 FREQENCY = 16.40 MHZ

PROGRAM DELIVERS THE GENERALIZED ADMITTANCE MATRICES FOR ALL MODI UP TO NN = 7 (Y2,Y3 ≠ 0)

6.2.3. PROGRAM PANB AND OUTPUT SAMPLE

```
E PROGRAM *PANB* , COMPUTATION OF THE NEAR FIELD COMPONENTS
C ******************************************************          PANB   1
E CONTROL CARDS                                                     PANB   2
PAN,3571,CM130000,CT500.                                            PANB   3
ATTACH,AMAT2,PW=3571.                                               PANB   4
CALL,S164M07,P=AMAT2,B=DISK.                                        PANB   5
FTN.                                                                PANB   6
LGO.                                                                PANB   7
PUBLIC,COLLECT.                                                     PANB   8
COLLECT,M=AMAT2.                                                    PANB   9
R HERE END OF RECORD CARD                                           PANB  10
C ****************                                                  PANB  11
      PROGRAM PANB (INPUT,OUTPUT,DISK,RESULT,TAPE1=INPUT,TAPE3=OUTPUT, PANB  12
     1TAPE6=DISK,TAPE7=RESULT)                                      PANB  13
C ****************                                                  PANB  14
C SOURCE PROGRAM IS DESCRIBED IN REPORT *THE SYRACUSE COMPUTER CODE PANB  15
C FOR RADIATION AND SCATTERING FROM BODIES OF REVOLUTION, EXTENDED FOR PANB  16
C NEAR FIELD COMPUTATIONS* BY R.M. BEVENSEE, MAY 1974,LAWRENCE      PANB  17
C LIVERMORE LABORATORY.                                             PANB  18
C MODIFICATIONS BY P.A. NEUKOMM AT BIOMECHANICS LABORATORY, SWISS FEDE- PANB  19
C RAL INSTITUTE OF TECHNOLOGY, PROVIDE THE E-FIELD VECTOR AT 9 TEST PANB  20
C POINTS NEAR THE BODY OF REVOLUTION BY SUMMING UP ALL NEEDED MODI  PANB  21
C FOR ALL AZIMUTHAL ANGLES. THE STORAGE REQUIREMENT IS LOWER THAN IN PANB  22
C THE ORIGINAL PROGRAM, THE CONTRIBUTION OF THE I-TH MODE IS PRINTED PANB  23
C IN ORDER TO OPTIMIZE THE COMPUTATION, A PROCEDURE FOR GRAPHING RE- PANB  24
C SULTS IS INCLUDED AND THE FINAL E-FIELD COMPONENTS(VERTICAL,HORIZON- PANB  25
C TAL,RADIAL) ARE STORED FOR EACH TEST POINT AND AZIMUTHAL ANGLE IN PANB  26
C THE FILE S164D9 IN THE COLLECT FILE AMAT2.                        PANB  27
C THIS PROGRAM HAS BEEN DIMENSIONED TO COMPUTE:                     PANB  28
C KK≤13,NP≤41,NPHI≤20,NT≤2,NTEST≤9,NNPHI≤37.                        PANB  29
C IN THIS PROGRAM IS NT=1, AND BY SELECTING ON THE DATA CARD *RUN=1, PANB  30
C RESP,RUN=2* THE DIRECT WAVE, RESP, THE GROUND REFLECTED WAVE IS RE- PANB  31
C GARDED FOR FIELD COMPUTATIONS.                                    PANB  32
C ATTENTION: SCALING IN THE PROGRAM: PHYSICAL DIMENSIONS 10 TIMES   PANB  33
C ACTUAL SIZE, FREQUENCY 10 TIMES LOWER THAN ACTUAL, FINAL OUTPUT:  PANB  34
C ACTUAL DATA IN ORIGINAL SCALE.                                    PANB  35
C ****************                                                  PANB  36
                                                                    PANB  37
      COMPLEX SYV(333),SYH(333),SYS(333)                            PANB  38
      DIMENSION PVTOT(09,2,37),PHTOT(09,2,37),PSTOT(09,2,37)        PANB  39
      DIMENSION GVTOT(09,2,37),GHTOT(09,2,37),GSTOT(09,2,37)        PANB  40
      COMPLEX ERTOT,ETTOT,EPTOT,EVTOT,EHTOT,ESTOT                   PANB  41
      COMPLEX COPHI(13,37),SIPHI(13,37)                             PANB  42
      COMPLEX ETR(13,9,2),ETT(13,9,2),ETP(13,9,2)                   PANB  43
      COMPLEX FTR(13,9,2),FTT(13,9,2),FTP(13,9,2)                   PANB  44
      DIMENSION PHI(37),SITN(20),COTN(20),DI(20),PHJ(37),THR(3)     PANB  45
      INTEGER D(61),E(37),TEXT(9),POL,RUN,JA,JB,JC                  PANB  46
      COMPLEX U, E3(02,041) ,E4(02,041) ,E1(02),E2(02),ESC(2,4),PP  PANB  47
      COMMON/A/BK,NN,TR(076),T(076),DR(2),DZ(2),AC(40),CA,CQ,       PANB  48
     1KG,NPHI,TP(076),U                                             PANB  49
      COMPLEX VVR(2,760),Y(1444),ZM(2,076),G(4764)                  PANB  50
      COMMON VVR,Y,ZM,G                                             PANB  51
      COMMON/B/RH(041),ZH(041),DH(041),TJ(19),R(041),ZS(041),       PANB  52
     1SV(041),CV(041),ANG(20),CSM(60)                               PANB  53
      COMMON/TEST/RT(4),ZST(4),SVT(4),CVT(4),TT(4),TRT(4)           PANB  54
      DIMENSION RTEST(20),ZTEST(20),DTEST(20),SINT(20),COST(20)     PANB  55
      U=CMPLX(0.,1.)                                                PANB  56
      ETA=376.707                                                   PANB  57
      PI=3.141593                                                   PANB  58
      PR=180./PI                                                    PANB  59
      REWIND 6                                                      PANB  60
      REWIND 7                                                      PANB  61
   50 READ(1,51)KK,NP,NPHI,NT,NTEST,NNPHI,BK,RUN                    PANB  62
   51 FORMAT(6I3,E14.7,2X,I2)                                       PANB  63
      IF(EOF (1)) 52,490                                            PANB  64
  490 CONTINUE                                                      PANB  65
      NST=NTEST*NNPHI                                               PANB  66
      READ(1,53)(RH(I),I=1,NP)                                      PANB  67
      READ(1,53)(ZH(I),I=1,NP)                                      PANB  68
   53 FORMAT(10F8.4)                                                PANB  69
      TEXT(1)=10HVERTIKAL                                           PANB  70
      TEXT(2)=10HHORIZONTAL                                         PANB  71
      TEXT(3)=10HRADIAL                                             PANB  72
      TEXT(4)=10HDIREKTE EI                                         PANB  73
      TEXT(5)=10HNSTRAHLUNG                                         PANB  74
      TEXT(6)=10H                                                   PANB  75
      TEXT(7)=10HREFLEKTIER                                         PANB  76
      TEXT(8)=10HTE EINSTRA                                         PANB  77
      TEXT(9)=10HHLUNG                                              PANB  78
      JA=RUN*3+1                                                    PANB  79
      JB=RUN*3+2                                                    PANB  80
      JC=RUN*3+3                                                    PANB  81
   76 WRITE(3,54)KK,NP,NPHI,NT,NTEST,NNPHI,BK,TEXT(JA),TEXT(JB),TEXT(JC)PANB  82
   54 FORMAT(1X//* KK=*,I3,* NP=*,I3,* NPHI=*,I3,* NT=*,I3,* NTEST=* PANB  83
     1,I3,* NNPHI=*,I3,* BK=*,E14.7,5X,R10,R10,R10)                 PANB  84
      WRITE(3,55)                                                   PANB  85
   55 FORMAT(1X/* RH*)                                              PANB  86
      WRITE(3,46)(RH(I),I=1,NP)                                     PANB  87
   46 FORMAT(1X,10F8.4)                                             PANB  88
      WRITE(3,56)                                                   PANB  89
   56 FORMAT(1X/* ZH*)                                              PANB  90
      WRITE(3,46)(ZH(I),I=1,NP)                                     PANB  91
      KL=1                                                          PANB  92
  126 IF((RH(1)-RH(NP)).NE.0..OR.(ZH(1)-ZH(NP)).NE.0.) GO TO 58     PANB  93
      KL=0                                                          PANB  94
      RH(NP+1)=RH(2)                                                PANB  95
      ZH(NP+1)=ZH(2)                                                PANB  96
      RH(NP+2)=RH(3)                                                PANB  97
      ZH(NP+2)=ZH(3)                                                PANB  98
      NP=NP+2                                                       PANB  99
   58 DO 57 I=2,NP                                                  PANB 100
      I2=I-1                                                        PANB 101
      RR1=RH(I)-RH(I2)                                              PANB 102
      RR2=ZH(I)-ZH(I2)                                              PANB 103
```

```
      DH(I2)=SQRT(RR1*RR1+RR2*RR2)
      ZS(I2)=.5*(ZH(I)+ZH(I2))
      R(I2)=.5*(RH(I)+RH(I2))
      SV(I2)=RR1/DH(I2)
      CV(I2)=RR2/DH(I2)
   57 CONTINUE
C BEREITSTELLUNG DES EINFALLS- UND REFLEKTIONSWINKELS
      DT=0.394
      DO 1 J=1,NT
      THR(J)=DT*(J-1) + 1.410
      IF(RUN.EQ.2) THR(J)=DT*J  + 1.410
    1 CONTINUE
      BK2=BK*BK
      P1=SQRT(BK2*BK2*ETA*ETA/4./PI**3)
      NM=(NP-3)/2
      NM4=NM*4
      NM2=NM*2
      NZ=NM2*NM2
      KG=NP-1
      DO 74 J=1,NM
      J2=2*(J-1)+1
      J3=J2+1
      J4=J3+1
      J5=J4+1
      J6=4*(J-1)+1
      J7=J6+1
      J8=J7+1
      J9=J8+1
      DEL1=DH(J2)+DH(J3)
      DEL2=DH(J4)+DH(J5)
      TP(J6)= DH(J2)/DEL1  $TP(J7)= DH(J3)/DEL1
      TP(J8)=-DH(J4)/DEL2  $TP(J9)=-DH(J5)/DEL2
      T(J6)=DH(J2)*DH(J2)/2./DEL1
      T(J7)=DH(J3)*(DH(J2)+DH(J3)/2.)/DEL1
      T(J8)=DH(J4)*(DH(J5)+DH(J4)/2.)/DEL2
      T(J9)=DH(J5)*DH(J5)/2./DEL2
   74 CONTINUE
      DO 75 J=1,NM4
      TR(J)=T(J)
   75 CONTINUE
  115 IF(KL.EQ.0) GO TO 78
      IF(RH(1)) 77,23,77
   77 DEL1=DH(1)+DH(2)
      TR(1)=DH(1)*(1.+(DH(2)+DH(1)/2.)/DEL1)
      TR(2)=DH(2)*(1.+DH(2)/2./DEL1)
   23 IF(RH(NP)) 79,78,79
   79 J1=(NM-1)*4+3
      J2=J1+1
      DEL2=DH(NP-2)+DH(NP-1)
      TR(J1)=DH(NP-2)*(1.+DH(NP-2)/2./DEL2)
      TR(J2)=DH(NP-1)*(1.+(DH(NP-2)+DH(NP-1)/2.)/DEL2)
   78 SS=0.
      DO 7 I=1,NM
      I1=2*(I-1)+1
      I2=I1+1
      SS=SS+DH(I1)+DH(I2)
      TJ(I)=SS
    7 CONTINUE
      DEL=TJ(NM)
      IF(KL.NE.0) DEL=DEL+DH(NP-2)+DH(NP-1)
      DEL=DEL/10.
      DO 8 J=1,NM
      TJ(J)=TJ(J)/DEL
    8 CONTINUE
      DO 42 J=1,NT
      E1(J)=0.
      E2(J)=0.
   42 CONTINUE
      IF(NTEST.EQ.0)GO TO 707
      READ(1,49)(RTEST(J),ZTEST(J),DTEST(J),J=1,NTEST)
   49 FORMAT(3F8.4)
      DO 708 J=1,NTEST
      RRT=SQRT(RTEST(J)**2+ZTEST(J)**2)
     .SINT(J)=RTEST(J)/RRT  $COST(J)=ZTEST(J)/RRT
  708 CONTINUE
  707 DP=PI/NPHI
      CA=BK*BK*ETA  $CQ=ETA
      DO 709 J=1,NPHI
      ANG(J)=(J-.5)*DP
  709 AC(J)=COS(ANG(J))
      DPI=PI/(NNPHI-1)
      DO 500 J=1,NNPHI
      PHI(J)=DPI*(J-1) $ PHJ(J)=PHI(J)*PR
      DO 501 M=1,KK
      NN=M-1
      COPHI(M,J)=   COS(NN*PHI(J))
      SIPHI(M,J)= U*SIN(NN*PHI(J))
  501 CONTINUE
  500 CONTINUE
      DO 502 I=1,NTEST
      ABSTA=SQRT(ZTEST(I)*ZTEST(I)+RTEST(I)*RTEST(I))
      SITN(I) = RTEST(I)/ABSTA      $  COTN(I) = ZTEST(I)/ABSTA
  502 CONTINUE
      DO 40 M=1,KK
      NN=M-1
      CALL PLANE(VVR,THR,NP,NT,1,R,ZS,SV,CV,T,TR)
      CALL PROGA

  127 READ(6)(Y(I),I=1,NZ)

      WRITE(3,112)NN
  112 FORMAT(*1*,*  O*,6X,*SIG OO*,6X,*MAG SOO*,6X,*SIG OO*,6X,
     1*MAG SOO*,10X,*MODE NN=*,I2)
      WRITE(3,113)
```

```
113 FORMAT(*+  -*,10X,*--*,11X,*--*,10X,*//*,11X,*//*)
    DO 41 L=1,NT
    L2=(L-1)*NM4
    DO 2 J=1,NM2
    E3(L,J)=0.
    E4(L,J)=0.
    DO 3 I=1,NM
    J1=J+(I-1)*NM2
    J2=J1+NM*NM2
    I1=I+L2
    I2=I1+NM
    I3=I1+NM2
    I4=I3+NM
    E3(L,J)=E3(L,J)+Y(J1)*VVR(1,I1)-Y(J2)*VVR(1,I2)
    E4(L,J)=E4(L,J)-Y(J1)*VVR(1,I3)+Y(J2)*VVR(1,I4)
  3 CONTINUE
  2 CONTINUE
    DO 43 J=1,NM2
    J1=J+L2
    J2=J1+NM2
    E1(L)=E1(L)+E3(L,J)*VVR(1,J1)
    E2(L)=E2(L)+E4(L,J)*VVR(1,J2)
 43 CONTINUE
    IF(NN) 44,45,44
 45 E1(L)=.5*E1(L)
    E2(L)=.5*E2(L)
 44 X1=THR(L)*PR
    X3=P1*CABS(E1(L))
    X2=X3*X3
    X5=P1*CABS(E2(L))
    X4=X5*X5
    WRITE(3,111) X1,X2,X3,X4,X5
111 FORMAT(1X,F6.2,4E12.4)
 41 CONTINUE
    IF(NTEST.EQ.0)GO TO 40
    DO 7100 ITE=1,NTEST
    WRITE(3,712)RTEST(ITE),ZTEST(ITE),DTEST(ITE)
712 FORMAT(/////4X,*RTEST=*,F8.4,4X,*ZTEST=*,F8.4,4X,*DTEST=*,F8.4,
   1   //)
    DR(1)=DTEST(ITE)*SINT(ITE)  $DZ(1)=DTEST(ITE)*COST(ITE)
    DR(2)=DZ(1)  $DZ(2)=-DR(1)
    FTEST=0.5/(PI*DTEST(ITE))
    IF(NN.EQ.0)FTEST=0.5*FTEST
    DO 706 IT=1,2
    CALL NEARZ(RTEST(ITE),ZTEST(ITE),DTEST(ITE),IT)
706 CALL PLANE(VVR,THR,5,NT,IT,RT,ZST,SVT,CVT,TT,TRT)
    DO 7101 L=1,NT
    X1=THR(L)*PR
    DO 702 IT=1,2
    ESC(IT,1)=CMPLX(0.,0.)  $ESC(IT,2)=CMPLX(0.,0.)
    ESC(IT,3)=CMPLX(0.,0.)  $ESC(IT,4)=CMPLX(0.,0.)
    DO 703 I=1,NM
    J1=I
    J2=I+NM2
    I1=I
    I2=I1+NM
    ESC(IT,1)=ESC(IT,1)-ZM(IT,J1)*E3(L,I1)-ZM(IT,J2)*E3(L,I2)
    ESC(IT,2)=ESC(IT,2)-ZM(IT,J1+NM)*E3(L,I1)-ZM(IT,J2+NM)*E3(L,I2)
    ESC(IT,3)=ESC(IT,3)-ZM(IT,J1)*E4(L,I1)-ZM(IT,J2)*E4(L,I2)
    ESC(IT,4)=ESC(IT,4)-ZM(IT,J1+NM)*E4(L,I1)-ZM(IT,J2+NM)*E4(L,I2)
703 CONTINUE
702 CONTINUE
    J1=(L-1)*4
    I1=J1+1  $I2=I1+1  $I3=I2+1  $I4=I3+1
    ERR  =FTEST*REAL(VVR(1,I1))  $ERI  =FTEST*AIMAG(VVR(1,I1))
    ETHR =FTEST*REAL(VVR(2,I1))  $ETHI =FTEST*AIMAG(VVR(2,I1))
    EPH1R=-FTEST*REAL(VVR(1,I2))  $EPH1I=-FTEST*AIMAG(VVR(1,I2))
    EPH2R=-FTEST*REAL(VVR(2,I2))  $EPH2I=-FTEST*AIMAG(VVR(2,I2))
    ETRR=ERR  $ETRI=ERI  $ETTHR=ETHR  $ETTHI=ETHI
    ETP1R=EPH1R  $ETP1I=EPH1I  $ETP2R=EPH2R  $ETP2I=EPH2I
    WRITE(3,704)X1
704 FORMAT(/10X,*EINC,*,1XF5.1,4X,*ETHETA INC*/)
    WRITE(3,705)ERR,ERI,EPH1R,EPH1I,ETHR,ETHI,EPH2R,EPH2I
705 FORMAT(1X,*ERAD=*,2E12.4,1X,*EPH=*,2E12.4,2X,*ETH=*,2E12.4,1X,
   1*EPH=*,2E12.4)
    ERR  =REAL(ESC(1,1))*FTEST  $ERI  =AIMAG(ESC(1,1))*FTEST
    ETHR =REAL(ESC(2,1))*FTEST  $ETHI =AIMAG(ESC(2,1))*FTEST
    EPH1R=REAL(ESC(1,2))*FTEST  $EPH1I=AIMAG(ESC(1,2))*FTEST
    EPH2R=REAL(ESC(2,2))*FTEST  $EPH2I=AIMAG(ESC(2,2))*FTEST
    WRITE(3,710)X1
710 FORMAT(/9X,*ESCAT,*,1XF5.1,4X,*ETHETA INC*/)
    WRITE(3,705)ERR,ERI,EPH1R,EPH1I,ETHR,ETHI,EPH2R,EPH2I
    ETRR=ETRR+ERR  $ETRI=ETRI+ERI  $ETTHR=ETTHR+ETHR
    ETTHI=ETTHI+ETHI  $ETP1R=ETP1R+EPH1R  $ETP1I=ETP1I+EPH1I
    ETP2R=ETP2R+EPH2R  $ETP2I=ETP2I+EPH2I
    ETR(M,ITE,L) = CMPLX(ETRR,ETRI)
    ETT(M,ITE,L) = CMPLX(ETTHR,ETTHI)
    EPR = (ETP1R+ETP2R)/2  $  EPI = (ETP1I+ETP2I)/2
    ETP(M,ITE,L) = CMPLX(EPR,EPI)
    WRITE(3,711)X1
711 FORMAT(/10X,*ETOT,*,1XF5.1,4X,*ETHETA INC*/)
    WRITE(3,705)ETRR,ETRI,ETP1R,ETP1I,ETTHR,ETTHI,ETP2R,ETP2I
    ERR  =-FTEST*REAL(VVR(1,I3))  $ERI  =-FTEST*AIMAG(VVR(1,I3))
    ETHR =-FTEST*REAL(VVR(2,I3))  $ETHI =-FTEST*AIMAG(VVR(2,I3))
    EPH1R=FTEST*REAL(VVR(1,I4))  $EPH1I=FTEST*AIMAG(VVR(1,I4))
    EPH2R=FTEST*REAL(VVR(2,I4))  $EPH2I=FTEST*AIMAG(VVR(2,I4))
    ETRR=ERR  $ETRI=ERI  $ETTHR=ETHR  $ETTHI=ETHI  $ETP1R=EPH1R
    ETP1I=EPH1I  $ETP2R=EPH2R  $ETP2I=EPH2I
    WRITE(3,714)X1
714 FORMAT(/10X,*EINC,*,1XF5.1,4X,*EPHI INC*/)
    WRITE(3,705)ERR,ERI,EPH1R,EPH1I,ETHR,ETHI,EPH2R,EPH2I
    ERR  =REAL(ESC(1,3))*FTEST  $ERI  =AIMAG(ESC(1,3))*FTEST
    ETHR =REAL(ESC(2,3))*FTEST  $ETHI =AIMAG(ESC(2,3))*FTEST
    EPH1R=REAL(ESC(1,4))*FTEST  $EPH1I=AIMAG(ESC(1,4))*FTEST
```

```
      EPH2R=REAL(ESC(2,4))*FTEST  $EPH2I=AIMAG(ESC(2,4))*FTEST          PANB 312
      WRITE(3,720)X1                                                    PANB 313
  720 FORMAT(/9X,*ESCAT,*,1XF5.1,4X,*EPHI INC*/)                        PANB 314
      WRITE(3,705)ERR,ERI,EPH1R,EPH1I,ETHR,ETHI,EPH2R,EPH2I             PANB 315
      ETRR=ETRR+ERR  $ETRI=ETRI+ERI  $ETTHR=ETTHR+ETHR                  PANB 316
      ETTHI=ETTHI+ETHI  $ETP1R=ETP1R+EPH1R  $ETP1I=ETP1I+EPH1I          PANB 317
      ETP2R=ETP2R+EPH2R  $ETP2I=ETP2I+EPH2I                             PANB 318
      FTR(M,ITE,L) = CMPLX(ETRR,ETRI)                                   PANB 319
      FTT(M,ITE,L) = CMPLX(ETTHR,ETTHI)                                 PANB 320
      FPR = (ETP1R+ETP2R)/2   $  FPI = (ETP1I+ETP2I)/2                  PANB 321
      FTP(M,ITE,L) = CMPLX(FPR,FPI)                                     PANB 322
      WRITE(3,721)X1                                                    PANB 323
  721 FORMAT(/10X,*ETOT,*,1XF5.1,4X,*EPHI INC*/)                        PANB 324
      WRITE(3,705)ETRR,ETRI,ETP1R,ETP1I,ETTHR,ETTHI,ETP2R,ETP2I         PANB 325
      WRITE(3,722)                                                      PANB 326
  722 FORMAT(////)                                                      PANB 327
 7101 CONTINUE                                                          PANB 328
 7100 CONTINUE                                                          PANB 329
   40 CONTINUE                                                          PANB 330
      F=3000.*BK/(2*PI)                                                 PANB 331
      DU=RH(20)/5. $ DA=ZH(41)/10. $ HO= ZTEST(1)/10.                   PANB 332
      PP = CMPLX(1.0E-32,1.0E-32)                                       PANB 333
      QQ = 1.0E-32                                                      PANB 334
      DO 508 ID=1,NTEST                                                 PANB 335
  508 DI(ID) = (RTEST(ID)-RH(22))*0.1                                   PANB 336
      DO 503 L=1,NT                                                     PANB 337
      X1=THR(L)*PR                                                      PANB 338
      DO 912 POL=1,2                                                    PANB 339
      WRITE(3,543)F,X1,TEXT(POL),HO,TEXT(JA),TEXT(JB),TEXT(JC)          PANB 340
  543 FORMAT(1H1,8X,*E I N F L U S S   D E R   A N Z A H L   B E R U E CPANB 341
     1K S I C H T I G T E N   M O D I   A U F   E T O T *,/1H0,13X,    PANB 342
     2*FREQUENZ =*,F6.1,* MHZ    EINSTRAHLUNG : WINKEL THETA = *,F5.1,  PANB 343
     3* GRAD    POLARISATION : *,R10,/1H ,13X,*ANTENNENHOEHE = *,F4.2,  PANB 344
     4* METER*,/1H0,13X,3R10,/)                                         PANB 345
  544 FORMAT(1H0,*TESTSEGMENT NR*,I3,*   ABSTAND DIST =* ,F5.2,* METER  PANB 346
     1  ROT.WINKEL PHI = *,F4.0,* GRAD*,/)                              PANB 347
  545 FORMAT(1H ,*MODE 0 BIS*,I2,* :  ERTOT =*,2E12.4,3X,*EPTOT =*,     PANB 348
     12E12.4,3X,*ETTOT =*,2E12.4)                                       PANB 349
      JDI=0                                                             PANB 350
      DO 504 ITE=1,NTEST                                                PANB 351
      WRITE(3,546)                                                      PANB 352
  546 FORMAT(/)                                                         PANB 353
      DO 505 J=1,NNPHI                                                  PANB 354
      IF(J.EQ.1.OR.J.EQ.37) WRITE(3,544) ITE,DI(ITE),PHJ(J)             PANB 355
      IF(J.EQ.19)           WRITE(3,544) ITE,DI(ITE),PHJ(J)             PANB 356
      ERTOT = CMPLX(0.,0.)                                              PANB 357
      ETTOT = CMPLX(0.,0.)                                              PANB 358
      EPTOT = CMPLX(0.,0.)                                              PANB 359
      IF(POL.EQ.1) 909,910                                              PANB 360
  909 DO 506 M=1,KK                                                     PANB 361
      NN=M-1                                                            PANB 362
      ERTOT  = ERTOT + ETR(M,ITE,L) * COPHI(M,J)                        PANB 363
      ETTOT  = ETTOT + ETT(M,ITE,L) * COPHI(M,J)                        PANB 364
      EPTOT  = EPTOT + ETP(M,ITE,L) * SIPHI(M,J)                        PANB 365
      IF(J.EQ.1.OR.J.EQ.37) WRITE(3,545) NN,ERTOT,EPTOT,ETTOT           PANB 366
      IF(J.EQ.19)           WRITE(3,545) NN,ERTOT,EPTOT,ETTOT           PANB 367
  506 CONTINUE                                                          PANB 368
      GO TO 913                                                         PANB 369
  910 DO 911 M=1,KK                                                     PANB 370
      NN=M-1                                                            PANB 371
      ERTOT  = ERTOT + FTR(M,ITE,L) * SIPHI(M,J)                        PANB 372
      ETTOT  = ETTOT + FTT(M,ITE,L) * SIPHI(M,J)                        PANB 373
      EPTOT  = EPTOT + FTP(M,ITE,L) * COPHI(M,J)                        PANB 374
      IF(J.EQ.1.OR.J.EQ.37) WRITE(3,545) NN,ERTOT,EPTOT,ETTOT           PANB 375
      IF(J.EQ.19)           WRITE(3,545) NN,ERTOT,EPTOT,ETTOT           PANB 376
  911 CONTINUE                                                          PANB 377
  913 CONTINUE                                                          PANB 378
      JDI=JDI+1                                                         PANB 379
      EVTOT = ERTOT * COTN(ITE) - ETTOT * SITN(ITE)                     PANB 380
      SYV(JDI) = EVTOT                                                  PANB 381
      EHTOT = EPTOT                                                     PANB 382
      SYH(JDI) = EHTOT                                                  PANB 383
      ESTOT = ERTOT * SITN(ITE) + ETTOT * COTN(ITE)                     PANB 384
      SYS(JDI) = ESTOT                                                  PANB 385
      IF(CABS(EVTOT).LT.QQ) EVTOT = PP                                  PANB 386
      IF(CABS(EHTOT).LT.QQ) EHTOT = PP                                  PANB 387
      IF(CABS(ESTOT).LT.QQ) ESTOT = PP                                  PANB 388
      GVTOT(ITE,L,J) = 20.*ALOG10(CABS(EVTOT))                          PANB 389
      GHTOT(ITE,L,J) = 20.*ALOG10(CABS(EHTOT))                          PANB 390
      GSTOT(ITE,L,J) = 20.*ALOG10(CABS(ESTOT))                          PANB 391
      PVTOT(ITE,L,J) = ATAN2(REAL(EVTOT),AIMAG(EVTOT))*PR               PANB 392
      PHTOT(ITE,L,J) = ATAN2(REAL(EHTOT),AIMAG(EHTOT))*PR               PANB 393
      PSTOT(ITE,L,J) = ATAN2(REAL(ESTOT),AIMAG(ESTOT))*PR               PANB 394
  505 CONTINUE                                                          PANB 395
  504 CONTINUE                                                          PANB 396
      WRITE(7)(SYV(I),I=1,NST)                                          PANB 397
      WRITE(7)(SYH(I),I=1,NST)                                          PANB 398
      WRITE(7)(SYS(I),I=1,NST)                                          PANB 399
      DO 918 I=1,3                                                      PANB 400
      J =(I*18)-17                                                      PANB 401
      WRITE(3,509) F,X1,DU,HO,TEXT(POL),DA,TEXT(1),TEXT(JA),TEXT(JB),   PANB 402
     1TEXT(JC)                                                          PANB 403
  509 FORMAT(1H1,11X,                                                   PANB 404
     1*A Z I M U T A L   S T R A H L U N G S   D I A G R A M M*,        PANB 405
     1     11X,*F R E Q U E N Z =  *,F6.1,*  M H Z*,/1H0,*KOERPER : VERTPANB 406
     2IKALER ROT.SYM. MENSCHMOD.   MESSANTENNE : PUNKTANTENNE AUF      EPANB 407
     3INSTRAHLUNG : WINKEL THETA = *,F5.1,* GRAD*,/1H ,10X,*DURCHMESSER PANB 408
     4 = *,F5.2,* METER*,21X,F4.2,* METER HOEHE *,20X,*POLARISATION = * PANB 409
     5,R10,/1H ,10X,*ACHSENLAENGE = *,F5.2,* METER*,21X,*PHI UND DIST VAPANB 410
     6R.*,    5X,*MESSANTENNE  : POLARISATION = *,R 10,/1H0,3R10,/)     PANB 411
      WRITE(3,553) PHJ(J)                                               PANB 412
  553 FORMAT(1H0,*ROTATIONSWINKEL PHI = *,F6.2,* GRAD*,/)               PANB 413
      WRITE(3,552)                                                      PANB 414
  552 FORMAT(1H ,*DIST    : ABSTAND DER MESSANTENNE VON DER KOERPEROBERFPANB 415
```

```
     1LAECHE  IN METER *,/1H , *PHI      : HORIZONTALER ROTATIONSWINKEL INPANB 416
     2 GRAD;  180 GRAD = SCHATTEN*,/1H ,*GAIN     : FELDSTAERKE BEI DER MEPANB 417
     3SSANTENNE  IN DB : 0 DB = MAX.FREESPACE*,/1H ,*PHASE   : PHASE DES PANB 418
     4MESSPUNKTES IN GRAD*,/1H0,                        22X,*AMPLITU* ,*PANB 419
     5DE DER FELDSTAERKE IM MESSPUNKT*,35X,*PHASENLAGE DER FELDSTAERKE IPANB 420
     6M MESSPUNKT*,/)                                                   PANB 421
      WRITE(3,562)                                                      PANB 422
  562 FORMAT(1H0,  *DIST    GAIN   PHASE -25 DB    -20 DB    -15 DB    -PANB 423
     110 DB      -5 DB      0 DB      +5 DB*,7X,*-180      - 90       0 PANB 424
     2  + 90      +180*,/)                                              PANB 425
  563 FORMAT(1H/,F4.0,2F8.2)                                            PANB 426
  567 FORMAT(1H+,23X,7(1H.,9X),2X,4(1H.,8X),1H.)                        PANB 427
  568 FORMAT(1H+,25X,61(R1))                                            PANB 428
  569 FORMAT(1H+,97X,37(R1))                                            PANB 429
      DO 512 ITE=1,NTEST                                                PANB 430
      WRITE(3,513) DI(ITE),GVTOT(ITE,L,J),PVTOT(ITE,L,J)                PANB 431
  513 FORMAT(1H/,F4.2,2F8.2)                                            PANB 432
      DO 514 NA = 1,61                                                  PANB 433
  514 D(NA)=1H                                                          PANB 434
      Q=GVTOT(ITE,L,J)                                                  PANB 435
      IF(Q.GT.5..OR.Q.LT.-25.) GO TO 515 $ Q = Q*2.                     PANB 436
      KV=IFIX(Q+50.5)                                                   PANB 437
      D(KV)=1RA                                                         PANB 438
  515 DO 526 NPH=1,37                                                   PANB 439
  526 E(NPH)=1H                                                         PANB 440
      B=PVTOT(ITE,L,J)/10.                                              PANB 441
      KVP=IFIX(B+19.0)                                                  PANB 442
      E(KVP)=1RP                                                        PANB 443
      WRITE(3,516)                                                      PANB 444
  516 FORMAT(1H+,24X,7(1H.,9X),2X,4(1H.,8X),1H.)                        PANB 445
      WRITE(3,517)(D(NL),NL=1,61)                                       PANB 446
  517 FORMAT(1H+,25X,61(R1))                                            PANB 447
      WRITE(3,531)(E(NPP),NPP=1,37)                                     PANB 448
  531 FORMAT(1H+,97X,37(R1))                                            PANB 449
  528 FORMAT(1H ,F4.2,20X,7(1H.,9X),2X,4(1H.,8X),1H.)                   PANB 450
      IF(ITE.EQ.3)WRITE(3,528) 0.20                                     PANB 451
      IF(ITE.EQ.4)WRITE(3,528) 0.30                                     PANB 452
      IF(ITE.EQ.5)WRITE(3,528) 0.40                                     PANB 453
      IF(ITE.EQ.5)WRITE(3,528) 0.45                                     PANB 454
      IF(ITE.EQ.6)WRITE(3,528) 0.55                                     PANB 455
      IF(ITE.EQ.6)WRITE(3,528) 0.60                                     PANB 456
      IF(ITE.EQ.7)WRITE(3,528) 0.70                                     PANB 457
      IF(ITE.EQ.7)WRITE(3,528) 0.75                                     PANB 458
      IF(ITE.EQ.8)WRITE(3,528) 0.85                                     PANB 459
      IF(ITE.EQ.8)WRITE(3,528) 0.90                                     PANB 460
      IF(ITE.EQ.8)WRITE(3,528) 0.95                                     PANB 461
  512 CONTINUE                                                          PANB 462
  918 CONTINUE                                                          PANB 463
  912 CONTINUE                                                          PANB 464
  503 CONTINUE                                                          PANB 465
   52 STOP                                                              PANB 466
      END                                                               PANB 467
```

```
                                                                        PANB 468
C ****************                                                      PANB 469
E SUBROUTINE                                                            PANB 470
      SUBROUTINE PLANE(VVR,THR,NP,NT,IT,R,ZS,SV,CV,T,TR)                PANB 471
      COMPLEX VVR(2,1),A5,A6,U                                          PANB 472
      COMMON/A/BK,NN                                                    PANB 473
      DIMENSION BJ(120),THR(1),FK(20),R(041),ZS(041),SV(041),CV(041),   PANB 474
     1T(076),TR(076)                                                    PANB 475
      U=CMPLX(0.,1.)                                                    PANB 476
      KG=NP-1                                                           PANB 477
      NM=KG/2-1                                                         PANB 478
      M2=NN+2                                                           PANB 479
      A5=2.*3.141593*U**(NN+1)                                          PANB 480
      NV=NM*4                                                           PANB 481
      FK(1)=1.                                                          PANB 482
      DO 153 J=1,M2                                                     PANB 483
      J1=J+1                                                            PANB 484
      FK(J1)=FK(J)*J                                                    PANB 485
  153 CONTINUE                                                          PANB 486
      DO 156 L=1,NT                                                     PANB 487
      L1=(L-1)*NV                                                       PANB 488
      CS=COS(THR(L))                                                    PANB 489
      SN=SIN(THR(L))                                                    PANB 490
      BCS=BK*CS                                                         PANB 491
      DO 302 J=1,KG                                                     PANB 492
      X=R(J)*BK*SN                                                      PANB 493
      J1=J                                                              PANB 494
      I1=NN                                                             PANB 495
      IF(I1) 303,304,303                                                PANB 496
  304 I1=I1+1                                                           PANB 497
      J1=J1+KG                                                          PANB 498
  303 DO 305 JJ=I1,M2                                                   PANB 499
      IF(X-1.E-5) 1,1,2                                                 PANB 500
    1 IF(JJ-1) 3,3,4                                                    PANB 501
    3 BJ(J1)=1.                                                         PANB 502
      GO TO 306                                                         PANB 503
    4 BJ(J1)=0.                                                         PANB 504
      GO TO 306                                                         PANB 505
    2 RH=X/2.                                                           PANB 506
      RH2=RH*RH                                                         PANB 507
      RH3=RH**(JJ-1)                                                    PANB 508
      BJ(J1)=RH3/FK(JJ)                                                 PANB 509
      SS=BJ(J1)                                                         PANB 510
    8 SST=SS*1.E-7                                                      PANB 511
      DO 155 K=1,20                                                     PANB 512
      SS=-SS*RH2/K/(K+JJ-1)                                             PANB 513
      BJ(J1)=BJ(J1)+SS                                                  PANB 514
      IF(ABS(SS)-SST) 306,306,155                                       PANB 515
  155 CONTINUE                                                          PANB 516
      WRITE(3,1000)                                                     PANB 517
 1000 FORMAT(11HSTOP AT 155)                                            PANB 518
      RETURN                                                            PANB 519
```

```
306 J1=J1+KG
305 CONTINUE
302 CONTINUE
    IF(NN) 307,308,307
308 DO 309 J=1,KG
    J1=J+2*KG
    BJ(J)=-BJ(J1)
309 CONTINUE
307 DO 300 J=1,NM
    J1=J+L1
    J2=J1+NM
    J3=J2+NM
    J4=J3+NM
    VVR(IT,J1)=0.
    VVR(IT,J2)=0.
    VVR(IT,J3)=0.
    VVR(IT,J4)=0.
    DO 301 I=1,4
    I1=2*(J-1)+I
    I4=4*(J-1)+I
    I2=I1+KG
    I3=I2+KG
    A6=(COS(ZS(I1)*DCS)+U*SIN(ZS(I1)*BCS))*A5
    BJ1=(BJ(I3)+BJ(I1))*.5
    BJ2=(BJ(I3)-BJ(I1))*.5
    VVR(IT,J1)=VVR(IT,J1)+A6*(CS*SV(I1)*BJ2+SN*CV(I1)*BJ(I2)*U)*T(I4)
    VVR(IT,J2)=VVR(IT,J2)+A6*CS*BJ1*U*TR(I4)
    VVR(IT,J3)=VVR(IT,J3)-A6*SV(I1)*BJ1*U*T(I4)
    VVR(IT,J4)=VVR(IT,J4)+A6*BJ2*TR(I4)


301 CONTINUE
300 CONTINUE
156 CONTINUE
    RETURN
    END

C ****************
E SUBROUTINE
    SUBROUTINE PROGA
    COMPLEX U
    COMMON/A/BK,NN,TR(076),T(076),DR(2),DZ(2),AC(40),CA,CQ,KG,
   1NPHI,TP(076),U
    COMMON/B/RH(041),ZH(041),DH(041),TJ(19),R(041),ZS(041),
   1SV(041),CV(041),ANG(20),CSM(60)
    COMPLEX VVR(2,760),Y(1444),ZM(2,076),G(4764)
    COMMON        VVR,Y,ZM,G
    N=KG/2
    NM=N-1
    NM2=NM*2
    NM4=NM*4
    NG=KG*KG
    M5=NN+2
    M6=NN+4
    FM=NN
    FM2=NN*NN
    PI=3.141593
    ETA=376.707
    DP=PI/NPHI
    M3=0
    DO 10 MM=M5,M6
    M1=MM-3
    M2=M3*NPHI
    DO 11 K=1,NPHI
    K1=M2+K
    CSM(K1)=DP*COS(M1*ANG(K))
 11 CONTINUE
    M3=M3+1
 10 CONTINUE
    RETURN
    END


C ****************
E SUBROUTINE
    SUBROUTINE REORD(K1,K3,L)
    DIMENSION K1(1),K3(1)
    DO 81 J=1,L
    K8=K3(J)
    K6=J
    DO 82 I=J,L
    IF(K3(I)-K8) 82,82,84
 84 K8=K3(I)
    K6=I
 82 CONTINUE
    K3(K6)=K3(J)
    K3(J)=K8
    K8=K1(K6)
    K1(K6)=K1(J)
    K1(J)=K8
 81 CONTINUE
    K3(L+1)=-1
    RETURN
    END

C ****************
E SUBROUTINE
    SUBROUTINE NEARZ(RTEST,ZTEST,DTEST,IT)
    COMPLEX GST(40),A3,A4,U
    DIMENSION RHT(5),ZHT(5),DHT(4),TPT(4)
    COMMON/TEST/RT(4),ZST(4),SVT(4),CVT(4),TT(4),TRT(4)
    COMMON/A/BK,NN,TR(076),T(076),DR(2),DZ(2),AC(40),CA,CQ,KG,
   1NPHI,TP(076),U
    COMMON/B/RH(041),ZH(041),DH(041),TJ(19),R(041),ZS(041),
```

```
     1SV(041),CV(041),ANG(20),CSM(60)
      COMPLEX VVR(2,760),Y(1444),ZM(2,076),GT(4764)
      COMMON        VVR,Y,ZM,GT
      DP=3.141593/NPHI
      NM=KG/2-1   $NM2=NM*2
      DO 2 I=1,5
      X1=I-3
      RHT(I)=X1*DR(IT) +RTEST
    2 ZHT(I)=X1*DZ(IT) +ZTEST
      DO 57 I=2,5
      I2=I-1
      RR1=RHT(I)-RHT(I2) $RR2=ZHT(I)-ZHT(I2)
      DHT(I2)=SQRT(RR1*RR1+RR2*RR2)
      ZST(I2)=.5*(ZHT(I)+ZHT(I2))  $RT(I2)=.5*(RHT(I)+RHT(I2))
      SVT(I2)=RR1/DHT(I2)
   57 CVT(I2)=RR2/DHT(I2)
      FM=NN  $FM2=NN*NN
      DO 16 J=1,KG
      DEL=.5*DH(J)  $DEL1=DH(J)*BK
      AA=DP*R(J)*DEL*BK
      DO 17 I=1,4
      Z3=ZS(J)-ZST(I)
      RR1= SV(J)*R(J)+CV(J)*Z3
      RR2=-SV(J)*RT(I)
      RR3=R(J)*R(J)+RT(I)**2+Z3*Z3
      RR4=-2.*R(J)*RT(I)
      X1=(R(J)-RT(I))**2+Z3**2
      YA=(RT(I)-R(J))*SV(J)+(ZST(I)-ZS(J))*CV(J)
      DELA2=X1-YA*YA
      IF(DELA2.NE.0.)GO TO 707
      DELA=0.  $GO TO 708
  707 DELA=SQRT(DELA2)
  708 DO 5 K=1,NPHI
      IF(K.NE.1.OR.DELA.GE.DTEST.OR.ABS(YA).GT.DEL)GO TO 7
      X=R(J)*DP
      YAA=DEL+YA  $YBB=DEL-YA
      YAA2=YAA*YAA  $YBB2=YBB*YBB
      XXA=SQRT(X*X+YAA2+DELA2)
      XXB=SQRT(X*X+YBB2+DELA2)
      XX1=SQRT(YAA2+DELA2)
      XX2=SQRT(YBB2+DELA2)
      W1=X*ALOG((YBB+XXB)/(-YAA+XXA))
      IF(XX2.EQ.0.)GO TO 801
      W1=W1+YBB*ALOG((X+XXB)/XX2)
  801 IF(XX1.EQ.0.)GO TO 802
      W1=W1+YAA*ALOG((X+XXA)/XX1)
  802 IF(DELA.EQ.0.)GO TO 803
      X1=X/DELA
      ATN=ATAN2((YBB*X1),XXB) + ATAN2((YAA*X1),XXA)
      W1=W1-DELA*ATN
  803 W1=0.5*W1/AA
      W2=-1.
      GST(1)=W1+U*W2
      GO TO 5
    7 YO=ABS(RR1+AC(K)*RR2)
      RD=RR3+RR4*AC(K)
      RK=BK*SQRT(RD)
      D2=RD-YO*YO
      Y1=YO-DEL   $Y2=YO+DEL
      R1=SQRT(Y1*Y1+D2)  $R2=SQRT(Y2*Y2+D2)
      IF(Y1)72,73,73
   72 TIN=ALOG((-Y1+R1)*(Y2+R2)/D2)
      GO TO 25
   73 TIN=ALOG((Y2+R2)/(Y1+R1))
   25 SN=SIN(RK)   $CS=COS(RK)
      GST(K)=(CS-U*SN)*(TIN-U*(BK*DH(J)-RK*TIN))/DEL1
    5 CONTINUE
      M3=(J-1)*KG+I
      DO 68 MM=1,3
      M1=MM-1  $M4=M1*NPHI   $M2=M1*KG*KG+M3
      GT(M2)=CMPLX(0.,0.)
      DO 13 K=1,NPHI
      K2=K+M4
   13 GT(M2)=GT(M2)+GST(K)*CSM(K2)
   68 CONTINUE
   17 CONTINUE
   16 CONTINUE
      DEL1=DHT(1)+DHT(2)
      DEL2=DHT(3)+DHT(4)
      TPT(1)=DHT(1)/DEL1  $TPT(2)=DHT(2)/DEL1
      TPT(3)=-DHT(3)/DEL2  $TPT(4)=-DHT(4)/DEL2
      TT(1)=DHT(1)*DHT(1)/2./DEL1
      TT(2)=DHT(2)*(DHT(1)+DHT(2)/2.)/DEL1
      TT(3)=DHT(3)*(DHT(4)+DHT(3)/2.)/DEL2
   74 TT(4)=DHT(4)*DHT(4)/2./DEL2
      TRT(1)=TT(1)  $TRT(2)=TT(2)  $TRT(3)=TT(3)  $TRT(4)=TT(4)
   78 DO 30 J=1,NM
      JL=(J-1)*NM2
      J3=(J-1)*4
      J1=2*(J-1)
      L1=J      $L2=L1+NM  $L3=J+NM2      $L4=L3+NM
      ZM(IT,L1)=CMPLX(0.,0.)  $ZM(IT,L2)=CMPLX(0.,0.)
      ZM(IT,L3)=CMPLX(0.,0.)  $ZM(IT,L4)=CMPLX(0.,0.)
      DO 70 JJ=1,4
      J2=J1+JJ  $J7=J3+JJ
      DO 71 II=1,4
      I2=II  $I7=II
      J4=(J2-1)*KG+I2
      NG=KG*KG
      J5=J4+NG $J6=J5+NG
      SS=SVT(I2)*SV(J2)  $CC=CVT(I2)*CV(J2)
      A3=.5*(GT(J6)+GT(J4))  $A4=.5*(GT(J6)-GT(J4))
      ZM(IT,L1)=ZM(IT,L1)+(CA*TT(I7)*T(J7)*(SS*A3+CC*GT(J5))-CQ*TPT(I7)
     1*TP(J7)*GT(J5))*U
```

```
      IF(NN.EQ.0)GO TO 706                                              PANB 728
  704 ZM(IT,L2)=ZM(IT,L2)+CA*SV(J2)*TT(I7)*T(J7)*A4 -FM*CQ*GT(J5)*TT(I7)PANB 729
     1*TP(J7)/RT(I2)                                                    PANB 730
  705 ZM(IT,L3)=ZM(IT,L3)-CA*SVT(I2)*TT(I7)*TR(J7)*A4                   PANB 731
      ZM(IT,L3)=ZM(IT,L3)+FM*CQ*GT(J5)*TPT(I7)*TR(J7)/R(J2)             PANB 732
  706 ZM(IT,L4)=ZM(IT,L4)+(CA*A3-FM2*CQ/RT(I2)/R(J2)*GT(J5))*TT(I7)*    PANB 733
     1TR(J7)*U                                                          PANB 734
   71 CONTINUE                                                          PANB 735
   70 CONTINUE                                                          PANB 736
   30 CONTINUE                                                          PANB 737
      RETURN                                                            PANB 738
      END                                                               PANB 739
                                                                        PANB 740
C ****************                                                      PANB 741
R HERE END OF RECORD CARD                                               PANB 742
E DATA CARDS                                                            PANB 743
E PARAMETER DESCRIPTION                                                 PANB 744
00804102000100903 7 0.3434808E+00  01     16.4 MHZ
E BODY DESCRIPTION                                                      PANB 746
  0.000   0.500   0.515   0.515   0.500   0.500   0.515   0.515   0.525   0.525
  0.575   0.600   0.625   0.660   0.710   0.780   0.925   1.050   1.050   1.000
  0.980   0.980   1.020   1.085   1.100   1.070   1.040   1.000   0.930   0.850
  0.630   0.480   0.490   0.620   0.760   0.850   0.870   0.820   0.700   0.500
  0.000
  0.000   0.000   0.350   0.760   1.270   1.740   2.180   2.580   3.120   3.680
  4.260   4.840   5.500   5.960   6.510   7.060   7.630   8.240   8.700   9.200
  9.740  10.270  10.770  11.340  11.820  12.270  12.550  12.820  13.190  13.510
 13.920  14.310  14.550  14.700  15.000  15.400  15.700  16.050  16.420  16.680
 16.800
E TEST POINT DESCRIPTION                                                PANB 757
  1.75   10.0   0.2
  2.25   10.0   0.2
  2.75   10.0   0.2
  3.75   10.0   0.2
  4.75   10.0   0.2
  6.25   10.0   0.2
  7.75   10.0   0.2
  9.25   10.0   0.2
 11.25   10.0   0.2
R HERE END OF RECORD CARD                                               PANB 767
ADD,S164D9,RESULT,RO.                                                   PANB 768
LIST                                                                    PANB 769
END                                                                     PANB 770
R HERE END OF INFORMATION CARD                                          PANB 771
```

RESULTS FROM PROGRAM * P A N B * (ONLY MODE NN = 1 SHOWN HERE)

```
KK=  8 NP= 41 NPHI= 20 NT=  1 NTEST=  9 NNPHI= 37 BK=  .3434808E+00   DIREKTE EINSTRAHLUNG

RH
  0.0000   .5000   .5150   .5150   .5000   .5000   .5150   .5150   .5250   .5250
   .5750   .6000   .6250   .6500   .7100   .7800   .9250  1.0500  1.0500  1.0000
   .9900   .9800  1.0200  1.0850  1.1000  1.0700  1.0400  1.0000   .9300   .8500
   .6300   .4800   .4900   .6200   .7600   .8500   .8700   .8200   .7000   .5000
  0.0000

ZH
  0.0000  0.0000   .3500   .7600  1.2700  1.7400  2.1800  2.5800  3.1200  3.6800
  4.2600  4.8400  5.5000  5.9600  6.5100  7.0600  7.6300  8.2400  8.7000  9.2000
  9.7400 10.2700 10.7700 11.3400 11.8200 12.2700 12.5500 12.8200 13.1900 13.5100
 13.9200 14.3100 14.5500 14.7000 15.0000 15.4000 15.7000 16.0500 16.4200 16.6800
 16.8000

   θ       SIG θθ      MAG Sθθ      SIG ØØ      MAG SØØ          MODE NN= 1
 80.79   .2021E+00   .4495E+00   .2399E-01   .1703E+00


 RTEST=  1.7500     ZTEST= 10.0000     DTEST=   .2000


        EINC,  80.8    ETHETA INC
ERAD=   .3090E+00  -.4579E+00 EPH=  -.8004E-01   .1306E+00  ETH=   .6659E-01   .1540E+00 EPH=  -.8002E-01   .1305E+00
        ESCAT,  80.8    ETHETA INC
ERAD=  -.8361E-01   .2103E+00 EPH=   .9599E-02  -.4437E-01  ETH=   .6585E-01   .5339E-01 EPH=   .7253E-02  -.4374E-01
        ETOT,  80.8    ETHETA INC
ERAD=   .2254E+00  -.2476E+00 EPH=  -.7044E-01   .8621E-01  ETH=   .1324E+00   .2074E+00 EPH=  -.7276E-01   .8679E-01
        EINC,  80.8    EPHI INC
ERAD=   .8618E-01  -.1406E+00 EPH=   .7427E+00   .4532E+00  ETH=   .4923E+00  -.8031E+00 EPH=   .7418E+00   .4548E+00
        ESCAT,  80.8    EPHI INC
ERAD=   .1430E-01  -.5590E-01 EPH=  -.2277E+00  -.2110E+00  ETH=   .1088E+00  -.4296E+00 EPH=  -.2358E+00  -.2149E+00
        ETOT,  80.8    EPHI INC
ERAD=   .1005E+00  -.1965E+00 EPH=   .5150E+00   .2442E+00  ETH=   .6011E+00  -.1233E+01 EPH=   .5060E+00   .2398E+00
```

```
RTEST=  2.2500     ZTEST= 10.0000     DTEST=    .2000
         EINC,  80.8     ETHETA INC
ERAD=   .3804E+00  -.5672E+00 EPH=  -.7773E-01   .1268E+00  ETH=   .2499E-01   .1952E+00 EPH=  -.7771E-01   .1268E+00
         ESCAT,  80.8     ETHETA INC
ERAD=  -.6107E-01   .1547E+00 EPH=   .1077E-01  -.3246E-01  ETH=   .4359E-01   .8401E-02 EPH=   .1021E-01  -.3246E-01
         ETOT,  80.8     ETHETA INC
ERAD=   .3193E+00  -.4126E+00 EPH=  -.6696E-01   .9434E-01  ETH=   .6858E-01   .2036E+00 EPH=  -.6750E-01   .9429E-01
         EINC,  80.8     EPHI INC
ERAD=   .1066E+00  -.1739E+00 EPH=   .6739E+00   .4130E+00  ETH=   .4735E+00  -.7724E+00 EPH=   .6731E+00   .4127E+00
         ESCAT,  80.8     EPHI INC
ERAD=   .7722E-02  -.5367E-01 EPH=  -.1253E+00  -.1573E+00  ETH=   .4680E-01  -.3026E+00 EPH=  -.1282E+00  -.1588E+00
         ETOT,  80.8     EPHI INC
ERAD=   .1143E+00  -.2275E+00 EPH=   .5486E+00   .2557E+00  ETH=   .5203E+00  -.1075E+01 EPH=   .5449E+00   .2539E+00

RTEST=  2.7500     ZTEST= 10.0000     DTEST=    .2000
         EINC,  80.8     ETHETA INC
ERAD=   .4403E+00  -.6618E+00 EPH=  -.7490E-01   .1222E+00  ETH=  -.2290E-01   .2419E+00 EPH=  -.7488E-01   .1221E+00
         ESCAT,  80.8     ETHETA INC
ERAD=  -.3916E-01   .1310E+00 EPH=   .1054E-01  -.2561E-01  ETH=   .2847E-01  -.1487E-01 EPH=   .1039E-01  -.2565E-01
         ETOT,  80.8     ETHETA INC
ERAD=   .4011E+00  -.5308E+00 EPH=  -.6436E-01   .9657E-01  ETH=   .5570E-02   .2271E+00 EPH=  -.6450E-01   .9649E-01
         EINC,  80.8     EPHI INC
ERAD=   .1240E+00  -.2024E+00 EPH=   .5910E+00   .3622E+00  ETH=   .4510E+00  -.7356E+00 EPH=   .5903E+00   .3619E+00
         ESCAT,  80.8     EPHI INC
ERAD=   .2830E-02  -.5085E-01 EPH=  -.8025E-01  -.1295E+00  ETH=   .1183E-01  -.2254E+00 EPH=  -.8149E-01  -.1301E+00
         ETOT,  80.8     EPHI INC
ERAD=   .1269E+00  -.2532E+00 EPH=   .5107E+00   .2327E+00  ETH=   .4628E+00  -.9610E+00 EPH=   .5088E+00   .2318E+00
```

```
RTEST=  3.7500     ZTEST= 10.0000     DTEST=    .2000
        EINC,  80.8     ETHETA INC
ERAD=   .5201E+00  -.7989E+00 EPH=  -.6786E-01   .1107E+00  ETH=  -.1280E+00   .3403E+00 EPH=  -.6785E-01   .1107E+00
        ESCAT,  80.8    ETHETA INC
ERAD=  -.7614E-02   .1009E+00 EPH=   .8189E-02  -.1848E-01  ETH=   .1096E-01  -.3195E-01 EPH=   .8230E-02  -.1849E-01
        ETOT,  80.8     ETHETA INC
ERAD=   .5125E+00  -.6980E+00 EPH=  -.5967E-01   .9223E-01  ETH=  -.1171E+00   .3084E+00 EPH=  -.5962E-01   .9219E-01
        EINC,  80.8     EPHI INC
ERAD=   .1488E+00  -.2428E+00 EPH=   .3911E+00   .2396E+00  ETH=   .3968E+00  -.6473E+00 EPH=   .3906E+00   .2396E+00
        ESCAT,  80.8    EPHI INC
ERAD=  -.6382E-02  -.4476E-01 EPH=  -.5228E-01  -.9951E-01  ETH=  -.2376E-01  -.1340E+00 EPH=  -.5255E-01  -.9966E-01
        ETOT,  80.8     EPHI INC
ERAD=   .1424E+00  -.2876E+00 EPH=   .3388E+00   .1401E+00  ETH=   .3731E+00  -.7813E+00 EPH=   .3381E+00   .1400E+00

RTEST=  4.7500     ZTEST= 10.0000     DTEST=    .2000
        EINC,  80.8     ETHETA INC
ERAD=   .5431E+00  -.8600E+00 EPH=  -.5931E-01   .9677E-01  ETH=  -.2291E+00   .4262E+00 EPH=  -.5932E-01   .9675E-01
        ESCAT,  80.8    ETHETA INC
ERAD=   .1356E-01   .7836E-01 EPH=   .5486E-02  -.1519E-01  ETH=  -.1875E-02  -.3572E-01 EPH=   .5552E-02  -.1520E-01
        ETOT,  80.8     ETHETA INC
ERAD=   .5566E+00  -.7826E+00 EPH=  -.5382E-01   .8158E-01  ETH=  -.2310E+00   .3905E+00 EPH=  -.5377E-01   .8155E-01
        EINC,  80.8     EPHI INC
ERAD=   .1589E+00  -.2593E+00 EPH=   .1619E+00   .9305E-01  ETH=   .3347E+00  -.5458E+00 EPH=   .1617E+00   .9931E-01
        ESCAT,  80.8    EPHI INC
ERAD=  -.1447E-01  -.3737E-01 EPH=  -.5175E-01  -.7912E-01  ETH=  -.3768E-01  -.8122E-01 EPH=  -.5179E-01  -.7916E-01
        ETOT,  80.8     EPHI INC
ERAD=   .1445E+00  -.2967E+00 EPH=   .1102E+00   .1393E-01  ETH=   .2970E+00  -.6271E+00 EPH=   .1099E+00   .2015E-01
```

```
RTEST=  6.2500     ZTEST= 10.0000     DTEST=    .2000
        EINC,  80.8     ETHETA INC
ERAD=   .4791E+00  -.8178E+00 EPH=  -.4470E-01   .7295E-01  ETH=  -.3352E+00   .4889E+00 EPH=  -.4473E-01   .7294E-01
        ESCAT,  80.8     ETHETA INC
ERAD=   .3226E-01   .4930E-01 EPH=   .1649E-02  -.1268E-01  ETH=  -.1819E-01  -.3144E-01 EPH=   .1709E-02  -.1269E-01
        ETOT,  80.8     ETHETA INC
ERAD=   .5114E+00  -.7685E+00 EPH=  -.4305E-01   .6027E-01  ETH=  -.3534E+00   .4575E+00 EPH=  -.4302E-01   .6025E-01
        EINC,  80.8     EPHI INC
ERAD=   .1480E+00  -.2415E+00 EPH=  -.1898E+00  -.1166E+00  ETH=   .2369E+00  -.3863E+00 EPH=  -.1898E+00  -.1161E+00
        ESCAT,  80.8     EPHI INC
ERAD=  -.2269E-01  -.2444E-01 EPH=  -.6023E-01  -.5011E-01  ETH=  -.4030E-01  -.3419E-01 EPH=  -.6020E-01  -.5012E-01
        ETOT,  80.8     EPHI INC
ERAD=   .1253E+00  -.2659E+00 EPH=  -.2500E+00  -.1667E+00  ETH=   .1966E+00  -.4205E+00 EPH=  -.2500E+00  -.1663E+00

RTEST=  7.7500     ZTEST= 10.0000     DTEST=    .2000
        EINC,  80.8     ETHETA INC
ERAD=   .3296E+00  -.6451E+00 EPH=  -.2948E-01   .4812E-01  ETH=  -.3542E+00   .4393E+00 EPH=  -.2951E-01   .4810E-01
        ESCAT,  80.8     ETHETA INC
ERAD=   .3873E-01   .2400E-01 EPH=  -.1855E-02  -.1362E-01  ETH=  -.2957E-01  -.1973E-01 EPH=  -.1809E-02  -.1064E-01
        ETOT,  80.8     ETHETA INC
ERAD=   .3683E+00  -.6211E+00 EPH=  -.3133E-01   .3749E-01  ETH=  -.3837E+00   .4195E+00 EPH=  -.3132E-01   .3746E-01
        EINC,  80.8     EPHI INC
ERAD=   .1128E+00  -.1841E+00 EPH=  -.4872E+00  -.2988E+00  ETH=   .1457E+00  -.2375E+00 EPH=  -.4871E+00  -.2984E+00
        ESCAT,  80.8     EPHI INC
ERAD=  -.2541E-01  -.1122E-01 EPH=  -.6401E-01  -.2055E-01  ETH=  -.3289E-01  -.7642E-02 EPH=  -.6398E-01  -.2056E-01
        ETOT,  80.8     EPHI INC
ERAD=   .8738E-01  -.1953E+00 EPH=  -.5512E+00  -.3194E+00  ETH=   .1128E+00  -.2451E+00 EPH=  -.5511E+00  -.3190E+00
```

```
RTEST=  9.2500    ZTEST= 10.0000    DTEST=   .2000
        EINC,  80.8    ETHETA INC
ERAD=   .1440E+00  -.3990E+00 EPH=  -.1530E-01   .2498E-01  ETH=  -.2799E+00   .2791E+00 EPH=  -.1532E-01   .2497E-01
        ESCAT,  80.8    ETHETA INC
ERAD=   .3604E-01   .3607E-02 EPH=  -.4735E-02  -.8093E-02  ETH=  -.3385E-01  -.4286E-02 EPH=  -.4706E-02  -.8120E-02
        ETOT,  80.8    ETHETA INC
ERAD=   .1800E+00  -.3954E+00 EPH=  -.2003E-01   .1689E-01  ETH=  -.3137E+00   .2748E+00 EPH=  -.2003E-01   .1685E-01
        EINC,  80.8    EPHI INC
ERAD=   .6487E-01  -.1059E+00 EPH=  -.6715E+00  -.4117E+00  ETH=   .7025E-01  -.1145E+00 EPH=  -.6715E+00  -.4116E+00
        ESCAT,  80.8    EPHI INC
ERAD=  -.2319E-01   .2557E-03 EPH=  -.5847E-01   .6708E-02  ETH=  -.2193E-01   .6349E-02 EPH=  -.5845E-01   .6702E-02
        ETOT,  80.8    EPHI INC
ERAD=   .4168E-01  -.1057E+00 EPH=  -.7300E+00  -.4050E+00  ETH=   .4832E-01  -.1081E+00 EPH=  -.7300E+00  -.4049E+00
RTEST= 11.2500    ZTEST= 10.0000    DTEST=   .2000
        EINC,  80.8    ETHETA INC
ERAD=  -.7773E-01  -.5859E-01 EPH=  -.3132E-03   .5290E-03  ETH=  -.7894E-01  -.3611E-01 EPH=  -.3266E-03   .5146E-03
        ESCAT,  80.8    ETHETA INC
ERAD=   .2379E-01  -.1381E-01 EPH=  -.6370E-02  -.3909E-02  ETH=  -.2787E-01   .1530E-01 EPH=  -.6963E-02  -.3937E-02
        ETOT,  80.8    ETHETA INC
ERAD=  -.5394E-01  -.7240E-01 EPH=  -.7283E-02  -.3380E-02  ETH=  -.1068E+00  -.2081E-01 EPH=  -.7289E-02  -.3422E-02
        EINC,  80.8    EPHI INC
ERAD=   .1462E-02  -.2470E-02 EPH=  -.6893E+00  -.4225E+00  ETH=   .1355E-02  -.2135E-02 EPH=  -.6893E+00  -.4226E+00
        ESCAT,  80.8    EPHI INC
ERAD=  -.1515E-01   .1044E-01 EPH=  -.3801E-01   .3307E-01  ETH=  -.7785E-02   .1231E-01 EPH=  -.3800E-01   .3308E-01
        ETOT,  80.8    EPHI INC
ERAD=  -.1368E-01   .7972E-02 EPH=  -.7273E+00  -.3394E+00  ETH=  -.6430E-02   .1018E-01 EPH=  -.7273E+00  -.3895E+00
```

E I N F L U S S   D E R   A N Z A H L   B E R U E C K S I C H T I G T E N   M O D I   A U F   E T O T

FREQUENZ = 164.0 MHZ   EINSTRAHLUNG : WINKEL THETA = 80.8 GRAD   POLARISATION : VERTIKAL
ANTENNENHOEHE = 1.00 METER

DIREKTE EINSTRAHLUNG

TESTSEGMENT NR 1   ABSTAND DIST = .08 METER   ROT.WINKEL PHI = 0. GRAD

MODE 0 BIS 0 :	ERTOT =	.1792E+00	-.1610E+00	EPTOT =	0.	0.	ETTOT =	.1321E+01	.4990E+00
MODE 0 BIS 1 :	ERTOT =	.4045E+00	-.4085E+00	EPTOT =	0.	0.	ETTOT =	.1454E+01	.7064E+00
MODE 0 BIS 2 :	ERTOT =	.4643E+00	-.3605E+00	EPTOT =	0.	0.	ETTOT =	.1418E+01	.7434E+00
MODE 0 BIS 3 :	ERTOT =	.4591E+00	-.3543E+00	EPTOT =	0.	0.	ETTOT =	.1412E+01	.7385E+00
MODE 0 BIS 4 :	ERTOT =	.4587E+00	-.3548E+00	EPTOT =	0.	0.	ETTOT =	.1413E+01	.7380E+00
MODE 0 BIS 5 :	ERTOT =	.4587E+00	-.3548E+00	EPTOT =	0.	0.	ETTOT =	.1413E+01	.7380E+00
MODE 0 BIS 6 :	ERTOT =	.4587E+00	-.3548E+00	EPTOT =	0.	0.	ETTOT =	.1413E+01	.7380E+00
MODE 0 BIS 7 :	ERTOT =	.4587E+00	-.3548E+00	EPTOT =	0.	0.	ETTOT =	.1413E+01	.7380E+00

TESTSEGMENT NR 1   ABSTAND DIST = .08 METER   ROT.WINKEL PHI = 90. GRAD

MODE 0 BIS 0 :	ERTOT =	.1792E+00	-.1610E+00	EPTOT =	0.	0.	ETTOT =	.1321E+01	.4990E+00
MODE 0 BIS 1 :	ERTOT =	.1792E+00	-.1610E+00	EPTOT =	-.8650E-01	-.7160E-01	ETTOT =	.1321E+01	.4990E+00
MODE 0 BIS 2 :	ERTOT =	.1194E+00	-.2090E+00	EPTOT =	-.8650E-01	-.7160E-01	ETTOT =	.1357E+01	.4620E+00
MODE 0 BIS 3 :	ERTOT =	.1194E+00	-.2090E+00	EPTOT =	-.9212E-01	-.7513E-01	ETTOT =	.1357E+01	.4620E+00
MODE 0 BIS 4 :	ERTOT =	.1189E+00	-.2094E+00	EPTOT =	-.9212E-01	-.7513E-01	ETTOT =	.1357E+01	.4615E+00
MODE 0 BIS 5 :	ERTOT =	.1189E+00	-.2094E+00	EPTOT =	-.9216E-01	-.7516E-01	ETTOT =	.1357E+01	.4615E+00
MODE 0 BIS 6 :	ERTOT =	.1189E+00	-.2094E+00	EPTOT =	-.9216E-01	-.7516E-01	ETTOT =	.1357E+01	.4615E+00
MODE 0 BIS 7 :	ERTOT =	.1189E+00	-.2094E+00	EPTOT =	-.9216E-01	-.7516E-01	ETTOT =	.1357E+01	.4615E+00

TESTSEGMENT NR 1   ABSTAND DIST = .08 METER   ROT.WINKEL PHI = 180. GRAD

MODE 0 BIS 0 :	ERTOT =	.1792E+00	-.1610E+00	EPTOT =	0.	0.	ETTOT =	.1321E+01	.4990E+00
MODE 0 BIS 1 :	ERTOT =	-.4620E-01	.8662E-01	EPTOT =	.2996E-07	.2480E-07	ETTOT =	.1189E+01	.2917E+00
MODE 0 BIS 2 :	ERTOT =	.1358E-01	.1346E+00	EPTOT =	.4450E-07	.1170E-09	ETTOT =	.1153E+01	.3287E+00
MODE 0 BIS 3 :	ERTOT =	.1876E-01	.1285E+00	EPTOT =	.3866E-07	-.3554E-08	ETTOT =	.1158E+01	.3336E+00
MODE 0 BIS 4 :	ERTOT =	.1830E-01	.1281E+00	EPTOT =	.3816E-07	-.2753E-08	ETTOT =	.1158E+01	.3330E+00
MODE 0 BIS 5 :	ERTOT =	.1827E-01	.1281E+00	EPTOT =	.3823E-07	-.2706E-08	ETTOT =	.1158E+01	.3330E+00
MODE 0 BIS 6 :	ERTOT =	.1827E-01	.1281E+00	EPTOT =	.3824E-07	-.2712E-08	ETTOT =	.1158E+01	.3330E+00
MODE 0 BIS 7 :	ERTOT =	.1827E-01	.1281E+00	EPTOT =	.3824E-07	-.2712E-08	ETTOT =	.1158E+01	.3330E+00

FOR THE TESTSEGMENTS NR. 2 TO 9 ONLY THE VALUES FOR PHI = 180° ARE SHOWN HERE

TESTSEGMENT NR 2 ABSTAND DIST = .13 METER ROT.WINKEL PHI = 180. GRAD

MODE 0 BIS 0 :	ERTOT =	.1708E+00	-.2555E+00	EPTOT =	0.	0.	ETTOT =	.1027E+01	.4182E+00
MODE 0 BIS 1 :	ERTOT =	-.1485E+00	.1570E+00	EPTOT =	.3267E-07	.2329E-07	ETTOT =	.9584E+00	.2145E+00
MODE 0 BIS 2 :	ERTOT =	-.4618E-01	.2349E+00	EPTOT =	.5274E-07	-.9806E-08	ETTOT =	.9044E+00	.2482E+00
MODE 0 BIS 3 :	ERTOT =	-.3520E-01	.2217E+00	EPTOT =	.4288E-07	-.1589E-07	ETTOT =	.9116E+00	.2572E+00
MODE 0 BIS 4 :	ERTOT =	-.3645E-01	.2206E+00	EPTOT =	.4183E-07	-.1418E-07	ETTOT =	.9127E+00	.2562E+00
MODE 0 BIS 5 :	ERTOT =	-.3654E-01	.2207E+00	EPTOT =	.4204E-07	-.1405E-07	ETTOT =	.9126E+00	.2561E+00
MODE 0 BIS 6 :	ERTOT =	-.3653E-01	.2207E+00	EPTOT =	.4205E-07	-.1407E-07	ETTOT =	.9126E+00	.2561E+00
MODE 0 BIS 7 :	ERTOT =	-.3653E-01	.2207E+00	EPTOT =	.4205E-07	-.1407E-07	ETTOT =	.9126E+00	.2561E+00

TESTSEGMENT NR 3 ABSTAND DIST = .18 METER ROT.WINKEL PHI = 180. GRAD

MODE 0 BIS 0 :	ERTOT =	.1673E+00	-.3229E+00	EPTOT =	0.	0.	ETTOT =	.8271E+00	.3707E+00
MODE 0 BIS 1 :	ERTOT =	-.2338E+00	.2079E+00	EPTOT =	.3344E-07	.2232E-07	ETTOT =	.8215E+00	.1436E+00
MODE 0 BIS 2 :	ERTOT =	-.5255E-01	.3212E+00	EPTOT =	.5807E-07	-.1791E-07	ETTOT =	.7441E+00	.1708E+00
MODE 0 BIS 3 :	ERTOT =	-.5307E-01	.2975E+00	EPTOT =	.4351E-07	-.2685E-07	ETTOT =	.7528E+00	.1860E+00
MODE 0 BIS 4 :	ERTOT =	-.6578E-01	.2951E+00	EPTOT =	.4162E-07	-.2378E-07	ETTOT =	.7550E+00	.1845E+00
MODE 0 BIS 5 :	ERTOT =	-.6602E-01	.2953E+00	EPTOT =	.4207E-07	-.2350E-07	ETTOT =	.7548E+00	.1842E+00
MODE 0 BIS 6 :	ERTOT =	-.6601E-01	.2954E+00	EPTOT =	.4211E-07	-.2355E-07	ETTOT =	.7548E+00	.1843E+00
MODE 0 BIS 7 :	ERTOT =	-.5600E-01	.2954E+00	EPTOT =	.4210E-07	-.2356E-07	ETTOT =	.7548E+00	.1843E+00

TESTSEGMENT NR 4 ABSTAND DIST = .23 METER ROT.WINKEL PHI = 180. GRAD

MODE 0 BIS 0 :	ERTOT =	.1683E+00	-.3972E+00	EPTOT =	0.	0.	ETTOT =	.5678E+00	.3197E+00
MODE 0 BIS 1 :	ERTOT =	-.3441E+00	.3008E+00	EPTOT =	.3194E-07	.2066E-07	ETTOT =	.6849E+00	.1130E-01
MODE 0 BIS 2 :	ERTOT =	-.5283E-01	.4930E+00	EPTOT =	.6393E-07	-.3142E-07	ETTOT =	.5437E+00	.9376E-02
MODE 0 BIS 3 :	ERTOT =	-.3731E-01	.4371E+00	EPTOT =	.3805E-07	-.4729E-07	ETTOT =	.5514E+00	.4564E-01
MODE 0 BIS 4 :	ERTOT =	-.4609E-01	.4292E+00	EPTOT =	.3346E-07	-.3980E-07	ETTOT =	.5581E+00	.4308E-01
MODE 0 BIS 5 :	ERTOT =	-.4717E-01	.4303E+00	EPTOT =	.3497E-07	-.3887E-07	ETTOT =	.5576E+00	.4210E-01
MODE 0 BIS 6 :	ERTOT =	-.4706E-01	.4304E+00	EPTOT =	.3511E-07	-.3911E-07	ETTOT =	.5575E+00	.4217E-01
MODE 0 BIS 7 :	ERTOT =	-.4704E-01	.4304E+00	EPTOT =	.3508E-07	-.3913E-07	ETTOT =	.5575E+00	.4218E-01

TESTSEGMENT NR 5 ABSTAND DIST = .33 METER ROT.WINKEL PHI = 180. GRAD

MODE 0 BIS 0 :	ERTOT =	.1744E+00	-.4105E+00	EPTOT =	0.	0.	ETTOT =	.3994E+00	.2847E+00
MODE 0 BIS 1 :	ERTOT =	-.3823E+00	.3720E+00	EPTOT =	.2826E-07	.1864E-07	ETTOT =	.6303E+00	-.1059E+00
MODE 0 BIS 2 :	ERTOT =	-.7186E-02	.6426E+00	EPTOT =	.6557E-07	-.4215E-07	ETTOT =	.4058E+00	-.1589E+00
MODE 0 BIS 3 :	ERTOT =	.7595E-01	.5392E+00	EPTOT =	.2657E-07	-.6606E-07	ETTOT =	.4032E+00	-.8702E-01
MODE 0 BIS 4 :	ERTOT =	.5513E-01	.5207E+00	EPTOT =	.1771E-07	-.5160E-07	ETTOT =	.4193E+00	-.8899E-01
MODE 0 BIS 5 :	ERTOT =	.5189E-01	.5240E+00	EPTOT =	.2144E-07	-.4932E-07	ETTOT =	.4190E+00	-.9198E-01
MODE 0 BIS 6 :	ERTOT =	.5232E-01	.5244E+00	EPTOT =	.2189E-07	-.5005E-07	ETTOT =	.4186E+00	-.9182E-01
MODE 0 BIS 7 :	ERTOT =	.5238E-01	.5244E+00	EPTOT =	.2177E-07	-.5012E-07	ETTOT =	.4186E+00	-.9177E-01

TESTSEGMENT NR 6 ABSTAND DIST = .53 METER ROT.WINKEL PHI = 180. GRAD

MODE 0 BIS 0 :	ERTOT =	.1811E+00	-.3547E+00	EPTOT =	0.	0.	ETTOT =	.2203E+00	.2142E+00
MODE 0 BIS 1 :	ERTOT =	-.3302E+00	.4138E+00	EPTOT =	.2087E-07	.1491E-07	ETTOT =	.5737E+00	-.2433E+00
MODE 0 BIS 2 :	ERTOT =	.1904E+00	.7752E+00	EPTOT =	.6228E-07	-.5259E-07	ETTOT =	.2070E+00	-.4016E+00
MODE 0 BIS 3 :	ERTOT =	.3447E+00	.5782E+00	EPTOT =	.2654E-08	-.8914E-07	ETTOT =	.1643E+00	-.2452E+00
MODE 0 BIS 4 :	ERTOT =	.2913E+00	.5315E+00	EPTOT =	-.1564E-07	-.5930E-07	ETTOT =	.2120E+00	-.2384E+00
MODE 0 BIS 5 :	ERTOT =	.2803E+00	.5429E+00	EPTOT =	-.5351E-08	-.5299E-07	ETTOT =	.2124E+00	-.2495E+00
MODE 0 BIS 6 :	ERTOT =	.2823E+00	.5450E+00	EPTOT =	-.3700E-08	-.5569E-07	ETTOT =	.2102E+00	-.2494E+00
MODE 0 BIS 7 :	ERTOT =	.2826E+00	.5447E+00	EPTOT =	-.4267E-08	-.5603E-07	ETTOT =	.2103E+00	-.2490E+00

TESTSEGMENT NR 7 ABSTAND DIST = .68 METER ROT.WINKEL PHI = 180. GRAD

MODE 0 BIS 0 :	ERTOT =	.1741E+00	-.2525E+00	EPTOT =	0.	0.	ETTOT =	.8880E-01	.1066E+00
MODE 0 BIS 1 :	ERTOT =	-.1942E+00	.3687E+00	EPTOT =	.1298E-07	.1085E-07	ETTOT =	.4725E+00	-.3129E+00
MODE 0 BIS 2 :	ERTOT =	.4232E+00	.7642E+00	EPTOT =	.5374E-07	-.5562E-07	ETTOT =	-.1785E-01	-.5808E+00
MODE 0 BIS 3 :	ERTOT =	.6357E+00	.4636E+00	EPTOT =	-.2413E-07	-.1034E-06	ETTOT =	-.1293E+00	-.3080E+00
MODE 0 BIS 4 :	ERTOT =	.5311E+00	.3745E+00	EPTOT =	-.5483E-07	-.5326E-07	ETTOT =	-.2529E-01	-.2763E+00
MODE 0 BIS 5 :	ERTOT =	.5044E+00	.4027E+00	EPTOT =	-.3294E-07	-.3984E-07	ETTOT =	-.1869E-01	-.3069E+00
MODE 0 BIS 6 :	ERTOT =	.5106E+00	.4092E+00	EPTOT =	-.2852E-07	-.4706E-07	ETTOT =	-.2598E-01	-.3079E+00
MODE 0 BIS 7 :	ERTOT =	.5119E+00	.4080E+00	EPTOT =	-.3042E-07	-.4823E-07	ETTOT =	-.2608E-01	-.3064E+00

TESTSEGMENT NR 8 ABSTAND DIST = .87 METER ROT.WINKEL PHI = 180. GRAD

MODE 0 BIS 0 :	ERTOT =	.1484E+00	-.1429E+00	EPTOT =	0.	0.	ETTOT =	-.4312E-02	-.2379E-01
MODE 0 BIS 1 :	ERTOT =	-.3160E-01	.2525E+00	EPTOT =	.5842E-08	.6938E-08	ETTOT =	.3094E+00	-.2986E+00
MODE 0 BIS 2 :	ERTOT =	.5702E+00	.6162E+00	EPTOT =	.4172E-07	-.5158E-07	ETTOT =	-.2420E+00	-.6434E+00
MODE 0 BIS 3 :	ERTOT =	.8531E+00	.2244E+00	EPTOT =	-.4850E-07	-.1069E-06	ETTOT =	-.4413E+00	-.2428E+00
MODE 0 BIS 4 :	ERTOT =	.5828E+00	.3421E-01	EPTOT =	-.9305E-07	-.3420E-07	ETTOT =	-.2518E+00	-.1654E+00
MODE 0 BIS 5 :	ERTOT =	.6309E+00	.1405E+00	EPTOT =	-.5401E-07	-.1027E-07	ETTOT =	-.2292E+00	-.2330E+00
MODE 0 BIS 6 :	ERTOT =	.5460E+00	.1559E+00	EPTOT =	-.4441E-07	-.2593E-07	ETTOT =	-.2487E+00	-.2383E+00
MODE 0 BIS 7 :	ERTOT =	.5499E+00	.1525E+00	EPTOT =	-.4942E-07	-.2900E-07	ETTOT =	-.2497E+00	-.2335E+00

TESTSEGMENT NR 9 ABSTAND DIST = 1.03 METER ROT.WINKEL PHI = 180. GRAD

MODE 0 BIS 0 :	ERTOT =	.8968E-01	-.2780E-01	EPTOT =	0.	0.	ETTOT =	-.6683E-01	-.1824E+00
MODE 0 BIS 1 :	ERTOT =	.1436E+00	.4460E-01	EPTOT =	-.1178E-08	.2524E-08	ETTOT =	.3998E-01	-.1616E+00
MODE 0 BIS 2 :	ERTOT =	.6234E+00	.2813E+00	EPTOT =	.2352E-07	-.3774E-07	ETTOT =	-.4478E+00	-.5126E+00
MODE 0 BIS 3 :	ERTOT =	.9262E+00	-.1776E+00	EPTOT =	-.6997E-07	-.9505E-07	ETTOT =	-.7570E+00	.2299E-01
MODE 0 BIS 4 :	ERTOT =	.5627E+00	-.3824E+00	EPTOT =	-.1315E-06	.5262E-08	ETTOT =	-.4217E+00	.1901E+00
MODE 0 BIS 5 :	ERTOT =	.5644E+00	-.2712E+00	EPTOT =	-.6244E-07	.4758E-07	ETTOT =	-.3552E+00	.3803E-01
MODE 0 BIS 6 :	ERTOT =	.5019E+00	-.2342E+00	EPTOT =	-.4107E-07	.1273E-07	ETTOT =	-.4093E+00	.1699E-01
MODE 0 BIS 7 :	ERTOT =	.5134E+00	-.2447E+00	EPTOT =	-.5496E-07	.4217E-08	ETTOT =	-.4154E+00	.3339E-01

A Z I M U T A L   S T R A H L U N G S   D I A G R A M M   F R E Q U E N Z = 164.0 M H Z

KOERPER : VERTIKALER ROT.SYM. MENSCHMOD.
DURCHMESSER = .20 METER
ACHSENLAENGE = 1.69 METER

MESSANTENNE : PUNKTANTENNE AUF
1.00 METER HOEHE
PHI UND DIST VAR.

EINSTRAHLUNG : WINKEL THETA = 80.0 GRAD
POLARISATION = VERTIKAL
MESSANTENNE : POLARISATION = VERTIKAL

DIREKTE EINSTRAHLUNG

ROTATIONSWINKEL PHI = 0.00 GRAD

DIST : ABSTAND DER MESSANTENNE VON DER KOERPEROBERFLAECHE IN METER
PHI : HORIZONTALER ROTATIONSWINKEL IN GRAD; 180 GRAD = SCHATTEN
GAIN : FELDSTAERKE BEI DER MESSANTENNE IN DB ; 0 DB = MAX.FREESPACE
PHASE : PHASE DES MESSPUNKTES IN GRAD

DIST	GAIN	PHASE
.08	-5.68	156.40
.13	-2.13	154.35
.18	-.20	150.98
.20		
.28	1.88	144.32
.30		
.38	2.06	137.1?
.40		
.45		
.53	2.29	123.81
.55		
.60		
.68	.47	103.95
.70		
.75		
.83	-1.95	70.02
.85		
.90		
.95		
1.03	-1.57	10.20

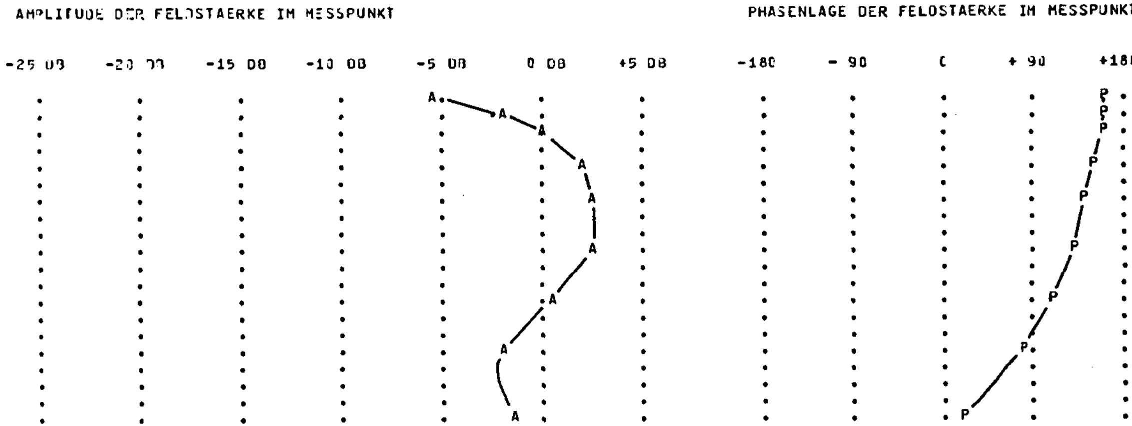

IN THIS PROGRAM THE VALUES ARE AVAILABLE FOR PHI = 5,10,15......180° (A1 POLARISATION VERT/HOR/RAD)
FOR AN INCIDENT WAVE WITH THETA(=VERTICAL) AND PHI(=HORIZONTAL) POLARISATION
SHOWN ARE HERE ONLY A1 VERTICAL/A2 VERTICAL FOR PHI = 0° AND 90°, RESP. 180° (NEXT PAGE)

DIST	GAIN	PHASE
.08	-10.21	-157.77
.13	-7.03	-157.28
.18	-5.01	-156.11
.20		
.28	-2.43	-152.69
.30		
.38	-.82	-148.52
.40		
.45		
.53	.70	-141.65
.55		
.60		
.68	1.53	-134.59
.70		
.75		
.83	1.88	-127.74
.85		
.90		
.95		
1.03	1.76	-119.51

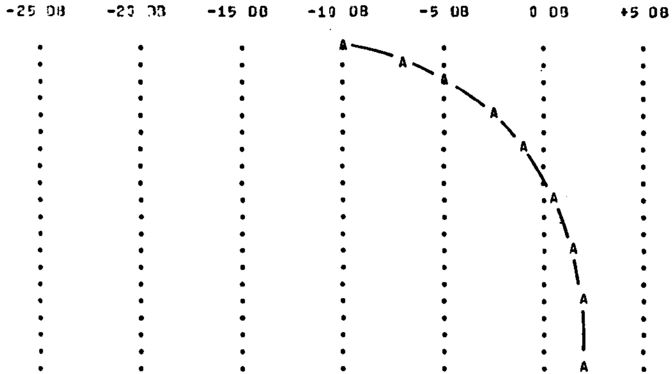

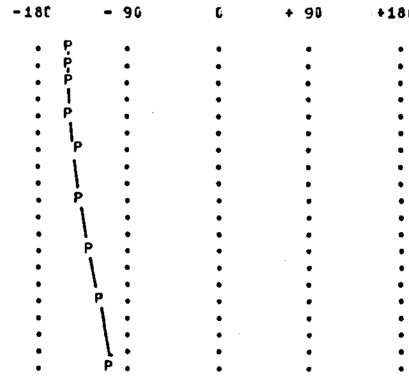

PHI = 180°

AMPLITUDE DER FELDSTAERKE IM MESSPUNKT

PHASENLAGE DER FELDSTAERKE IM MESSPUNKT

DIST	GAIN	PHASE
.08	-14.23	-69.27
.13	-10.92	-56.02
.18	-9.02	-48.19
.20		
.28	-6.82	-31.71
.30		
.38	-5.52	-14.46
.40		
.45		
.53	-4.33	12.18
.55		
.60		
.68	-3.59	39.50
.70		
.75		
.83	-3.09	67.36
.85		
.90		
.95		
1.03	-2.59	104.64

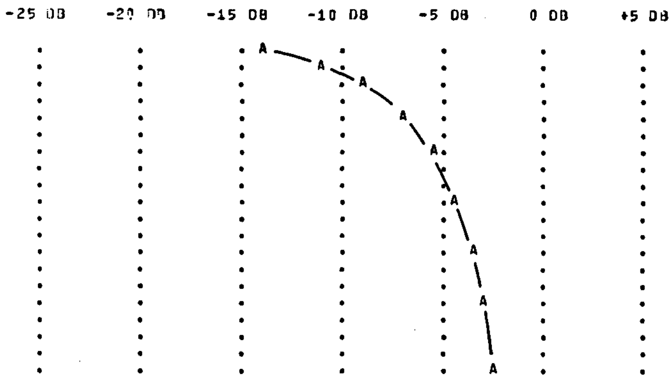

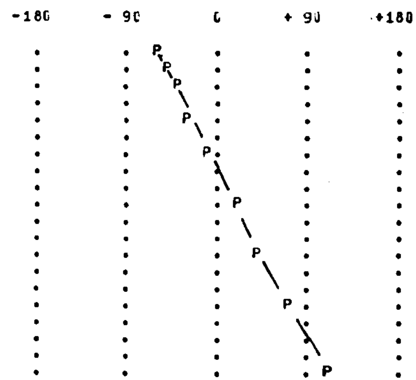

16.2.4. PROGRAM PANC, DATA CARDS FOR TEST BODIES FZYL, MANMOD 1 AND MANMOD 2, FIELD HOMOGENEITY RESULTS WITH FZYL

```
E PROGRAM *PANC*, COMPUTATION OF THE HOMOGENEITY OF THE FIELDS
E ****************************************************************
E CONTROL CARDS
PAN,3571,CM70000,CT5.
FTN.
ATTACH,HOMOG.
CALL,F100D5, P=HOMOG,B=DISK.
LGO.
R HERE END OF RECORD CARD
C ****************
      PROGRAM PANC (INPUT,OUTPUT,DISK,TAPE1=INPUT,TAPE3=OUTPUT,
     XTAPE6=DISK)
C ****************
C THIS PROGRAM IS AN EXTENSION TO PROGRAM PANB AND COMPUTES THE FIELD
C HOMOGENEITY ALONG A DIPOLE ANTENNA (2H=0.1M) ORIENTED (P1) VERTICALLY,
C HORIZONTALLY OR RADIALLY, SPACED  (DAT= 0.1M)  FROM THE BODY SURFACE
C AND FOR BOTH INCIDENT FIELD POLARIZATIONS (P2).
C THE OUTPUT IS A TABLE WITH FOLLOWING INFORMATIONS:
C PHI: HORIZONTAL ROTATION ANGLE (AZIMUTHAL ANGLE)
C GAIN CENTER: FIELD COMPONENT AT THE CENTER POINT OF THE ANTENNA
C PHASE CENTER: PHASE OF THE FIELD COMPONENT AT THE CENTER POINT
C MEAN ERROR: LOGARITHMIC DIFFERENCE (DELTA U) BETWEEN THE INDUCED
C VOLTAGE (CENTER E * 2H) AND THE ACTUAL INDUCED VOLTAGE ( INTEGRAL E
C FROM -H TO +H)
C MAXIMUM GAINVAR: LOGARITHMIC DIFFERENCE (SMALL DELTA E) BETWEEN THE
C FIELDS AT THE ENDS OF THE DIPOLE ANTENNA.
C MAXIMUM PHASEVAR: DIFFERENCE (SMALL DELTA PHI) BETWEEN THE PHASES
C OF THE FIELDS AT THE ENDS OF THE DIPOLE ANTENNA.
C PRIOR TO THE RUN OF THIS PROGRAM PANC THE FOLLOWING COMPUTATIONS
C ARE NEEDED:
C Y-MATRICES WITH PROGRAM HARRA (FZYL DATA SET, MODEL FREQUENCY 10 MHZ,
C MODI 0 TO 7)
C FIELD POINTS WITH PROGRAM PANB (FZYL DATA SET, MODEL FREQUENCY 10 MHZ,
C KK=8, RUN=1, NTEST=5, TESTSEGMENTS 2.25 10.0 0.2 / 1.75 10.0 0.2 /
C 2.75 10.0 0.2 / 2.25  9.5 0.2 / 2.25 10.5 0.2)
C THE RESULTS OF PANB SHOULD BE STORED IN THE FILE F100D5 IN THE COLLECT
C FILE HOMOG.
C ****************

      COMPLEX SYV(185),SYH(185),SYS(185)
      REAL F,DA,DU,HO,X1
      INTEGER TEXT(2),POL,NNPHI
      COMPLEX PP
      DIMENSION DI(5)
      READ(1,10) F
   10 FORMAT(2X,F5.1)
      DA=1.8 $ DI(1)=0.1 $ DU=0.25 $ HO=1.0 $ X1=80.8
      NNPHI=37 $ NST=185
      PI=3.141593
      CS= (DU/2.+DI(1))*PI/(NNPHI-1)
      FAC=DI(1)/(4.*CS)
      PP= CMPLX(1.0E-32,1.0E-32)
      QQ=1.0E-32 $ Q=10000.
      PR=180./PI
      TEXT(1) =10HVERTICAL
      TEXT(2)=10HHORIZONTAL
      REWIND 6
      DO 701 POL=1,2
      READ(6)(SYV(I),I=1,NST)
      READ(6)(SYH(I),I=1,NST)
      READ(6)(SYS(I),I=1,NST)
  520 FORMAT(1H1,1X,
     1*A Z I M U T H A L  R A D I A T I O N  P A T T E R N  F R E Q U E
     2N C Y*,I4,* M H Z*,/1H0,1X,*HOMOGENEITY CHECK OF THE FIELD ALONG A
     3 0.1 METER DIPOLE ANTENNA*/1H0,1X,*TESTBODY: ROT.SYM.CYLINDER*,8X,
     4*FIELD POINT*,7X,*INCIDENT WAVE*/1H ,11X,
     5*AXIAL LENGTH =*,F5.2,* M    DAT =*,F4.2,* M*,7X,*POLAR. = *,R10/1H
     6 ,11X,*DIAMETER      =*,F5.2,* M    HB  =*,F4.2,* M*,7X,*THETA  =*,
     7F5.1,* DEG*,/)
  521 FORMAT(1H0,1X,5X,
     1*VERTICAL POLARIZED ANTENNA*,13X,*RADIAL POLARIZED ANTENNA*/1H0,1X
     2,*PHI  GAIN   PHASE  MEAN  MAXIMUM MAXIMUM*,4X,
     3       *GAIN   PHASE  MEAN  MAXIMUM MAXIMUM*/1H ,1X,5X,
     4       *CENTER CENTER ERROR GAINVAR PHASEVAR*,3X,
     5       *CENTER CENTER ERROR GAINVAR PHASEVAR*)
  524 FORMAT(1H0,1X,5X,
     1*HORIZONTAL POLARIZED ANTENNA*,11X,*RADIAL POLARIZED ANTENNA*/1H0,
     21X,*PHI  GAIN   PHASE  MEAN  MAXIMUM MAXIMUM*,4X,
     3       *GAIN   PHASE  MEAN  MAXIMUM MAXIMUM*/1H ,1X,5X,
     4       *CENTER CENTER ERROR GAINVAR PHASEVAR*,3X,
     5       *CENTER CENTER ERROR GAINVAR PHASEVAR*)
  522 FORMAT(1H ,1X,
     1*DEG  DB      DEG     DB     DB       DEG*,8X,
     2      *DB     DEG     DB     DB       DEG*,/)
  523 FORMAT(1H ,1X,I3,2X,F5.1,1X,F6.1,2X,F5.2,1X,F5.1,1X,F6.1,7X,
     1                   F5.1,1X,F6.1,2X,F5.2,1X,F5.1,1X,F6.1)
      WRITE(3,520) IFIX(F),DA,DI(1),TEXT(POL),DU,HO,X1
      IF(POL.EQ.2) GOTO 1
      WRITE(3,521) $ GOTO 2
    1 WRITE(3,524) $ GOTO 2
    2 CONTINUE
      WRITE(3,522)
      DO 700 J=1,NNPHI
      IH1=J-2 $ IH2=J+2 $ NC=NNPHI-1
      IF(J.EQ.1)  IH1=J+2 $ IF(J.EQ.2)  IH1=J
      IF(J.EQ.NC) IH2=J   $ IF(J.EQ.NNPHI)  IH2=J-2
      ITE1 = J
      ITE2 = J+NNPHI
      ITE3 = J+NNPHI*2
      ITE4 = J+NNPHI*3
      ITE5 = J+NNPHI*4
      JJJ  = (J*5)-5
```

```
      IF(POL.EQ.1) GOTO 4                                        PANC 103
      SYV(ITE1)=SYH(ITE1)                                        PANC 104
      SYV(ITE5)=SYH(IH1)                                         PANC 105
      SYV(ITE4)=SYH(IH2)                                         PANC 106
    4 CONTINUE                                                   PANC 107
      IF(CABS(SYV(ITE1)).LT.QQ)  SYV(ITE1)=PP                    PANC 108
      IF(CABS(SYV(ITE5)).LT.QQ)  SYV(ITE5)=PP                    PANC 109
      IF(CABS(SYV(ITE4)).LT.QQ)  SYV(ITE4)=PP                    PANC 110
      IF(CABS(SYS(ITE1)).LT.QQ)  SYS(ITE1)=PP                    PANC 111
      IF(CABS(SYS(ITE3)).LT.QQ)  SYS(ITE3)=PP                    PANC 112
      IF(CABS(SYS(ITE2)).LT.QQ)  SYS(ITE2)=PP                    PANC 113
      AMV1=CABS(SYV(ITE1)) $ AMR1=CABS(SYS(ITE1))                PANC 114
      AMV5=CABS(SYV(ITE5)) $ AMR3=CABS(SYS(ITE3))                PANC 115
      AMV4=CABS(SYV(ITE4)) $ AMR2=CABS(SYS(ITE2))                PANC 116
      PV1=ATAN2(REAL(SYV(ITE1)),AIMAG(SYV(ITE1)))*PR             PANC 117
      PV5=ATAN2(REAL(SYV(ITE5)),AIMAG(SYV(ITE5)))*PR             PANC 118
      PV4=ATAN2(REAL(SYV(ITE4)),AIMAG(SYV(ITE4)))*PR             PANC 119
      PR1=ATAN2(REAL(SYS(ITE1)),AIMAG(SYS(ITE1)))*PR             PANC 120
      PR3=ATAN2(REAL(SYS(ITE3)),AIMAG(SYS(ITE3)))*PR             PANC 121
      PR2=ATAN2(REAL(SYS(ITE2)),AIMAG(SYS(ITE2)))*PR             PANC 122
      DPV1=ABS(PV5-PV4) $ DPV2=360.-DPV1                         PANC 123
      DPR1=ABS(PR3-PR2)$ DPR2=360.-DPR1                          PANC 124
      IF(ABS(DPV2).LT.ABS(DPV1)) DPV1=DPV2 $ DPV=ABS(DPV1)       PANC 125
      IF(ABS(DPR2).LT.ABS(DPR1)) DPR1=DPR2 $ DPR=ABS(DPR1)       PANC 126
      IF(POL.EQ.1) GOTO 5                                        PANC 127
      D1=AMV1-AMV5 $ D2=AMV1-AMV4                                PANC 128
      AMV5=AMV1-D1*FAC $ AMV4=AMV1-D2*FAC                        PANC 129
      IF(AMV5.LT.QQ) AMV5=QQ $ IF(AMV4.LT.QQ) AMV4=QQ            PANC 130
      DPV=DPV*FAC                                                PANC 131
    5 CONTINUE                                                   PANC 132
      AV1=20.*ALOG10(AMV1) $ AR1=20.*ALOG10(AMR1)                PANC 133
      AV5=20.*ALOG10(AMV5) $ AR3=20.*ALOG10(AMR3)                PANC 134
      AV4=20.*ALOG10(AMV4) $ AR2=20.*ALOG10(AMR2)                PANC 135
      EAV=20.*ALOG10((4.*AMV1)/(AMV5+AMV4+2.*AMV1))              PANC 136
      EAR=20.*ALOG10((4.*AMR1)/(AMR3+AMR2+2.*AMR1))              PANC 137
      DAV=ABS(AV5-AV4) $ DAR=ABS(AR3-AR2)                        PANC 138
      IF(AV1.GT.-50.) GOTO 8                                     PANC 139
      AV1=Q $ PV1=Q $ EAV=Q $ DAV=Q $ DPV=Q                      PANC 140
    8 CONTINUE                                                   PANC 141
      IF(AR1.GT.-50.) GOTO 9                                     PANC 142
      AR1=Q $ PR1=Q $ EAR=Q $ DAR=Q $ DPR=Q                      PANC 143
    9 CONTINUE                                                   PANC 144
      WRITE(3,523) JJJ,AV1,PV1,EAV,DAV,DPV,AR1,PR1,EAR,DAR,DPR   PANC 145
  700 CONTINUE                                                   PANC 146
  701 CONTINUE                                                   PANC 147
      END                                                        PANC 148
R HERE END OF  RECORD CARD                                       PANC 149
E DATA CARD                                                      PANC 150
  100.0 MHZ                                                      PANC 151
R HERE END OF  INFORMATION CARD                                  PANC 152
```

D A T A   C A R D S : T E S T B O D Y   D E S C R I P T I O N

```
TESTBODY FZYL: CYLINDER WITH ROUND CAPS

RH (X-COMPONENT RADIUS)
  0.0000  0.4735  0.8738  1.1488  1.2499  1.2500  1.2500  1.2500  1.2500  1.2500
  1.2500  1.2500  1.2500  1.2500  1.2500  1.2500  1.2500  1.2500  1.2500  1.2500
  1.2500  1.2500  1.2500  1.2500  1.2500  1.2500  1.2500  1.2500  1.2500  1.2500
  1.2500  1.2500  1.2500  1.2500  1.2500  1.2500  1.2499  1.1488  0.8738  0.4735
  0.0000

ZH (Z-COMPONENT HIGHT)
  0.0     0.0932  0.3586  0.7574  1.2293  1.7150  2.2007  2.6863  3.1720  3.6577
  4.1434  4.6290  5.1147  5.6004  6.0861  6.5717  7.0574  7.5431  8.0288  8.5144
  9.0001  9.4858  9.9714 10.4571 10.9428 11.4285 11.9141 12.3998 12.8855 13.3712
 13.8568 14.3425 14.8282 15.3139 15.7995 16.2852 16.7707 17.2426 17.6414 17.9068
 18.0000


TESTBODY MANMOD1: HUMAN BODY,FRONT VIEW, ROTATIONAL SYMMETRIC

RH (X-COMPONENT RADIUS)
  0.0000  0.7000  0.6700  0.6500  0.7500  0.9000  1.0700  1.1500  1.2300  1.2800
  1.2600  1.3000  1.3300  1.3800  1.4400  1.5100  1.5800  1.6500  1.6600  1.6600
  1.6800  1.6100  1.5300  1.4500  1.4500  1.4800  1.5000  1.5500  1.6000  1.7000
  1.7000  1.7000  1.2500  0.8500  0.6500  0.6500  0.8200  0.8500  0.7600  0.5000
  0.0000

ZH (Z-COMPONENT HIGHT)
  0.0000  0.0000  0.4700  0.9500  1.4200  1.8500  2.3000  2.7800  3.2000  3.6700
  4.1000  4.6000  5.0300  5.4900  6.0000  6.4200  6.8400  7.3300  7.8000  8.2700
  8.7400  9.2000  9.7000 10.1700 10.6300 11.1100 11.6000 12.0500 12.5000 12.9400
 13.3600 13.8000 14.0000 14.2500 14.6500 15.1500 15.5800 16.0000 16.4100 16.6500
 16.8000


TESTBODY MANMOD2: HUMAN BODY, SIDE VIEW, ROTATIONAL SYMMETRIC

RH (X-COMPONENT RADIUS)
  0.000   0.500   0.515   0.515   0.500   0.500   0.515   0.515   0.525   0.525
  0.575   0.600   0.625   0.660   0.710   0.780   0.925   1.050   1.050   1.000
  0.980   0.980   1.020   1.085   1.100   1.070   1.040   1.000   0.930   0.850
  0.630   0.480   0.490   0.620   0.760   0.850   0.870   0.820   0.700   0.500
  0.000

ZH (Z-COMPONENT HIGHT)
  0.000   0.000   0.350   0.760   1.270   1.740   2.180   2.580   3.120   3.680
  4.260   4.840   5.500   5.960   6.510   7.060   7.630   8.240   8.700   9.200
  9.740  10.270  10.770  11.340  11.820  12.270  12.550  12.820  13.190  13.510
 13.920  14.310  14.550  14.700  15.000  15.400  15.700  16.050  16.420  16.680
 16.800
```

A Z I M U T H A L   R A D I A T I O N   P A T T E R N   F R E Q U E N C Y   65 M H Z

HOMOGENEITY CHECK OF THE FIELD ALONG A 0.1 METER DIPOLE ANTENNA

TESTBODY: ROT.SYM.CYLINDER, AXIAL LENGTH = 1.80 M, DIAMETER = .25 M — FIELD POINT: DAT = .10 M, HB =1.00 M — INCIDENT WAVE: POLAR. = VERTICAL, THETA = 80.8 DEG

PHI	VERTICAL POLARIZED ANTENNA					RADIAL POLARIZED ANTENNA				
DEG	GAIN CENTER DB	PHASE CENTER DEG	MEAN ERROR DB	MAXIMUM GAINVAR DB	MAXIMUM PHASEVAR DEG	GAIN CENTER DB	PHASE CENTER DEG	MEAN ERROR DB	MAXIMUM GAINVAR DB	MAXIMUM PHASEVAR DEG
0	-19.4	-167.8	.01	1.0	6.5	-1.7	-27.3	-.32	4.3	4.1
5	-19.4	-167.5	.01	1.0	6.6	-1.7	-27.3	-.32	4.3	4.1
10	-19.6	-166.6	.01	.9	6.7	-1.7	-27.5	-.31	4.3	4.0
15	-19.8	-165.0	.00	.9	7.0	-1.7	-27.7	-.31	4.3	4.0
20	-20.1	-162.6	-.00	.9	7.5	-1.7	-28.1	-.31	4.4	3.9
25	-20.5	-159.4	-.01	.8	8.0	-1.7	-28.6	-.31	4.4	3.7
30	-21.0	-155.2	-.02	.7	8.7	-1.7	-29.2	-.31	4.4	3.6
35	-21.5	-149.7	-.03	.5	9.4	-1.7	-29.9	-.31	4.4	3.4
40	-22.0	-142.8	-.05	.3	10.0	-1.7	-30.6	-.30	4.4	3.2
45	-22.5	-134.4	-.07	.0	10.3	-1.7	-31.5	-.30	4.4	2.9
50	-22.8	-124.3	-.09	.3	10.0	-1.7	-32.5	-.30	4.5	2.6
55	-22.9	-112.8	-.10	.6	8.8	-1.7	-33.5	-.29	4.5	2.3
60	-22.7	-100.9	-.11	.9	6.9	-1.7	-34.5	-.29	4.5	1.9
65	-22.2	-89.3	-.11	1.0	4.5	-1.7	-35.7	-.28	4.4	1.5
70	-21.4	-78.8	-.11	1.0	2.4	-1.7	-36.8	-.28	4.4	1.2
75	-20.5	-69.8	-.10	.9	.6	-1.6	-37.9	-.27	4.4	.8
80	-19.5	-62.2	-.09	.8	.6	-1.6	-39.1	-.26	4.4	.4
85	-18.5	-55.8	-.08	.6	1.5	-1.5	-40.2	-.25	4.3	.1
90	-17.5	-50.5	-.07	.5	2.0	-1.4	-41.3	-.25	4.3	.2
95	-16.7	-46.0	-.06	.4	2.3	-1.3	-42.4	-.24	4.2	.5
100	-15.8	-42.2	-.06	.3	2.5	-1.2	-43.3	-.23	4.1	.7
105	-15.1	-38.9	-.05	.2	2.6	-1.1	-44.3	-.22	4.1	.9
110	-14.4	-36.0	-.05	.1	2.6	-1.0	-45.1	-.22	4.0	1.0
115	-13.8	-33.4	-.04	.1	2.6	-.9	-45.9	-.21	3.9	1.1
120	-13.2	-31.2	-.04	.0	2.6	-.8	-46.6	-.20	3.9	1.1
125	-12.7	-29.2	-.04	.0	2.5	-.7	-47.2	-.19	3.8	1.1
130	-12.3	-27.5	-.03	.1	2.4	-.6	-47.7	-.19	3.7	1.1
135	-11.9	-25.9	-.03	.1	2.4	-.5	-48.2	-.18	3.7	1.1
140	-11.5	-24.6	-.03	.1	2.3	-.4	-48.6	-.18	3.6	1.0
145	-11.2	-23.4	-.03	.1	2.3	-.3	-48.9	-.17	3.6	.9
150	-10.9	-22.4	-.03	.2	2.2	-.2	-49.2	-.17	3.5	.9
155	-10.7	-21.5	-.03	.2	2.2	-.1	-49.4	-.17	3.5	.8
160	-10.5	-20.9	-.03	.2	2.1	-.1	-49.6	-.16	3.5	.7
165	-10.4	-20.3	-.03	.2	2.1	-.0	-49.8	-.16	3.4	.7
170	-10.3	-20.0	-.02	.2	2.1	-.0	-49.9	-.16	3.4	.6
175	-10.3	-19.7	-.02	.2	2.0	.0	-49.9	-.16	3.4	.6
180	-10.2	-19.7	-.02	.2	2.0	.0	-49.9	-.16	3.4	.6

A Z I M U T H A L   R A D I A T I O N   P A T T E R N   F R E Q U E N C Y   65 M H Z

HOMOGENEITY CHECK OF THE FIELD ALONG A 0.1 METER DIPOLE ANTENNA

TESTBODY: ROT.SYM.CYLINDER, AXIAL LENGTH = 1.80 M, DIAMETER = .25 M — FIELD POINT: DAT = .10 M, HB =1.00 M — INCIDENT WAVE: POLAR. = HORIZONTAL, THETA = 80.8 DEG

PHI	HORIZONTAL POLARIZED ANTENNA					RADIAL POLARIZED ANTENNA				
DEG	GAIN CENTER DB	PHASE CENTER DEG	MEAN ERROR DB	MAXIMUM GAINVAR DB	MAXIMUM PHASEVAR DEG	GAIN CENTER DB	PHASE CENTER DEG	MEAN ERROR DB	MAXIMUM GAINVAR DB	MAXIMUM PHASEVAR DEG
0	-3.1	59.1	.09	0.0	0.0	*****	******	*****	*****	******
5	-3.2	59.2	.09	.3	1.0	-18.6	64.7	-.17	2.1	6.7
10	-3.3	59.5	.09	.7	1.9	-12.6	64.9	-.17	2.1	6.6
15	-3.4	60.0	.09	1.1	2.9	-9.1	65.2	-.17	2.1	6.5
20	-3.7	60.6	.08	1.4	3.9	-6.7	65.5	-.17	2.1	6.3
25	-4.0	61.5	.08	1.9	4.8	-4.8	66.0	-.17	2.1	6.1
30	-4.4	62.5	.08	2.3	5.8	-3.4	66.6	-.17	2.1	5.8
35	-4.9	63.7	.08	2.8	6.8	-2.2	67.2	-.17	2.1	5.4
40	-5.5	65.2	.08	3.3	7.8	-1.2	68.0	-.17	2.1	5.1
45	-6.2	66.8	.08	4.0	8.8	-.4	68.8	-.17	2.1	4.6
50	-7.0	68.6	.08	4.8	10.0	.3	69.7	-.17	2.1	4.2
55	-8.0	70.7	.08	5.8	11.4	.9	70.6	-.17	2.0	3.7
60	-9.2	73.0	.08	7.1	13.3	1.4	71.7	-.17	2.0	3.2
65	-10.6	75.8	.07	9.0	16.3	1.8	72.8	-.17	2.0	2.7
70	-12.4	79.1	.06	12.2	22.1	2.1	73.9	-.17	2.0	2.1
75	-14.8	83.5	.01	18.7	38.4	2.4	75.0	-.17	2.0	1.5
80	-18.1	90.4	-.51	29.9	115.1	2.6	76.2	-.17	2.0	.9
85	-23.3	105.9	-3.69	9.7	188.9	2.7	77.4	-.17	2.0	.3
90	-29.5	169.5	-8.75	.1	199.5	2.7	78.7	-.17	2.0	.3
95	-23.1	-128.2	-3.62	9.9	188.4	2.7	79.9	-.17	2.0	.9
100	-18.0	-112.9	-.50	30.3	113.0	2.6	81.1	-.17	2.0	1.5
105	-14.7	-106.1	.01	18.6	37.9	2.4	82.3	-.17	2.0	2.1
110	-12.4	-101.7	.06	12.2	21.9	2.2	83.4	-.17	2.0	2.7
115	-10.5	-98.4	.07	9.0	16.2	1.9	84.5	-.17	2.0	3.2
120	-9.1	-95.7	.08	7.1	13.2	1.5	85.6	-.17	2.0	3.8
125	-7.9	-93.3	.08	5.8	11.3	1.0	86.6	-.17	2.0	4.3
130	-6.9	-91.3	.08	4.8	9.9	.4	87.6	-.17	2.0	4.8
135	-6.1	-89.5	.08	4.0	8.7	-.3	88.5	-.17	2.0	5.2
140	-5.3	-87.9	.08	3.4	7.7	-1.1	89.3	-.17	2.0	5.6
145	-4.8	-86.5	.08	2.8	6.7	-2.1	90.1	-.17	2.0	6.0
150	-4.3	-85.3	.08	2.3	5.7	-3.3	90.7	-.17	2.0	6.3
155	-3.9	-84.3	.09	1.9	4.8	-4.8	91.3	-.17	2.0	6.6
160	-3.5	-83.4	.09	1.5	3.8	-6.6	91.7	-.17	2.0	6.8
165	-3.3	-82.8	.09	1.1	2.9	-9.0	92.1	-.17	2.0	7.0
170	-3.1	-82.3	.09	.7	1.9	-12.5	92.4	-.17	2.0	7.1
175	-3.0	-82.0	.09	.4	1.0	-18.5	92.5	-.17	2.0	7.2
180	-3.0	-81.9	.09	0.0	0.0	*****	******	*****	*****	******

FZYL 65 MHz

A Z I M U T H A L   R A D I A T I O N   P A T T E R N   F R E Q U E N C Y   75 M H Z

HOMOGENEITY CHECK OF THE FIELD ALONG A 0.1 METER DIPOLE ANTENNA

TESTBODY: ROT.SYM.CYLINDER — AXIAL LENGTH = 1.80 M, DIAMETER = .25 M
FIELD POINT — DAT = .10 M, HB =1.00 M
INCIDENT WAVE — POLAR. = VERTICAL, THETA = 80.8 DEG

PHI	VERTICAL POLARIZED ANTENNA					RADIAL POLARIZED ANTENNA				
DEG	GAIN CENTER DB	PHASE CENTER DEG	MEAN ERROR DB	MAXIMUM GAINVAR DB	MAXIMUM PHASEVAR DEG	GAIN CENTER DB	PHASE CENTER DEG	MEAN ERROR DB	MAXIMUM GAINVAR DB	MAXIMUM PHASEVAR DEG
0	-10.0	157.3	.02	.5	1.7	-.9	2.5	-.31	4.1	2.0
5	-10.0	157.3	.02	.5	1.7	-.9	2.5	-.31	4.1	2.0
10	-10.1	157.5	.02	.5	1.6	-.9	2.4	-.31	4.1	2.1
15	-10.2	157.7	.02	.5	1.6	-.9	2.2	-.31	4.1	2.1
20	-10.4	158.1	.02	.5	1.6	-.9	2.0	-.30	4.1	2.1
25	-10.6	158.6	.02	.5	1.5	-1.0	1.7	-.30	4.1	2.1
30	-10.9	159.2	.02	.5	1.4	-1.1	1.3	-.30	4.2	2.1
35	-11.2	159.9	.03	.5	1.3	-1.1	.8	-.30	4.2	2.1
40	-11.6	160.7	.03	.5	1.2	-1.2	.3	-.30	4.2	2.1
45	-12.1	161.6	.03	.4	1.1	-1.3	-.4	-.29	4.2	2.1
50	-12.6	162.6	.03	.4	1.0	-1.4	-1.1	-.29	4.2	2.0
55	-13.2	163.7	.03	.4	.8	-1.4	-1.9	-.29	4.3	1.9
60	-14.0	164.8	.04	.4	.7	-1.5	-2.8	-.28	4.3	1.8
65	-14.8	166.1	.04	.4	.5	-1.6	-3.8	-.28	4.3	1.6
70	-15.7	167.6	.05	.4	.2	-1.7	-4.9	-.27	4.3	1.4
75	-16.8	169.1	.05	.4	.1	-1.7	-6.0	-.26	4.3	1.2
80	-18.1	170.8	.06	.3	.4	-1.8	-7.2	-.26	4.3	.9
85	-19.6	172.8	.07	.3	.9	-1.8	-8.5	-.25	4.3	.6
90	-21.4	175.3	.09	.2	1.5	-1.8	-9.7	-.24	4.3	.3
95	-23.8	178.5	.11	.0	2.3	-1.9	-11.0	-.24	4.2	.0
100	-27.0	-176.5	.15	.3	3.6	-1.9	-12.3	-.23	4.2	.3
105	-31.7	-165.8	.23	1.2	5.3	-1.8	-13.5	-.22	4.1	.6
110	-39.3	-122.3	.06	3.8	12.0	-1.8	-14.7	-.22	4.1	.8
115	-35.3	-40.6	-.46	.7	18.0	-1.8	-15.9	-.21	4.0	1.0
120	-29.5	-21.7	-.23	1.0	9.5	-1.7	-17.0	-.20	3.9	1.2
125	-26.0	-15.1	-.15	1.0	6.4	-1.7	-18.0	-.20	3.9	1.3
130	-23.6	-11.4	-.11	.9	4.9	-1.6	-18.9	-.19	3.8	1.4
135	-21.8	-9.0	-.09	.9	4.0	-1.5	-19.7	-.18	3.7	1.4
140	-20.5	-7.2	-.07	.8	3.4	-1.5	-20.4	-.18	3.7	1.4
145	-19.4	-5.8	-.06	.8	3.0	-1.4	-21.1	-.17	3.6	1.4
150	-18.6	-4.7	-.06	.8	2.7	-1.4	-21.6	-.17	3.6	1.4
155	-17.9	-3.8	-.05	.8	2.5	-1.3	-22.0	-.17	3.5	1.4
160	-17.4	-3.1	-.05	.8	2.3	-1.3	-22.4	-.16	3.5	1.3
165	-17.0	-2.6	-.05	.8	2.2	-1.2	-22.7	-.16	3.4	1.3
170	-16.8	-2.2	-.04	.7	2.1	-1.2	-22.9	-.16	3.4	1.3
175	-16.6	-2.0	-.04	.7	2.1	-1.2	-23.0	-.16	3.4	1.3
180	-16.6	-1.9	-.04	.7	2.0	-1.2	-23.0	-.16	3.4	1.3

A Z I M U T H A L   R A D I A T I O N   P A T T E R N   F R E Q U E N C Y   75 M H Z

HOMOGENEITY CHECK OF THE FIELD ALONG A 0.1 METER DIPOLE ANTENNA

TESTBODY: ROT.SYM.CYLINDER — AXIAL LENGTH = 1.80 M, DIAMETER = .25 M
FIELD POINT — DAT = .10 M, HB =1.00 M
INCIDENT WAVE — POLAR. = HORIZONTAL, THETA = 80.8 DEG

PHI	HORIZONTAL POLARIZED ANTENNA					RADIAL POLARIZED ANTENNA				
DEG	GAIN CENTER DB	PHASE CENTER DEG	MEAN ERROR DB	MAXIMUM GAINVAR DB	MAXIMUM PHASEVAR DEG	GAIN CENTER DB	PHASE CENTER DEG	MEAN ERROR DB	MAXIMUM GAINVAR DB	MAXIMUM PHASEVAR DEG
0	-3.2	54.7	.09	0.0	0.0	*****	******	*****	*****	******
5	-3.2	54.8	.09	.3	1.1	-18.6	61.3	-.18	2.2	7.7
10	-3.3	55.1	.09	.7	2.3	-12.6	61.5	-.18	2.2	7.6
15	-3.5	55.7	.09	1.1	3.4	-9.1	61.8	-.18	2.1	7.4
20	-3.7	56.5	.08	1.4	4.5	-6.7	62.2	-.18	2.1	7.2
25	-4.0	57.5	.08	1.9	5.6	-4.8	62.7	-.18	2.1	6.9
30	-4.4	58.7	.08	2.3	6.7	-3.4	63.4	-.17	2.1	6.6
35	-4.9	60.1	.08	2.8	7.9	-2.2	64.2	-.17	2.1	6.2
40	-5.5	61.8	.08	3.3	9.0	-1.2	65.0	-.17	2.1	5.8
45	-6.2	63.6	.08	4.0	10.3	-.3	66.0	-.17	2.1	5.3
50	-7.0	65.8	.08	4.8	11.7	.4	67.0	-.17	2.1	4.8
55	-8.0	68.2	.08	5.8	13.3	1.0	68.1	-.17	2.1	4.3
60	-9.2	70.9	.08	7.1	15.6	1.5	69.3	-.17	2.1	3.7
65	-10.7	74.1	.07	9.0	19.0	1.9	70.5	-.17	2.1	3.1
70	-12.5	78.0	.06	12.0	25.8	2.2	71.8	-.17	2.1	2.4
75	-14.8	83.1	-.01	17.9	44.0	2.4	73.2	-.17	2.1	1.8
80	-18.0	91.1	-.58	24.5	115.2	2.6	74.5	-.17	2.1	1.1
85	-22.9	108.6	-3.53	9.2	182.8	2.7	75.9	-.17	2.1	.4
90	-28.1	168.5	-7.61	.2	194.3	2.8	77.3	-.17	2.1	.3
95	-22.8	-133.3	-3.43	9.7	182.0	2.7	78.7	-.17	2.0	1.0
100	-17.9	-116.3	-.56	25.0	112.3	2.6	80.1	-.17	2.0	1.6
105	-14.7	-108.4	-.02	17.8	43.1	2.5	81.4	-.17	2.0	2.3
110	-12.3	-103.3	.05	12.0	25.4	2.2	82.8	-.17	2.0	3.0
115	-10.5	-99.5	.06	9.0	18.8	1.9	84.0	-.17	2.0	3.6
120	-9.1	-96.3	.07	7.1	15.4	1.5	85.3	-.17	2.0	4.2
125	-7.9	-93.6	.08	5.8	13.1	1.1	86.5	-.17	2.0	4.8
130	-6.9	-91.3	.08	4.8	11.5	.5	87.6	-.17	2.0	5.3
135	-6.0	-89.2	.08	4.0	10.1	-.2	88.6	-.17	2.0	5.8
140	-5.3	-87.3	.08	3.4	8.8	-1.1	89.5	-.17	2.1	6.3
145	-4.7	-85.7	.08	2.8	7.7	-2.0	90.4	-.17	2.1	6.7
150	-4.2	-84.3	.08	2.3	6.6	-3.2	91.1	-.17	2.1	7.1
155	-3.8	-83.1	.09	1.9	5.5	-4.7	91.8	-.17	2.1	7.4
160	-3.5	-82.2	.09	1.5	4.4	-6.5	92.3	-.17	2.1	7.6
165	-3.2	-81.4	.09	1.1	3.3	-9.0	92.7	-.17	2.1	7.8
170	-3.1	-80.9	.09	.7	2.2	-12.4	93.0	-.17	2.1	8.0
175	-3.0	-80.5	.09	.4	1.1	-18.4	93.2	-.17	2.1	8.1
180	-2.9	-80.4	.09	0.0	0.0	*****	******	*****	*****	******

FZYL 75 MHz

FZYL 100 MHz

A Z I M U T H A L R A D I A T I O N P A T T E R N F R E Q U E N C Y 100 M H Z

HOMOGENEITY CHECK OF THE FIELD ALONG A 0.1 METER DIPOLE ANTENNA

TESTBODY: ROT.SYM.CYLINDER
AXIAL LENGTH = 1.80 M
DIAMETER = .25 M

FIELD POINT
DAT = .10 M
HB =1.00 M

INCIDENT WAVE
POLAR. = VERTICAL
THETA = 80.8 DEG

	VERTICAL POLARIZED ANTENNA					RADIAL POLARIZED ANTENNA				
PHI DEG	GAIN CENTER DB	PHASE CENTER DEG	MEAN ERROR DB	MAXIMUM GAINVAR DB	MAXIMUM PHASEVAR DEG	GAIN CENTER DB	PHASE CENTER DEG	MEAN ERROR DB	MAXIMUM GAINVAR DB	MAXIMUM PHASEVAR DEG
0	-5.8	167.3	.00	.3	1.1	-3.1	18.1	-.15	3.2	1.8
5	-5.8	167.4	.00	.3	1.1	-3.1	18.1	-.15	3.2	1.8
10	-5.8	167.7	.00	.3	1.1	-3.2	18.0	-.15	3.2	1.7
15	-5.9	168.2	.00	.3	1.2	-3.2	18.0	-.15	3.2	1.6
20	-6.0	168.9	.00	.3	1.2	-3.3	17.9	-.15	3.2	1.4
25	-6.1	169.7	.00	.3	1.2	-3.4	17.7	-.16	3.3	1.1
30	-6.3	170.8	.00	.3	1.2	-3.4	17.5	-.16	3.3	.9
35	-6.5	172.0	.00	.3	1.2	-3.5	17.3	-.16	3.4	.5
40	-6.8	173.4	.00	.3	1.2	-3.7	16.9	-.17	3.4	.2
45	-7.0	175.0	.00	.2	1.2	-3.8	16.5	-.17	3.5	.1
50	-7.3	176.8	.01	.2	1.2	-3.9	16.0	-.18	3.6	.5
55	-7.7	178.8	.01	.2	1.2	-4.1	15.3	-.19	3.7	.8
60	-8.1	-179.1	.01	.2	1.2	-4.2	14.5	-.19	3.7	1.0
65	-8.5	-176.7	.01	.2	1.2	-4.4	13.6	-.20	3.8	1.2
70	-8.9	-174.2	.01	.2	1.1	-4.5	12.5	-.21	4.0	1.4
75	-9.4	-171.5	.01	.2	1.1	-4.7	11.3	-.22	4.1	1.4
80	-10.0	-168.6	.01	.2	1.0	-4.8	9.9	-.23	4.2	1.4
85	-10.5	-165.4	.01	.2	.8	-4.9	8.4	-.24	4.3	1.2
90	-11.2	-162.0	.01	.1	.7	-5.0	6.8	-.25	4.3	1.0
95	-11.8	-158.2	.01	.1	.4	-5.1	5.1	-.26	4.4	.7
100	-12.6	-154.2	.01	.1	.1	-5.1	3.3	-.27	4.4	.3
105	-13.3	-149.8	.01	.1	.2	-5.2	1.6	-.28	4.5	.1
110	-14.1	-144.9	.01	.1	.6	-5.1	-.2	-.28	4.5	.5
115	-14.9	-139.6	.01	.2	1.1	-5.1	-1.9	-.29	4.5	.8
120	-15.6	-133.7	.01	.2	1.6	-5.1	-3.6	-.30	4.5	1.2
125	-16.4	-127.3	.01	.3	2.2	-5.0	-5.1	-.31	4.4	1.4
130	-17.1	-120.3	.00	.4	2.7	-4.9	-6.5	-.31	4.4	1.6
135	-17.7	-113.0	-.00	.5	3.0	-4.8	-7.8	-.32	4.3	1.8
140	-18.3	-105.4	-.01	.7	3.2	-4.7	-8.9	-.32	4.3	1.9
145	-18.6	-98.0	-.01	.8	3.2	-4.6	-9.8	-.33	4.2	1.9
150	-18.9	-91.0	-.01	.9	3.0	-4.5	-10.7	-.33	4.2	1.9
155	-19.0	-84.8	-.02	1.1	2.6	-4.4	-11.4	-.33	4.1	1.9
160	-19.1	-79.5	-.02	1.1	2.1	-4.4	-11.9	-.33	4.1	1.9
165	-19.1	-75.3	-.02	1.2	1.7	-4.3	-12.3	-.33	4.1	1.8
170	-19.0	-72.3	-.02	1.2	1.4	-4.3	-12.6	-.33	4.1	1.8
175	-19.0	-70.5	-.02	1.3	1.2	-4.2	-12.8	-.33	4.1	1.8
180	-19.0	-69.9	-.02	1.3	1.1	-4.2	-12.9	-.33	4.0	1.8

A Z I M U T H A L R A D I A T I O N P A T T E R N F R E Q U E N C Y 100 M H Z

HOMOGENEITY CHECK OF THE FIELD ALONG A 0.1 METER DIPOLE ANTENNA

TESTBODY: ROT.SYM.CYLINDER
AXIAL LENGTH = 1.80 M
DIAMETER = .25 M

FIELD POINT
DAT = .10 M
HB =1.00 M

INCIDENT WAVE
POLAR. = HORIZONTAL
THETA = 80.8 DEG

	HORIZONTAL POLARIZED ANTENNA					RADIAL POLARIZED ANTENNA				
PHI DEG	GAIN CENTER DB	PHASE CENTER DEG	MEAN ERROR DB	MAXIMUM GAINVAR DB	MAXIMUM PHASEVAR DEG	GAIN CENTER DB	PHASE CENTER DEG	MEAN ERROR DB	MAXIMUM GAINVAR DB	MAXIMUM PHASEVAR DEG
0	-3.5	43.7	.09	0.0	0.0	*****	******	*****	*****	******
5	-3.5	43.8	.09	.4	1.5	-18.6	53.3	-.17	2.3	11.1
10	-3.6	44.3	.09	.7	3.1	-12.7	53.5	-.17	2.3	10.9
15	-3.8	45.1	.09	1.1	4.6	-9.2	53.9	-.17	2.3	10.7
20	-4.0	46.1	.08	1.5	6.2	-6.8	54.5	-.17	2.3	10.4
25	-4.3	47.5	.08	1.9	7.7	-4.9	55.2	-.17	2.2	10.1
30	-4.7	49.2	.08	2.3	9.3	-3.4	56.1	-.17	2.2	9.6
35	-5.2	51.1	.08	2.8	10.8	-2.2	57.1	-.17	2.2	9.1
40	-5.8	53.4	.08	3.3	12.5	-1.2	58.2	-.17	2.2	8.5
45	-6.5	56.0	.08	4.0	14.2	-.4	59.5	-.17	2.2	7.9
50	-7.3	58.9	.08	4.7	16.1	.4	60.9	-.17	2.2	7.2
55	-8.3	62.3	.08	5.7	18.5	1.0	62.4	-.17	2.2	6.5
60	-9.5	66.1	.07	7.0	21.6	1.5	63.9	-.17	2.1	5.7
65	-10.9	70.5	.06	8.7	26.4	1.9	65.6	-.17	2.1	4.8
70	-12.7	75.9	.04	11.4	35.4	2.2	67.3	-.17	2.1	4.0
75	-14.9	83.0	-.07	15.7	57.3	2.5	69.1	-.17	2.1	3.1
80	-17.9	93.9	-.72	17.3	115.4	2.7	70.9	-.17	2.1	2.2
85	-22.1	115.5	-3.06	7.9	168.4	2.8	72.7	-.17	2.1	1.3
90	-25.2	166.5	-5.39	.4	180.4	2.9	74.5	-.17	2.1	.4
95	-21.7	-144.7	-2.87	8.9	166.2	2.8	76.4	-.17	2.1	.5
100	-17.6	-124.4	-.68	18.1	109.9	2.8	78.2	-.17	2.1	1.4
105	-14.6	-114.0	-.10	15.7	54.6	2.6	80.0	-.17	2.1	2.3
110	-12.3	-107.1	.01	11.5	34.1	2.4	81.7	-.17	2.1	3.2
115	-10.5	-101.9	.04	8.9	25.5	2.1	83.4	-.17	2.1	4.0
120	-9.1	-97.6	.06	7.1	20.8	1.7	85.0	-.17	2.1	4.8
125	-7.9	-94.0	.07	5.9	17.7	1.2	86.6	-.17	2.1	5.5
130	-6.8	-90.8	.07	4.9	15.4	.6	88.0	-.17	2.1	6.3
135	-6.0	-88.0	.08	4.1	13.5	-.1	89.4	-.17	2.1	6.9
140	-5.3	-85.5	.08	3.5	11.8	-.9	90.6	-.18	2.1	7.5
145	-4.7	-83.4	.08	2.9	10.2	-1.9	91.7	-.18	2.1	8.1
150	-4.1	-81.5	.08	2.4	8.7	-3.1	92.7	-.18	2.1	8.6
155	-3.7	-79.9	.09	1.9	7.2	-4.5	93.5	-.18	2.1	9.0
160	-3.4	-78.7	.09	1.5	5.8	-6.4	94.2	-.18	2.1	9.3
165	-3.1	-77.7	.09	1.1	4.3	-8.8	94.8	-.18	2.1	9.6
170	-3.0	-77.0	.09	.7	2.9	-12.2	95.1	-.18	2.1	9.8
175	-2.8	-76.5	.09	.4	1.4	-18.2	95.4	-.18	2.1	9.9
180	-2.8	-76.4	.09	0.0	0.0	*****	******	*****	*****	******

A Z I M U T H A L R A D I A T I O N P A T T E R N F R E Q U E N C Y 125 M H Z

HOMOGENEITY CHECK OF THE FIELD ALONG A 0.1 METER DIPOLE ANTENNA

TESTBODY: ROT.SYM.CYLINDER — AXIAL LENGTH = 1.80 M — DIAMETER = .25 M
FIELD POINT — DAT = .10 M — HB =1.00 M
INCIDENT WAVE — POLAR. = VERTICAL — THETA = 80.8 DEG

PHI	VERTICAL POLARIZED ANTENNA					RADIAL POLARIZED ANTENNA				
DEG	GAIN CENTER DB	PHASE CENTER DEG	MEAN ERROR DB	MAXIMUM GAINVAR DB	MAXIMUM PHASEVAR DEG	GAIN CENTER DB	PHASE CENTER DEG	MEAN ERROR DB	MAXIMUM GAINVAR DB	MAXIMUM PHASEVAR DEG
0	-4.5	161.8	.00	.3	1.2	-1.1	15.8	-.12	3.2	2.6
5	-4.5	161.9	.00	.3	1.2	-1.1	15.8	-.12	3.2	2.6
10	-4.5	162.3	.00	.3	1.2	-1.1	15.8	-.12	3.2	2.5
15	-4.6	162.9	.00	.3	1.2	-1.1	15.8	-.12	3.2	2.3
20	-4.7	163.7	.00	.3	1.2	-1.2	15.8	-.13	3.2	2.1
25	-4.8	164.8	.00	.3	1.2	-1.2	15.9	-.13	3.3	1.8
30	-5.0	166.1	.00	.3	1.2	-1.3	15.9	-.13	3.3	1.5
35	-5.2	167.6	.00	.3	1.2	-1.4	15.9	-.14	3.4	1.2
40	-5.4	169.4	.00	.2	1.2	-1.5	15.8	-.15	3.4	.8
45	-5.7	171.3	.00	.2	1.2	-1.6	15.7	-.15	3.5	.4
50	-5.9	173.5	.00	.2	1.2	-1.7	15.5	-.16	3.5	.0
55	-6.3	175.9	.00	.2	1.1	-1.8	15.2	-.17	3.6	.4
60	-6.6	178.5	.00	.2	1.1	-1.9	14.9	-.17	3.7	.7
65	-7.0	-178.7	.00	.2	1.0	-2.1	14.4	-.18	3.8	1.0
70	-7.4	-175.7	.00	.2	.9	-2.2	13.8	-.19	3.9	1.3
75	-7.9	-172.5	.00	.2	.7	-2.3	13.1	-.20	4.0	1.5
80	-8.4	-169.0	.00	.2	.5	-2.4	12.3	-.21	4.1	1.6
85	-9.0	-165.3	.00	.2	.3	-2.5	11.3	-.22	4.2	1.6
90	-9.5	-161.4	.00	.2	.0	-2.6	10.3	-.24	4.3	1.6
95	-10.2	-157.1	.00	.2	.4	-2.7	9.1	-.25	4.3	1.4
100	-10.8	-152.6	.00	.2	.8	-2.7	7.9	-.26	4.4	1.2
105	-11.5	-147.7	.00	.2	1.3	-2.7	6.7	-.27	4.4	1.0
110	-12.2	-142.4	.00	.2	1.9	-2.7	5.5	-.28	4.5	.8
115	-13.0	-136.7	.00	.3	2.5	-2.7	4.2	-.29	4.5	.5
120	-13.7	-130.5	.00	.4	3.2	-2.7	3.0	-.30	4.5	.3
125	-14.4	-123.8	.00	.5	3.8	-2.6	1.9	-.31	4.5	.1
130	-15.0	-116.8	-.00	.7	4.2	-2.6	.8	-.32	4.5	.1
135	-15.6	-109.4	-.00	.9	4.5	-2.5	-.1	-.33	4.4	.2
140	-16.0	-102.0	-.01	1.1	4.5	-2.4	-1.0	-.34	4.4	.3
145	-16.4	-94.8	-.01	1.3	4.2	-2.4	-1.7	-.34	4.4	.3
150	-16.6	-88.0	-.01	1.5	3.7	-2.3	-2.3	-.35	4.3	.3
155	-16.7	-81.9	-.01	1.6	3.0	-2.2	-2.9	-.35	4.3	.3
160	-16.8	-76.8	-.01	1.7	2.3	-2.2	-3.3	-.35	4.3	.2
165	-16.8	-72.8	-.01	1.8	1.6	-2.1	-3.6	-.36	4.3	.2
170	-16.8	-69.8	-.02	1.8	1.1	-2.1	-3.9	-.36	4.3	.2
175	-16.8	-68.1	-.02	1.9	.8	-2.1	-4.0	-.36	4.2	.2
180	-16.8	-67.5	-.02	1.9	.7	-2.1	-4.0	-.36	4.2	.1

A Z I M U T H A L R A D I A T I O N P A T T E R N F R E Q U E N C Y 125 M H Z

HOMOGENEITY CHECK OF THE FIELD ALONG A 0.1 METER DIPOLE ANTENNA

TESTBODY: ROT.SYM.CYLINDER — AXIAL LENGTH = 1.80 M — DIAMETER = .25 M
FIELD POINT — DAT = .10 M — HB =1.00 M
INCIDENT WAVE — POLAR. = HORIZONTAL — THETA = 80.8 DEG

PHI	HORIZONTAL POLARIZED ANTENNA					RADIAL POLARIZED ANTENNA				
DEG	GAIN CENTER DB	PHASE CENTER DEG	MEAN ERROR DB	MAXIMUM GAINVAR DB	MAXIMUM PHASEVAR DEG	GAIN CENTER DB	PHASE CENTER DEG	MEAN ERROR DB	MAXIMUM GAINVAR DB	MAXIMUM PHASEVAR DEG
0	-4.0	31.5	.09	0.0	0.0	*****	******	*****	*****	******
5	-4.0	31.7	.09	.4	2.0	-18.9	45.2	-.18	2.5	14.2
10	-4.1	32.3	.09	.7	4.1	-12.9	45.5	-.18	2.5	14.0
15	-4.3	33.3	.09	1.1	6.1	-9.4	46.0	-.18	2.5	13.8
20	-4.6	34.7	.09	1.5	8.2	-7.0	46.7	-.18	2.4	13.4
25	-4.9	36.5	.08	1.9	10.2	-5.1	47.6	-.18	2.4	12.9
30	-5.3	38.8	.08	2.3	12.3	-3.6	48.7	-.18	2.4	12.3
35	-5.8	41.4	.08	2.8	14.4	-2.4	50.0	-.18	2.4	11.7
40	-6.4	44.4	.08	3.4	16.6	-1.4	51.5	-.18	2.4	10.9
45	-7.1	47.9	.07	4.0	18.9	-.5	53.1	-.18	2.3	10.1
50	-7.9	51.8	.07	4.7	21.5	.2	54.8	-.17	2.3	9.2
55	-8.9	56.2	.07	5.6	24.7	.8	56.7	-.17	2.3	8.3
60	-10.0	61.3	.06	6.8	28.8	1.4	58.7	-.17	2.2	7.3
65	-11.4	67.2	.05	8.4	35.1	1.8	60.8	-.17	2.2	6.2
70	-13.1	74.4	.00	10.6	46.4	2.2	62.9	-.17	2.2	5.1
75	-15.3	83.8	-.16	13.3	70.2	2.4	65.2	-.17	2.2	4.0
80	-18.0	97.7	-.83	12.7	115.9	2.7	67.4	-.17	2.2	2.9
85	-21.2	122.3	-2.53	6.2	155.1	2.8	69.7	-.17	2.1	1.8
90	-22.9	165.4	-3.72	.9	165.3	2.9	72.0	-.17	2.1	.6
95	-20.5	-154.4	-2.24	8.0	150.2	2.9	74.3	-.17	2.1	.5
100	-17.2	-132.4	-.73	14.0	106.4	2.8	76.6	-.17	2.1	1.6
105	-14.5	-119.7	-.18	13.5	63.8	2.7	78.8	-.17	2.1	2.7
110	-12.3	-111.0	-.04	10.8	42.8	2.5	81.0	-.17	2.1	3.7
115	-10.6	-104.3	.01	8.6	32.6	2.2	83.1	-.17	2.1	4.8
120	-9.1	-98.8	.04	7.1	26.6	1.8	85.1	-.17	2.1	5.7
125	-7.9	-94.1	.05	5.9	22.6	1.3	87.0	-.18	2.1	6.7
130	-6.9	-90.1	.06	5.0	19.6	.7	88.8	-.18	2.1	7.5
135	-6.0	-86.5	.07	4.2	17.1	.1	90.4	-.18	2.1	8.4
140	-5.3	-83.4	.07	3.6	14.9	-.8	91.9	-.18	2.1	9.1
145	-4.7	-80.7	.08	3.0	12.9	-1.7	93.3	-.18	2.1	9.8
150	-4.1	-78.4	.08	2.5	10.9	-2.9	94.5	-.18	2.1	10.4
155	-3.7	-76.4	.09	2.0	9.0	-4.4	95.5	-.18	2.1	10.9
160	-3.3	-74.8	.09	1.6	7.2	-6.2	96.4	-.18	2.1	11.3
165	-3.1	-73.6	.09	1.2	5.4	-8.6	97.1	-.18	2.1	11.6
170	-2.9	-72.7	.09	.8	3.6	-12.1	97.6	-.18	2.2	11.9
175	-2.8	-72.2	.10	.4	1.8	-18.1	97.9	-.18	2.2	12.0
180	-2.7	-72.0	.10	0.0	0.0	*****	******	*****	*****	******

FZYL 125 MHz

FZYL 300 MHz

AZIMUTHAL RADIATION PATTERN FREQUENCY 300 MHZ

HOMOGENEITY CHECK OF THE FIELD ALONG A 0.1 METER DIPOLE ANTENNA

TESTBODY: ROT.SYM.CYLINDER — AXIAL LENGTH = 1.80 M, DIAMETER = .25 M
FIELD POINT — DAT = .10 M, HB =1.00 M
INCIDENT WAVE — POLAR. = VERTICAL, THETA = 80.8 DEG

PHI	VERTICAL POLARIZED ANTENNA					RADIAL POLARIZED ANTENNA				
DEG	GAIN CENTER DB	PHASE CENTER DEG	MEAN ERROR DB	MAXIMUM GAINVAR DB	MAXIMUM PHASEVAR DEG	GAIN CENTER DB	PHASE CENTER DEG	MEAN ERROR DB	MAXIMUM GAINVAR DB	MAXIMUM PHASEVAR DEG
0	.6	93.6	-.00	.1	7.3	-12.7	118.2	-.54	5.1	31.0
5	.6	93.8	-.00	.1	7.3	-12.6	118.2	-.53	5.1	30.6
10	.6	94.6	-.00	.1	7.3	-12.5	118.2	-.51	5.1	29.4
15	.5	95.9	-.00	.1	7.3	-12.2	118.2	-.47	5.1	27.6
20	.4	97.7	-.00	.1	7.3	-11.8	118.3	-.43	5.1	25.2
25	.3	100.0	-.00	.1	7.4	-11.4	118.5	-.39	5.0	22.4
30	.1	102.7	-.00	.1	7.4	-10.9	118.9	-.34	4.9	19.4
35	-.1	106.0	-.00	.1	7.5	-10.4	119.5	-.30	4.8	16.5
40	-.3	109.7	-.00	.1	7.5	-9.8	120.4	-.27	4.6	13.7
45	-.6	113.9	-.00	.1	7.6	-9.2	121.6	-.24	4.4	11.2
50	-.9	118.4	-.00	.0	7.6	-8.6	122.9	-.22	4.2	9.1
55	-1.2	123.4	-.00	.0	7.7	-8.0	124.6	-.20	4.0	7.4
60	-1.6	128.8	-.00	.0	7.7	-7.4	126.4	-.19	3.8	6.1
65	-2.0	134.5	-.00	.0	7.8	-6.8	128.5	-.19	3.7	5.2
70	-2.5	140.5	-.00	.0	7.9	-6.3	130.7	-.19	3.5	4.7
75	-3.0	146.8	-.00	.1	7.9	-5.8	133.0	-.19	3.4	4.4
80	-3.5	153.4	-.00	.1	8.0	-5.3	135.3	-.19	3.3	4.4
85	-4.1	160.2	-.00	.1	8.1	-4.9	137.7	-.19	3.2	4.6
90	-4.7	167.2	-.00	.2	8.2	-4.6	140.0	-.19	3.2	4.9
95	-5.4	174.4	-.00	.2	8.2	-4.3	142.3	-.20	3.2	5.3
100	-6.1	-178.2	-.00	.3	8.3	-4.0	144.6	-.20	3.2	5.7
105	-6.9	-170.6	-.00	.3	8.4	-3.8	146.6	-.21	3.2	6.1
110	-7.8	-162.8	-.00	.4	8.4	-3.6	148.6	-.21	3.3	6.5
115	-8.7	-154.7	-.01	.5	8.3	-3.5	150.3	-.21	3.3	6.7
120	-9.7	-146.1	-.01	.6	8.2	-3.4	151.9	-.22	3.4	6.9
125	-10.8	-137.0	-.01	.8	7.8	-3.4	153.3	-.22	3.5	6.9
130	-11.9	-127.2	-.01	.9	7.2	-3.3	154.4	-.22	3.6	6.7
135	-13.0	-116.5	-.01	1.1	6.2	-3.3	155.4	-.22	3.7	6.5
140	-14.1	-104.9	-.00	1.2	4.7	-3.3	156.1	-.23	3.8	6.1
145	-14.9	-92.5	-.01	1.2	2.8	-3.4	156.7	-.23	3.9	5.7
150	-15.5	-79.8	-.01	1.2	.7	-3.4	157.2	-.23	4.0	5.2
155	-15.9	-67.8	-.01	1.1	1.1	-3.4	157.5	-.23	4.0	4.6
160	-16.0	-57.3	-.01	.9	2.3	-3.4	157.7	-.24	4.1	4.1
165	-15.9	-48.9	-.01	.7	3.0	-3.4	157.8	-.24	4.1	3.7
170	-15.8	-43.0	-.01	.5	3.3	-3.5	157.9	-.24	4.1	3.4
175	-15.7	-39.4	-.01	.4	3.4	-3.5	157.9	-.24	4.1	3.2
180	-15.7	-38.2	-.01	.4	3.4	-3.5	157.9	-.24	4.1	3.1

AZIMUTHAL RADIATION PATTERN FREQUENCY 300 MHZ

HOMOGENEITY CHECK OF THE FIELD ALONG A 0.1 METER DIPOLE ANTENNA

TESTBODY: ROT.SYM.CYLINDER — AXIAL LENGTH = 1.80 M, DIAMETER = .25 M
FIELD POINT — DAT = .10 M, HB =1.00 M
INCIDENT WAVE — POLAR. = HORIZONTAL, THETA = 80.8 DEG

PHI	HORIZONTAL POLARIZED ANTENNA					RADIAL POLARIZED ANTENNA				
DEG	GAIN CENTER DB	PHASE CENTER DEG	MEAN ERROR DB	MAXIMUM GAINVAR DB	MAXIMUM PHASEVAR DEG	GAIN CENTER DB	PHASE CENTER DEG	MEAN ERROR DB	MAXIMUM GAINVAR DB	MAXIMUM PHASEVAR DEG
0	-1.7	-84.4	.16	0.0	0.0	#####	######	#####	#####	######
5	-1.8	-84.2	.16	.7	2.5	-21.8	-37.6	-.32	2.2	44.5
10	-2.0	-83.4	.16	1.4	4.9	-15.8	-36.6	-.31	2.2	44.0
15	-2.3	-82.2	.16	2.1	7.4	-12.3	-34.9	-.31	2.2	43.2
20	-2.8	-80.5	.15	2.9	9.8	-9.9	-32.6	-.30	2.2	42.2
25	-3.4	-78.4	.15	3.7	12.3	-8.0	-29.6	-.30	2.2	40.8
30	-4.2	-75.7	.14	4.8	14.8	-6.5	-26.0	-.29	2.3	39.1
35	-5.2	-72.6	.13	6.0	17.3	-5.2	-21.8	-.27	2.3	37.2
40	-6.4	-69.0	.11	7.6	20.0	-4.2	-17.1	-.26	2.3	34.9
45	-8.0	-64.8	.07	9.8	23.1	-3.3	-11.9	-.25	2.3	32.4
50	-10.0	-60.0	.02	13.3	27.2	-2.5	-6.2	-.23	2.4	29.6
55	-12.5	-54.5	-.07	21.5	35.4	-1.8	-.2	-.22	2.4	26.6
60	-16.1	-47.6	-.66	(631.2)	105.0	-1.1	6.2	-.20	2.4	23.5
65	-21.9	-37.0	-3.74	14.3	222.2	-.6	12.8	-.19	2.4	20.2
70	-35.9	22.4	#####	2.7	213.3	-.1	19.6	-.17	2.3	16.7
75	-24.5	131.0	-4.40	6.9	214.4	.4	26.4	-.16	2.3	13.3
80	-18.8	144.9	.14	(626.9)	180.2	.8	33.3	-.15	2.3	9.9
85	-15.8	154.6	.65	17.9	54.4	1.1	40.1	-.15	2.2	6.5
90	-14.0	164.0	.51	9.1	50.2	1.4	46.8	-.14	2.2	3.1
95	-12.9	173.7	.38	5.5	52.6	1.5	53.4	-.14	2.1	.1
100	-12.1	-175.7	.25	3.6	56.8	1.7	59.7	-.13	2.1	3.1
105	-11.6	-164.1	.11	2.6	61.7	1.7	65.8	-.13	2.0	6.1
110	-11.2	-151.4	-.03	2.2	66.2	1.7	71.7	-.13	2.0	8.8
115	-10.9	-137.8	-.16	2.4	69.0	1.6	77.2	-.13	2.0	11.4
120	-10.4	-123.7	-.24	3.0	69.3	1.3	82.4	-.13	1.9	13.9
125	-9.7	-109.9	-.25	3.6	66.4	1.0	87.2	-.14	1.9	16.2
130	-8.9	-97.0	-.20	4.1	61.0	.6	91.7	-.14	2.0	18.3
135	-8.0	-85.6	-.13	4.4	53.8	-.0	95.8	-.14	2.0	20.2
140	-7.1	-75.8	-.06	4.4	45.9	-.8	99.5	-.14	2.0	22.0
145	-6.2	-67.6	.01	4.1	38.3	-1.7	102.8	-.15	2.0	23.5
150	-5.5	-60.9	.06	3.7	31.2	-2.8	105.6	-.15	2.1	24.9
155	-4.8	-55.5	.09	3.1	24.9	-4.2	108.1	-.15	2.1	26.1
160	-4.2	-51.3	.12	2.5	19.2	-6.0	110.1	-.15	2.1	27.0
165	-3.8	-48.1	.14	1.9	14.0	-8.4	111.7	-.15	2.1	27.8
170	-3.5	-45.9	.15	1.3	9.1	-11.8	112.8	-.15	2.2	28.3
175	-3.3	-44.5	.15	.6	4.5	-17.8	113.5	-.16	2.2	28.7
180	-3.2	-44.1	.16	0.0	0.0	#####	######	#####	#####	######

A Z I M U T H A L R A D I A T I O N P A T T E R N F R E Q U E N C Y 425 M H Z

HOMOGENEITY CHECK OF THE FIELD ALONG A 0.1 METER DIPOLE ANTENNA

TESTBODY: ROT.SYM.CYLINDER — AXIAL LENGTH = 1.80 M — DIAMETER = .25 M
FIELD POINT — DAT = .10 M — HB =1.00 M
INCIDENT WAVE — POLAR. = VERTICAL — THETA = 80.8 DEG

PHI	VERTICAL POLARIZED ANTENNA					RADIAL POLARIZED ANTENNA				
DEG	GAIN CENTER DB	PHASE CENTER DEG	MEAN ERROR DB	MAXIMUM GAINVAR DB	MAXIMUM PHASEVAR DEG	GAIN CENTER DB	PHASE CENTER DEG	MEAN ERROR DB	MAXIMUM GAINVAR DB	MAXIMUM PHASEVAR DEG
0	2.6	47.1	.00	.0	8.0	-15.6	-97.4	-.97	5.9	65.4
5	2.5	47.5	.00	.0	8.0	-15.6	-97.0	-.96	5.9	65.0
10	2.5	48.5	.00	.0	8.0	-15.7	-95.9	-.93	5.9	63.9
15	2.4	50.2	.00	.0	8.0	-15.8	-94.2	-.88	5.9	62.1
20	2.3	52.6	.00	.0	7.9	-15.9	-91.8	-.82	5.9	59.5
25	2.2	55.7	.00	.0	7.9	-16.0	-88.8	-.75	5.8	56.3
30	2.1	59.4	.00	.0	7.8	-16.2	-85.5	-.66	5.8	52.5
35	1.9	63.8	.00	.1	7.8	-16.5	-81.9	-.57	5.7	48.3
40	1.6	68.8	.00	.1	7.7	-16.9	-78.2	-.49	5.5	43.8
45	1.4	74.4	.00	.1	7.7	-17.3	-74.7	-.40	5.3	39.3
50	1.1	80.5	.00	.1	7.7	-17.9	-71.7	-.33	5.1	34.8
55	.7	87.3	.00	.1	7.7	-18.6	-69.7	-.26	4.9	30.8
60	.4	94.5	.00	.2	7.8	-19.5	-69.3	-.21	4.7	27.4
65	-.1	102.3	.00	.2	7.9	-20.5	-71.5	-.17	4.6	25.2
70	-.5	110.4	.00	.2	8.0	-21.5	-77.8	-.16	4.3	24.7
75	-1.0	119.0	.00	.3	8.2	-22.2	-88.9	-.16	3.8	25.4
80	-1.5	128.0	.00	.3	8.5	-21.9	-103.0	-.17	2.9	24.9
85	-2.1	137.2	.00	.3	8.7	-20.6	-115.4	-.17	2.0	21.5
90	-2.7	146.7	.00	.3	9.0	-18.8	-123.3	-.15	1.4	16.7
95	-3.4	156.3	.00	.3	9.4	-17.0	-127.0	-.14	1.1	12.1
100	-4.1	166.0	.00	.3	9.7	-15.3	-128.0	-.13	1.0	8.2
105	-4.9	175.8	.00	.3	10.1	-13.8	-127.3	-.13	1.0	4.8
110	-5.7	-174.4	.01	.3	10.6	-12.6	-125.5	-.13	1.1	1.9
115	-6.6	-164.7	.01	.3	11.0	-11.5	-123.2	-.14	1.2	.6
120	-7.6	-154.9	.01	.3	11.6	-10.6	-120.6	-.14	1.4	2.8
125	-8.7	-145.0	.01	.3	12.2	-9.8	-117.9	-.15	1.5	4.7
130	-9.9	-134.9	.01	.3	13.0	-9.2	-115.2	-.16	1.8	6.4
135	-11.2	-124.2	.00	.2	14.1	-8.7	-112.7	-.17	2.0	7.9
140	-12.7	-112.8	-.00	.2	15.3	-8.3	-110.3	-.18	2.2	9.1
145	-14.1	-100.0	-.01	.0	16.8	-8.0	-108.2	-.19	2.5	10.1
150	-15.5	-85.7	-.03	.3	18.2	-7.7	-106.3	-.20	2.7	10.9
155	-16.6	-70.2	-.05	.7	19.0	-7.5	-104.7	-.21	2.9	11.5
160	-17.2	-54.8	-.06	1.1	18.6	-7.4	-103.4	-.22	3.1	12.0
165	-17.4	-41.5	-.07	1.4	17.4	-7.3	-102.4	-.22	3.3	12.3
170	-17.4	-31.6	-.08	1.6	15.9	-7.2	-101.6	-.23	3.4	12.5
175	-17.3	-25.7	-.08	1.7	15.0	-7.2	-101.2	-.23	3.5	12.6
180	-17.2	-23.7	-.08	1.7	14.6	-7.1	-101.1	-.23	3.5	12.7

A Z I M U T H A L R A D I A T I O N P A T T E R N F R E Q U E N C Y 425 M H Z

HOMOGENEITY CHECK OF THE FIELD ALONG A 0.1 METER DIPOLE ANTENNA

TESTBODY: ROT.SYM.CYLINDER — AXIAL LENGTH = 1.80 M — DIAMETER = .25 M
FIELD POINT — DAT = .10 M — HB =1.00 M
INCIDENT WAVE — POLAR. = HORIZONTAL — THETA = 80.8 DEG

PHI	HORIZONTAL POLARIZED ANTENNA					RADIAL POLARIZED ANTENNA				
DEG	GAIN CENTER DB	PHASE CENTER DEG	MEAN ERROR DB	MAXIMUM GAINVAR DB	MAXIMUM PHASEVAR DEG	GAIN CENTER DB	PHASE CENTER DEG	MEAN ERROR DB	MAXIMUM GAINVAR DB	MAXIMUM PHASEVAR DEG
0	1.6	-132.6	.12	0.0	0.0	*****	******	*****	*****	******
5	1.5	-132.4	.12	.5	2.8	-20.5	-98.2	-.26	2.2	50.4
10	1.4	-131.5	.12	1.0	5.5	-14.5	-97.1	-.26	2.2	49.8
15	1.2	-130.2	.12	1.5	8.2	-11.0	-95.2	-.26	2.1	48.9
20	.8	-128.3	.12	2.1	10.6	-8.6	-92.7	-.25	2.1	47.6
25	.4	-126.0	.12	2.7	12.7	-6.8	-89.4	-.25	2.0	46.0
30	-.2	-123.2	.13	3.5	14.4	-5.4	-85.3	-.24	1.9	44.2
35	-1.0	-120.2	.12	4.3	15.5	-4.2	-80.6	-.24	1.7	42.1
40	-1.9	-117.0	.12	5.4	15.8	-3.3	-75.2	-.23	1.6	39.8
45	-3.0	-113.8	.10	6.7	14.7	-2.5	-69.0	-.23	1.5	37.3
50	-4.4	-110.8	.07	8.5	11.2	-2.0	-62.1	-.22	1.4	34.7
55	-6.1	-108.6	-.00	10.7	2.7	-1.5	-54.4	-.22	1.3	32.0
60	-8.3	-108.2	-.20	13.3	16.7	-1.1	-46.1	-.22	1.3	29.2
65	-11.0	-111.6	-.80	13.3	53.9	-.9	-36.9	-.21	1.3	26.2
70	-14.2	-123.9	-2.12	8.1	89.3	-.7	-27.1	-.21	1.3	23.0
75	-16.2	-150.9	-3.07	1.9	100.3	-.6	-16.6	-.20	1.4	19.5
80	-15.1	-178.3	-1.87	4.1	87.6	-.5	-5.6	-.20	1.5	15.8
85	-12.7	169.6	-.33	8.9	50.1	-.3	5.9	-.19	1.6	11.7
90	-10.7	167.3	.31	8.7	8.8	-.2	17.5	-.18	1.7	7.3
95	-9.4	169.7	.46	6.0	15.3	-.1	29.1	-.17	1.9	2.6
100	-8.6	174.7	.47	3.4	29.1	.0	40.4	-.16	1.9	2.1
105	-8.2	-178.4	.44	1.3	39.0	.2	51.2	-.16	2.0	6.8
110	-8.1	-169.9	.36	.3	48.2	.3	61.4	-.15	2.0	11.4
115	-8.4	-159.7	.23	1.5	58.3	.3	70.8	-.15	2.0	15.6
120	-8.8	-147.4	.03	1.9	69.4	.3	79.5	-.16	2.0	19.5
125	-9.3	-132.6	-.23	1.5	80.0	.1	87.3	-.16	2.0	23.1
130	-9.6	-115.4	-.48	.2	87.1	-.1	94.4	-.17	2.0	26.3
135	-9.6	-96.8	-.58	1.5	87.8	-.5	100.7	-.17	2.0	29.2
140	-9.0	-79.0	-.49	3.2	81.3	-1.1	106.3	-.18	2.0	31.7
145	-8.1	-63.7	-.29	4.4	69.5	-1.9	111.2	-.18	2.1	34.0
150	-7.0	-51.5	-.09	4.8	55.5	-2.9	115.4	-.19	2.1	35.9
155	-6.1	-42.2	.05	4.5	42.3	-4.2	118.9	-.19	2.1	37.6
160	-5.2	-35.4	.14	3.8	31.1	-5.9	121.8	-.19	2.2	38.9
165	-4.5	-30.4	.19	2.9	21.8	-8.3	124.0	-.19	2.2	39.9
170	-4.1	-27.1	.22	2.0	13.8	-11.7	125.6	-.20	2.2	40.7
175	-3.8	-25.1	.23	1.0	6.7	-17.6	126.5	-.20	2.3	41.1
180	-3.7	-24.5	.24	0.0	0.0	*****	******	*****	*****	******

FZYL 425 MHz

16.2.5. ADDITIONAL RESULTS FROM FIELD COMPUTATIONS WITH FZYL, MANMOD 1 AND MANMOD 2

EFFECT OF THE FREQUENCY ON THE DIRECTIVE RADIATION PATTERN (EXTENSION)

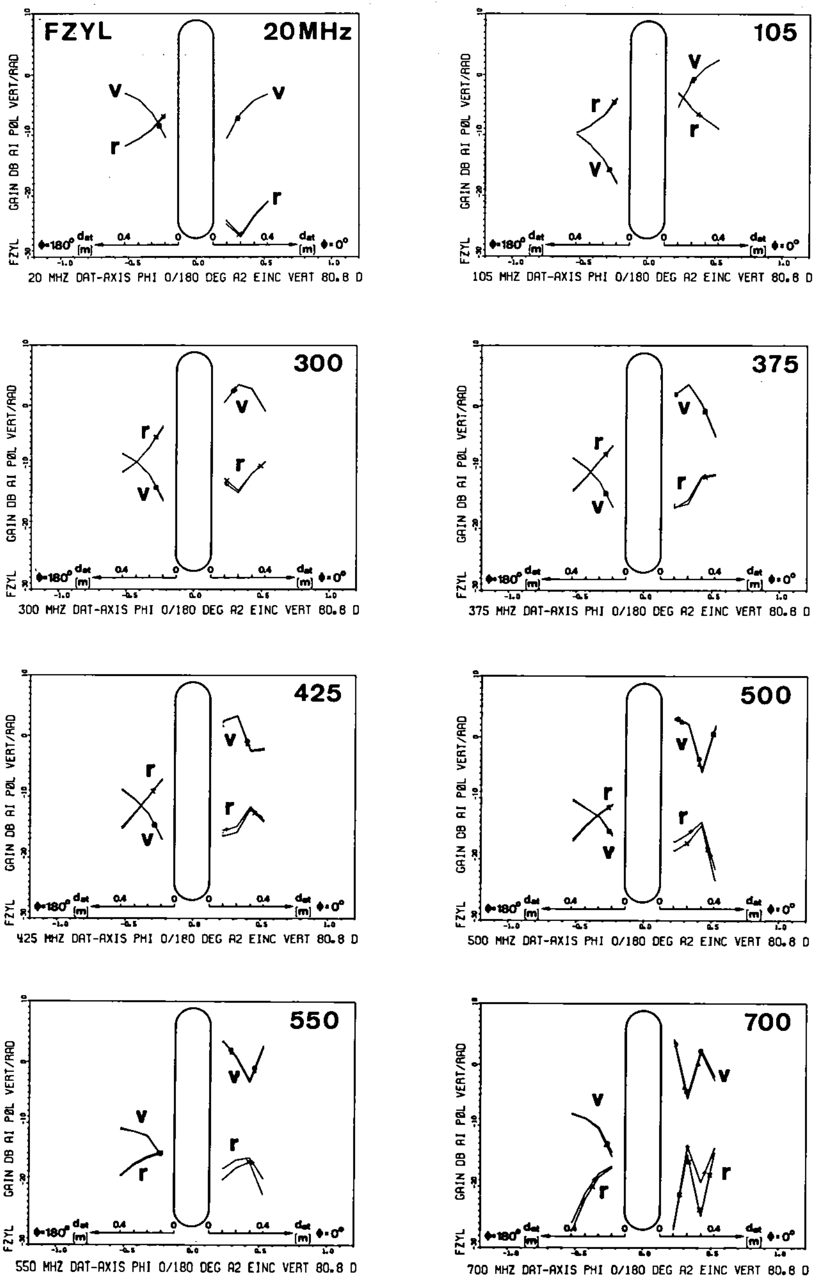

FIGURE 78d Field components E_v and E_r versus d_{at} at $\phi = 0$ and 180^0, with the parameter f 20 to 700 MHz. Constant: p_2 = vertical, $\theta_i = 80.8^0$, $h_B = 1.0$ m.

EFFECT OF THE FREQUENCY ON THE AZIMUTHAL RADIATION PATTERNS (EXTENSION)

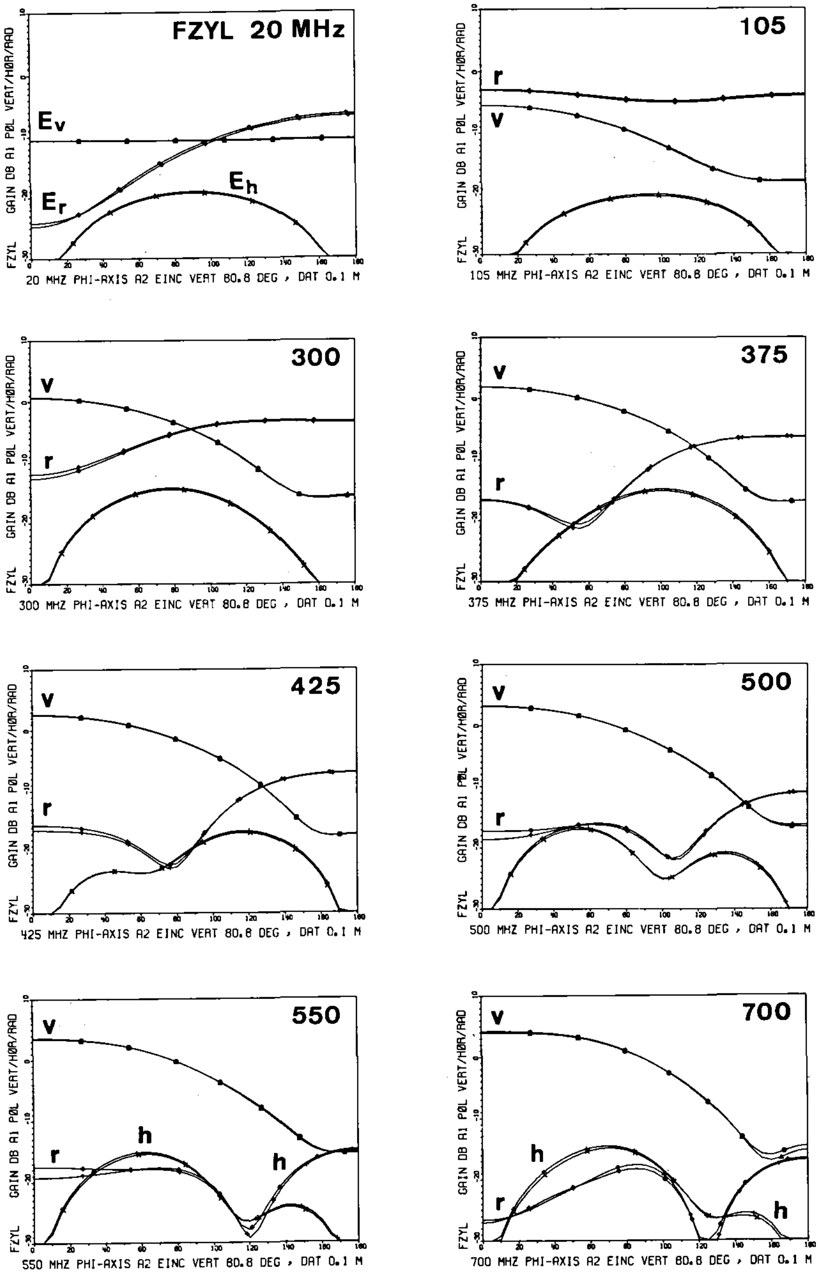

FIGURE 77d Field components E_v, E_r and E_h versus ϕ with the parameter f 20 to 700 MHz. Constant: $d_{at} = 0.1$ m, p_2 = vertical, $\theta_i = 80.8^o$, $h_B = 1.0$ m.

Leer - Vide - Empty

AZIMUTHAL RADIATION PATTERNS IN THE 11 MHz RANGE

- FZYL : 11 MHz
- MANMOD 1 : 15 MHz
- MANMOD 2 : 15 MHz

The three figures show the azimuthal radiation patterns of the field components E_v, E_r and E_h at d_{at} = 0.1, 0.2, 0.3 and 0.4 m.

Effect of the body shape:

- E_v varies only within 2 dB
- E_r varies extremely, especially at small d_{at}
- E_h varies only within 2 dB

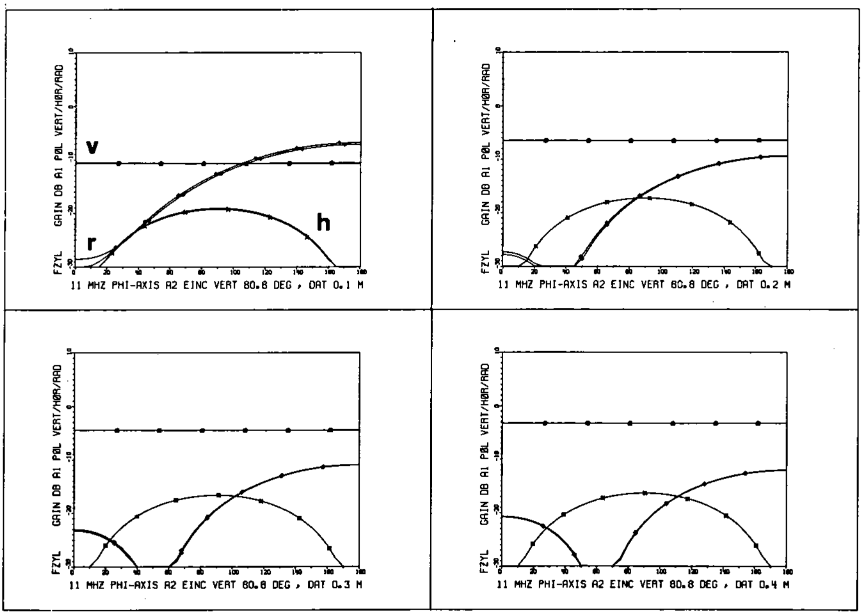

FIGURE 100a Azimuthal radiation pattern FZYL at 11 MHz.

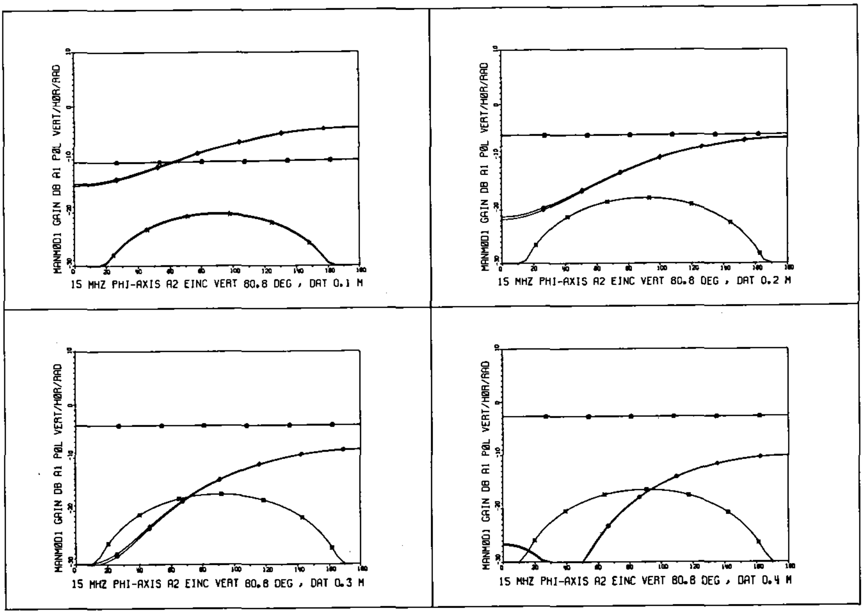

FIGURE 100b Azimuthal radiation pattern MANMOD1 at 15 MHz.

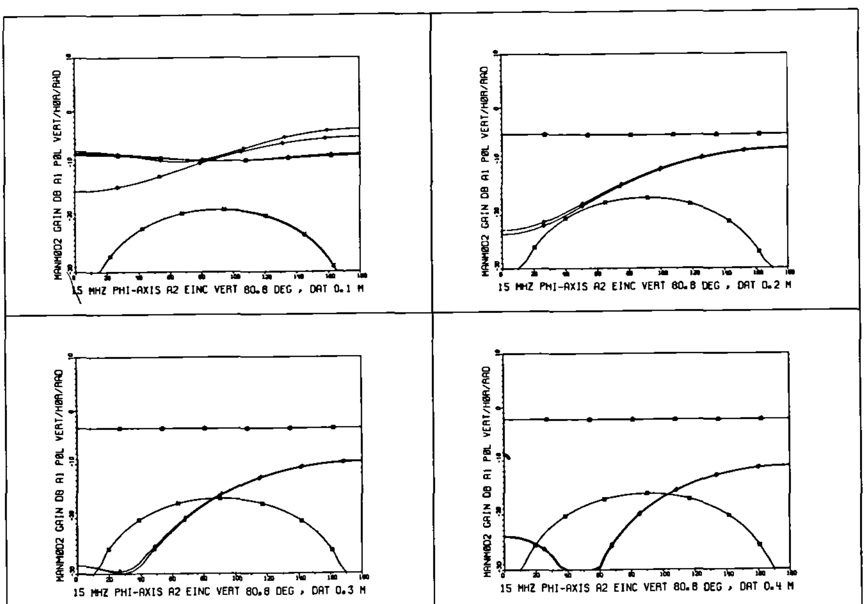

FIGURE 100c Azimuthal radiation pattern MANMOD2 at 15 MHz.

AZIMUTHAL RADIATION PATTERNS IN THE 50 MHz RANGE

- FZYL : 50 MHz
- MANMOD 1 : 50 MHz
- MANMOD 2 : 50 MHz

The three figures show the azimuthal radiation patterns of the field components E_v, E_r and E_h at d_{at} = 0.1, 0.2, 0.3 and 0.4 m .

Effect of the body shape:

- E_v varies only within 2.5 dB
- E_r varies only within 2.5 dB
- E_h varies only within 2.0 dB

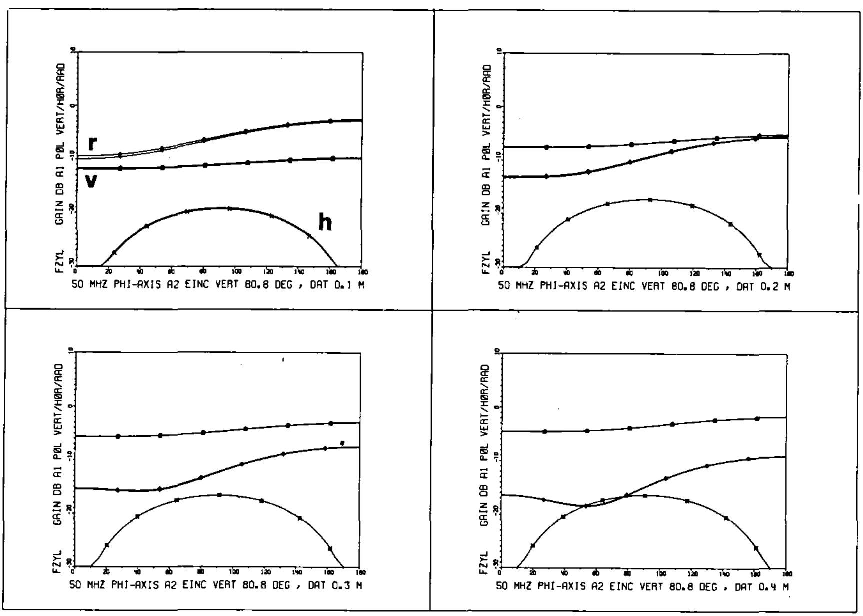

FIGURE 101a Azimuthal radiation patterns FZYL at 50 MHz.

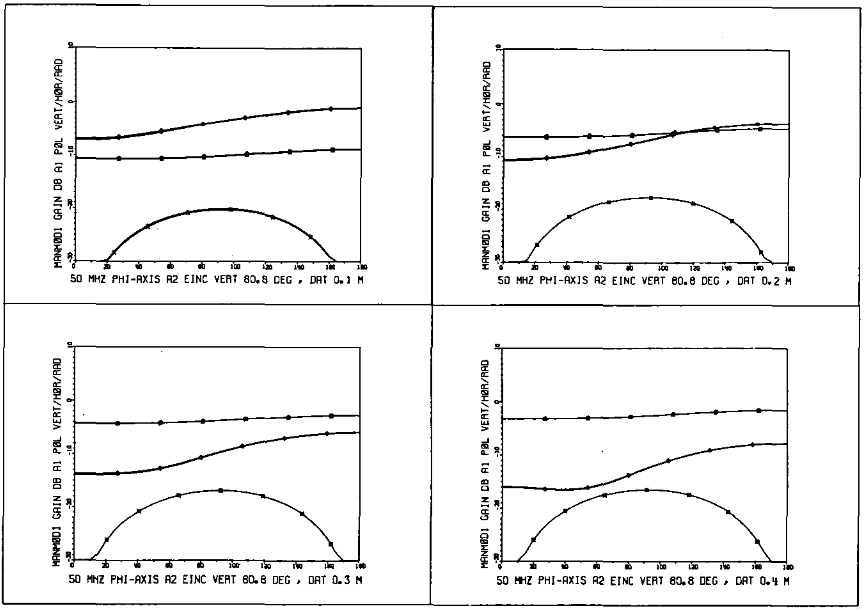

FIGURE 101b Azimuthal radiation patterns MANMOD1 at 50 MHz.

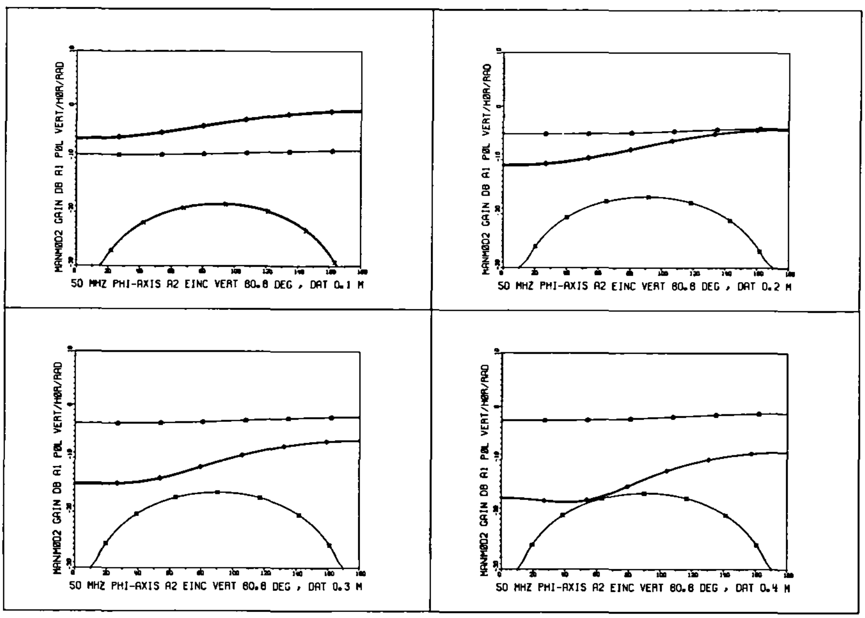

FIGURE 101c Azimuthal radiation patterns MANMOD2 at 50 MHz.

AZIMUTHAL RADIATION PATTERNS IN THE 75 MHz RANGE

- FZYL : 75 MHz
- MANMOD 1 : 75 MHz
- MANMOD 2 : 80 MHz

The three figures show the azimuthal radiation patterns of the field components E_v, E_r and E_h at d_{at} = 0.1, 0.2, 0.3 and 0.4 m.

Effect of the body shape:

- E_v varies extremely between FZYL 75 MHz and MANMOD 1 75 MHz, but E_v varies less (about 10 dB) between FZYL 75 MHz and MANMOD 2 80 MHz.
- E_r is almost constant versus ϕ and the amplitude varies within 5 dB between the three bodies at constant d_{at}.
- E_h varies only within 1 dB

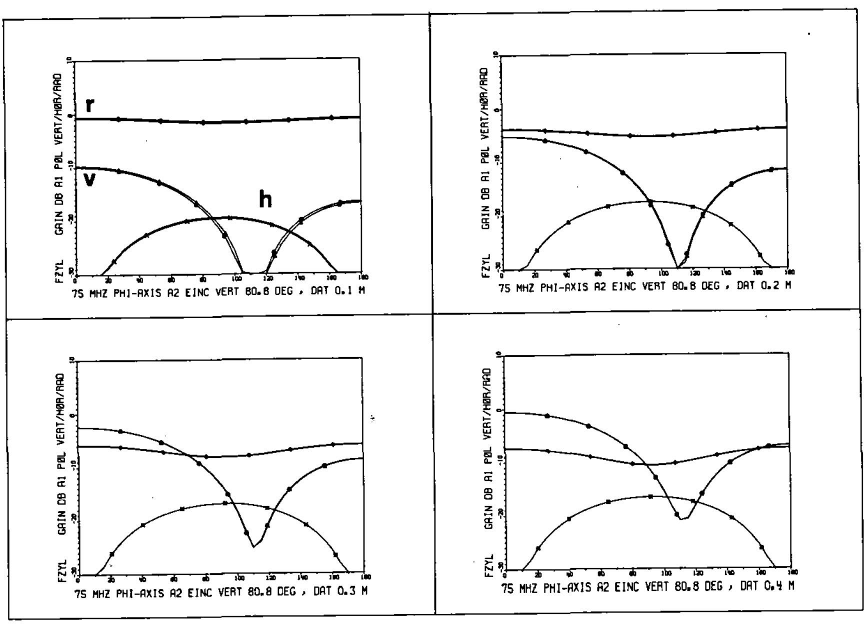

FIGURE 102a Azimuthal radiation patterns FZYL at 75 MHz.

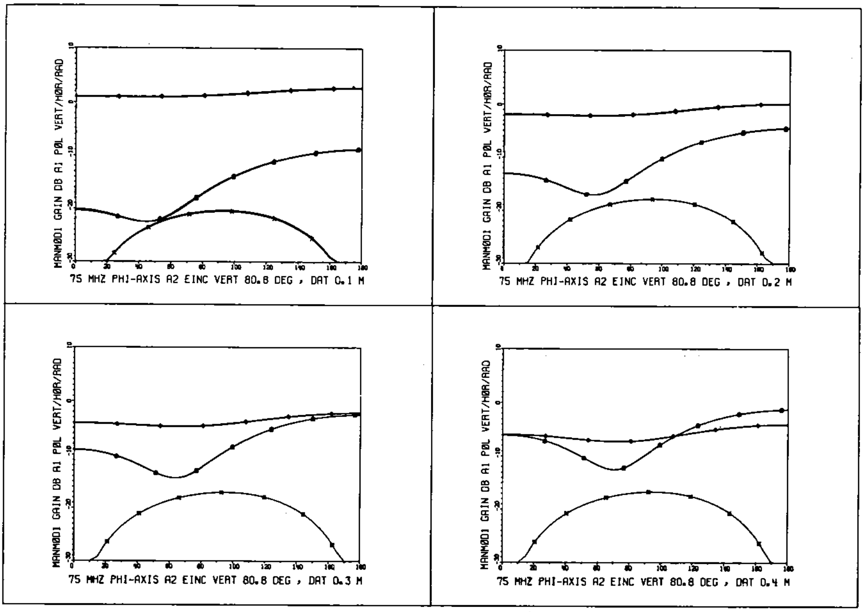

FIGURE 102b Azimuthal radiation patterns MANMOD1 at 75 MHz.

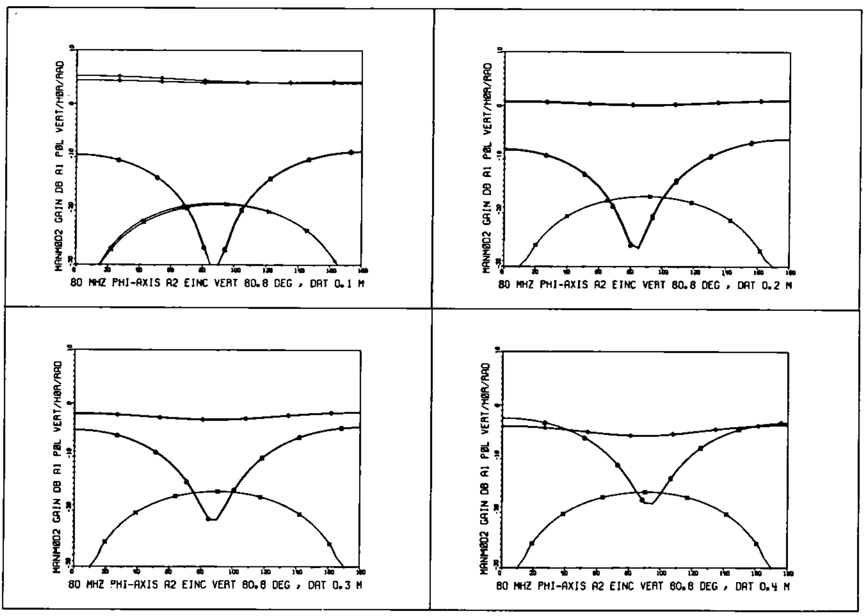

FIGURE 102c Azimuthal radiation patterns MANMOD2 at 80 MHz.

AZIMUTHAL RADIATION PATTERNS IN THE 85 MHz RANGE

- FZYL : 85 MHz
- MANMOD 1 : 90 MHz
- MANMOD 2 : 90 MHz

The three figures show the azimuthal radiation patterns of the field components E_v, E_r and E_h at d_{at} = 0.1, 0.2, 0.3 and 0.4 m.

Effect of the body shape:

- E_v varies very much between FZYL 85 MHz and MANMOD 1 90 MHz (12 dB), but E_v varies less between FZYL 85 MHz and MANMOD 2 90 MHz (3 dB)
- E_r is almost independent on ϕ and differs in amplitude within 5 dB between the three bodies
- E_h varies only within 2 dB

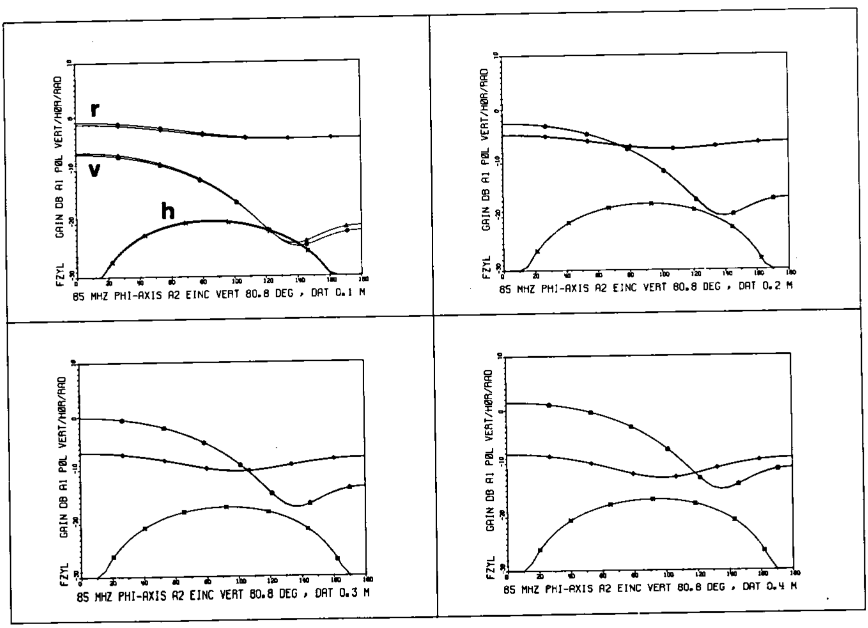

FIGURE 103a Azimuthal radiation patterns FZYL at 85 MHz.

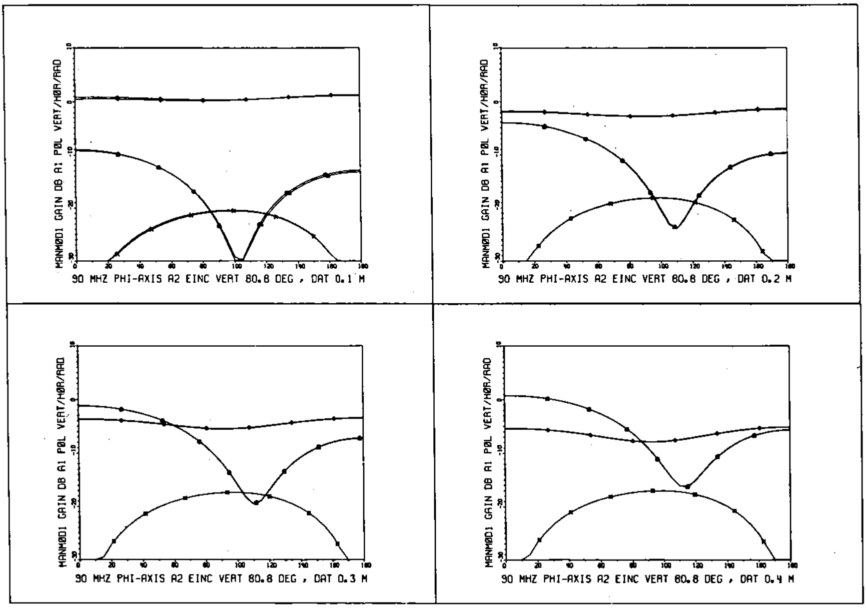

FIGURE 103b Azimuthal radiation patterns MANMOD 1 at 90 MHz.

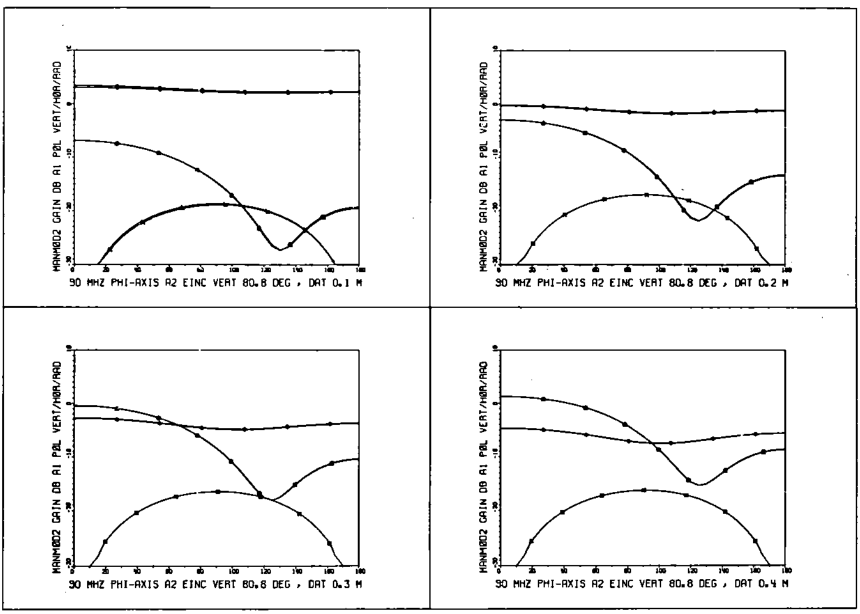

FIGURE 103c Azimuthal radiation patterns MANMOD 2 at 90 MHz.

AZIMUTHAL RADIATION PATTERNS IN THE 200 MHz RANGE

- FZYL : 200 MHz
- MANMOD 1 : 200 MHz
- MANMOD 2 : 200 MHz

The three figures show the azimuthal radiation patterns of the field components E_v, E_r and E_h at d_{at} = 0.1, 0.2, 0.3 and 0.4 m.

Effect of the body shape:

- E_v varies within 5 dB
- E_r is almost independent on ϕ up to d_{at} = 0.3m and varies only 3 dB between the three bodies. At d_{at} = 0.4 E_r becomes dependent on ϕ and varies within 5 dB between the three bodies.
- E_h varies within 10 dB and develops two peaks, especially with MANMOD 1

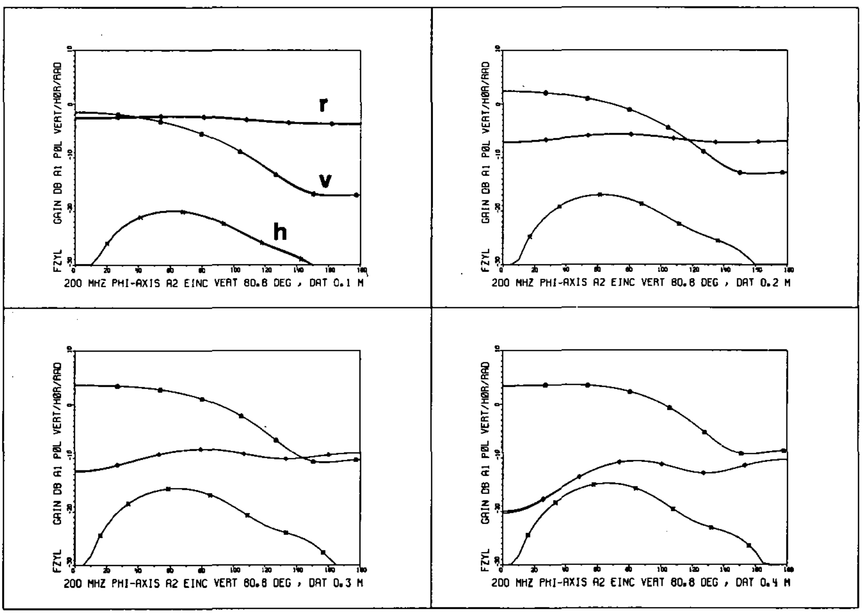

FIGURE 104a Azimuthal radiation patterns FZYL at 200 MHz.

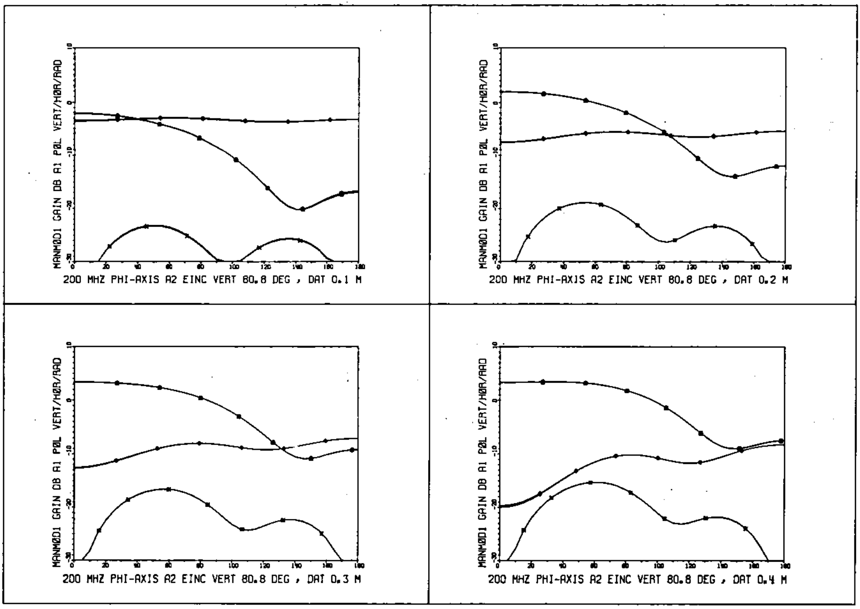

FIGURE 104b Azimuthal radiation patterns MANMOD1 at 200 MHz.

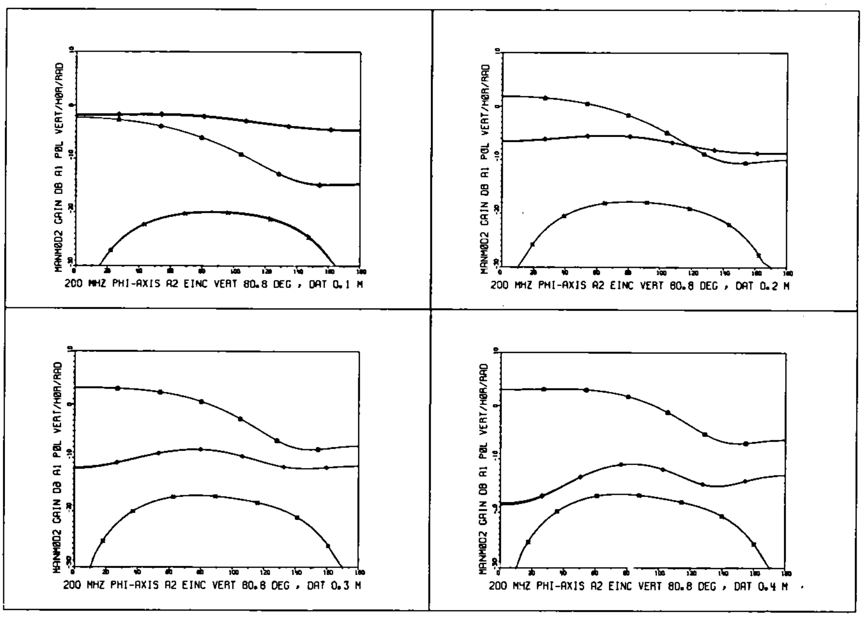

FIGURE 104c Azimuthal radiation patterns MANMOD2 at 200 MHz.

AZIMUTHAL RADIATION PATTERNS IN THE 800 MHz RANGE

- FZYL : 800 MHz
- MANMOD 1 : 800 MHz
- MANMOD 2 : 800 MHz

The three figures show the azimuthal radiation patterns of the field components E_v, E_r and E_h at d_{at} = 0.1, 0.2, 0.3 and 0.4 m.

The accuracy of the results are very doubtful, because the computer program limitations have been exceeded at this high frequency (see section 10.3.4.).

Effect of the body shape:

- E_v varies within 6 dB
- E_r varies within 16 dB
- E_h changes very much in wave form and amplitude

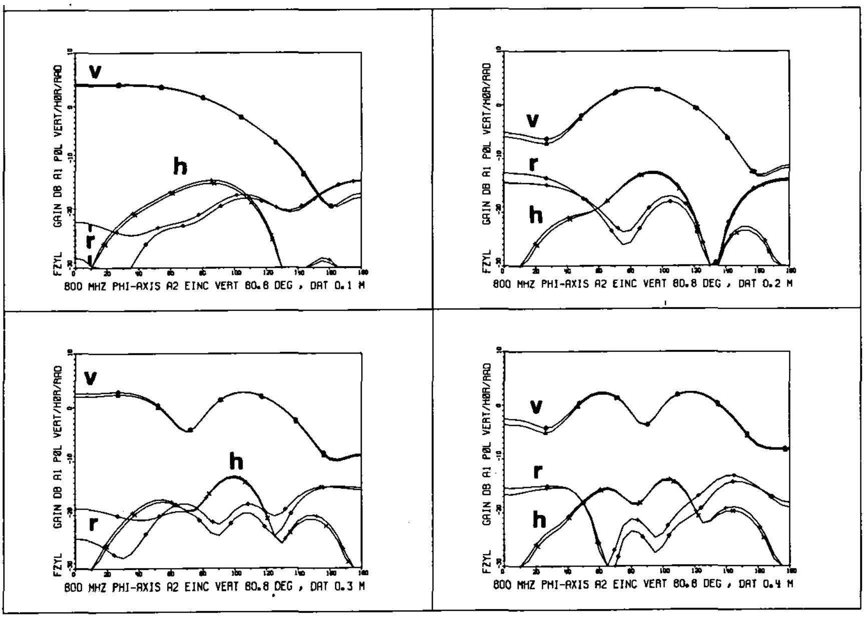

FIGURE 105a Azimuthal radiation patterns FZYL at 800 MHz.

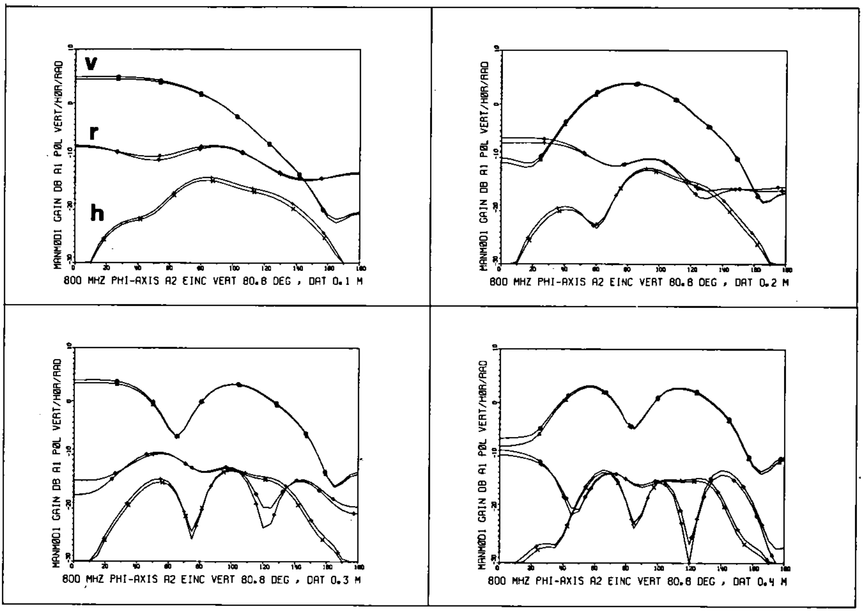

FIGURE 105b Azimuthal radiation patterns MANMOD 1 at 800 MHz.

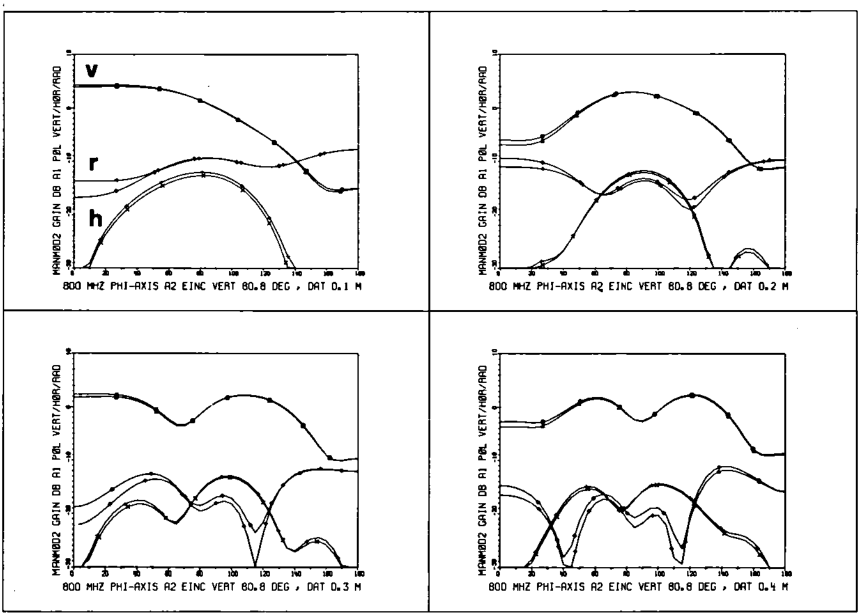

FIGURE 105c Azimuthal radiation patterns MANMOD 2 at 800 MHz.

L E B E N S L A U F

28. 7. 1943	Geboren in Baden (AG)
1950 - 1955	Primarschule in Wettingen (AG)
1955 - 1958	Bezirksschule in Baden und Wettingen
1958 - 1959	Oberrealsschule der Kantonsschule Zürich Stadt
1959 - 1963	Lehre als Maschinen-Schlosser bei Brown, Boverie & Cie
1963 - 1966	Teilzeit-Arbeit als FEAM bei Brown, Boverie & Cie und zweiter Bildungsweg bei der Akademikergemeinschaft in Zürich, Eidgenössische Matura, Typus C
1966 - 1970	Studium der Elektrotechnik an der Abt. III B der ETH Zürich. Hilfs-Assistent am Lehrstuhl für Apparatebau der Elektrotechnik der ETH Zürich, Industrietätigkeit. Abschluss als Dipl. El. Ing. ETH
seit 1971	Leiter der Gruppe Messtechnik am Laboratorium für Biomechanik der ETH Zürich
1974	Organisator und Chairman des Second International Symposium on Biotelemetry, Davos, May 20-24, 1974
1974 - 1976	Vice-president der International Society on Biotelemetry und seither member of the scientific council
seit 1978	Beirat der Schweizerischen Gesellschaft für Biomedizinische Technik, Mitglied des Schweizerischen Fachkommission FK-62 der IEC-SEV, Experte des Internationalen TC-62 der IEC (Probleme der Biotelemetrie)